PARTIAL DISCHARGE MEASUREMENTS IN HIGH VOLTAGE MOTORS

by

John G. Buchan BSc (Hons)

This thesis is submitted in partial fulfilment of the requirements of the Council for National Academic Awards for the Degree of Doctor of Philosophy (PhD).

Sponsoring Establishment :

School of Electronic and Electrical Engineering
Robert Gordons Institute of Technology
Schoolhill
Aberdeen AB9 1FR

Collaborating Establishment :

Britoil plc
150 St. Vincent Street
Glasgow G2 5LJ

September 1987.

DECLARATION

I hereby declare that this thesis is a record of work undertaken by myself, that it has not been the subject of any previous application for a degree, and that all sources of information have been duly acknowledged.

During this research the following course was attended :

1. Short course on computer-aided electromagnetic field analysis, SERC Rutherford-Appelton Laboratories, Oxford, 1983.

John G. Buchan BSc (Hons)

September 1987.

INDEX

ACKNOWLEDGEMENTS

In these ackowledgements , I first of all give thanks to my director of studies , Mr. David G. Edwards for his well appreciated supervision and help throughout the period of study .

I am also very grateful to the Science and Engineering Research Council for financial assistance during the research and to Britoil plc for industrial sponsorship.

It is also with great appreciation that I thank my wife Christine for her support and encouragement and endeavour to proof-read the thesis and for the times she sent me upstairs to work on this report - thank you .

Thanks also must go to my mum and dad for their encouragement and moral support throughout my long college years .

I am also very thankful for the time given to write some of this thesis at McDermott Engineering Aberdeen ; especially to Walter Abernethy , my boss . Thanks also to Graeme Dow and Michael Tracy for the CAD drawings in the report .

I also express thanks to Miss Gillian Stephen for typing a large portion of this report from my sometimes unreadable hand-writing .

Thanks also to Philip Robertson of William Whyte, Chemist for the developing and printing of photographs and oscillograms in the thesis.

Finally , I cannot forget to thank our two little boys , John and Paul, for their thoughtfulness in going to their beds early(ish) to help dad complete his book .

My help comes from the Lord, who
made heaven and earth .

(Psalm 121:2)

ABSTRACT

PARTIAL DISCHARGE MEASUREMENTS IN HIGH VOLTAGE MOTORS

by

JOHN G. BUCHAN

The work presented in this thesis is concerned with the development of an on-line technique for detecting and locating partial discharges in the stator winding of a high voltage electrical machine . This technique forms part of an on-line health monitoring strategy for the insulation of high voltage machines . Existing diagnostic techniques and partial discharge measurement systems are reviewed . The requirement for an on-line partial discharge location technique is discussed .

An experimental investigation was carried out into the propagation characteristics of partial discharge pulses within a model stator winding . This allowed identification of the main propagation characteristics which were used as the basis for the development of a partial discharge location technique .

In the development of a location technique , a means of on-line detection of discharge signals at the motor terminals is required . A study was therefore made on the use of the Rogowski coil for the non-invasive measurement of partial discharges .

A partial discharge location system was developed based on the correlation of partial discharge pulses detected at the two ends of a motor phase winding . The performance of the location system was investigated by injecting artificially generated discharge pulses into the model stator winding . Further verification of the ability of the technique to locate the position of discharges was done by injecting high voltage discharges .

The final part of the research work was to develop a theoretical model to predict the propagation behaviour of partial discharge pulses in the stator winding of an electrical machine . The effect of electromagnetic propagation through the endwinding region is incorporated in the model of two adjacent coils in a winding .

CHAPTER ONE

INTRODUCTION

1.1 Introduction

The induction motor is an essential piece of equipment in any industrial process . It provides the necessary power to mechanical plant such as pumps and compressors which are used in the extraction and processing of a product .

The sudden and unexpected failure of an induction motor may have catastrophic consequences , with , the loss of plant production ; damage to the motor and other valuable ancillary equipment ; and the danger of injury to plant personnel . This is especially true in the offshore oil and gas industry in which men and machines work in the harsh enviroment of a North Sea production platform , where the risk of explosion exists from the release of hydrocarbon gases into confined areas .

Losses in revenue from oil and gas production involve large amounts of money in addition to the repair and replacement costs of critical equipment which are particularly high in relation to land based industries . Reliability and availability of the induction motor which is critical to a process is therefore of paramount importance .

A number of surveys have been conducted in both onshore and offshore industries to establish the frequency and types of failure of large induction motors . The results of three independent surveys are presented here .

In a survey conducted by Robert Gordons Institute of Technology [1], on 82 high voltage induction motors operated by onshore and offshore industrial organisations , a total of 94 failures were recorded in a group of 52 motors . A total of 30 motors experienced no failures . The motor ratings varied from 425 kW up to 6.3 MW and supply voltages ranged from 2.3 kV to 13.8 kV . It is notable that 98 percent of these machines were direct-on-line started .

A very much larger survey was performed under the sponsorship of the Electric Power Research Institute [2] . This survey investigated the failures in generator and motor units in 65 power generation plants which represented a total of 168 generators and 6312 motors . Of the motor sample population , 3863 motors were rated at 200 kW and above whilst 1952 motors ranged from 75 kW to 200 kW ,(the remaining 497

motors ratings were not reported) . Supply voltages varied from 460 V and 575 V for low voltage motors , and between 2.3 kV and 13.2 kV for high voltage motors .

From a population of 6312 motors a total of 1474 failures occured in a group of 1052 motors . A further breakdown of these figures shows that a total of 1002 failures occured in a group of 673 motors rated 200 kW and above , and a total of 406 failures occured in a group of 327 motors rated from 75 kW to 200 kW . This represents an overall failure rate of 3.1 percent of the motors per year .

The third survey was conducted by Shell U.K. Exploration and Production [3] , which operates 10 offshore installations in the North Sea . The survey covers 158 motors rated between 335 kW and 9.24 MW supplied by voltages at 4.16 kV and principally 6.6 kV . Although no detail is provided on the number of failures and failed machines , the reported failure rates of motors are significantly higher than those in motors in onshore plants , typically between 12 and 20 percent . This underlines the increased problem of machine reliability on offshore installations due to the harsh operating enviroment .

From the information presented in these surveys it can be seen that there are a significant amount of motor failures , in both land and offshore industries , to warrant the introduction of some effective measures to increase the levels of machine availability .

This objective can be achieved in the following ways :

i. Improvement of the machine design by the manufacturer to meet the requirements of a particular operator's application. This will improve motor reliability and therefore increase plant availability .

ii. The introduction of an intelligent maintenance strategy to reduce the probability of motor failure .

It is the latter of these measures which forms the basis of this study .

1.2 Maintenance Philosophies

Existing maintenance strategies can be classified into three distinct categories [4] , which are discussed in the following sections .

1.2.1 Run to Break Maintenance

Machines are run continuously until failure occurs and are subsequently repaired and recommissioned . This is obviously a crude method of operation and not recommended for important plant motors .

1.2.2 Regular Preventative Maintenance

Machines are shut down for inspection at regular , planned time intervals to reduce the chance of unplanned outages . This type of maintenance is the common practice of operators of production platforms . The main problem lies in the choice of the optimum maintenance interval . Too frequent maintenance is wasteful in lost production time and increases the risk of introducing problems during overhaul which may lead to premature breakdown of the motor . Too long an interval increases the number of machine failures during operation . By experience , a compromise between the two can be achieved but this does not ensure that failure of machines will not occur .

This philosophy equates to that of a doctor giving a patient periodic checks . Whilst the screening process increases the chances of diagnosis of a serious illness , it will be unable to detect a rapid deterioration in the patient's health .

1.2.3 Condition Based Maintenance

Condition based maintenance is a predictive maintenance strategy in which the condition of failure-prone components of the machine are monitored . This method relies on monitoring relevant motor parameters whilst the motor is running to assess the condition or health of the motor . If the parameters indicate that the machine is progressing towards a potentially critical condition , then the machine can be taken off line at the next planned outage for remedial action .

On-line condition monitoring is approached in one of two ways . The

first is through 'Trend Analysis' in which an assessment of the machines condition can be found by observing the trend in the magnitude of a measured parameter to provide an indication of possible failure . This technique is used in conjunction with information obtained from case histories of the machine or other machines .

The second approach assumes an in depth knowledge of the relationship between the parameter measured and the integrity of the component which causes the motor to fail .

By applying a condition-based maintenance strategy the optimum time interval for machine examination can be obtained since this depends on the health of the machine which is continuously monitored . Application of condition monitoring to machines , according to a study by the Department of Industry [4] , has been proved to have the following benefits to the industrial operator :-

i. Increased plant availability resulting in greater output from the capital invested .
ii. Reduced maintenance costs .
iii. Improved safety .
iv. More efficient plant operation .

1.2.4 Condition Monitoring Techniques

The first step in the application of a condition monitoring strategy to a rotating electrical machine is the identification of the type of faults which occur in normal service . As the motor is an electromechanical device it is possible to classify fault mechanisms into one of three categories as follows : electrical , mechanical and electromechanical .

1.3 Basic Motor Failure Mechanisms

Failure which is purely electrical in nature is associated with those faults which occur in the stator windings of the machine . Failure which is purely mechanical in nature is due to faults which occur in the mechanical components of the machine , that is , the bearings and the rotor . Failure which is classed as electromechanical is a result of a fault in a mechanical component due to an electrical stress and vice versa . An example of this is the gradual wear of bearing

surfaces from spark erosion which is caused by circulating currents in the rotor shaft and bearings of the machine .

The surveys on motor failures conducted by R.G.I.T. and the E.P.R.I. have shown that the majority of machine failures are due to the development of faults in three major components of the motor : the stator winding , the bearings and the rotor . Results from these surveys , (shown in table 1.1) , indicate that around 40 percent of machine breakdowns are attributed to failure of the bearings and a similar percentage is attributed to failure of the stator winding . This is followed by rotor failures which accounts for 4.25 and 9 percent of motor breakdowns .

Machine Component	Percentage of Failures	
	RGIT Survey	EPRI Survey
Bearings	44.68	41
Stator Winding	44.68	36
Rotor	4.25	9
Other	6.39	14

Figure 1.1 : Percentage Failures of Major Components

1.3.1 Bearing Failure

Bearing failures are a direct result of one of three fault mechanisms and these are :

i. Rotor shaft vibrations .
ii. Bearing currents .
iii. Inadequate lubrication .

Excessively high levels of vibration transmitted to the bearing from the rotor shaft inevitably lead to bearing failure . Vibration monitoring systems are widely available to detect abnormally high levels of vibration [5] .

Bearing currents are circulating currents that flow through the rotor shaft , bearing assembly and pedestals , and the machine baseplate [6]. They are generated from voltages induced in the rotor shaft by

radial magnetic asymmetries in the machine . The flow of bearing currents causes sparking at the bearing surfaces which results in the formation of small pits from the removal of small fused metal particles . A further consequence is the deterioration of the lubricant by the discharge process and contamination from metal particle debris .

The majority of bearing assemblies are not suitable for an on-line monitoring technique and are therefore subject to periodic examination off line .

One technique , applicable to plain bearings which have an oil circulation system only , is the particle debris monitor . Magnetic and conducting particles entrained in the oil may be detected and quantified , in terms of size and number [7] .

1.3.2 Rotor Failure

Rotor – related failures are a result of the following fault mechanisms :

i. Broken rotor bars and cracked bar/end ring joint .
ii. Static and dynamic rotor eccentricity .

Fractures can occur in the conducting bars of a squirrel cage rotor winding at the point where the rotor bar is joined to the end ring , [8] . These fractures or breaks are a result of a number of mechanisms .

In an operating condition where there is a surge in the rotational torque exerted on the rotor , for example when the motor is started direct on line , the torsional force exerted on the end-ring stresses the bar/end ring joint . Fracture of this joint ensues through metal fatigue . The conductors adjacent to the broken bar carry additional current which causes the conductors to overheat . Subsequently , the overheating causes differential thermal expansion of the bars which stresses the bar/end ring joints . This condition becomes progressively worse as more fractures appear in the rotor until breakdown occurs . Serious damage to the stator core and end-windings can happen if a bar or bar fragments are freed .

Another source of rotor bar overheating is high resistance brazed or welded bar/end ring joints . Current redistribution results in localised heating in rotor bars adjacent to the bar with the high resistance joint .

A motor with broken rotor bars exhibits torque pulsations , speed fluctuations and abnormal vibration which can damage the rotor and the bearings .

A monitoring technique , [1] , has been developed which is capable of discriminating between the effects caused by high resistance bar/end ring joints and the number of broken rotor bars . This information is obtained from a frequency spectrum analysis of either the motor supply current , axial flux , end winding leakage flux or stator core vibration .

Static rotor eccentricity is the condition in a motor caused by stator ovality or incorrect alignment of the rotor and stator axes , whereby the airgap length varies . The position of minimum airgap length is fixed in space . Fluctuation in the airgap length introduces pulsating electromagnetic forces , (unbalanced magnetic pull) , which initiates abnormal vibration . This results in damage to the bearings of the machine .

Dynamic eccentricity is similar , in that the centre of the rotor is not at the centre of rotation which means the minimum airgap revolves with the rotor . Bearing movement and flexing of the rotor shaft from dynamic disturbances are responsible for this form of eccentricity .

A combination of static and dynamic eccentricity promotes large unbalanced magnetic forces in the airgap which can cause serious damage to the machine in the form of rub between rotor and stator surfaces .

It is possible to detect and assess the severity of static and dynamic eccentricty in machines , [9] , by analysis of the frequency spectrum of signals derived from the supply current and the stator frame vibration . This technique can be incorporated in an overall condition monitoring system .

1.3.3 Stator Winding Failure

Failure of the stator winding occurs by breakdown of the stator insulation through a combination of degradation mechanisms and abnormal motor operating conditions . The former is discussed in section 1.5 of this chapter .

The various abnormal operating conditions that contribute to the breakdown of the stator insulation are : too frequent starting , stalling , unbalanced supply or single phasing , and overloading .

These operational faults are generally adequately protected against by the use of over-current and thermal relays , thermistors located in the core and by negative phase sequence relays for single phasing faults [10] .

1.4 High Voltage Machine Insulation Systems

A knowledge of insulation systems employed in high-voltage stator windings is necessary to an understanding of breakdown processes within these systems .

In general , high voltage machine stator coils are form wound . A strand of copper is wrapped in a layer , or layers , of micaceous insulation . Traditionally , this was constructed from the lapping of mica flakes or splittings bonded to a paper/fabric/glass cloth backing tape using a resin binder . This has been replaced by mica paper which is formed from splitting small mica flakes into tiny particles , which are then formed into sheets mica paper of by settling the particles from suspension , rather like a paper making process . The resin binder may be applied at this stage by impregnation to give a resin-filled mica tape . Refer to reference 12 for a more detailed account .

Once formed , the coil is wound in a number of layers of mica tape impregnated in resin and heat cured to give a consolidated high voltage insulation system which has high dielectric and thermal strength . A typical coil insulation system is shown in figure 1.4.1 .

Up until the 1960's , the binding medium used was a natural resin ; either shellac or bitumen . These resins were applied to the

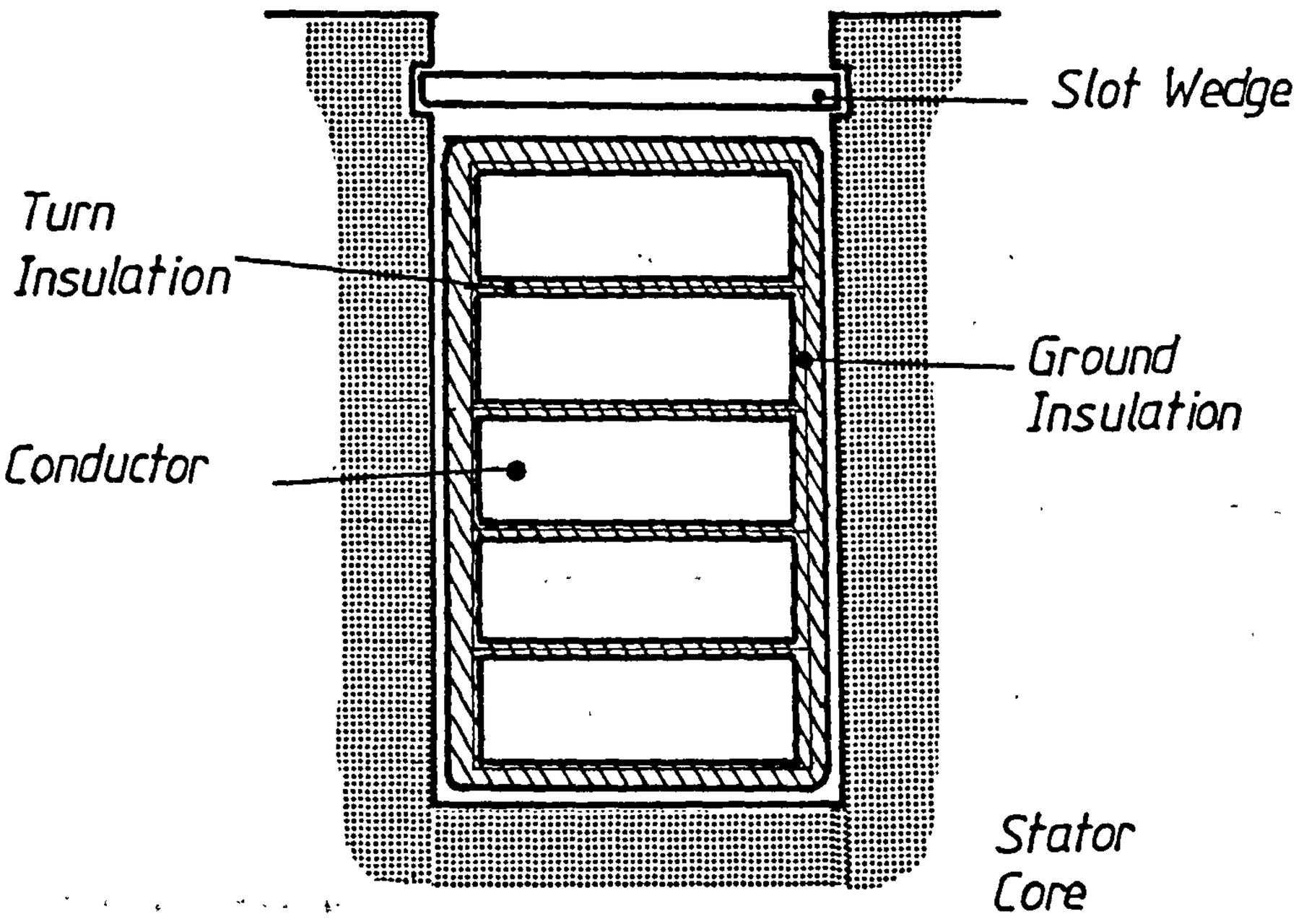

Figure 1.4.1 – Typical High Voltage Machine Winding Insulation System

mica flake and backing tape in liquid form as hard resin suspended in a solvent which required the removal of the solvent before the resin could set . These natural resins are thermoplastics , and consequently become pliable and plastic at high temperatures . This restricted their use to machines having a class B , (130 deg C) ,thermal rating .

However , in the 1950's new synthetic resins were developed , such as polyester and epoxy resins which are thermosetting polymers . Synthetic resins have higher working temperatures than natural resins in that they preserve their mechanical properties at higher temperatures . This meant that machines constructed with synthetic resin-bonded insulation could operate at higher temperatures . As a consequence greater power output could be obtained from a machine of a given frame size , thus making the use of synthetic resins more economically attractive .

In high voltage motors the slot- bar portion of the stator coil is coated in a partially conductive layer of colloidal graphite paint or carbon-impregnated tape to prevent the occurrence of harmful slot discharges by eliminating the build up of high stress regions .

In addition the area of the coil which emerges form the stator core in to the endwinding space is a region of high electric field stress due to the sharp discontinuity in conductor and dielectic . This region is covered in a stress grading semi-conductive paint which effectively smoothes the discontinuity in the electric field by the flow of leakage currents through this semi-conductive paint [12] .

1.5 Insulation breakdown mechanisms

An understanding of the mechanisms, whereby machine stator insulation breaks down, is a necessary prerequisite to the development of an on-line insulation monitoring and diagnostic technique .

It is possible to identify six modes of failure in a 3-phase stator winding of a machine [11] , and these are indicated on the diagram in figure 1.5.1 . Each of these faults result in a flow of short-circuit current in the machine winding from a breakdown in the turn or ground insulation .

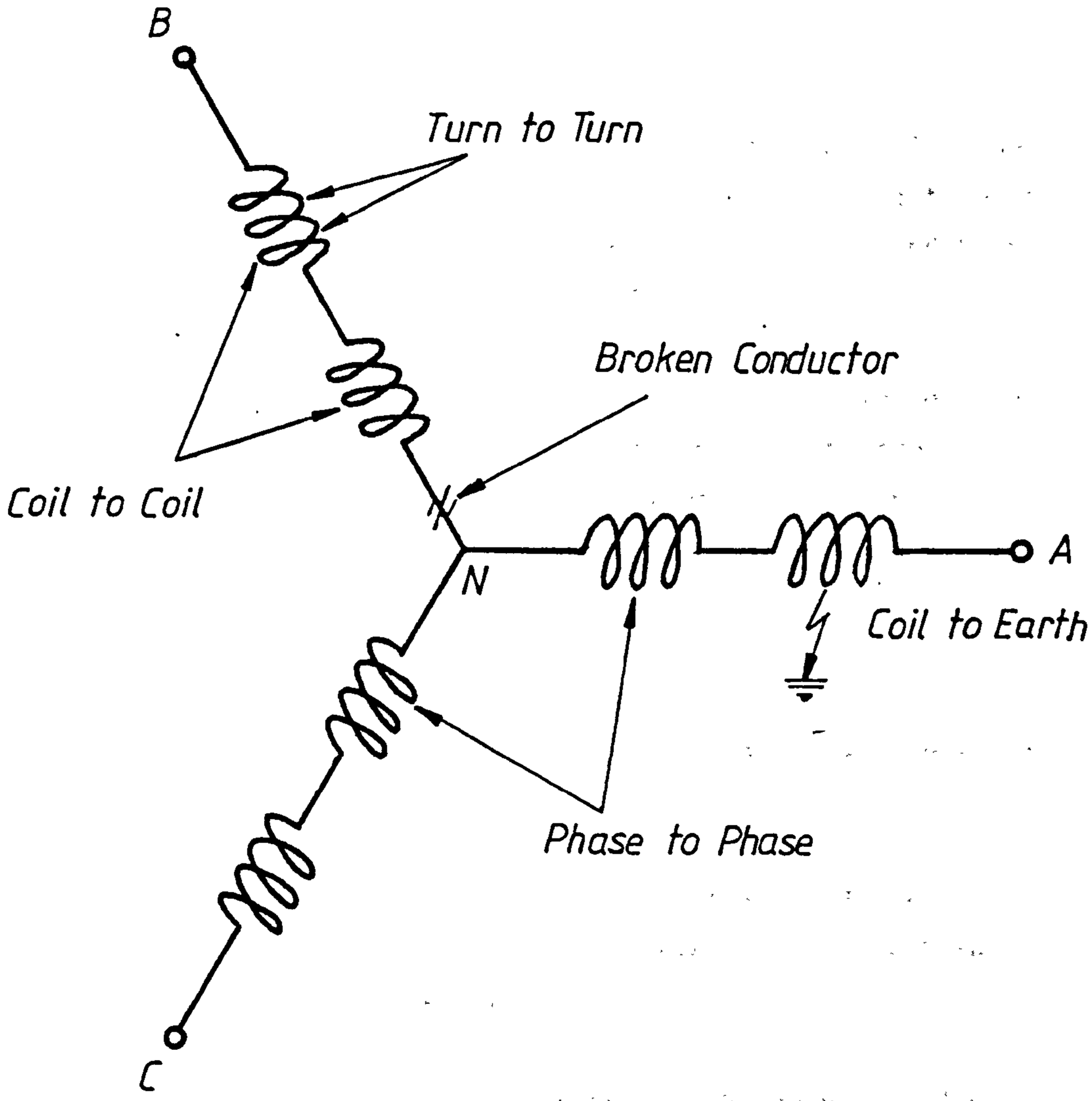

Figure 1.5.1 - Failure Modes in High Voltage Machine Stator Winding

Machine insulation breaks down when subjected to a combination of three principal stress and deterioration processes which are classified as follows:-

i. Thermal
ii. Mechanical
iii. Electrical

The severity of individual stresses can vary substantially and depends on a number of factors : the size of the machine ; type of insulation ; end-winding bracing system ; machine operating conditions and so on .

The degradation processes caused by each type of stress is reviewed with particular reference to present generation thermosetting insulation and in comparison to older thermoplastic insulation systems .

1.5.1 Thermal stress

Thermal stresses in machine insulation can take two forms ; iso-thermal and thermal cycling .

In the case of iso-thermal stress the insulation deteriorates gradually over a long period of time which is observed by a decline in the dielectric strength of the insulation [13] .

Deterioration is a result of heat generated at the copper conductor surface at normal operating temperatures which has to be dissipated through the main ground insulation to the iron in the stator core and the air in the endwindings . Heat dissipated in the insulation causes embrittlement by depolymerisation of the binding resin and eventual localised cracking . Loss of adhesion of the mica tape to the copper is also observed which accounts for the slight swelling in the stator bar observed in functional ageing tests performed on epoxy resin/mica paper [14] .

A similar degradation process occurs in natural resin/mica flake insulation from thermal stressing [15] . The natural resins loose their thermoplastic quality and become brittle . However during normal service temperatures the resins become pliable and the

insulation swells .

Thermal cycling of the insulation occurs during normal motor service when a change in load takes place or when the motor is tripped and re-started . Variations in temperature and the differences between the thermal expansion coefficients of the copper conductors and the ground insulation causes relative axial movement between the copper and insulation . These axial movements from thermal expansion and contractions, mechanically stress the insulation , especially at the interface of the slot bar and the end-windings , and promote the development of tape separation or 'girth cracking' which leads to the eventual failure of the insulation [16] . In addition , shear stresses at the copper/insulation interface cause a loss in adhesion of the insulation to the copper conductors .

These problems are associated more with older thermoplastic insulations . Tests show , [13,14] , that the epoxy thermosetting resin insulation systems exhibit a high resistance to thermal cycling stresses . This is because epoxy resin/mica paper insulation has a similar thermal expansion coefficient to copper thus the insulation tends to move axially with the copper conductor [15,17] .

Thermal cyclic stress is also responsible for damage done to the partially conductive paint coating on the slot bar causing it to flake [18] .

It has also been suggested that localised heating at points of contact between the partially conductive coating and the slot leads to degradation of small areas of the coating . The displacement currents which flow through the insulation are conducted along the partially conductive coating to the core . If the point of contact between the coating and the core is relatively small the current passing through this area causes heat to be dissipated which thermally degrades the coating material [19].

1.5.2 Mechanical stress

The stator windings of an electrical machine are subjected to electromagnetic forces created by the interaction of the current carried by the winding conductors and the magnetic field in which conductors are situated . As both current and magnetic field vary

sinusoidally at the supply frequency , the electromagnetic forces generated vary sinusoidally at twice the supply frequency . These cyclic forces cause the slot and end-winding conductors to vibrate at twice the supply frequency . Maximum forces are generated in a winding when two phases carry equal and opposite currents .

In order to eliminate damaging vibration the bar is supported continuously along the length of the slot by wedges in core slots to prevent radial motion of the bar in the slot , and packing material to prevent motion between insulation and the core surfaces . This is a particular requirement for hard thermosetting insulated bars which do not provide a uniform fit of the bar within the core slot . Older thermoplastic insulated coils conform to the contour of the slot and provide a wedge tight fit as the insulation expands at service temperature [17] .

A poor fit or damage to the packing material in the presence of the vibration will cause abrasion of the partially conductive layer and the mainwall insulation and a loosening of the wedge and packing material . Loosening of wedges and packing material in turn, accelerates the abrasion of the coil insulation surface .

The end-windings are supported with one or more bracing rings which are positioned close to the coil nose and secured to the individual coil with resinated glass fibre tape or cord . Each coil is separated from adjacent coils with bracing blocks . Movements in the end-windings however are more pronounced due to the fact that they are fixed at the slot end and are allowed a number of degrees of freedom . The movements from vibration tend to be in the radial and circumferential directions as shown in figure 1.5.2 . Vibration causes abrasion of the insulation where the tape or cord binds the coils together and to the bracing ring , [3] , which may result in the eventual fracture and failure of the main insulation . It is also responsible for fatigue fracture of the copper connections between coils . Arcing at the fracture position ensues leading to the breakdown of the insulation from overheating .

Mechanical stresses in the end-windings from vibration are particularly high during start-up of the machine [20] . During this period the winding conductors carry as much as seven times the normal running current . This gives rise to electromagnetic forces in the

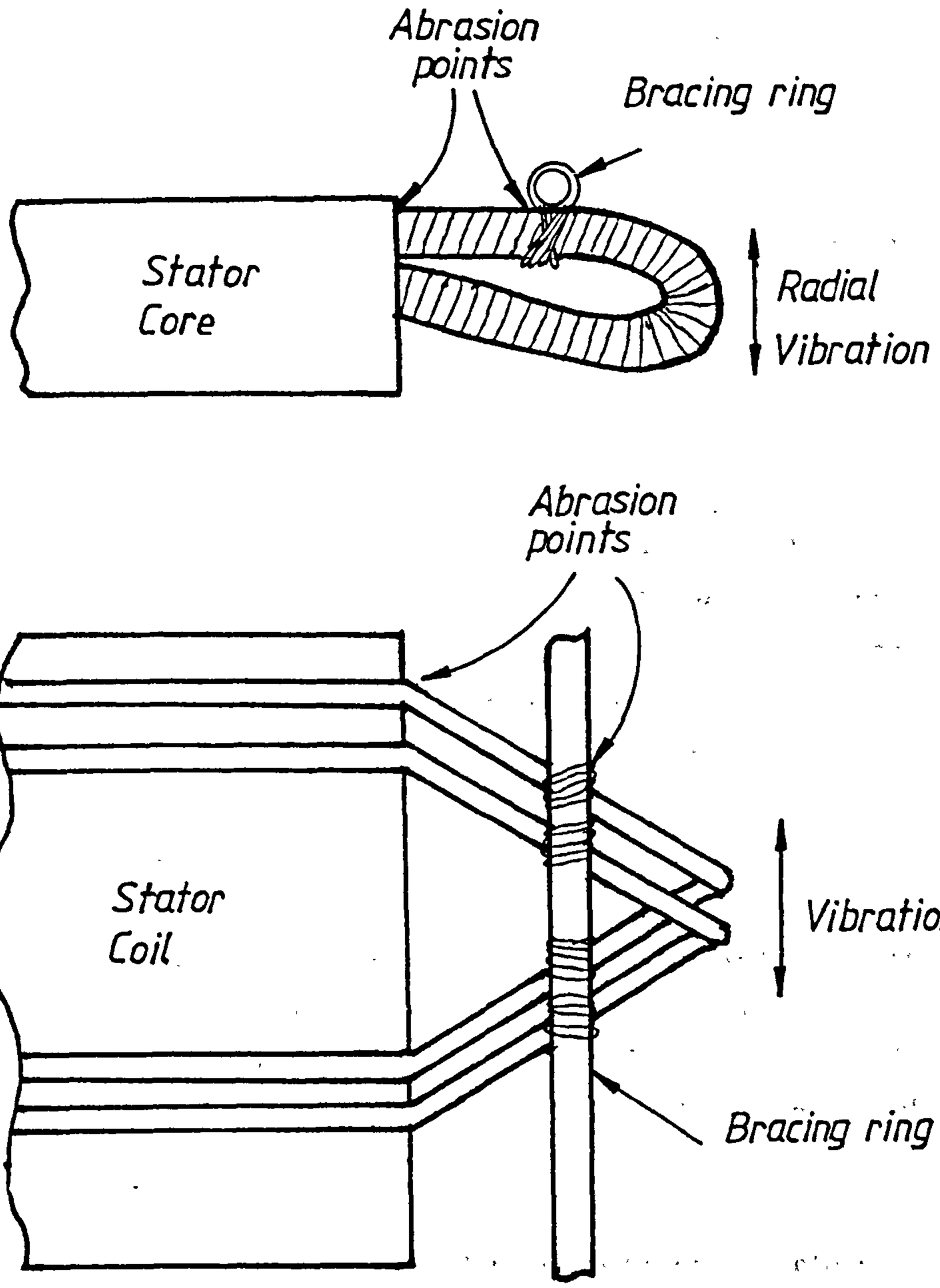

Figure 1.5.2 - Endwinding Vibration

endwindings that are as much as 49 times the magnitude experienced during normal service . The forces are such that individual coils experience larger movements and more severe abrasion than in normal running conditions . After a large number of starts the vibration causes fatigue cracking of the copper at the coil connections .

1.5.3 Electrical stress

Electrical stress in a machine winding occurs from external and internal processes and are categorised as follows :-

i. Dielectric stress .
ii. Partial discharges .

Dielectric stress occurs from the application of a high voltage across a small insulation space causing a steep voltage gradient that stresses the mainwall and interturn insulation . This voltage is either the normal sinusoidal supply voltage applied to the machine or an externally generated , steep-fronted , voltage surge .

1.5.3.1 System voltage surges

Voltage surges generated in power distribution systems from switching operations are frequent and severely stress the insulation of high voltage machines , resulting in the possible breakdown of the insulation . These switching transients may be placed in one of two categories .

In the first category are steep-fronted transients which place severe stress on the interturn insulation , whilst in the second category are large overvoltages, which are lower-frequency transients, that severely stress the mainwall insulation .

Steep-fronted transients occur when an arc is struck during the closure of the contacts of a circuit-breaker , termed a pre-strike , and the opening of contacts , termed a restrike . Restriking transients are a rare occurence , while prestriking transients are very frequent and occur during every contact closure [21] .

During circuit breaker closure, one of the poles will close initially, followed shortly by closure of the second and third poles . The first

pole closure will result in a steep-fronted voltage transient of, at worst, an amplitude equal to the peak phase to earth voltage . This surge then propagates to the motor terminals where it is increased to twice the phase voltage , due to the much greater surge impedance of the motor compared with the cable . When the surge impinges on the other two phase windings a resonant oscillation occurs which may reach 2 times the phase voltage at the terminals of each phase . Under these conditions , the voltage across the second and third poles of the breaker will approach $(2.0 + 0.5)V_{ph}$. If at this instant in time a pre-strike occurs across the second or third pole a steep-fronted transient is injected in the motor cable, which can double to 5 times phase voltage at the motor terminals .

In circuit breakers which can interrupt the arc current very quickly, multiple prestrikes can take place before contact closure thus subjecting the machine winding to a number of steep-fronted transients (see figure 1.5.3) . This is a particular problem with the use of vacuum circuit breakers . The wavefront duration of the prestriking transient is very short, in the region of 0.2 μsec to 1 μsec [21] . As a result a large proportion (as much as 80 to 90 percent) of the incident surge wavefront is distributed across the line end coil of the motor due to the propagation time in the winding. This causes high interturn voltages which stress the interturn insulation . Any localised weak points will be overstressed , followed by breakdown of the interturn insulation and winding failure . Moreover during the steepest wavefront conditions , under 600 nsec , the largest interturn voltage occurs in the neutral end turn of the line coil [21].

Large switching over-voltages can be produced by current chopping when a circuit breaker opens . The magnitude of this overvoltage is proportional to the product of the level of current chopped and the system surge impedance , (that of the supply cable and motor) , [23] . This severly stresses the ground insulation of the machine.

1.5.3.2. Partial Discharges

Partial discharges are essentially low energy electrical discharges which cause insulation breakdown by a gradual erosion process . These discharges occur internally and externally to the insulation .

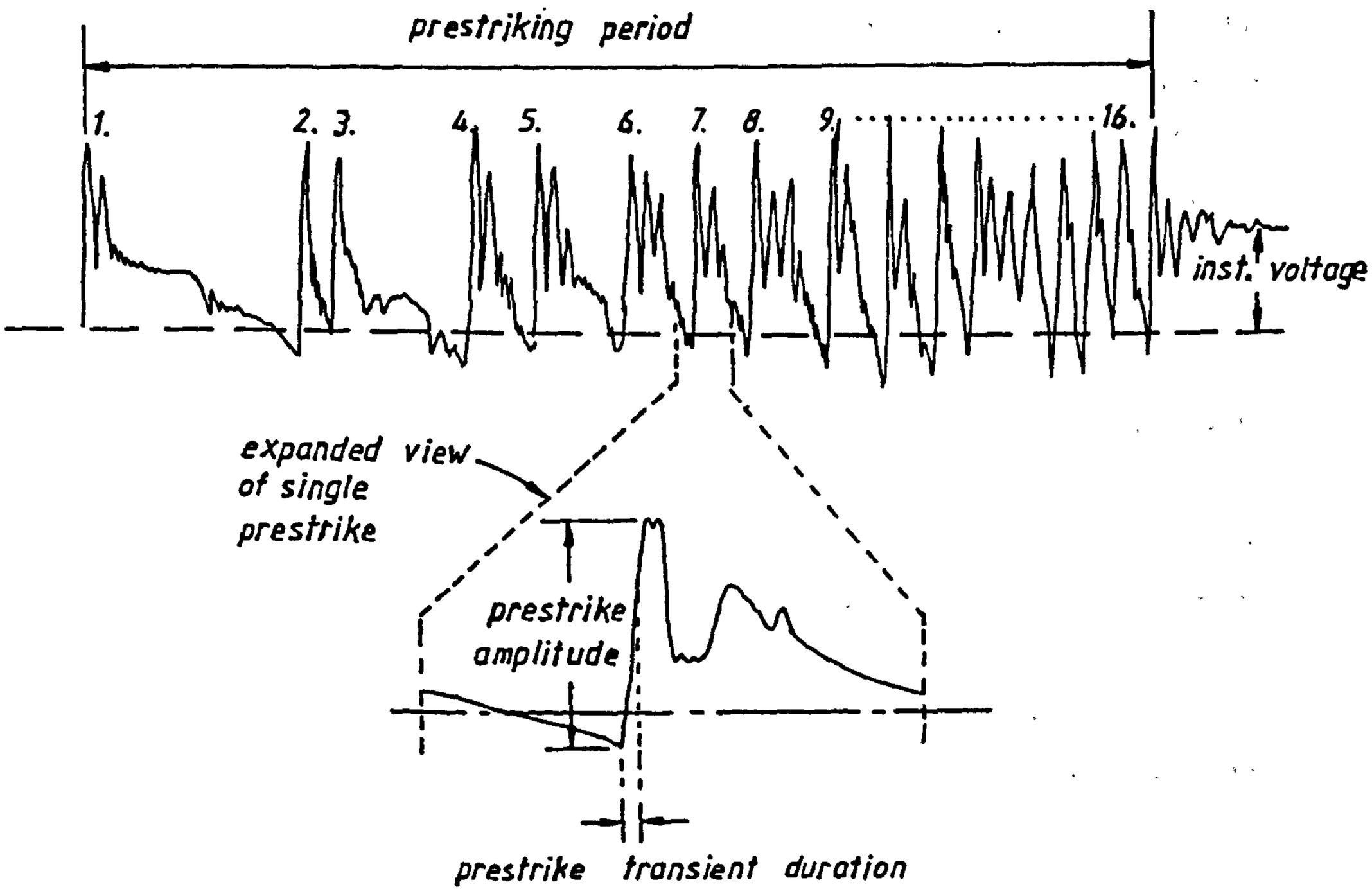

Figure 1.5.3 - Typical Prestrike Transients from Vacuum Circuit Breaker

Internal discharges take place in small voids or cavities in the insulation which are formed when air is trapped in small quantities during the curing and pressing process of coils at the manufacturing stage. In the air space of a cavity the electric field strength is higher than that across the solid insulation due to the difference in the dielectric permittivities . The relative permittivity of air, ϵ_o , is equal to unity while the permittivity of a mica paper/epoxy resin composite dielectric , ϵ_r , varies between 5 and 7 such that the electric stress across the cavity is :-

$$E_c = \frac{\epsilon_r}{\epsilon_o} . E_s \qquad \ldots.(1.1)$$

which can be as much as 7 times the electric stress, in the dielectric. The other contributory factor determining the magnitude of electric stress enhancement and distortion of the electric field within a cavity is the shape of the cavity , [24] , and the presence of charge or semi-conducting deposits on the surface of the cavity, [25] .

If, under normal working stress, the voltage across the cavity exceeds the breakdown potential of the gas, a discharge between opposite surfaces of the cavity will be established. The voltage across the cavity is then quickly restored . Under alternating voltage stress this process is repeated and a number of discharges occur on each half cycle. This sequence of discharge breakdown within a cavity is explained with reference to the simple model of a disk shaped cavity of thickness t, contained in a solid dielectric of thickness d, see figure 1.5.4 .

In the electrical circuit analogue [26], the cavity is represented by a capacitance C_c , the dielectric above and below the cavity is represented by a capacitance C_b and a capacitance C_a corresponds to the remaining dielectric. It follows that

$$C_b = \frac{\epsilon_o . \epsilon_r . A}{(d-t)} \qquad \text{and} \qquad C_c = \frac{\epsilon_o . A}{t} \qquad \ldots.(1.2)$$

where A is the surface area of the cavity .

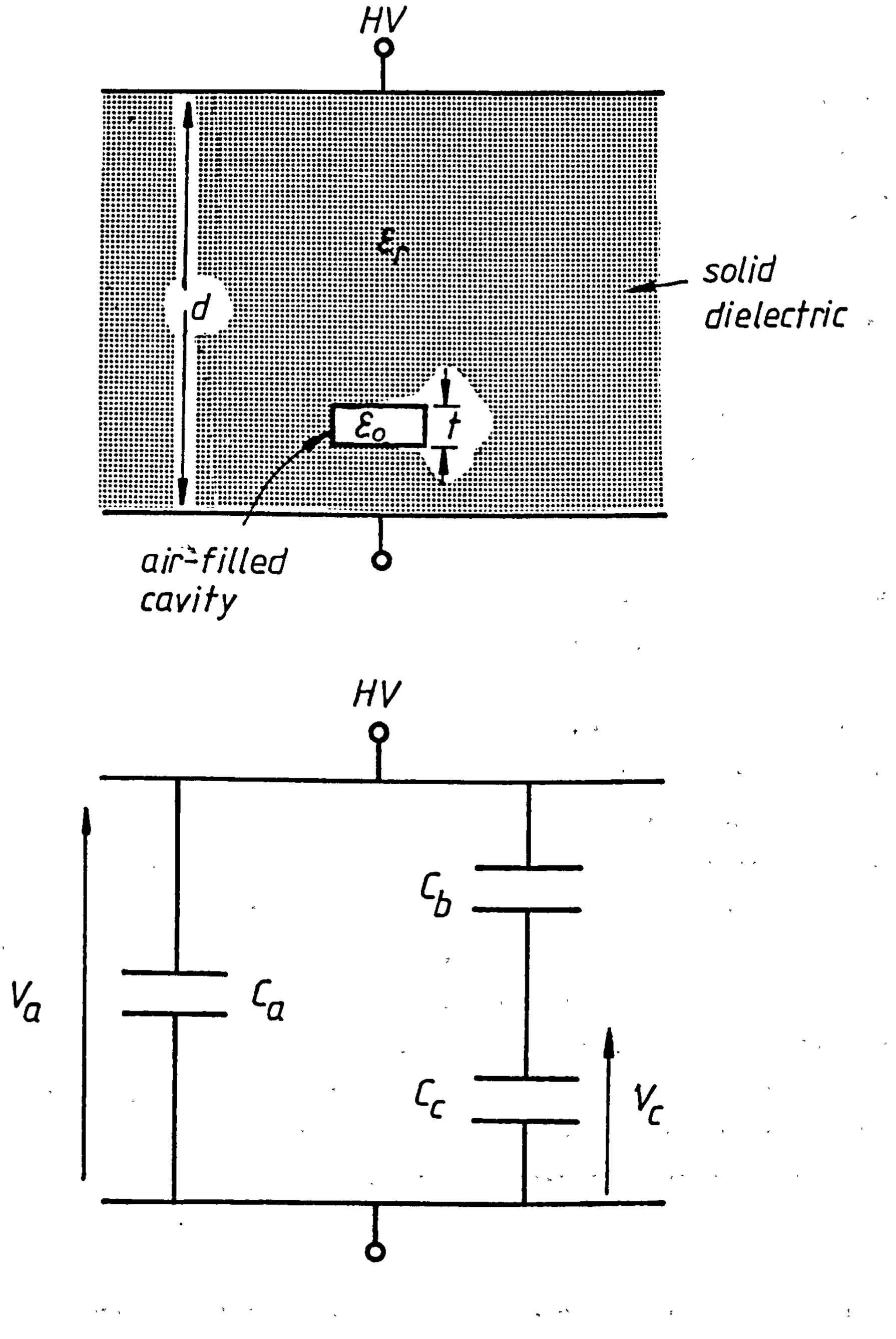

Figure 1.5.4 - Simple Model of Internal Air Filled Cavity in a Homogeneous Dielectric

The voltage Vc, developed across the cavity is therefore :

$$V_c = \frac{C_b}{(C_c+C_b)} . V_a = \frac{V_a}{1 + 1/\epsilon_r(d/t-1)} \quad \ldots.(1.3)$$

As the voltage rises during the positive half cycle of the supply the voltage across the cavity rises in accordance with equation (1.3). Once the voltage Vc exceeds the breakdown potential of the cavity , +u , a discharge occurs and the voltage collapses in the cavity to a voltage level of +v . Once the voltage level reaches +v the discharge finishes . The voltage across the cavity then builds up with the applied voltage Va . A second discharge occurs when the voltage in the cavity reaches +u and the sequence of events is repeated. Thus a number of discharges are produced on the rising portion of the positive half cycle. A similar behaviour is observed on the negative half cycle in which discharges occur when the cavity voltage exceeds -u . The sequence of discharges is shown, with respect to the applied a c voltage for a single cycle , in figure 1.5.5 .

The main erosion mechanism is through electron and ion bombardment of the cavity surfaces. Electrons and ions impinging on the surfaces cause deterioration of the surface materials by the scission or breaking of chemical bonds and high localised surface temperatures, [25] . The application of an alternating voltage causes alternate ion and electron bombardment of cavity walls. Erosion may not take place at the same site on a cavity surface since discharges occur at different positions in the cavity . This is due to the high surface resistivity which promotes charge accumulation at a discharge site when the cavity is only partially discharged. The remnant charge distorts the electric field and forces the next discharge to occur at a different place on the surface .

In addition to particle bombardment, the surface of a cavity can be attacked from active discharge bi-products such as ozone, O_3 , and nitric oxides, NO_2.

Studies performed on samples of epoxy resins, [27] , have shown that large crystalline growths, oxalic acid, are deposited on the surface of cavities and that these formations intensify surface erosion. Similarily, investigations on the degradation mechanisms of mica subjected to internal discharges, (having energies of 10^{-8} and 10^{-6}

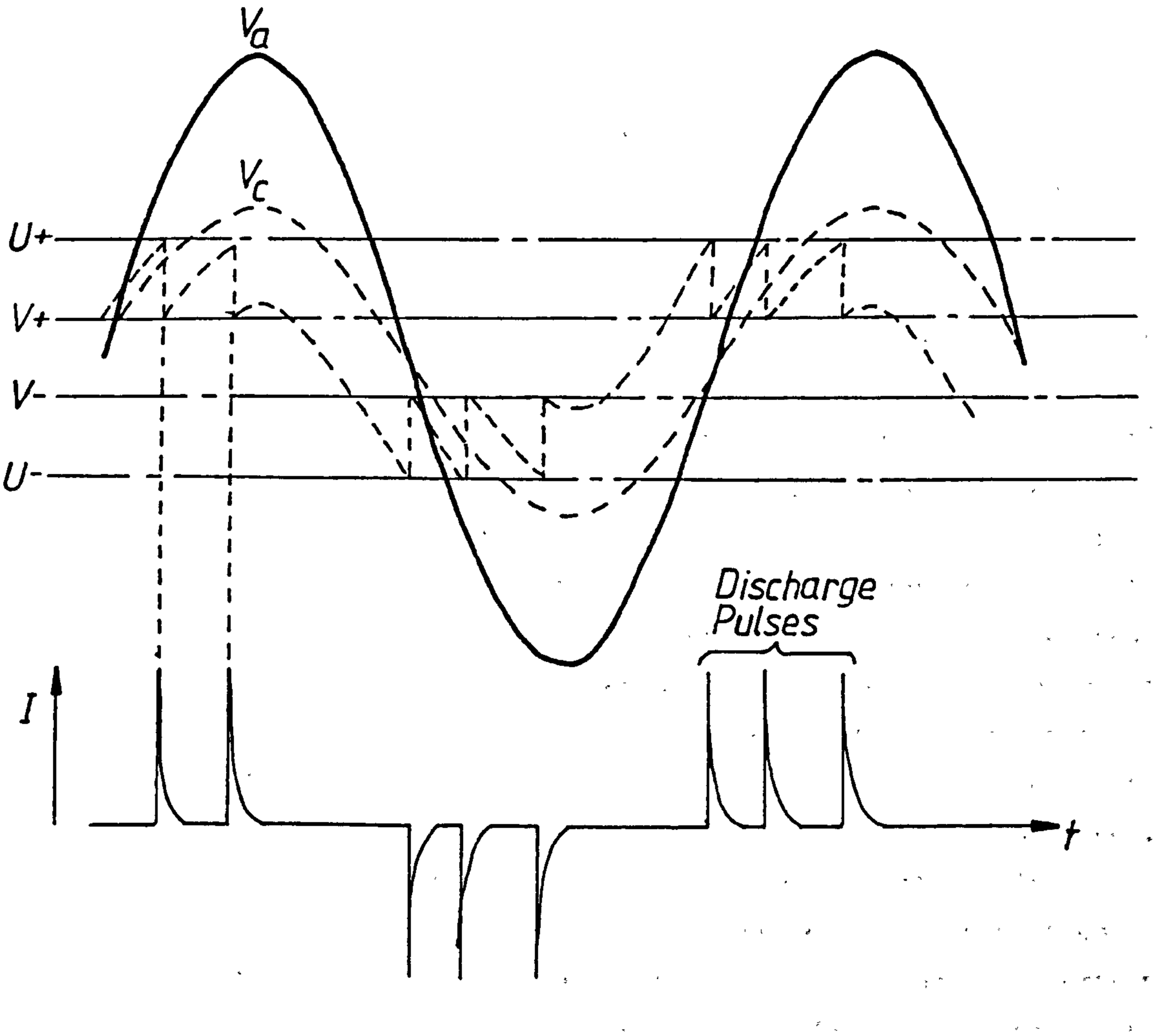

Figure 1.5.5 - Sequence of Discharges in an Internal Cavity under Alternating Voltage Stress

μJoules), have shown that the crystalline structure of mica collapses with the formation of cracks and splitting of surface layers . This deterioration process is accelerated by the nitric acid formed by the discharges [28] .

The net effect of all these degradation mechanisms is a slow erosion of the cavity surfaces and the material as a whole thereby reducing the dielectric strength of the insulation.

Internal partial discharge erosion of high voltage machine insulation has been the greatest problem for older thermoplastic natural resin insulation which swells in service causing de-lamination and void formation. Mica paper/synthetic resin insulation systems are well consolidated from heat pressing and curing and remain so during service so that the presence of internal cavity discharges is greatly reduced. However, motor failure has occured , [29] , from breakdown of the turn insulation in the endwindings. The presence of a groundwall insulation puncture in the endwinding, evidence of overheating at the breakdown site and no evidence of mechanical abrasion suggest the failure has been induced by partial discharges. Internal discharges occur in cavities which develop at the interface of the turn and main wall insulation. The main wall insulation is very resistant to discharge attack but the much thinner interturn insulation is less resistant to erosion . Eventually the turn insulation fails creating a short circuit between turns. This leads to excessive overheating of the adjacent main wall insulation from the mains frequency current at the point of short circuit. Failure of the main wall insulation ensues.

External discharges take the form of slot discharges in the core and surface discharges in the endwinding.

Slot discharges occur in the air space between the stator bar and the iron core and along the surface of the coil. Insulation systems of resin/mica paper are particularly vulnerable to slot discharges since these insulations are rigid and do not swell in normal service as do natural resin bonded insulations. Consequently the partially conductive surface coating makes positive electrical contact with the slot sides at intermittent intervals requiring extensive use of packing material to compensate for this. Two forms of slot discharge have been identified in high voltage motors and generators, [30] ,

which are characterised by the discharge initiation mechanism and the damage which results. The first form is a low intensity discharge which occurs at sites of damage or removal of the partially conductive coating even though electrical contact is maintained between the slot bar surface and the core.

At locations along the slot bar surface which are not in contact with the core, a surface potential is allowed to build up from displacement currents flowing through the mainwall insulation along the surface coating to the earth point of contact. The potential development depends on the resistivity of the partially conducting coating and the magnitude of the displacement currents. Calculations of resistivities for uniform conductive coatings have shown that surface potentials of only a few volts are developed. Even with departures of 80% from the manufacturers recommended resistivity, the potential developed at the bar surface is insufficient to cause slot discharge. However, if the partially conducting coating is damaged and small areas of coating are removed slot discharge activity will occur.

Damage may occur in service when abrasion between the slot bar surface and core laminations results from bar vibration when loose wedges and excessive clearances are present. It is also possible that excessive heating at the points of contact may lead to degradation of small regions of the surface coating [19] .

The high resistivity of the main wall insulation, at the free surface where the coating has been removed, allows development of high surface voltages. If the surface potential is sufficiently high, partial discharges will bridge the air gap between the insulation and the core or pass across the insulation surface to the surrounding surface coating. Surface discharges from the free surface to the conductive coating are established when the air gap is sufficiently large to cause the stress across the surface to be the greatest. The miniumium air gap for this has been shown to be approximately 0.15 mm for a circular bare surface of radius 1 mm or greater, on an 11 kV coil [30].

Surface discharges of this sort cause erosion of the partially conducting coating and extension of the bare surface. Similarly, at smaller separations the stress between the bare surface and the core is greatest and slot discharges between these points result. Slot

discharges of this type damage both the surface insulation and iron core but do not affect the surface coating .

Low intensity slot discharges have magnitudes in the range 1000 to 10,000pC , [31] , which can erode the surface layer resin exposing the glass fibre and mica. Abrasion of this glass fibre and mica layer from mechanical vibration of the bar in the slot cell can leave the second layer of resin open to discharge erosion and the process repeats .

The second form of slot discharge is very much more intense. It occurs when the slot bar and conductive coating are totally isolated from the iron core when contact is lost from excessive vibration and loose wedges. When the slot bar becomes isolated there is a capacitive voltage division across the insulation and air gap which may cause breakdown of the intervening air space producing a high intensity arc discharge. Discharge magnitudes characteristic of this type of discharge are in excess of 10,000pC and may be greater than 100,000pC [33] . Temperatures generated at the point of discharge may be as high as 1000 deg C which causes rapid erosion of the main wall insulation with the formation of erosion pits.

Surface discharges occur in the endwindings in the presence of contamination materials deposited on the endwinding surface of the machine. Typical contaminants are : oil from bearing leaks, water from a highly humid atmosphere or sea water , (as in the case of a motor on an offshore installation).

These contaminants allow the passage of excessive leakage currents which promote development of tracking and surface discharges at points of high stress. In the extreme case surface discharges can promote the breakdown of the insulation .

It has been shown in the discussion that a cumulative effect of thermal, mechanical and electrical stresses cause gradual degradation and final breakdown of the insulation of high voltage machine stators and this is conveniently summarised in the block diagram in figure 1.5.6 .

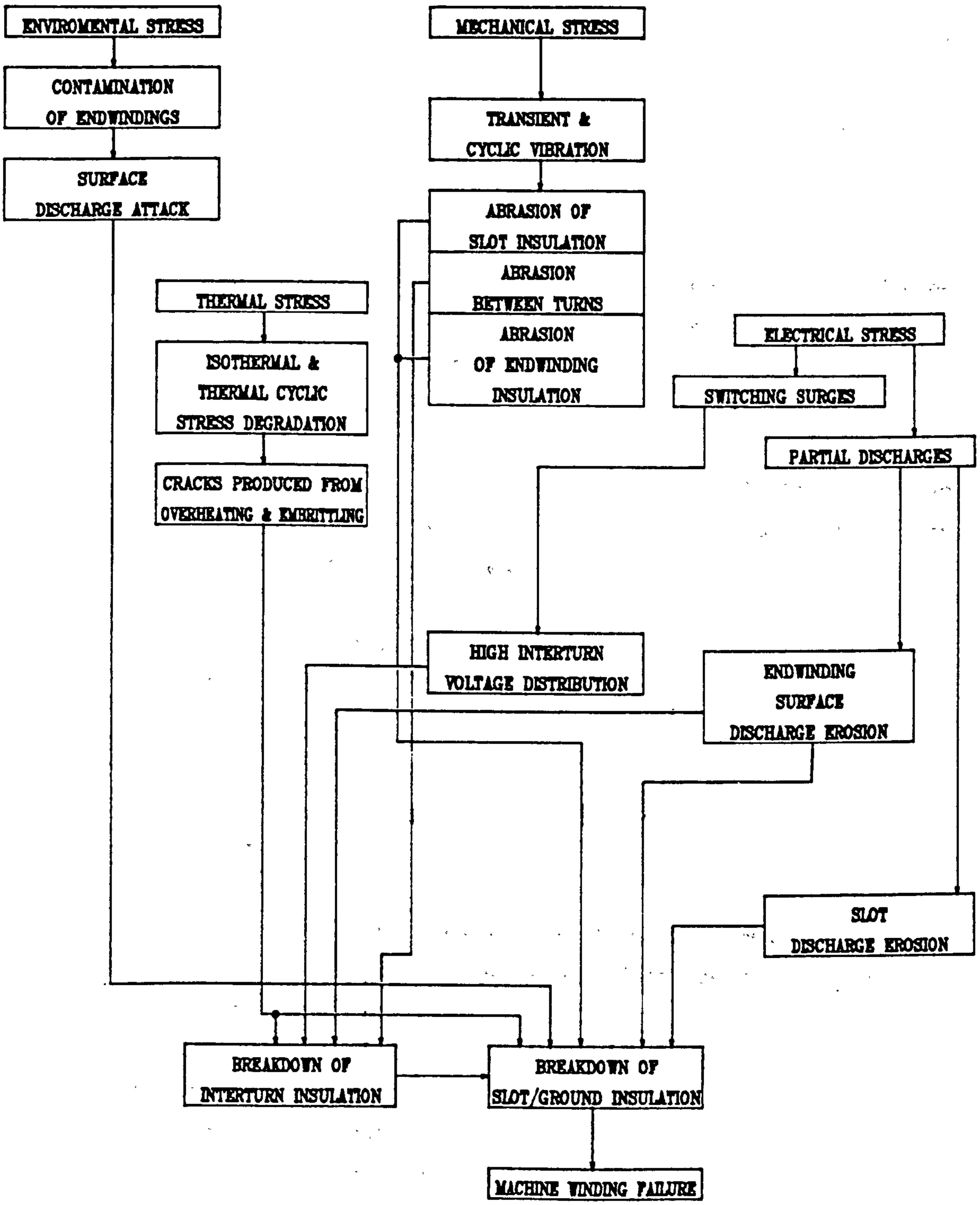

Figure 1.5.6 - Summary of Stator Winding Insulation Breakdown Mechanisms

1.6 High Voltage Insulation Diagnostic Measurements.

The purpose of diagnostic measurements is to assess the condition or health of high voltage insulation from observable phenomena which may be related to or give a measure of the insulation integrity.

The significance of partial discharges in determining the life of high voltage insulation is well recognised and observation of partial discharge phenomena yield by far the most information regarding the integrity of insulation, especially localised deterioration.

Although, it is recognised that measurements of insulation resistance and polarisation index , [32] , give useful information on the degree of surface contamination and dryness of the insulation and general state of the insulation, these measurements are limited in the assessment of the condition of the insulation.

Partial discharges are caused by rapid movement of electrical charge and hence energy changes, which are observable from the secondary physical effects these energy changes produce :-

i. Electrical current pulses.
ii. Dielectric losses.
iii. E.M. radiation.
iv. Light emissions.
v. Sound emissions.
vi. Chemical reactions.

Insulation diagnostic measurements are based on the measurements of one of these effects of partial discharge and are generally classified into the following categories :-

i. Integrated measurements
ii. Resolved measurements
iii. Radio interference measurements.

1.6.1 Integrated measurements.

Integrated measurements provide a quantitative measurement of dielectric loss or energy dissipation within the insulation structure. Dielectric loss is due to three main causes and these are : the

residual leakage current which arises from the conductivity of the dielectric : polarisation loss and the loss incurred by internal partial discharges.

1.6.1.1 Loss Tangent Measurements

A lossy dielectric is modelled conventionally , [26] , by either a series or parallel combination of a capacitor and resistor as shown in figure 1.6.1.1. Considering the parallel circuit equivalent only, the dielectric is represented by an ideal capacitance Cp and the dielectric loss is represented by a resistor, Rp. Under a.c. voltage stress the phasor relationships between voltage and current are shown in figure 1.6.1.2 .

Energy dissipated per cycle of supply voltage is thus a product of the ohmic current Ir and the applied voltage V.

$$P = I_r.V$$

In practical measurements the value of tan δ is measured which can be related to the power loss in the dielectric,

$$P = \omega C_p V^2 \tan\delta \qquad \ldots.(1.4)$$

since tan δ is defined as,

$$\tan\delta = \frac{Ir}{Ic} = \frac{1}{\omega CpRp} \qquad \ldots.(1.5)$$

δ is termed the dielectric loss angle and the tangent of the angle is termed the loss tangent or dissipation factor.
The measurement of loss tangent is normally performed using an a.c. bridge device such as the Schering bridge shown in figure 1.6.1.3. In the high voltage arms of the bridge are the specimen (winding) capacitance C_1 and a loss free standard capacitance C_2 .
Capacitance C_4 and resistance R_3 are variable to provide the controls to balance the bridge, and with resistance R_4 constitute the low voltage arms of the bridge. The high voltage supply is at mains frequency.

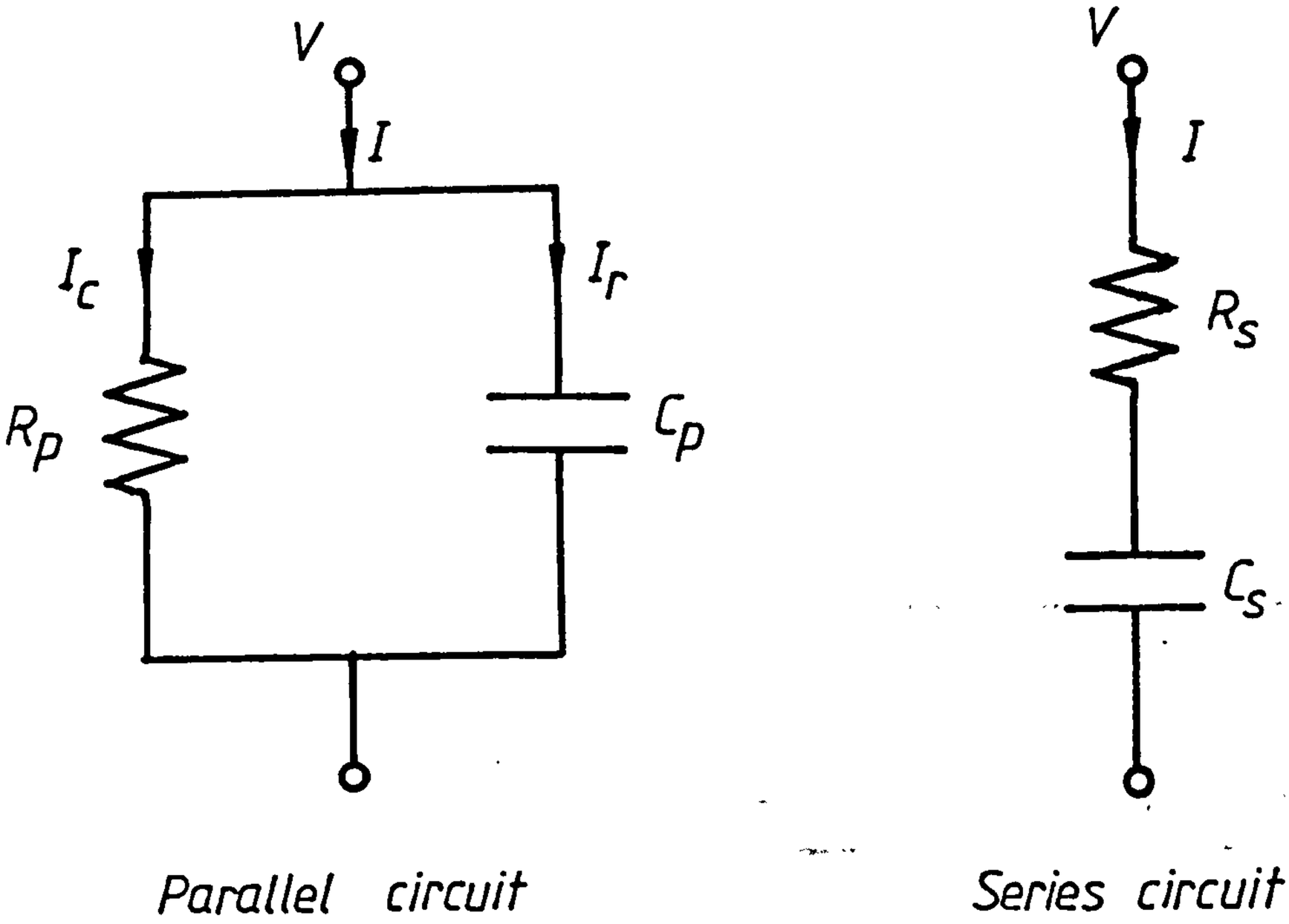

Figure 1.6.1.1 - Equivalent Circuits for Lossy Dielectric

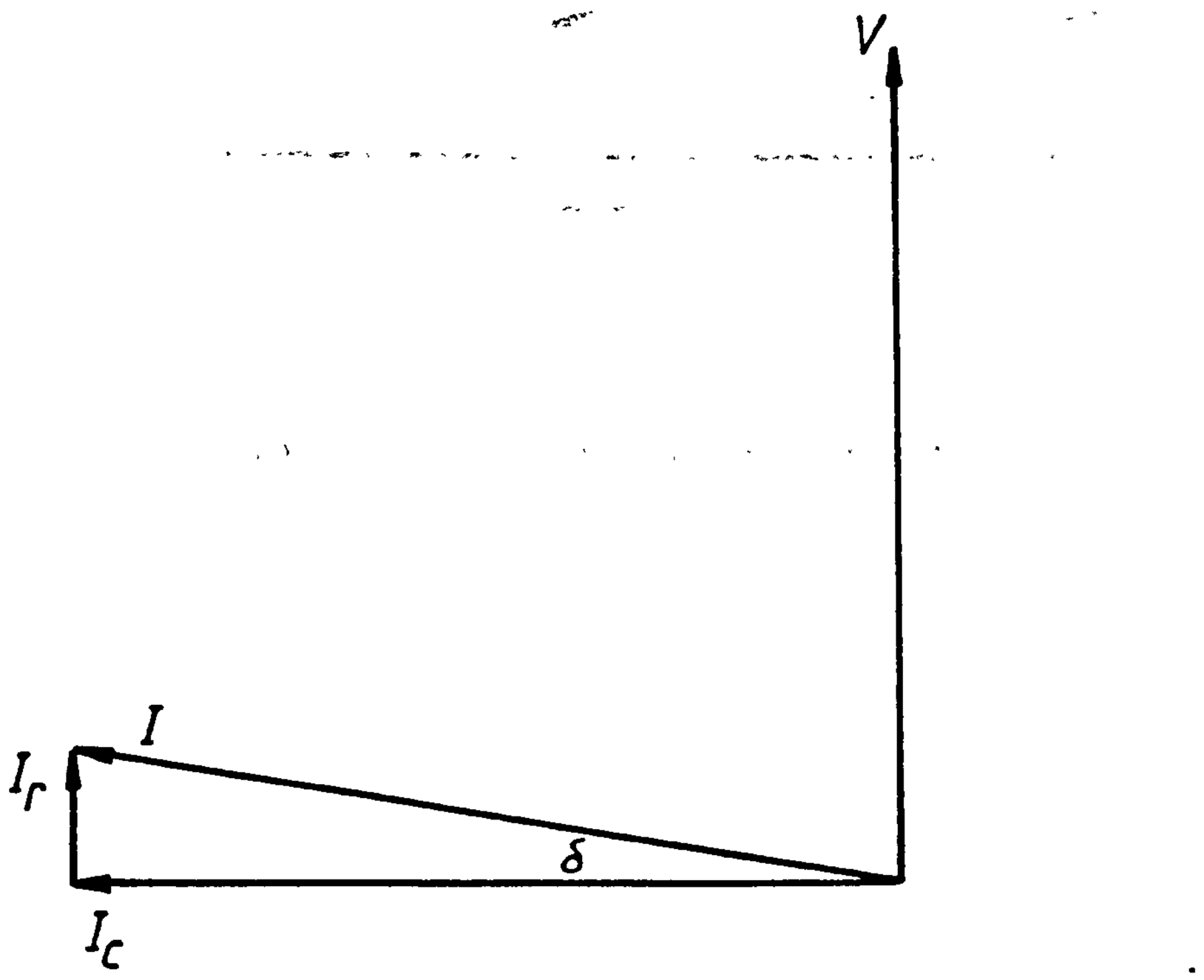

Figure 1.6.1.2 - Phasor Relationships in Dielectric

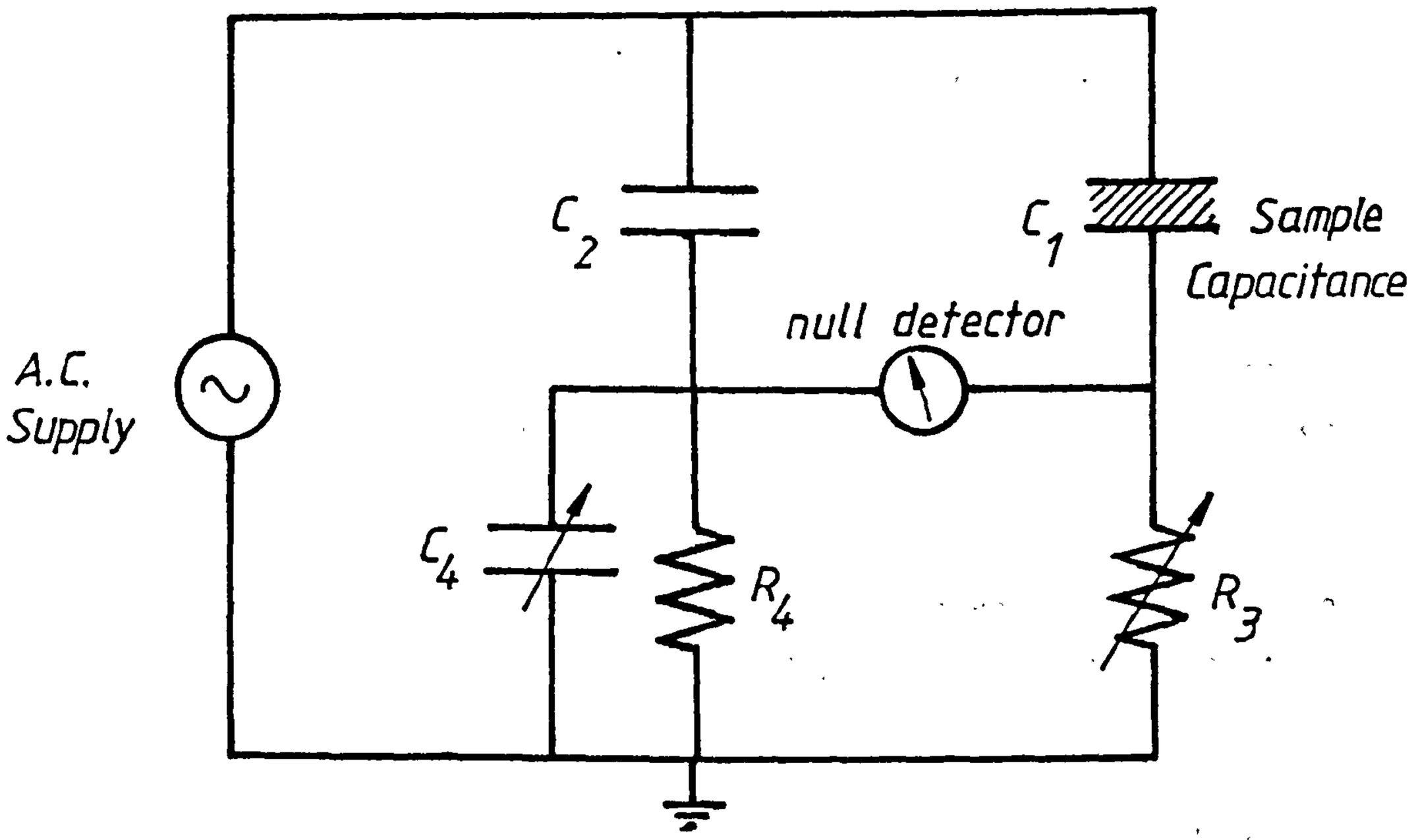

Figure 1.6.1.3 - Schering Bridge Circuit

At bridge balance position the ratio of bridge impedances is given by the equation,

$$\frac{Z_1}{Z_3} = \frac{Z_2}{Z_4} \qquad \ldots.(1.6)$$

From this relationship the capacitance of the test dielectric can be obtained , which is ;

$$C_1 = C_2 . \frac{R_4}{R_3} \qquad \ldots.(1.7)$$

The loss tangent is then calculated from the following relationship ,

$$\tan\delta = \omega . R_4 . C_4 \qquad \ldots.(1.8)$$

Several other a.c. bridge circuits are available which measure capacitance and loss tangent . One widely used in measurements on insulation systems is the Ampere-turn or transformer ratio-arm bridge [38] .

The presence of supply frequency harmonics may cause difficulty in achieving bridge balance conditions depending on the detector's response to these harmonic frequencies [36] .

In a homogeneous insulation the loss tangent has a fixed value independent of the applied voltage which may exhibit a slight increase with temperature. Loss tangent is therefore a measure of the quality of an insulation subject to residual and polarisation dielectric energy loss. However in a non-homogeneous insulation containing internal cavities a change in the tanδ characteristic is observed with the applied voltage. As the supply voltage is raised internal partial discharges will occur at the inception voltage, Vi . A corresponding increase in the loss tangent value occurs at this point. Further increase in applied voltage results in a gradual increase in the loss tangent, a characteristic termed tip-up, which is shown in the graph in figure 1.6.1.4.

Along with the increase in tanδ with increasing voltage is an increase in the capacitance C of the insulation due to the short

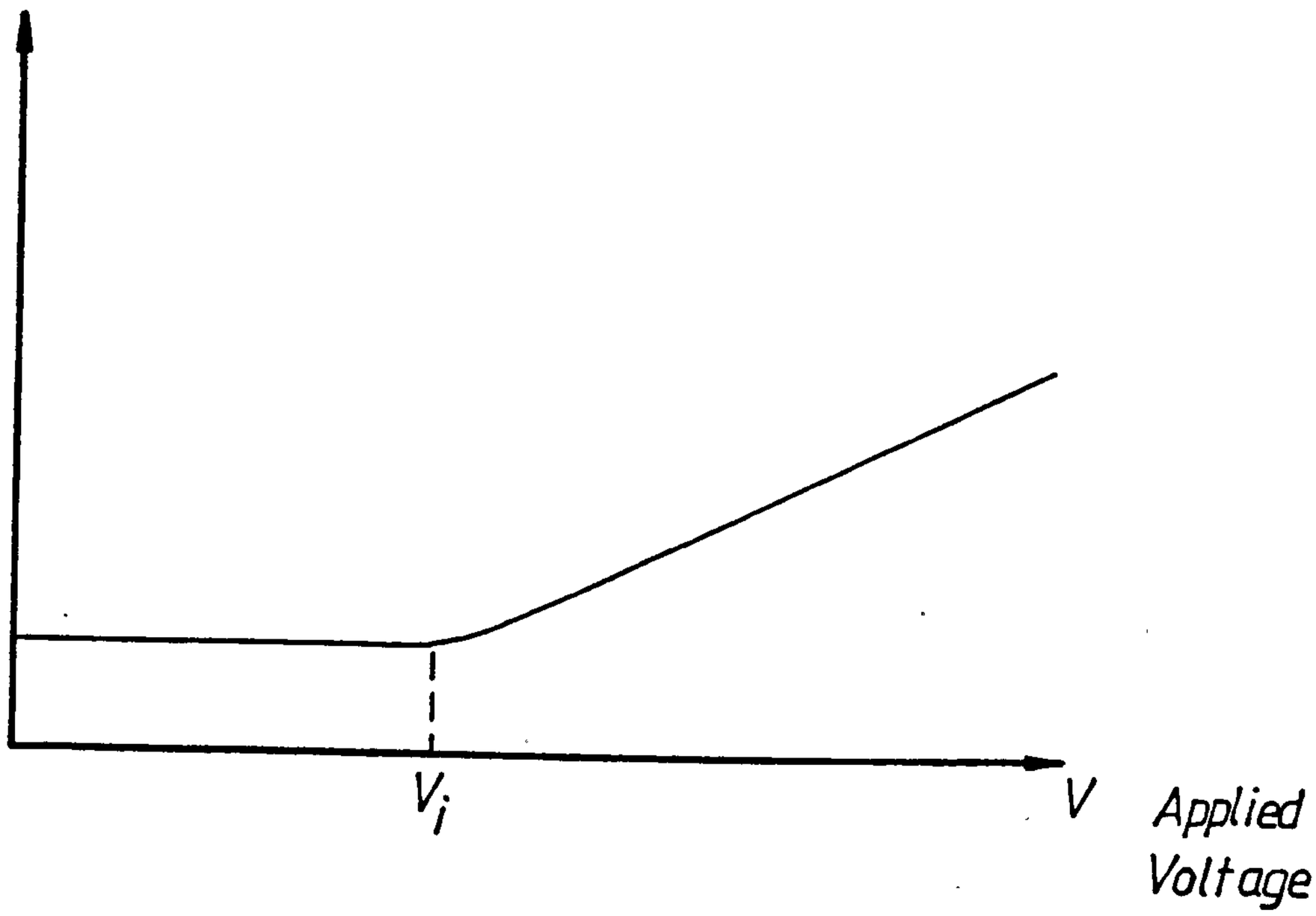

V_i - Discharge inception voltage

Figure 1.6.1.4 - Loss Tangent Tip-Up Characteristic

circuit effect partial discharges have on the capacitance of internal cavities [34] .

A measurement of the degree of tip-up as a result of internal discharges can be expressed in terms of the index $\Delta \tan \delta$ which is defined over a voltage interval ΔV.

In accordance with acceptance standards for individual coils, [35], $\tan \delta$ is measured at 0.2 Vi increments up to the rated line voltage of the machine V_L and $\Delta \tan \delta$ is defined with respect to a voltage interval of 0.2 V_L . The use of $\Delta \tan \delta$ as a measure of the integrity of an insulation, however requires great care especially in its application to machine winding insulation systems [36] .

A more useful term in diagnostic measurement is the integrated energy dissipated per cycle through internal discharges which can be obtained from the loss tangent curve and is expressed approximately by the relationship [37] :

$$Jc = 2\pi V^2 (C.\tan\delta - C_i.\tan\delta_i) \quad \ldots\ldots(1.9)$$

This can be expressed as energy dissipated per cycle per unit of capacitance for ease of comparison of measurements between insulation systems and is therefore [32] ,

$$Jc = 2\pi V^2 (C.\tan\delta - C_i.\tan\delta_i)/C_i \quad \ldots\ldots(1.10)$$

1.6.1.2 Dielectric Loss Anaylser

The dielectric loss analyser (D.L.A.) is basically a capacitive bridge device which provides a c.r.t. display of charge transfer against voltage. It was developed concurrently by separate researchers Simons et al , [39] , and Dakin et al [40] .

The basic circuit is shown in figure 1.6.1.5 in which C_1 is a loss free standard capacitance, C_2 is the specimen, C_3 and R_4 are the bridge balance controls and the ratio arm capacitance is C_4 . Capacitors C_3 and C_4 are relatively large to limit the voltage across the low voltage arms of the bridge to a few hundred volts. A reference voltage from the supply is derived from a potential divider and applied to the horizontal (X - plates) plates of the c.r.t. The

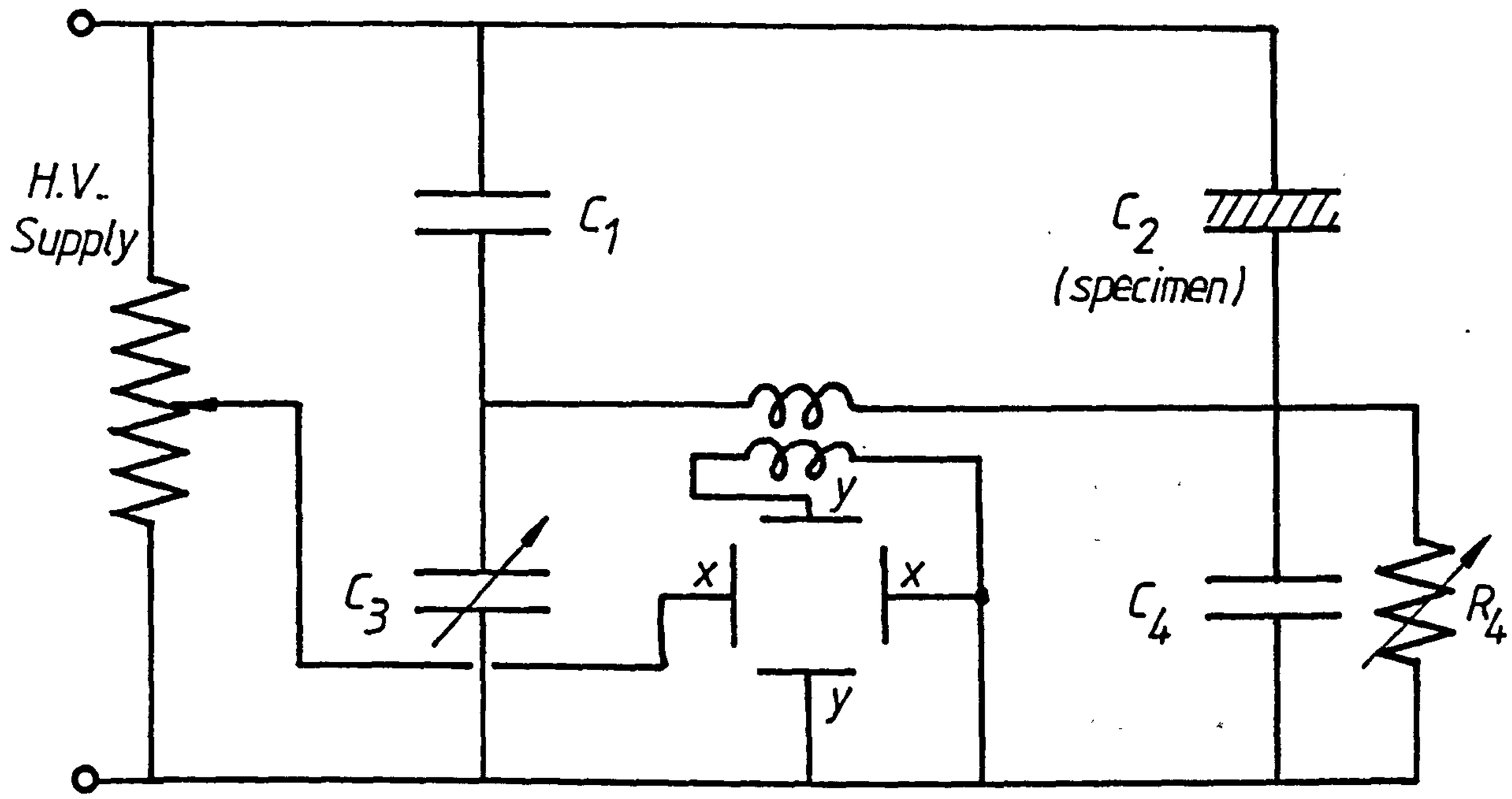

Figure 1.6.1.5 - Dielectric Loss Analyser Circuit

bridge is balanced by adjusting the values of C_3 and R_4 . R_4 compensates for the losses in the specimen.

At balance condition, the c.r.t. trace displays a horizontal line. As the supply voltage is increased, partial discharges occur. Each discharge results in an accumulated charge being deposited on the plates of capacitor C_4 with a simultaneous step in voltage impressed across the high impedance transformer.

A voltage amplifier is incorporated to improve bridge sensitivity. This voltage is thus developed across the vertical Y - plates of the c.r.t. The accumulated effect of all discharges during one cycle of the supply is a loop trace which has a rhomboid shape.

Figure 1.6.1.6 shows the development of this shape from the waveforms applied to the plates of the c.r.t. where point A is the discharge inception point.

The vertical height of the rhomboid corresponds to the total charge transfer during one half cycle which is Qm . Similarly the base of the rhomboid is equal to twice the peak inception voltage, that is $2\sqrt{2}$ V_i . Integrated discharge is energy therefore given by the area of the loop trace expressed per unit of capacitance as:

$$Jc = 2\sqrt{2}.V_i.\frac{Qm}{C_2} \quad \text{(joules/pFcycle)} \qquad \ldots\ldots(1.11)$$

In addition to this quantities the dielectric loss analyser yields the specimen capacitance and the loss tangent values.

Tests on machine windings are normally conducted off - line with the use of a high voltage test transformer which is used to allow measurements of integrated discharge energy, loss tangent and capacitance at steps in supply voltage of $0.2V_L$ to rated line voltage. The integrated energy and loss tangent versus voltage characteristics are obtained for each phase winding and the complete winding , [32] , from which an assessment of the general condition of the insulation can be made.

Records of the loop traces observed during tests yield additional diagnostic information such as endwinding contamination which is

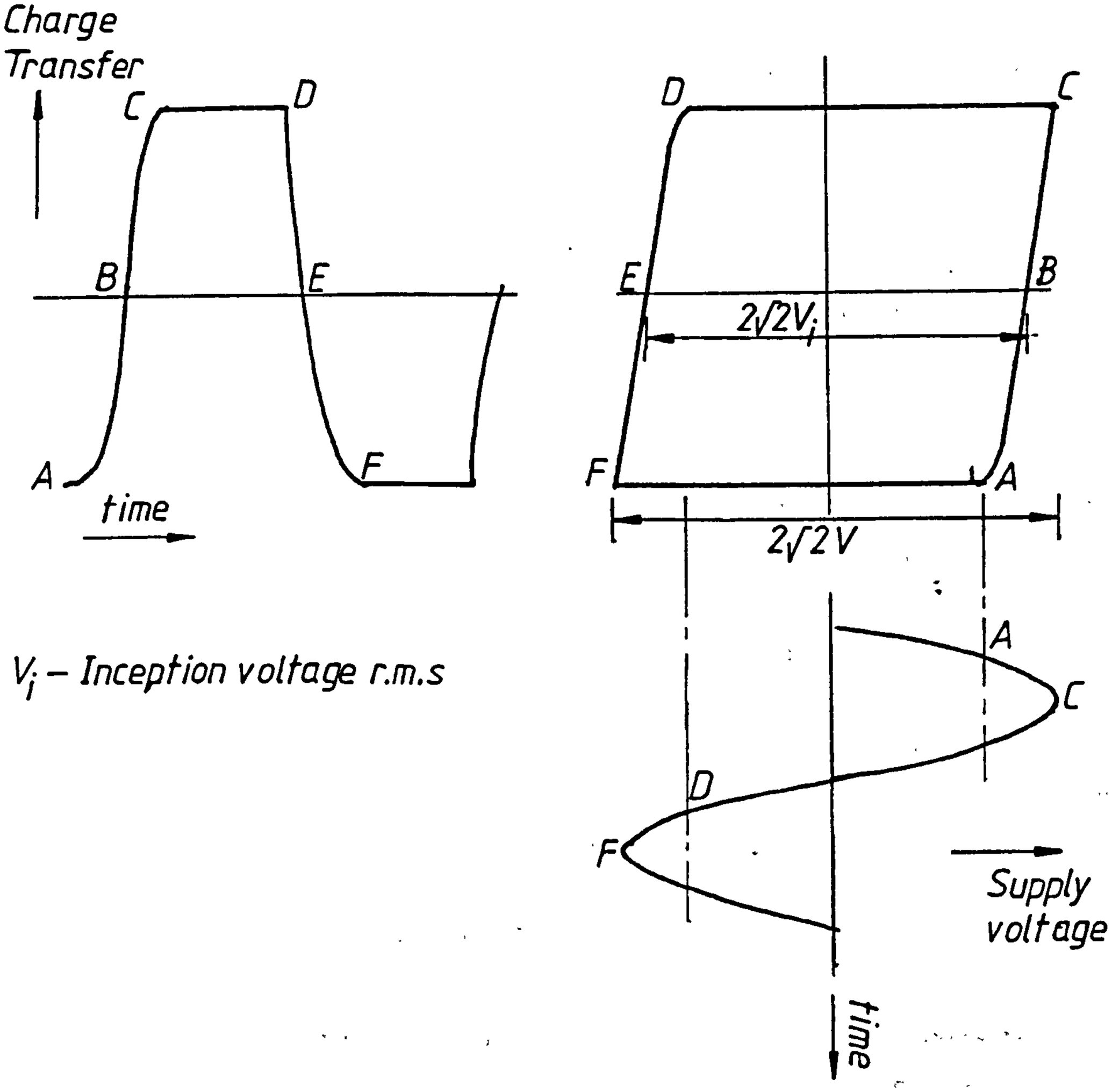

V_i – Inception voltage r.m.s

Figure 1.6.1.6 - Dielectric Loss Analyser Loop Trace

observed as a ripple effect distorting the rhomboid or the presence of large slot discharges which appear as irregularities on the inclined portions of the loop trace. Interpretation of loop traces in this manner however, requires considerable operator skill and experience.

The dielectric loss analyser does provide useful additional diagnostic information to loss tangent measurement and has the advantange that loss energy measurements from discharge processes can be separated from inherent dielectric losses. However being an integrated measurement system it can only provide a measurement of overall insulation integrity and is not capable of detecting localised degradation mechanisms . Slot discharge activity which is a principle erosion process in modern synthetic resin bonded insulations , can only be detected if these discharges are widespread throughout the winding .

A recent development in the D.L.A. , [41] , is the addition of a discharge pulse measurement system whereby large slot discharge pulses are detected using a resonant circuit and superimposed on the loop trace display. This aids measurement of discharge inception voltage and indicates the magnitude of large slot discharges.

It is therfore a very useful diagnostic tool especially for older natural resin bonded insulation systems which are more susceptible to damage from internal cavity discharge attack.

1.6.2 Resolved measurements

Resolved measurements involve the detection and measurement of individual partial discharges. This may be achieved by optic and acoustic techniques but by far the most useful and practical method is electrical detection. In this type of detection partial discharges may be measured by means of a detection circuit connected to the terminals of the specimen.

1.6.2.1 Partial Discharge Pulses

Before discussing the various methods of partial discharge detection it is beneficial to examine the characteristics of individual partial discharge current pulses since measurements are based on these . Discharge pulse shapes are dependent on the mechanism of discharge

present and this is related to the electrode physical arrangement .

Broadly speaking there are three general types of discharge that occur in high voltage equipment and these are as follows :-

i. Corona discharges.
ii. Surface discharges.
iii. Internal discharges.

Corona discharges occur at sharp points or protrusions on high voltage conductor surfaces between the point and the surrounding air due to the high electric field stress around the point . At low inception voltages , the discharges occur on the negative half cycle of the supply . The resulting current pulse shape is characterised by a steep rising front followed by a long exponentially decaying tail . These pulses are called Trichel pulses . Peak currents vary from 0.5 to 2 mA , rise times vary from 1.3 to 1.8 nsec and durations are in the range of 100 to 160 nsec for a point electrode radius of curvature of 0.12 mm [71] .

Much larger and less frequent discharges occur on the positive half cycle at higher inception stresses and involve a streamer type discharge mechanism . The rise times of these pulses are in the region of 2 nsec , peak current varies from around 1.5 to 3.5 mA whilst pulse durations lie between 160 to 220 nsec for electrode separations greater than 35 mm . Smaller electrode separations result in slightly shorter pulse durations due to transit times of ion particles .

Surface discharges occur both on the positive and negative polarity half cycles of the supply . In general, pulses are very similar in shape to those of corona discharge pulses with a fast rise time front and exponential tail . Typical rise times are in the region of between 2 and 3 nsec . However the amplitude and duration of the pulse varies considerably depending on the surface resistivity , whether or not contaminants are present . Measured durations vary from 50 to 500 nsec for uniform electrode/dielectric arrangements [72,74] .

Internal discharges occur in small cavities within a solid dielectric and vary in nature depending on the discharge mechanism which is operative . Obviously these are very complicated phenomena and only

generalisations are discussed in this section .

A single electron avalanche forms the basis of a discharge across the gap between opposite faces of the cavity .

Depending on the gap separation , voltage ,surface resistivity etc., in the cavity a Townsend-like discharge occurs at low over-voltages and a streamer-like discharge is predominant at high over-voltages . Over-voltage being defined as the magnitude of voltage across the cavity above the minimum breakdown potential of the cavity [75] .

In a Townsend type discharge the current pulse has a theoretical pulse shape as shown in figure 1.6.2.1 in which the current due to the electron avalanche lasts for approximately between 250 and 800 picoseconds , (normally less than 1 nsec.) . The positive ion current is more rectangular in shape and of a much longer duration [73,75] . Observed pulse durations lie between 20 and 300 nanoseconds, [75] , depending on the gap separation .

Streamer-like discharges , self sustaining discharges , are characterised by a larger and longer duration pulses which are Gaussian in shape . However there is very little quantitative information on these discharges .

In general partial discharges are widely different in shape, magnitude, and duration . These factors depend on the discharge mechanism present . However it can be said of all partial discharges that they have very short rise times and varying durations such that signal frequencies of concern in measurement may extend from tens of kilohertz up to a few gigahertz . This makes accurate measurement of the discharge current pulse itself impractical as such wideband measurement introduces considerable problems . The capacitance of the test specimen and associated circuit resistances and capacitance limit the effective response time of the measuring circuit making it extremely difficult to measure current pulses .

A derived quantity known as the apparent charge of a partial discharge is however measureable . This is best explained with reference to the simple model of a dielectric containing a cavity as shown in figure 1.5.4 .

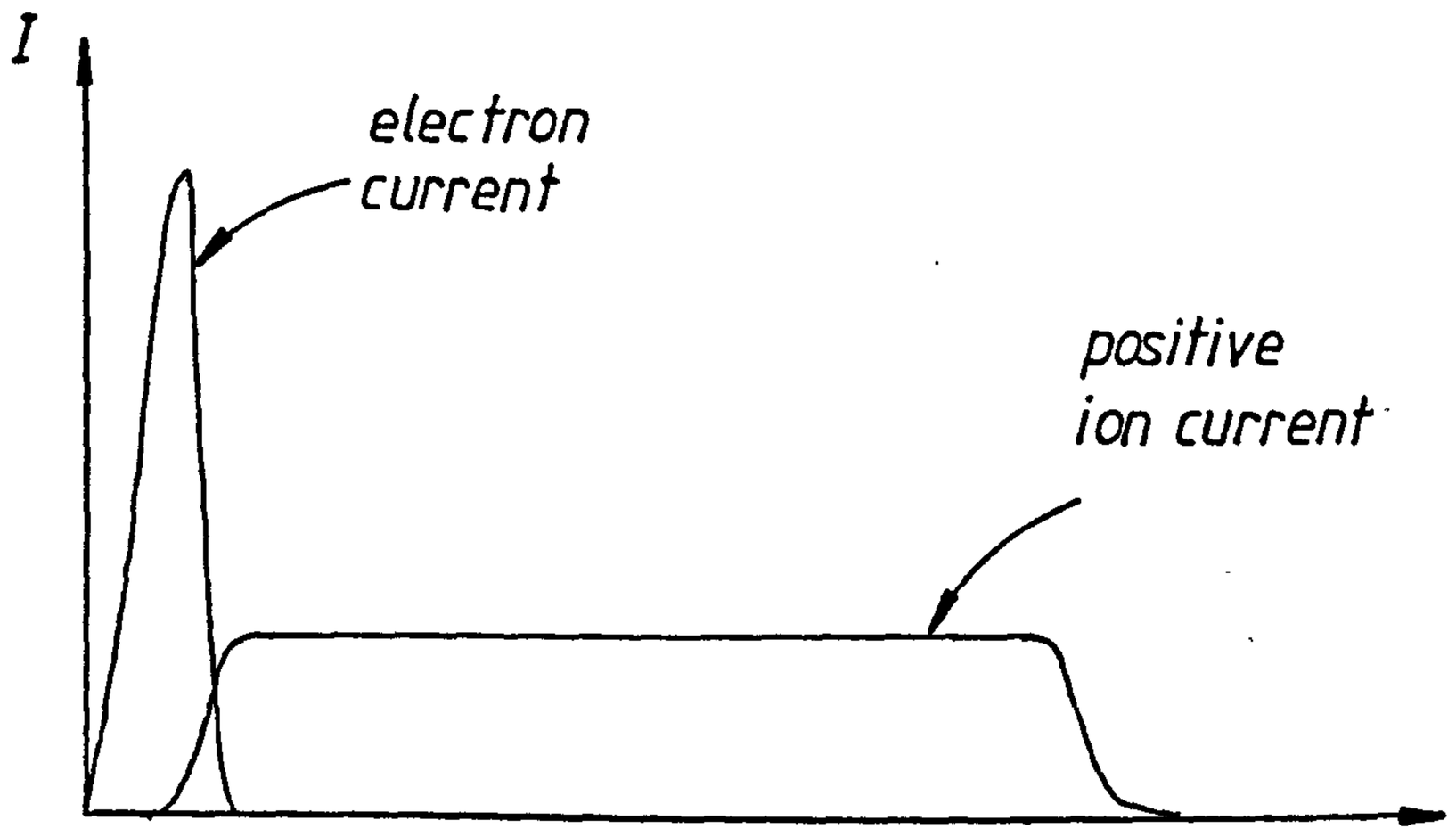

Figure 1.6.2.1 - Theoretical Current Pulse Shape for Internal Partial Discharge

When a discharge takes place in the specimen, electrical charge is lost to the system which causes a small change in the specimen capacitance, δC, and a voltage drop across the terminals of the specimen given by the expression,

$$\delta V = \frac{Cb}{Ca + Cb} . \delta V_c \qquad \ldots.(1.12)$$

Charge is subsequently restored to the specimen from the high voltage source. The charge transfered is given by

$$q = (Ca + Cb). \delta V_t \qquad \ldots.(1.13)$$

Substitution of equation (1.12) into the above equation gives

$$q_a = Cb . \delta V_c \qquad \ldots.(1.14)$$

The quantity, q_a, is referred to as the apparent charge of the partial discharge. Although q_a is not equal to the true charge transfer in the discharge q_c given by,

$$q_c = Cc . \delta V_L \qquad \ldots.(1.15)$$

the two quantities are related [42] . The charge measured at the terminals is less than the actual charge transfer in the cavity due to the smaller series capacitance Cb.

1.6.2.2 Partial Discharge Measurement Circuits.

There are three basic partial discharge detection circuits and these are shown in the diagrams of figure 1.6.2.2 . In each circuit Ct represents the specimen capacitance, $\simeq$(Ca + Cb), C_k is a discharge free coupling or blocking capacitor , Zm (Zm') is a measuring impedance and Z is a discharge free low-pass filter in the h.v. supply connection.

The a.c. bridge circuit shown is known as a balanced detector circuit. At balance the ratio of the bridge arm impedances are equal and the power frequency signal is reduced to zero at the detection amplifier terminals. Normally the detection impedances Zm and Zm' are a parallel resistor and capacitor combination which are adjusted to

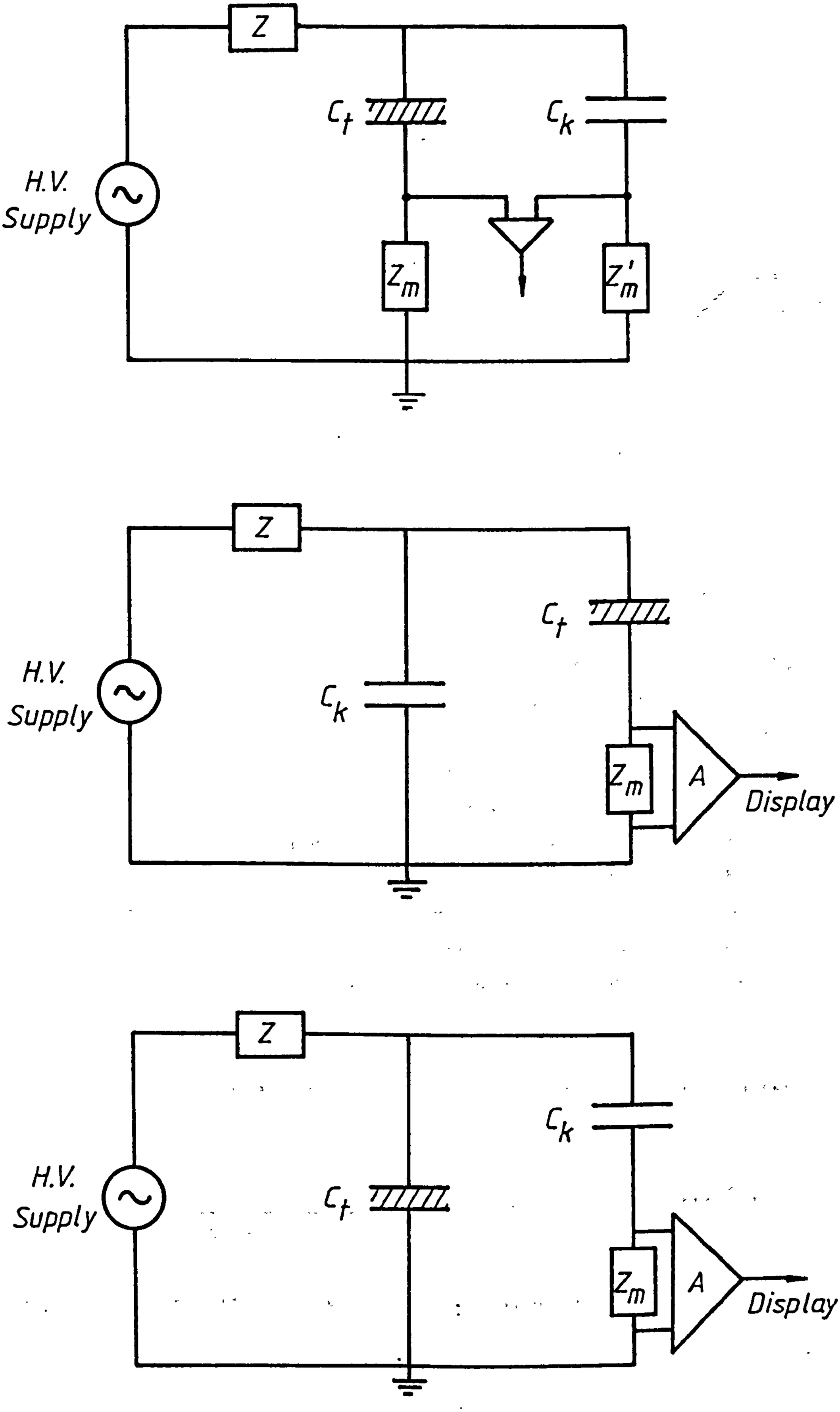

Figure 1.6.2.2 - Basic Discharge Detection Circuits

obtain the balance condition. Any discharge in the test specimen will result in a pulse detected by the differential amplifier detector. These pulses may then be further processed and displayed. The bridge coupling capacitor Ck must be discharged free to prevent spurious discharge detection . Ck need not have a capacitance value the same as the test specimen , Ct.

An advantage in the use of this circuit arrangement is that spurious pulse or discharge signals conducted via the h.v. supply or electromagnetically coupled into the bridge arms are cancelled at the detector thus providing a degree of common mode interference suppression.

The two other detector circuits are termed 'straight' partial discharge detector circuits.

In the first circuit , the measuring impedance , Zm, is connected in series with the test specimen, C_t , both of which are in turn connected in parallel with a discharge free coupling capacitor Ck, across the h.v. supply. The impedance, Z, is a low pass filter which isolates the measurement circuit during a discharge event and affords protection against spurious pulses, from the h.v. supply, entering the detection circuit. The measuring impedance, Zm, is generally a passive resonant circuit comprising a parallel resistor R, inductor L and detection capacitance Cd, as shown in figure 1.6.2.3. When a discharge of magnitude, q , occurs in the test specimen an instantaneous change in voltage is produced across the detection capacitance Cd determined by the capacitive voltage distribution in the circuit [43] .

A discharge q produces a change in voltage across the specimen given by,

$$\delta V_t = \frac{q}{Ct + CkCd/(Ck + Cd)} \qquad \ldots.(1.16)$$

since Cd and Ck are effectively in series across the specimen Ct.

This voltage is distributed across Cd and Ck in accordance with the expression,

$$\delta V_d = \frac{Ck}{Cd + Ck} . \delta V_t \qquad \ldots.(1.17)$$

Therefore the instantaneous detector voltage is given by ,

$$\delta V_d = \frac{q}{Ct + Cd + Ct\ (Cd/Ck)} \qquad \ldots.(1.18)$$

The step in detector voltage is followed by a damped oscillation, as shown in figure 1.6.2.4 which is expressed in the time response across the detector terminals given by,

$$V_d(t) = \frac{q}{C} e^{-\alpha t} \left[\cos\beta t - \frac{\alpha}{\beta} \sin\beta t\right] \qquad \ldots.(1.19)$$

where $\alpha = 1/2RC$; $\beta = \sqrt{(1/LC - \alpha^2)}$

C is the total capacitance seen by the detector input and is given by

$$C = Cd + Ct.Ck/(Ct + Ck) \qquad \ldots.(1.20)$$

In the second straight discharge detector circuit the measuring impedance is connected in series with the coupling capacitor across h.v. supply which is in parallel with the test specimen. This circuit responds to a partial discharge pulse in the same manner as the previous circuit and similar equations for the circuit response may be derived. The main difference and advantage in the use of this detector circuit is that the test specimen may be connected to earth at one terminal which might be a requirement of the apparatus being tested.

The detected discharge pulses are amplified and observed on an oscillographic display having an elliptical time base that depicts a cycle of the power supply voltage. Typical displays are shown in figure 1.6.2.5 . A positive and negative marker pulse indicate the position of the rising portion of the positive and negative half cycles of the supply respectively. The magnitude of individual discharges is quantified by comparing the peak crest amplitudes with

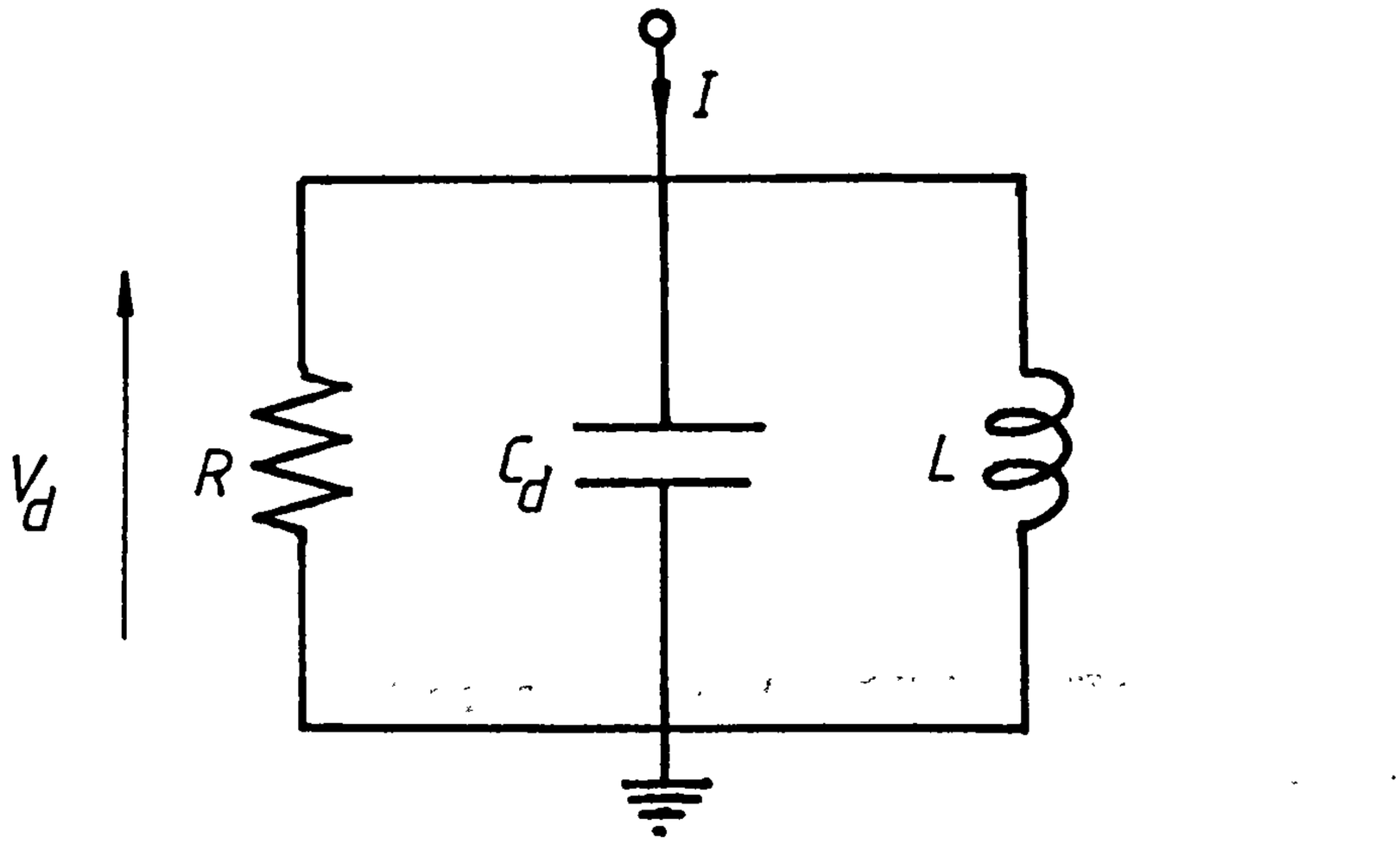

Figure 1.6.2.3 - Passive Resonant Detector Circuit

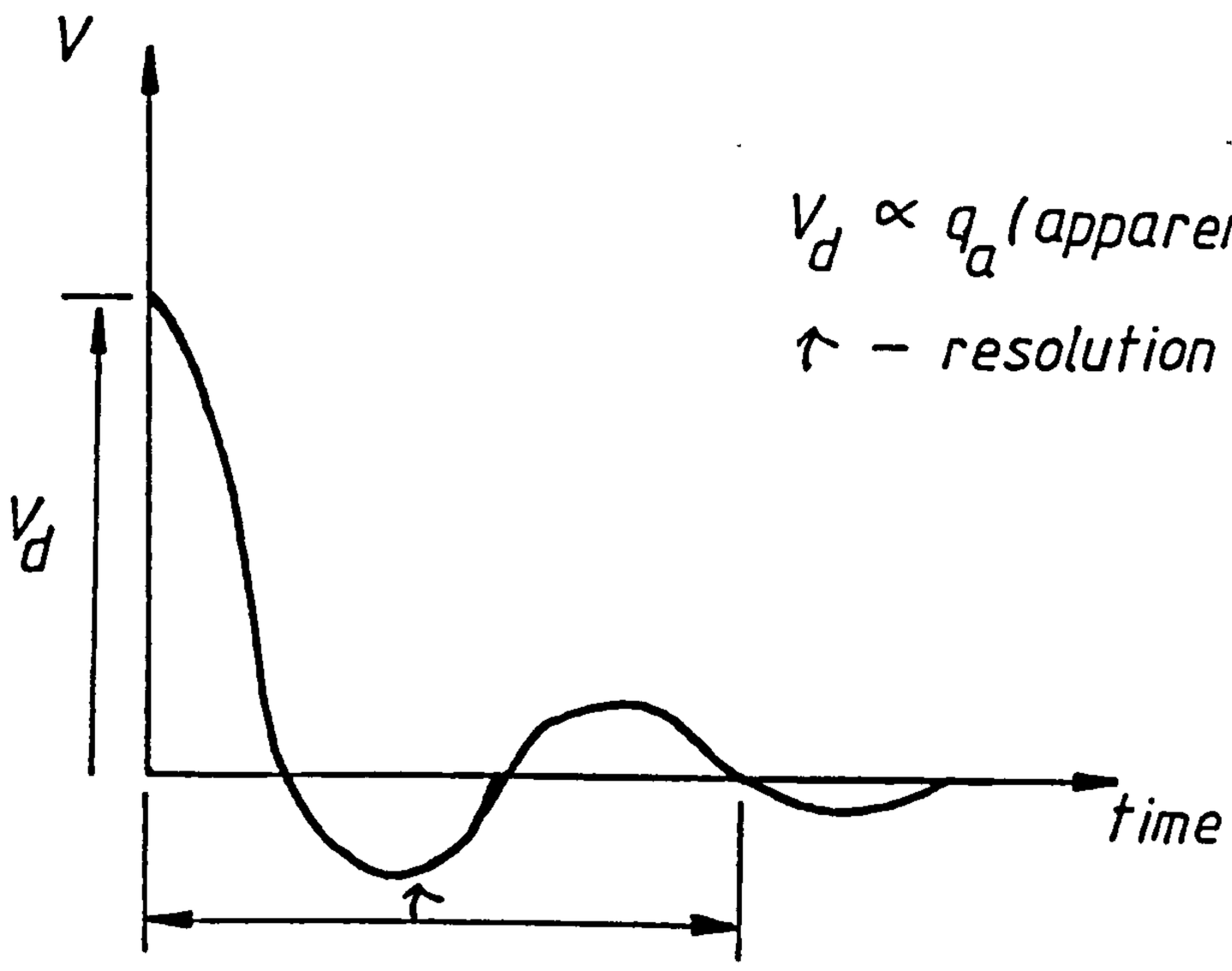

$V_d \propto q_a$ (apparent charge)

τ – resolution time

Figure 1.6.2.4 - Response of Detector Circuit

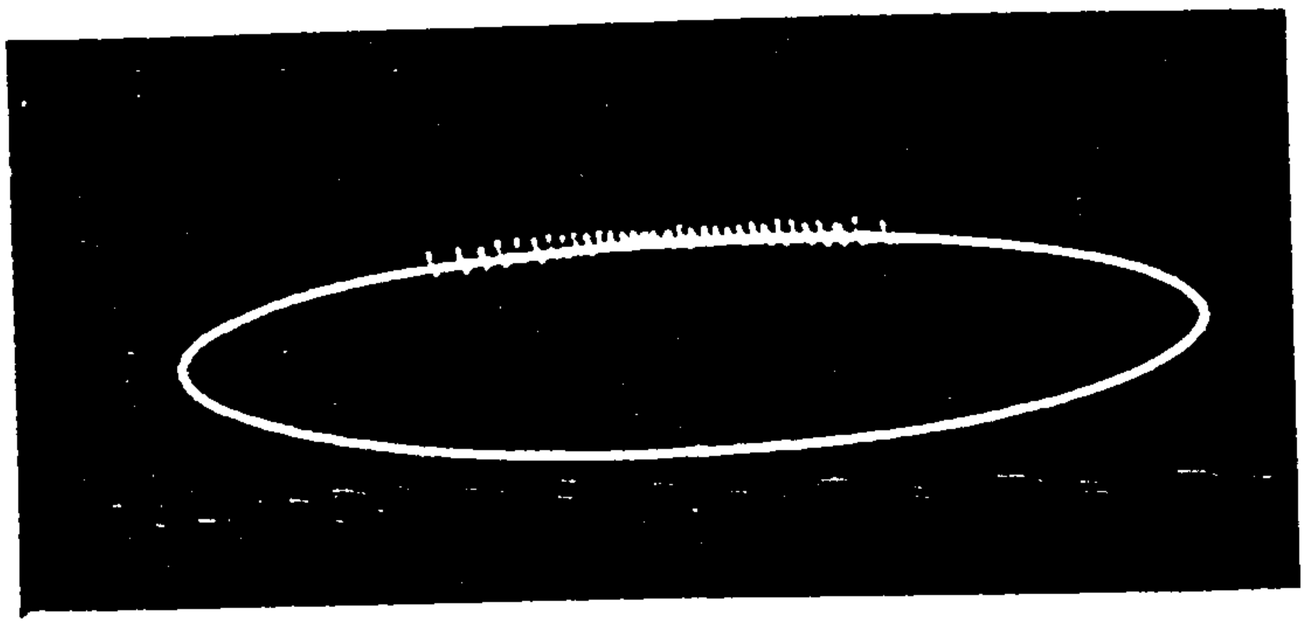

Negative Corona Discharge

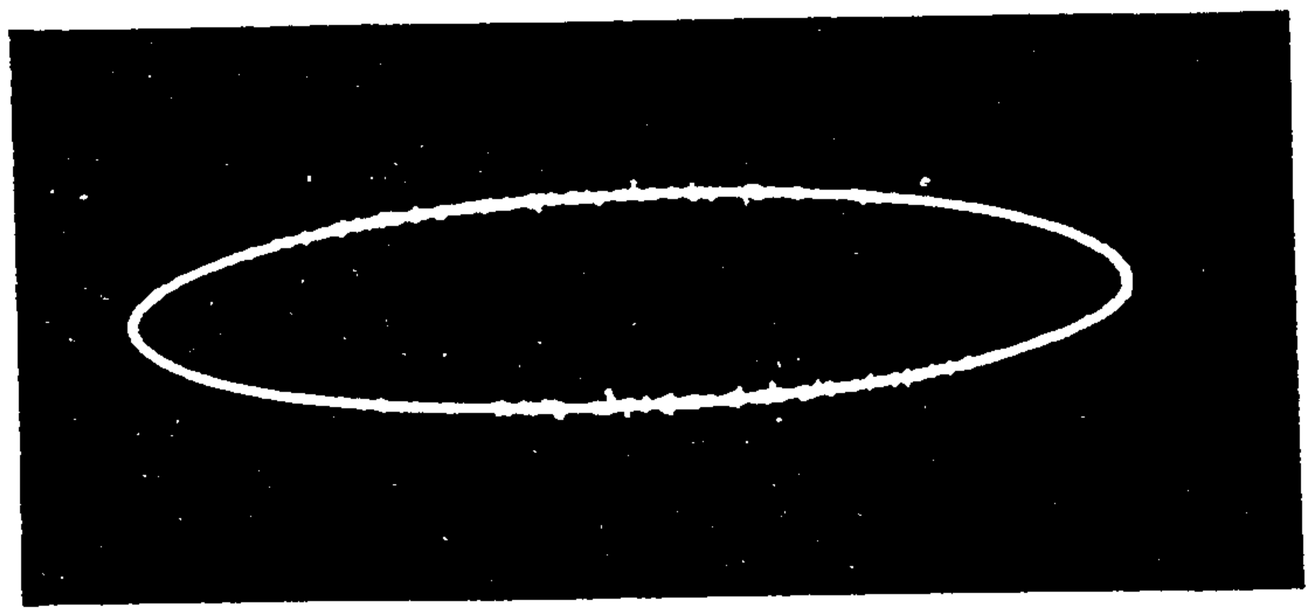

Internal Discharge at inception V_i

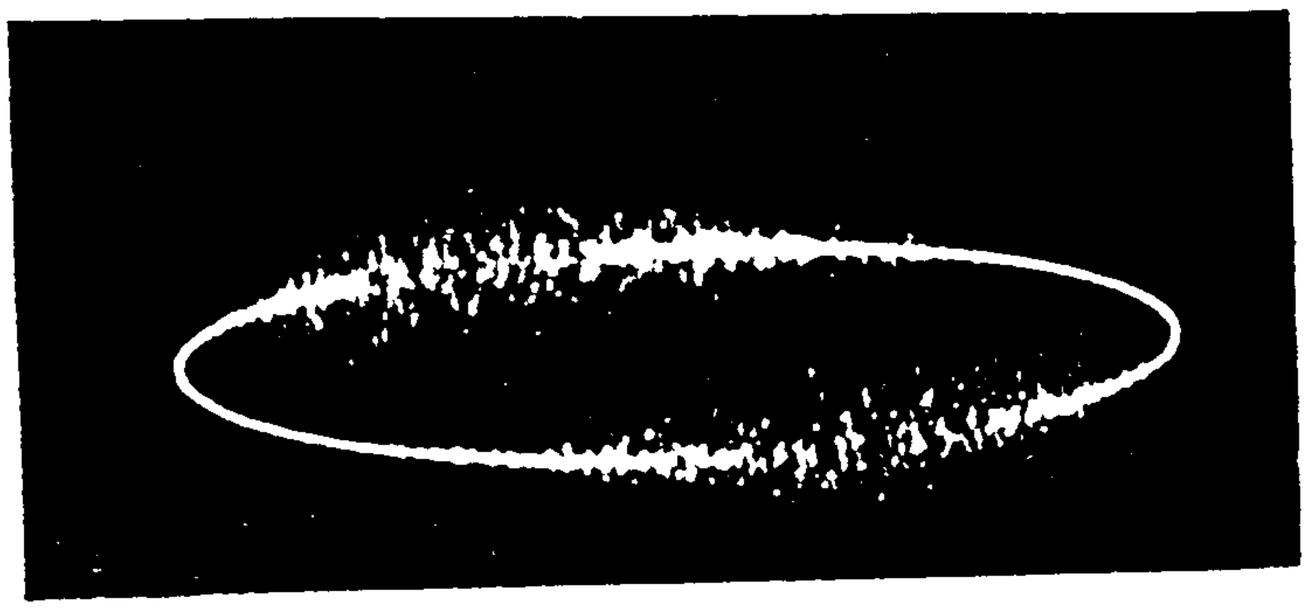

Internal Discharge at twice inception $2V_i$

Figure 1.6.2.5 - Typical Discharge Pulse Display Patterns from Resolved Discharge Detector

that of a calibration pulse . The calibration pulse is derived by injecting a pulse of charge of known magnitude into the discharge detection circuit by means of a discharge calibration circuit. This circuit generally comprises a voltage step generator and a series capacitance Co connected to the detection circuit in the positions shown in figure 1.6.2.6. The simulated discharge pulse has a magnitude of

$$q_o = C_o V_o \qquad \ldots.(1.21)$$

where V is the injected pulse voltage [44] .

Calibrators connected to the low voltage terminals of the detector circuit are classified as indirect calibrators whilst those connected to the high voltage terminals are termed direct calibrators.

Secondary calibration standards , [45] , are also sometimes used and consist of real discharges generated in a point to hemi-sphere electrode system, (see photograph in figure 1.6.2.7).

The discharges produced are negative point corona discharges and are characterised by their very regular magnitude.

Two distinct advantages of a resolved pulse measurement system , using an elliptic time based display , is the ability to identify, from the trace, the following :-

i. Partial discharge mechanisms.
ii. Interference sources.

Figure 1.6.2.5 shows the difference in pulse patterns obtained from a point corona source and a cavity discharge source by the magnitude and position with respect to the supply cycle. Other discharge mechanisms such as a cavity adjacent to a conductor or a surface discharge are identified by their characteristic pulse patterns which is useful in diagnostic work [46] .

Secondly, the source of interference external to the discharge test circuit can be identified on the detector display by the pulse characteristics that are peculiar to the interference mechanism present.

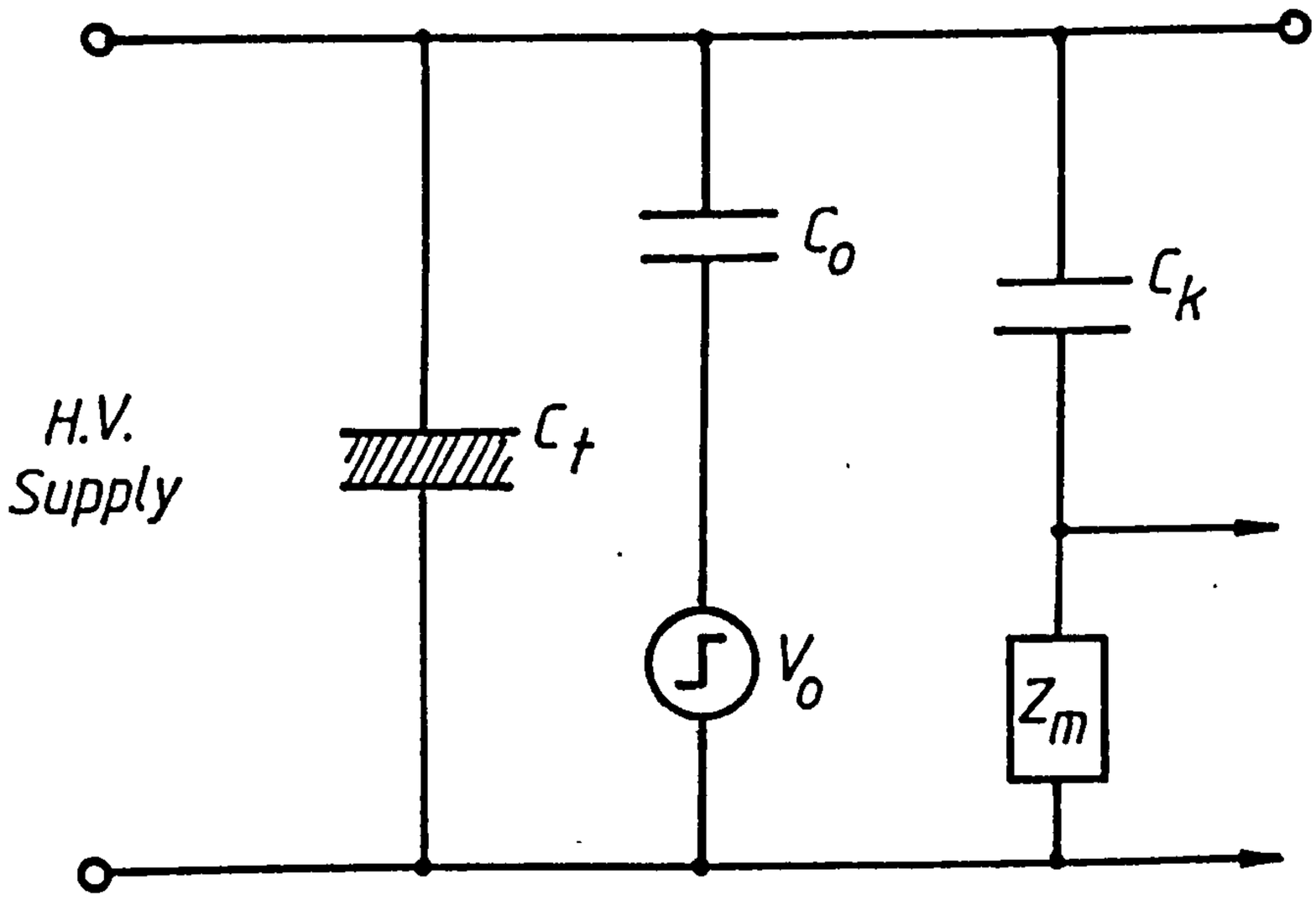

a) Direct Calibration Circuit

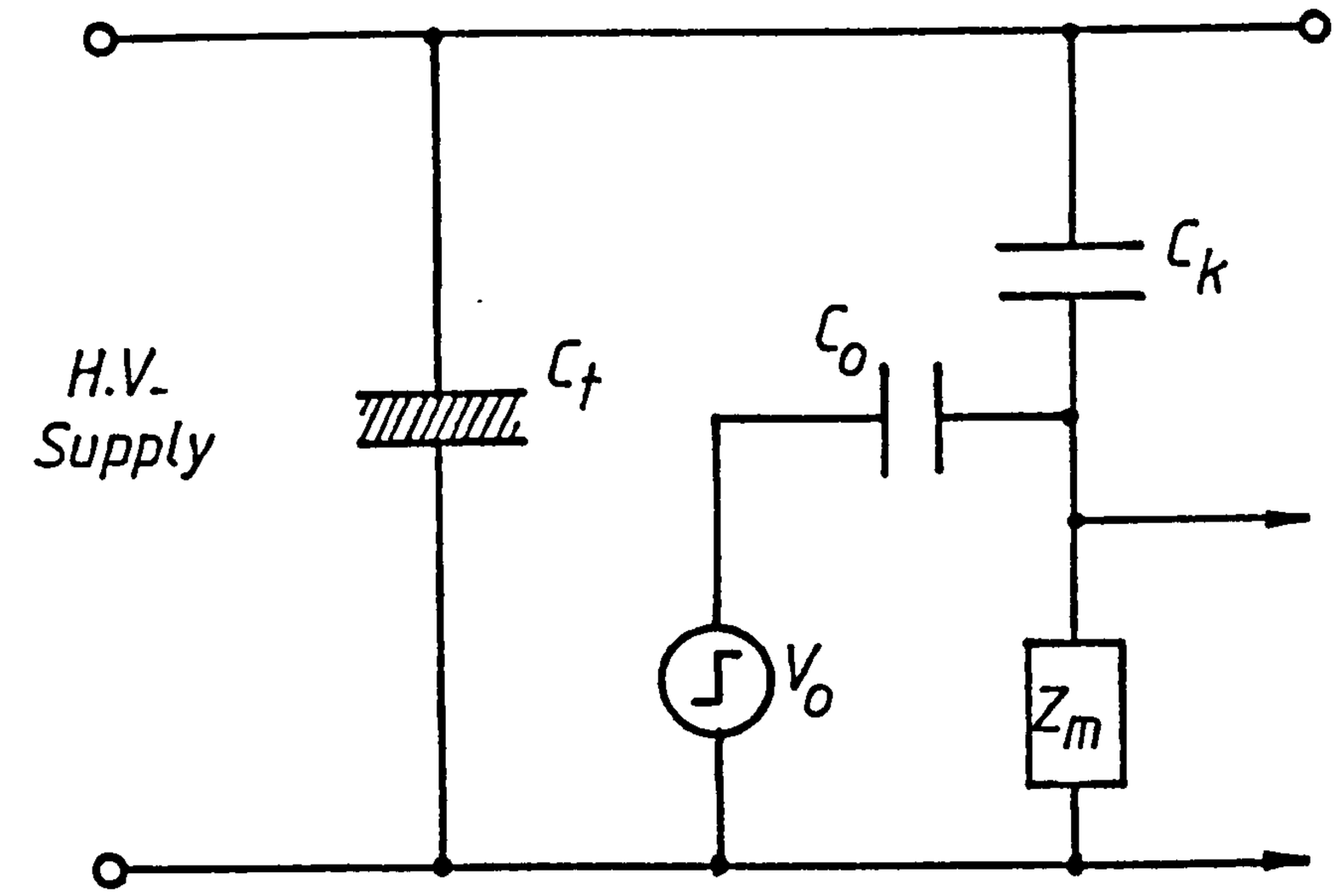

b) Indirect Calibration Circuit

Figure 1.6.2.6 - Basic Discharge Detector Calibration Circuits

Figure 1.6.2.7 - Point to Hemi-sphere Secondary Discharge Source

Examples of three types of common interference pulse patterns are shown in the diagrams of figure 1.6.2.8 which include interference signals from radio broadcasts, thyristor controllers and fluorescent lighting.

It is the level of interference that determines the ultimate sensitivity of the discharge detection system , and control of interference is therefore of prime importance ; especially in an industrial enviroment where noise levels are likely to be high. The interference originates from one of two sources : external signals and unwanted discharge signals generated in the test circuit .

In the first category, the interference signal is coupled to the test circuit in one or more of four modes, (see figure 1.6.2.9) , outlined as follows :-

Electrostatic coupling - interference enters the test circuit via a path formed by stray capacitance. Circuits with low capacitance samples are most susceptible to this coupling mechanism.

Electromagnetic coupling - the loop formed in the test circuit allows interference signals to be electromagnetically induced in the test circuit.

Earth coupling - resistance in the earth path of the test circuit and multiple earth connections , causes unwanted voltages at the detector from interference currents flowing in the earth path.

Coupling via the high voltage supply - the path interference enters the test circuit is through the mains supply line. These signals may be eliminated by the use of a low pass filter in the high voltage supply line.

Techniques to reduce and possibly eliminate interference signals include the extensive use of screening, single point earthing, mains filtering and discharge free components and are outlined in reference [47] .

Special techniques have been developed which suppress interference which cannot be reduced by conventional methods to allow site measurements to be taken with greater sensitivity. One techinque

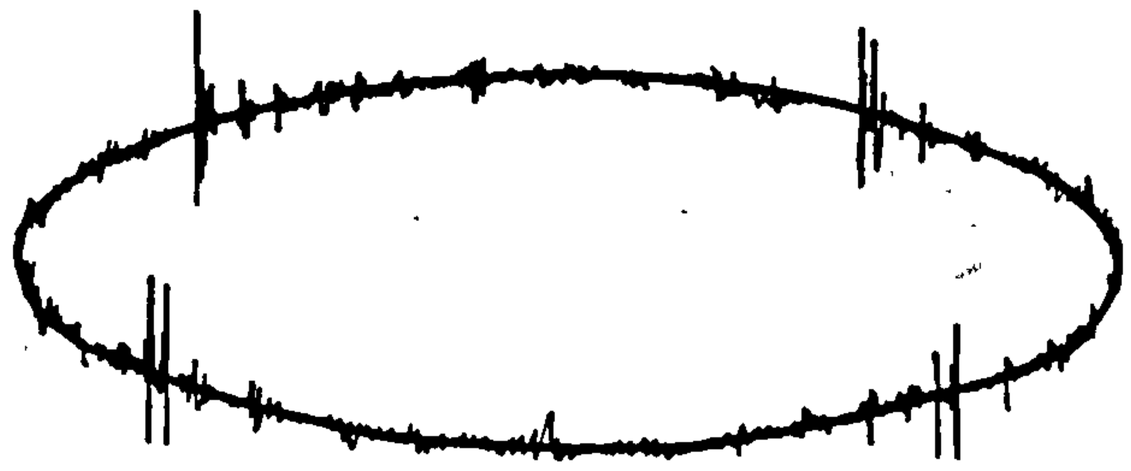

Thyristor Controller

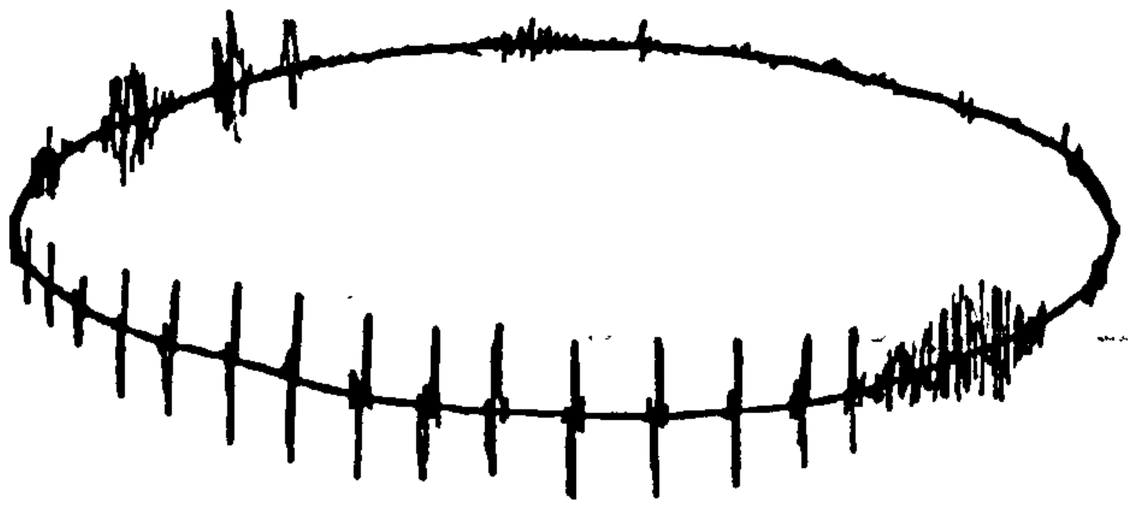

Fluorescent Lighting

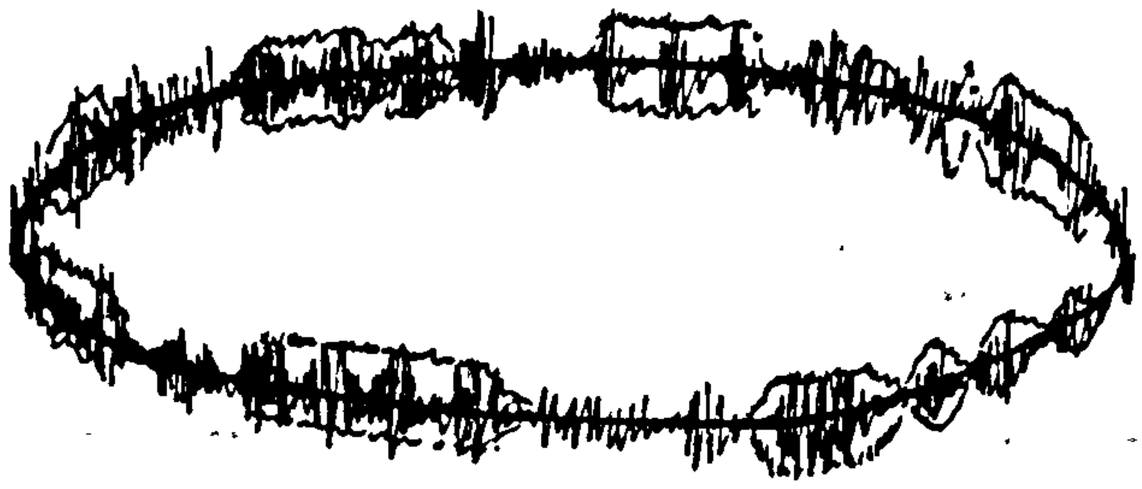

Radio Broadcast

Figure 1.6.2.8 - Common Interference Pulse Patterns

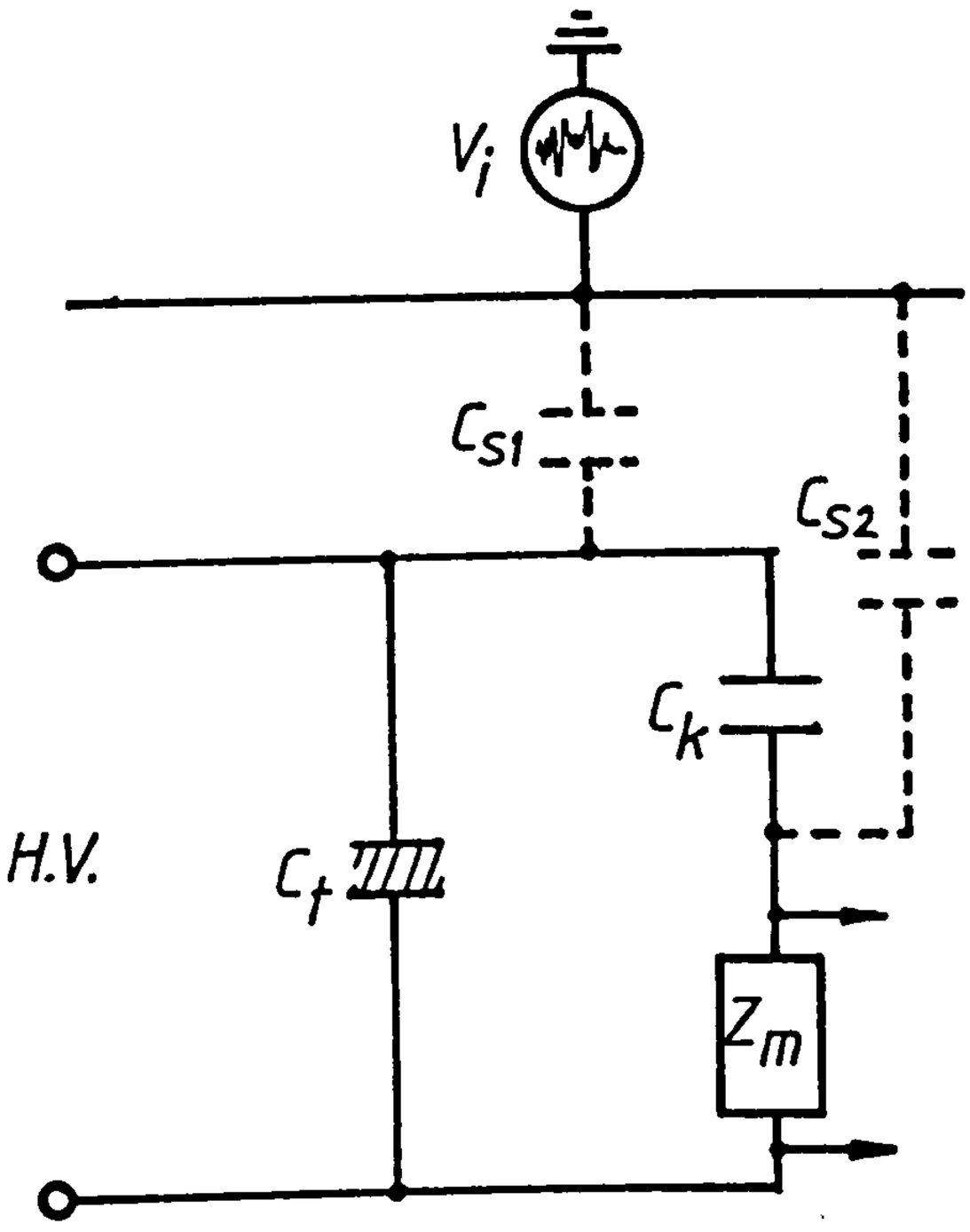

a) Electrostatic Coupling

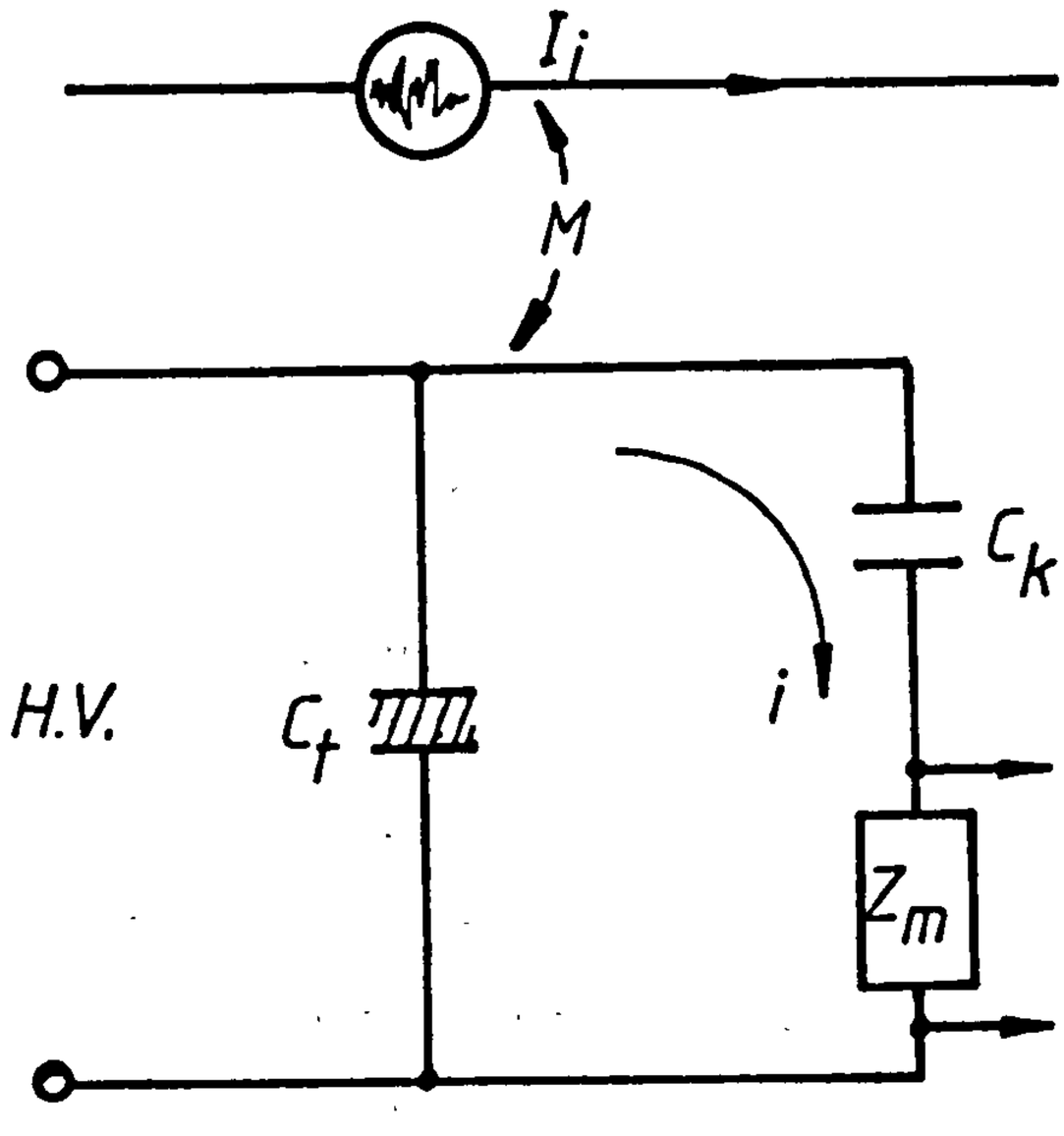

b) Electromagnetic Coupling

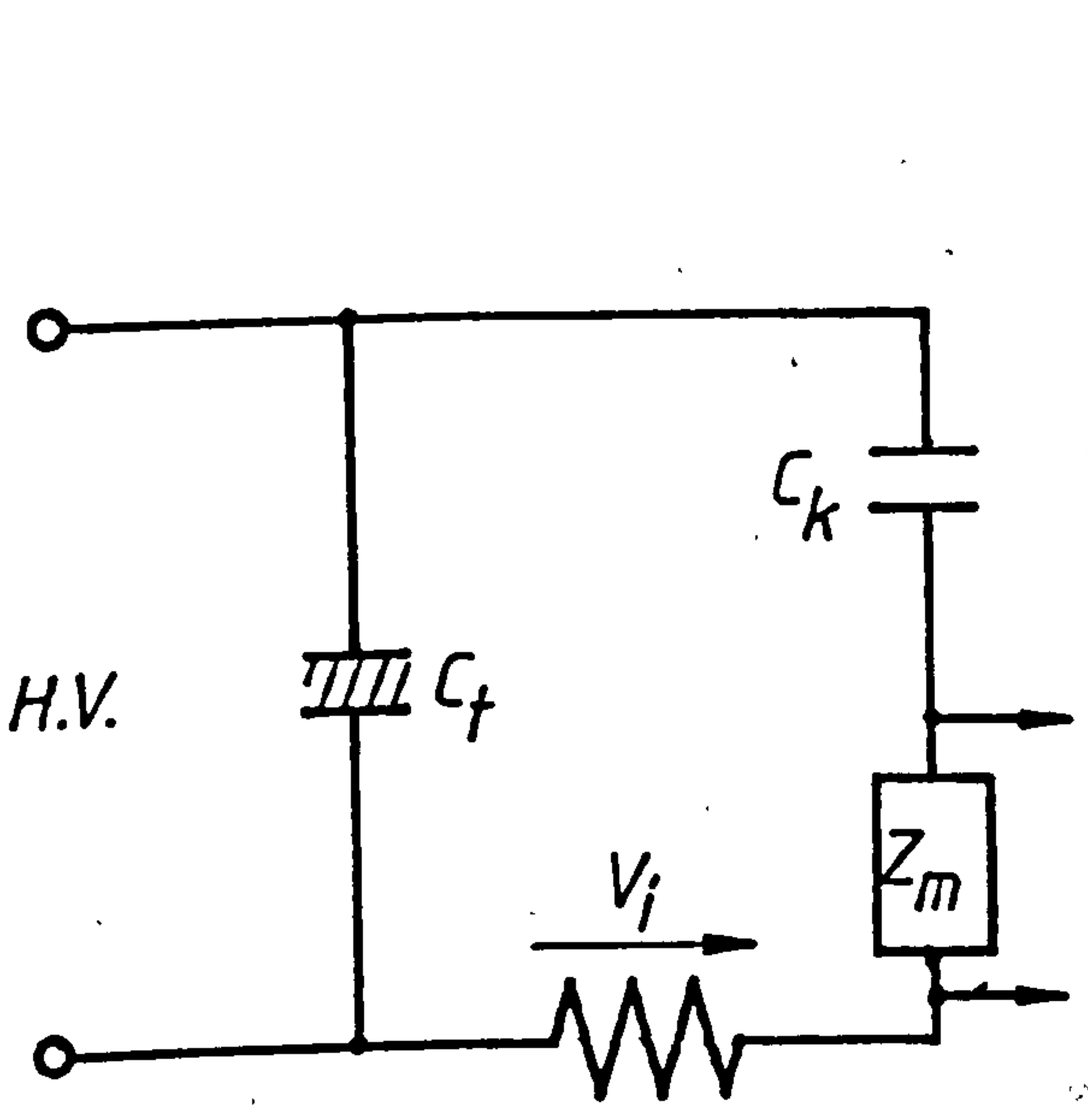

c) Earth Path Coupling

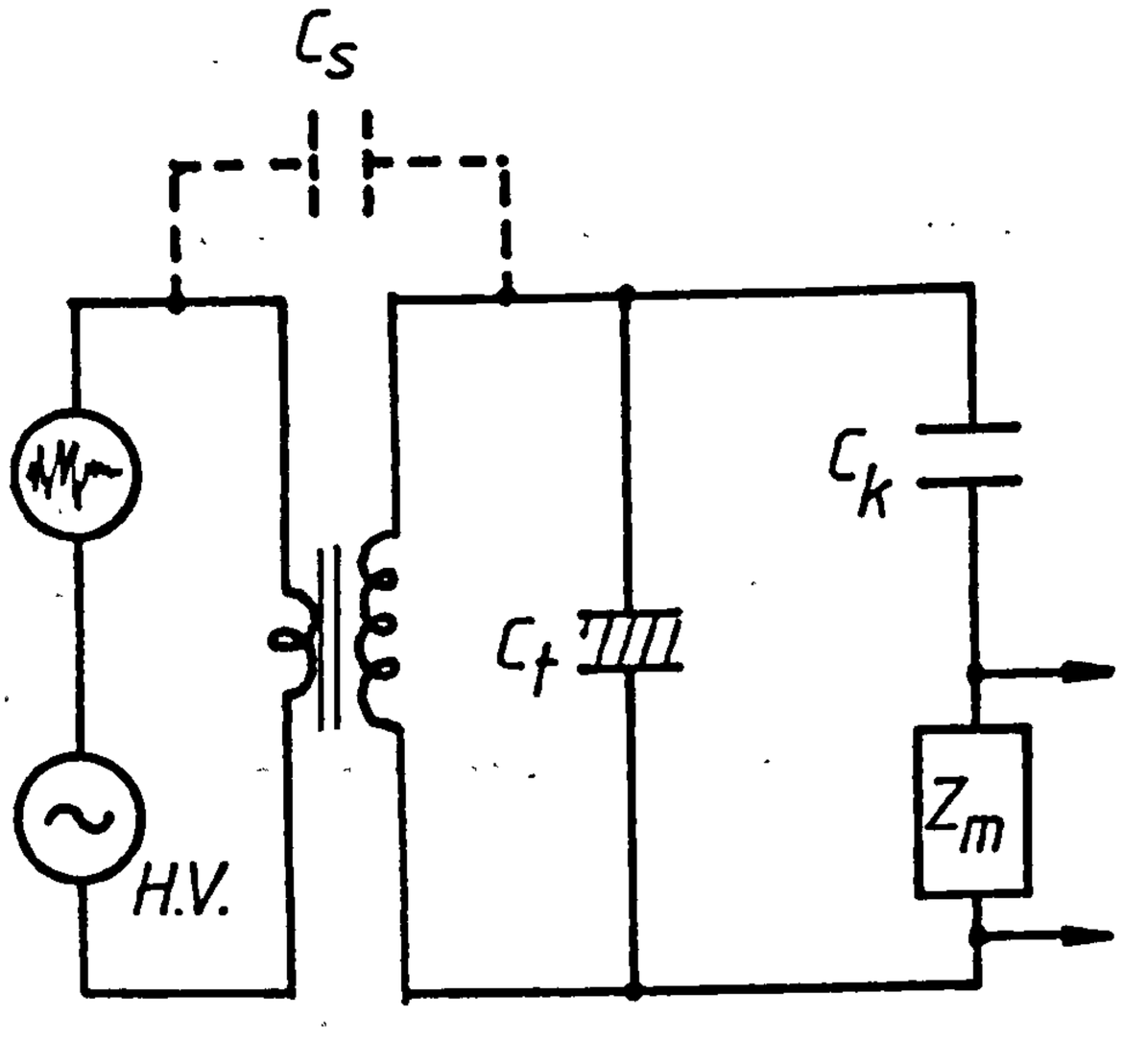

d) Coupling via H.V. Source

Figure 1.6.2.9 - Interference Coupling Mechanisms in Discharge Detection Circuits

rejects unwanted signals which are random in nature by the use of signal averaging methods [48] . The main disadvantage of this method is that it cannot reject spurious pulses which occur at a fixed position on the supply cycle.

Another technique that provides rejection of this type of interference is the pulse discrimination system , [49] , which is based on a balanced detection circuit. Common mode noise signals that pass through both arms of the detection circuit are rejected on a polarity discrimination basis by coincidence logic circuits.

1.6.2.3 Partial Discharge Measurements in H.V. Machines.

The value of using partial discharge measurements to monitor the condition of stator winding insulation depends on the type of insulation system examined and more importantly the mechanism of deterioration. Older generation natural resin bonded mica flake insulation experiences degradation by discharge erosion of internal cavities. These internal discharges are most intense in the line end coils of the phase winding and the repetition rate is such that individual discharges are not recognisable due to the limited resolution of commercial discharge detectors such as the ERA Mk III which has a pulse resolution time of about 20 μsec. Superposition of discharge pulses makes it difficult to interpret the measurements. However the photographs of the discharge patterns and measurements of the maximum discharge present can be compared over a period of time to yield information that indicates an increase in the overall discharge activity and peak level.

Probably the more useful application of partial discharge testing is to modern synthetic resin bonded mica paper insulation systems. This type of insulation is more consolidated than natural resin bonded insulation and therefore exhibits a greater resistance to erosion by internal discharges.

Failure is likely to occur through erosion of the mainwall insulation by slot discharges and surface discharges in the endwindings. High discharge magnitudes are indicative of slot discharge activity. Discharge peak magnitudes of between 1000 pC and 10,000 pC are characteristic of slot discharges from bare areas of the partially conductive coating and in excess of 10,000pC, and as large as 100,000

pC, are associated with slot discharges that occur when the shield is isolated from the slot.

In addition, a feature which is indicative of surface discharges in the endwinding region is that surface discharges have large magnitudes, typically 50,000 pC , [50] , and occur intermittently on the positive half-cycle of the supply voltage. Surface discharges also have the characteristic that their magnitudes increase proportionately with the applied voltage stress [25] .

Discrimination between slot, surface and internal discharge sources is therefore possible from their respective discharge pulse characteristics. Partial discharge measurements in this case have a distinct advantage over the dielectric loss analyser system as it is inherently insensitive in discrimination between different discharge mechanisms .

A recent development , [41] , in the dielectric loss analyser by the addition of a discharge pulse detection facility, whereby discharge pulses are displayed superimposed on the normal D.L.A. loop trace , is seen as an attempt to improve its discrimination capability.

Nevertheless, it is difficult to make quantitative measurements, apart from peak discharge magnitudes, from normal elliptical time base displays on discharge detectors. One technique, when used in conjunction with discharge detection systems, does provide quantitative information on partial discharge activity by recording the magnitudes and repetition frequencies of all discharges present. Pulse height analysis as it is termed may provide the basis for a very useful diagnostic technique [57] .

1.6.2.4 Pulse Height Distribution Analysis

Pulse height analysis was developed fundamentally for use in nuclear pulse spectrometry in which the statistical behaviour of radiation particles is studied [51] .

A pulse height distribution is basically a histogram of the frequency of occurence of a distribution of pulse heights or amplitudes in a train of pulses, whether these represent radiation particles having energies in eV or partial discharges having magnitudes in pC.

The first to recognise the importance of pulse height analysis in partial discharge measurements was Starr and Johnstone [52] .

In their system a single channel pulse height analyser is used to count the number of pulses whose amplitude lie in an interval or window about a preset pulse height. This process is repeated over a range of pulse heights to obtain the pulse amplitude distribution. The single channel analyser basically detects pulses within a voltage window (or channel) of fixed width by means of upper and lower voltage level discriminators, and subsequently counts them. Modern pulse height analysers have multiple channels which are distributed over a given signal range, normally 10 Volts. Multi-channel pulse height analysers as they are termed are basically fast analogue to digital converters with a memory, to store the pulse counts for each channel.

Commercially available analysers have typically, 1024,2048,4096 and 8192 channels which permits very sensitive measurements of pulse amplitudes since channel apertures are extremely small. Resolution between individual pulses is governed by the 'dead time' of the analyser, which is the time taken to process a single pulse. Multichannel analysers are therefore very suitable for use in partial discharge measurements.

A practical example of a pulse height distribution is shown in figure 1.6.2.10 . The sample is a small air filled , cylindrical cavity with a diameter of 2 mm and depth of 1.5 mm which is formed by a circular hole in a sheet of synthetic resin-bonded paper , sandwiched between two sheets of synthetic resin-bonded mica flakes . It can be observed that the measured distribution is exponential in shape which would be expected of an internal cavity discharge . In contrast , the pulse height distribution obtained from a negative corona discharge source , as shown in figure 1.6.2.11 , shows the very regular discharge magnitude which characterises this type of discharge . This subject is treated in greater depth in references [54,55] .

In this way the pulse height distribution in partial discharge measurements can be seen to provide a wealth of information on the discharge mechanism and its intensity since any change in the discharge process is reflected in the pulse height distribution.

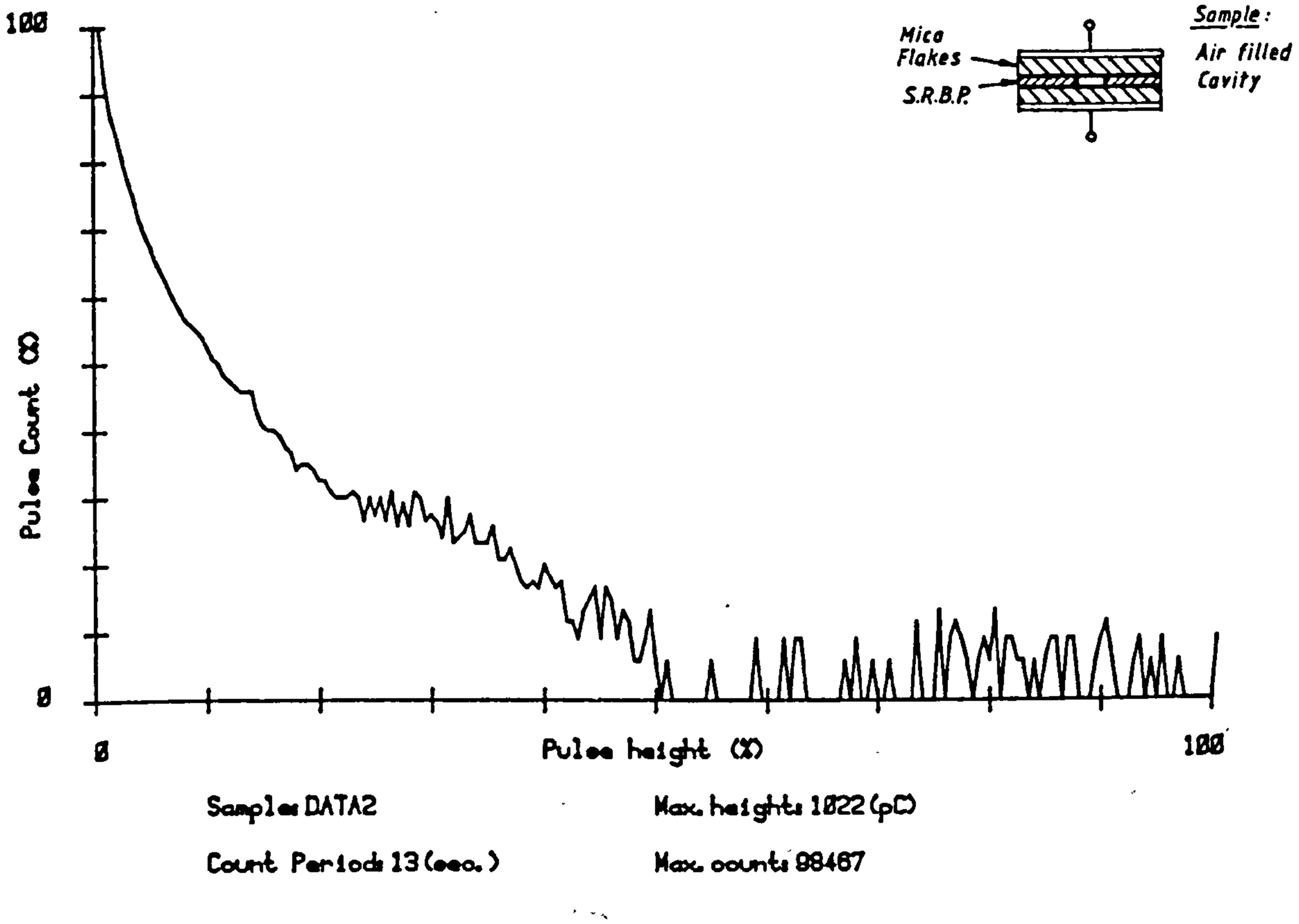

Figure 1.6.2.10 - Pulse Height Distribution from Internal Air-Filled Cavity

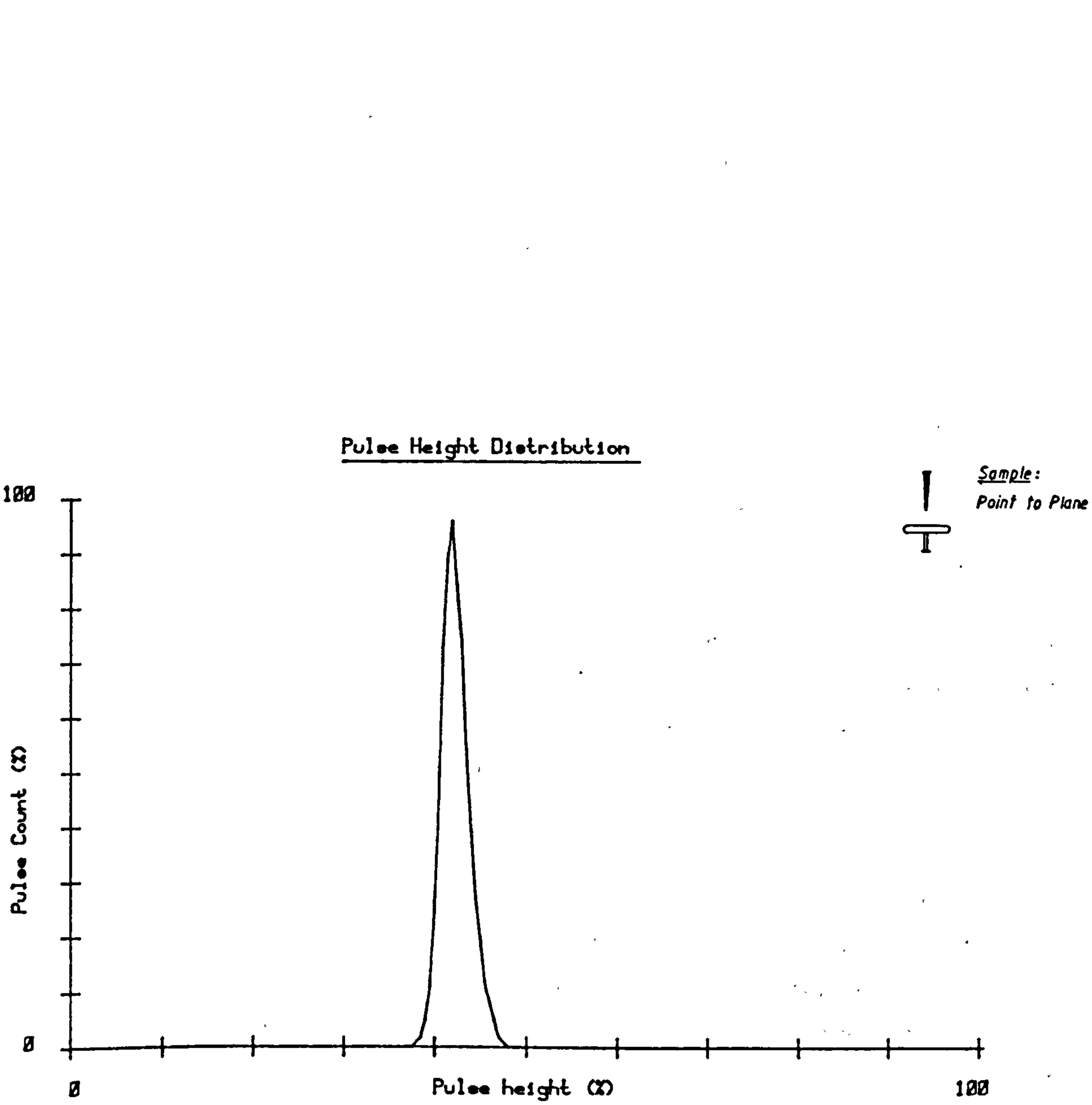

Figure 1.6.2.11 - Pulse Height Distribution from Point Corona Source

So far single discharge sites have been discussed. However, in a machine winding there are multiple discharge sources distributed throughout the winding, in particular in the line end coils where activity is the greatest. Pulse height analysis applied with discharge detection measurements at the machine terminals therefore results in a superposition of all discharge activity in one pulse amplitude distribution. Separation of each discharge distribution is impossible unless it is possible to examine localised areas of the winding.

Functional ageing experiments on samples of machine coils and stator bars have shown that changes in the pulse amplitude distribution occur over a period of time and that certain relationships between discharge pulse distributions and deterioration progression can be made [56] . Results on coil sections with no simulation of the stator core ,(packing and wedging), at electric stresses between 2 kV/mm and 8kV/mm indicate a change in the pulse amplitude distribution in which the maximum apparent discharge magnitude varies and the number of relatively large discharges changes with time .

It is clear that pulse height analysis is potentially a very valuable tool, when used in conjuction with partial discharge detection techniques, to assess the condition of the insulation of high voltage machine windings. This is born out by the fact that pulse distribution analysis has been successfully applied in an on-line insulation condition monitoring system to generators in Ontario Hydro, [57] .

In this system the discharge pulses are coupled to the pulse height analyser by permanently installed capacitors connected to the line end of each phase of the generator winding. Both positive and negative pulses are processed by the analyser. The pulse height distributions obtained are used as a fingerprint such that any deterioration of the winding insulation is gauged by a comparison of pulse distribution fingerprints. Generally this means an overall increase in the area under the distribution curve. This trend analysis technique can successfully diagnose the loss of insulation integrity. Furthermore the pulse height distributions permit identification of the discharge mechanism causing the deterioration.

High intensity slot discharge, as outlined previously, is identified by the large magnitudes of discharge pulses and by a pulse distribution characteristic which is possibly load dependent. When the generator load is increased the partial discharge activity is increased . This is explained by the fact that increasing load causes increased stator bar vibration hence greater slot discharge activity. Associated with these features is a difference in the pulse distributions of positive and negative pulses.

In a similar fashion, a low intensity slot discharge which occurs on bare areas of the semi-conducting coating is identified by the same polarity effect in the pulse distributions. However, these discharges exhibit no dependence on the generator load. Internal partial discharges are identified by the fact that the positive and negative discharge activity is very similar.

As well as the use of pulse height distribution analysis to fingerprint partial discharge activity other techniques such as pulse interval distributions, (which is the distribution of time intervals between consecutive pulses), and pulse phase distributions (which is the distribution of time occurrence of pulses after the start of the supply cycle), may contribute more information towards diagnosis of insulation health [58] .

1.6.3 Frequency Spectrum Measurements.

Frequency spectrum analysis is fundamentally the measurement of electromagnetic interference voltage levels over a broadband of frequency which can extend from 10kHz up to as high as 1500 MHz . Measurement of EM interference is performed by either a radio noise meter or a spectrum analyser. The radio noise meter is designed to cover frequencies between 10kHz and 30MHz whereas the spectrum analyser operation extends up to ultra-high frequencies.

A radio noise meter is basically a tuneable narrow bandpass filter, (typically a 9 kHz passband), based on a superheterodyne receiver. The output of the filter is fed to a quasi-peak voltmeter which provides an indication of discharge level in microvolts. It is possible in purely capacitive test objects to calibrate the detector voltage in picocoulombs of apparent charge [65] . However, the relationship between the voltmeter reading and the apparent charge is

dependent on the repetition rate of the discharge pulses.

The interference voltage is not directly relatable to the apparent charge of a discharge within a stator winding since the frequency response of the winding is very complex. A partial discharge at a point within the winding is subject to frequency dependent attenuation before it is detected at the terminals and also excites resonances at certain frequencies, which makes calibration impracticable.

Certain studies have developed successful models of the frequency response of large motors and generators based on lumped parameter circuits , [59] , and on simple transmission line resonance theory, [60] . These investigations aid the interpretation of frequency spectrum signatures from measurements on motors and generators.

The true value of frequency spectrum analysis in partial discharge detection is to indicate the presence and intensity of any discharge activity by a comparison of frequency spectrum signatures.

One technique has been developed to detect on-line the presence of partial discharges and in particular arcing faults in large turbine generators, caused by broken stator winding conductors, by monitoring the level of radio frequency noise over a band width between 10kHz and 30 MHz [61] . The r.f. currents produced by discharges in the winding and external interference sources flow in the neutral connection of the generator winding and are sensed by a wide-band current transformer and radio noise meters which cover the frequency range required (see figure 1.6.3.1). Noise level is measured in microvolts quasi-peak over the frequency spectrum. Frequency spectrum signatures from different machines are compared and from this an average spectrum signature is obtained which represents the general noise level from a healthy machine.

A very similar technique , [62] , employs a current transformer in the neutral connection of the generator and a spectrum analyser to measure the level of noise in the frequency range 14 kHz to 1000 MHz. In general results show that machines generate a characteristic noise spectrum and similar machines produce similar spectra. Healthy machines generate spectra with relatively low levels of wideband noise. However, in machines which have high levels of slot discharge the amplitudes of spectral frequencies increase .

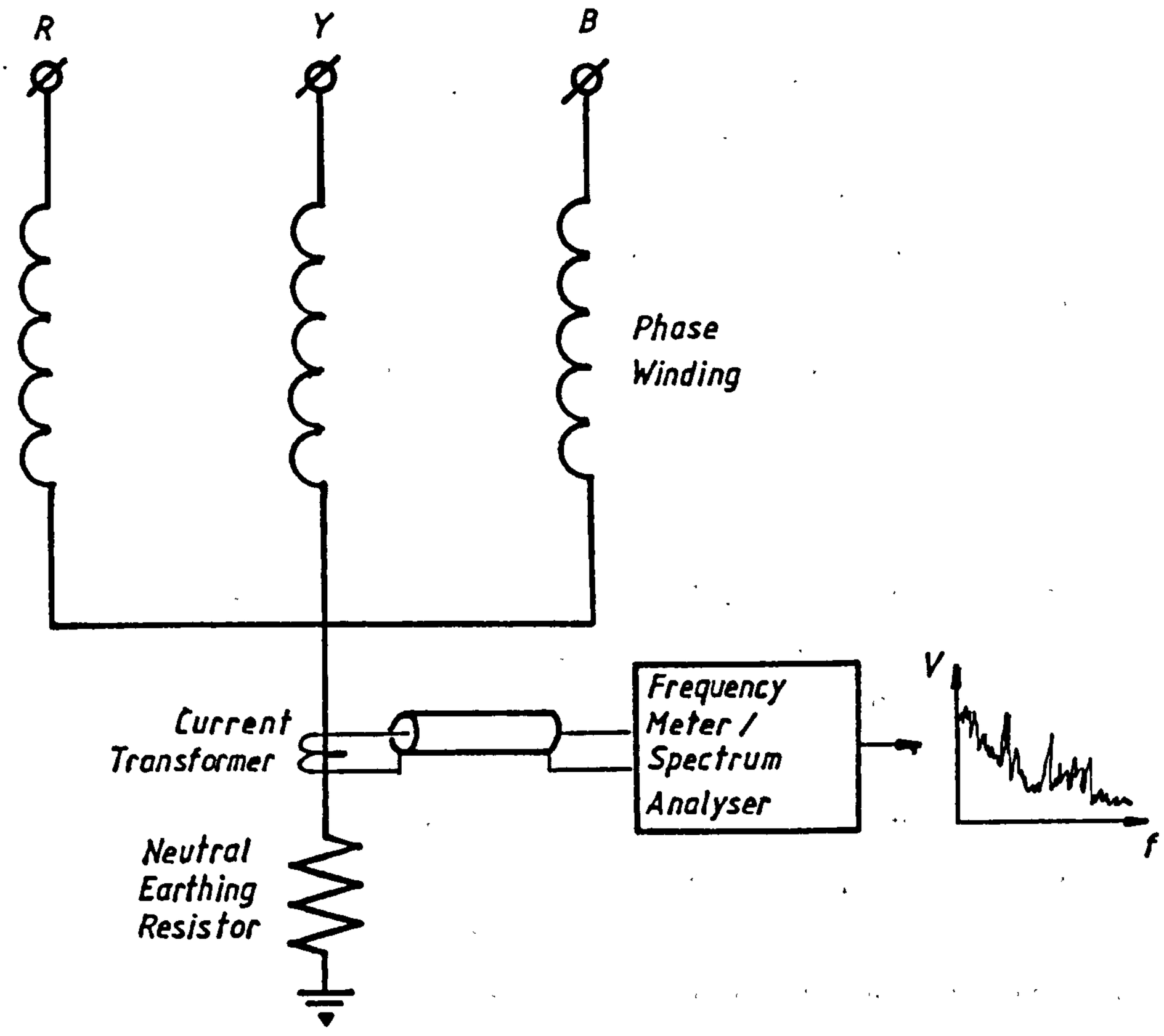

Figure 1.6.3.1 - Radio Frequency Neutral Earth Current Monitoring

Measurements indicate that slot discharge activity may be identified by an increase in spectral frequency amplitudes in the low frequency range, below 1 MHz .

A fundamental limitation of the system is the inability to discriminate between signals originating in the test machine and those generated in other equipment, (transformers, bus-sections and other machines), since externally generated noise signals are detected in the neutral line. Isolating a signal source requires additional testing.

The system developed by the CERL , [31] , is applied to h.v. motors . A split-core current transformer is situated at the switchgear side of the feeder cable and radio frequency currents generated by discharges are detected over the frequency range 500kHz to 700 kHz and indicated as a quasi-peak voltage level. Slot discharges are the principal deterioration mechanism monitored since an oscilloscope is used in conjuction with the radio noise meter, displays intermittent high level discharges.

Another detection system developed by the CEGB , [63] , relies on the use of an r.f. loop probe , [64] , developed to detect noise voltage levels from discharges, over the frequency band from 300 MHz to 1500 MHz. The probe is basically circular loop 70 mm in diameter which senses changes in the magnetic field enclosed by the loop over a wide band of frequencies. It is inherently insensitive, (-60dB below midband), at frequencies below 1 MHz. In an on-line system the probe may be situated near to a line end connection of the winding or a number of probes may be positioned at intervals around the winding to give a discharge location capability. A spectrum analyser is used to determine the level of noise in the frequency range.

The u.h.f. band of 300 MHz to 1500 MHz is adopted since noise signals generated from slot discharges extend into this frequency range. Noise signals generated from corona discharges and exciter sparking have a much lower frequency content, and aerial borne interference from radio broadcast stations occur in the v.h.f. band from 30 MHz to 300 MHz which, to a great extent, is attenuated by the machines metal enclosure. Discharge activity is identified by a general increase in the spectral frequencies amplitudes. Changes by as much as 20dB in

signal level have been detected by the technique.

As can be seen from previous investigations frequency spectrum analysis provides useful diagnostic information and can supplement other on-line diagnostic techniques.

1.6.4 Partial Discharge Location Techniques.

As well as detecting the presence of partial discharges and providing an indication of the type and intensity of discharges it is potentially useful to be able to locate the position of discharge sources within a machine winding structure. Moreover, by examination of regions of the stator winding a picture of the discharge activity distributed along the winding length can provide information that may permit diagnosis of a fault condition and its position on the winding. In addition to the diagnostic information provided, an advantage of a discharge location technique is that the level of interference signals, that cloud the discharge pattern, from other plant and external noise sources is greatly reduced.

Existing location techniques appled to h.v. electrical machines are classified in one of two categories as follows :-

i. Probe techniques.
ii. Travelling wave techniques.

1.6.4.1 Probe Techniques

All probe techniques to measure partial discharges in the machine slot region are intrusive , as in most instances the rotor of the machine must be removed to access the stator winding. The machine must therefore be off-line to perform tests . However , this is not a problem when the probes used are mounted in the endwindings [31] .

An electromagnetic probe technique is described by Dakin et al, [66] , consists basically of a sensing coil wound on an iron , half-toroid, core which straddles the slot of a machine stator core as shown in figure 1.6.4.1. The iron of the stator core therefore forms the other half of the magnetic circuit. High frequency current pulses from discharges in the slot are detected by the coil. Hence the probe behaves like a high frequency current transformer with a single turn

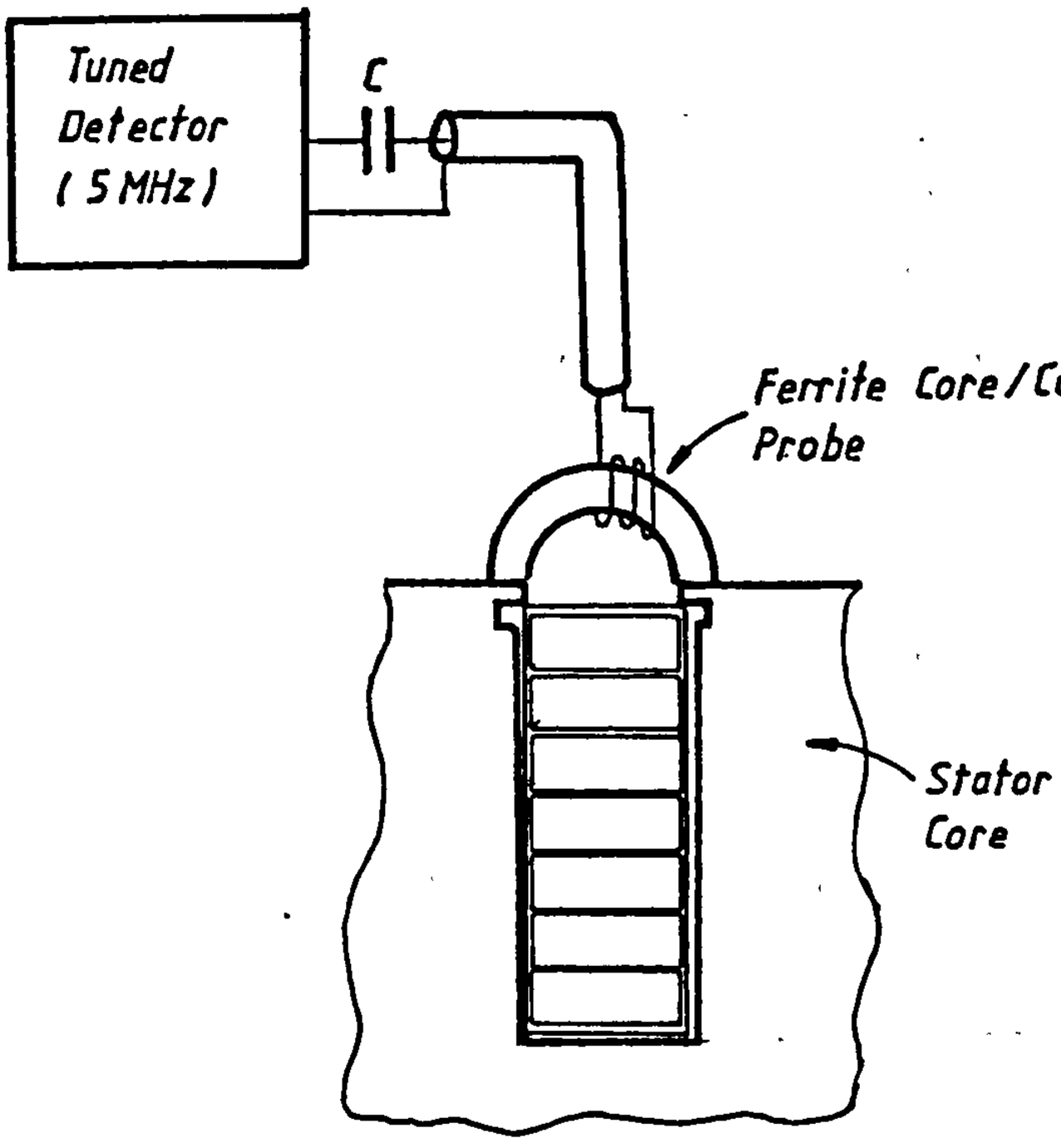

Figure 1.6.4.1 - Electromagnetic Probe Technique

primary, (the coil conductor), and multi-turn secondary. The probe coil inductance and associated cable and detector input capacitance are selected to obtain circuit resonance at a frequency of around 5 MHz . At this frequency, pulses travelling in the winding from a discharge site , are attenuated rapidly such that the sensitivity of the probe falls quickly with distance from the discharge site. The probe is therefore sensitive to discharges in a small slot region in the vicinity of the probe. Adopting a lower resonant frequency of 1 MHz, for example, has been shown to increase the probes sensitivity to discharges at localities further away thus reducing the probes location selectivity .

The discharge pulses detected by the coil are fed to the detector amplifier which is tuned to the circuit resonant frequency to obtain optimum sensitivity. A radio noise meter is used to provide a quasi-peak voltage measurement. By scanning each slot in the machine sequentially a distribution of partial discharge activity is obtained which indicates the regions of highest discharge intensity.

Calibration of the probe is achieved whilst the winding is de-energised, by injecting a calibration pulse through a foil electrode, coupling capacitor which is wound on a portion of the coil at the interface of the slot and endwinding regions. Sensitivities obtained are approximately 0.019 μV/pC .

This technique is particularly suited to locating slot discharges in machine windings and is used extensively in the U.S.A. and Canada, [67] .

A similar technique developed by the CEGB , [31] , allows measurement of discharge levels in the endwindings of machine stators by measurement of the discharge currents in the intercoil connecting links.

1.6.4.2 Travelling Wave Techniques

The winding of an electrical machine is a distributed component and as such it behaves as a very complex transmission line at frequencies whose wavelength is comparable to the length of the winding conductor. Signals travel in the stator winding with a finite velocity. Knowing the time taken for a pulse to propagate from a location in the winding

to the winding terminals and the propagation velocity it is possible to determine the position of the pulse source. This principle provides the basis of all travelling wave location techniques.

One technique, used to locate the source of discharges in a machine winding , [68] , relies on an analysis of the spectral frequency phase relationships in a discharge pulse observed at the winding terminals. An artificial discharge pulse is injected at one end of a stator bar and observed at the opposite end. A digital storage oscilloscope stores the pulse waveform detected at the output. Subsequently, the relative magnitudes of the harmonic components of the waveforms are evaluated along with their respective phase angles relative to the fundamental frequency of pulse. The phase angle of the nth harmonic relative to the fundamental frequency, along with a knowledge of the variation of the winding capacitance with frequency, is sufficient to determine the location of the discharge source. The particular nth harmonic chosen for analysis of the discharge position is the one whose magnitude is significantly higher than the next higher, ((n+1)th), harmonic. The technique is dependent on the knowledge of the variation of capacitance with frequency.

Until now, no partial discharge location technique for electrical machine stator windings has been developed based on the time domain behaviour of pulses. Although, such techniques have been applied to the testing of transformers , [69,70] , in which the difference in time delays incurred by the pulses detected at the winding terminals is used to determine the position of the discharge source.

It is the purpose of this study to develop a technique for the location of partial discharges in the stator windings of electrical machines to complement existing partial discharge measurements .

CHAPTER TWO

DISCHARGE PULSE PROPAGATION IN H.V. MACHINE STATOR WINDINGS

2.1 Propagation of Partial Discharge Pulses in Stator Windings

When a partial discharge takes place , whether it is a surface discharge or an internal discharge in the slot or endwinding region , a rapid injection of electrical charge occurs , and results in current pulses flowing in conductors local to the point of discharge . These high frequency current pulses propagate to both ends of a phase winding where they are transmitted and reflected at the respective junctions .

A knowledge of the manner in which high frequency pulses propagate in high voltage stator windings is a necessary prerequisite in partial discharge measurements to the following :

i. The development of a technique capable of locating the position of partial discharge sites in a phase winding .

ii. The accurate measurement of partial discharge magnitudes from measurements made at the motor winding terminals .

Until recently , there have been very few published investigations on the propagation of partial discharge pulses in the stator windings of high voltage machines . Studies have been performed in other high voltage systems which are subject to partial discharges such as h.v. transformers [76,77] and h.v. power cables [78] .

Similar studies have also been done on h.v. machine stator windings but with pulse waveforms representative of lightning and switching surges , [22] , which have provided much useful information .

One investigation on the propagation of discharge pulses in waterwheel generator stator windings , [79] , gave some information on pulse attenuation in these windings but no detailed results on the propagation behaviour . Another study by Miller et al. , [80] , performed a frequency analysis of partial discharges propagating in a motor winding to give details on the attenuation of harmonic frequencies of the pulse with distance of propagation . However , the investigation by Wilson et al. ,[81] , is the most detailed and the most relevant to the study of the behaviour of discharge pulses in machine stator windings . In this study the basic mode of pulse propagation is outlined together with information regarding pulse

velocities and attenuation . Tests were performed on a number of high voltage machines and results of experiments on a 6.6 kV ; form wound motor and on a 22 kV generator winding were discussed .

Two basic modes of pulse propagation are identified . In the series mode the winding behaves like a simple transmission line in which the a pulse has a finite propagation velocity and is subject to attenuation. In the second mode , a portion of the pulse travels through the winding virtually unhindered and without appreciable time delay . The path of propagation is through the endwinding conductors by electromagnetic coupling . This mode occurs at higher pulse frequencies , above a certain cut-off frequency . These results are similar to the findings of the study on the propagation characteristics of partial discharge pulses in motor windings described in the following sections .

2.2 Stator Winding Test Rig

The model phase winding used for experimentation is constructed from a group of fourteen , 7 - turn coils supported in a wooden cradle which has the slotted profile of a stator core as shown in the photograph in figure 2.2.1 . A sheet of copper is formed over the teeth of the wooden frame to represent the iron core of a machine . This model is valid , since the depth of penetration of flux at a frequency of 100 kHz is 53 μm , (conductivity of sheet steel is taken to be 3.6 $\mu\Omega^{-1}m^{-1}$). Therefore at higher frequencies, the ferromagnetic properties of the iron of a stator core has negligible effect on the propagation of electromagnetic signals within the stator winding . The inductance of the slot portion of a stator coil becomes independent of frequency above 100 kHz .

The rotor of the machine is considered to have negligible influence on the pulse propagation behaviour at the frequencies encountered in partial discharge pulses due to the skin effect and the fact that an appreciable air gap exists between the stator and rotor surfaces . Therefore the rotor is not simulated by the model .

Each coil in the model is of a form wound construction in which 2 parallel conductors are wound to form a 7 turn coil in a double-stack conductor arrangement . By connecting the parallel conductors at the coil ends the coil is made to behave electrically as a 7 turn coil .

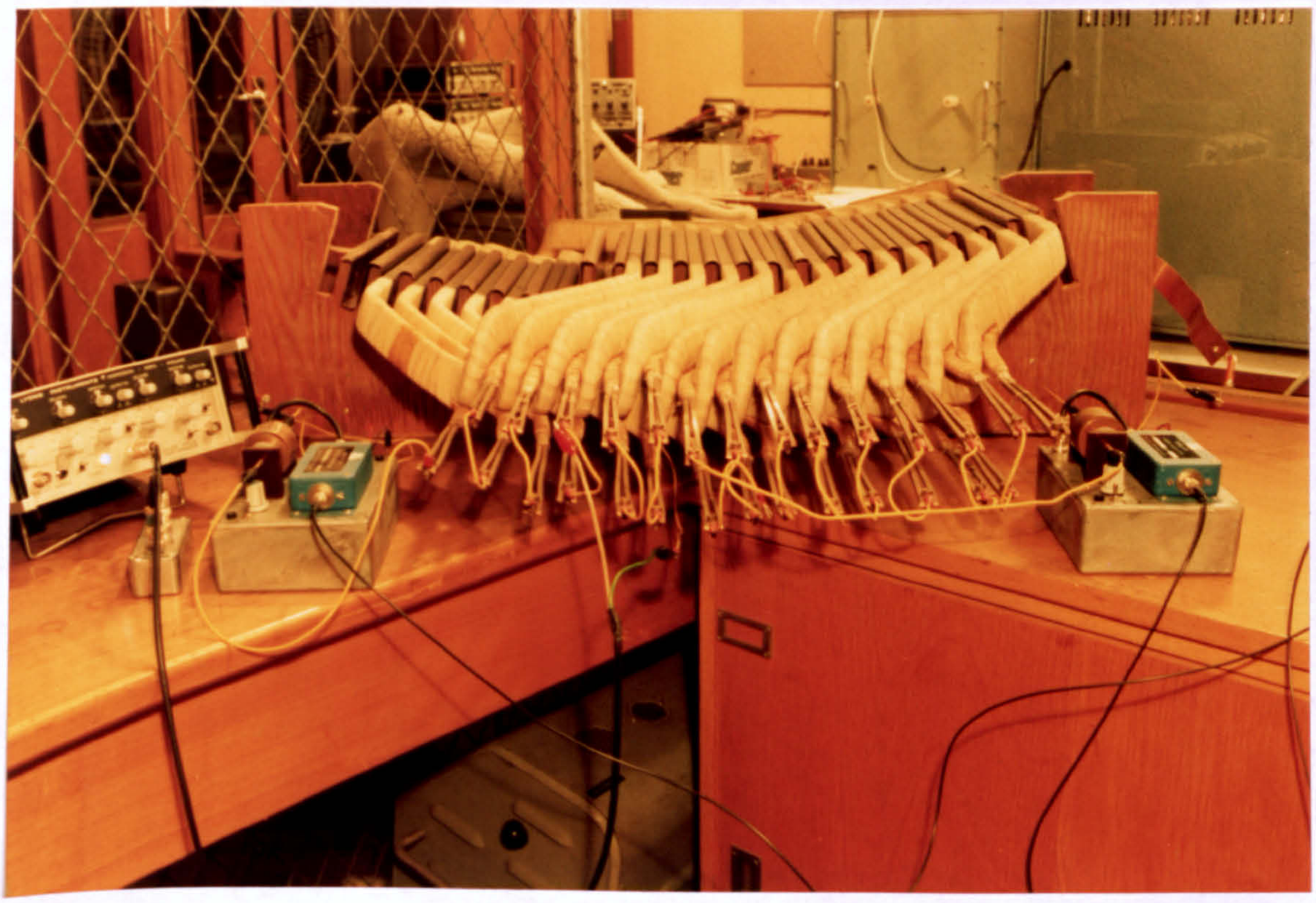

Figure 2.2.1 - Motor Phase Winding Test Rig

The coils are typical of those used in high voltage motors rated at 6.6 kV and are insulated to class F standard with epoxy resin bonded mica paper tape to give an interturn insulation thickness of 0.62 mm and a main slot insulation thickness of 1.9 mm . The slot portion is painted with a colloidal graphite paint which extends 20 mm beyond the core ends . Voltage grading paint at the slot ends overlaps the graphite paint by 13 mm and extends a further 40 mm into the endwinding region . The endwinding is finished with one layer of flexible epoxy sealing tape .

The coils are lap connected to form a double layer phase winding which has a coil pitch of 9 slots . Connections are made with a brass nut and bolt arrangement and short lengths of copper wire . In this manner access for oscilloscope measurements is achieved at test points on the coil interconnections and winding terminations .

Partial discharge pulses are simulated with a pulse generator which injects a train of rectangular pulses through a calibration coupling capacitor into the coil interconnections or the winding terminations . In some instances , pulses from the pulse generator are fed directly to the winding injection points to observe the behaviour of voltage pulses in the winding to enable identification of the important propagation characteristics . Pulse amplitudes from the pulse generator are variable in the range of 0 to 20 volts , and pulse rise time is adjustable from 10 nsec. to 1000 nsec to allow simulation of most partial discharge pulse features .

Voltage measurements are made with low capacitance oscilloscope probes whilst current measurements are made using a Rogowski coil , which is basically an air-cored current transformer , at the coil interconnections and winding terminals . A typical test arrangement is shown in the diagram of figure 2.4.1 ,(page 89).

To simulate the effect of discontinuity of impedance at the winding terminations , the model phase winding is terminated in a variable resistor at each end , which is adjustable in the range of 0 to 1000 ohms . This covers the terminating conditions that are likely to occur in a machine .

In a star connected winding , the line end will be connected to the power supply system through a length of power cable which has

typical surge impedance values of between 20 and 50 ohms [21] . This is much less than the effective surge impedance of machine windings which are typically between 100 and 5000 ohms [21]. The neutral end however is connected to the junction of the two other phase windings and so behaves effectively as an impedance of half the phase winding surge impedance , (refer to figure 2.2.2) .

In the case of a delta connected winding both terminals of a phase winding are at the junction of the two other phase windings and the supply cable as shown in figure 2.2.3 . The effective surge impedance at the winding termination is the resultant of these .

The terminating resistors in the phase winding model are not representative of the surge impedances of other phase windings or power cables in the strictest sense , since they do not simulate the effects of pulses reflected back into the phase winding from the opposite end of the power supply cable or the other phase windings . In the case of pulses reflected at the opposite ends of the other phase windings , it is sufficient to model these as a discrete impedance as attenuation of pulses in these windings is likely to reduce reflected pulses to an extent that their influence is negligible . However , pulses reflected at the switchgear end of a supply connection cable undergo a small degree of attenuation since modern power cables exhibit low loss transmission characteristics . In addition , supply cables to high voltage motors are often 3-phase armoured cables so that the single phase connecting cable is not a simple transmission line but includes mutual impedances between the phase conductors .

The use of a discrete impedance to model the supply cable is therefore of limited value for the reasons mentioned . However , this does not exclude the use of a discrete component to model the reflection characteristics of a junction of one or more surge impedances which is important in determining the pulse transmission behaviour in a machine stator winding . For the purposes of this investigation the phase winding model is sufficient in its representation of a phase winding in a real machine .

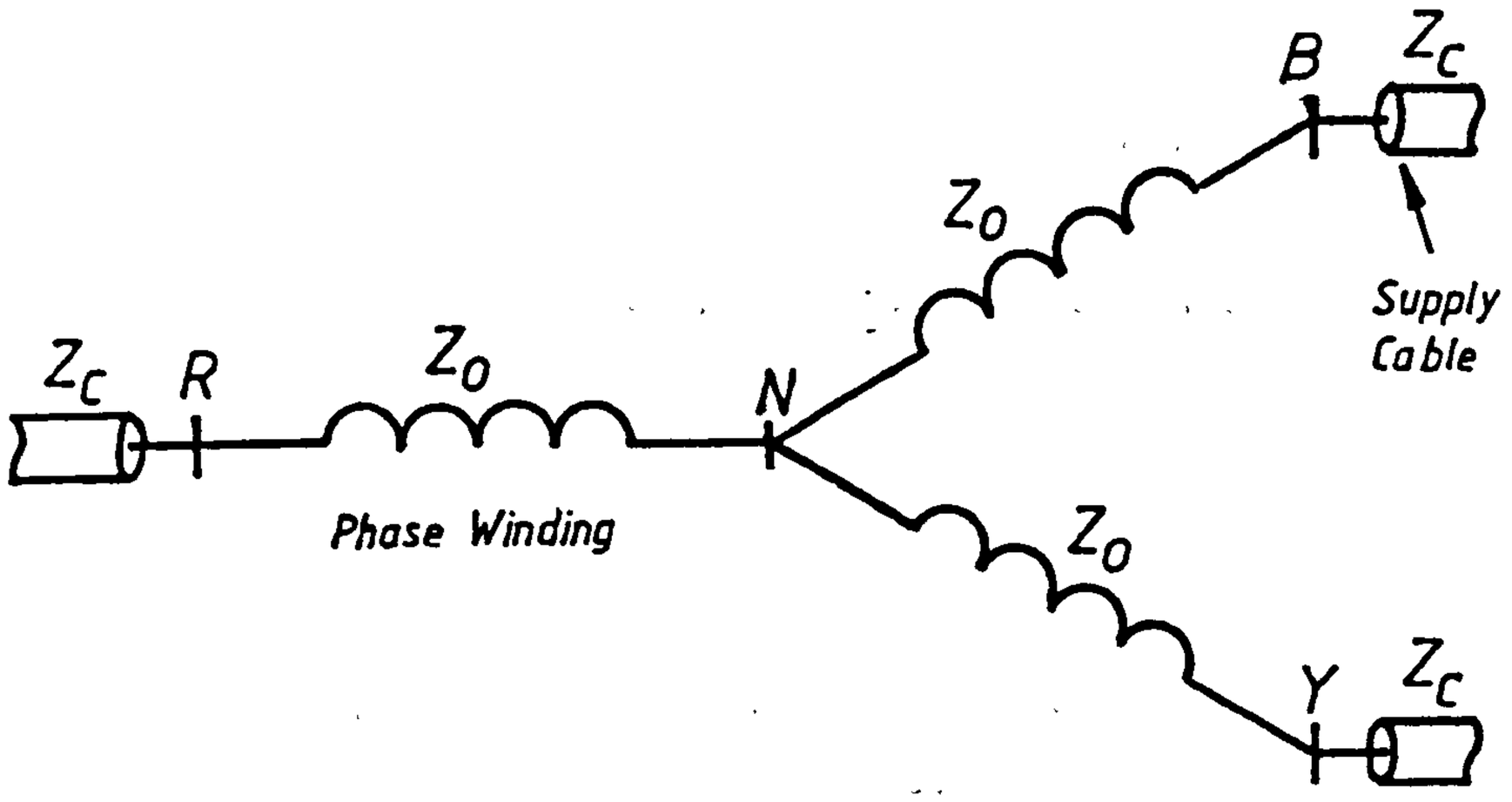

Figure 2.2.2 - Star connected winding

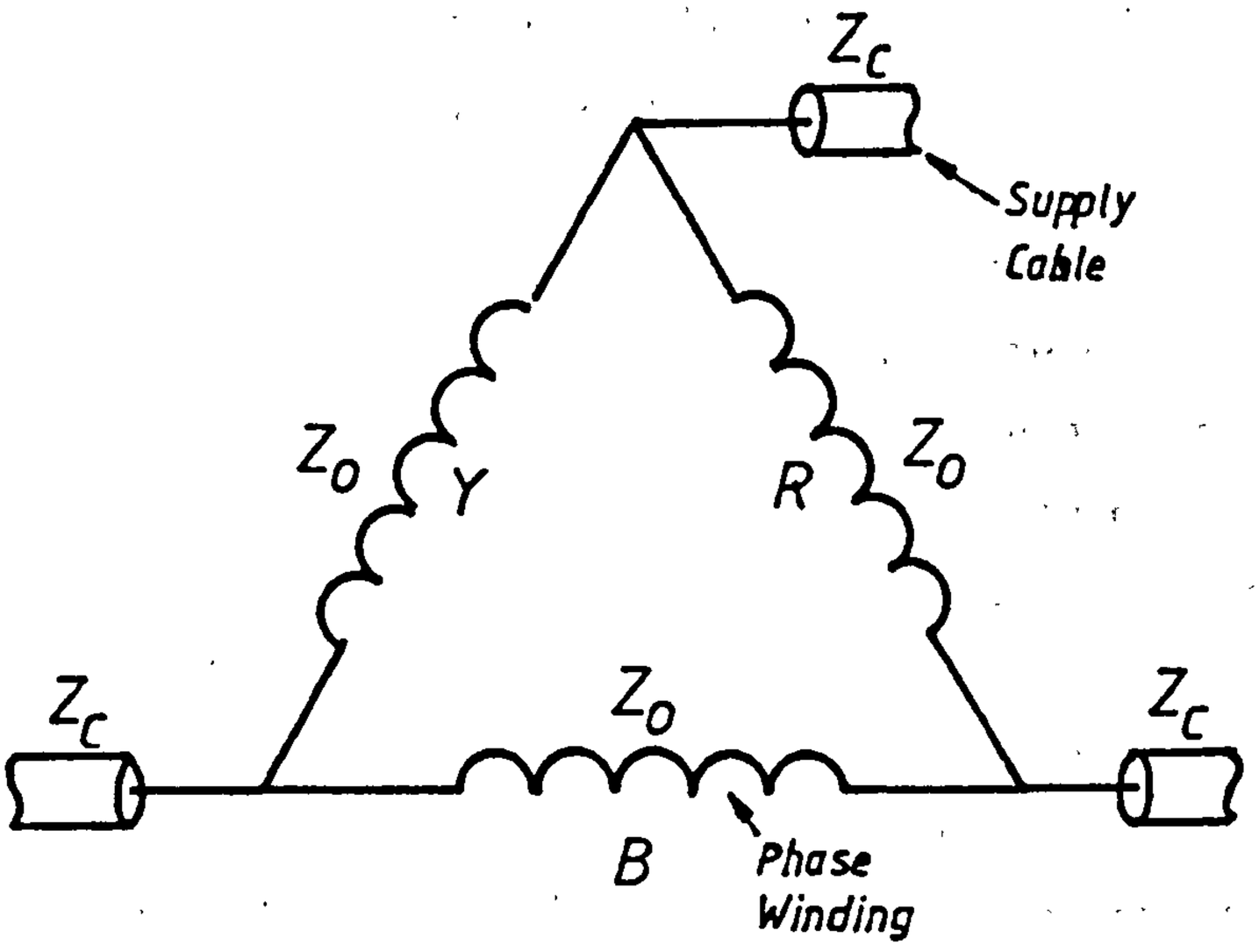

Figure 2.2.3 - Delta connected winding

2.3 Propagation of Steep-Fronted Pulses in a Single Stator Coil

To gain an appreciation of how fast rise-time , short duration pulses such as partial discharge pulses propagate in high voltage motor windings , an examination of their behaviour in a single stator coil was undertaken initially . By doing so , the influence of the remainder of the winding could be ignored initially to allow an assessment of the main propagation characteristics . In addition , this approach makes it possible to explain more readily the complex behaviour of electromagnetic pulses travelling in a stator winding transmission system as a whole .

Partial discharge pulses have widely differing shapes depending on the discharge mechanism present , which in the stator winding of a h.v. motor may be an internal cavity type discharge , a slot discharge or an endwinding surface discharge . However , common to each type of discharge is the rapid rise-time of the pulse which contains high frequency signal components . A rise-time as short as 1 nanosecond is possible for small internal cavity discharges , (refer to section 1.6.2.1 of chapter one) , which corresponds to signal components having frequencies extending up to 1000 MHz . A more realistic rise-time which may be expected will be in the region of 10 nsec or greater which is associated with frequency components of around 100 MHz and below . The durations of pulses vary considerably , from say 100 nsec to a few tens of microseconds , which places the lower end of the frequency spectrum in to the 100 kHz region . The investigation must therefore determine the propagation of electromagnetic pulses with a frequency spectrum that extends over the signal bandwidth outlined above . This is achieved by using rectangular pulses having a short rise-time and reasonably long duration .

Pulses derived from a pulse generator were injected at the source end of a stator coil and observed at the output which is terminated in a resistance of 300 ohms , see figure 2.3.1 . This resistance is approximately equal to the characteristic impedance of the stator winding and so represents the remainder of the winding . The pulses used had a rise-time of 10 nsec and a duration of 10 μsec so that a wide bandwidth of signal frequencies are generated , from 100 kHz up to 100 MHz . Figure 2.3.2 shows the waveform observed at the output of a single coil when a rectangular pulse of the type described above was

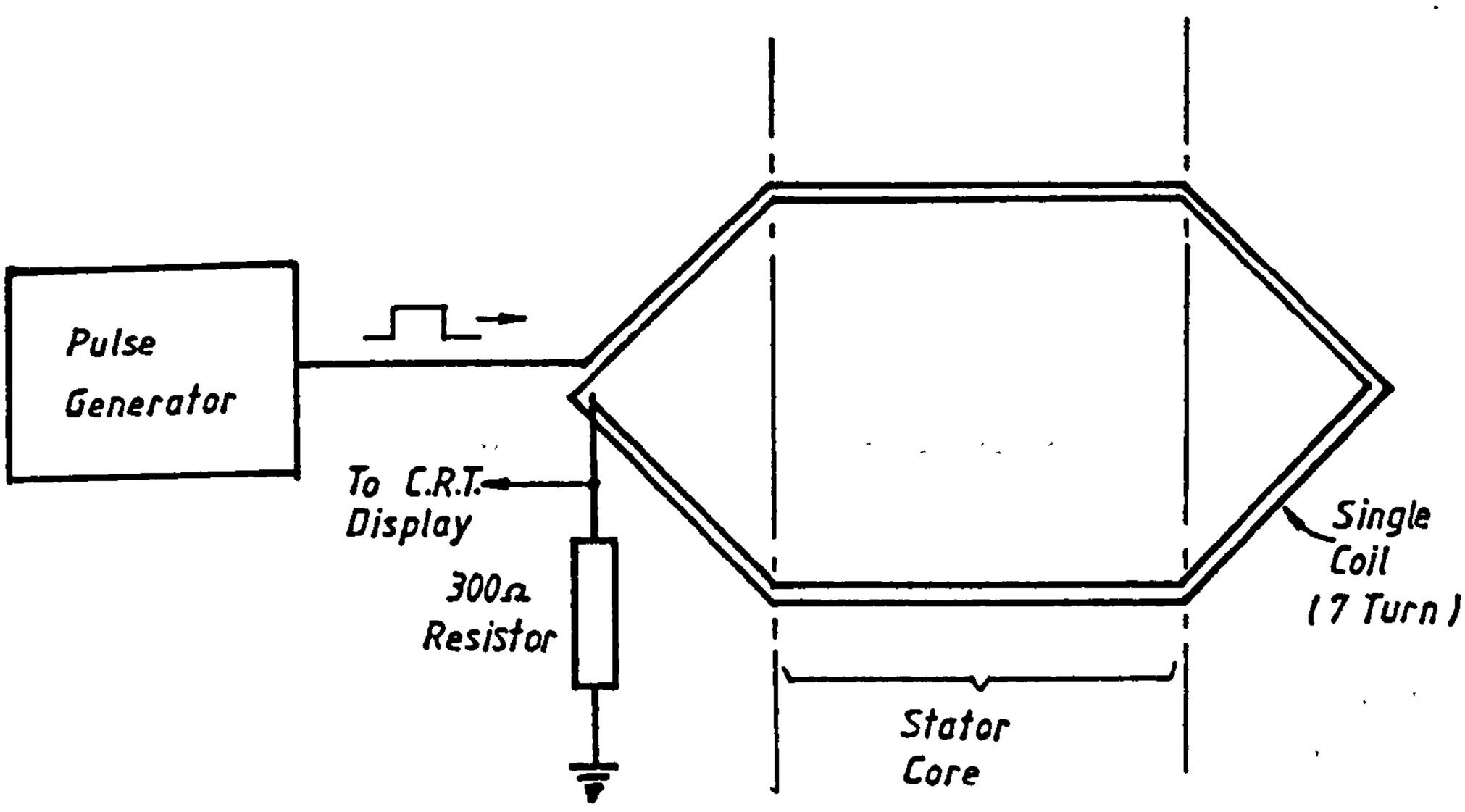

Figure 2.3.1 - Single Stator Coil Test Circuit

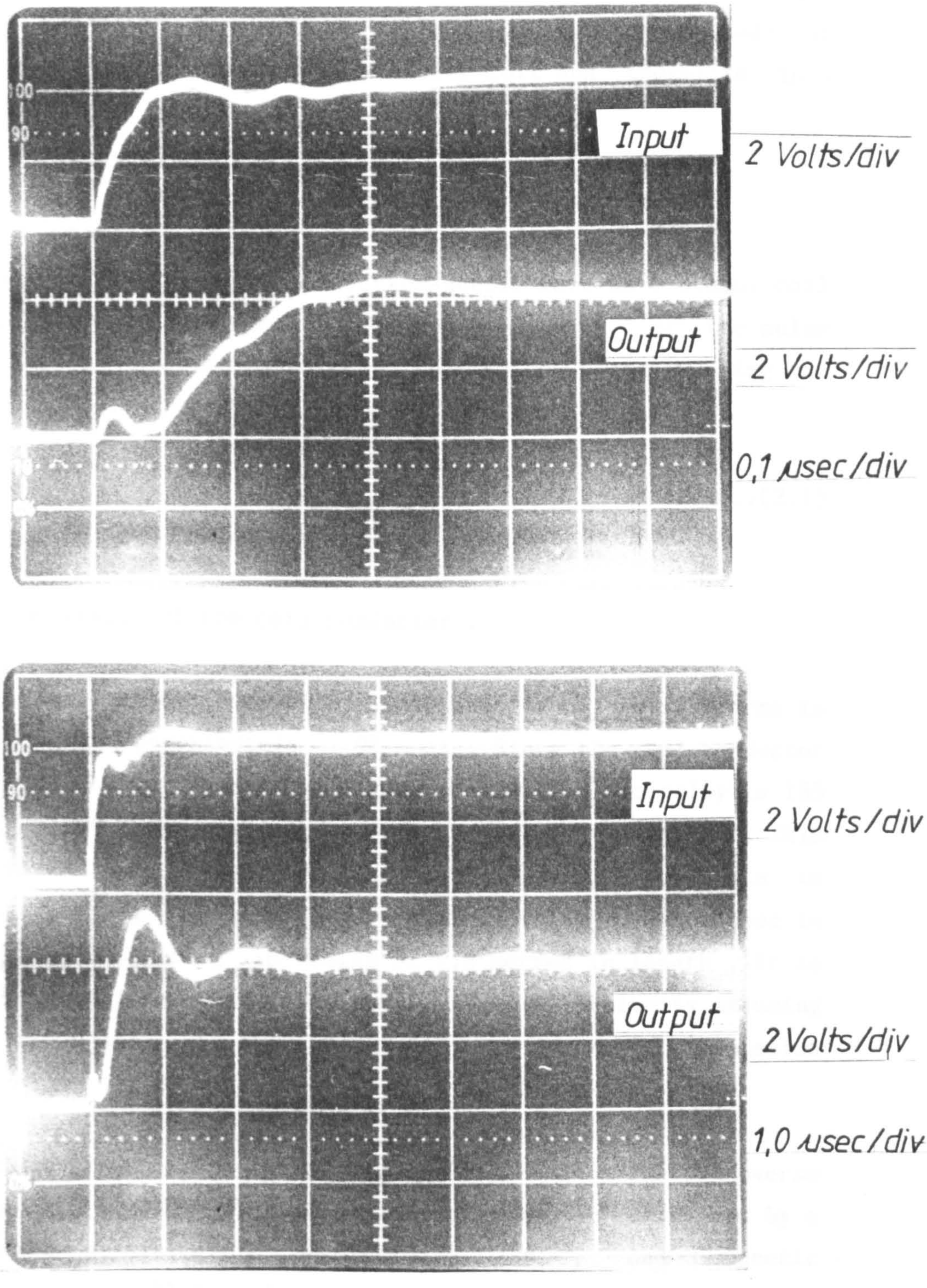

Figure 2.3.2 - Response of Single Coil to Steep-Fronted Pulse

It is apparent from the waveform that appears at the coil output that the pulse has incurred some time delay in passing through the coil . The wave therefore travels through each turn in the coil with a measureable speed of propagation . This is the main mode of electromagnetic wave propagation in a stator coil and therefore in a machine winding .

2.3.1 Velocity of Propagation in a Stator Coil

The propagation velocity of an electromagnetic wave in a stator coil is obtained from measurement of the transit time t_c of the pulse wavefront through a coil and relating this to the velocity using the simple expression ,

$$v = \frac{d}{t_c} \qquad \text{.....(2.1)}$$

where d is the length of the coil conductor .

The transit time through the coil , as measured from the waveforms in figure 2.3.2 , is approximately 90 nsec . Since the coil conductor length is 11.95 metres the corresponding propagation velocity is 133 m/μsec which is 44 percent of the speed of light in a vacuum . This is in the same region as has been found in similar experiments in motor stator windings , [81] , which yielded a value of 156 m/μsec in a phase winding comprising 18 coils of 2.8 metres in length . It is possible to relate this to a calculated value of velocity assuming that wave propagation is similar to that in a lossless transmission line .

In a lossless transmission line a wave propagating in the transverse electromagnetic , (TEM) , mode along a conductor surrounded by a medium having a dielectric permittivity , ϵ_r , and magnetic permeability , μ_r , will travel at a speed given by the expression ,

$$v = \frac{c}{\sqrt{\epsilon_r . \mu_r}} \qquad (c = 3 \times 10^8 \, ms^{-1}) \qquad \text{.....(2.2)}$$

At the signal frequencies of interest the value of $\mu_r = 1$, as eddy currents induced in the stator core will limit the extent of penetration of the magnetic field into the iron , or in the case of

the model , the copper . This depth is approximately 53 μm at a frequency of 100 kHz for a core constructed of sheet steel , (refer to section 2.2) .

To calculate the propagation velocity therefore , it is necessary to determine the relative permittivity of the coil insulation . The manner in which this is done, is to compare the value of the capacitance of a single coil which is measured , with that calculated from a knowledge of the conductor/dielectric geometry.

First, consider the calculated value of capacitance. It is only practical to calculate the capacitance to earth in the slot region of the coil since the geometry of the electric field around the slot conductors is well defined and uniform and approximates to that of a parallel plate capacitor arrangement. Consider the cross section of the slot as shown in figure 2.3.1.1. The total capacitance of the two slot portions of a single coil is given by the expression.

$$C = \frac{2.(2.\epsilon_0.\epsilon_r(k_s w)}{b_i} + \frac{7.\epsilon_0.\epsilon_r(2k_s a))}{b_i} \qquad \ldots\ldots(2.3)$$

The first term in the equation is the contribution to the capacitance of the electric field between top and bottom conductor/slot wall surfaces whilst the second term represents the contribution to the capacitance of each of the conductors to the adjacent slot wall.

The above expression is an approximation and assumes that the insulation extends from the conductor to the slot wall ; the electric field terminates at the outer surface of the insulation at the top of the slot and that electric field fringing effects are negligible. From the coil manufacturers specification and measurements the slot bar parameters are as follows :-

a	-	conductor height	=	$4.075.10^{-3}$ m
b	-	interturn insulation thickness	=	$0.6096.10^{-3}$ m
b_i	-	main insulation thickness	=	$2.1532.10^{-3}$ m
w	-	conductor width	=	$8.8916.10^{-3}$ m
k_s	-	slot length	=	0.270 m

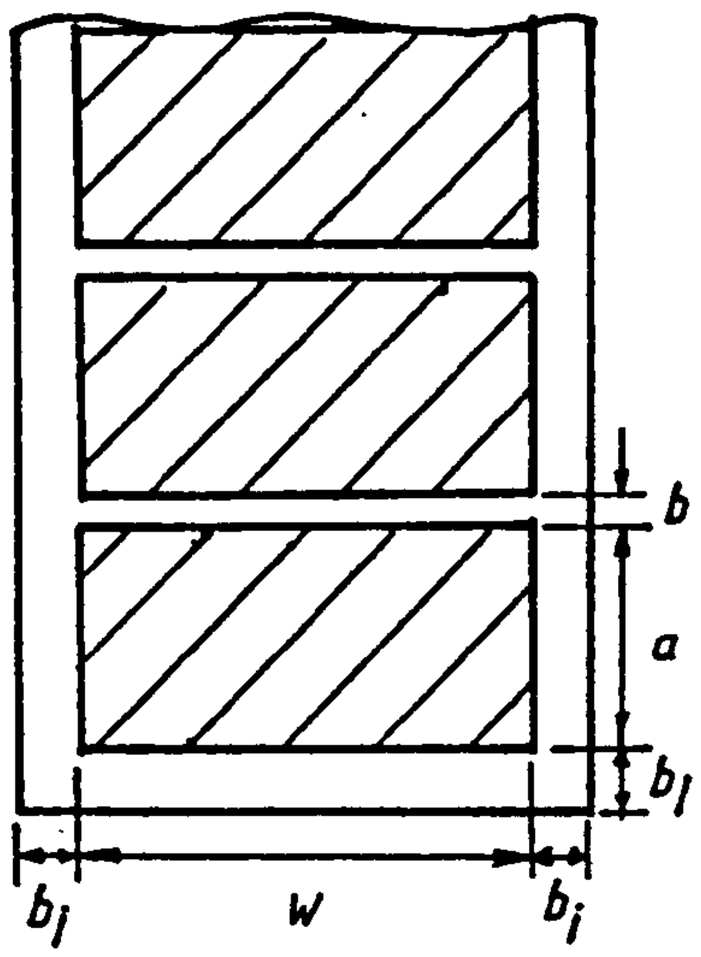

a - conductor height

b - interturn insulation thickness

b_i - main insulation thickness

w - conductor width

k_s - slot length

Figure 2.3.1.1 - Stator Coil Slot Dimensions

The capacitance of the slot portion of a single coil from calculation based on these parameters is $(180).\epsilon_r$ pFarads . However, from measurement of the total coil capacitance using an a.c. bridge at a frequency of 10kHz the capacitance is 1244pF . Of course , some of this value must be attributed to the capacitance of the endwindings to earth which is estimated at 50pF , (a value taken from the measured capacitance between adjacent coils), so that the measured slot capacitance is taken to be 1194pF . It follows therefore, that the relative permittivity of the dielectric is obtained by equating the measured and calculated values of slot capacitance hence :

$$(180).\epsilon_r = 1194$$

$$\therefore \quad \epsilon_r = \frac{1194}{180} = 6.6$$

Based on the dielectric permittivity of 6.6, the calculated wave velocity in the slot is given by

$$v = \frac{c}{\sqrt{\epsilon_r}} = \frac{3.10^8}{\sqrt{6.6}} = 116.7 \text{ m/}\mu\text{sec}$$

In the endwinding region , the conductor is surrounded by the main insulation and an air space so that the effective relative permittivity in this region is between unity , for air , and 6.6 for the insulation . The velocity of propagation is therefore expected to be higher in the endwinding region as a result . The effective transit time through the coil and apparent wave velocity may be calculated assuming an air dielectric in the overhang .

The transit time through a coil with a total conductor length of d_e in the endwinding and a total conductor length of d_s in the slot is given by the expression ,

$$Tc = \frac{1}{(c/\sqrt{\epsilon_r})}.ds + \frac{1}{c}.de$$

For the coil d_e = 8.17 m and d_s = 3.78 m , therefore the transit time through the coil is 59.6 nsec . The apparent wave velocity in the coil as a whole is therefore 200 m/μsec . This value may be calculated from the expression for the apparent wave velocity which is :

$$v = c.\frac{(1 + d_e/d_s)}{(\sqrt{\epsilon_r} + d_e/d_s)}$$

The measured wave velocity as determined previously is 132.9 m/μsec, which is considerably lower than expected . Velocity in the endwinding conductors must therefore be closer to the velocity of propagation in the slot such that the effective dielectric permittivity in the endwinding region is similar to the slot region value .

In a recent study , [23] , a single stator coil is modelled as a multi-conductor transmission line system, with junctions at the interface between the slot and overhang regions . In the analysis a single velocity of propagation is assumed , that is a velocity based on the relative permittivity of the coil insulation . Predicted waveforms correlate closely with those measured and therefore indicate that the wave velocity in the coil overhang is much lower than would be expected and indeed approaching the velocity in the slot .

An experiment performed which supports this , entailed extending the earth plane of the core over the endwinding conductors by wrapping the coil endwinding in an aluminium foil which is in contact with the core . This effectively makes the dielectric permittivity constant along the entire coil length such that , assuming a relative permittivity of 6.6 , the expected transit time through the coil is 102 nsec .

A rectangular fast risetime pulse was input at one end of the coil and observed at the other terminal as before . Figure 2.3.1.2 shows the output waveform obtained for the extended earth coil , along with the waveform obtained from a normal coil .

It can be seen from a comparison of the two , that there is little measureable difference in the waveforms . The pulse transit time through the coil with the extended earth is 105 nsec., which corresponds to a wave velocity of 113.8 m/μsec . This compares well with the calculated value of 102 nsec . However, the difference between the transit time through the normal and the extended earth coil is only 15 nsec . If this difference were due to the increase in speed of propagation in air in the endwinding region then it would be approximately 42.4 nsec . This is the difference between the transit

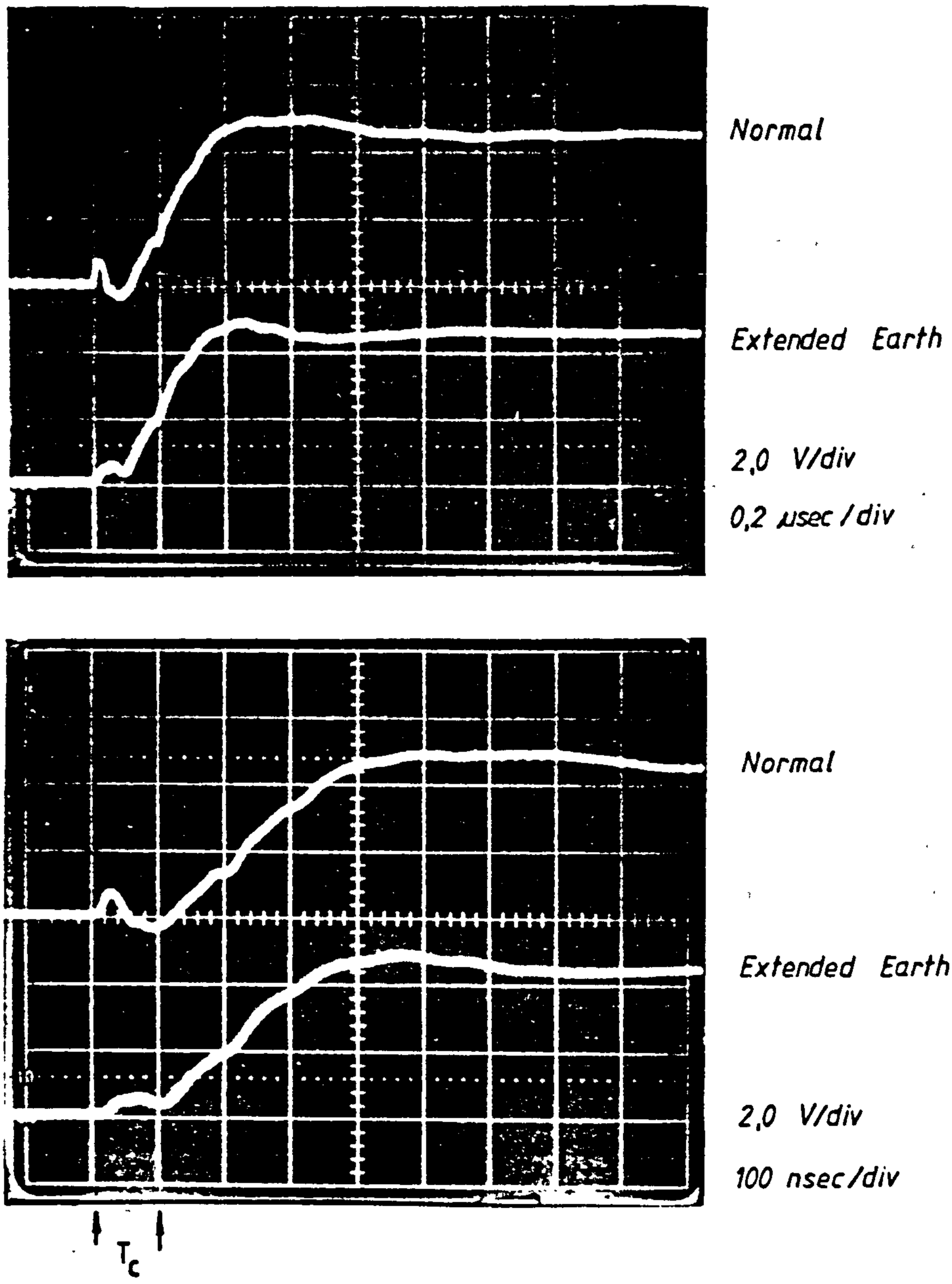

Figure 2.3.1.2 - Response of Single Coil To a Steep-Fronted Pulse (With and Without Extended Earth)

time through the coil with the extended earth , 102 nsec. , and the transit time through a coil with an endwinding having a relative permittivity equal to that of air , (59.6 nsec) . Since this is not the case , the speed of propagation in the endwinding must be significantly less than the velocity through a conductor situated in air . This confirms that electromagnetic waves travel at a speed approaching the speed of propagation in the slot region of a stator coil .

2.3.2 Frequency Response of a Single Stator Coil

The waveform observed at the output of a single coil in response to the injection of a fast rise time rectangular pulse shows a significant increase in the wavefront duration from 10 nsec to around 200 nsec . This is characteristic of a low pass filter circuit in which signals above a certain passband of frequencies are attenuated progressively as the signal frequency increases . To confirm that this is the case, the frequency response of the coil was obtained by measuring the ratio of the output signal amplitude to the amplitude of a sinusoidal input signal over a frequency range from 100 kHz to 30 MHz . The test circuit arrangement is identical to the circuit in figure 2.3.1 with the exception that a sinusoidal signal generator is used as the source .

The normalised frequency response characteristic in figure 2.3.2.1 shows that the coil does indeed behave like a low pass filter circuit. Signals in the frequency range below 1.2 MHz pass through the coil virtually unattenuated . However , as the frequency is increased above 1.2 MHz the signal is attenuated , which is observed as a fall off in the gain as the frequency increased . The gain in the response of the stator coil continues to decrease over a 2MHz frequency band until at a frequency of 3 MHz the signal is attenuated to approximately 15 % of the input amplitude .

The cut off frequency of the stator coil is defined as the frequency at which the gain is 0.707 times ,(-3 dB below), the low frequency gain . From figure 2.3.2.1 the cut off frequency is 1.45 MHz and defines the signal bandwidth of the stator coil .

As the frequency is increased further a number of resonances occur at frequencies of 7 MHz, 10 MHz and 24 MHz . These resonant frequencies

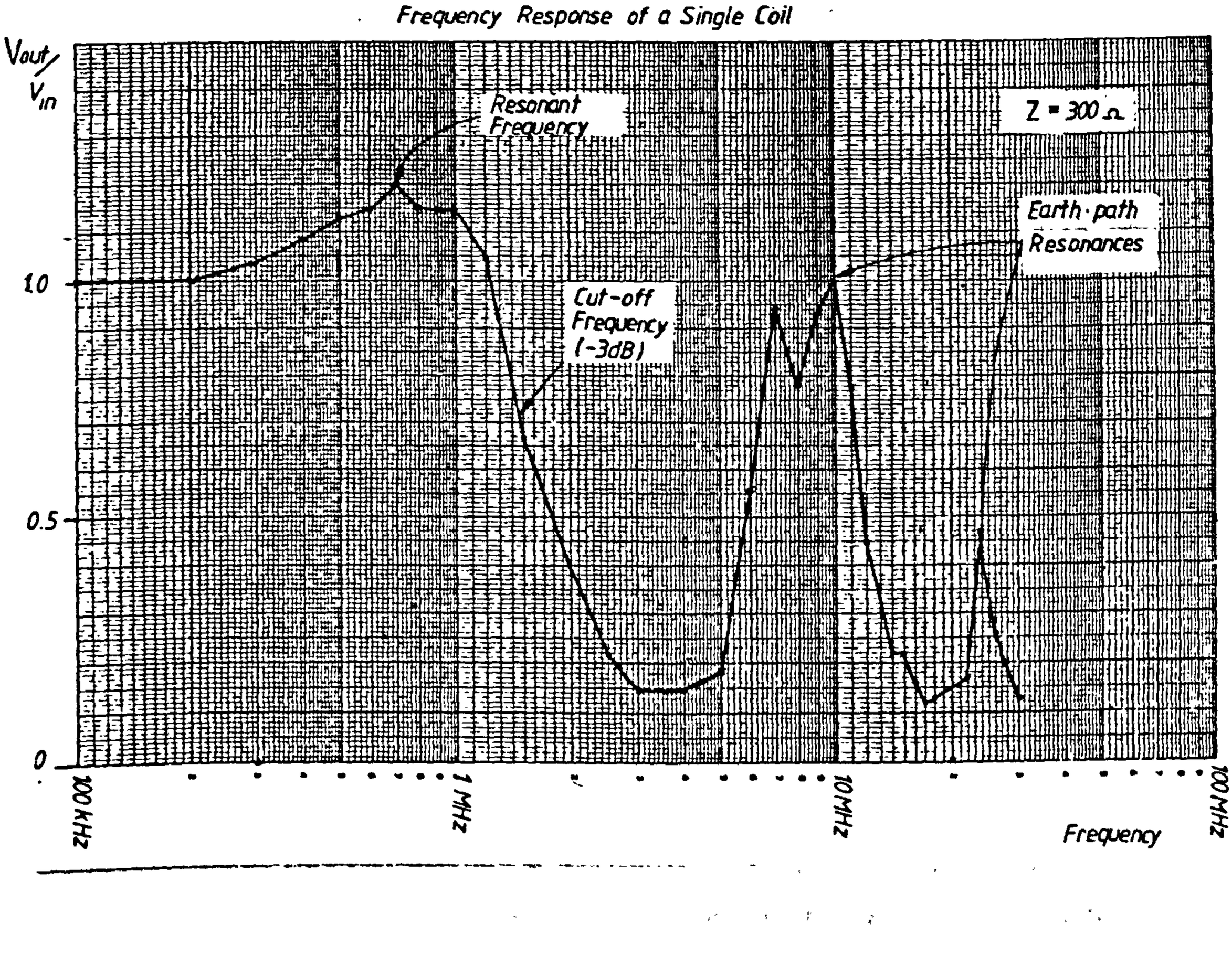

Figure 2.3.2.1 - Frequency Response of a Single Stator Coil

are manifested in the observed coil output waveform as high frequency oscillations . The resonant oscillations, however , are not coil resonances but are associated with the earth circuit since these remain on the output waveform even when the coil terminals are connected together to prevent propagation through the coil .

It is also observed that the frequency response peaks at a frequency of 700 kHz which corresponds the resonant frequency of the coil . The frequency response characteristic can be explained with reference to the very simplified equivalent circuit for a single stator coil which is shown in figure 2.3.2.2 , in which L is the series coil inductance and C is the capacitance to ground in the slot portion of the coil . The resistance R is the termination resistance which is 300 ohms .

The circuit has a tranfer function given by equation (2.4) below ,

$$\frac{V_0(s)}{V_i(s)} = \frac{1/LC}{s^2 + (1/CR)s + 1/LC} \qquad \ldots.(2.4)$$

which can be expressed by the characteristic equation for a second order system ,

$$\frac{V_0(s)}{V_i(s)} = \frac{\omega^2}{s^2 + 2\zeta\omega s + \omega^2} \qquad \ldots.(2.5)$$

where $\omega = 1/\sqrt{(LC)}$ and $\zeta = (LC)/2R$.

ω is the natural frequency of the circuit and ζ is the damping factor .

The frequency response of the simplified equivalent circuit for a second order system is very similar to the measured response in that it has a low pass characteristic with a resonant peak close the upper frequency limit . The resonant frequency can be calculated from the equation for ω . L is the coil self inductance and has a measured value of 49 μH and C is the slot capacitance which is 1194 pF . The resonant frequency of the coil is therefore given by ,

$$f = \frac{\omega}{2\pi}$$

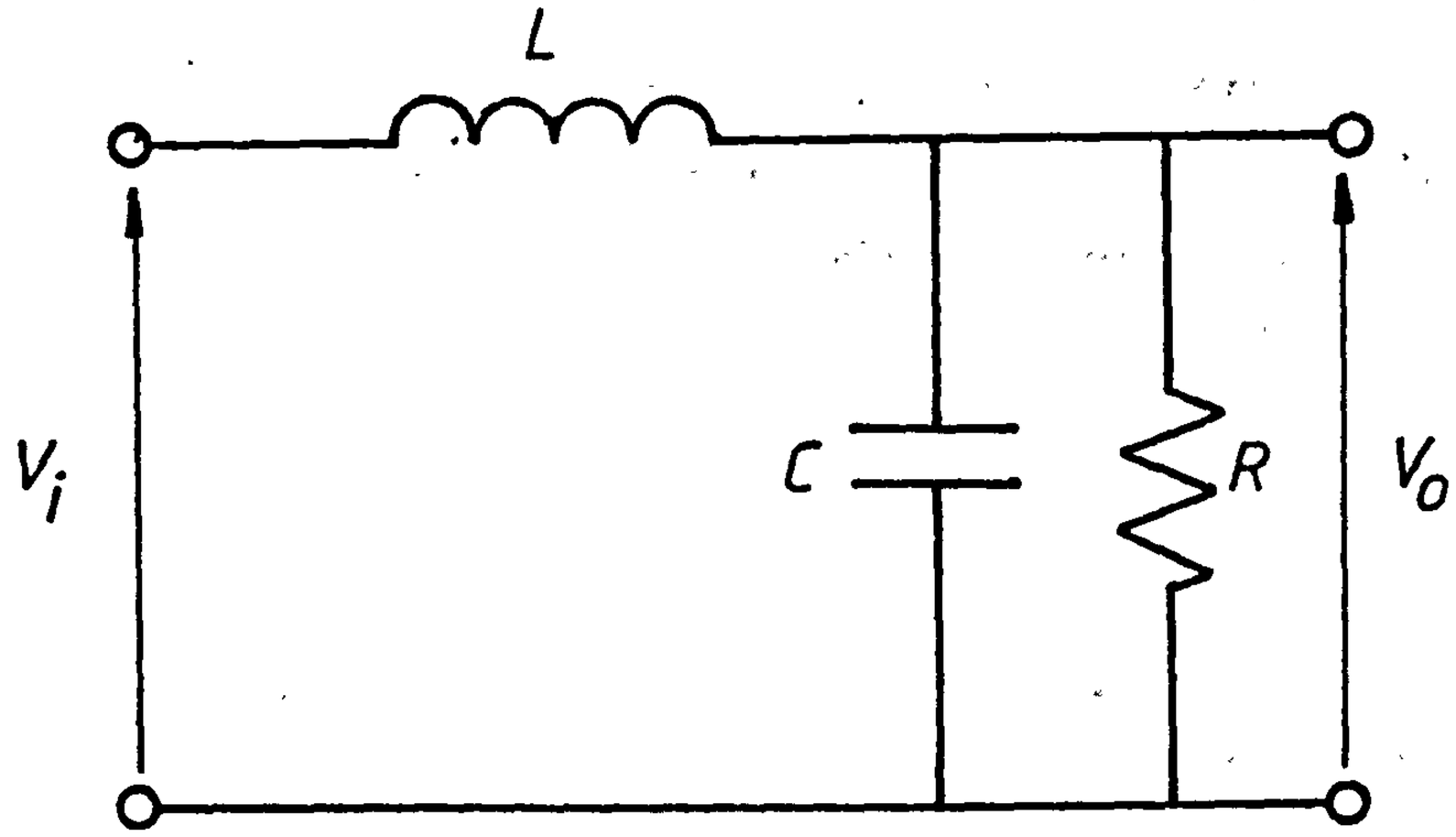

L – Coil Self Inductance

C – Coil Slot Capacitance

R – Terminal Resistance

Figure 2.3.2.2 – Simplified Equivalent Circuit for Single Stator Coil

which , for the values of L and C , is approximately 658 kHz .

This compares well with the frequency of 700 kHz obtained from the frequency response characteristic and shows this resonant frequency is due to the interaction of the coil self inductance , L, and the coil capacitance to earth in the slot , C .

The presence of a resonant condition in the frequency response is indicative of a system with little damping . In the equivalent circuit for the stator coil the level of damping is controlled principally by the circuit terminal resistance R , which is expressed in the term for the damping factor , ζ . Thus reducing the circuit resistance R causes the damping factor and hence system damping to increase . This is shown in the frequency response characteristic in figure 2.3.2.3 in which the terminal resistance is 20 ohms . There is no indication of resonance in the response due to the increased damping in the circuit .

The degree of damping in the circuit affects the pulse rise time ; by increasing the damping the rise time is increased . In the case when a resonant oscillation occurs on the pulse response waveform the rise time is difficult to measure , however the time to the peak of the oscillation is approximately one quarter cycle of the natural frequency which is given by the equation ,

$$T = \frac{1}{4\omega}$$

For a natural frequency of 700 kHz , the rise time to the first peak is 350 nsec, which correlates with the value of 360 nsec observed on the waveform in figure 2.3.1.2 .

It is shown in this section that a single stator coil behaves like a low pass filter such that signals are subject to frequency dependent attenuation due to the self inductance and the slot capacitance of the coil . However , this does not take into account the effect of interturn mutual inductance and interturn capacitance in determining the response of a stator coil .

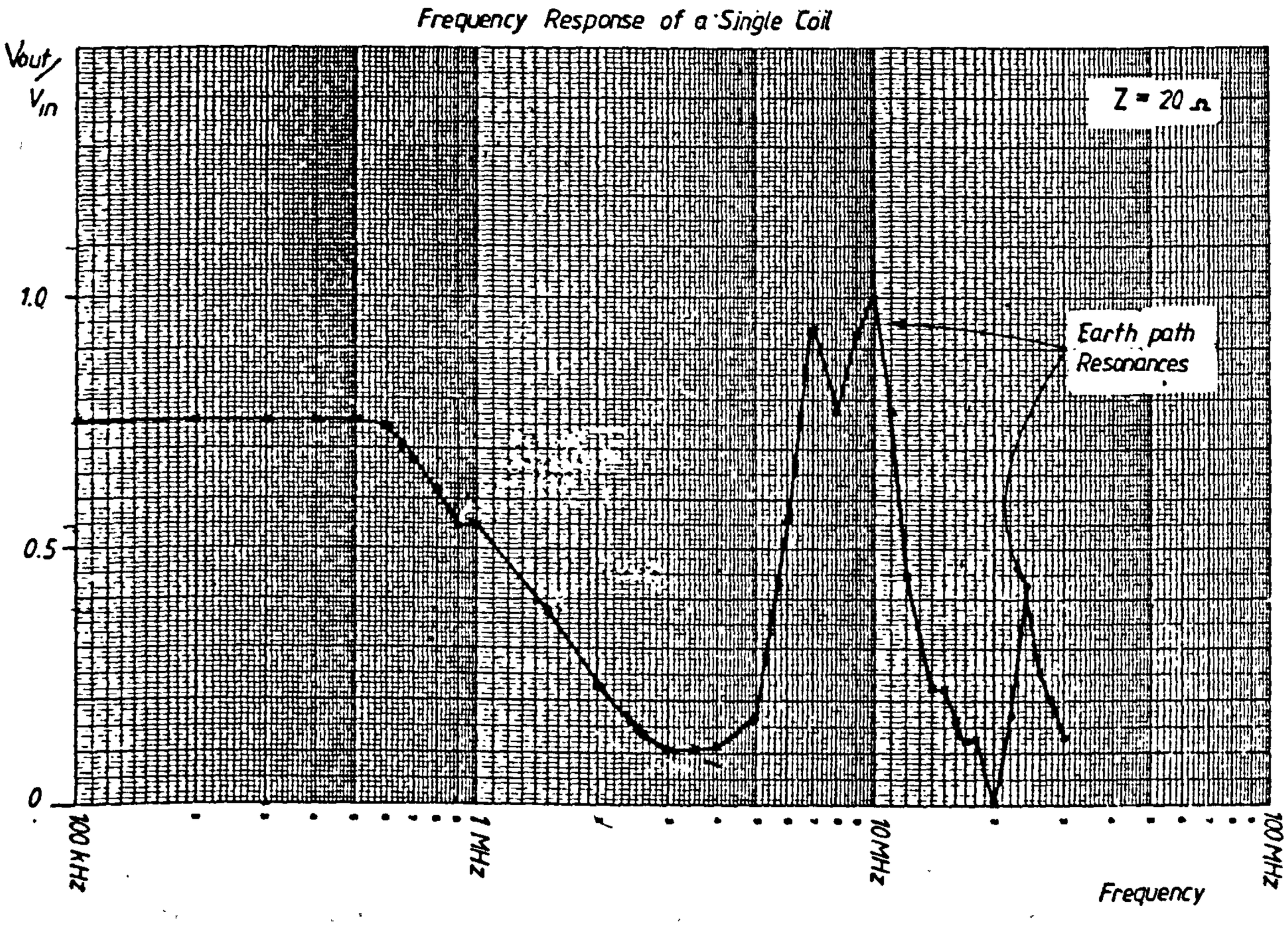

Figure 2.3.2.3 - Frequency Response of Single Coil Terminated in a 20 ohm Impedance

In the study of steep fronted wave propagation in the line end coil of a machine by Wright et al , [23] , two modes of wave propagation are identified within a single stator coil . Waves travel along the coil conductor as in a transmission line in the first mode of propagation . In the second mode , the interturn capacitance and mutual inductance are responsible for the coupling of signals between adjacent turns of the coil . This coupling between turns is stronger at higher frequencies since the reactance of the interturn capacitance and mutual inductance is small . For example, the capacitance between two adjacent turns in the stator coil is given by the expression ,

$$C = \frac{\epsilon_0 . \epsilon_r w . l}{b_i} \qquad \ldots.(2.6)$$

where l is the length of a turn conductor . The turn capacitance is 1.45 nF based on the coil dimensions in figure 2.3.1.1 .
At a frequency of 1.57 MHz the impedance between two adjacent turns due to interturn capacitance becomes comparable with the impedance of the turn self inductance ,(7 μH) .

2.4 Propagation of Steep-Fronted Pulses in a Phase Winding

In the same manner as for a single stator coil , the transmission characteristics of a complete phase winding may be obtained from the response of the winding to a fast rise time rectangular pulse . Pulses derived from a pulse generator were injected at the source end of the phase winding and observed at the inter-coil connections along the winding on a 60 MHz bandwidth oscilloscope , see figure 2.4.1. Both ends of the winding were initially terminated in a resistance of 300 ohms . This value of resistance was selected to be representative of the characteristic impedance of the winding so that reflections at the terminals of the winding were eliminated . The pulses injected in this first experiment had a duration of 100 μsec and a rise time of 10 nsec. , so that the winding was subjected to signal frequencies in the range 10 kHz up to 100 MHz . Figure 2.4.2 shows the waveforms observed at the coil interconnections when a fast-fronted pulse was injected at the source end of the winding .

A general observation which can be made from the waveforms in figure 2.4.2 , is that the main pulse propagates along the winding with finite velocity as in a simple transmission line . As the pulse

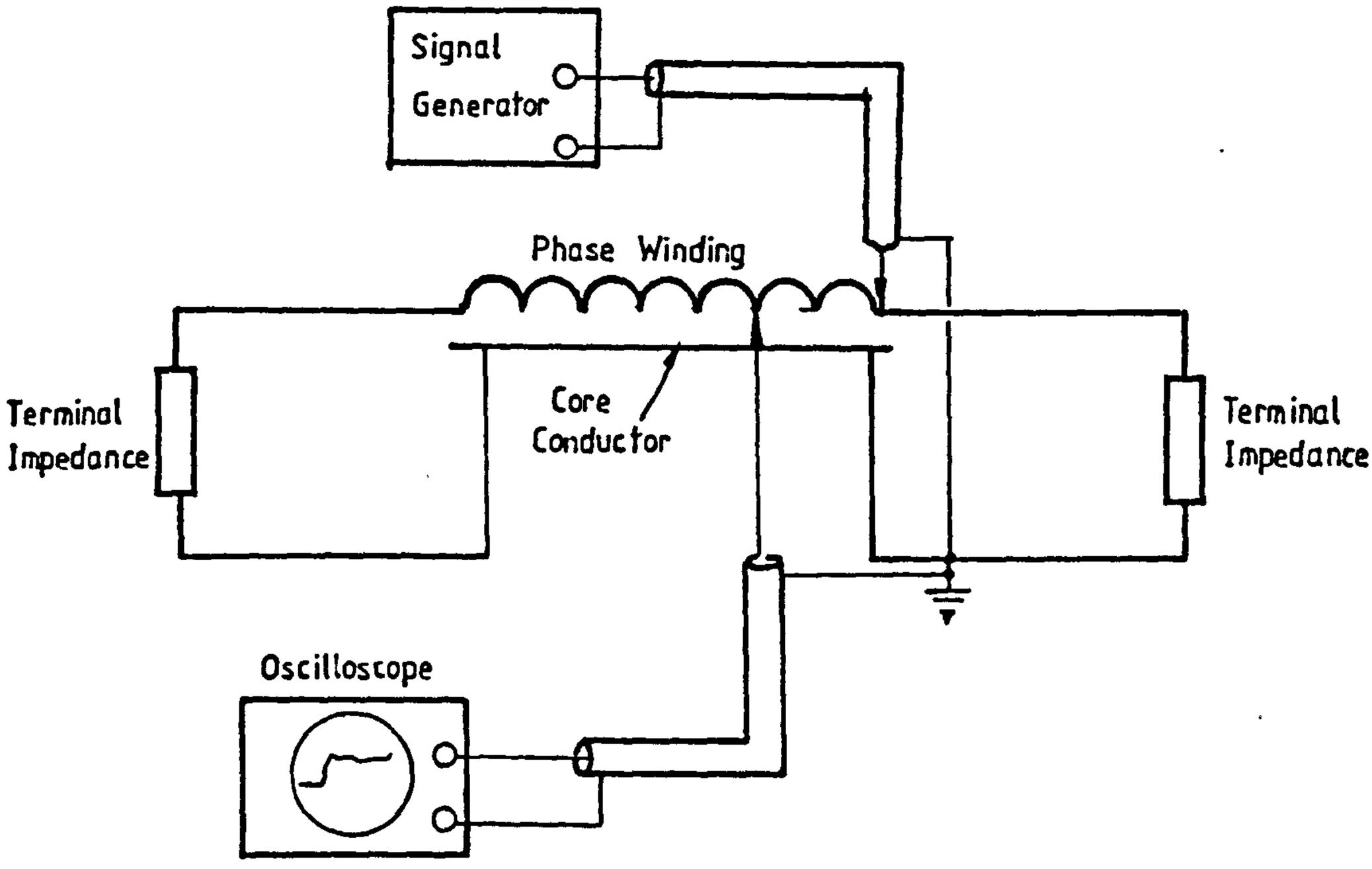

Figure 2.4.1 - Phase Winding Test Circuit

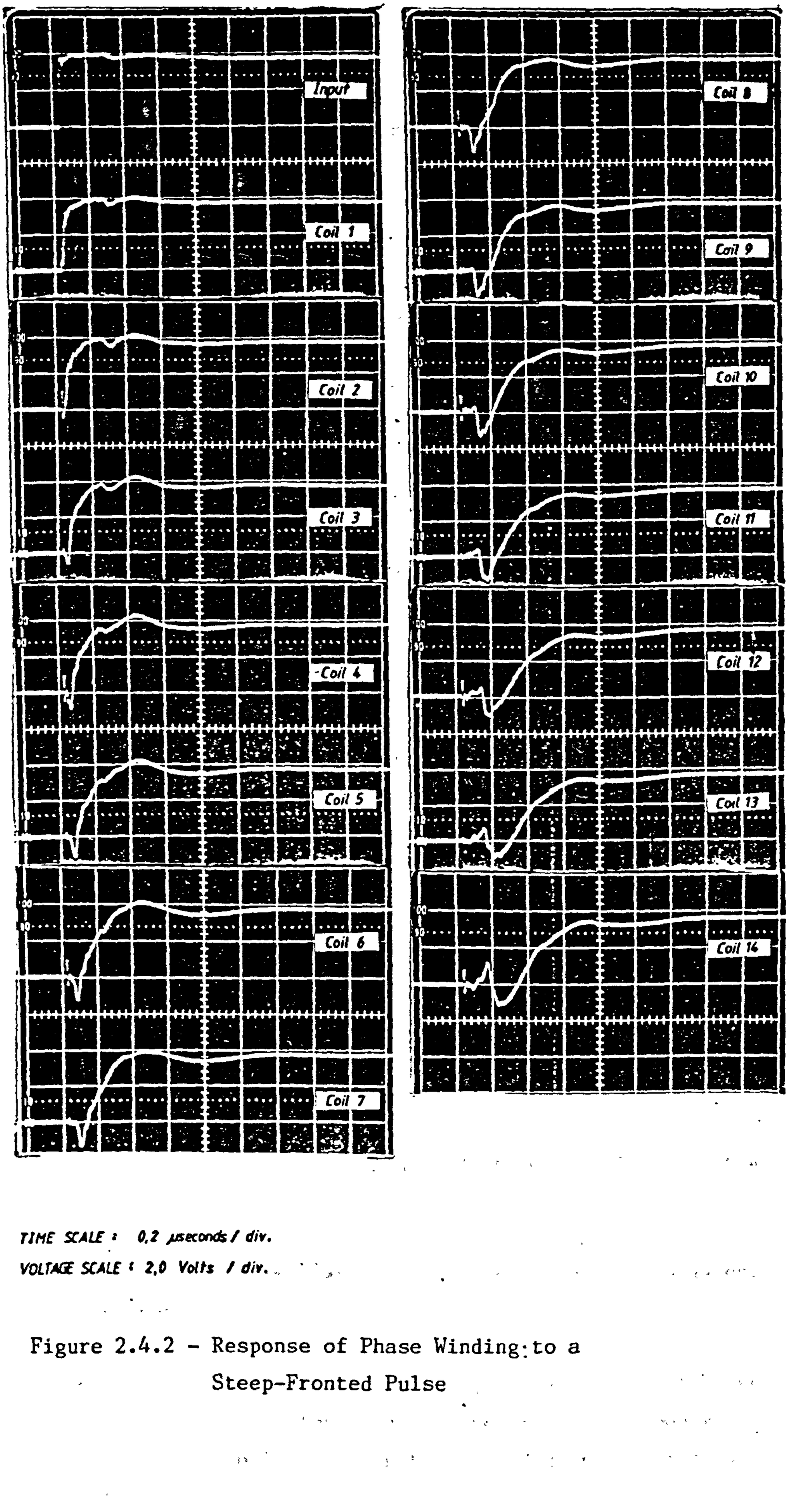

TIME SCALE : 0,2 μseconds / div.

VOLTAGE SCALE : 2,0 Volts / div.

Figure 2.4.2 - Response of Phase Winding to a Steep-Fronted Pulse

propagates through the winding structure the wavefront grows less steep and increases in duration . This is a result of the cumulative effect of a number of stator coils connected in series , each of which acts like a low pass filter to the spectrum of signals contained in the pulse .

In addition to the main pulse wavefront , the waveforms in figure 2.4.2 show that another pulse of opposite polarity precedes the main wavefront as it passes through the winding . This negative polarity pulse begins to develop after the main pulse wavefront has travelled through the first three coils in the winding . It is seen to have a much steeper wavefront than the main pulse and this short rise time is virtually constant as the negative wavefront travels through the winding . This behaviour indicates that the negative pulse contains relatively high frequency components which propagate through the winding with a higher velocity than the main pulse .

Considering the forementioned transmission characteristics of the negative pulse , it can be deduced that a second mode of wave propagation must take place in the stator winding . Further investigation shows that higher frequency signals travel through the endwindings of the stator coils by electromagnetic coupling between adjacent coil endwindings . This is discussed in greater depth in section 2.5 of this chapter .

Three separate modes of wave propagation are therefore identified and are as follows :-

i. Simple transmission line propagation in which waves travel in the TEM (Transverse Electromagnetic) mode .

ii. Interturn mutual capacitive and inductive coupling within a single stator coil .

iii. Intercoil electromagnetic coupling through adjacent endwindings .

Consider first of all the main transmission line mode of wave propagation . The basic parameters that define propagation behaviour in this mode are wave velocity and attenuation over the frequency range of interest .

Velocity of propagation based on time interval measurements taken from the waveforms in figure 2.4.2 , is very difficult to estimate since the pulse is considerably distorted as it penetrates the winding, by secondary modes of wave propagation and by the dispersion in the wave velocity that occurs with frequency . If the transit time through a coil or number of coils is defined by the time interval between the moment the pulse wavefront enters the winding to the point on the wave at which the main wavefront begins to rise , the velocity of propagation can be estimated over the winding length . Based in this definition of transit time the velocity of propagation is calculated at every second coil along the winding and is shown in figure 2.4.3 .

Coil No.	Transit time (μsec.)	Velocity (m/μsec.)
2	200	119.5
4	400	119.5
6	610	117.5
8	890	107.4
10	1100	108.6
12	1500	95.6
14	1800	92.9

Figure 2.4.3 - Estimated Wave Velocities through a Phase Winding

The estimated velocities in figure 2.4.3 indicate that the wave velocity is reduced with increasing depth of travel into the winding . Since the higher frequency signal components of the pulse are attenuated through each coil in the winding , it is the low frequency components that pass through the winding with little attenuation along the conduction path . It is these lower frequency components that form the main pulse , and predominate increasingly as the wave travels deeper into the winding . This would suggest that low frequency signals travel at a lower velocity since there is a reduction in the wave velocity with greater depth of penetration into the winding .

Measurement of the wave velocity of sinusoidal signals over the frequency range 10 kHz to 3.4 MHz is shown in figure 2.4.4 and confirms this to be the case . Propagation velocity is measured by

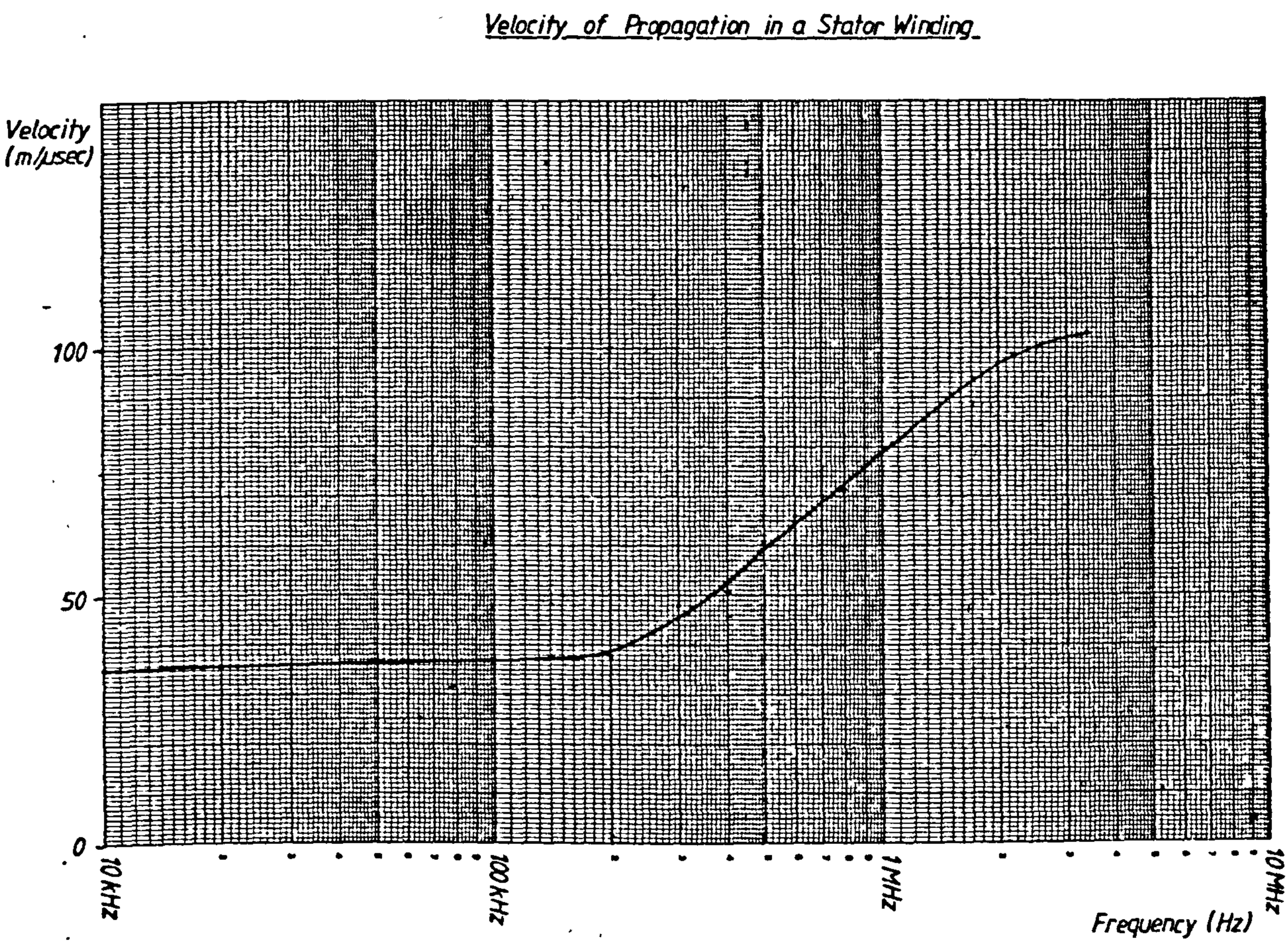

Figure 2.4.4 - Velocity of Propagation in a Phase Winding

recording the transit time of a sinusoidal signal , derived from a sinewave generator , through the phase winding at certain frequencies. Progression of the sine wave can be observed at each of the coil interconnections along the winding .

At frequencies below 200 kHz signals travel at a speed of approximately 38 m/μsec . As the frequency is increased , the velocity rises almost linearly up to a frequency of 2 MHz . Thereafter the characteristic shows the wave velocity increases less rapidly and reaches a ceiling value of 103 m/μsec at a frequency of 3.4 MHz . Above this frequency , signals undergo considerable attenuation such that no useful measurement of wave velocity can be made since the upper limit of signal propagation is reached .

The velocity of propagation at the upper frequency limit approaches a velocity of 116 m/μsec which corresponds to propagation in a conductor having an insulation with a relative permittivity of 6.6 , that of the winding insulation .

At much lower frequencies , below 200 kHz , the velocity of propagation (38 m/μsec) is much lower and represents a velocity of travel determined by the lumped effect of the winding self inductance and the slot capacitance to earth . This is in the region of values quoted in studies of surge propagation in machine windings , [21,22] , and may be calculated using the equation developed by R.Rudenberg [82] which is ,

$$v = \frac{n.(k + s)}{LC} \qquad \ldots.(2.7)$$

where, n - number of turns per coil.
k - length of slot conductor (m) .
s - length of one endwinding section (m).
L - self inductance of one endwinding section (μH).
C - capacitance to earth of a single slot section (pF).

For a single coil the total measured self inductance is 49 μH and the total measured capacitance to earth in the slot is 1194 pF, which result in values of 24.5 μH and 597 pF respectively for L and C . The parameters k and s have lengths of 0.27 m and 0.583 m respectively . This gives a calculated wave velocity of 49.4 m/μsec , which is in the

region of the measured value of 38 m/μsec .

It can be seen therefore , at low frequencies the velocity of propagation is determined by the lumped effect of endwinding inductance and slot capacitance , and is similar to propagation in an artificial transmission line constructed from discrete elements of series inductance and shunt capacitance . The variation in wave velocity over the frequency range of 100 kHz to 3.4 MHz is therefore seen as a transition in the mode of wave propagation . At low frequencies , the endwinding inductance and slot capacitance behave like lumped elements in a transmission line . As frequency is increased , the influence of electromagnetic coupling in the endwindings increases . The winding also behaves more like a distributed structure since the wavelength of higher frequency components becomes comparable to or less than the length of the winding . Thus the gradual increase in the wave velocity indicates the increased influence of the endwinding coupling mode of wave propagation .

2.4.1 Frequency Response of a Motor Phase Winding

A phase winding has a similar response over a wide bandwidth of signal frequencies to a single stator coil, in that it behaves like a low pass filter network .

As before, a sinusoidal wave generator was connected to the source end of the winding and a 300 ohm resistor at the other end as shown in figure 2.4.1 . The frequency response characteristic was obtained by measuring the ratio of the output voltage , Vo , to the input voltage, Vin , over a range of frequencies extending from 10 kHz up to 30 MHz. The frequency response characteristic obtained is shown in figure 2.4.1.1 .

The response clearly indicates an increase in the attenuation of the signal through the winding as the signal frequency is increased until at a frequency of around 3.8 MHz virtually no signal is detected at the winding output . This represents a distinct cut-off frequency . Wave propagation is permitted by the winding structure at frequencies below this cut-off , but no wave penetration takes place in the winding above this frequency . This low pass characteristic is the cumulative effect of the stator coils connected in series , each of

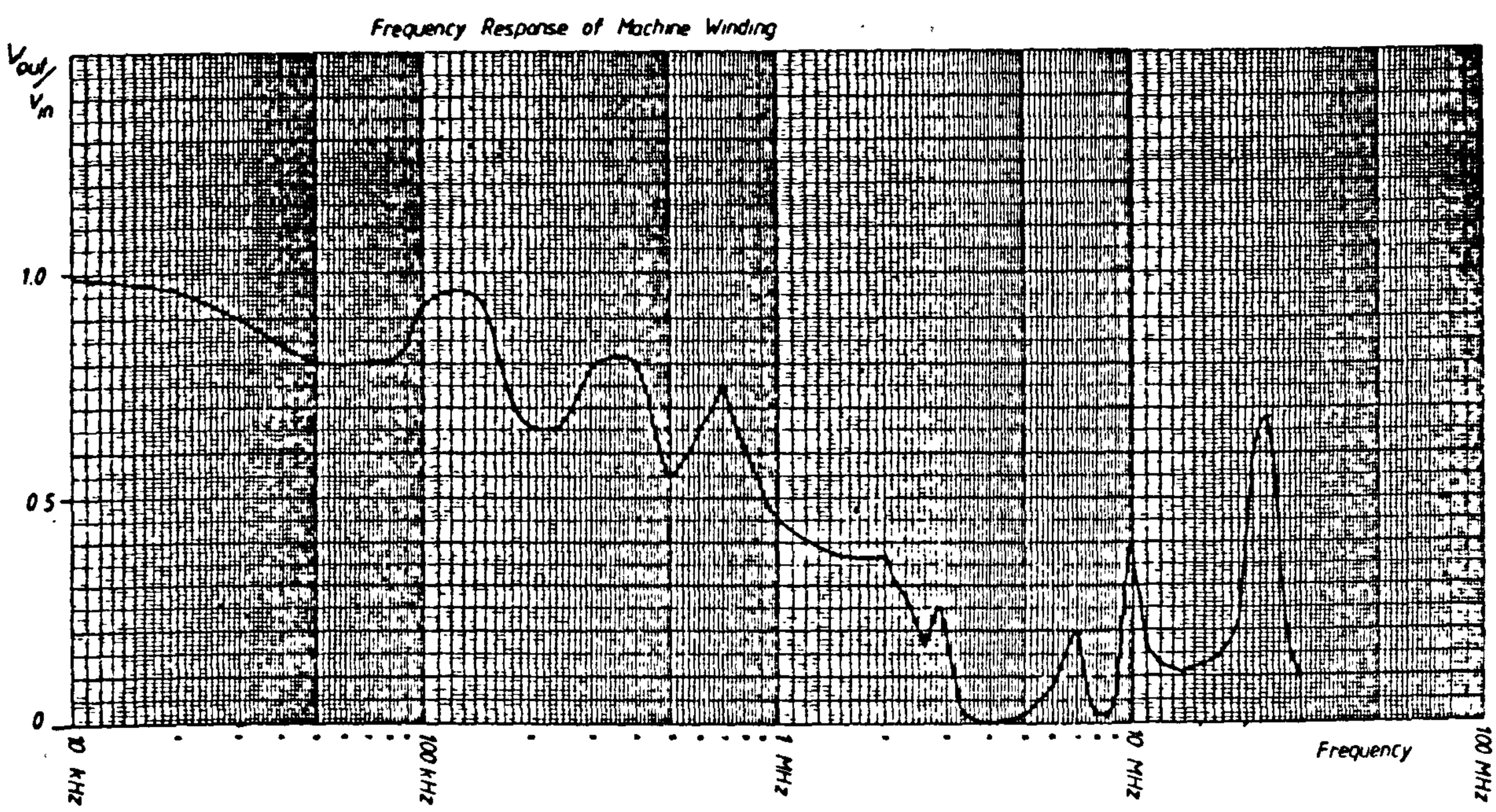

Figure 2.4.1.1 - Frequency Response of a Phase Winding

which behaves like a low pass filter circuit due to the series self inductance and shunt capacitance of a coil . The frequency response of a phase winding is therefore generally similar to the response of a single stator coil .

Superimposed on the frequency response characteristic are three peaks which correspond to winding resonances , and occur at 120 kHz, 350 kHz, and 700 kHz . These are transmission line resonances which occur when the winding is terminated at either end by an impedance that is not equal to the characteristic impedance of the winding . In this case the winding was terminated at both ends in an impedance value lower than the characteristic impedance such that resonant oscillations had half wavelengths that were multiples of the winding length . This is discussed in greater detail in section 2.4.2 .

At frequencies of 7 MHz, 10 MHz and 24 MHz resonance peaks are observed in the response characteristic in figure 2.4.1.1 . Indeed these are signal resonances and appear as high frequency oscillations on the pulse waveforms in figure 2.4.2 at the instant the input pulse is injected into the winding and are observed at each of the winding interconnections . Since these high frequency signals occur instantaneously at each coil connection it must follow that they travel by an alternative path other than along the winding conductor . It is the earth path that supports the propagation of these signals since the signals are affected by any changes in the earth path . These resonant peaks on the frequency response must therefore be ignored in the analysis of the propagation phenomena .

2.4.2 Influence of Winding Termination Impedance

The phase winding has an effective characteristic impedance of around 300 ohms . The value of this characteristic impedance can be calculated approximately from the equation (2.8) , assuming the winding acts as a simple transmission line . Obviously this is an over-simplification and does not take into account the effect of endwinding and interturn coupling within a winding .

$$Z = \sqrt{\frac{L}{C}} \qquad \ldots(2.8)$$

L is the self inductance of the winding per unit length and is calculated as follows :-

$$L = \frac{\text{Total winding inductance}}{\text{Winding length}} = \frac{14.49.10^{-6}}{167.3} = 4.1\ \mu H/m$$

C is the shunt capacitance of the winding per unit length and is obtained as follows :-

$$C = \frac{\text{Total shunt capacitance}}{\text{Winding length}} = \frac{14.1194.10^{-12}}{167.3} = 99.9\ pF/m$$

The characteristic impedance is calculated at 202.6 ohms and is reasonably close to the measured value of around 300 ohms .

When the winding is terminated in a resistance equal to the winding impedance there is minimum reflection of the pulse at the terminals and so little distortion appears on the pulse waveform . If however , the terminating resistance is altered from the characteristic impedance value , reflection of the main pulse occurs at the discontinuity . The magnitude of the reflected wave depends on the ratio of the terminal impedance to the winding impedance . Figure 2.4.2.1 shows the response of the phase winding to a step input pulse when the terminal impedance at one end of the winding is an open-circuit . This represents a terminating condition in which the winding is effectively a free boundary at one end to electromagnetic waves . In this condition the step input wave excites the winding into a state of resonance .

On the waveforms observed there appears to be a number of resonant oscillations superimposed on the response . The main resonant oscillation is seen in the waveform in figure 2.4.2.1 to have a period of oscillation of 18 μsec corresponding to a frequency of 55.5 kHz . The other single frequency oscillations observed occur at higher frequencies than the fundamental . These resonances are clearly shown on the frequency response characteristic in figure 2.4.2.2 in which the winding is terminated in one end in an open-circuit . Four distinct resonance peaks occur at frequencies of 55 kHz, 180 kHz, 290 kHz, and 750 kHz . The amplitude of each resonance decreases with increasing signal frequency . These represent transmission line resonances due to the internal reflection of waves within the winding.

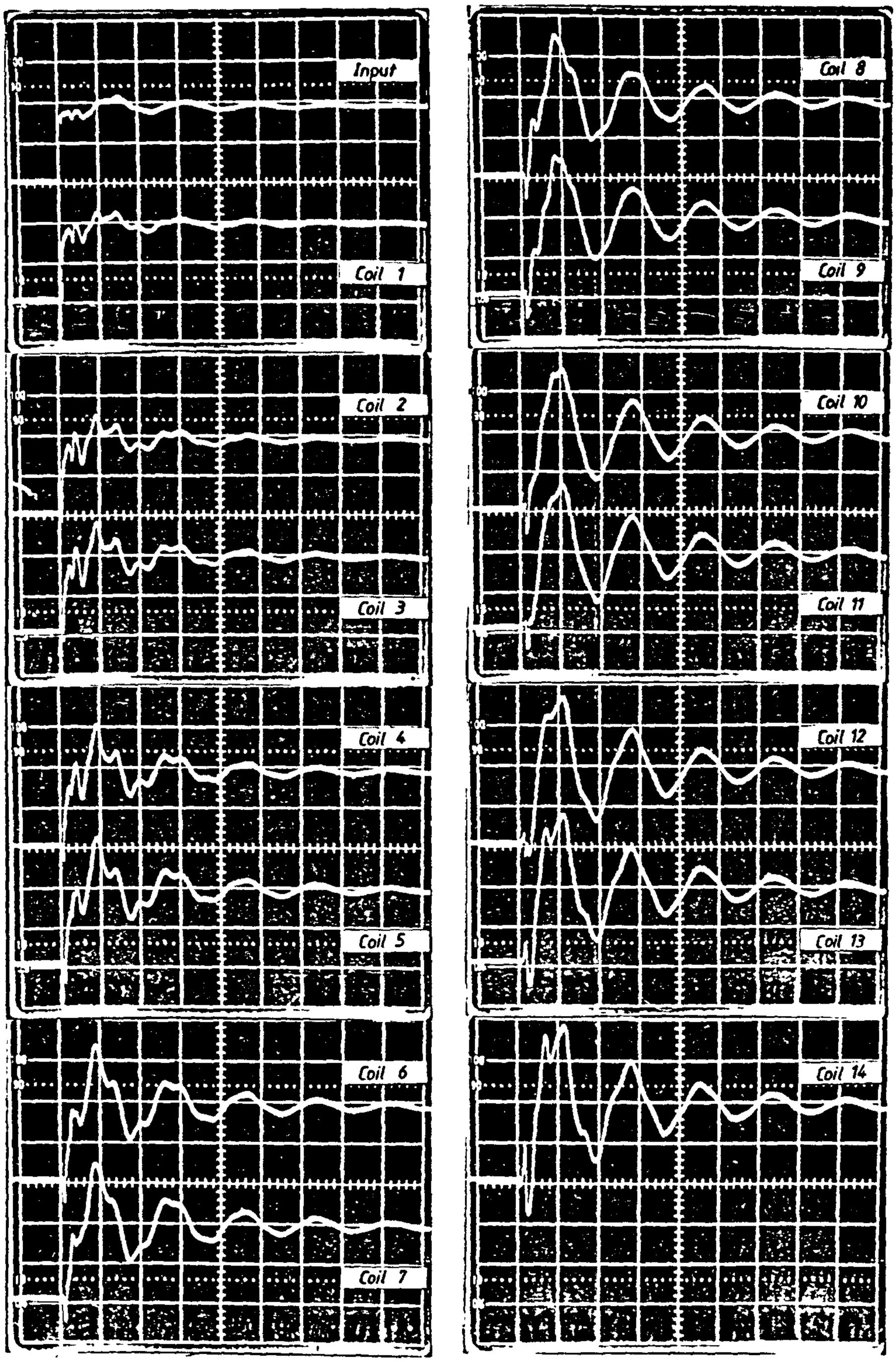

Time Scale : 10µsec / div

Voltage Scale : 0,5 V / div

Figure 2.4.2.1 - Response of Phase Winding to a Steep-Fronted Pulse (One Terminal Open-Circuit)

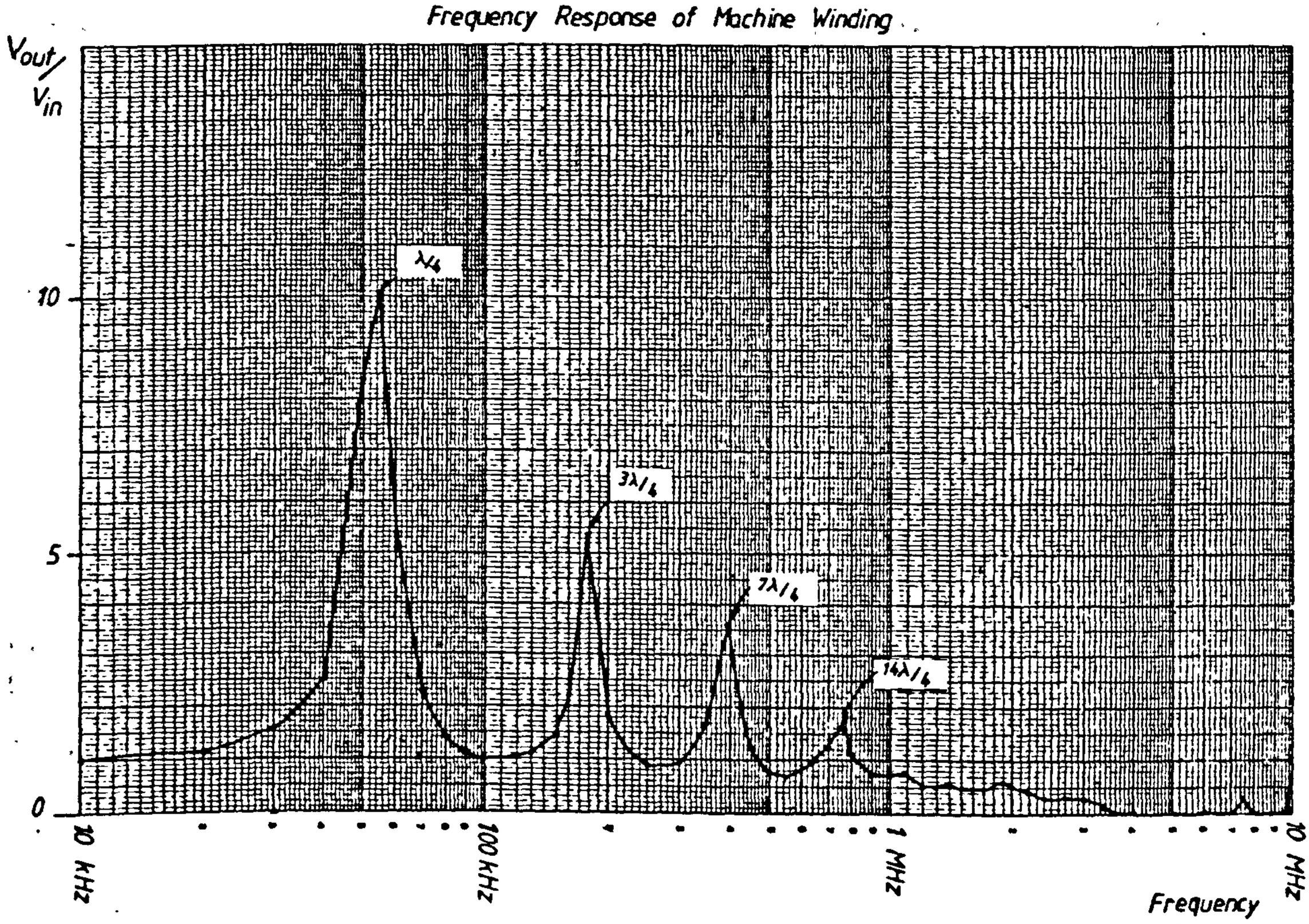

Figure 2.4.2.2 - Frequency Response of Phase Winding with One Terminal Open-Circuited

Since the winding is open-circuited at one end and terminated in a very low impedance at the other by the signal generator source impedance , the winding presents a free boundary at one end and a fixed boundary at the other to electromagnetic waves . Under these terminating constraints the winding will exhibit transmission line resonance at frequencies when the electrical length of the winding is an odd multiple of one quarter wavelength of the signal oscillation .

The first resonance at 55 kHz occurs when the winding length equals one quarter wavelength of the wave oscillation . This can be calculated from the fundamental relationship ; $v = f.\lambda$. The velocity of propagation at lower frequencies has been measured at 38 m/μsec for the fundamental mode of wave propagation and the length of the fourteen coil winding is 167.3 metres . Therefore if one quarter wavelength equals the winding length , then the wavelength of the signal at resonance must be 669.2 metres . The calculated resonant frequency is therefore ,

$$f = \frac{v}{\lambda} = \frac{38.10^6}{669.2} = 56.8 \text{ kHz}$$

If the same calculation is applied to successive odd multiples of one quarter wavelength , it can be shown that the winding resonances observed occur at n = 1,3,7 and 14 quarter wavelengths . The measured and calculated resonant frequencies are given in table 2.4.2.3 .

No. of Quarter Wavelengths (n)	Wavelength (m)	Measured Resonant Frequency (kHz)	Calculated Resonant Frequency (kHz)
1	669.2	55	56.8
3	223.0	176	170.3
7	95.6	395	397.5
14	47.8	765	794.9

Figure 2.4.2.3 - Calculated and Measured Resonant Frequencies in a Phase Winding

The observed winding resonances occur at integral multiples of the number of stator coils with the exception of the one at 3 quarter wavelengths . At a resonant frequency of 765 kHz , one quarter

wavelength is equal to the length of a single stator coil .

Similar behaviour is observed when the stator winding is terminated in both ends by a low impedance compared to the winding impedance . To obtain any voltage measurements the winding is terminated in a resistance of 20 ohms which is considered to represent a short-circuit condition at that termination .

Figure 2.4.2.4 shows the response of the winding when it is subjected to a step input wave . The main wave is distorted by single frequency oscillations superimposed on the wave as it progresses through the winding structure . These oscillations are transmission line resonances caused by internal wave reflections and have a period of oscillation related to the transit time through the winding and hence to the winding length . Also present on the first few waveforms is a decay in the amplitude of the rectangular pulse .

The winding at low frequency behaves fundamentally as a lumped inductance element which in this case is connected to earth at one terminal and in series with a low impedance to the signal source at the other ,(see figure 2.4.2.5). The circuit behaves like a high pass filter since the winding reactance increases with frequency . This explains the decay in the waveform . The time constant of this decay is determined by the ratio of the winding inductance to the circuit resistance .

The transmission line resonances are obtained from the measurement of the frequency response characteristic for the winding which is seen in figure 2.4.2.6 . A number of winding resonances occur over the frequency range 10 kHz to the upper frequency limit of wave propagation , 3.4 MHz . These winding resonant oscillations have half wavelengths that are multiples of the winding length since the winding terminations represent fixed boundaries to electromagnetic waves . Only half wavelengths are possible therefore .

The first resonance is at a frequency of 115 kHz and corresponds to an oscillation which has a half wavelength that is equal to the winding length . To confirm this , the resonant frequency is calculated as before, using the expression ; $v = f.\lambda$ and a measured wave velocity of 38 m/μsec . The half wavelength is 167.3 metres and therefore the wavelength is 334.6 metres . This gives a calculated resonant

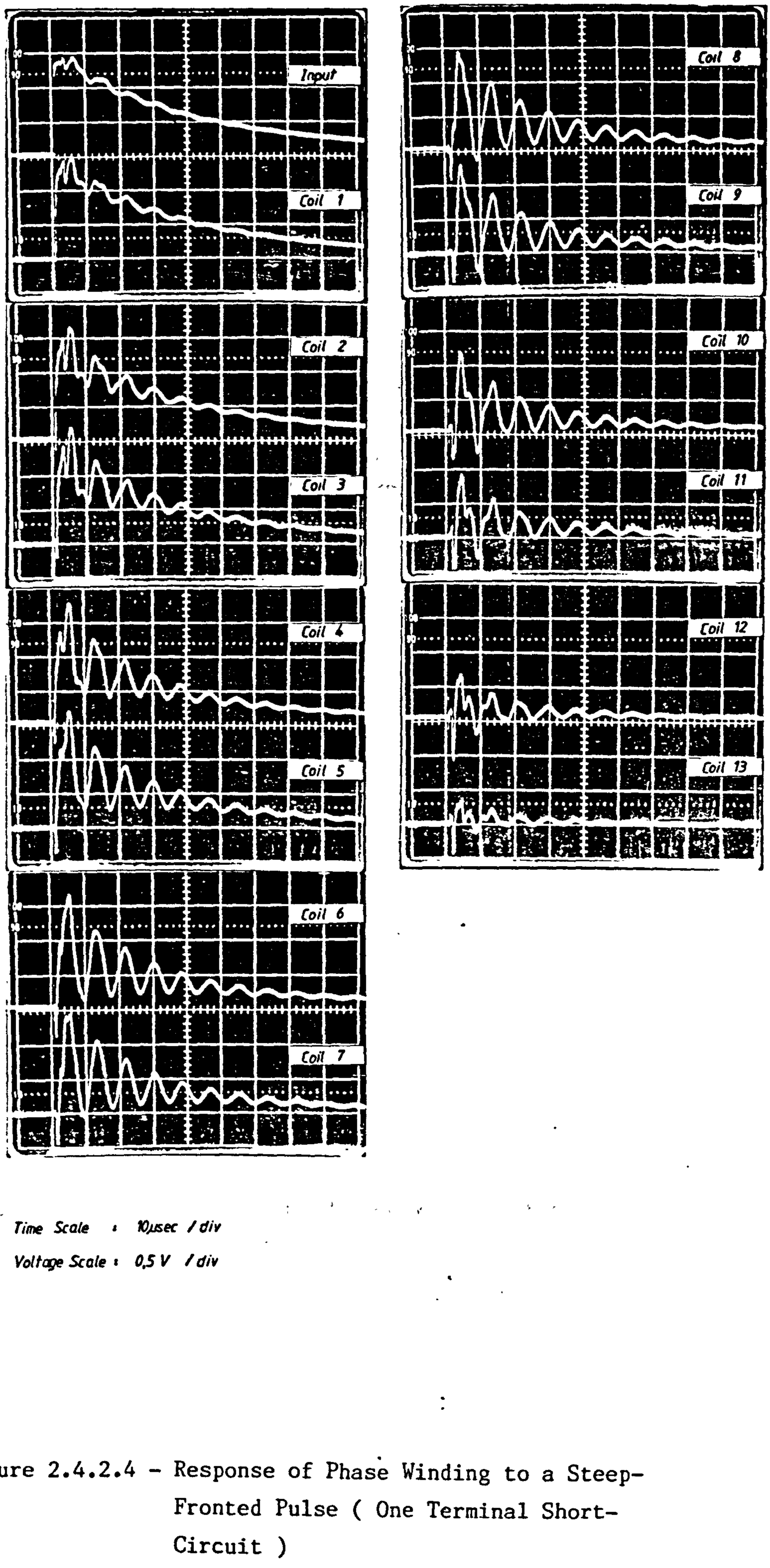

Figure 2.4.2.4 - Response of Phase Winding to a Steep-Fronted Pulse (One Terminal Short-Circuit)

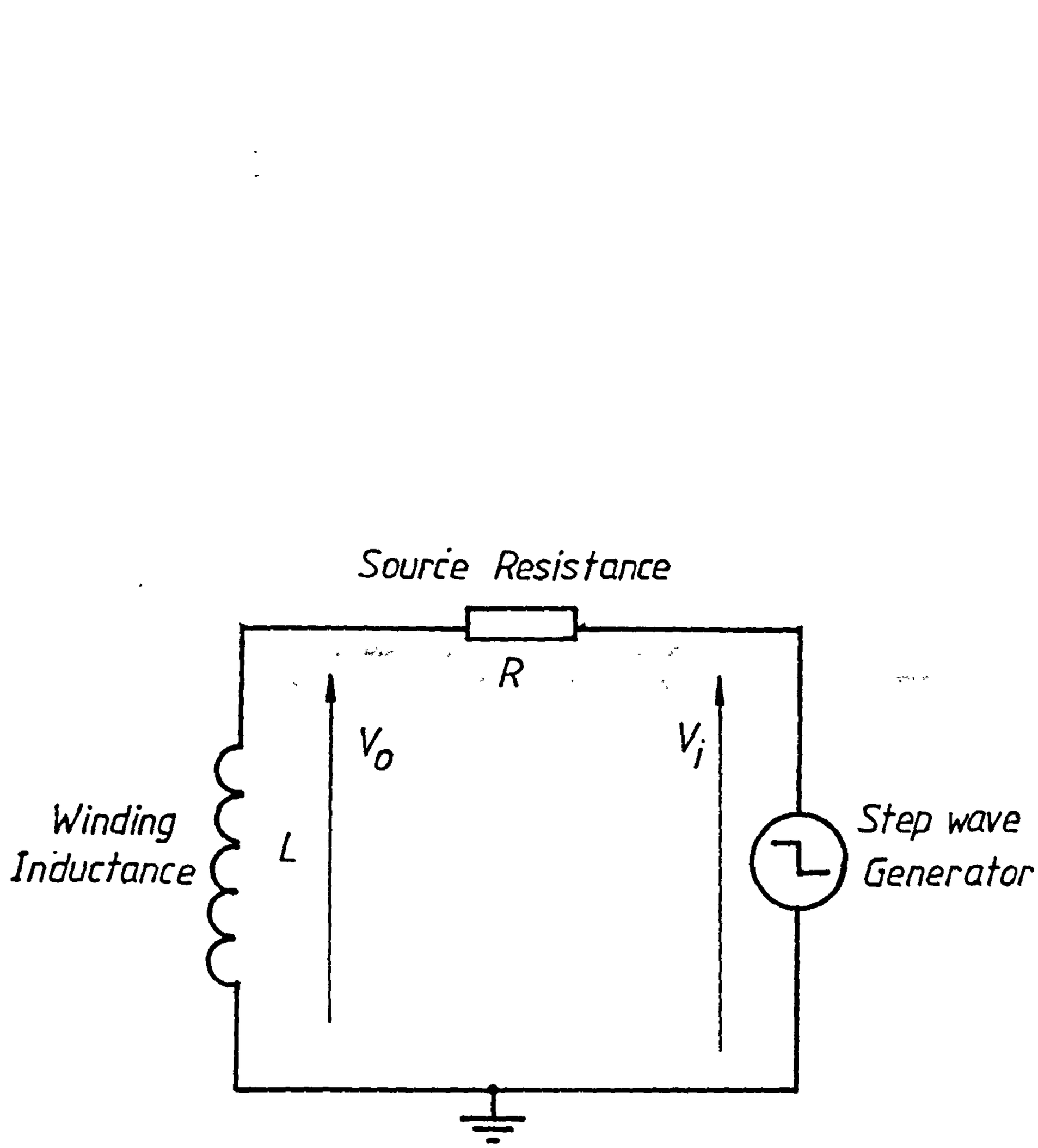

Figure 2.4.2.5 - Low Frequency Equivalent Circuit of Phase Winding

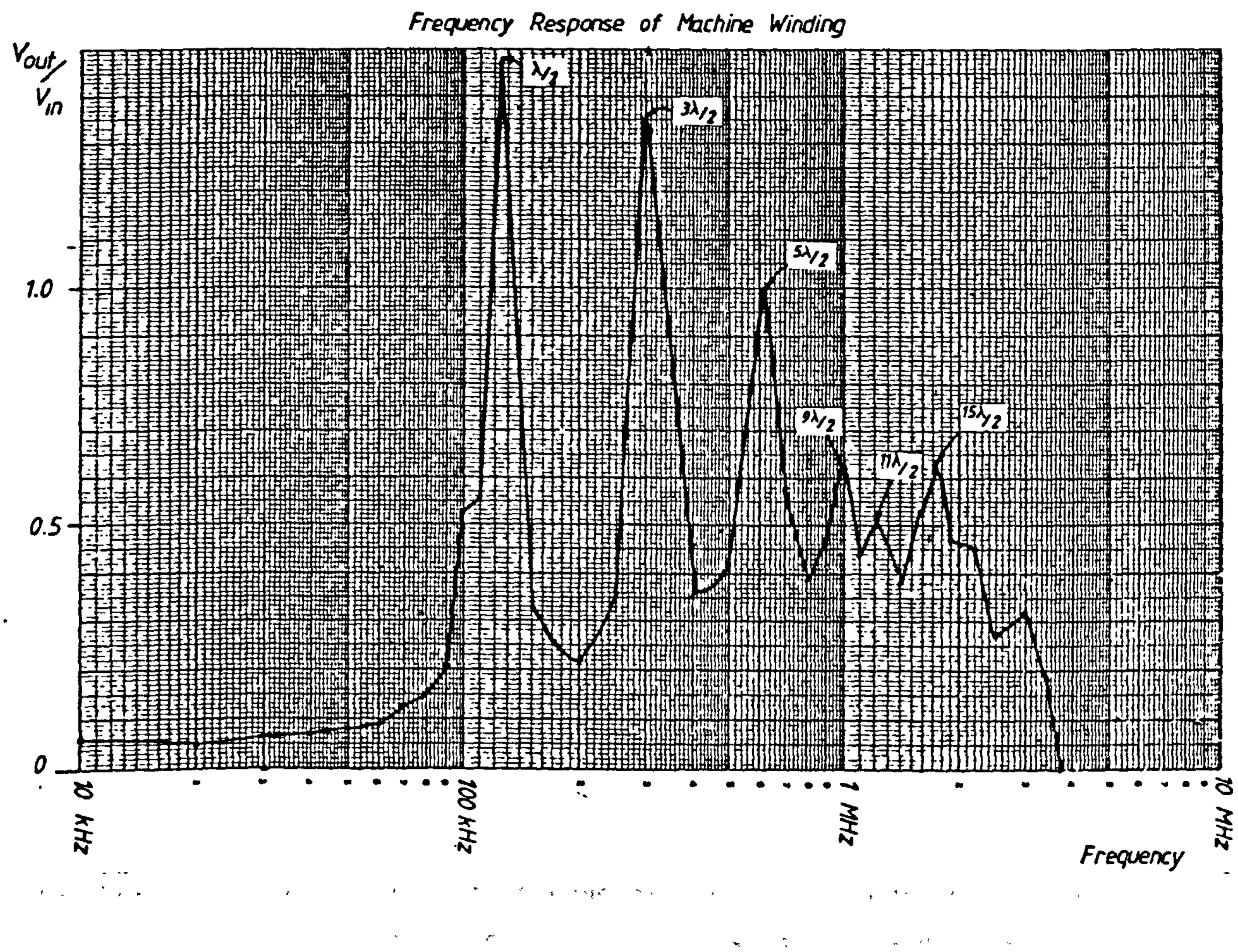

Figure 2.4.2.6 - Frequency Response of Phase Winding with One Terminal Short-Circuited

frequency of 113.5 kHz , which correlates well with the measured value . The fundamental resonance in the winding occurs at this frequency as can be seen by the predominant oscillation in the waveforms in figure 2.4.2.4 .

The other resonant frequencies can be shown to occur when n = 1,3,5,9,11, and 15 times the half wavelength of the resonant oscillation . Calculated and measured values for these resonant frequencies are given in the table in figure 2.4.2.7 for comparison .

No. of Half Wavelengths (n)	Wavelength (m)	Measured Resonant Frequency (kHz)	Calculated Resonant Frequency (kHz)
1	334.6	115	113.5
3	111.5	310	340.7
5	66.9	605	568.0
9	37.2	1000	1022.0
11	30.4	1210	1249.2
15	22.3	1700	1703.5

Figure 2.4.2.7 - Calculated and Measured Resonant Frequencies in a Phase Winding

The winding resonances that occur at n = 1,3, and 5 half wavelengths coincide with the resonant peaks observed in figure 2.4.1.1 . This implies that both winding termination impedances are lower than the winding impedance at these frequencies . Therefore the impedance discontinuity at each end of the winding is responsible for resonances observed at these frequencies in figure 2.4.1.1 .

Another observation from the frequency response characteristic in figure 2.4.2.6 , is that below 100 kHz , signals measured at the end close to the short-circuit termination are small in relation to the main input signal amplitude . At these lower frequencies each coil behaves like a lumped inductance element with an associated reactance at the signal frequency . Consequently there is a linear distribution in the voltage to earth across the winding , from the source terminal to the terminal at earth potential . The signal observed at each coil interconnection is therefore a fraction of the input signal amplitude.

2.5 Electromagnetic Coupling in the Endwindings

It has been established that an electromagnetic pulse travels along the winding conductor with a finite speed of propagation , however a portion of the pulse arrives at the output of each coil a short time before the main travelling wave pulse and with a negative polarity . In the following discussion , simple experiments show that this negative pulse is tranferred through each coil by a complex interaction of conduction along the winding conductor and electromagnetic coupling between the endwinding conductors of adjacent coils in the winding .

The simplest way to determine if significant coupling exists between coils is to eliminate conduction along the winding conductor by creating an open-circuit between any two coils . In the circuit arrangement in figure 2.4.1 an open-circuit was introduced between the first and second coils in the winding . Both disconnected terminals were terminated in a 300 ohm resistor to minimise the influence of pulse reflections on the pulse waveforms to give a clear picture of the pulse transfer mechanism involved . A pulse having a fast rise time of 10 nsec and a duration of 100 μsec was injected at the input to the first coil in the winding from a pulse generator with low source impedance .

The response at the input to coil 2 , in figure 2.5.1 , shows that a significant portion of the injected pulse is coupled from the first coil to the second coil . The amplitude of the coupled pulse is 30 percent of the amplitude of the injected pulse which indicates a strong mutual coupling between the first two coils in the winding . Since the core is an effective barrier to electrostatic fields and magnetic fields at high frequencies , there is negligible coupling between the slot conductors of adjacent coils and so the only path available to signals is through the endwinding turns of adjacent coils.

The question of which coupling mechanism is operative , electric or magnetic field coupling arises , and to what extent each contributes to the mutual coupling between coils . It is expected that the electric field coupling between neighbouring coils is weak because the air gap separating two adjacent coil conductors in the overhang region is relatively large , (15 mm) , compared to the dielectric

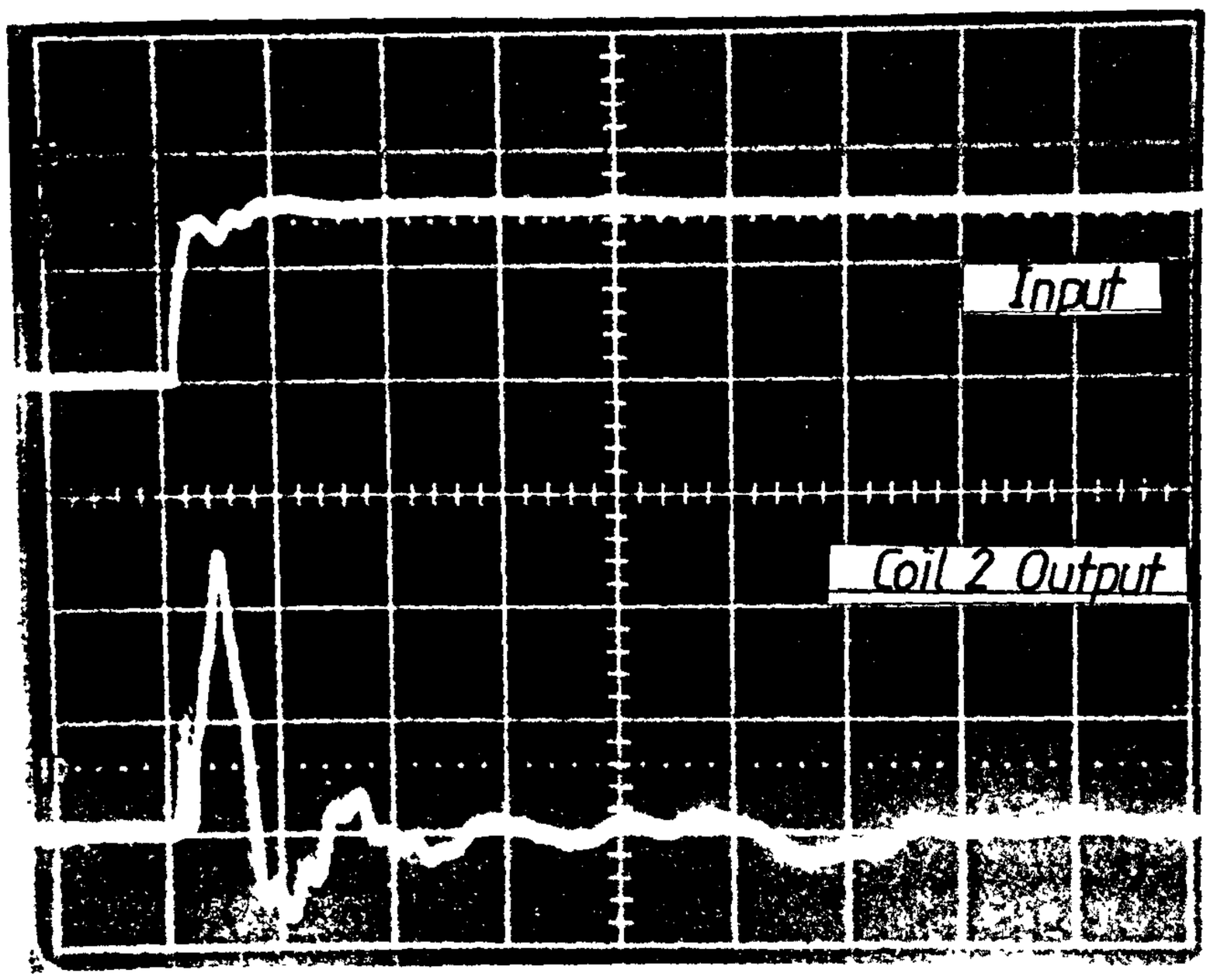

2 V/div

0,5 V/div

0,5 μsec/div

Figure 2.5.1 - Response at Input to Second Coil
(Open-Circuit Between First Two Coils)

thickness, (2.5 mm) , such that the intercoil coupling capacitance is small . Measurement of this capacitance gives a value of 50 pF . On the other hand the magnetic field coupling is stronger due to the close proximity of turn conductors in the overhang which means the mutual inductance between neighbouring coils must be relatively high in comparison with the coil self inductance . Bridge measurement ,(at a frequency of 100 kHz), of the mutual inductance between adjacent coils in a coil group supports this assumption . The results are shown in the table in figure 2.5.2.

Between Coils	Measured Mutual Inductance (uH)	Ratio of M/L
1-2	23.3	0.475
1-3	15.8	0.322
1-4	10.4	0.212

Figure 2.5.2 - Mutual Inductance between adjacent coils

The measured self inductance L , is 49 μH at 100 kHz .

These measurements show that the mutual inductance between adjacent coils is a significant percentage of the coil self inductance , even between coils 1 and 4 which are displaced by 3 slots .

To support these assumptions , the first coil in the winding was wrapped in an aluminium foil which acted as an electrostatic shield but allowed penetration of the magnetic field . Pulses were fed into the input of the first coil and the pulse waveform at the input to coil 2 was recorded , see figure 2.5.3 . There is no appreciable change in the amplitude or form of the mutually coupled pulse compared to figure 2.5.1, and it is therefore be concluded that there is negligible electric field coupling between adjacent coils in a winding of this type . The mechanism of pulse transfer between coils is almost entirely through magnetic field coupling . Figure 2.5.4 shows how significant magnetic coupling is still present when the first coil is moved away a short distance (100 mm) from the second coil.

Further investigation of the electromagnetic coupling mechanism between adjacent coils provides an understanding of the second mode of wave propagation . The previous test arrangement was used as shown in

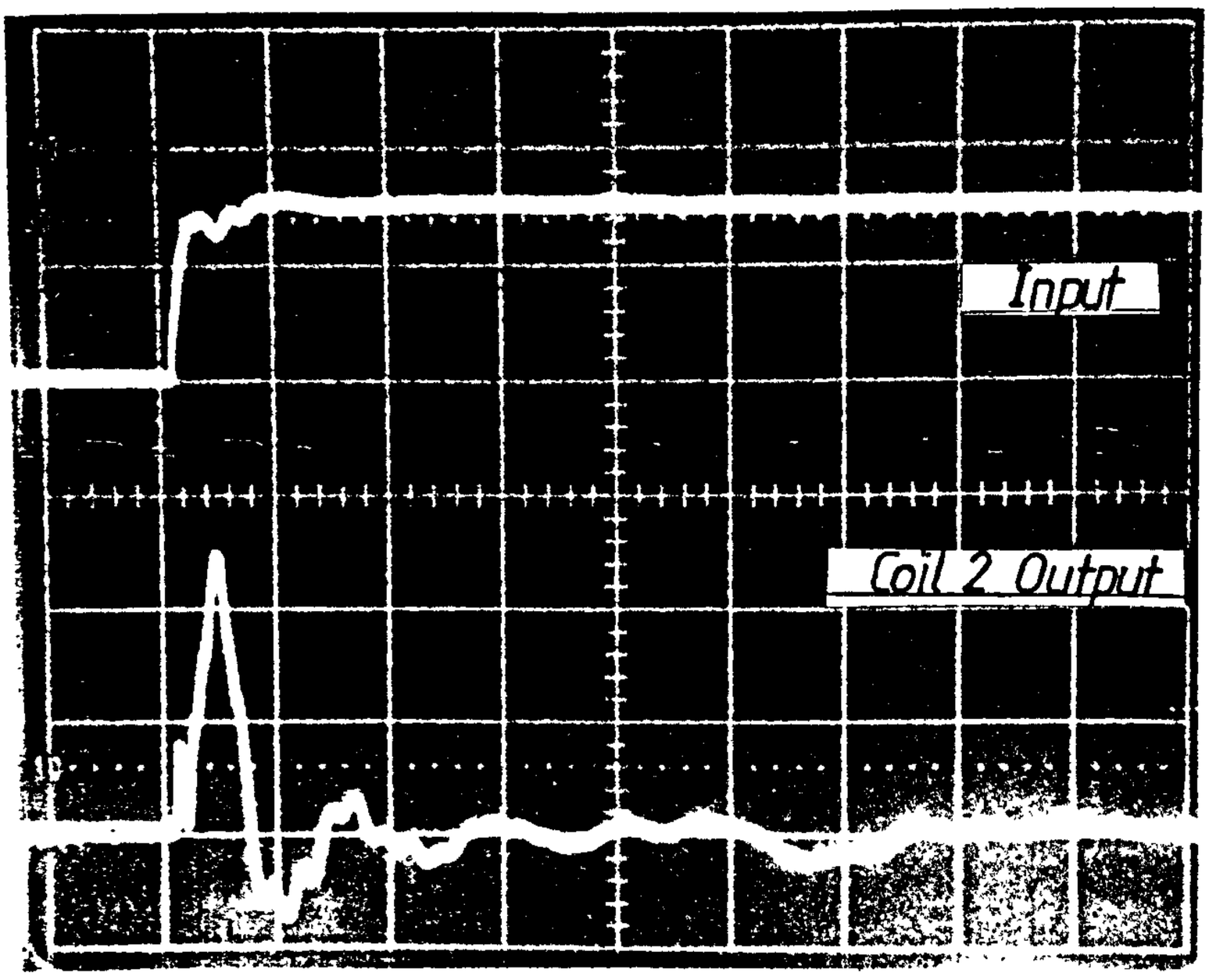

Figure 2.5.3 - Response at Input to Second Coil when First Coil is Electrostatically Shielded

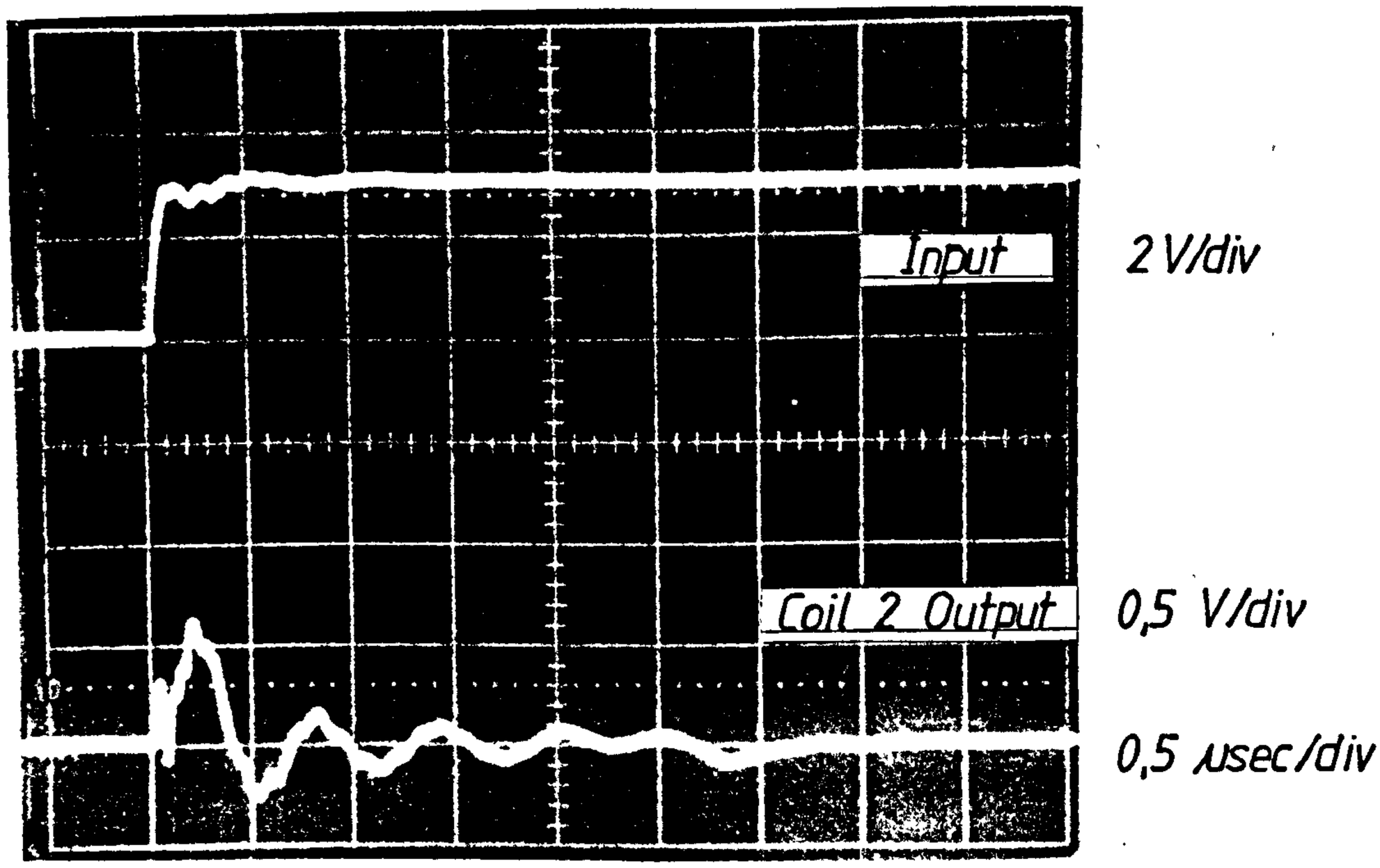

Figure 2.5.4 - Response when First Coil is Moved Away from Second Coil

figure 2.4.1 , and the pulse waveforms at the outputs of coils at intervals along the winding are recorded as shown in figure 2.5.5 .

The first trace in the sequence shows , as before in figure 2.5.1, that a very signifcant portion of the pulse injected into the winding is transferred to the second coil in the group , and occurs instantaneously . It is then followed by a number of oscillations which arise from a transmission line resonance effect . In addition to these oscillations there is a reflection of the coupled pulse at the end of the winding, which has undergone considerable attenuation and distortion . The time between the beginning of the coupled pulse and its reflection from the end terminal is approximately 3.0 μsec which for a distance travelled of 310.7 metres (twice 13 coil lengths) corresponds to a velocity of propagation of 103.5 m/μsec . This value for velocity compares with the value of 108.6 m/μsec computed from measurement of the time between the wavefront of the pulse observed at the outputs of coils 2 and 4 , which is 220 nsec .

It is seen therefore , that the pulse transferred by magnetic coupling to the second coil, travels through the remainder of the winding with a velocity approaching : $v = c/\sqrt{\epsilon_r}$.

However , if the output waveform of coil 4 is examined it can be seen that a pulse having negative polarity appears almost immediately and follows the initial pulse induced in coil 2 which has travelled through coils 2 and 3 . This pulse must have been electromagnetically induced in coil 4 by currents circulating in the endwinding turns of both coils 1 and 2 . The amplitude of the pulse is 13.5 percent of the injected pulse amplitude which confirms that the mutual inductive coupling between coil 1 and coil 4 is weaker than between coil 1 and coil 2 , approximately 50 percent which is in line with the measured mutual inductances given in figure 2.5.2 . This is expected , since the area of overlap between endwinding conductors , (hence mutual inductance), in coils 1 and 4 is smaller as the coils are displaced by three slots.

Similar behaviour is observed at the output of coils 10, 12 and 14 where a progressively smaller pulse is induced in these coils almost instantaneously in time . For example , The wavefront of the induced pulse in the last coil in the winding is seen to appear only 200 nsec after the wavefront of the injected pulse at the source end

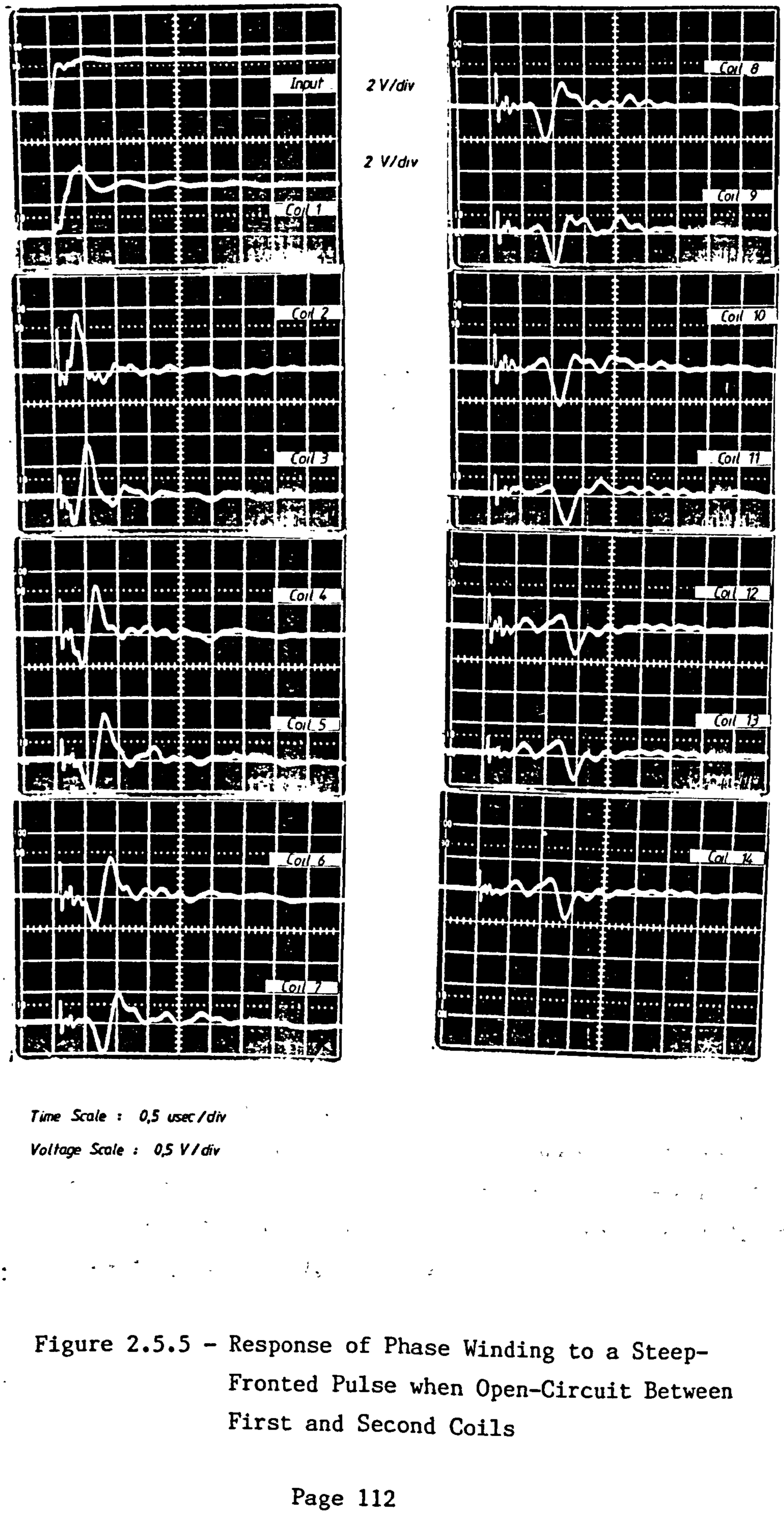

Figure 2.5.5 - Response of Phase Winding to a Steep-Fronted Pulse when Open-Circuit Between First and Second Coils

of the winding .

Each of the pulses induced simultaneously in a number of coils , propagate in both directions within the winding at a velocity of approximately 110 m/μsec . These travelling pulses then interfere either constructively or destructively with other pulses such that a number of oscillations are observed on each of the waveforms in figure 2.5.5 .

2.5.1 Frequency Response of Endwinding Coupled Signals

From an examination of the waveforms of figure 2.5.5 it is possible to infer two properties of the signals that take part in the second mode of wave propagation in windings . The first observation is that the signals transferred by endwinding coupling are limited to a narrow bandwidth of frequencies as can be seen from the pulse induced in the second coil in the winding in the first trace in figure 2.5.5 . This pulse has the appearance of a damped oscillation which is characteristic of the response of a narrowband circuit to a step input . The second is that signals are relatively high frequency, which is deduced from the period of oscillation of the coupled pulse which corresponds to a frequency of approximately 1.4 MHz .

Frequency response measurements support these observations from waveforms. Measurements were performed on the same circuit arrangement as in figure 2.4.1 with the exception that a sinusoidal wave generator was used in place of the step wave generator . Figure 2.5.1.1 displays the frequency response of the winding which is normalised to the amplitude of the input signal .

Signal propagation through endwinding coupling is indeed restricted to a narrow bandwidth of signal frequencies . As is shown in the frequency response, endwinding coupling begins at signal frequencies just above 100 kHz . The amplitude of the induced signal rises with increasing frequency up to a maximum at a frequency of around 1.5 MHz and falls off thereafter more rapidly until at a frequency of 3.6 MHz there is no endwinding coupling .

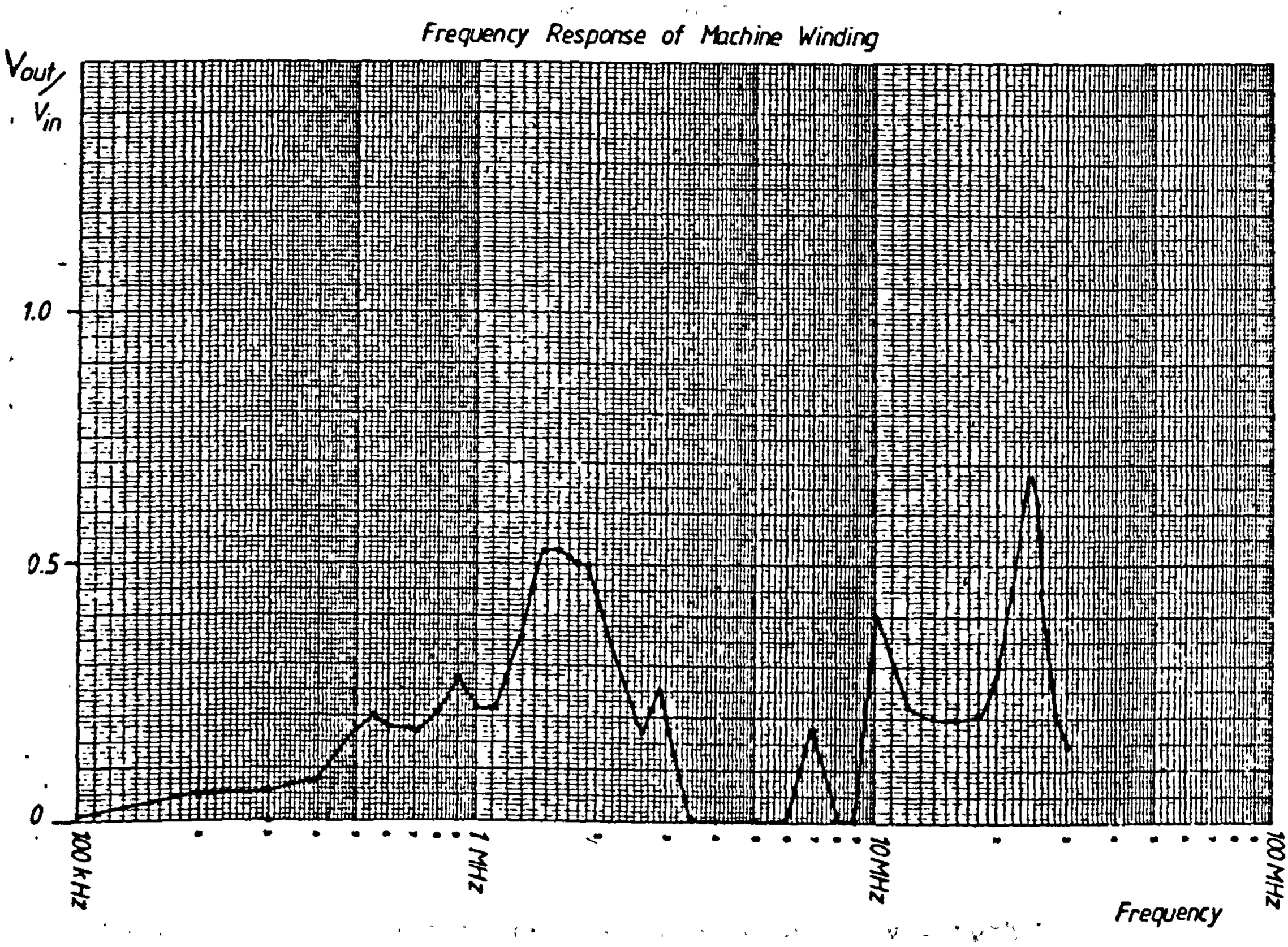

Figure 2.5.1.1 – Frequency Response of Phase Winding when : Open-Circuit Between First and Second Coils

The gradual rise in the amplitude of the coupled signal with increase in frequency is expected , as the induced e.m.f. in the second coil due to the magnetic flux linking the first and second coils is proportional to the rate of change in the currents flowing in the first coil which is expressed in the relationship ,

$$e = M.\frac{di}{dt} \qquad \text{.....(2.9)}$$

Since $i(t) = I \sin(\omega t)$ the equation becomes ,

$$e = M.\omega.I \cos(\omega t)$$

The induced voltage in the second coil is therefore proportional to the mutual inductance and the frequency ω .

The upper frequency cut-off is a result of the low pass filter characteristic of each stator coil .

The peak in the frequency response corresponds to the damped oscillation observed in the waveform in figure 2.5.5 which has a frequency of oscillation of approximately 1.5 MHz . It is possible to relate the wavelength at this frequency to the length of the winding through the relationship : $v = f.\lambda$, assuming the velocity of propagation is given by , $v = c/\sqrt{\epsilon_r}$. As before , the boundary conditions at the ends of the winding can be defined . At the input to the second coil in the winding is an open-circuit, and at the opposite end, the winding is terminated in a 300 ohm resistor which represents a low impedance. The total length of the winding involved is therefore 155.35 m, (13 coils length) , which is the length of winding between the two boundaries . Under these terminating conditions , only resonances with quarter wavelengths that are multiples of the winding length can exist .

The wavelength of the signal at a frequency of 1.5 MHz moving at a velocity of 116 m/μsec is 77.3 metres which is half the effective length of the winding , 155.35 m . Two wavelengths of the signal at 1.5 MHz occupy the winding length .

Other resonance peaks are observed in the frequency response and these have wavelengths which can be related to the effective winding length

and the given boundary conditions and are summarised in the table in figure 2.5.1.2 .

Number of Wavelengths	Frequency calculated	Frequency measured
3/4	560 kHz	550 kHz
5/4	933 kHz	900 kHz
2	1.49 MHz	1.5 MHz
4	2.98 MHz	2.9 MHz

Figure 2.5.1.2 - Relationship between calculated and measured resonant frequencies and wavelengths in motor winding .

This resonance behaviour is even more distinct if the winding is open-circuited at each coil interconnection . The frequency response for this condition is shown in figure 2.5.1.3 .

It is observed that there are a greater number of resonance peaks in the response which are evenly spaced along the frequency axis . The positions of the resonant frequencies can be calculated as before assuming a wave velocity of 116 m/μsec as before . However in this case the effective boundary conditions are difficult to define since open-circuits exist at each coil interconnection on the winding . It is therefore assumed , intuitively , that the boundaries are at the winding ends and that these terminations , the signal generator source impedance of 50 ohms and the 300 ohm resistor represent fixed boundaries at the frequencies concerned . The length of conductor between the boundary points is therefore the length of the winding which is 167.3 m .

The table in figure 2.5.1.4 shows that the resonant frequencies have wavelengths and half wavelengths which are integral multiples of the length of the winding .

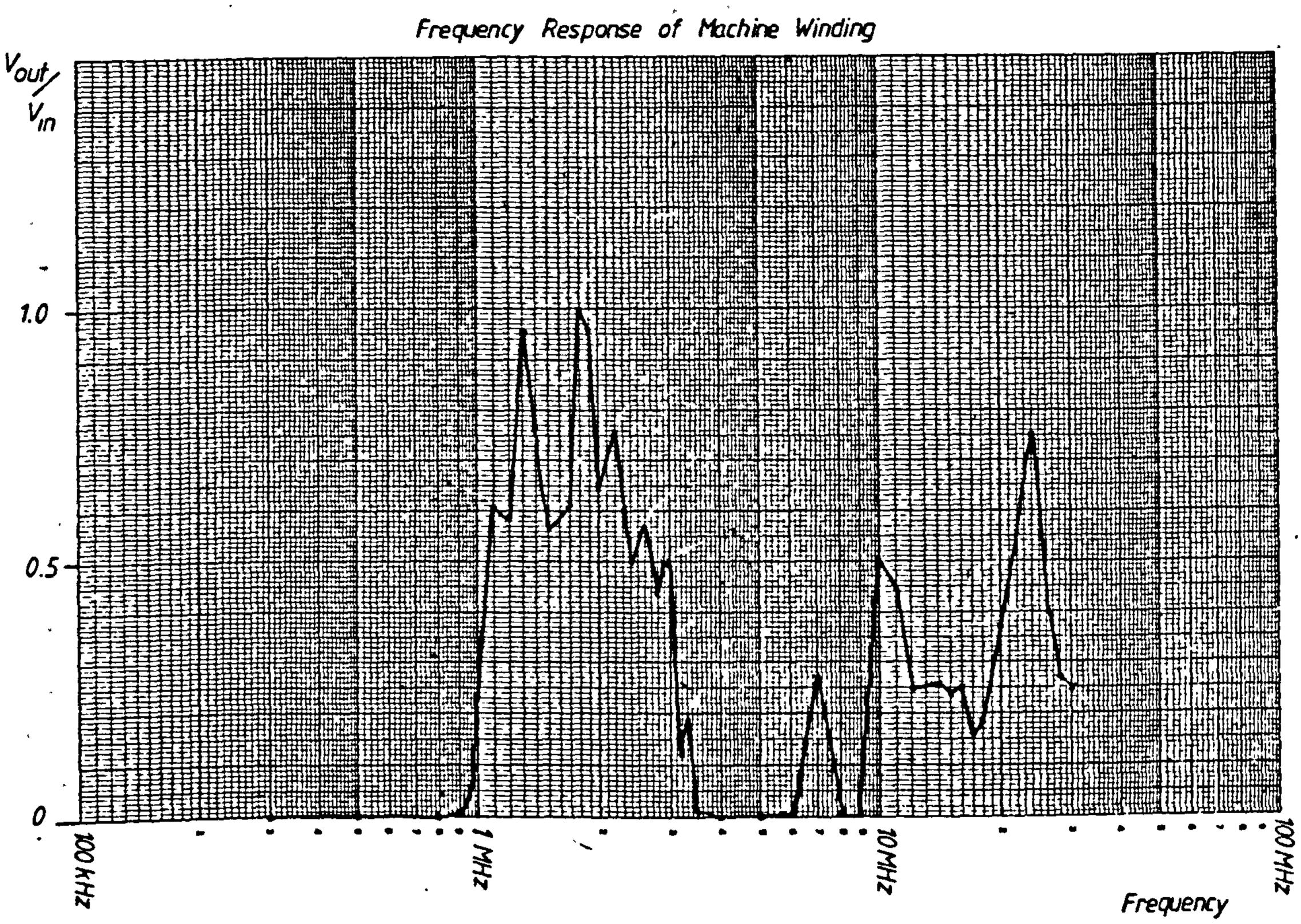

Figure 2.5.1.3 - Frequency Response of Phase Winding
(Open-Circuit Between All Coils)

No. of Wavelengths	Frequency calculated (MHz)	Frequency measured (MHz)
3/2	1.05	1.10
2	1.38	1.30
5/2	1.73	1.80
3	2.31	2.20
7/2	2.43	2.60
4	2.77	2.90
5	3.28	3.30

Figure 2.5.1.4 - Calculated and measured resonant frequencies related to wavelengths in motor winding .

Calculated resonant frequencies compare fairly well with those of the measured values and each successive resonance occurs when every half wavelength is an integral multiple of winding length so that the assumption of two fixed boundaries at the winding terminations is justified.

Another general feature of the frequency response is that the lower cut-off frequency is considerably higher at 1 MHz than in the case when only one open-circuit exists . In addition the slope of the response as the frequency is increased from 900 kHz to 1.1 MHz is extremely steep . The upper cut-off frequency is the same as in the case of a single open-circuit between the first and second coils , and is the upper frequency limit of signal propagation in a single coil . The passband for signals coupled through the endwindings between adjacent coils is therefore limited to a well defined range of frequencies between 1 MHz and 3 MHz .

The frequency response outlined in the preceding paragraphs is reflected in the pulse waveforms recorded at the output of each coil in the winding as shown in figure 2.5.1.5 . In the first trace , which is taken at the output of the second coil , it is possible to observe a few of the oscillations that are associated with the resonant frequencies seen in the frequency response characteristic . The first oscillation to occur has a period of 550 nsec which corresponds to a predominant resonant frequency of 1.8 MHz . This is followed by a higher frequency oscillation with a period of

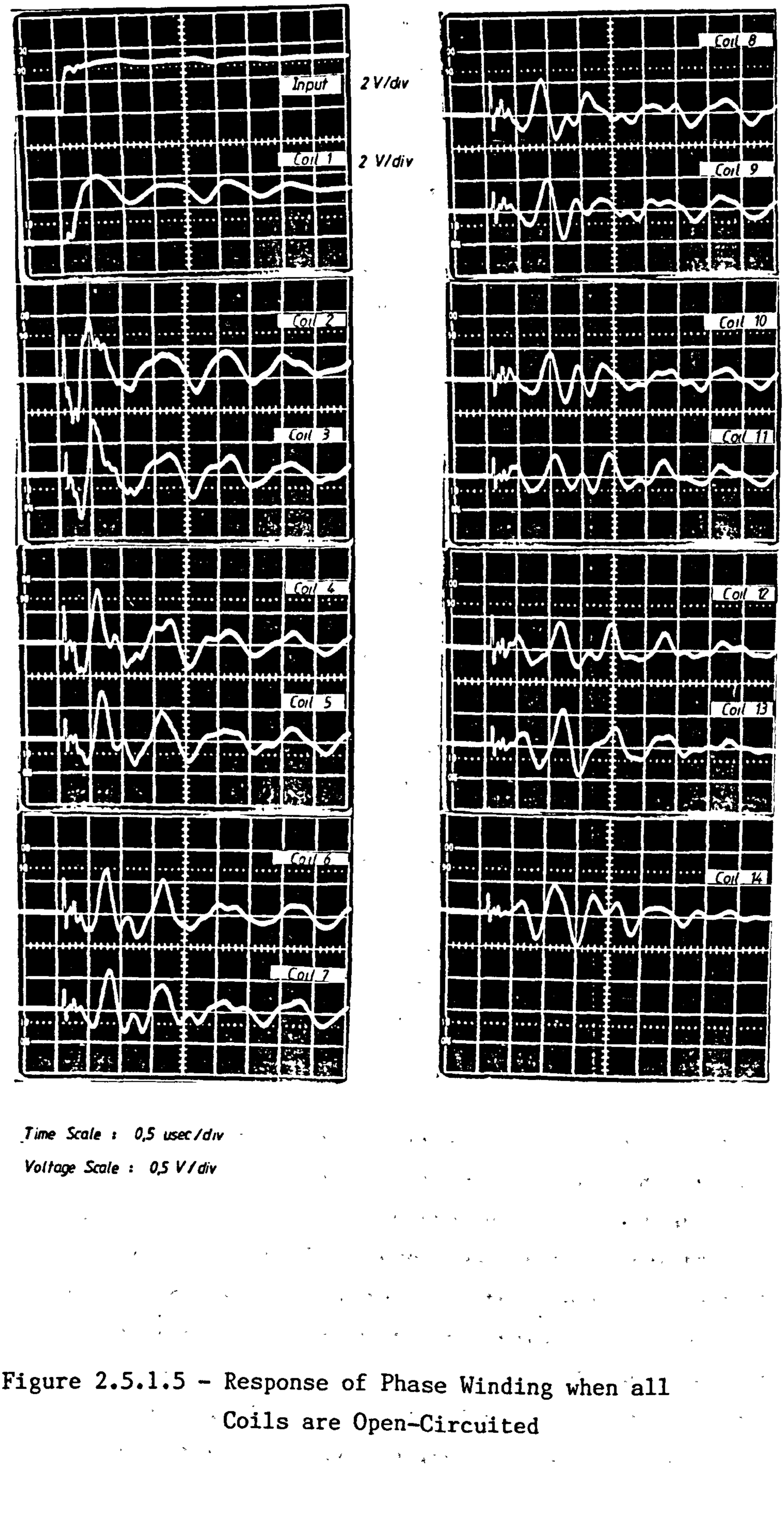

Figure 2.5.1.5 - Response of Phase Winding when all Coils are Open-Circuited

450 nsec which is corresponds to a frequency of 2.2 MHz . Similarly , the much lower frequency oscillation observed is at 1.1 MHz .

Finally , in the frequency responses obtained from both circuit arrangements , the resonant peaks at 7 , 10 and 24 MHz due to earth path propagation are still present and bare no relation to the second mode of wave propagation .

2.6 Partial Discharge Pulse Propagation in a Phase Winding

For the purpose of investigating the propagation characteristics of partial discharge pulses , a repetitive , regular discharge source is required which therefore excludes the use of a real discharge source . Partial discharges were therefore simulated by a low voltage rectangular pulse generator . The circuit used to derive artificial discharge pulses is shown in figure 2.6.1 and comprises a pulse generator that feeds rectangular pulses through a 500 pF coupling capacitor and coaxial cable into the winding . The capacitor effectively differentiates the step pulse to give a fast rise time pulse with an exponential decay on the pulse tail .A signal diode eliminates the negative polarity pulse created by the differentiation of the falling edge of the rectangular input pulse . The circuit therefore provides a source of regular , positive polarity , discharge shaped pulses . Initially the winding is terminated at both ends by the characteristic impedance of the winding , 300 ohms , and the discharge pulse source is connected at one end of the winding .

The waveforms in figure 2.6.2 show the discharge pulse as it propagates through the winding at each coil interconnection . At the input, the pulse has the ideal discharge pulse shape and has a duration of approximately 1 μsec and a rise time of 10 nsec .

Propagation of this type of pulse is very similar to the behaviour of a fast-fronted rectangular pulse as described in section 2.4 . The lower frequency components of the pulse propagate in the transmission line mode at a velocity of 38 m/μsec as observed from the pulse transit time through coils . As the main low frequency portion of the pulse travels through the winding it exhibits a progressive deterioration in the pulse wavefront and a gradual increase in the duration of the pulse . The frequency dependent attenuation is responsible for this behaviour since the winding has a low pass filter

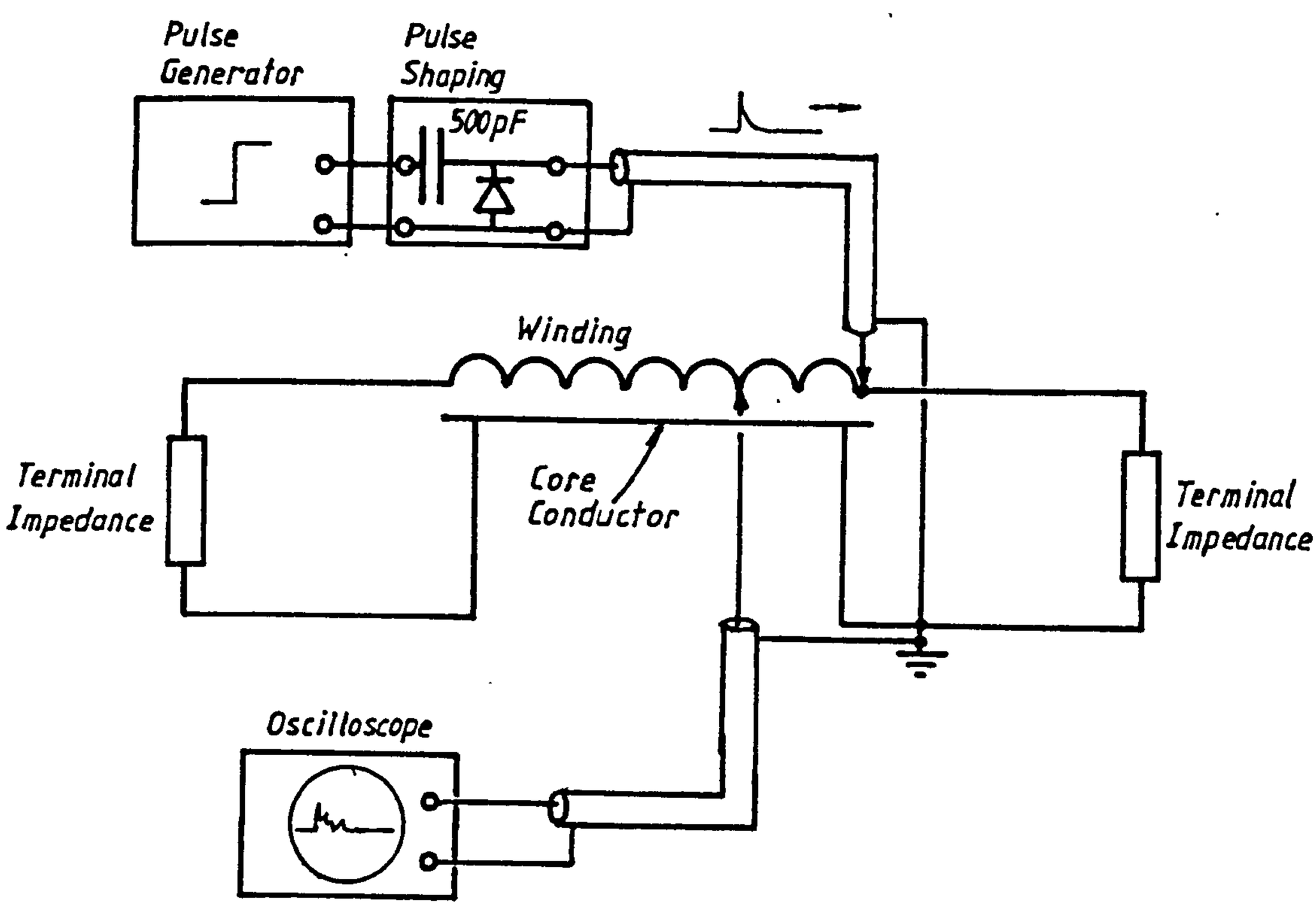

Figure 2.6.1 - Artificial Discharge Pulse
Injection Test Circuit

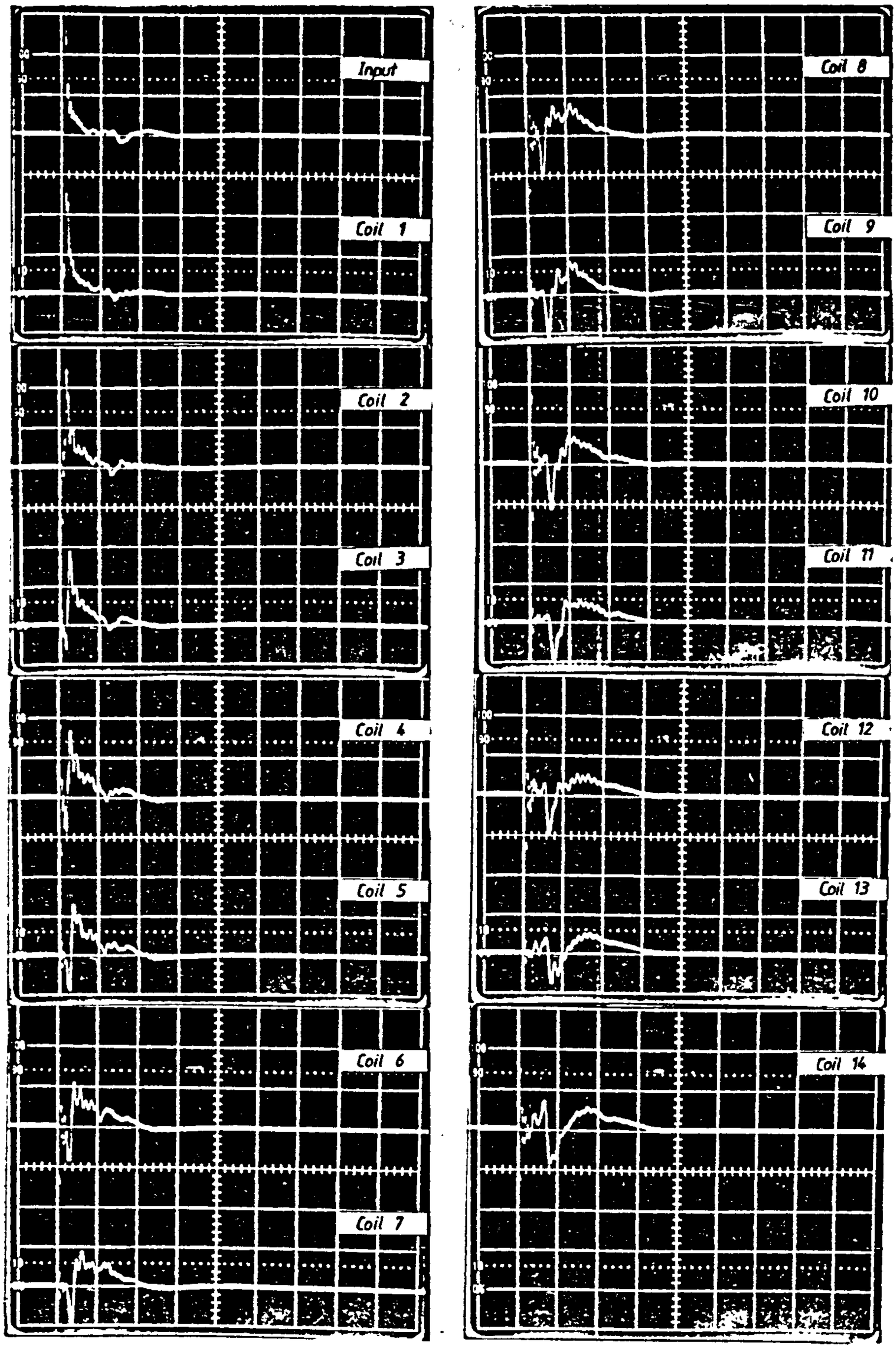

Time Scale : 2,0 μsec / div

Voltage Scale : 0,5 V / div

Figure 2.6.2 - Response of Phase Winding to Discharge Pulse

characteristic . The high frequency components of the pulse travel through the winding with a much greater velocity of approximately 105 m/μsec and form the fast rise-time , short duration , negative wave seen on the waveforms . Propagation of the high frequency wave must therefore be through the endwinding path created by the electromagnetic coupling between coils . Two distinct modes of wave propagation with differing wave velocities can be distinguished therefore .

In addition to the characteristics discussed , reflections of the pulse at the winding terminals are also observed on the waveforms . On the input pulse , a positive polarity pulse reflection is seen after about 3.2 μsec which corresponds to two wave transit times through the winding . The progressive movement of this reflection towards the main pulse is observed at consecutive coil connections until at coil 14 the reflected pulse is seen to precede the main travelling pulse .

2.6.1 Influence of Winding Terminating Impedance

Pulse reflections inevitably occur when the winding is terminated in an impedance other than the winding impedance . Figure 2.6.1.1 shows the waveforms seen at each of the coil interconnections when a discharge pulse is injected at one end of the winding whilst the other end is terminated in an open-circuit .

Immediately it can be seen that pulse reflections occur at the impedance discontinuity . In the first trace , the input pulse appears initially and is followed by two separate pulse reflections . The first reflection has a higher frequency content and occurs after a time delay of 3.2 μsec which corresponds to twice the travel time through the winding at a velocity of 105 m/μsec . This must therefore be the reflection of the wave that travels through the endwinding structure . The much lower frequency , longer duration , pulse follows the main input pulse after a time delay of approximately 6 μsec and corresponds to the slower travelling wave reflected at the open-circuit terminal . Both pulse reflections travel in the opposite direction to the main pulse since both reflected pulses occur at a smaller time delay after the main pulse as it progresses deeper into the winding . At about half way into the winding , the first high frequency pulse reflection converges with the main travelling pulse .

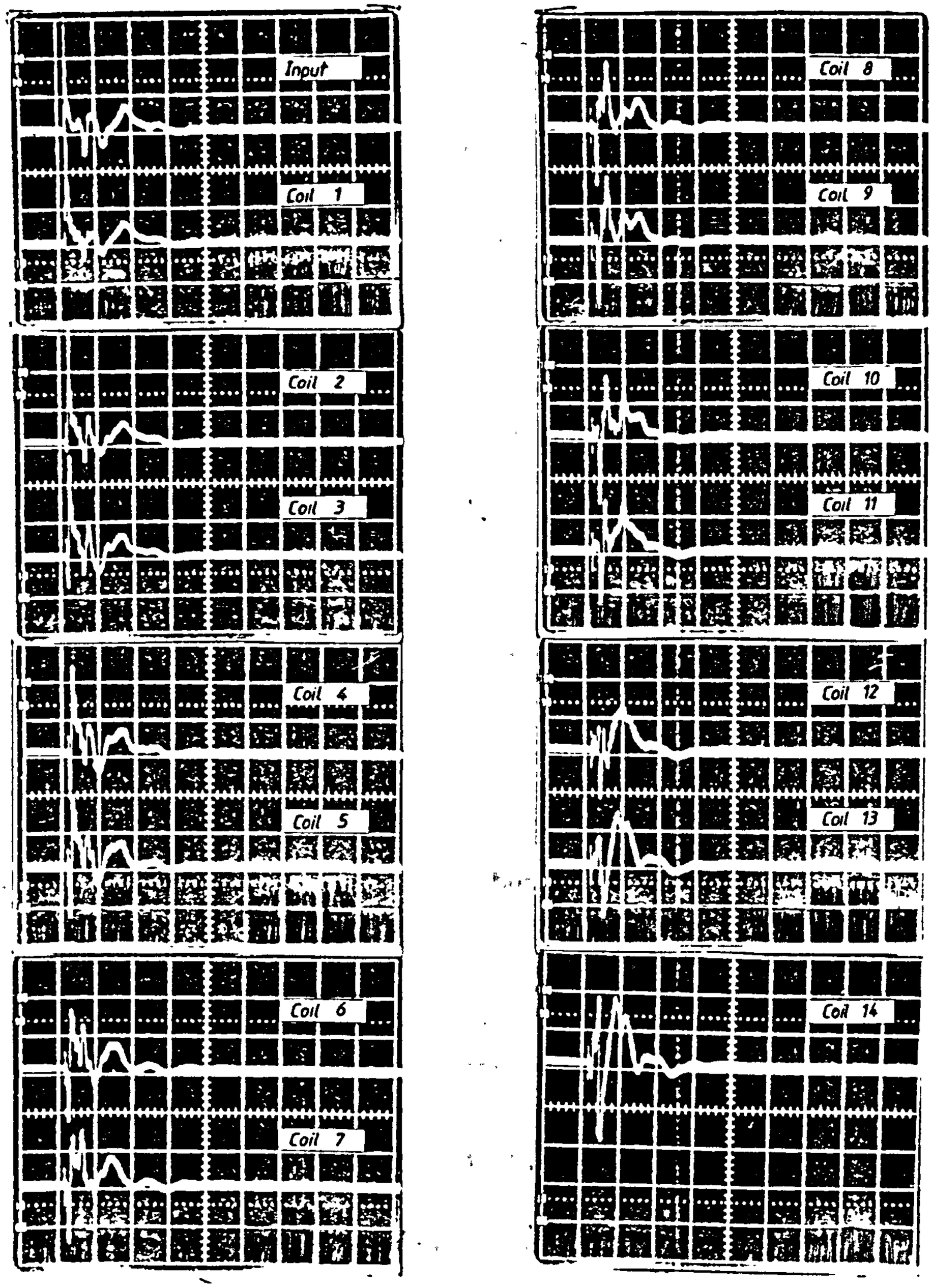

TIME SCALE : 4,0 μseconds / div.

VOLTAGE SCALE : 2,0 Volts / div.

Figure 2.6.1.1 – Response of Phase Winding (Open-Circuit at One Terminal)

Similar behaviour is observed when the winding is terminated at one end in a short-circuit . Figure 2.6.1.2 shows the waveforms recorded at each coil interconnection when a discharge pulse is injected at the input to coil 1 .

The main pulse is followed by two separate pulse reflections . The first has a higher frequency content than the second and occurs 3.2 μsec after the main pulse . This must be the reflection , at the short-circuit terminal, of the wave that travels through the endwindings. The reflected pulse that follows this occurs at a time delay of 6 μsec after the main pulse and is reflected with negative polarity at the short-circuit terminal . This is the reflection of the low frequency wave which travels at a lower velocity , around 38 m/μsec .

Reflections of this nature can be expected when real discharges take place in a machine winding since a phase winding is always terminated by two other phase windings or by the supply feeder cable to the machine . The influence of these reflections on pulse location within a phase winding are discussed in chapter four .

2.7 Partial Discharge Measurements in Motor Windings

The stator winding of an electrical machine is a distributed circuit, and as a result, partial discharge pulses are subject to distortion and attenuation before they reach the winding terminals . The degree of this attenuation is dependent on frequency . Above a certain cut-off frequency , measured at 3.4 MHz , virtually no wave propagation takes place in the winding and therefore the bandwidth of any partial discharge system is limited to this range .

Below the upper frequency limit , the greatest sensitivity in the measurement of partial discharge magnitude may be obtained . The sensitivity is a maximum in the frequency range 10 kHz to 100 kHz since attenuation of the signal is less than - 1.9 dB,(a reduction of 20 % in the signal), as shown in the frequency response characteristic in figure 2.4.1.1 . Signals above 100 kHz experience a gradual increase in the level of attenuation up to the upper frequency 3.4 MHz . The lower limit of signal detection is limited only by the level of signal interference generated by low frequency disturbances , typically from harmonics of the power supply frequency . Commercial

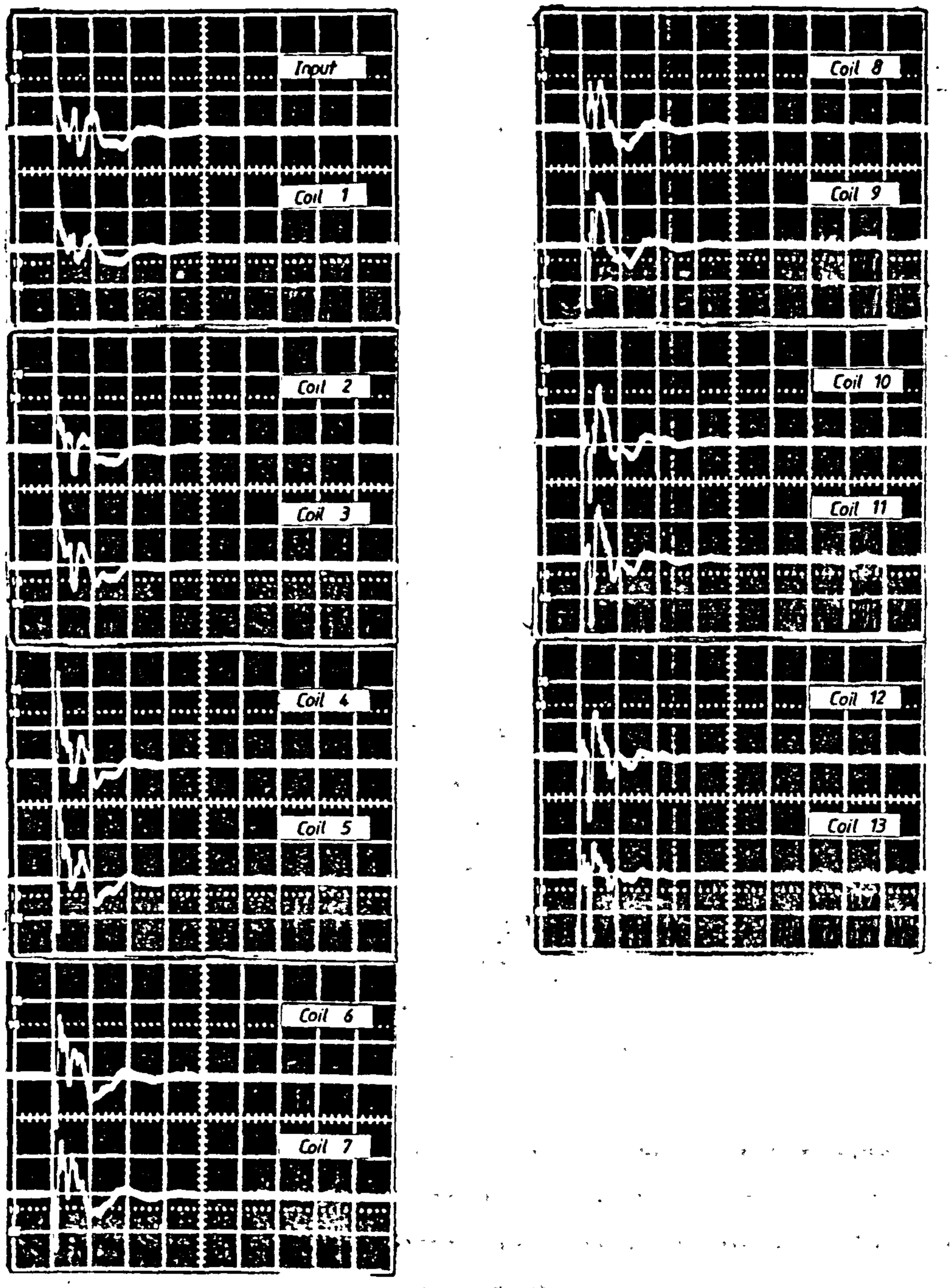

Figure 2.6.1.2 - Response of Phase Winding (Short-Circuit at One Terminal)

instruments such as the ERA discharge detector have a lower frequency limit of around 20 kHz .

Since the most suitable frequency range for discharge measurements has been established the choice remains whether to adopt a narrowband detector or a wideband detector and what type of detection device to use at the motor terminals . The latter is discussed in greater depth in chapter three of this report .

If a narrowband detector is selected the resonant frequency of the detection impedance may be varied over the frequency range 10 kHz to 100 kHz to obtain maximum signal sensitivity . Commercially available detectors, such as the ERA Mk III discharge detector, have a resonant frequency that may be set at a frequency in the range 30 kHz to 100 kHz and an amplifier which has a bandwidth between 10 kHz and 250 kHz. This type of detector is most suitable for the measurement of discharge pulse magnitude . However , there are difficulties in applying partial discharge measurements to stator windings using a narrowband detector Figure 2.7.1 shows the response of this type of detector to a source of negative point corona discharge pulses injected at each of the coil interconnections along the winding . In this case the winding is terminated in an impedance of 150 ohms at the neutral end to represent a star connected phase winding . The detector is an ERA Mk III discharge detector located at the line end of the winding which is terminated in an impedance of 300 ohms .

As the discharge source is positioned progressively farther away from the detector , the measured peak signal magnitude falls from 100 % to 42% at a distance of 10 coils from the detector terminal . When the source of discharges is connected at a distance greater than 10 coils from the detector, the measured signal magnitude is increased until at the neutral end the observed signal magnitude is greater than the injected value . This characteristic is due to the constructive interference of the pulse reflected at the neutral terminal with the pulse that travels directly to the detector terminal from the discharge source . This behaviour has been reported by other investigators [81] . Obviously care must be taken in the interpretation of partial discharge measurements in motor windings using a narrowband detector for the forementioned reasons .

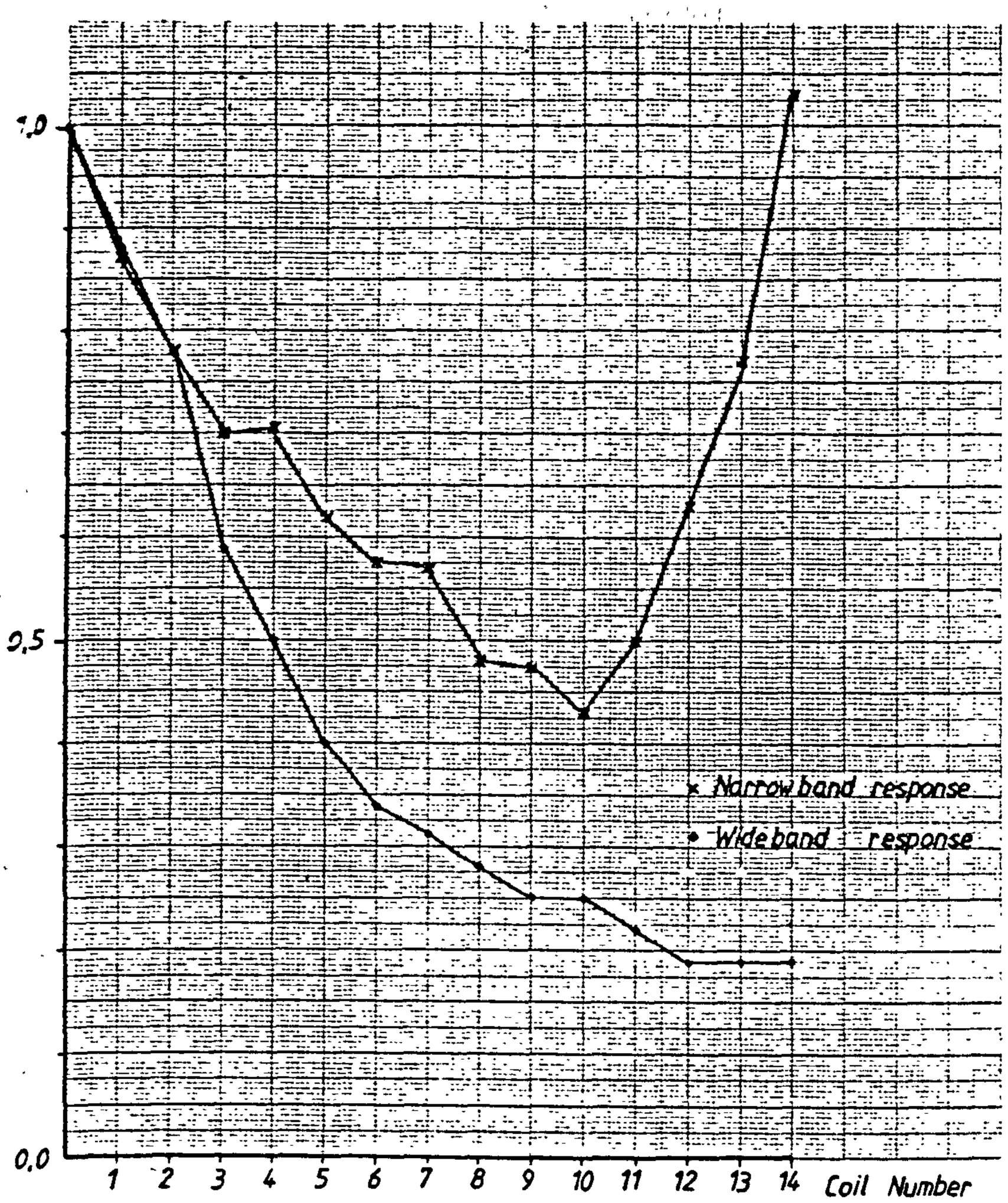

Figure 2.7.1 - Response of Narrow and Wide Band Detectors to Partial Discharge Pulses

Wideband detection is much less affected by pulse reflections but experiences greater attenuation of the signal through the winding . Figure 2.7.1 shows the amplitude of a negative point corona discharge pulse with distance from the detection terminal .

Attenuation of the pulse is greatest over the first six coils in the winding . In this length of winding the pulse is reduced to 30 % of the initial discharge amplitude , (-10.45 dB of attenuation) . After this, attenuation is much less with increasing distance from the detector terminal . By this time the pulse has travelled more than six coils length and the high frequency components of the pulse have been attenuated, leaving the low frequency pulse which incurs a much lower degree of attenuation . This may not be prohibitive in measurements of partial discharges since most discharge activity takes place in the line end coils of a machine due to the linear distribution of supply voltage across the winding .

Both narrowband and wideband discharge measurements can be applied to high voltage motor windings knowing the limitations involved with either system .

2.7.1 Basis for a Discharge Location Technique

The travelling wave behaviour of high frequency pulses in machine stator windings can be used as a basis for a location technique for partial discharges . The results of experiments with artificial discharge pulses show that two separate modes of wave propagation exist . Both of these phenomena provide scope for the development of a location technique based on pulse transit time through the winding .

CHAPTER THREE

THE ROGOWSKI COIL IN PARTIAL DISCHARGE MEASUREMENTS

3.1 Partial Discharge Couplers

A partial discharge detection system requires the use of non-invasive devices to couple the discharge signals from the test apparatus to the ground station . These partial discharge couplers can be located at the line and neutral ends of the motor phase windings .

Operation of these devices rely on the changes in the electric, (capacitive measurement), or magnetic, (inductive measurement), field coupling caused by the discharge signal.

3.1.1 Capacitive Couplers

Capacitive couplers have been in service in the power generation utilities of Ontario Hydro , Canada , as part of an insulation diagnostic system since 1976 , [57]. The couplers are permanently installed to allow on-line testing of the machine . Two types are in existence at present :

Loop type - These are fabricated from a length of single core, h.v., armoured power cable which is formed into a loop. The core conductor is connected to the machine terminals at a convenient point. The cable armour then acts as the low voltage side of a capacitor. It is typically 1-2m long and has a capacitance of around 80-160 pF.

End-cap type - This is a conventional foil capacitor contained in a moulded plastic housing which is taped to the stator endwinding and has much smaller dimensions for installation in confined areas.

In both devices, a matched coaxial cable is used to connect the capacitive coupler to the signal processing instrument. Power frequency signals are also, to a large extent, filtered out by the coupler.

3.1.2 Inductive Couplers

Until recently, the ferrite cored current transformer has been used as an inductive coupler in partial discharge measurements . A broadband response is attainable, between 100 kHz and 10 MHz , with adequate sensitivity. It has however, certain disadvantages and these are :

i. Sensitivity depends on the permeability of the magnetic core and any air gap in the iron path severely reduces the current transformer's output . It is therefore necessary to machine the faces of the core at the slit position, and to provide an adequate clamping arrangement.

ii. Power frequency currents in the secondary winding are high and will subsequently affect the amplifier stage.

A device which is gaining acceptance as a partial discharge coupler is the Rogowski coil. The Rogowski coil is basically an air-cored current transformer and consequently requires a large number of turns to provide comparable sensitivity . It has the advantage of a simple construction, since it may be wound on any non-magnetic former , and exhibits superior power frequency signal rejection. These useful qualities of the Rogowski coil makes it desirable for use in a discharge detection system.

Most publications have examined the behaviour of the Rogowski coil as a current monitor in measurement systems involving high-energy electron beams [83]. The following sections represent a detailed investigation on the theory and application of the Rogowski coil in partial discharge detection.

3.2 The Rogowski Coil

The Rogowski coil, sometimes referred to as the Rogowski loop , is a device which allows non-intrusive measurement of fast rise-time pulsed currents [83,84,85] . It was first developed by W. Rogowski in 1912 [86].

As its name suggests, the Rogowski coil is essentially a thin solenoid bent round to form a closed loop, normally a toroid, making an aperture through which the current to be measured is passed. A voltage is electromagnetically induced in the coil by any time varying current threading the loop aperture which, provided the coil is properly terminated, is an analogue of the current pulse.

The Rogowski coil offers distinct advantages over other current monitoring devices in that:

The loop is only sensitive to currents that thread the aperture, and a

fixed relationship exists between the current to be measured and the developed voltage, which makes the Rogowski coil simple to calibrate .

No direct connection to the monitored circuit is necessary, allowing complete isolation from high voltages and spurious earth loop currents.

No significant energy transfer takes place in measurements permitting non-invasive measurements to be made.

It has the inherent ability to reproduce the voltage analogue of a current pulse with a rise time in the nanosecond or even sub-nanosecond range.

3.3 Rogowski Coil Theory

Consider the toroidal Rogowski coil , in figure 3.3.1 , which has a total of N minor turns each with cross-sectional area S and assume :

i. The magnetic flux density B is constant over the whole of the section S.

ii. The coil is uniformly wound such that the winding density N/l is constant.

iii. Each turn is normal to the magnetic field vector H.

Any time varying magnetic field, established by a current i_p threading the loop aperture, will link with the minor turns of the loop and induce an e.m.f. given by :

$$e = N.\frac{d\phi}{dt} \qquad \ldots.(3.1)$$

which can be shown from the Biot-Savart law to be :

$$e = \mu_0.\mu_r.\frac{N.S.di_p}{l \quad dt}$$

where $\mu_0.\mu_r.N.S/l$ is the mutual inductance of the closed loop , from

which,

$$e = M.\frac{di_p}{dt} \qquad \ldots.(3.2)$$

This equation shows that the voltage induced in the coil is the time derivative of the current i_p being monitored. Some integration process is therefore required to obtain a signal which is proportional to the current .

Let the coil be terminated by loading resistance R for which an equivalent circuit is shown in figure 3.3.2 .

An induced voltage e(t) will drive a coil current i_p (t) through the self inductance L and coil resistance R_o of the loop and develop a voltage v_m (t) across the burden resistance R . The circuit neglects the effective stray capacitance shunting R from subsequent signal processing circuitry.

A differential equation can be written from Kirchoff's voltage law which describes the circuit behaviour given by ;

$$e(t) = v_i(t) + v_m(t)$$

which is ,

$$M.\frac{di_p}{dt} = L.\frac{di_s}{dt} + i_s.(R + R_o) \qquad \ldots.(3.3)$$

From this equation it may be seen that, depending on the relative magnitudes of the voltages $v_i(t)$ and $v_m(t)$ and hence on the respective values of inductive reactance and circuit resistance, the coil current $i_s(t)$ can be made proportional either to the driving current $i_p(t)$ or to its time derivative di_p/dt.

If, first of all, the coil reactance dominates the circuit impedance, hence voltage distribution, then $\omega L \gg (R + R_o)$ and we can assume that $i_s.(R + R_o) = 0$. This results in the expression :

$$M.\frac{di_p}{dt} = L.\frac{di_s}{dt}$$

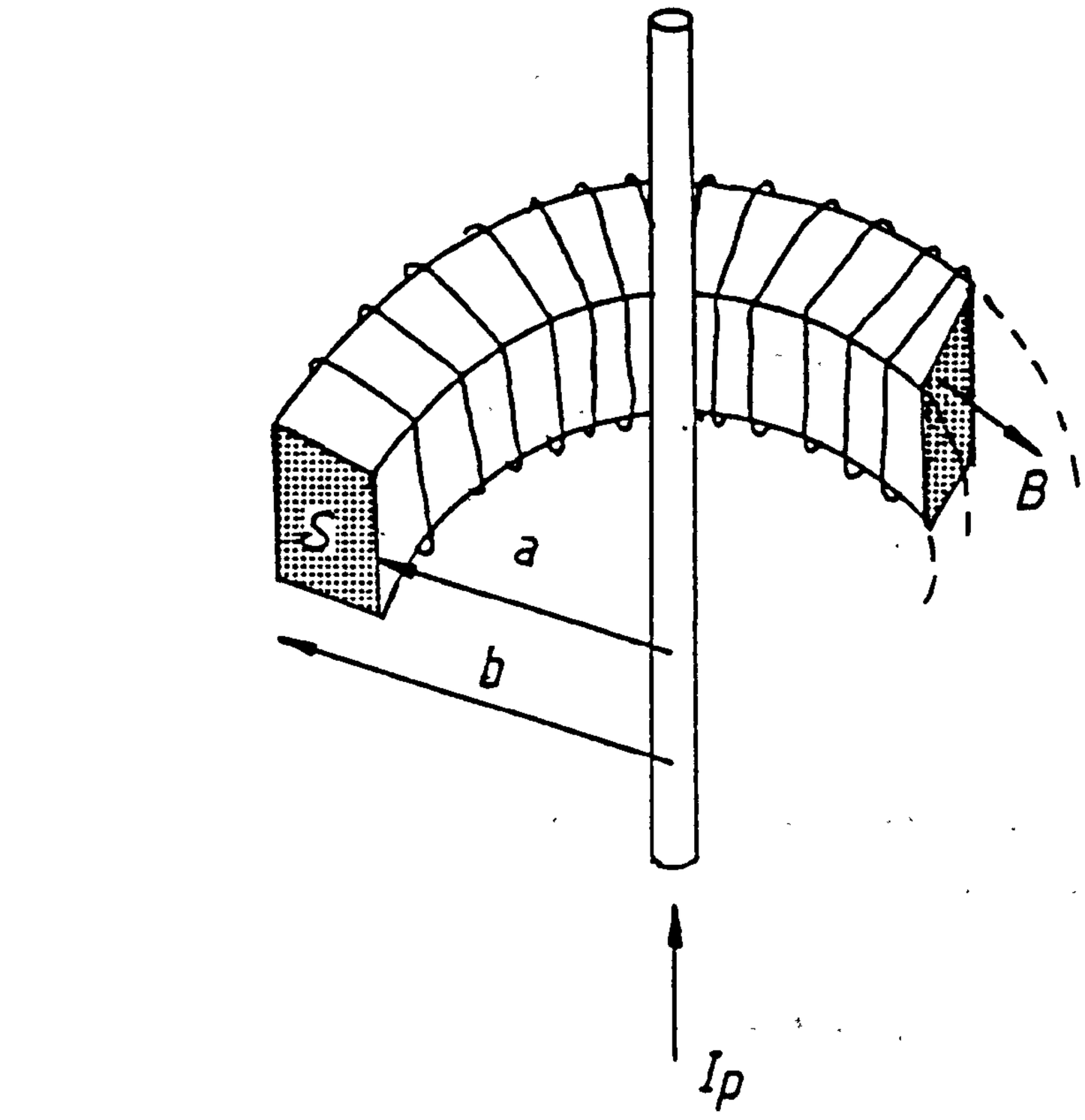

Figure 3.3.1 - Rogowski Coil

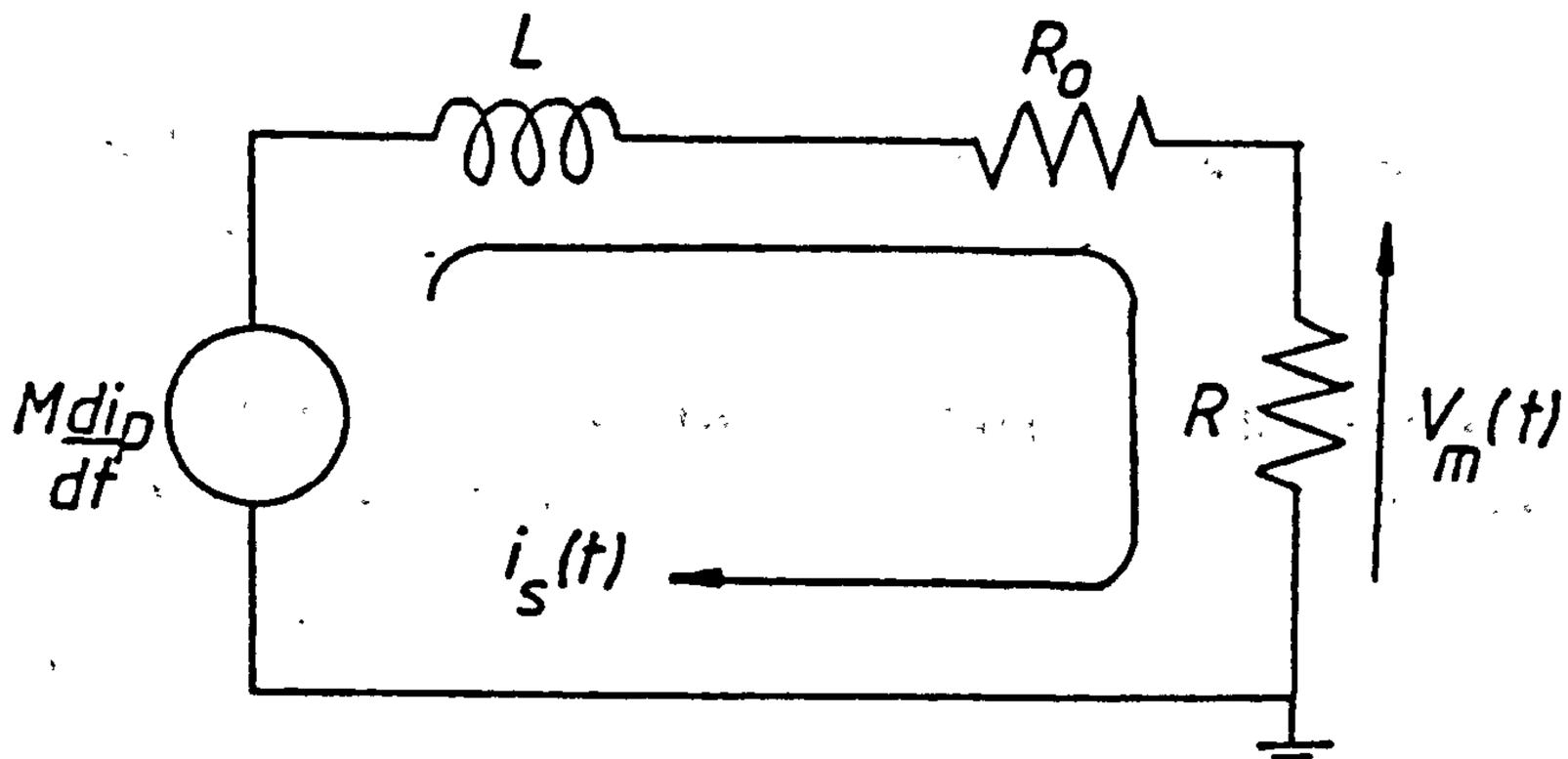

Figure 3.3.2 - Rogowski Coil Equivalent Circuit

which on integrating w.r.t. time becomes :

$$M.i_p(t) = L.i_s(t)$$

Since the self inductance of the coil is $L = \mu_0 .\mu_r .N.S./l$, and a similar expression exists for M, then it follows, to a good approximation, that :

$$i_s(t) = \frac{i_p(t)}{N} \qquad \ldots.(3.4)$$

This represents the basic relationship between the primary and secondary currents in a current transformer with a 1:N turns ratio.

The resultant voltage across the load resistor R becomes :

$$v_m(t) = i_s(t).R$$

and so ,

$$v_m(t) = i_p(t).\frac{R}{N} \qquad \ldots.(3.5)$$

Thus, the measured voltage $v_m(t)$ is made proportional to the monitored current $i_p(t)$ through the turns ratio and the load resistance value.

This particular mode of operation is associated with a 'Self Integrating' Rogowski coil.

If, on the other hand, the load resistor is large and dominates the circuit impedance, then , $(R + R_0) \gg \omega L$, and it can be assumed that,

$$L.\frac{di_s}{dt} = 0$$

from which ,

$$M.\frac{di_p(t)}{dt} = i_s(t).(R + R_0)$$

This results in an expression for $v_m(t)$,

$$v_m(t) = M.\frac{di_p(t)}{dt} \qquad \ldots.(3.6)$$

The voltage $v_m(t)$ is therefore equal to the induced voltage e(t) and is proportional to the time derivative of the current $i_p(t)$.

In this mode of operation the coil is termed a 'Differentiating' Rogowski coil.

Although this simple analysis of the Rogowski coil behaviour indicates that two distinct modes of operation exist; differentiating and self integrating , in practice, the category into which one places a particular coil configuration depends on the coil circuit parameters (R, R_o , and L) and on the duration of the pulse . This statement is best illustrated by a discussion of the coil's response to a rectangular pulse with an instantaneous rise time.

Consider the equivalent circuit of the Rogowski coil and load in which each element is replaced by its Laplace transform representation.

The corresponding circuit equation is given by :

$$E(s) = sM.I_p(s) = sL.I_s(s) + I_s(s).(R + R_o)$$

however, $V_m(s) = I_s(s).R$ and so,

$$\frac{V_m(s)}{I_p(s)} = \frac{sM.R}{sL + (R + R_o)} \qquad \ldots.(3.7)$$

is obtained, which is the transfer function of the coil.

Applying a step in the primary current $I_p(s) = I_p/s$, and deriving the time domain solution , the response of the coil is found to be :

$$v_m(t) = I_p.\frac{R}{N}.\exp(-R.t/L) \qquad \ldots.(3.8)$$

True differentiation of a step function results in an impulse (Dirac - delta) function with the same amplitude as the step . However, the

response of the Rogowski coil only approximates to this case with an exponentially decaying pulse, the shorter the time constant $L/(R + R_0)$, the closer the approximation to an impulse.

On the other hand, if the time constant of the coil is large in comparison to the duration of the applied step the response will be an approximate reproduction of the pulse with a degree of pulse 'tilt'. These properties are demonstrated in the photographs of oscilloscope traces in figure 3.3.3 .

The traces show the response of a Rogowski coil with self inductance $L = 50\,\mu H$ and load resistance $R = 50\Omega$ to a primary current pulse of $1.5\,\mu sec$ duration .

3.3.1 Frequency Response

The response of the Rogowski coil to a step function reveals that the device has a poorer response at lower frequencies, as predicted .

The frequency domain transfer function of the Rogowski coil is obtained from the circuit equation (3.7) by the substitution $s = j\omega$ to give :

$$|Z(\omega)| = \frac{V_m(\omega)}{I_p(\omega)} = \frac{j\omega.M.R}{j\omega L + (R + R_0)}$$

The transfer function $|Z(\omega)|$ may then be expressed in decibels by,

$$|Z(\omega)| = \frac{R/N}{(1 + (\omega_0/\omega)^2)^{1/2}} \qquad ....(3.9)$$

From this expression it follows that the amplitude response $|Z(\omega)|$ falls with decreasing frequency at a rate of - 20db per decade . At the frequency where the coil reactance equals the loop resistance there is a - 3db drop from the constant midband value of gain $|Z(\omega)|$ which is R/N, see figure 3.3.1.1 . In terms of time domain response, this corresponds to a 'sag' or 'tilt' in the coils response to a rectangular pulse i_p given by the expression :

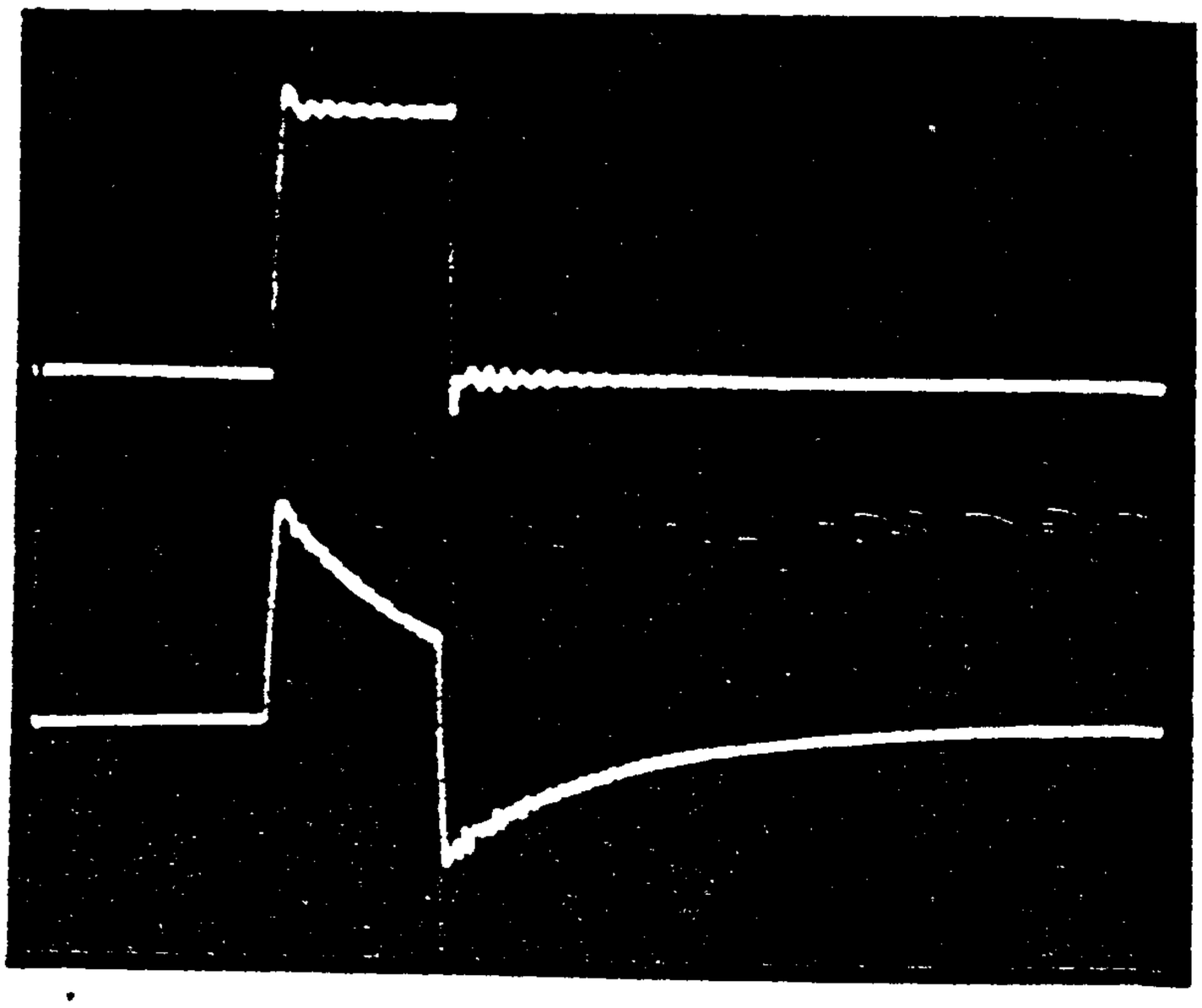

Figure 3.3.3 - Pulse Tilt in Rogowski Coil Response

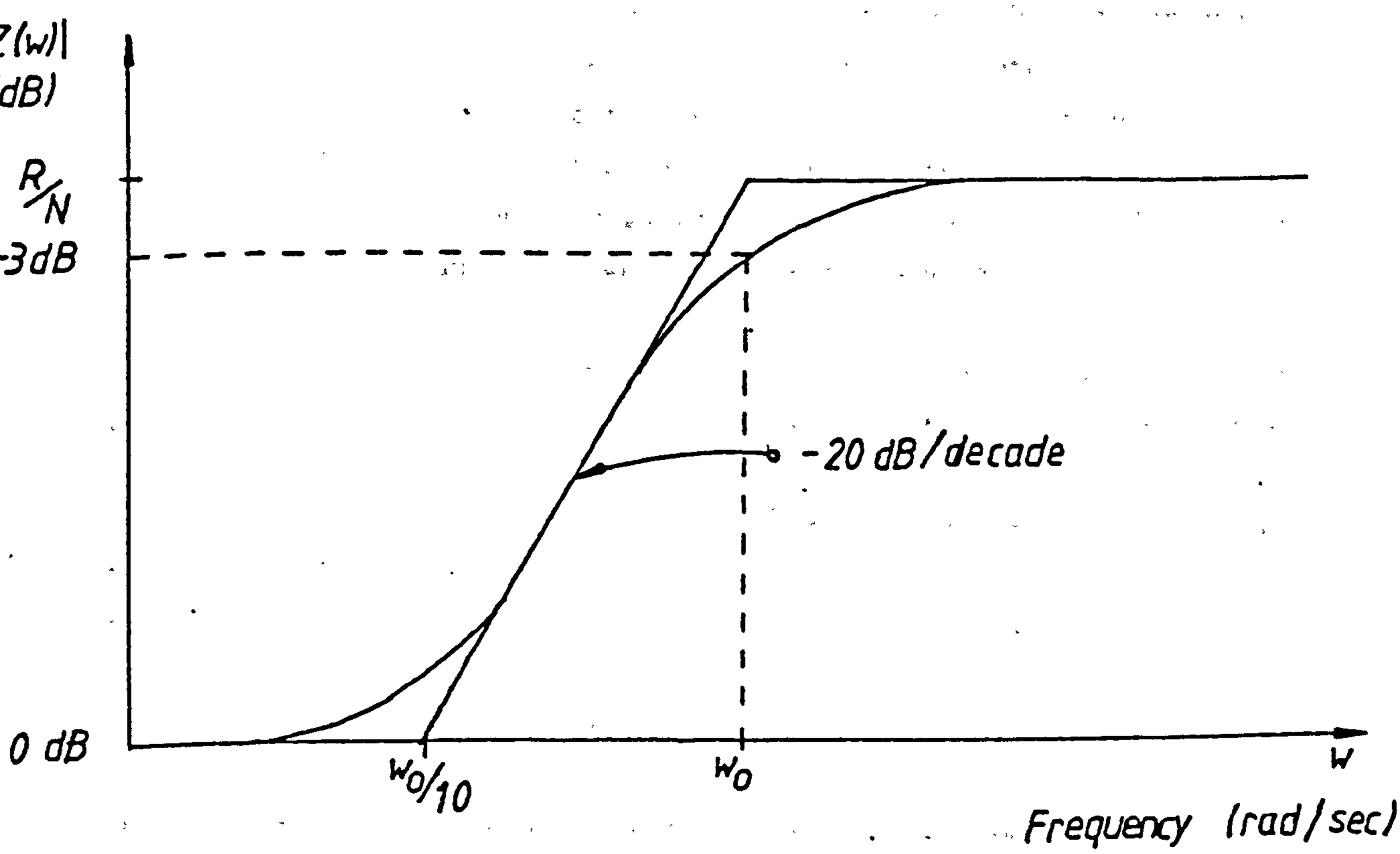

Figure 3.3.1.1 - Frequency Response of Rogowski Coil

$$\% \text{ tilt} = \frac{R.t_p}{L} \times 100$$

where t_p is the width of the input pulse . This is typical of the behaviour of a high pass filter circuit.

The high frequency cut-off region is difficult to define since stray capacitances and inductances can result in spurious resonances before reaching the cut-off frequency. These unwanted signals are normally eliminated by placing the Rogowski coil in a metallic shield.

3.4 Shielding the Rogowski Coil

The Rogowski coil is normally encased in a metallic shield which is connected to earth potential for two reasons which are discussed here.

3.4.1 Electrostatic Coupling

Voltage fluctuations on conductors in the region of the Rogowski coil cause variations in the local electric field . These interference voltages are coupled into the coil circuit via the mutual capacitances that link the neighbouring circuits, giving rise to currents flowing in the coil in addition to the main induced current. Diagram 3.4.1 shows these interference signals electrostatically coupled from the primary current conductor as well as external sources.

To prevent capacitive coupling of signals, the coil is situated in a metallic housing which is connected to earth potential thus providing a path for unwanted signals to earth. The electrostatic shield must allow magnetic flux associated with the primary current to link with the coil and this is achieved by incorporating a continuous slit in the shield wall, (see figure 3.4.2) .

3.4.2 Transmission Line Behaviour

When the toroidal Rogowski coil is placed in a conductive shield, a the coil has a uniformly distributed capacitance to the shield which; for fast rise time primary current pulses, makes the coil behave like a transmission line, so that signals induced in the winding take a finite time to propagate to the coil terminations .

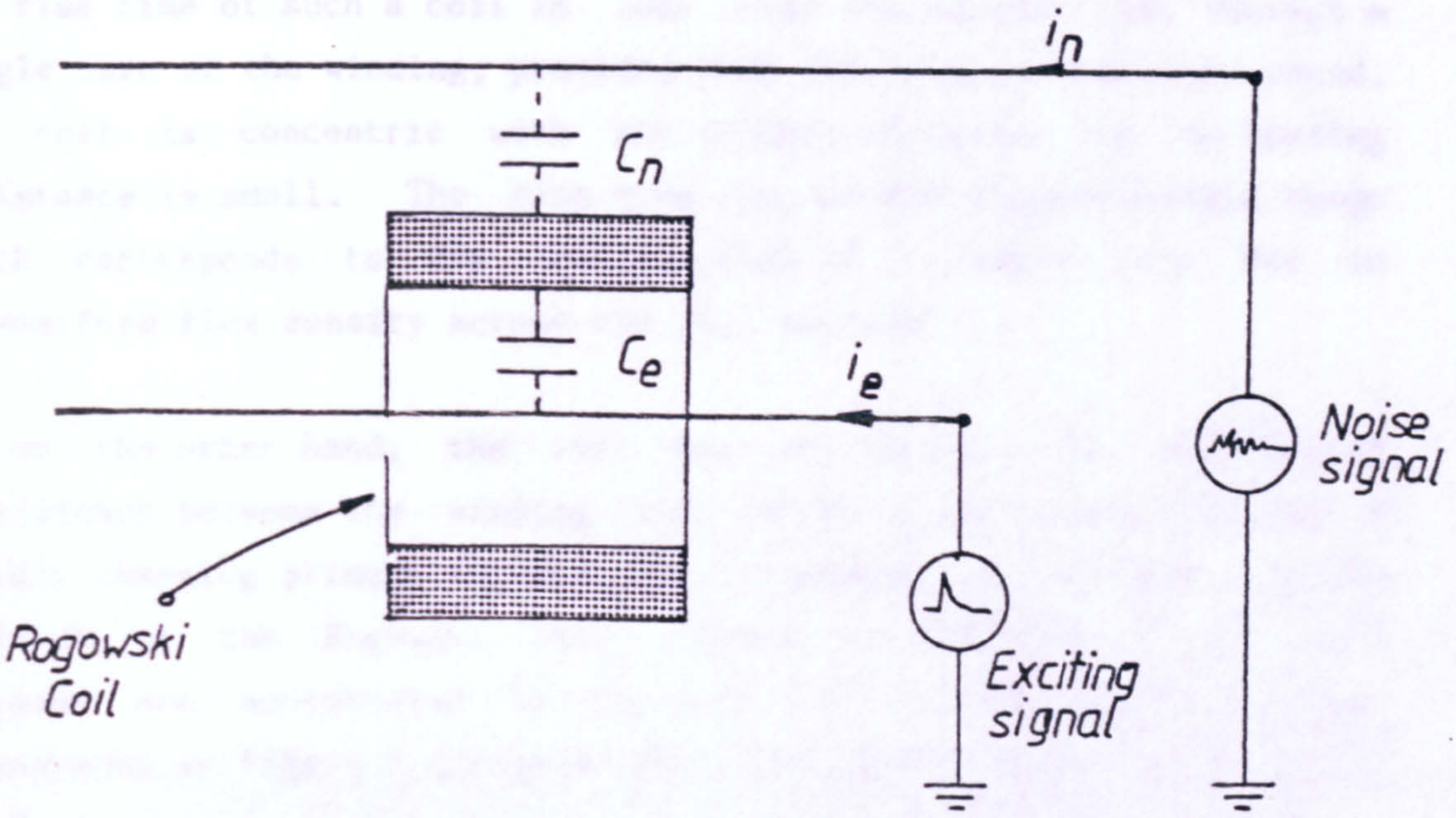

Figure 3.4.1 - Electrostatic Coupling

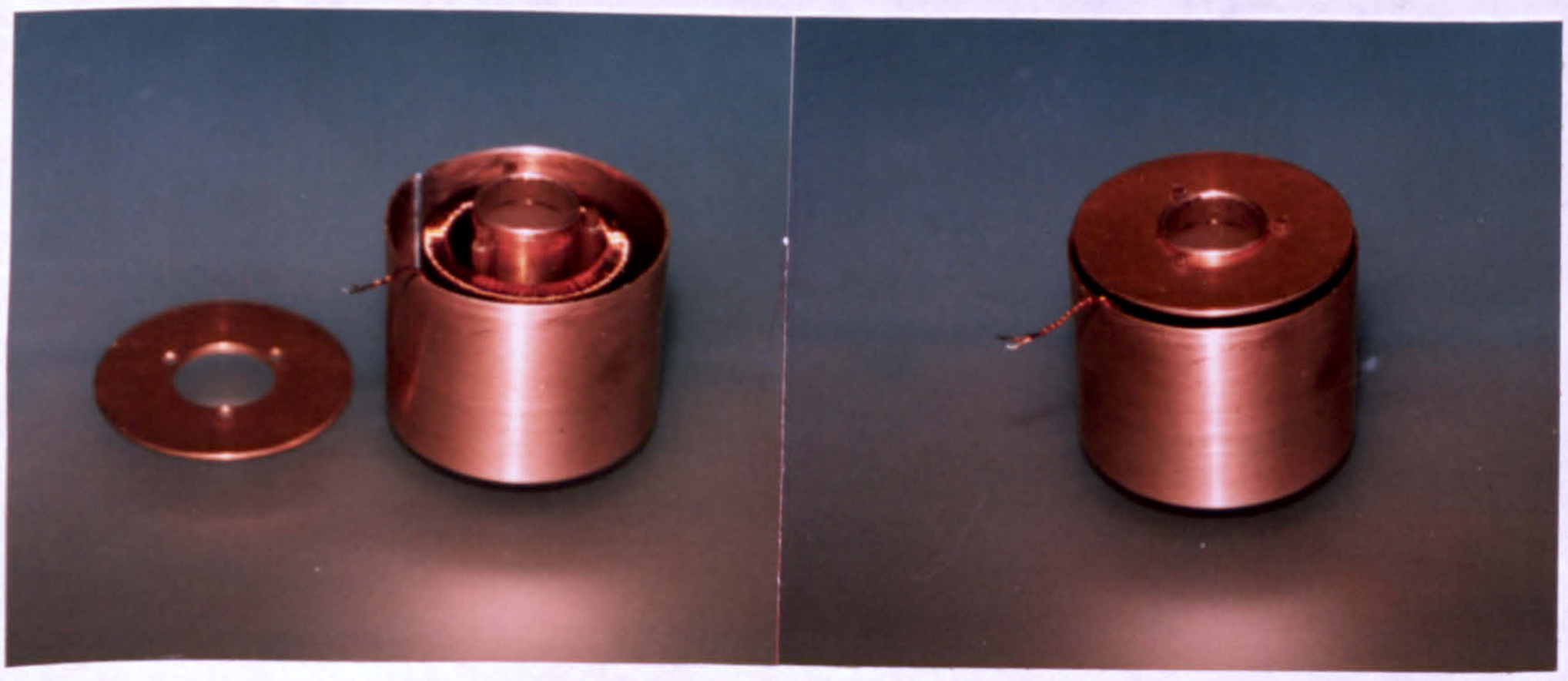

Figure 3.4.2 - Shielded Rogowski Coil

The rise time of such a coil is less than the transit time through a single turn of the winding, provided that the coil is uniformly wound, the coil is concentric with the primary conductor and the loading resistance is small. The rise time is in the sub-nanosecond range which corresponds to the response time of a single turn due to non-uniform flux density across the coil section .

If on the other hand, the coil has no shield, the distributed capacitance between the winding and earth is non-uniform so that a rapidly changing primary voltage causes transient oscillations in the response of the Rogowski coil. These oscillations in the coil response are accentuated if the coil is asymmetrically excited. Photographs in figure 3.4.3 show this behaviour in the coil output waveform.

A more detailed analysis of the high frequency response of the Rogowski coil may be found in references [83,84,85] .

3.5 Wideband Current Measurement

For truly wideband current measurement the Rogowski coil must faithfully pass all frequency components in the monitored pulse with equal amplitude and phase properties , at both high and low frequencies such that fast rising edges and wide pulses are reproduced accurately in the analogue voltage signal $v_m(t)$. These requirements can be met by both the differentiating and the self integrating Rogowski coil with certain constraints.

3.5.1 Differentiating Rogowski Coil

It is possible to use a differentiating coil as a wideband current monitoring device if an integration is performed on the output signal. The integrator can be a passive RC circuit or an active circuit . However, practical difficulties arise in the implementation of such a system and these are outlined as follows :

i. Active integration ;

Amplifier drift due to an offset input signal results in errors in the integrated signal.

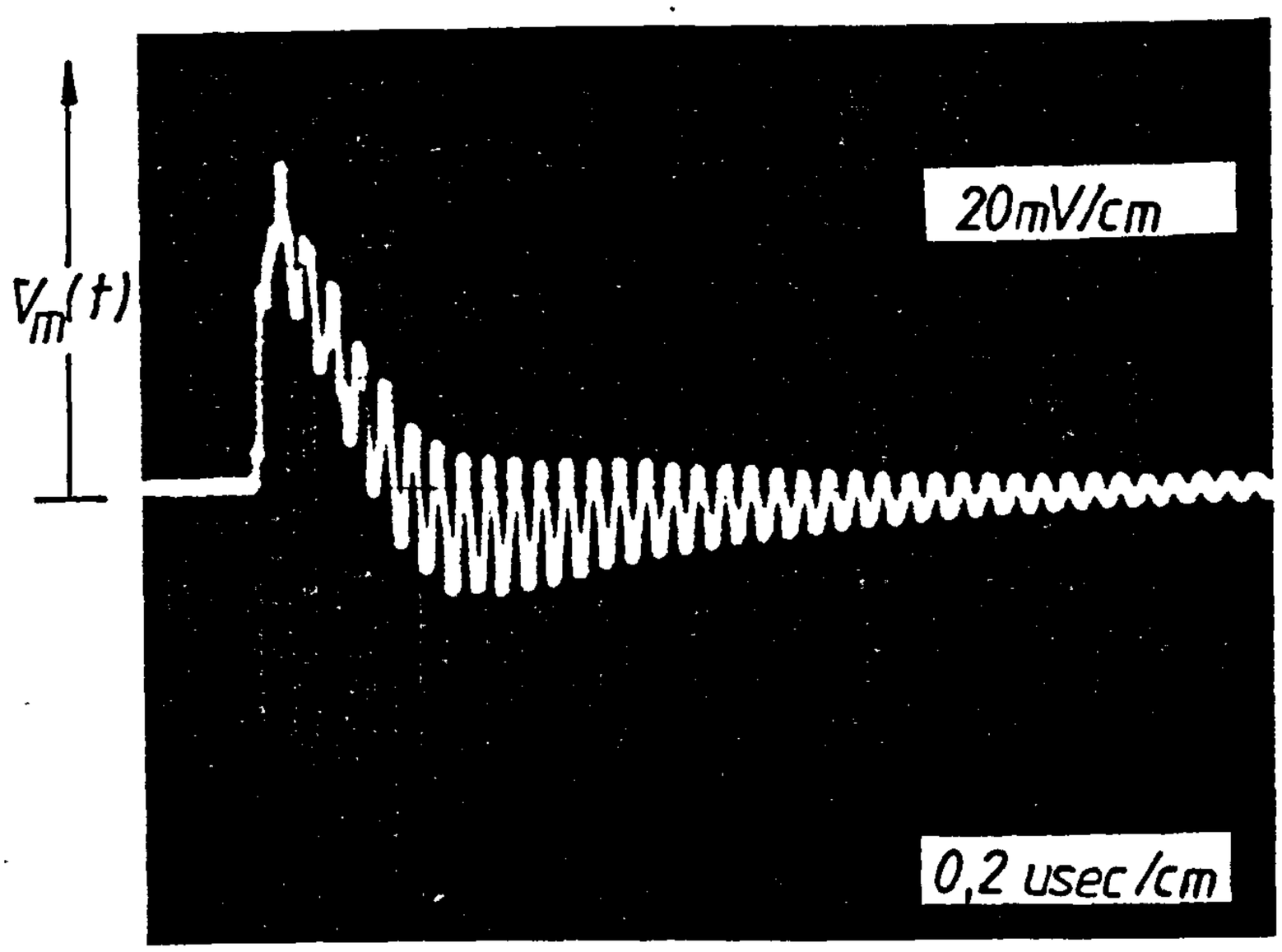

Figure 3.4.3 - Response of Rogowski Coil with
No Electrostatic Shield

ii. Passive integration ;

This method suffers from very low sensitivity due to attenuation from the high resistance and capacitance values required in the integrator.

Another problem common to both systems is in the choice of load resistance across the coil since any stray capacitance shunting the resistor will eventually dominate the load impedance and place a restriction on the upper limit in load resistance value, and hence maximum signal level.

3.5.2 Self Integrating Rogowski Coil

From experience the self integrating coil is the simplest to implement and is very suitable for monitoring rapid events . A full analysis of its behaviour is therefore presented in the following section , with a special emphasis on the characteristics which make the self integrating coil useful in partial discharge studies.

3.6 Partial Discharge Measurements

Partial discharges give rise to rapid movements of charge within an associated electrical circuit. Discharges are detected by monitoring the current pulses that originate from the discharge site. These pulses are ideally exponential decays having rise times less than a few nanoseconds and fall times ranging from a few nanoseconds to tens of microseconds . A Rogowski coil can be designed to have a frequency response characteristic appropriate to the measurement of such pulses.

3.6.1 Response of Self Integrating Coil to a Discharge Pulse

It is beneficial to know the exact transient response of a self integrating coil to a typical discharge signal for the purpose of extracting meaningful information as well as establishing confidence in the ability of the coil to process correctly such signals.

A decaying exponential pulse is taken as fairly representative of most real discharge current pulses. Simulation of different discharge mechanisms is achieved by varying the amplitude and the decay time of

this type of pulse.

Experiments were performed on a test circuit utilising a squarewave pulse generator to drive an RC network to simulate a discharge pulse as shown in figure 3.6.1.1 .

The pulse generator also had a facility to change the pulse rise time, and the pulse decay time was controlled by the circuit time constant, determined by the values of resistance R and capacitance C.

The typical response of a self integrating Rogowski coil with a 1 usec time constant, (L = 50 μH and R = 50Ω), to an exponential pulse with a time constant of 75 nsec is shown in the oscilloscope trace in figure 3.6.1.2. This demonstrates the negative 'dip' that occurs on the response when driven by a current pulse with a decay time much less than the time constant, $L/(R + R_0)$, of the Rogowski circuit.

This property of the response is derived theoretically from the time domain solution of the Rogowski coil equivalent circuit voltage equation (3.3) excited by a function of the form :

$$i_p(t) = I_p.\exp(-t/T_1) \qquad ....(3.10)$$

where T_1 is the time constant of the simulated discharge pulse and T_2 is the time constant of the coil.

The solution for the output voltage $v_m(t)$ is given by :

$$v_m(t) = I_p.\frac{R}{N}\left[\frac{-\exp(-t/T_1)}{(T_1/T_2-1)} - \frac{\exp(-t/T_2)}{(T_2/T_1-1)}\right] \qquad ....(3.11)$$

$$T_1 \neq T_2$$

Examination of equation (3.11) shows that the output voltage has two exponential components. The first component is dependent on the pulse time constant, and the second, on the coil self inductance and burden resistance.

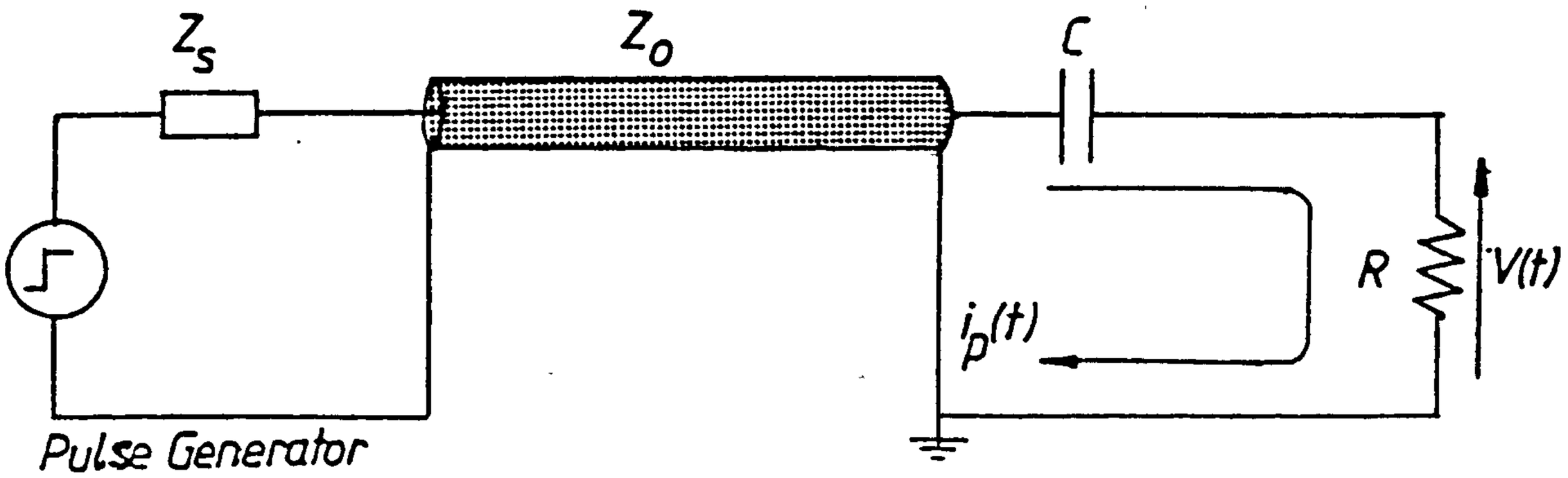

Figure 3.6.1.1 - Discharge Simulation Circuit

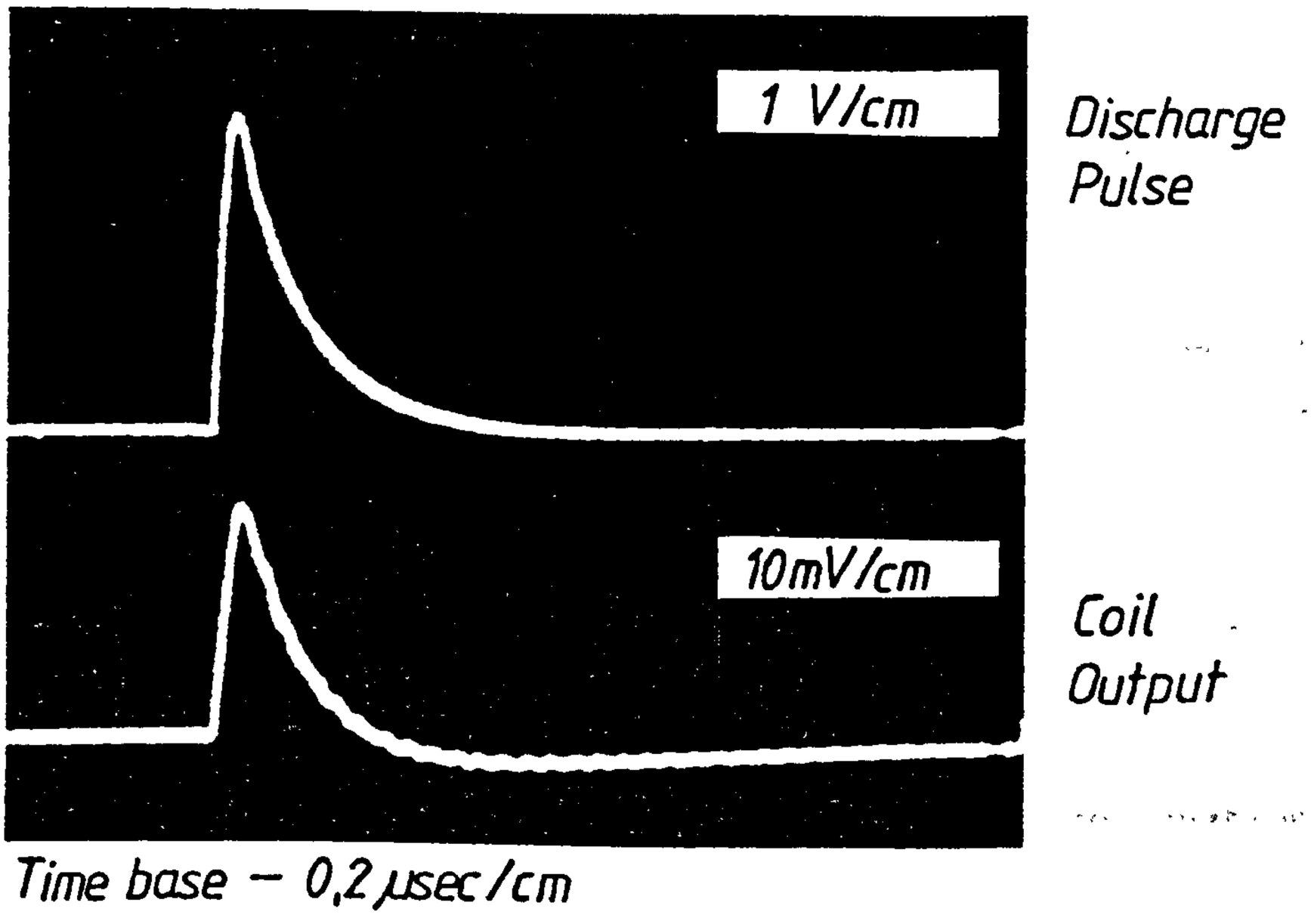

Figure 3.6.1.2 - Response of Rogowski Coil to Typical Discharge Pulse

If the condition when $T_2 \gg T_1$ is examined it can be seen that $(T_1/T_2-1) = -1$ and $(T_2/T_1-1) = T_2/T_1$ so that the second term is negligible and the expression reduces to :

$$v_m(t) = I_p.\frac{R}{N}.\exp(-t/T_1) = i_p(t).\frac{R}{N}$$

which is a direct analogue of the measured signal.

When the original pulse $I_p.\exp(-t/T_1)$ is compared with the coil waveform it is seen that the output signal $v_m(t)$ differs in magnitude and time constant. The coil response to the artificial discharge pulse is characterised by reduced amplitude , more rapid decay and negative overshoot .

These properties are displayed in the graph of the coil's response as a function of the ratio the pulse and coil time constants T_2/T_1,(see figure 3.6.1.3) .

The zero crossing point, t_0, is calculated by equating the expression (3.11) to zero. The result for $T_1 \neq T_2$ is given by ,

$$t_o = \frac{T_1.T_2.}{(T_1-T_2)} \ln\left[\frac{-(T_1/T_2-1)}{(T_2/T_1-1)}\right] \quad \ldots.(3.12)$$

Similarily the point of the negative minimum is obtained by differentiating equation (3.11) and equating the result to zero from which, for $T_1 \neq T_2$,

$$t_{min} = \frac{T_1.T_2.}{(T_1-T_2)} \ln\left[\frac{-T_1.(T_1/T_2-1)}{T_2.(T_2/T_1-1)}\right] \quad \ldots.(3.13)$$

The negative overshoot is then found by substitution into equation (3.11) .

The design of a self integrating coil for a particular application is achieved by the use of equations 3.11, 3.12, and 3.13 .

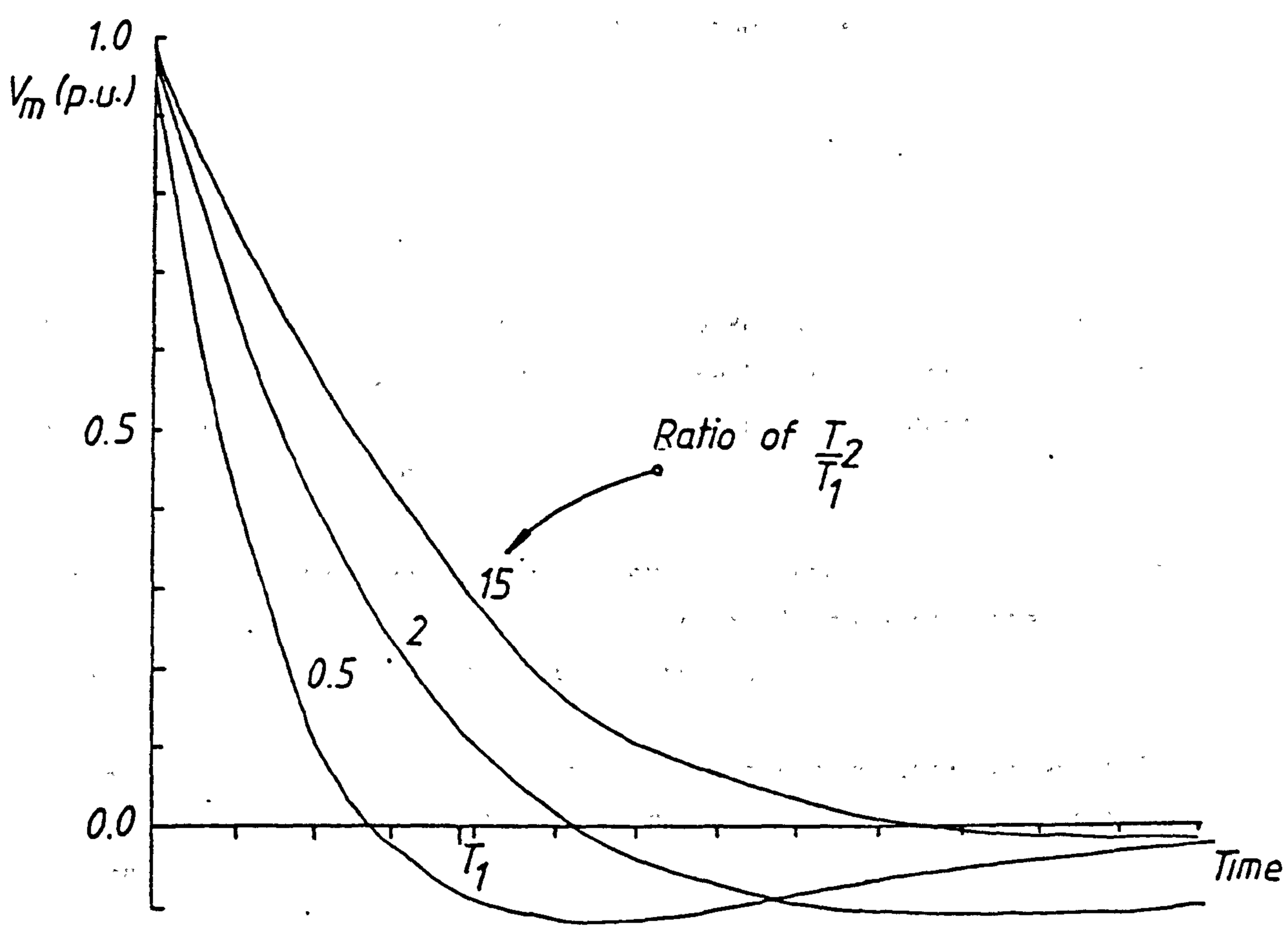

Figure 3.6.1.3 - Theoretical Response of Rogowski Coil

3.6.2 Charge Measurement with the Rogowski Coil

Modern discharge detection techniques invariably calibrate the magnitudes of detected pulses in terms of picocoulombs of charge since this is independent of the actual discharge current pulse shape . It is also reasonable to expect that damage to the insulation is related to the quantity of charge transferred in the discharge.

In wideband detection systems the charge content, q , is found by integrating the current signal $i_p(t)$ in the manner :

$$q_c = \int_0^t i_p(t).dt$$

This is achieved with a self integrating Rogowski coil by integrating the voltage signal $v_m(t)$ with a passive RC integrator circuit which has a time constant T_i , much greater than the duration of the discharge current pulse .

Consider the charge measurement scheme in figure 3.6.2.1 in which the output signal $v_m(t)$ is coupled via a coaxial cable from the point of measurement to a passive integrator circuit.

Assuming $v_m(t)$ is a true analogue of the discharge current pulse $i_p(t)$, and that the integrator has a high enough input impedance to ignore loading effects then ,

$$U(t) = \frac{1}{R_i.C_i} \int_0^{t'} v_m(t).dt$$

where t' is the pulse duration . However,

$$v_m(t) = i_p(t).\frac{R}{N}$$

$$U(t) = \frac{R}{N.R_i.C_i} \int_0^t i_p(t).dt$$

The output voltage of the integrator is therefore proportional to the charge contained in the pulse q_c . The charge q_c is given by the peak value of the output voltage U(t),so that :

$$q_c = U_{peak}(t)$$

Typical waveforms of the current pulse signal $v_m(t)$ and the corresponding output signal U(t) of the integrator circuit to an exponential type discharge pulse are shown in figure 3.6.2.2 . The peak value of U(t) gives the charge contained in the discharge pulse which is the area under the pulse $v_m(t)$.

3.7 Practical Design of a Wideband Rogowski Coil

The Rogowski coil is very simple to construct since any suitable non-magnetic material can be used to form the core . In the design used in this study , enamelled copper wire is wound on to a synthetic resin-bonded paper tube to form the coil which is then enclosed in a copper shield. The leads extending from the coil ends are twisted to cancel any stray field components which might couple unwanted signals into the coil circuit. Alternatively, a thin coaxial cable may be connected to the coil ends very close to the winding.

The parameters used to design a Rogowski coil for a particular application are discussed in the following sections .

3.7.1 Calculation of Self and Mutual Inductance

Owing to the simple geometry of the coil, expressions for self and mutual inductance of the toroid may be developed which form useful design parameters.

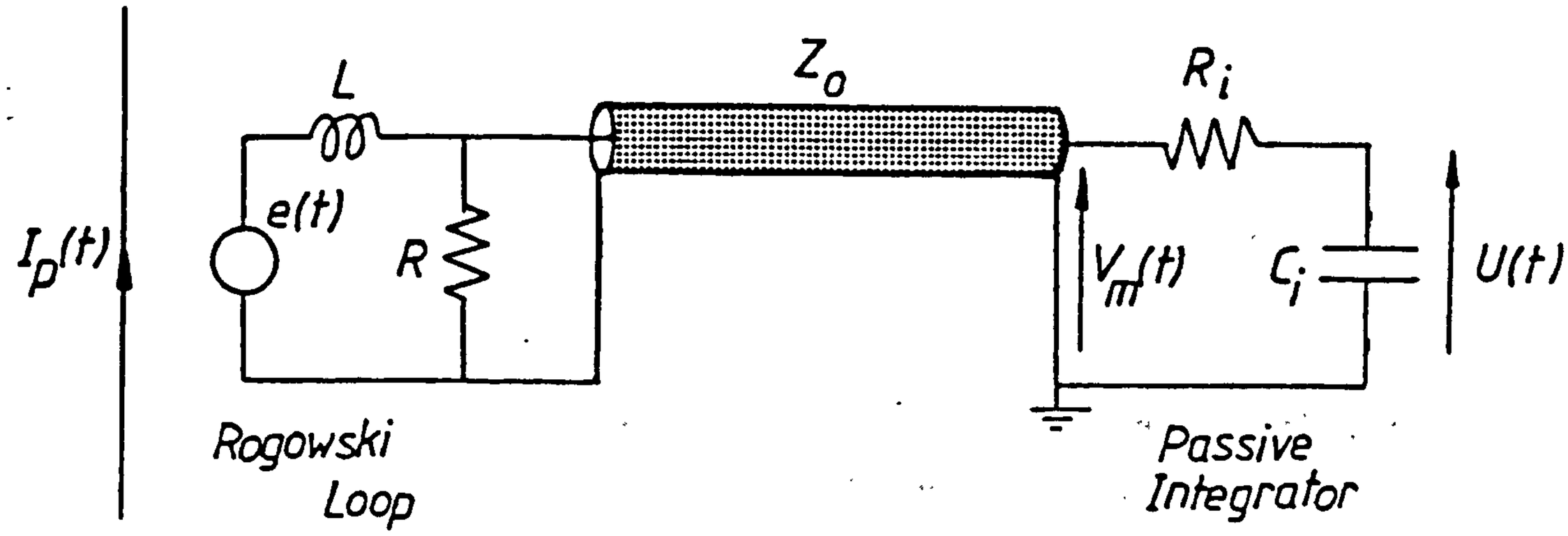

Figure 3.6.2.1 - Charge Measurement Circuit

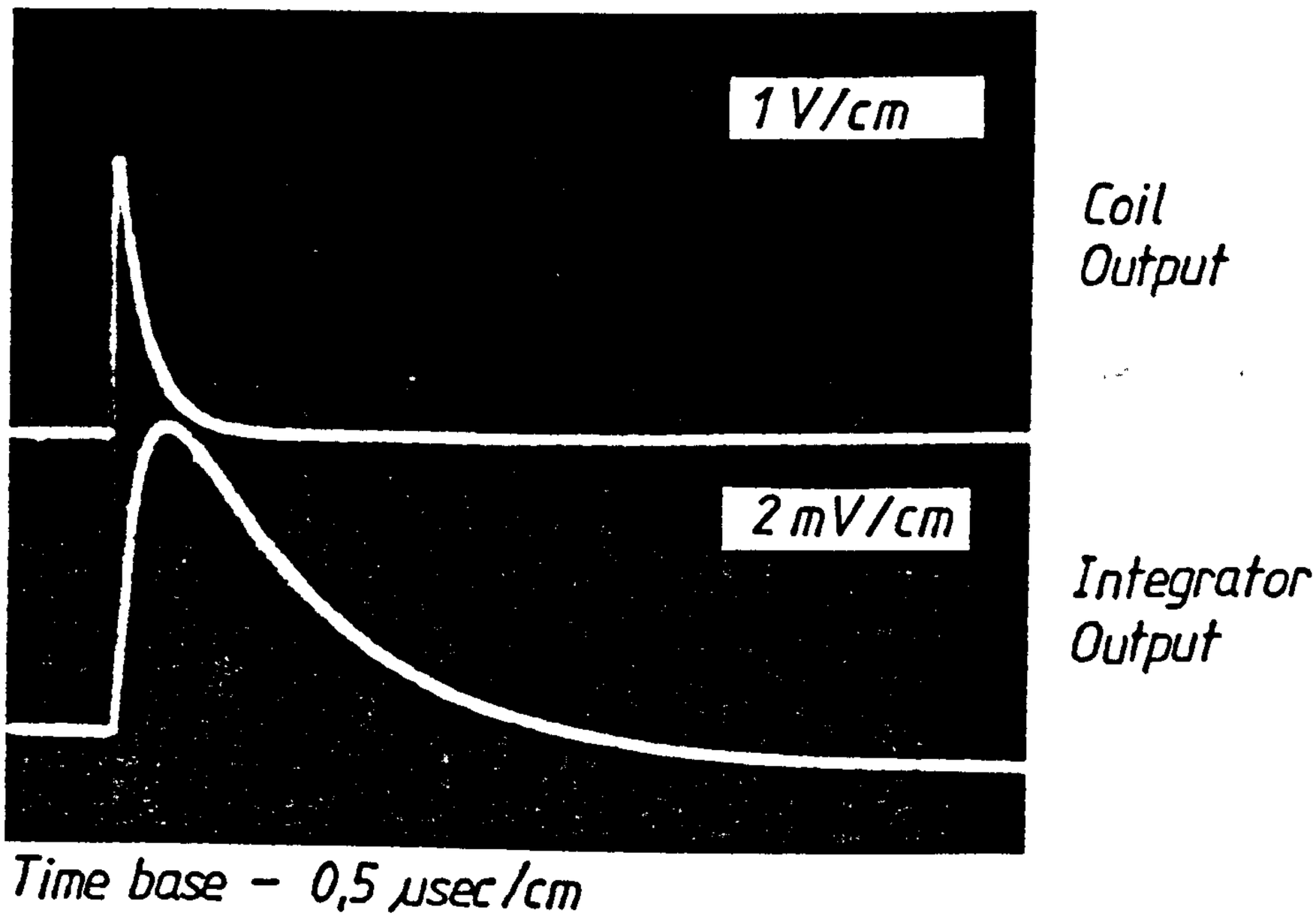

Figure 3.6.2.2 - Charge and Current Pulse Waveforms

The general expression for the self inductance is :

$$L = \frac{N.\phi}{i} \qquad \ldots.(3.14)$$

which is the magnetic flux , ϕ , per unit current i, linking N turns of the conductor.

If an elemental annulus with infinitesimally small width ,dr, is considered the field strength may be obtained from Amperes law ,

$$\oint dH.dl = N.I$$

thus,

$$H = \frac{N.I}{2\pi r}$$

therefore the flux density must be ,

$$B = \mu_0\mu_r\frac{N.I}{2\pi r} \qquad \ldots.(3.15)$$

The flux passing through the elemental section is :

$$d\phi = \mu_0\mu_r\frac{N.I.1.dr}{2\pi r}$$

The total flux in the coil is found by integrating $d\phi$ between the limits r = a and r = b which is :

$$= \mu_0\mu_r\frac{N.I}{2\pi}.1\int_a^b \frac{dr}{r}$$

$$= \frac{2.N.I.1.}{10^7}\ln(b/a)$$

Substituting this result into the expression (3.14), the equation for

the self inductance of the toroid is given by :

$$L = \frac{2.N^2.l}{10^7} \ln(b/a) \qquad \ldots.(3.16)$$

The mutual inductance is given by :

$$M = \frac{N_2.\phi_2}{I_1}$$

but since there is no leakage flux perfect coupling dictates that

$$N_1.I_1 = N_2.I_2$$

from which,

$$M = \frac{N_2.\phi_2.N_1}{I_2\ N_2} = L.\frac{N_1}{N_2}$$

The mutual inductance is simply the self inductance divided by the turns ratio N_1/N_2 and is therefore :

$$M = \frac{2.N.l}{10^7} \ln(b/a) \qquad \ldots.(3.17)$$

3.7.2 Decay Time Constant

The time constant of the coil is crucial in the measurement of fast current pulses since it has been shown that it determines the maximum signal pulse duration without pulse tilt . In most cases it may be calculated quite accurately from the relationship :

$$T = \frac{L}{(R + R_0)} = \frac{2.N.l}{(R + R_0).10^7} \ln(b/a)$$

provided the load resistance is much larger than the coil resistance. However, in the situation in which coil size is limited, limiting the self inductance L value, and a good low frequency response is desired, the load resistance may be of the order of the coil resistance or less. This necessitates calculation of the effective

coil resistance at frequencies at which the current flow is restricted to a layer at the surface of the conductor due to skin effect . The depth of this layer is frequency dependent and is given by the expression at a frequency f :

$$S = \frac{1}{\sqrt{\sigma.\pi.\mu.f}} \qquad \sigma \text{ - conductivity } (\Omega^{-1}m^{-1})$$

If the winding conductor is regarded as a planar slab of material of uniform dimensions, a depth of S, and assuming negligible interaction between adjacent coil turns, the effective coil resistance is expressed as :

$$R = \frac{\text{length of slab}}{\text{conductivity x cross sectional area}}$$

$$= \frac{L}{2.\sigma.\pi.r.S}$$

$$= \frac{N.(1 + (b-a))}{\sigma.\pi.r.S} \qquad \ldots.(3.18)$$

If the pitch of the winding is small then an additional increase in the effective coil resistance will occur from an eddy current modification of the current density distribution in one turn due to the magnetic fields established by neighbouring turns - proximity effect . A full treatment of the calculation and measurement of coil resistance is supplied in reference [87] .

3.7.3 Power Frequency Sensitivity

A prerequisite for on-line partial discharge detection systems , is the ability to attenuate power frequency related signals to sufficiently low levels to prevent unduly large signals entering sensitive low voltage circuits . The response of the self integrating Rogowski coil to low frequencies, power frequency and associated harmonic components, is discussed in this section .

Computation of the peak and r.m.s. magnitude of the power frequency and power harmonic signals can be obtained readily from the frequency domain transfer function of the coil,

$$V_m = I_p . |Z(\omega)|$$

$$= I_p . \frac{R/N}{(1 + (\omega_0/\omega)^2)^{1/2}}$$

In the design of a Rogowski coil it may be necessary to compromise between the requirement to reject power frequency related signals and that to capture the low frequency end of the pulse spectrum .

3.7.4 Design Parameters

The design parameters for one particular coil, (figure 3.3.1), are :

N	= 200 turns	R	= 50 Ω
a	= $11.25.10^{-3}$ m	R_i	= 15 kΩ
b	= $14.75.10^{-3}$ m	C_i	= 100 pF
l	= 21.10^{-3} m. (mean circumference of coil)		

These values with the equations in the earlier part of the chapter yield :

Parameter	Calculated	Measured
Self Inductance (L)	45.5 μH	45.8 μH
Time Constant (L/R)	0.89 μsec	0.85 μsec
Current Sensitivity (V_m/I_p)	0.312 mV/mA	0.309 mV/mA
Charge Sensitivity (U/q_c)		5.67 μV/pC
t_o	210.0 nsec	250.0 nsec
t_{min}	420.0 nsec	450.0 nsec

The simple geometry of the coil is such that calculated and measured performances are in very close agreement .

3.8 Narrowband Current Measurement

In certain instances it may be desirable to perform current measurements in a restricted bandwidth of signal frequencies. This is achieved with the aid of a Rogowski coil connected to an energy storage element , a capacitor, and a resistive damping element .

The response will be a damped oscillation in response to a current impulse, the frequency of oscillation being dependent on the reactive components,

$$f = \frac{1}{2\pi\sqrt{LC}}$$

This type of measurement has the advantages of greater sensitivity, in terms of output signal level for a given current pulse amplitude ,and freedom from spurious external and circuit resonances, (provided these exist at frequencies well above or below the centre frequency of the coil circuit) . The amplitude response depends essentially on the peak value of the primary current and not on pulse shape .

Narrowband current monitoring devices using Rogowski coils are simple to construct, and two circuit configurations may be adopted for this. The Rogowski coil may be connected as the inductive element in either a series or parallel resonant circuit , (see figure 3.8.1). Choice of which circuit to be used depends on the particular centre frequency desired, whether a high or low frequency. This is outlined in the following discussion.

The effect that stray capacitance, C_{sf}, has on each circuit determines which of the two configurations is to be adopted since the combination of C_{sf} and the fixed capacitance, C', along with the self inductance, L, of the loop , determines the resonant frequency.

In the parallel resonant circuit the total capacitance is given by :

$$C = C' + C_{sf} \quad :$$

C_{sf} will limit the lowest value of effective capacitance C and so place a restriction on the upper limit in resonant frequency . The

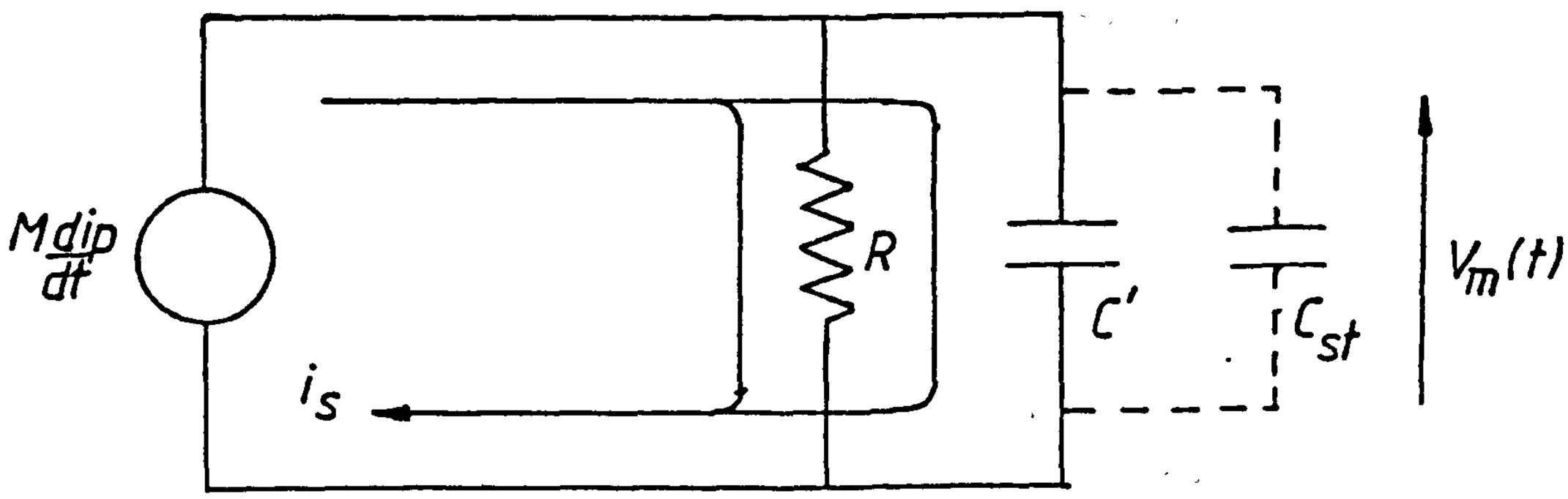

Parallel Circuit

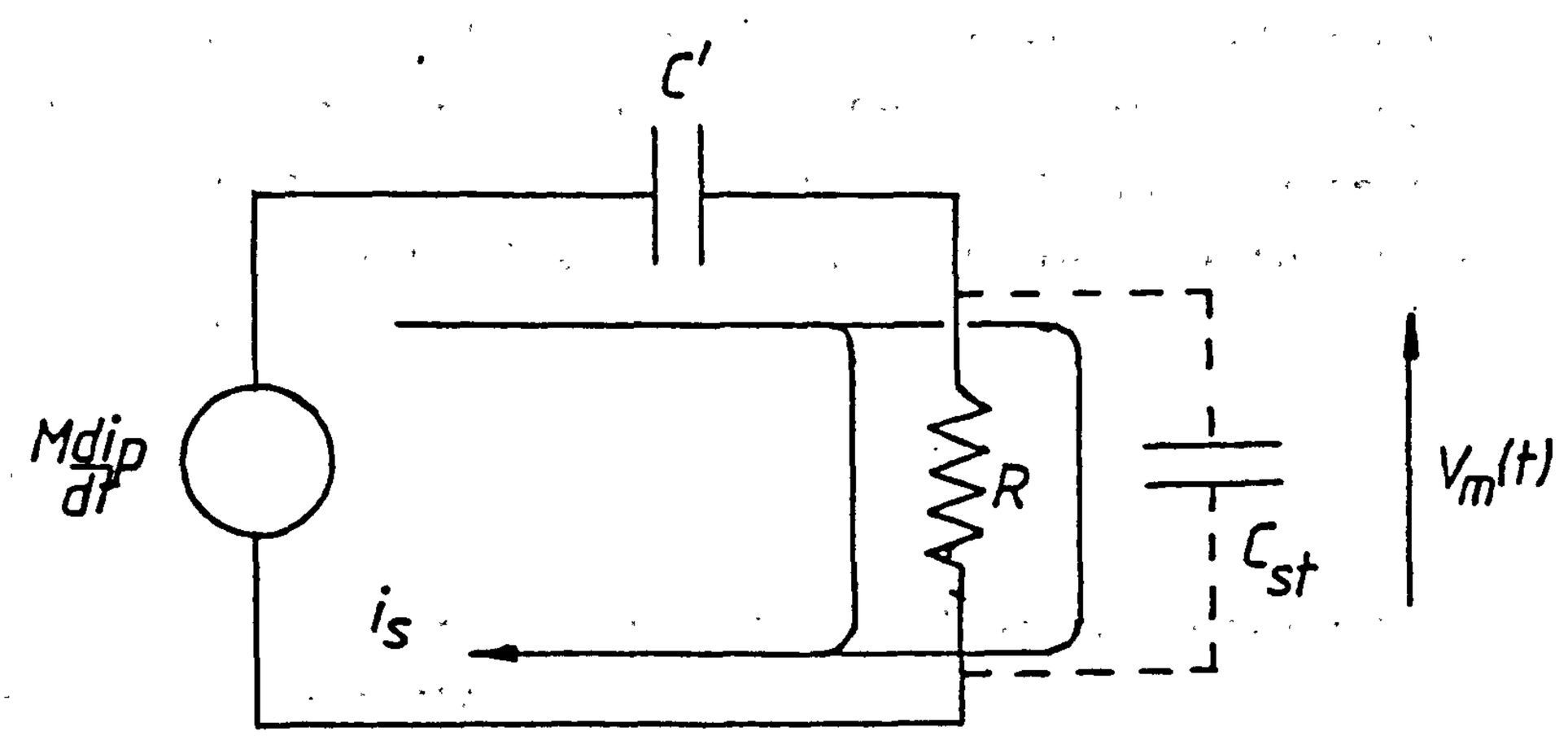

Series Circuit

Figure 3.8.1 - Parallel and Series Circuit Arrangements

parallel circuit is therefore most applicable to measurements at relatively low resonant frequencies.

The series resonant circuit on the other hand, has a total circuit capacitance of,

$$C = \frac{C'.C_{st}}{(C' + C_{st})} = \frac{C'}{(1 + C'/C_{st})}$$

It is seen from the equation above, that as the stray capacitance increases the denominator approaches unity and the total capacitance $C = C'$. The series configuration may therefore be used when a high centre frequency is desired without any appreciable effect from stray capacitance. It may be noted that any stray capacitance across the terminating resistor, R, will restrict the maximum value of R since it will dominate the load impedance as R is increased , thus limiting signal sensitivity.

3.8.1 Calibration of Narrowband Coils

The peak magnitude of the first half cycle in the oscillatory response of a narrowband Rogowski coil is related to the peak value of primary circuit current. This relationship differs for the two circuit configurations and may be determined from a Laplace transform treatment of each circuit to obtain the transient response to a step function in the monitored current $i_p(t)$.

3.8.1.1 Parallel Circuit Response

The parallel circuit transfer function, derived from an examination of the equivalent circuit is given by,

$$V_m(s) = I_p(s). \frac{k.s}{s^2 + (1/RC)s + (1/LC)} \quad \ldots.(3.19)$$

where $k = 1/N.C$, C is the total circuit capacitance and N is the number of coil minor turns.

Solution of this equation to a step in current $I_p(s) = I_p/s$ will result in an overdamped or underdamped response depending on the quadratic in the denominator. If the roots are complex :

$$\left[\left[\frac{1}{2RC}\right]^2 - \frac{1}{LC}\right]^{1/2} < 0$$

The transient solution to the equation is then given by ,

$$v_m(t) = \frac{I_p}{\omega.N.C} .\exp(-at)\sin(\omega t) \qquad ....(3.20)$$

where, $\omega = \left[\frac{1}{2RC} - \frac{1}{LC}\right]^{1/2}$ and $a = \frac{1}{2RC}$

This response function is shown in figure 3.8.1.1 .

It is a damped sinusoidal function for which v (t) = 0 at time t = 0, rising to a first peak at t = $\pi/2\omega$ of,

$$\hat{v}_m(t) = \frac{I_p}{\omega.N.C} .\exp(-\pi\omega/RC) \qquad ....(3.21)$$

which is the expression used to calibrate the device in terms of the peak value of output signal $v_m(t)$ corresponding to the peak value in the monitored current $i_p(t)$.

3.8.1.2 Series Circuit Response

A similar expression for the transfer function of the series circuit can be obtained and is given by :

$$V_m(s) = I_p(s). \frac{k.s^2}{s^2 + (R/L)s + (1/LC)} \qquad ....(3.22)$$

where k = R/N

Again the solution of this equation depends on the roots of the quadratic in the denominator. The underdamped solution has complex roots when,

$$\left[\left[\frac{R}{2L}\right]^2 - \frac{1}{LC}\right]^{1/2} < 0$$

and is given by equation,

$$v_m(t) = I_p.\frac{R}{N}.\exp(-at)(\cos(\omega t) - \frac{a}{\omega}.\sin(\omega t)) \qquad \ldots.(3.23)$$

where $a = R/2L$ and $\omega = \left[\left[\frac{R}{2L}\right]^2 - \frac{1}{LC}\right]^{1/2}$

In this function, $v_m(t)$ has an instantaneous value of $I_p.R/N$ at time $t = 0$, (see figure 3.8.1.2), and follows a damped cosinusoidal function thereafter. This follows from the assumption of an instantaneous rise in primary current $i_p(t)$, inducing an infinite voltage across the circuit inductance L allowing current through L to develop a voltage $I_p.R/N$ across the terminating resistor R. Of course a real current pulse will have finite rise time and will therefore modify the resultant waveform. However, at sufficiently rapid rise times in $i_p(t)$, (negligibly small in comparison to the period of oscillation),C will contribute negligible circuit impedance. The self inductance L will dominate circuit impedance and voltage distribution such that a current $i_s(t)$, (secondary circuit current), will be made proportional to $i_p(t)$. A voltage $I_p.R/N$ will result across R.

For longer current pulse rise times the output signal $v_m(t)$ will appear to rise in step with the monitored signal from zero and follow a damped sinusoidal function form thereafter, similar to the response of the parallel circuit . The oscilloscope traces in figure 3.8.1.3 illustrate this ambiguity in oscillatory pulse shape for different pulse rise times.

The calibration of the series circuit can be achieved with the aid of the equation :

$$\hat{v}_m = I_p.\frac{R}{N} \qquad \ldots.(3.24)$$

which relates the initial peak in the signal $v_m(t)$ to the peak value in the current monitored, $i_p(t)$.

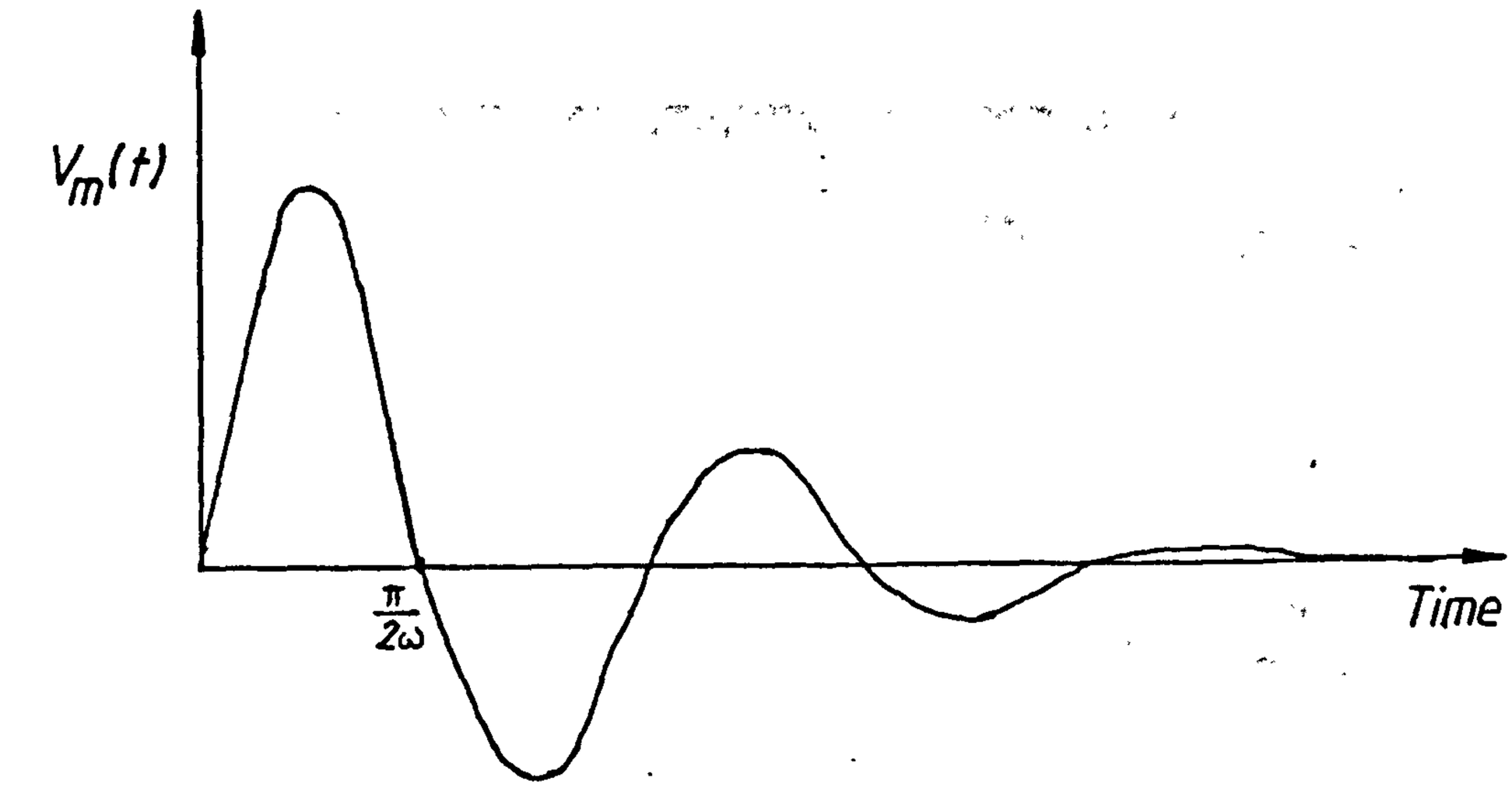

Figure 3.8.1.1 - Parallel Circuit Response

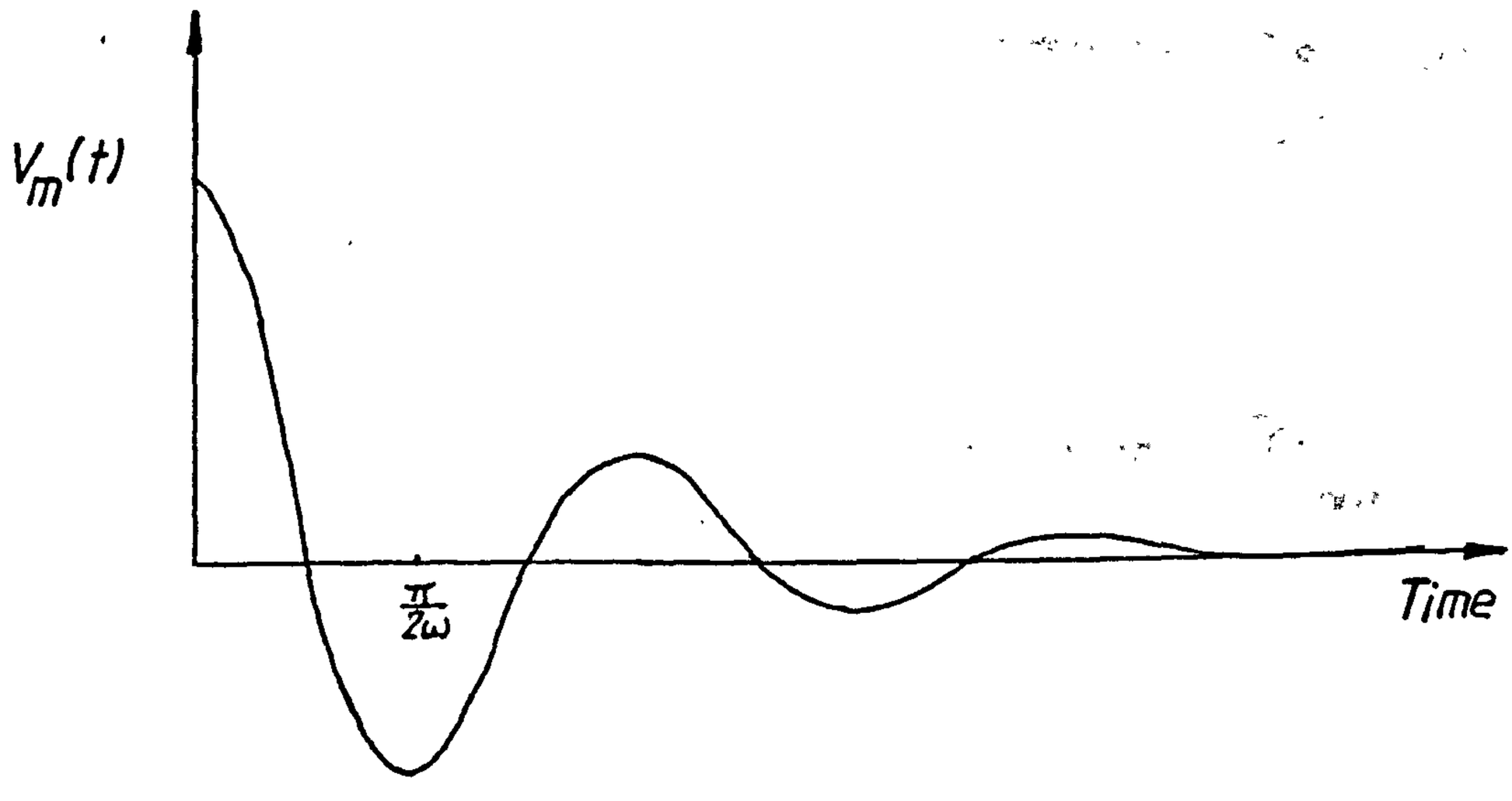

Figure 3.8.1.2 - Series Circuit Response

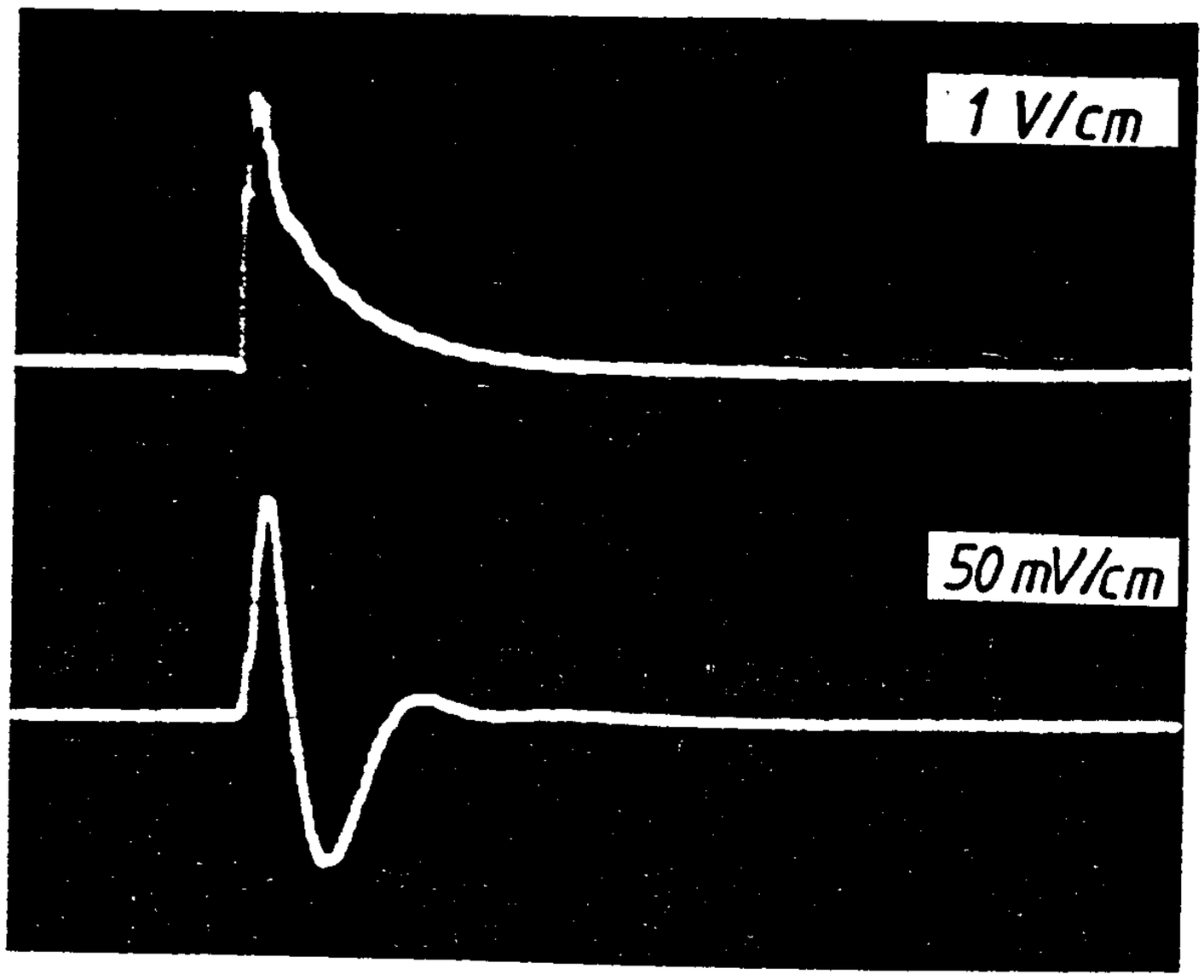

Fast Rise time Input Pulse

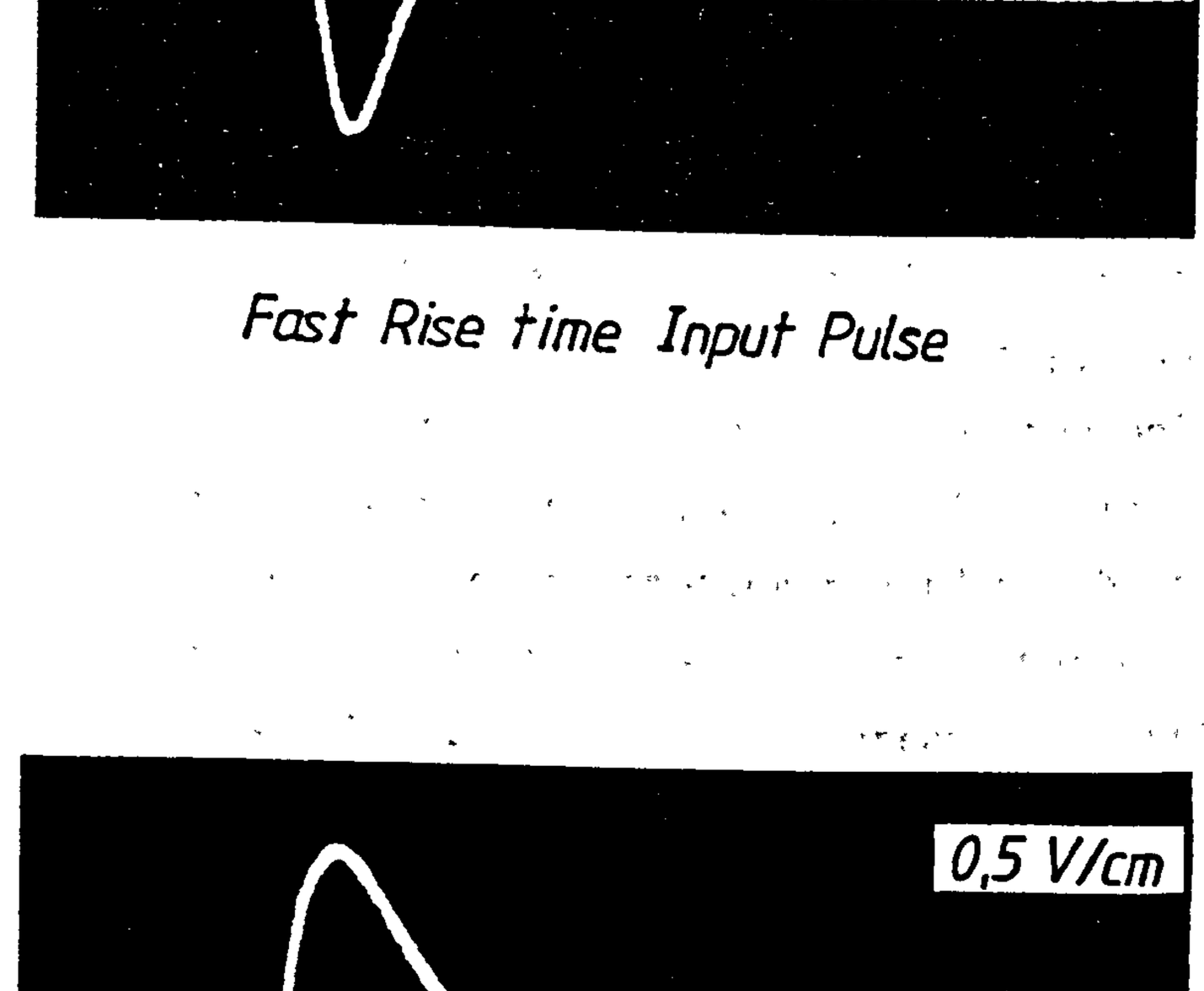

Slow Rise time Input Pulse

Time Base - 0,2 μsec

Figure 3.8.1.3 - Response of Series Circuit to Fast and Slow Rise Time Pulses

3.9 Charge Measurement with Narrowband Coils

Charge is defined as the integral of the current i(t), and if the current is a pulse, the integration time must exceed the pulse duration. The charge contained in the waveform depends on the shape of the current pulse which requires faithful reproduction of the current i(t). The narrowband Rogowski coil does not possess this ability and accurate charge measurements are not possible although, under certain conditions semi-quantitative measurement can be made.

In the following discussion only the series resonant circuit response is considered for brevity since conclusions drawn from the analysis are applicable to the parallel circuit.

For a rectangular current pulse I_p of duration T the charge contained is simply the product of these two variables. The transient time domain response of the resonant circuit to a step, however, is a damped oscillation the amplitude of which is related only to the peak current $i_p(t)$ through equation (3.24) . The amplitude of the oscillatory pulse contains no information regarding the time duration, T , of the monitored current i_p (t), and charge measurement is therefore not possible . If the current i_p (t) were an exponential function , $i_p(t) = I_p \exp(-t/T)$ with a time constant, T, the charge in the pulse would, from the integration, be

$$q_c = \int_0^t I_p.\exp(-t/T).dt$$

be ,

$$q_c = I_p.T.(1 - \exp(-t/T))$$

Assuming the integration time t is longer than the pulse duration, the charge transferred would be given by the simple expression,

$$\therefore \quad q_c = I_p.T$$

In partial discharge measurements this relationship could be used to calibrate the peak amplitude in the narrowband coil response, $\hat{v}_m(t)$, provided that

i. The partial discharge current pulse has an exponential decay form with an instantaneous rise time.

ii. Current pulses all have the same time constant of decay.

This is difficult to establish in practice and care must be taken in the interpretation of results based on these assumptions .

CHAPTER FOUR

DEVELOPMENT AND PERFORMANCE OF A PARTIAL DISCHARGE LOCATION SYSTEM

4.1 Principle of Location Technique.

As discussed previously, a partial discharge generates two electromagnetic pulses which propagate from the discharge site to the two ends of a phase winding . A motor winding connected to a high voltage supply will have a large number of discharge sites distributed along its length . Pulses generated at these sites travel to the line and neutral ends of the winding . An observer at the terminals will see a train of pulses which are random in height and spacing in time, (as shown in figure 4.1.1). The correlation of these two pulse trains forms the basis of the location technique .

Consider, as shown in figure 4.1.1, a discharge occurs at a site on the winding close to one end . The pulses generated at the discharge site will arrive at the line and neutral terminals after time delays of τ_1 and τ_2 ,respectively . A delay difference of $(\tau_1 - \tau_2)$ separates the two pulses and it is this relationship which is used to locate the position of the discharge source.

Since the pulse trains are time varying functions $v_1(t)$ and $v_2(t)$, a cross-correlation function between the two can be defined as a function of the delay difference , τ . This is given by the relationship :

$$R_{12}(\tau) = \lim_{T\to\infty} \frac{1}{T} \int_0^T v_1(t).v_2(t+\tau)dt \qquad .....(4.1)$$

Assuming that the winding is lossless and distortion free and a partial discharge source generates a signal f(t) and $v_1(t)$ and $v_2(t)$ are the voltage signals detected at the line end and neutral end respectively, then ; $v_1(t) = f(t-\tau_1)$ and $v_2(t) = f(t-\tau_2)$. The cross correlation function is then,

$$R_{12}(\tau) = \lim_{T\to\infty} \frac{1}{T} \int_0^T f(t-\tau_1).f(t-\tau_2+\tau)dt \qquad .....(4.2)$$

If now a change of variable $t' = t - \tau_1$ is made , the integral becomes

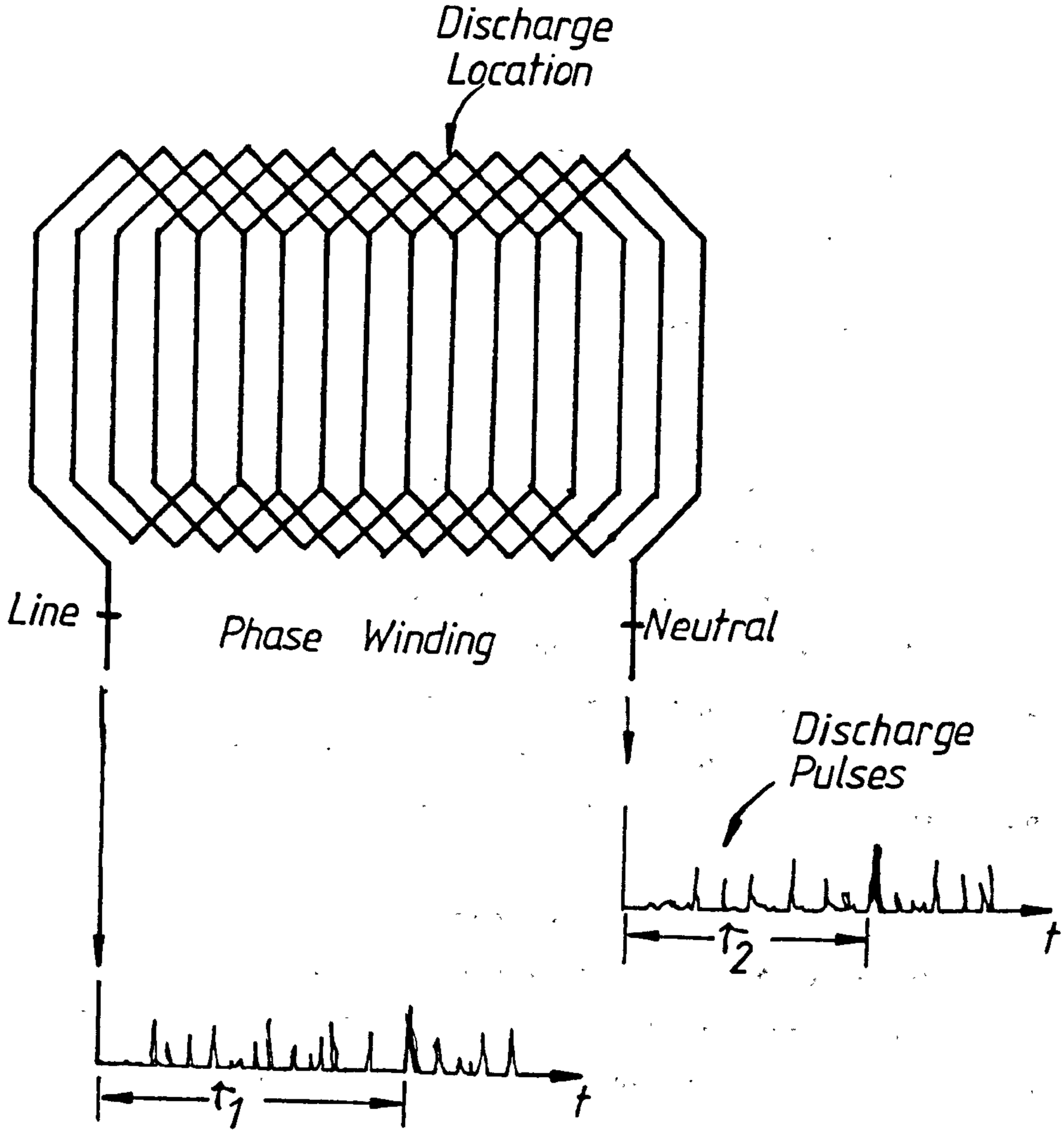

Figure 4.1.1 – Discharge Pulse Trains from Phase Winding

$$R_{12}(\tau) = \lim_{T\to\infty} \frac{1}{T} \int_0^T f(t').f\,(t'+\tau + (\tau_1-\tau_2))dt \quad .....(4.3)$$

The cross-correlation function is defined as a function of the time delay difference $(\tau_1 - \tau_2)$.

If the discharge source is in the centre of the winding , then $\tau_1 = \tau_2$ and τ becomes zero . This transforms the expression (4.3) into the autocorrelation function given by ,

$$R_{ff}(\tau) = \lim_{T\to\infty} \frac{1}{T} \int_0^T f(t').f(t'-\tau)dt \quad .....(4.4)$$

The autocorrelation function has the property that it always becomes a maximum at $\tau = 0$.

To illustrate the properties of the cross-correlation function consider the signals observed at the winding terminals, originating from a single discharge source , to be ideal impulses that are rectangular in shape and separated by a time difference τ'. The resulting cross-correlation function is simply the area under the curve $v(t).v(t+\tau)$ graphed as a function of the variable τ. This is shown diagramatically in figure 4.1.2 which shows the cross-correlation function is a maximum at $(\tau_1 - \tau_2)$. The cross-correlation function is therefore a shifted auto-correlation function $R_{ff}\ (\tau - \tau_2 + \tau_1)$, which peaks at a delay $\tau' = (\tau_1 - \tau_2)$. A display of the cross-correlation function will therefore indicate the delay difference $(\tau_1 - \tau_2)$, which is the basis of the location philosophy.

If d_1 represents the distance of the discharge source from the line-end terminal and v is the velocity of pulse propagation then ,

$$\tau_1 = \frac{d_1}{v} \quad \text{and} \quad \tau_2 = \frac{(L - d_1)}{v} \quad .....(4.5)$$

where L is the length of the winding . The delay difference τ is

given by ,

$$\tau_2 - \tau_1 = \frac{(L - 2d_1)}{v} \qquad \text{.....(4.6)}$$

A simple rearrangement of the above expression yields the distance of the discharge source from the line end .

$$d_1 = L - \frac{(\tau_1 - \tau_2).v}{2} \qquad \text{.....(4.7)}$$

The value of L and v may be measured while the cross-correlation function provides $(\tau_1 - \tau_2)$. Thus a display of the cross-correlation function, essentially determines the location of discharge sources in a winding from the position of the correlation peaks .

Partial discharges occuring external to the winding will also produce correlation peaks in the cross-correlation function . However these discharge sources and other spurious noise sources may be ignored if only those time delay differences less than $\tau = L/v$ are considered . More precisely , delay differences in the interval $-\tau/2 < 0 > + \tau/2$ since $\tau = 0$ represents the centre of the motor winding .

So far, the principle of cross-correlation as a location technique has been discussed in relation to ideal pulses travelling in a distortion free , lossless transmission line . In practice , as has been demonstrated in chapter two , discharge pulses propagating in a motor winding undergo considerable distortion and frequency dependent attenuation causing the wavefront of the pulse to lengthen . Added to this is the influence introduced by pulse reflections at winding terminations and the superposition effects of pulses separated by very short time intervals . Under these conditions the pulse shape is distorted considerably and would necessarily mean that derivation of a cross-correlation function would be impractical . However, since it is only the time delay difference ,τ, between the arrival of pulse pairs that is of concern in the location of discharges , the only information required is that of the time at which pulses occur . In other words the instant in time that the leading edge of the pulse occurs relative to the other discharge pulses .

The way in which this information is obtained is to detect the

position in time when the pulse waveform rises above a certain threshold level . This is termed threshold detection in that the threshold level is set at a pre-determined level between the expected upper limit of noise level and well below the pulse peak . Thus a train of pulses emerging from a winding terminal is threshold detected , amplified and limited to produce a train of unipolar, rectangular pulses , of varying widths but with the time position information preserved . This type of operation relates to a class of detectors referred to as non-parametric detectors . Non-parametric detectors do not depend on the parameters of the process which are subject to unknown variations and widely varying characteristics [88] .

Returning to the cross-correlation function in expression (4.2) the voltage signals $v_1(t) = f(t - \tau_1)$ and $v_2(t) = f(t - \tau_2)$ are replaced by the threshold detected functions $SGN_1(t)$ and $SGN_2(t)$. Consider the two signals described by

$$\begin{aligned} SGN_1(t - \tau_1) &= 0 , \quad t < \tau_1 \\ &= 1 , \quad \tau_1 < t < (\tau_1 + T_1) \\ &= 0 , \quad t > (\tau_1 + T_1) \end{aligned} \qquad \text{.....(4.8)}$$

$$\begin{aligned} \text{and} \quad SGN_2(t - \tau_2) &= 0 , \quad t < \tau_2 \\ &= 1 , \quad \tau_2 < t < (\tau_2 + T_2) \\ &= 0 , \quad t > (\tau_2 + T_2) \end{aligned} \qquad \text{.....(4.9)}$$

which are typical . T_1 and T_2 are the pulse durations of $SGN_1(t-\tau_1)$ and $SGN_2(t-\tau_2)$ respectively .

The resulting cross-correlation function $R_{12}(\tau)$ is described by the function ,

$$\begin{aligned} R_{12}(\tau) &= 0 , \quad \tau < (\tau_1 - \tau_2) - T_1 \\ &= 1/T , \quad (\tau_1 - \tau_2) - T_1 < \tau < (\tau_1 - \tau_2) \\ &= T_1/T, \quad (\tau_1 - \tau_2) < \tau < (\tau_2 - \tau_1) + (T_2 - T_1) \\ &= -1/T, \quad (\tau_1 - \tau_2) + (T_2 - T_1) < \tau < (\tau_2 - \tau_1) + T_2 \\ &= 0 , \quad \tau > (\tau_2 - \tau_1) + T_2 \end{aligned} \qquad \text{.....(4.10)}$$

as shown in figure 4.1.2 . The function is a trapezoid with a base $(T_1 + T_2)$ and top $(T_2 - T_1)$. If the pulses have equal widths, $(T_1 = T_2)$, then $T_2 - T_1 = 0$ and the function becomes a triangle which has its apex at $\tau = (\tau_2 - \tau_1)$. This is the auto-correlation function R_{ff} .

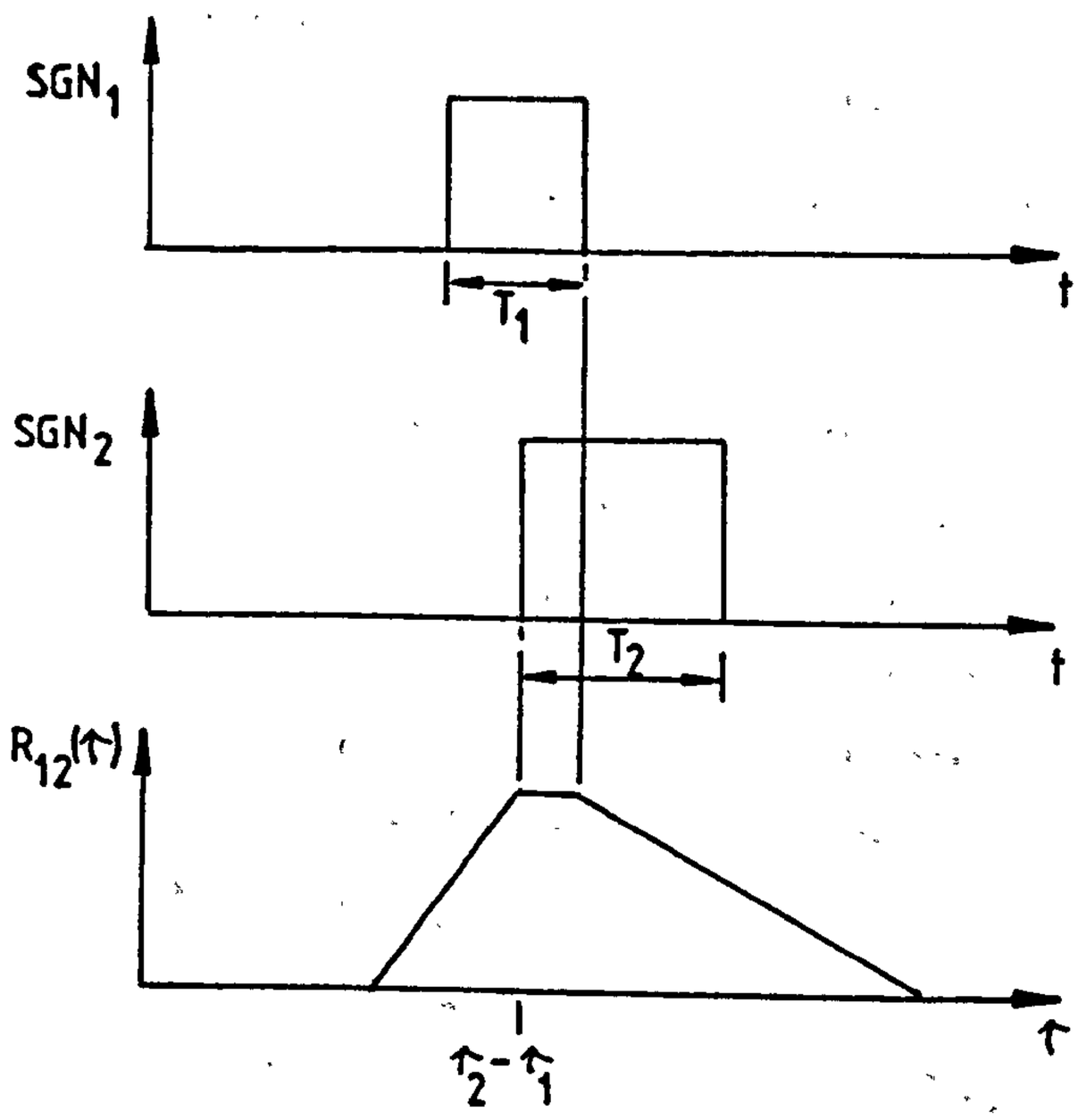

Figure 4.1.2 - Cross Correlation Function

Although information regarding the shape of the partial discharge signals has been ignored it remains that the cross-correlation of the threshold detected signals provides an indication of the time delay difference $,(\tau_2-\tau_1),$ which then may be related to the location of the discharge source in the winding .

4.2 Implementation of Cross-Correlation

In order to obtain the cross-correlation function it is necessary to compare the polarities of the pulses detected at the two ends of the winding as a function of delay $,\tau,$ between the two channels . The way in which this is achieved is described with reference to the schematic block diagram in figure 4.2.1 , which shows the whole instrument system .

The analogue pulse signals emerging form the line and neutral ends of the winding are detected by the Rogowski coils . These signals are then amplified and transmitted to the signal processing instrumentation via two separate fibre optic transmission links , where they are directed in to a programmable delay line , one in each channel . Each programmable delay line delays the analogue signal in the range 0 to τ_{max}, (τ_{max} being the maximum delay in the delay line), in delay increments of τ_{inc} . In this manner , the differential delay $\tau=(\tau_2-\tau_1)$ may be varied in the range , $-\tau_{max}<0<\tau_{max}$, in steps of τ_{inc}. Thus , for a given delay setting , τ_s , pulse signals in channels 1 and 2 will be delayed $(\tau_2-\tau_1)$ with respect to one another . Consequently , pulses originating from a location on the winding corresponding to a delay difference $(\tau_2-\tau_1)$ at the line and neutral terminals , will arrive at the same instant in time at the outputs of the programmable delay lines .

The pulse trains are passed to a time coincidence unit which indicates the presence of two pulses arriving at the same instant in time . When two pulses are coincident in time , corresponding to a particular point on the winding , one pulse is passed through by a coincidence logic pulse to a multi-channel analyser that counts the coincident pulses , and stores the result in memory . All other non-coincident pulses , corresponding to discharge sources at other positions on the winding , are ignored . In this way time correlation of pulse trains provide the location of the discharge source .

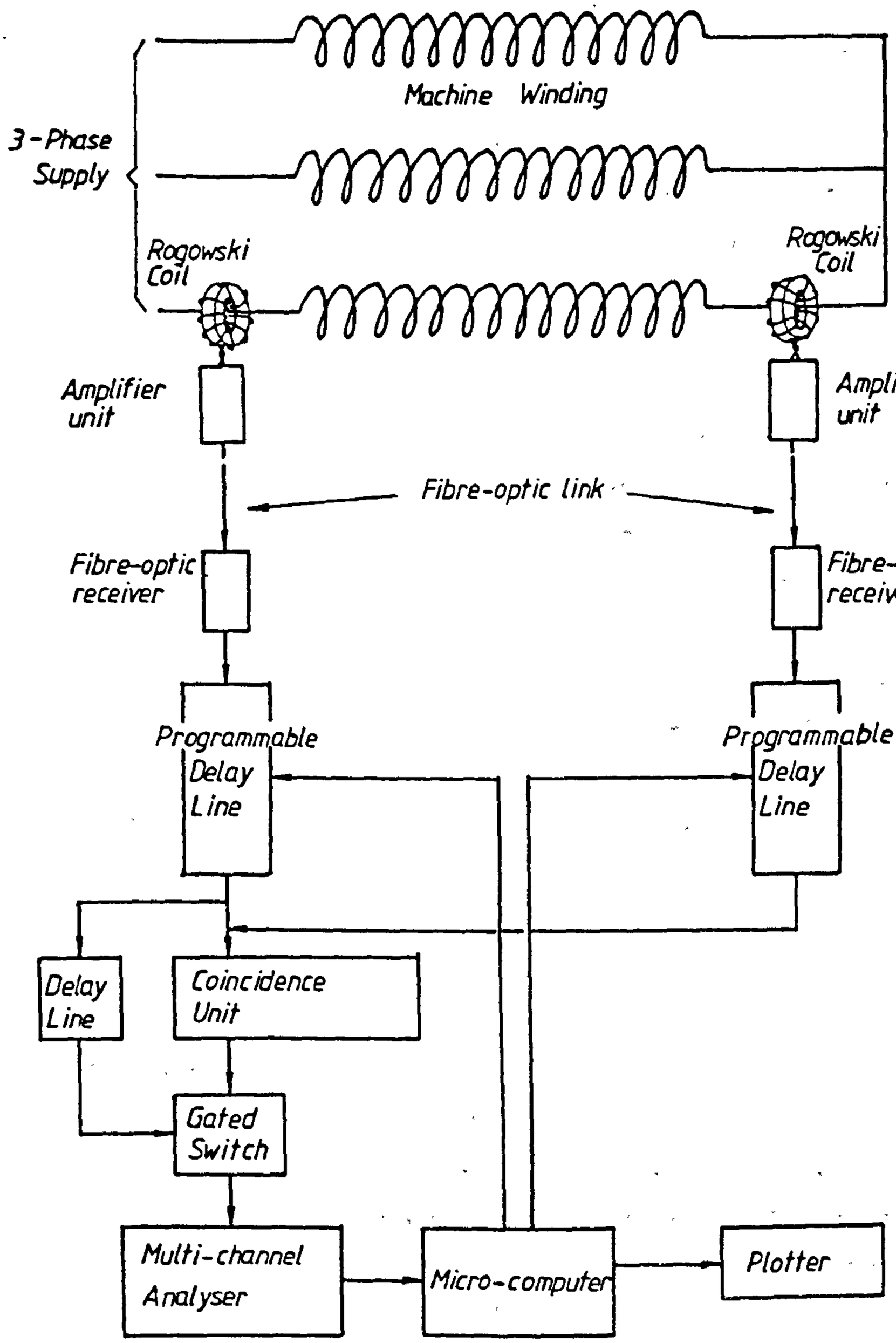

Figure 4.2.1 - Instrumentation System

A microcomputer is used to supervise the delay line switching sequence so that the range of time delay differences corresponding to a distribution of set positions on the winding is covered . At each individual delay setting, (location on the winding), the number of coincident pulses are counted in the multi-channel analyser in a memory channel corresponding to that particular delay setting, hence discharge location. The dwell time on each delay setting is determined by the micro-computer which may be programmed to any value in increments of 1 millisecond to allow sufficiently long samples times .

By sequential switching of the programmable delay lines to observe incremental points on the winding, it is possible to scan the entire winding . From a scan a histogram of correlated pulse counts against differential delay $(\uparrow_2 - \uparrow_1)$, and therefore winding location, is produced. In doing so , the cross-correlation function is derived which provides an indication of partial discharge activity with position along the length of the motor winding . This is shown on the display of the multi-channel analyser in figure 4.2.2 for a single discharge source generated artificially. The following sections outline the design of the main components of the location instrument system as shown in the schematic diagram in figure 4.2.1 .

4.2.1 Discharge Detection Unit

Partial discharge current pulses are detected by a Rogowski coil. The signals are amplified in a 120 MHz wideband amplifier which has two complimentary outputs . Current signals are taken from the inverted output via a short length of coaxial cable whilst non-inverted signals are fed into a passive R - C integrator circuit to derive signals proportional to the apparent charge, q . The gain of the amplifier is continuously variable over a range of 10 to 400 . A voltage follower circuit forms the subsequent stage to minimise loading of the integration capacitor and provide a sufficiently low output impedance to drive long lengths of coaxial cable and subsequent stages. A fibre-optic link is used to connect the detection unit to the ground station equipment and provides the necessary high-voltage isolation requirement and eliminates earth loop interference . Figure 4.2.1.1 shows the detection unit in block diagram form .

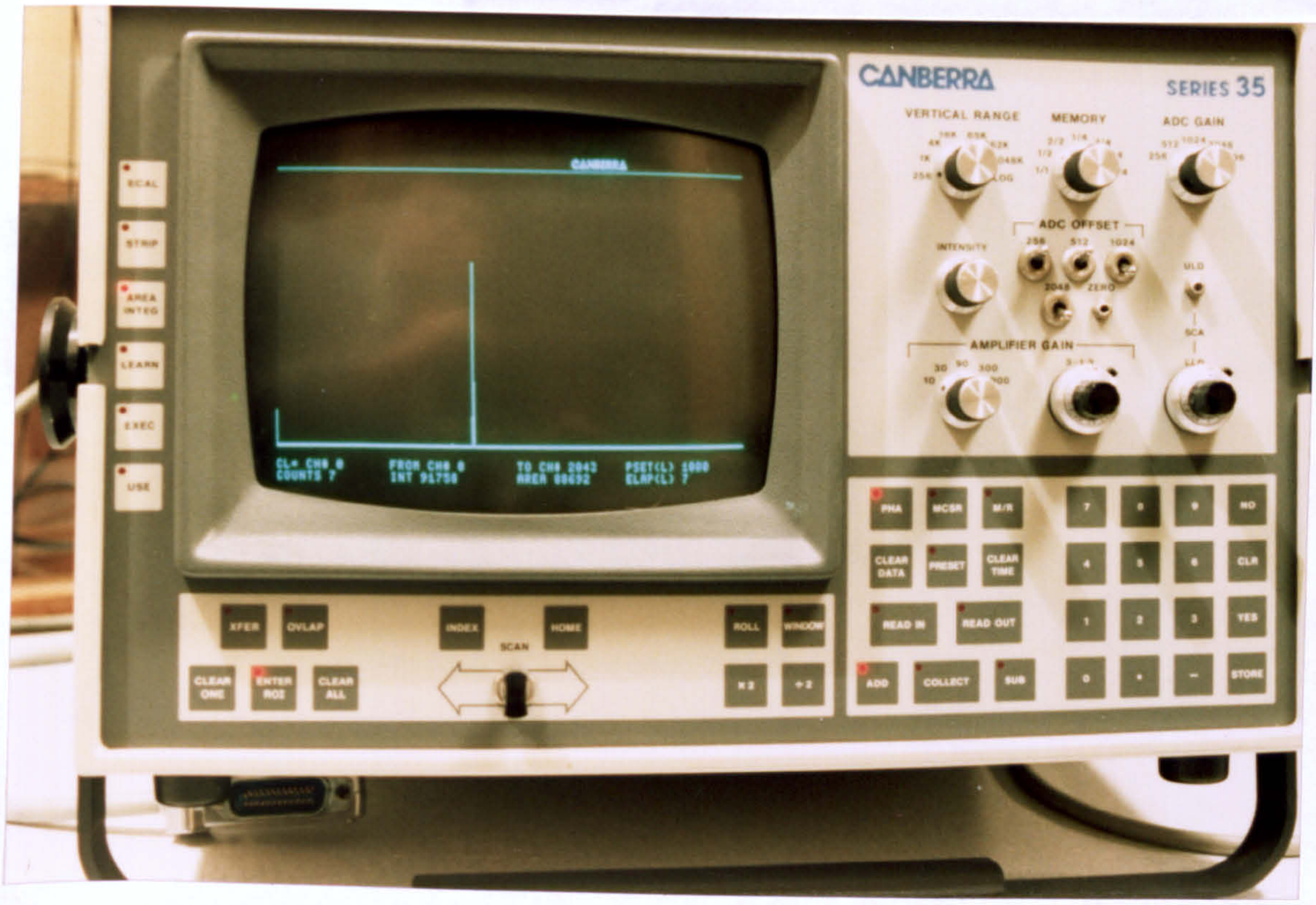

Figure 4.2.2 - Multi-channel Analyser Display

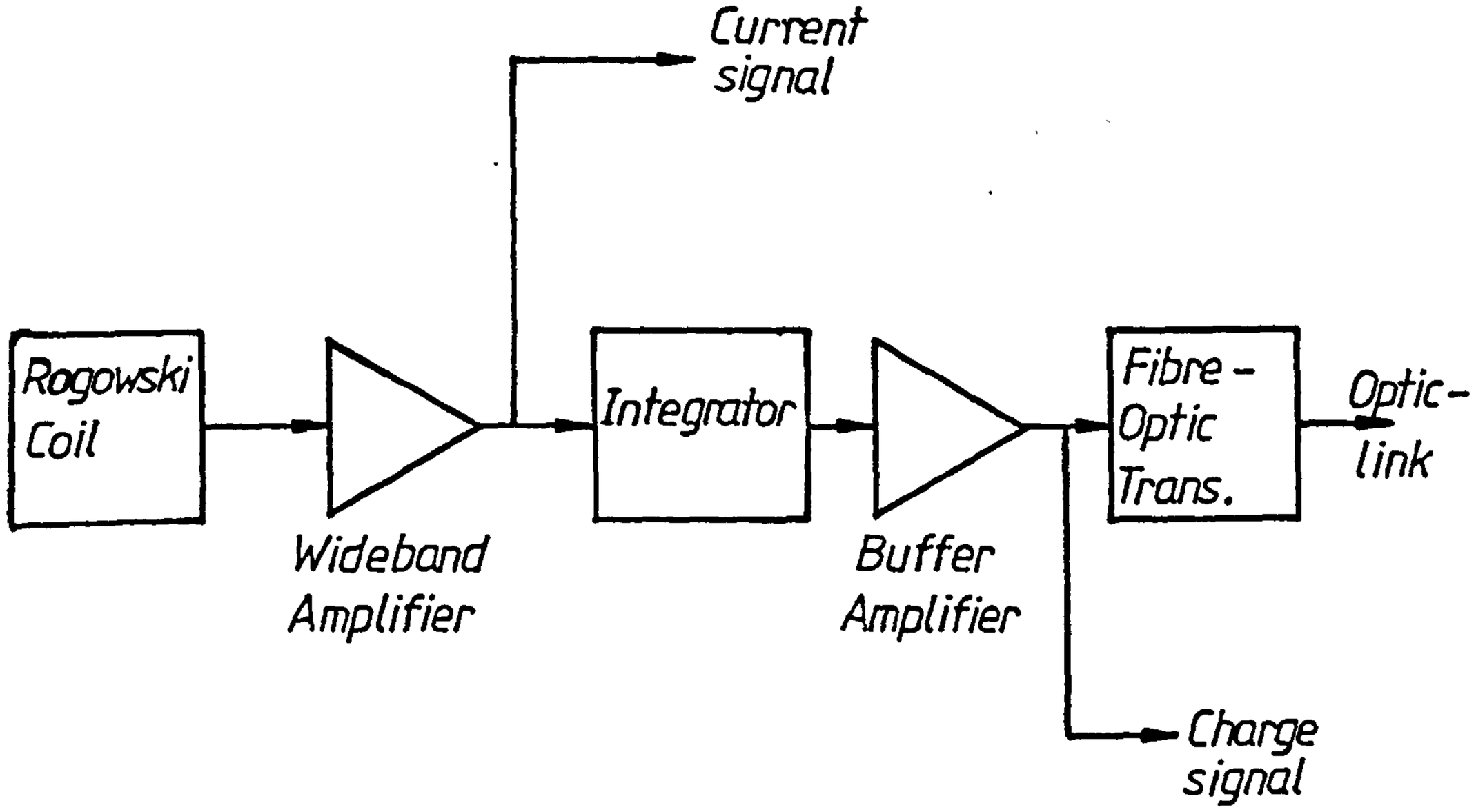

Figure 4.2.1.1 - Discharge Detection Unit

The fibre-optic transmitter and the amplifier circuits require isolated power supplies at voltages of +5V/0V and +5V/-5V respectively. These are provided by two separate battery supplies mounted with the fibre-optic transmitter and pulse amplifier in an integral unit shown in the photograph in figure 4.2.1.2 . The fibre-optic link receiver is mounted in the pulse location instrument and has a voltage follower circuit with sufficient capability of driving directly the programmable delay line unit.

4.2.2 Programmable Analogue Delay line.

The delay of an electrical signal is most easily done in a two-wire transmission line in which the signal travels as an electromagnetic wave at a finite speed . The velocity of propagation is a characteristic of the transmission line configuration and is always below that of light in a vacuum , c .

In general, a signal will travel at a speed

$$v = \frac{1}{\sqrt{L.C}} \qquad (ms^{-1})$$

in a two-wire transmission line with inductance L and capacitance C per unit length of line . If the relative magnetic permeability μ_r is assumed to be unity then the speed of propagation will be dependent on the geometry of the line and on the relative permittivity of the dielectric ϵ_r . The delay time therefore , of a signal in a length of transmission line x is

$$T = x.\sqrt{L.C} \qquad (\text{ sec. })$$

Various configurations of the two conductor line are commercially available, however only three geometries are of particular use in the construction of an analogue delay line for relatively wideband signals and these are ;

i. Coaxial line
ii. Helical line
iii. Microstrip line

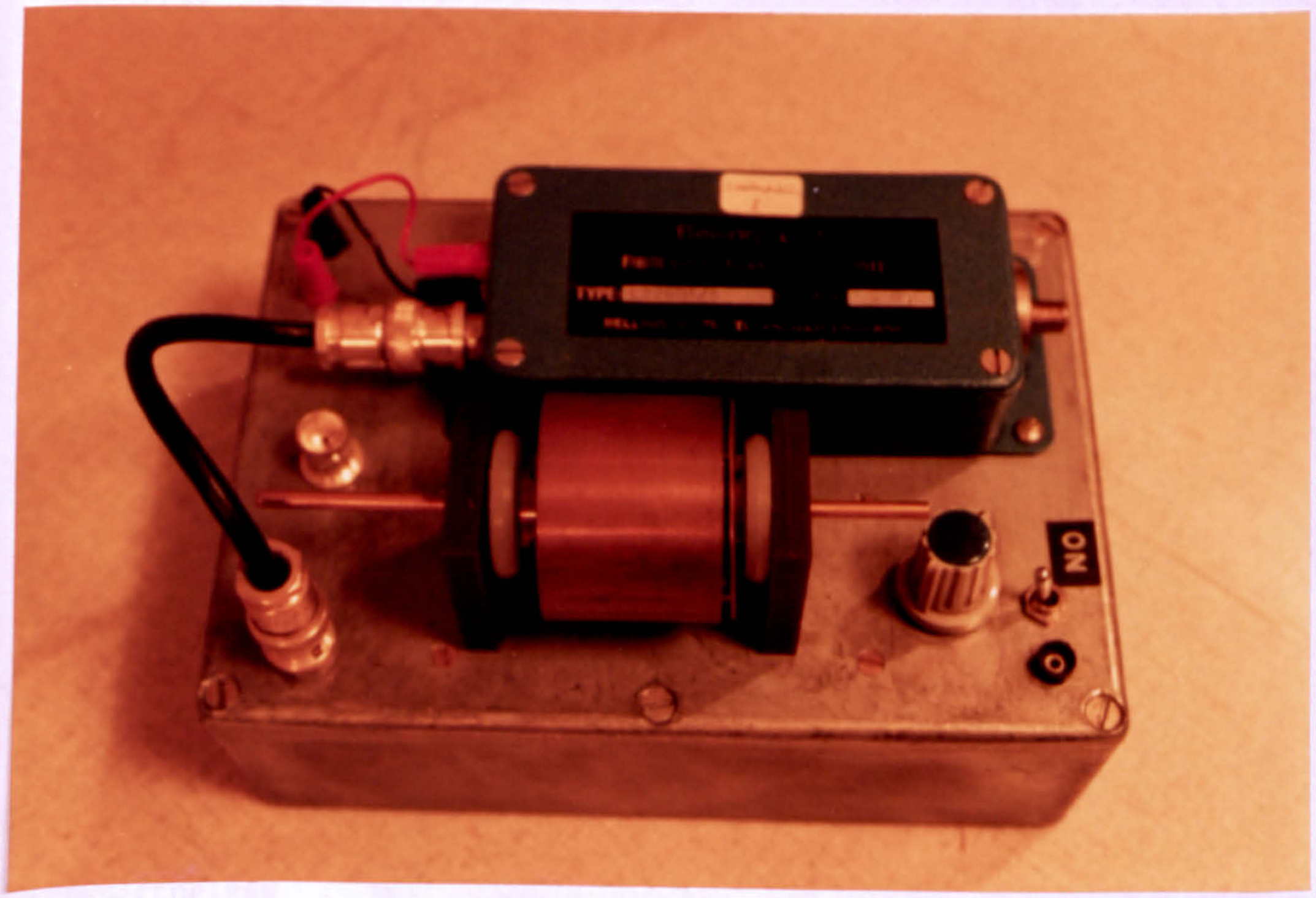

Figure 4.2.1.2 - Discharge Detection Unit

The eventual selection of delay medium depends not only on delay time considerations but on an appraisal of each line on the basis of other criteria such as attenuation , signal bandwidth , frequency dependent distortion, ease of termination and volume occupied per unit of length of delay. The relevant characteristics of each of the forementioned delay lines are examined in the following sections .

4.2.2.1 Coaxial line.

The coaxial line construction has the advantage that electric and magnetic fields are restricted to within the sheath thus eliminating radiation losses and shielding the line from external interference signals .

Modern coaxial cables have dielectrics of polystyrene, polyethylene or P.T.F.E. (polytetraflouroethene) , which have relative permittivities of about 2.3 . This corresponds to a propagation velocity of about 0.2 m/nsec , which is a time delay of 5 nsec per metre run of cable . The coaxial cable is well suited to small delays whilst for long delays the length and weight of line can be prohibitive , ie. a 1 μsec delay requires a 200 metre cable .

The coaxial line also has a broad bandwidth for signal frequencies of up to a few hundred megahertz for short cable runs, (a few metres) , while for longer lengths the rise time of the signal is progressively increased due to the transmission line losses in the cable .

Nevertheless , the coaxial line does provide a suitable medium for discharge type pulses which are processed prior to the delay line stage in the instrument .

4.2.2.2 Helical line

The helical line is basically of the same construction as the coaxial cable with the exception that the inner conductor is replaced with a helical conductor formed on a dielectric or ferrite core .

This configuration allows construction of lines with very high characteristic impedance and very long delays per unit length of cable since the self inductance L can be made a relatively large value . Typical commercially available cables have impedances ranging from

$Z^{\cdot}$ = 100Ω to 4000Ω and delays of T = 23 nsec/m to 3.3 μsec/m which have dielectric and ferrite loaded cores . These delay times and impedances seem very impressive but these cables are restriced in their available bandwidth since they suffer from phase distortion due to the interturn capacitive coupling which is frequency dependent . The maximum effective bandwidth of these cables with no appreciable distortion is about 1 MHz [89,90] .

Another problem associated with helical lines is the manner in which the line is terminated since at the cable ends the effective inductance decreases hence the characteristic impedance falls towards the ends . There are techniques to compensate for this mismatch at low frequencies but reflections inevitably occur at high frequencies .

4.2.2.3 Microstrip line

The microstrip line has a very simple construction in which a copper track or conductor is etched on the dielectric substrate of a double sided printed circuit board . The conducting plane on the other board side is utilised for the earth conductor . A long line may be fabricated on a large board by 'meandering' the track taking care that adjacent tracks have sufficient separation . This is to prevent pulse feed forward by the capacitive and inductive coupling between adjacent conductors , resulting in pulse distortion [91].

Propagation is not strictly TEM and characteristic parameters are usually designed using computer programs . However , a good approximation to the characteristic impedance may be given by the expression [92] :-

$$Z = \sqrt{\frac{L}{C}} = \frac{377}{\sqrt{\epsilon_r}} \left|\frac{h}{w}\right|$$

where h is the dielectric thickness,(in metres), and w is the width of the track conductor,(in metres) .

The velocity of propagation depends on the relative permittivity of the dielectric used for the printed circuit board . For a dielectric of epoxy-resin/ glass fibre , ϵ_r = 2.6 , which gives a velocity of 186 m/μsec and a delay of 5.4 nsec/metre [92] .

An advantage of this type of transmission line system is the flexibility in design and the ease of mounting components directly on the line whereas in coaxial lines there is some difficuly as to what technique is best for termination . There is however , little to be gained in terms of storage space for large delay lines . In addition to this , there is no shielding from external interference (radiated or closely coupled signals) . Apart from this the stripline constitutes a viable option for the delay of electromagnetic signals .

4.2.2.4 Fibre-Optic Transmission Line

The use of a fibre-optic cable to delay an analogue signal has the advantage that it is free from electromagnetic interference , which is a necessity in partial discharge measurements . Bandwidth is virtually unrestricted and attenuation is in the region of -5 dB/km . However, due to the multiple modes of internal reflection within a cable and frequency dependent velocity of propagation , distortion of the pulse in the form of pulse 'jitter' occurs when long distances of travel are involved . In addition to this , transmitter and receiver devices are required at the ends of the optical cable for signal conversion .

From a comparison of the analogue signal delay lines available , the coaxial cable is selected as the delay medium on its overall superior characteristics .

The programmable delay line developed comprises eight, binary weighted lengths of low loss (6.23 dB/km) , coaxial cables which are connected by a set of sixteen relay contacts . These are mercury-wetted relays which have a very low contact resitance of 75 mΩ to prevent excessive pulse amplitude attenuation in the delay line . The circuit in figure 4.2.2.1 of the programmable delay line shows that each of the cable lengths can be switched into or out of the delay line by a pair of single-pole changeover contact relays . Connections are made from the cable ends to the relay contacts via a coaxial plug and socket arrangement . In this manner the length of the delay is varied from zero to the maximum in 256 steps . Each delay increment corresponds to the delay in the smallest length of cable which is: 4.39 nsec and the maximum delay is therefore 1.68μseconds .

Over the maximum length of the delay line some frequency dependent distortion of the pulse does occur in the form of an increase in the

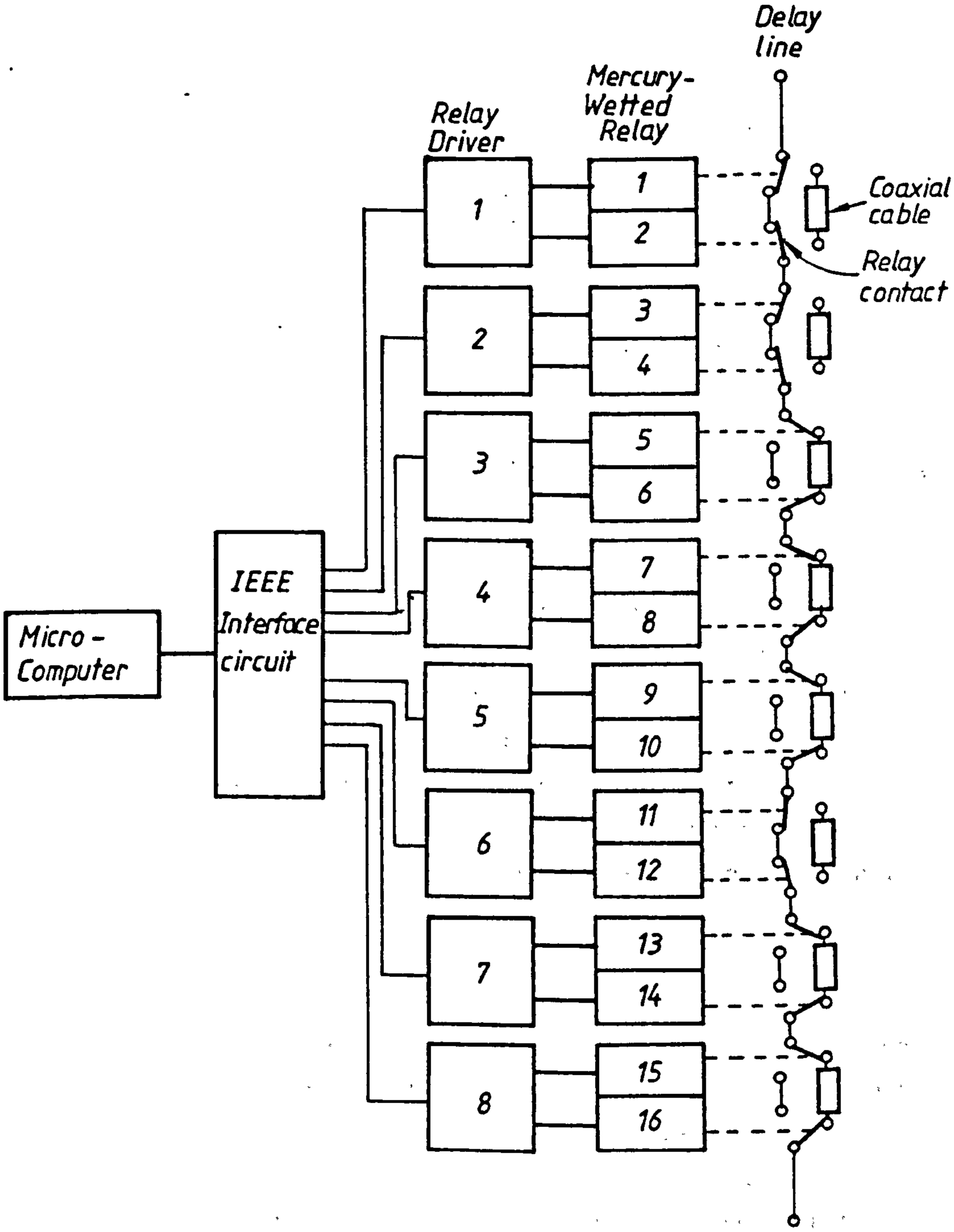

Figure 4.2.2.1 - Programmable Delay Line

rise time ,(hence fall time) , of the pulse . Oscilloscope traces in figure 4.2.2.2 show the influence of 382.5 metres of delay cable on a 10 μsec, (20nsec rise time), pulse . Rise time has increased to 400 nsec through the line . This does not adversely effect the location technique as the pulse is distorted in the winding and post-integrated before it enters the delay line.

Control of the programmable delay line is achieved by a microcomputer through a specially designed interface circuit . Communication protocol between the microcomputer and the interface circuit is that of the IEEE - 488 instrument bus standard . The interface circuit basically allows the microcomputer to change the status of each pair of relay contacts connected to an appropriate delay line section .

An 8 - bit binary code entered from the microcomputer terminal is received by the interface circuit and subsequently presented on 8 control lines to relay coil driver circuits , see diagram 4.2.2.1 . A set of two relay drivers are controlled by a single control line . These two relay drivers in turn energise or de-energise the coils of two relays which terminate the ends of a length of delay line . Therefore, a single logic level 1 on a control line switches a binary weighted delay line section into the delay line whilst a logic level 0 bypasses the delay line section . The least significant bit (LSB) of the binary code controls the shortest delay line section whilst the most significant bit (MSB) controls the longest delay line section .

4.2.3 Coincidence Unit

A time coincidence detector is basically a logical AND gate, see figure 4.2.3.1 , whose inputs are two (or more) ideally rectangular logic pulses . These store the time information regarding the position in time of the discharge pulse in their leading or trailing edges . When two pulses from separate pulse trains are coincident in time a logic pulse is output from the gate .

If δ_1, and δ_2 are the widths of the pulses then the coincidence resolution time is simply given by ,

$$\tau_c = \delta_1 + \delta_2 \qquad \ldots.(4.11)$$

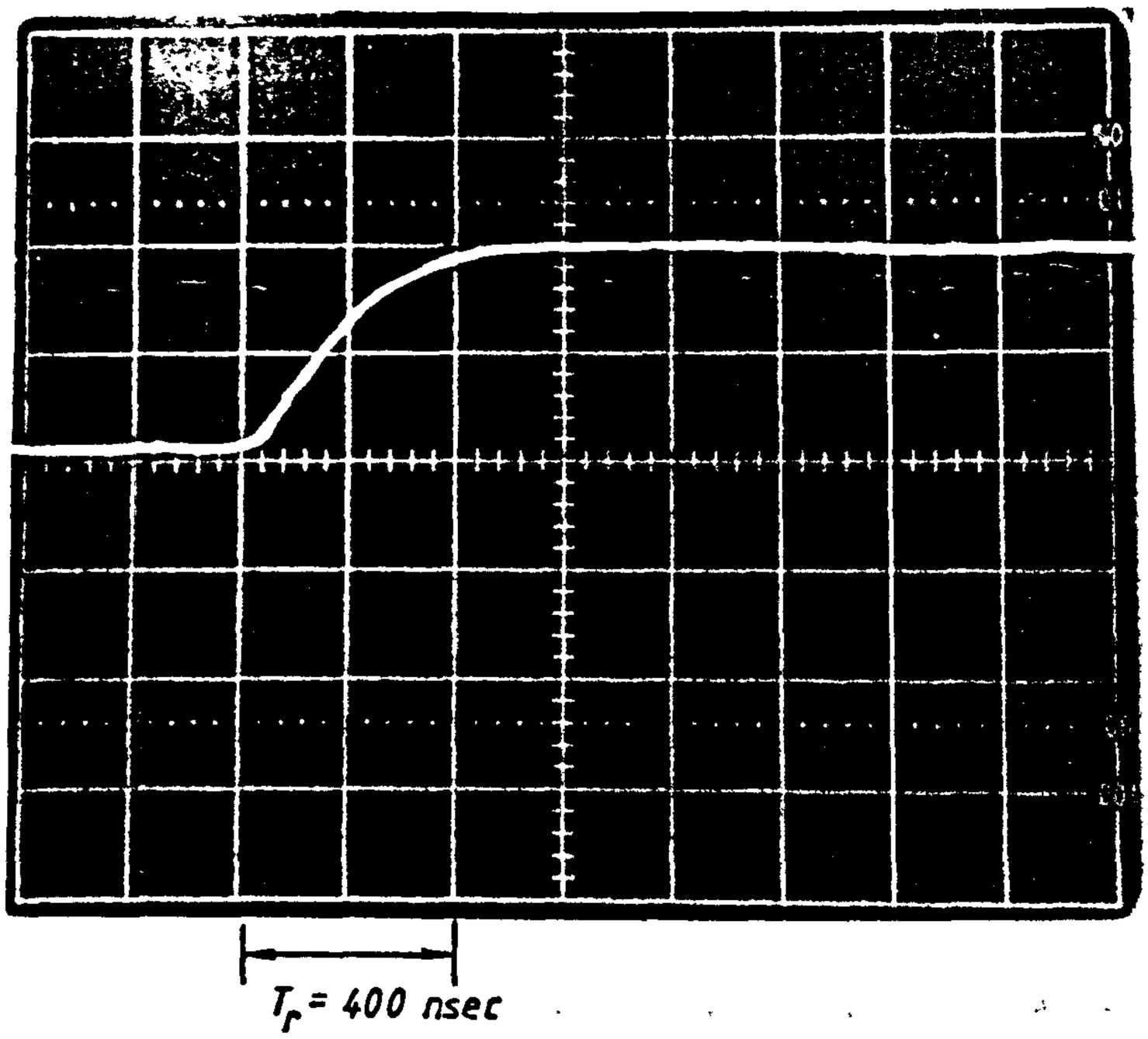

Figure 4.2.2.2 - Pulse Distortion in Delay Line

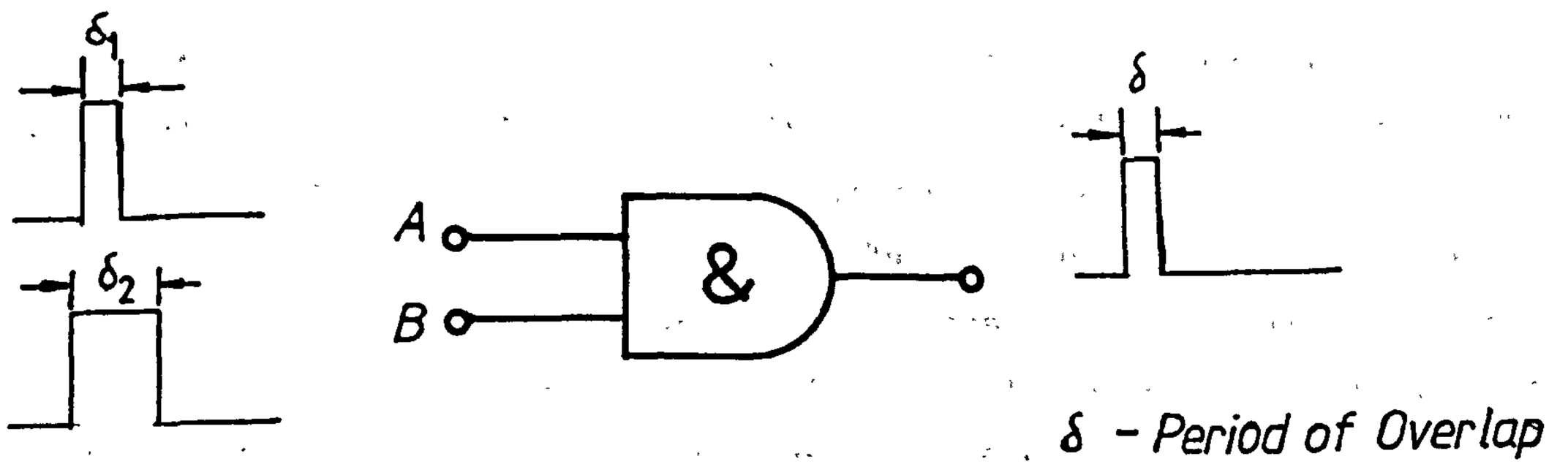

Figure 4.2.3.1 - Coincidence Detection

The implementation of this principle is described with reference to the block diagram of the coincidence unit in figure 4.2.3.2 . Each section of the coincidence unit is described in more detail in the following paragraphs .

4.2.3.1 Polarity Selection

The analogue pulses from the output of the programmable delay line are developed across a 75 ohm matched terminating impedance . Pulses are then passed through a unity gain amplifier which has complementary outputs . The two outputs are connected to a single-pole changeover, analogue switch . This provides the coincidence unit with the facility to select either positive or negative polarity pulses, which is desirable in a partial discharge measurement system .

4.2.3.2 Threshold Detection

After polarity selection , the pulses are passed to a time discrimination circuit which detects the occurrence of the leading edge of the analogue pulse . Several techniques can achieve this [93,94], however the method adopted here relies on the detection of the instant in time when the positive rising edge of the pulse exceeds a threshold level . This level is normally just above that of the noise level in the system .

The threshold detector is basically a high speed comparator circuit which amplifies and limits the differential signal at its input . The inverting input is set at a d.c. voltage level which is variable . This is the threshold level control . The non-inverting input receives the pulse signals for comparison purposes . A positive signal transition above the threshold at the input results in the output going to saturation level . Conversely , the output level falls to zero when the input signal falls below the threshold level . The result is a logic pulse of duration dependent on threshold crossing interval .

This technique of level discrimination is problematic when noise is superimposed on the signal . Noise signal transitions at the threshold level results in multiply transitions at the output of the discriminator, which results in what is termed pulse jitter . The manner in which this is overcome is to apply positive feedback to the

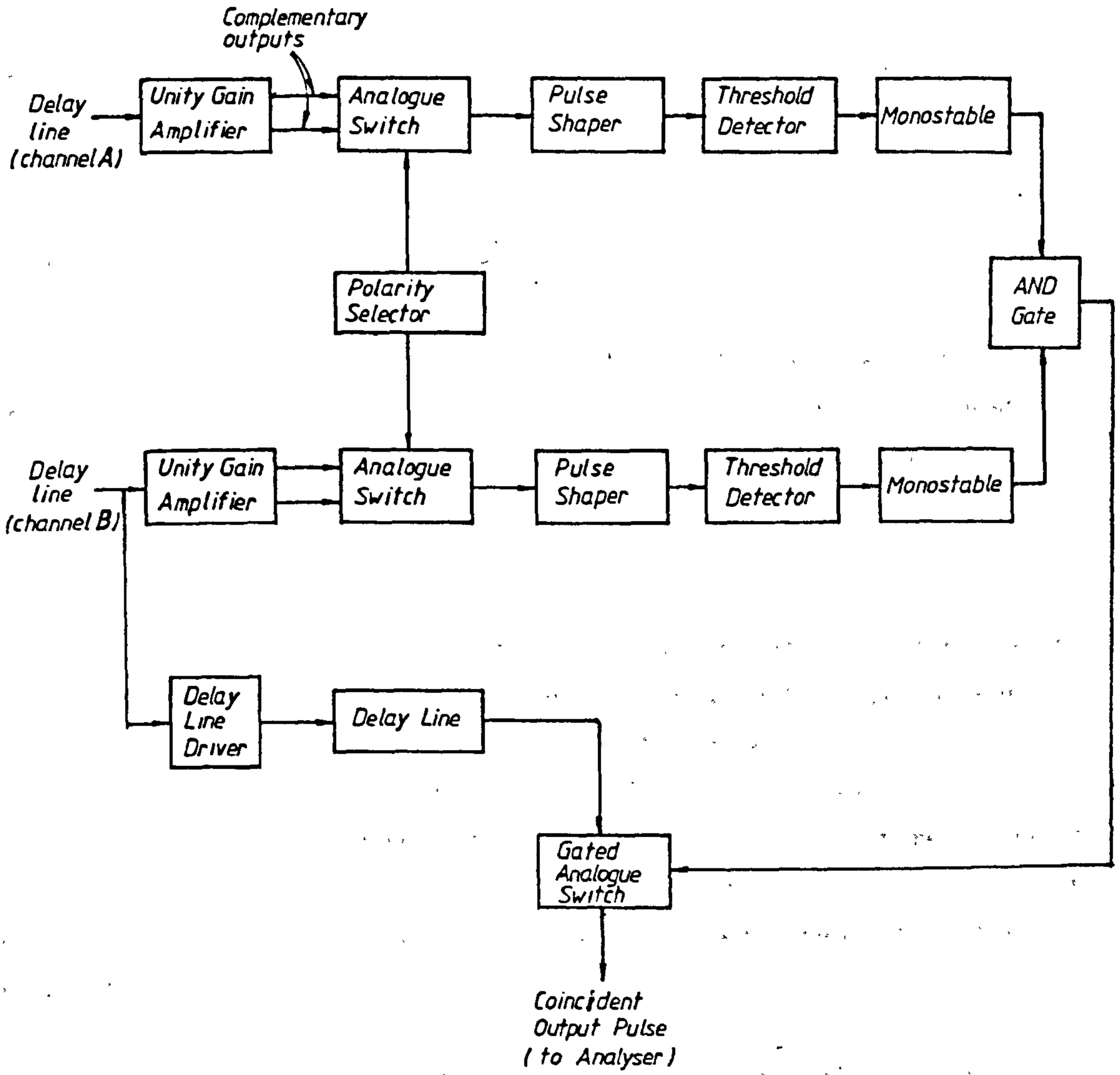

Figure 4.2.3.2 - Block Diagram of Coincidence Detector

comparator . In doing so , hysteresis is introduced into the device's operation . Once a positive transition above the lower hysteresis level takes place at the input, the output rapidly switches to a saturation level . Should the input signal fall below the upper threshold level and fail to reach the hysteresis lower limit , as in the case of spurious noise the output will remain as before . Only when the signal falls through the hysteresis upper limit and below the threshold level can the output revert to zero logic level, (see figure 4.2.3.2.1 . This hysteresis band , in which signal excursions at the input about the threshold level do not affect the output state , is variable between 10 mV and 50 mV about the threshold level depending on the noise present .

4.2.3.3 AND Gate Coincidence Circuit

The variable width pulses from the threshold detector are converted to logic pulses with constant duration , δ , by a monostable multi-vibrator circuit . Resolution of the coincidence operation is 2δ which is 20 nsec since δ is set at the minimum duration of 10 nsec.

Pulses from the monostable circuit in the two channels are directed to a logic AND gate which produces a logic pulse when the two pulses at the inputs are coincident . The width of the gated pulse is equal to the overlap interval of the two input pulses , (see figure 4.2.3.1). In practice the input pulses from the monostables are not rectangular but have a finite rise and fall time . As a consequence the overlap period is shorter and the corresponding coincidence resolution time is less, approximately 15 nsec .

The logic pulse from the AND gate is used to control a high speed analogue switch . When the switch receives a gating signal from the AND gate the discharge pulses from the output of one of the programmable delay line channels is directed through a cable driver circuit to the multi-channel analyser . Discharge signals are fed to the gated switch through a fixed delay line which delays the signals to compensate for the propagation delays of logic signals through the coincidence circuit , (approximately 90 nsec.) .

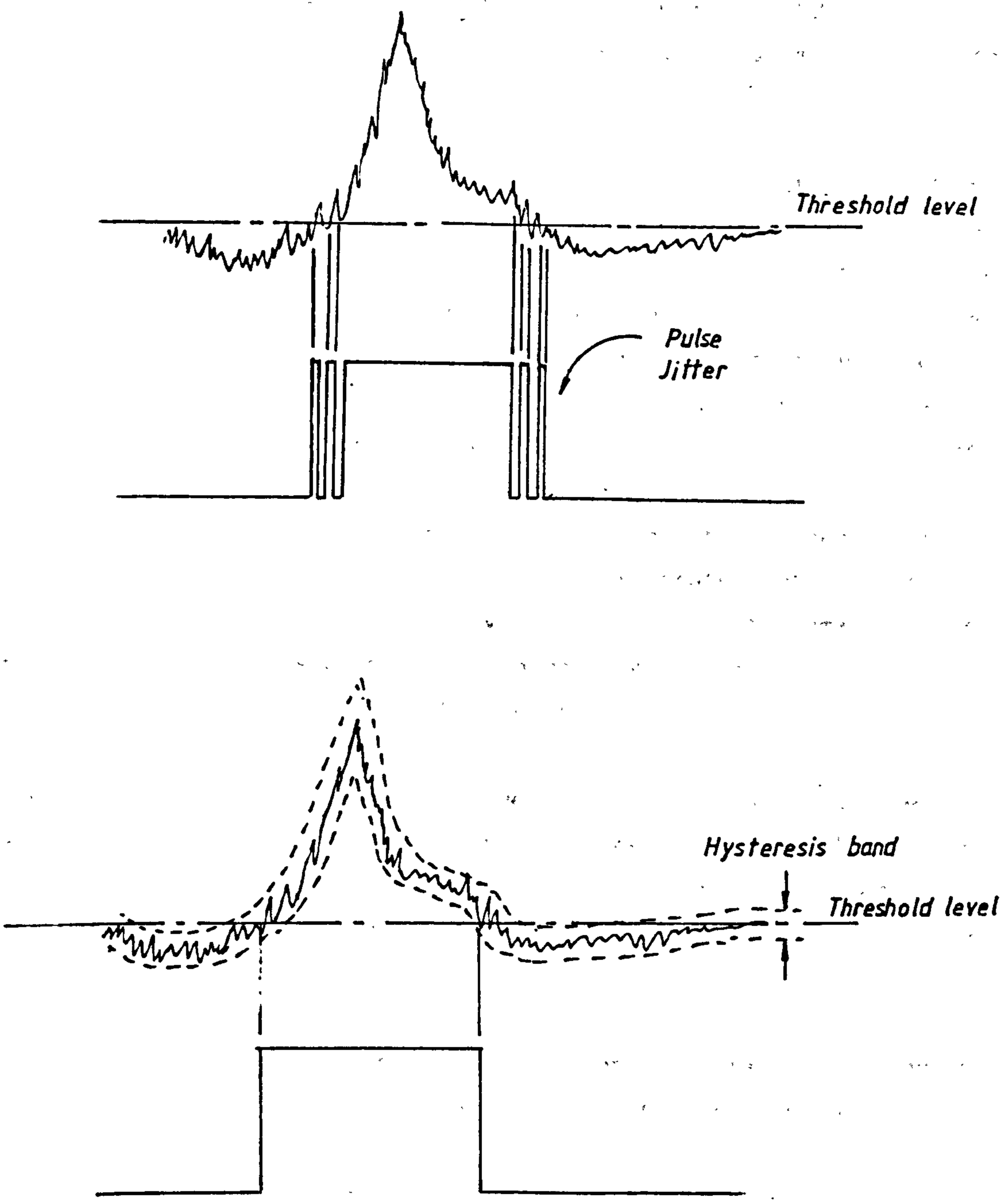

Figure 4.2.3.2.1 - Effect of Hysteresis on Threshold Detection

4.2.3.4 Amplitude and Rise Time Walk

Two detrimental effects on the accuracy of leading edge time discrimination are amplitude and rise time walk [93] . These effects are described with reference to the diagrams in figure 4.2.3.4.1 .

Amplitude walk occurs when pulses have different amplitudes, and are coincident in time, cross the threshold level of the discriminator at different times . As a result the output logic pulses differ in time of origin as the amplitude changes . Rise time walk is a similar behaviour in leading edge discriminators in which pulses are coincident and are of constant amplitude . However, due to different rise times, the pulses cross the threshold level at different times and result in timing errors in the logic pulses . The graph in figure 4.2.3.4.2 shows the discriminator's characteristics when pulses of variable height and rise times are discriminated at a constant threshold level of 100 mV . As would be expected the smallest time errors (or walk) occurs with pulses whose rise time is short and whose amplitude to threshold level ratio is great .

The effects of amplitude and rise time walk are seen as not being a real problem to the coincidence circuit since it is the relative time error,(between channels), that affects the coincidence operation . Only when pulses presented to the discriminators in each channel differ greatly in amplitude and rise time .

Techiques to reduce walk error include constant fraction timing and extrapolated leading edge timing methods outlined in reference 93.

4.2.4 Multi-Channel Analyser : Modes of Operation

The two modes in which multichannel analyser operates are :-

i. Multi-Channel Scaling .
ii. Pulse Height Analysis .

The first of these , multi-channel scaling , is when the analyser stores the number of pulses above a preset amplitude threshold level within a specified time interval , termed the instrument's dwell time. This is repeated for consecutive time intervals in a sample period

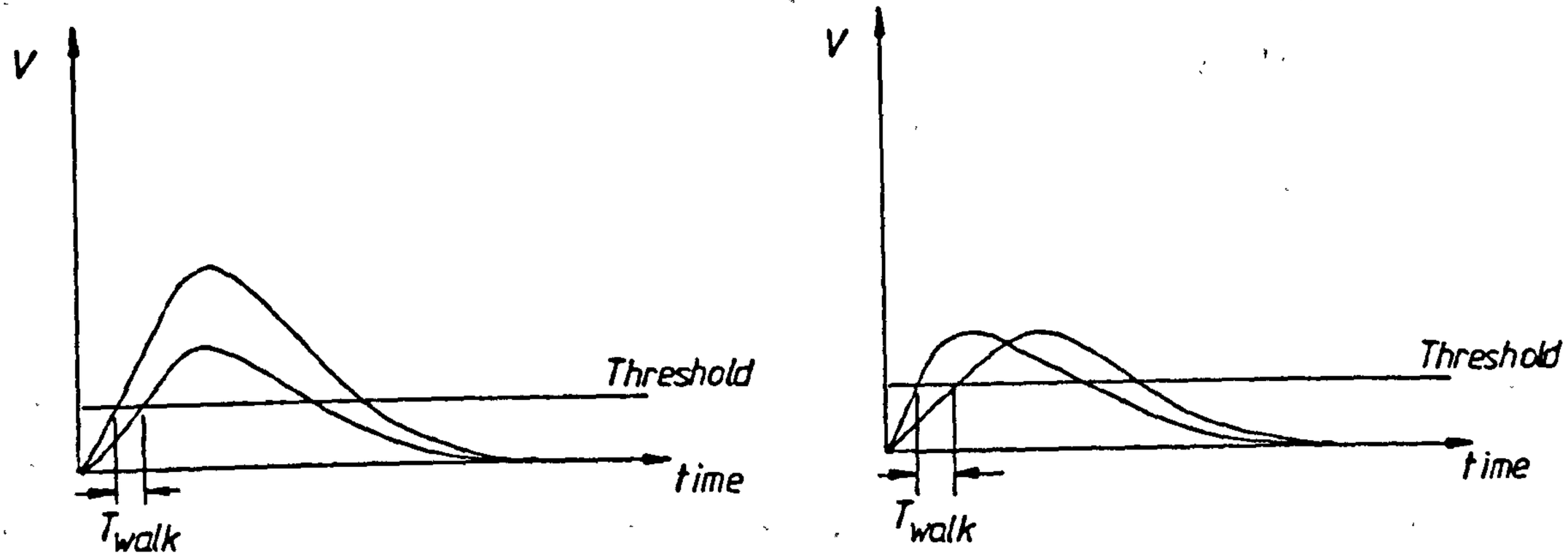

Amplitude walk

Rise-time walk

Figure 4.2.3.4.1 - Amplitude and Risetime Walk

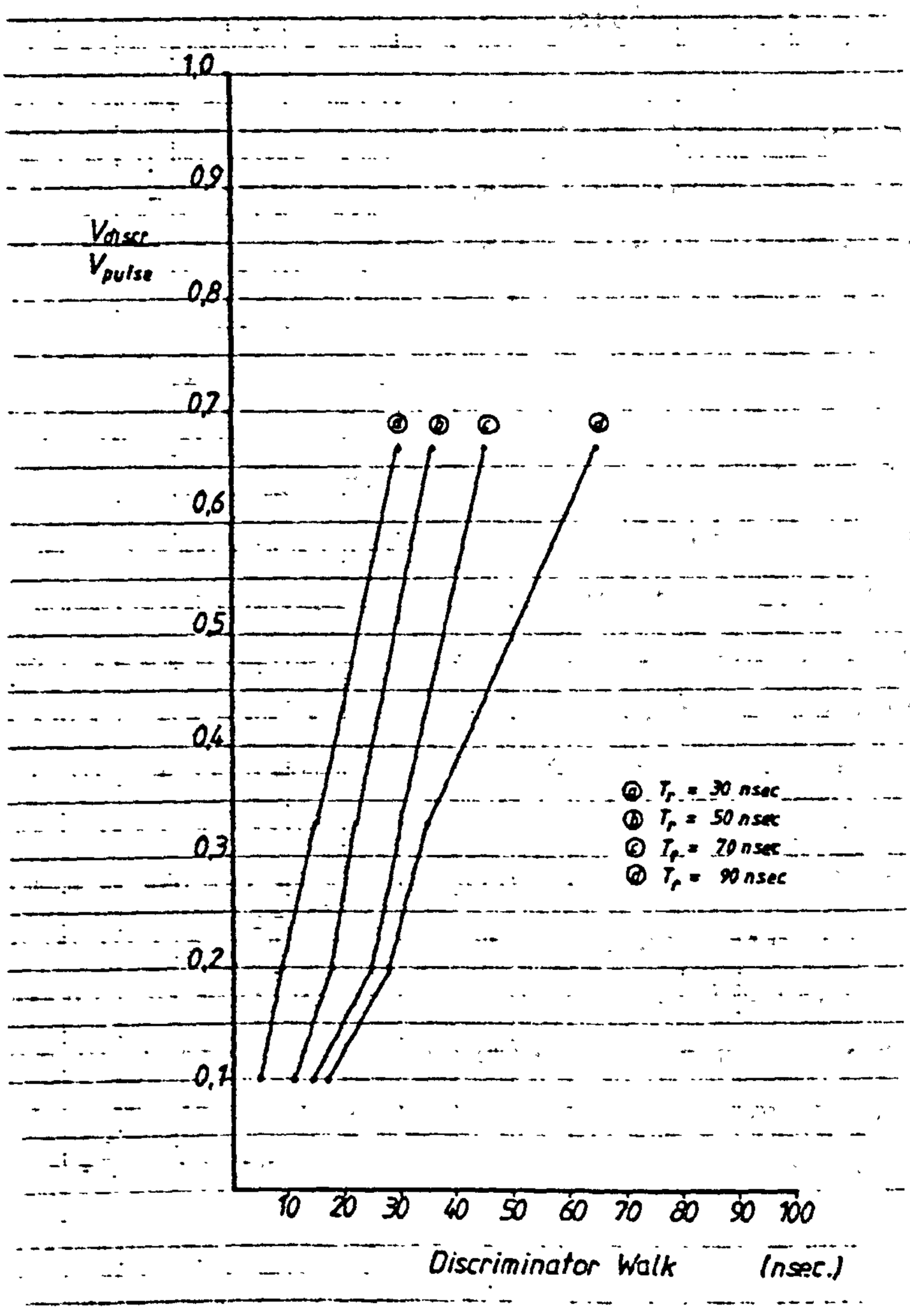

Figure 4.2.3.4.2 - Threshold Discriminators Characteristics

until all memory positions, (channels), are filled . In the correlation scan of the winding each of the memory channels are used to store the number of pulses at a particular location on the winding. To perform this function the analyser requires three signals ; an MCS (multi-channel scaling) start; an MCS reset and a channel advance signal . These control signals are derived from the micro-computer interface cicuit .

The MCS start and reset signals are taken from the address handshake line which goes to a logic zero when the interface is addressed, and to a logic one (high) when reset. However, the interface is addressed each time a byte of data is sent , for a period of 4 msec, (see logic timing diagram in figure 4.2.4.1 . To prevent premature MCS reset an inhibit circuit, (see figure 4.2.4.2), ignores the transition of the address handshake line to reset status for a period of 4.5 msec. Two output monostable circuits control the duration of the MCS start and reset signals ; approximately 2 μsec .

The channel advance signal is derived from the interface receive status signal line. When the interface is addressed this signal line is asserted and a monostable circuit is triggered . The output of the monostable controls the channel advance function and has a pulse duration of around 2 μsec.

Therefore each time the programmable delay line is addressed to change the delay setting , the multi-channel analyser receives a signal to step to the next channel . In this manner each delay setting corresponds to a separate channel in the analyser's memory such that a scan of the winding can be performed . Sequential stepping through every delay setting is software controlled from the microcomputer .

In the pulse height analysis mode, pulses are counted according to their amplitude. The pulse amplitude range is sub-divided into a number of pulse height intervals ; this number depends on the number of memory channels in the multi - channel analyser. The result is a frequency distribution of pulse amplitudes . The amplitude may be calibrated in picocoulombs of charge for partial discharge measurements .

It is the intention to utilise the pulse height analysis technique to assess the magnitude and severity of a particular discharge mechanism

having used the scanning technique to ascertain the point on the winding which has the highest level of discharge activity. Discussion of this is given in more detail in chapter one .

4.2.5 Data Transfer and Presentation

Multi-channel scaling and pulse height distribution data is transferred from the multi-channel analyser to the microcomputer via an RS-232 data highway , (at 19200 baud) . A high speed buffer memory in the microcomputer interface stores the data from a single analyser distribution under the control of a data aquisition program . A special image specifier program is then used to retrieve the useful data from the buffer memory by removing the control and data sequencing characters . The scan or distribution is then stored in a permanent storage medium in a specified data file for subsequent processing . Once stored , the data file may be retrieved for display on the microcomputer screen or to produce a hard copy on a plotter .

The instrumentation system , M.I.C.A. : Machine Insulation Condition Analyser , described in the preceding sections is shown in the photograph in figure 4.2.5.1 .

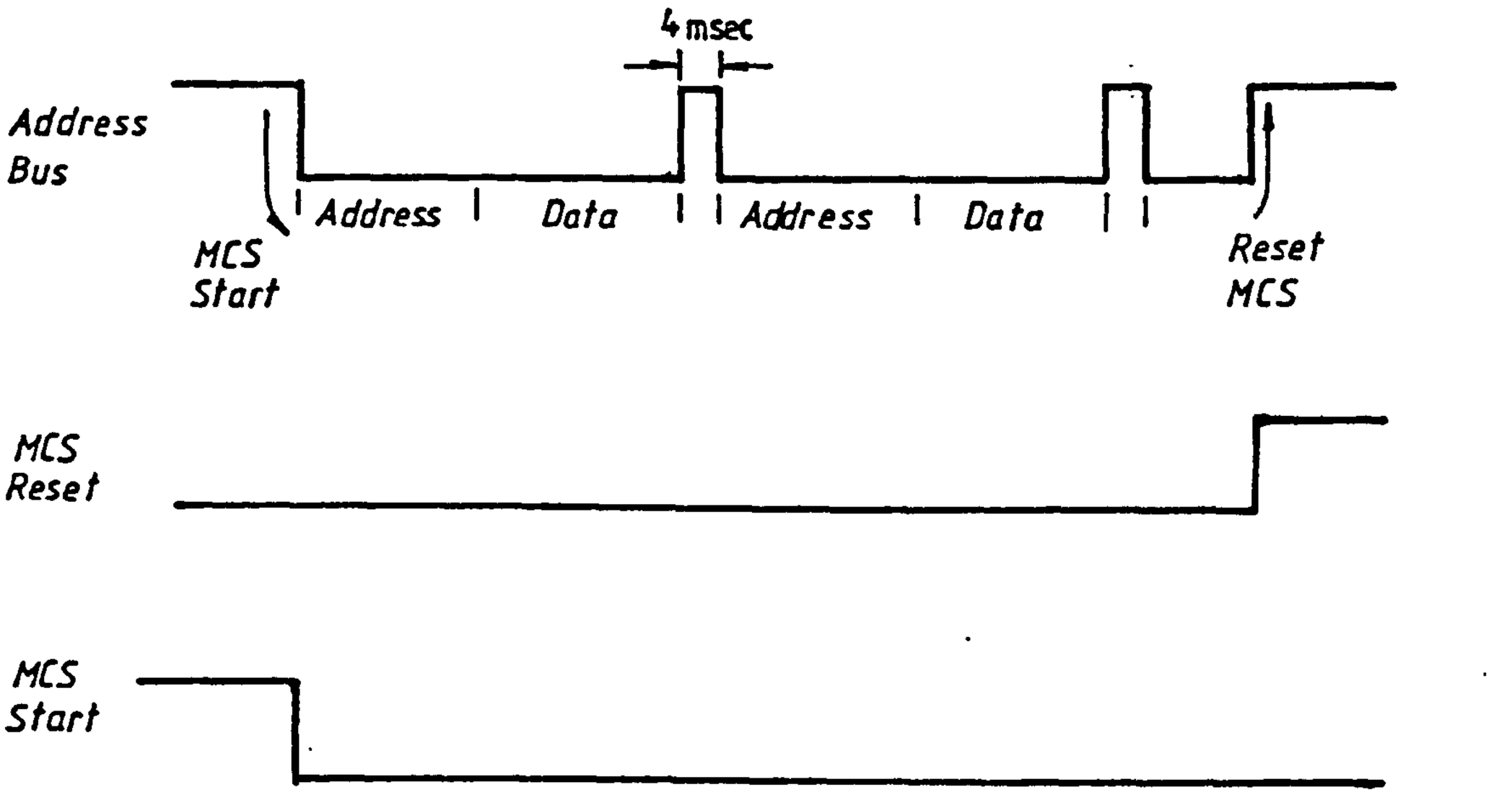

Figure 4.2.4.1 - Logic Timing Diagram

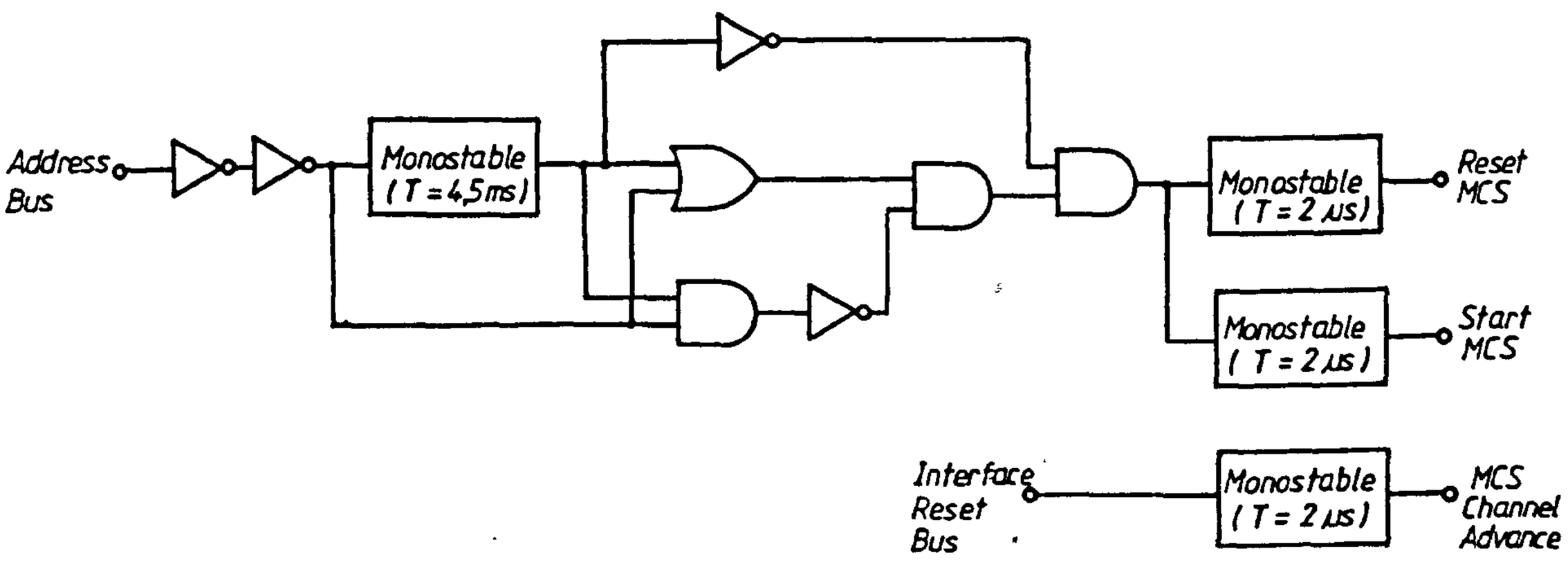

Figure 4.2.4.2 - Scan Control Circuit

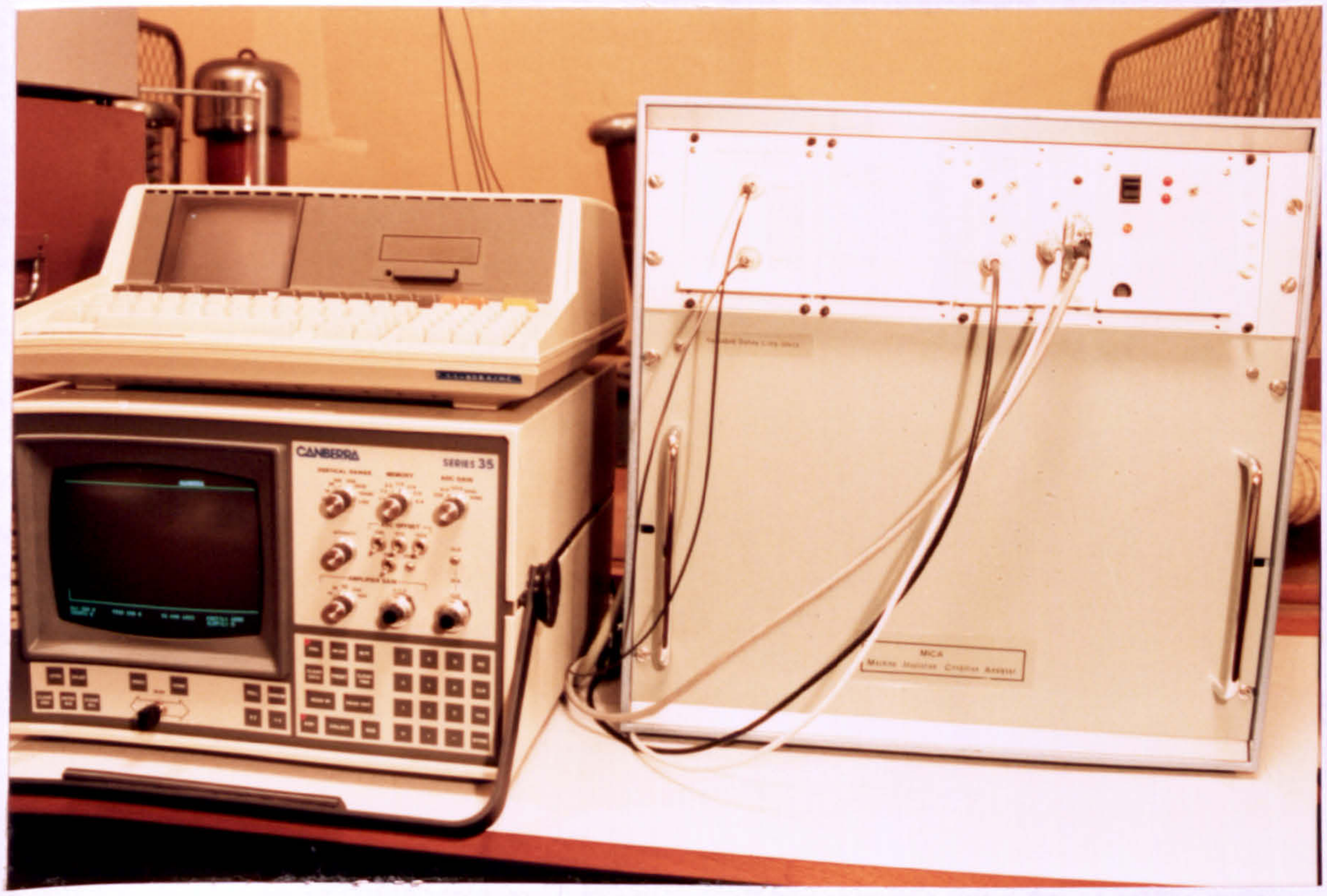

Figure 4.2.5.1 - MICA : Machine Insulation Condition Analyser

4.3 Results from Correlation Experiments

The following sections detail the results of tests designed to assess the behaviour of MICA with respect to accuracy of location under various modes of pulse injection and terminating impedance configurations.

Investigation is restricted to tests performed on a model winding comprising six stator coils. The experimental circuit is shown in figure 4.3.1 , where intercoil connections , (points of pulse injection), are numbered from c1 to c7 and the terminating impedance, Z, is variable in the range 0 to 1000 ohms .

Tests are divided into two categories as follows :-

i. Pulses injected from an artificial source.
ii. Pulses injected from a high voltage source.

4.4 Artificial Discharge Source Injection

Discharge pulses are derived from the circuit shown in figure 4.3.1. The artificial discharge pulses are unipolar, decaying exponential, pulses; the charge content, of which , is determined by the coupling capacitance and the peak voltage of the rectangular input pulse. Thus, a 5000 pC discharge is produced with a pulse amplitude of 10 volts and 500 pF capacitor .

4.4.1 Matched Termination Impedances.

In this first test, the winding is terminated at both ends in a matched impedance of 330 ohms . The correlation scan of the winding is shown in figure 4.4.1.1 which represents the superposition of separate correlation scans of the winding for pulses injected at each of the coil interconnections and at the terminations.

The location peaks are equally spaced along the axis and the width of the peaks are no greater than 2 delay line increments. Temporal resolution of location is therefore no greater than 13 nsec propagation time in the winding which corresponds to a spacial accuracy of approximately 1.4 metres of the winding length .

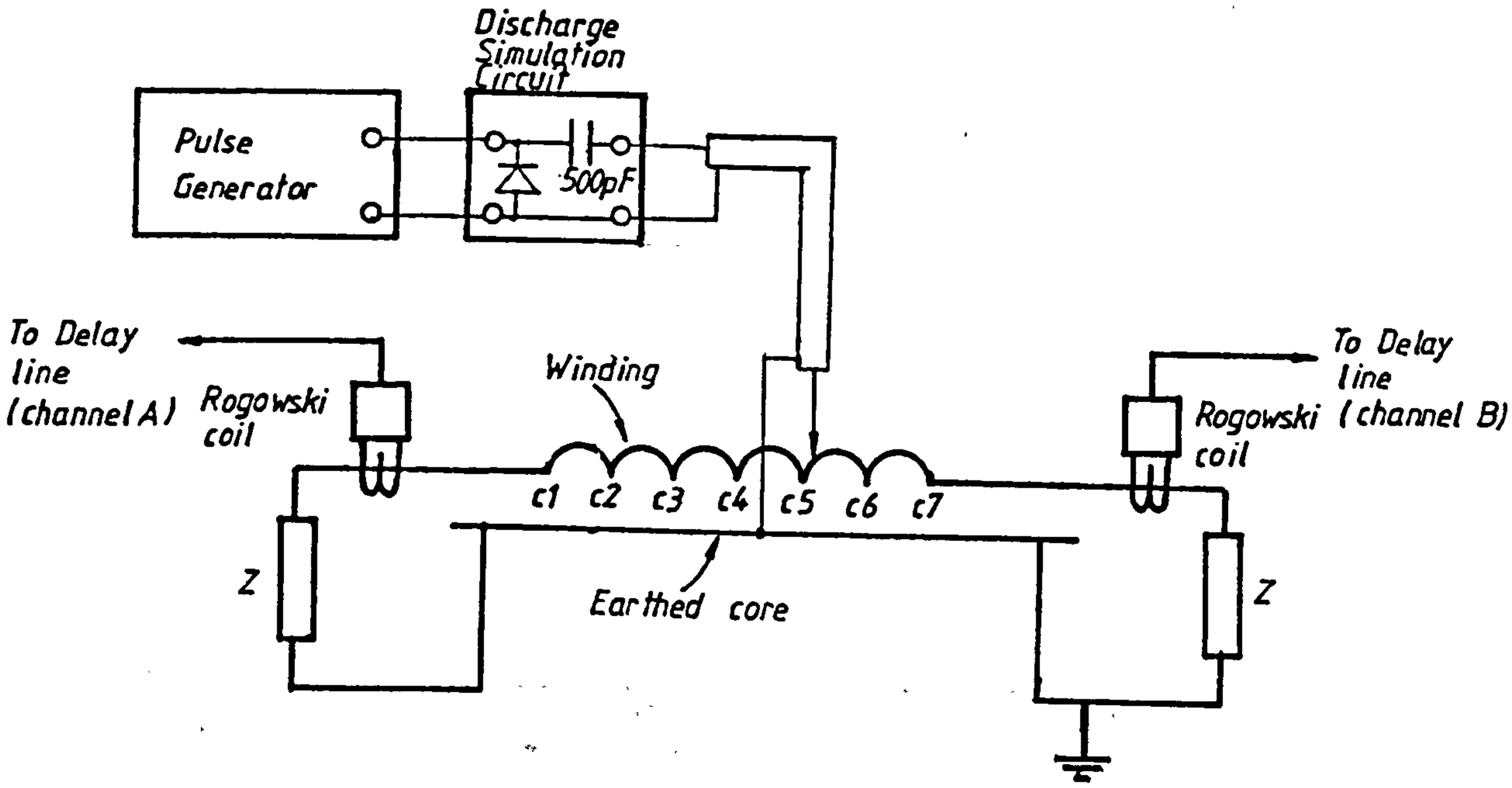

Figure 4.3.1 - Discharge Injection Test Circuit

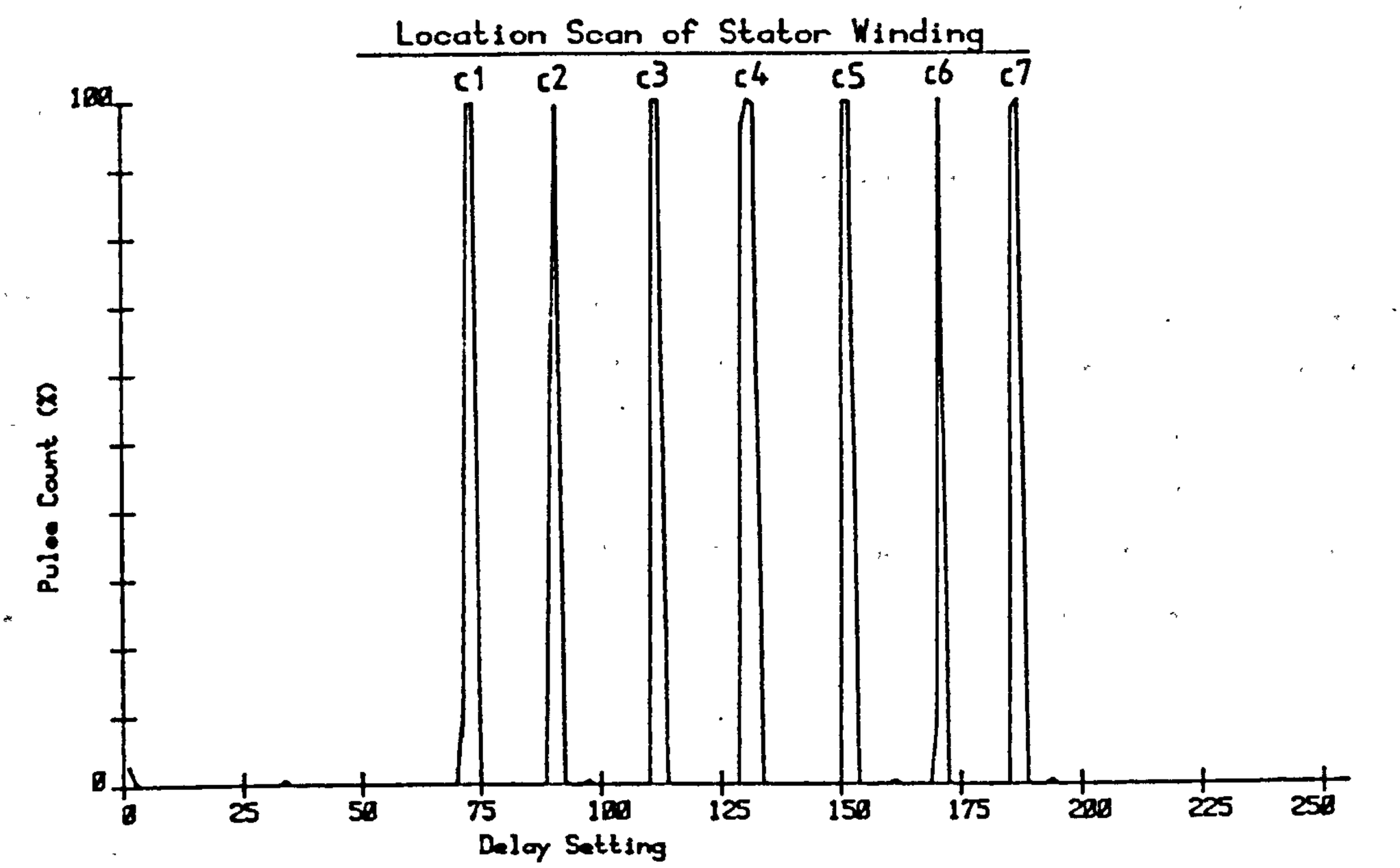

Figure 4.4.1.1 – Scan of Winding with Matched Terminating Impedances

The position of the discharge source may be related to the location peak on the scan through a simple expression . It is recalled that at a particular discharge source location, pulses will arrive at the winding terminals with a differential delay time, td . For coincidence to occur this delay difference must equal the differential delay in the programmable delay lines. Therefore it can be stated that :

$$\pm t_d = t_1 (D_1 - D_2) \qquad \ldots(4.12)$$

where, D_1 - delay line setting in channel A .

D_2 - delay line setting in channel B .

The delay through a unit length of cable (delay increment) , t_1, is fixed at the measured value of 6.5 nsec. The differential delay, td, may have positive or negative values depending on which half of the winding the discharge source is located . Since there are 256 possible delay settings in each of the programmable delay lines it follows that $D_2 = 256 - D_1$. Rearranging the expression 4.12 , we obtain :

$$\pm t_d = t_1 (2D_1 - 256)$$

from which it follows that,

$$D_1 = \pm \frac{t_d}{2t_1} + 128 \qquad \ldots(4.13)$$

Therefore, knowing the differential delay, td, from pulse propagation measurements it is possible to calculate the expected delay setting. The delay setting corresponds to channel position on the scan plot on the multi-channel analyser .

The maximum delay difference is equal to the propagation time through the complete winding. Substitution of this value into equation 4.13 for positive and negative differential delays, determines the channel positions of the winding terminals, hence the boundaries of the location scan.

In the scan of a winding with six coils the delay through the winding is observed to be approximately 750 nsec. This places the terminals of the winding at channel positions 70 and 185. The channel

positions of the remaining peaks on the location scan in figure 4.4.1.1, are given in table 4.4.1.2 .

To verify the accuracy in the position of these peaks the actual time differences between the arrival of the pulses in either channel were obtained from waveform observations, and are given in table 4.4.1.2 . From the time delay differences , expression 4.13 is used to calculate an expected channel position for each pulse source location.

Pulse injection Point	Channel Position Observed	Expected	Delay difference td observed (nsec)
c1	72	61	770
c2	90	89	520
c3	111	110	230
c4	131	128	0
c5	152	145	230
c6	170	168	520
c7	186	187	770

Figure 4.4.1.2 - Calculated and Measured Scan Locations

Error in the observed location peak positions is on average 3 channel positions which corresponds to a temporal error of 19.5 nsec and a spatial error of 2.1 m of the winding length. This error approximately 2.9 % of the total length of the winding.

In each of the correlation scans performed the pulse repetition frequency is 4.2 kHz which is a pulse repetition period of 238 μsec. The sample period at each channel position during a scan is 250 msec ,(set by the microcomputer), so that the expected pulse count at the location peaks is 1050 pulse, i.e.

$$n = \text{p.r.f.} \times \text{channel sample time} \quad \ldots\ldots(4.14)$$

The observed pulse count for one of the peaks, which is representative of each of the other peaks, is 1090 pulses. This difference in pulse count is due to errors in the measurement of the values of channel sample time and pulse repetition rate .

4.4.2 Effect of Discrimination Levels on Discharge Location

In this experiment the influence of varying the discrimination levels in the coincidence detector on the accuracy of the location technique is investigated. As in the experiment detailed in section 4.4.1. a scan is obtained for each position of pulse injection, with the exception that the discrimination level on one channel input to the coincidence unit is changed.

In the experiment of section 4.4.1 the discrimination voltage levels were as follows :-

Channel A - 150 mV.
Channel B - 120 mV.

which is a discrimination level difference of 30mV . In this experiment the level in channel A is increased to give settings of :

Channel A - 200 mV.
Channel B - 120 mV.

The effect which is expected from a change in discrimination level in one channel is explained with reference to the diagrams in figure 4.4.2.1 .

In the first diagram, pulses originate close to channel A and as a result pulses with fast rise times are seen at channel A and slower rise time pulses at channel B, due to pulse distortion through the winding. By increasing the discrimination level on channel A the point of coincidence is effectively shifted by time t_c which corresponds to a shift in delay setting to obtain coincidence. This results in a shift of the position of the location peaks towards the position of channel B on the location scan.

When pulses are injected closer to the termination monitored by channel B the pulses observed in channel A have longer rise times. As a consequence, a greater shift in the location peaks is expected due to the longer wavefront of pulses observed in channel A. The shift in the position of peaks, is likewise, towards the position of the winding termination connected to channel B . This is due to the fact that the delay introduced into channel A must be reduced to

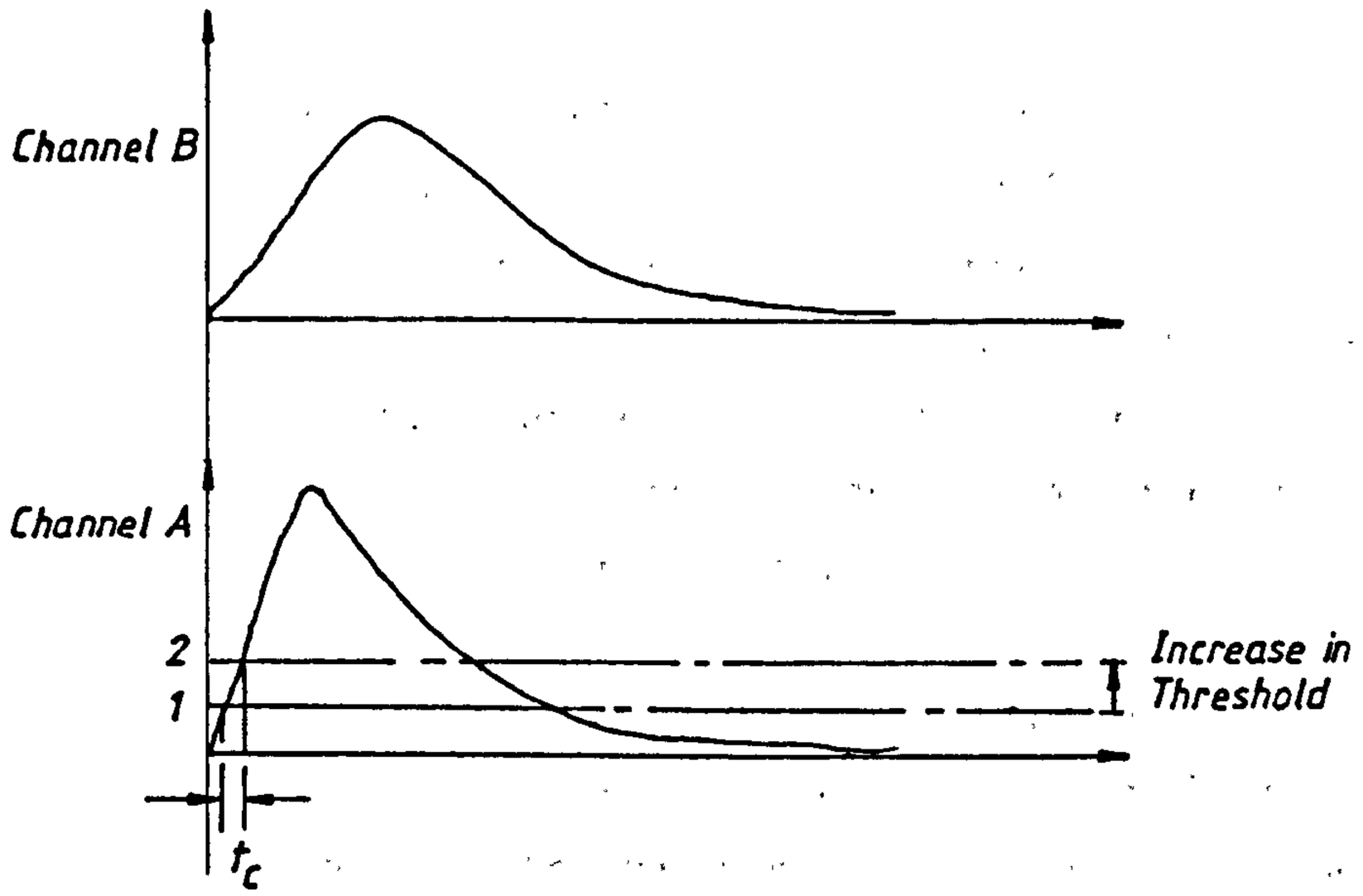

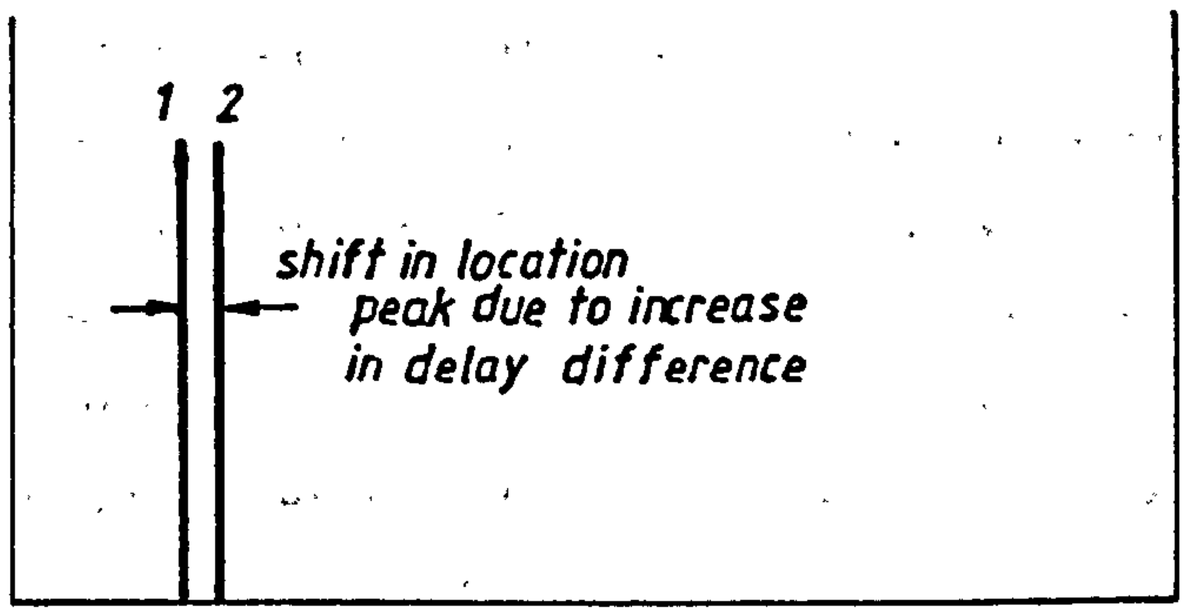

Figure 4.4.2.1 - Effect of Changing Threshold Level on Location Scan

obtain pulse coincidence.

The scan shown in figure 4.4.2.2 does indicate a shift in the spectrum of location peaks towards the position of channel B , but does not show a progressively larger shift of peaks when pulses are injected closer to channel B . The reason for this is explained as follows. When pulses are injected close to channel B , longer pulse rise times are seen at the terminal connected to channel A . It is this difference in pulse rise time that results in the greater shift in the position of location peaks . However , pulses in channel B are delayed for a proportionately longer time than pulses in channel A to obtain coincidence , so that at the output of the programmable delay lines there is a considerably smaller difference in pulse rise times in each channel. The compensating effect of the delay lines is to produce a smaller shift in the location peak distribution .

In each of the correlation scans the pulse repetition frequency of injected pulses is 4.2 kHz , which for a sample period at each delay increment of 250 msec gives an expected maximum pulse count at the location peaks of 1050 pulses . The observed value is 1084 pulses which is approximately the same value for each of the location peaks , showing good repeatability in the instruments pulse interval resolution .

4.4.3 Influence of Winding Terminations on Location

In a star connected high voltage motor the phase winding is not terminated in an impedance which matches its own , but at one terminal, by two other phase windings and at the other terminal by the cable connecting the motor to the supply . It is therefore necessary to investigate the behaviour of MICA under different terminating conditions to assess the usefullness of the device in a practical situation . Two tests are performed to determine the effect of mis-matched termination impedance on the location capabilities of the instrument .

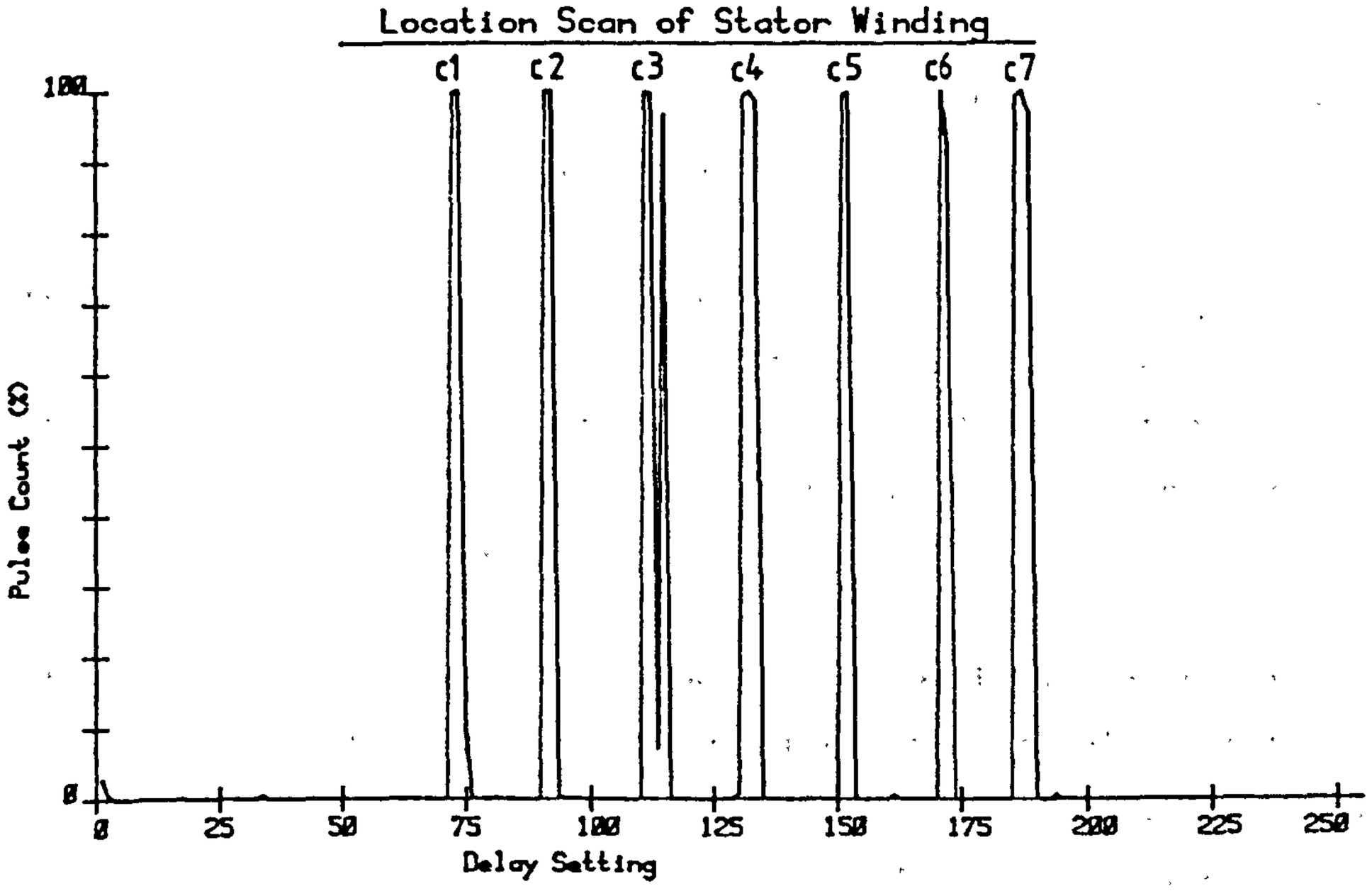

Figure 4.4.2.2 - Scan of Winding with Altered Threshold Level in Discriminator

The experiment in section 4.4.1 is repeated for terminating impedance configurations as follows :-

i. Terminal c1 is terminated in a 20 ohm impedance, which is representative of a power cable characteristic impedance. Terminal c7 is terminated in the winding impedance of 300 ohms .

ii. Terminal c1 is terminated in an impedance of 20 ohms . Terminal c7 is terminated in an impedance of 150 ohms , which represents the junction of the other two phase windings at the star point .

The result of the collective location scans for the first terminating impedance configuration is shown in the scan in figure 4.4.3.1 . The reason , that only six location peaks are recorded , is that , at the point where the pulses are injected across a 20 ohm impedance the pulse generator is overloaded .

The repetition frequency of injected pulses is as in the previous tests , 4.2 kHz , which for a sample period at each delay position of 250 msec. , gives an expected pulse count of 1050 pulses . The maximum pulse count observed is 1079 which is approximately the pulse count in all of the location scan peaks .

The position of the location peaks are given in the table in figure 4.4.3.2 for both the expected and observed values . Expected location positions are calculated from expression 4.13 which assumes a knowledge of pulse propagation characteristics for the termination conditions described .

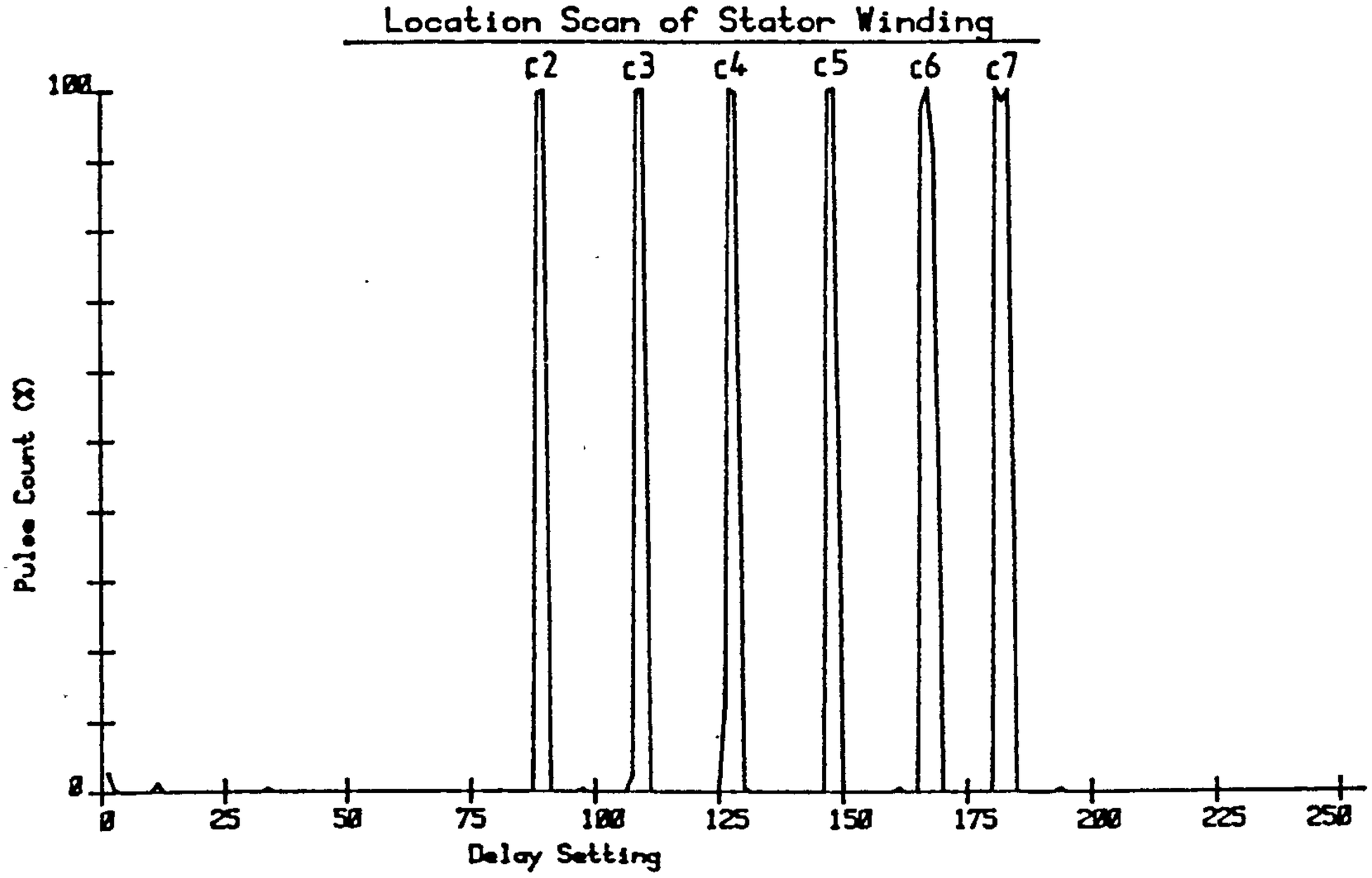

Figure 4.4.3.1 - Scan of Winding - 20/300 ohm Terminating Impedances

Pulse Injection Point	Channel Position Observed	Expected	Delay Difference t Observed (nsec.)
c2	89	85	505
c3	108	105	300
c4	127	128	0
c5	148	148	260
c6	167	171	560
c7	182	183	720

Figure 4.4.3.2 - Calculated and Measured Locations

A comparison of the positions of corresponding location peaks in the scans for matched terminations in figure 4.4.1.1 and these results show that the introduction of a low impedance termination at one end of the winding causes a shift in the true location peak positions towards the low impedance terminal position . This shift in location peaks is progressively larger for pulse injection points closer to the matched impedance terminal .

The magnitude of this shift indicates the error in the location position introduced by the low impedance , which is given in the table in figure 4.4.3.3 .

Pulse Injection Point	Location Peak Shift	Location Error (metres)
c2	1	0.7
c3	3	2.1
c4	4	2.8
c5	4	2.8
c6	3	2.1
c7	4	2.8

Figure 4.4.3.3 - Error in Scan Locations

A maximum shift of 4 channel positions occurs , which corresponds to an error in the true location of 2.8 metres of the winding length , (or two coil turns) .

In this second experiment , the winding is terminated in an impedance of 20 ohms at one end and 150 ohms at the other . Pulses are injected at a pulse repetition frequency of 4.2 kHz to give an expected pulse count of 1050 pulses . For a delay setting dwell time of 250 msec the measured pulse count is 1086 , which is approximately the pulse count in each scan .

The distribution of the location peaks from each of the winding scans is shown in figure 4.4.3.4 . Similar to the previous scans the width of the location peaks is no greater than two delay increments , which is 1.4 metres of the winding length . The positions of the location peaks on the scan are close to the predicted positions taken from the pulse propagation measurements for the particular terminating impedance conditions . The observed and expected locations are given in the table in figure 4.4.3.5 .

Pulse Injection Point	Channel Position		Delay Difference t (nsec.)
	Observed	Expected	
c2	88	85	560
c3	107	105	300
c4	126	128	0
c5	145	151	300
c6	165	171	560
c7	182	186	750

Figure 4.4.3.5 - Calculated and Measured Locations

By introducing an impedance of 150 ohms at one end of the winding and a 20 ohms impedance at the opposite end , the effect on the resulting scan is a shift in the positions of the location peaks towards the low impedance terminal of the winding . This displacement of the location peaks is slightly greater than in the previous experiment which leads to the conclusion that the presence of asymmetric terminating impedance accentuates the displacement of the location positions of discharge sources towards the low impedance end of the winding . The magnitudes of the shift in the location peaks relative to the matched termination case , taken as reference , is shown in figure 4.4.3.6 .

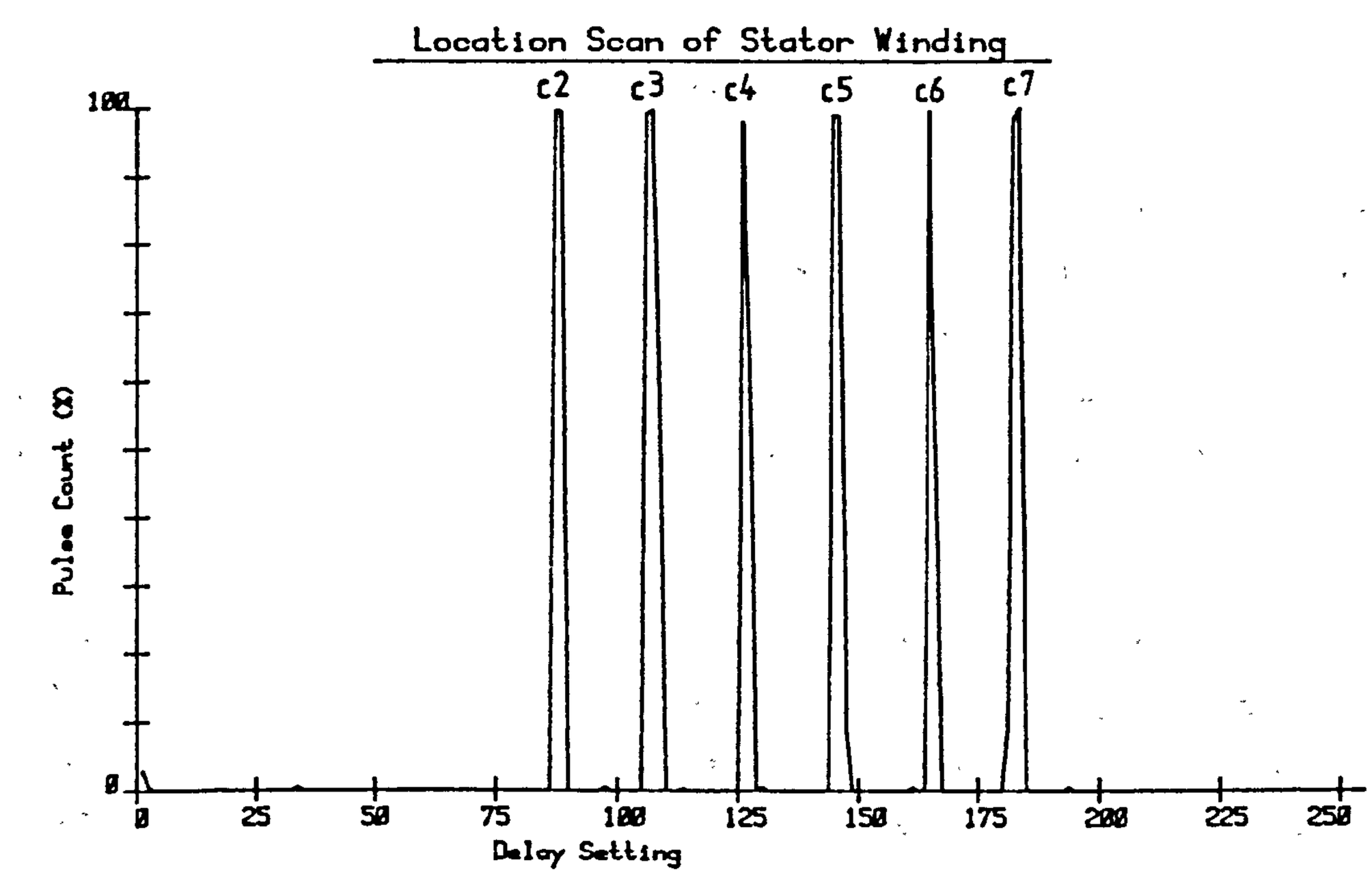

Figure 4.4.3.4 - Scan of Winding - 20/150 ohm Terminating Impedances

Pulse Injection Point	Location Peak Shift	Location Error (metres)
c2	2	1.4
c3	4	2.8
c4	5	3.5
c5	7	4.9
c6	5	3.5
c7	4	2.8

Figure 4.4.3.6 - Error in Locations

As seen from the table , the error in discharge location is a maximum two coils distance from the high impedance terminal of the winding . It is an error of 4.9 metres of winding length which is about three coil turns . The reason for this behaviour is due entirely to the influence of the terminating impedances on the shape of the injected pulse , in particular its wavefront .

It is concluded from these experiments that any discontinuity in impedance at the winding terminals results in a displacement of the location positions of discharge sources on the scan . In addition this displacement is governed by the presence of a relatively low impedance at one winding terminal which causes a shift in the scan location peaks towards the low impedance terminal position .

4.4.4 Effect of Endwinding Pulse Injection

Hitherto , artificial discharge pulses have been injected into the coil interconnections . In this experiment the pulses are injected into the winding at an intermediate point in each coil endwinding opposite the coil connections . The purpose of this test is to determine what effect the mode of pulse injection has on the position of discharge locations on a scan .

Pulses from a pulse generator are coupled into the endwinding of a coil through a coupling capacitor constructed from a narrow strip of aluminium foil wrapped around the coil conductor stack . The width of the foil section is 40 mm and the distance around the periphery of the coil conductors is 115 mm .

It is assumed that for these dimensions and at the signal frequencies of concern , (less than 200 MHz) , the coil conductor stack may be regarded as a single conductor . In this case the foil will act as one electrode of a parallel plate capacitor with the coil conductors acting as the other electrode . From these assumptions the following expression may be used to calculate the value of the coupling capacitance .

$$C = \frac{\epsilon_0 \epsilon_r A}{d}$$

d - main insulation thickness in the endwinding which is 2mm.
A - area of the foil capacitor plate .

The estimated coupling capacitance is therefore 135 pF . Pulses from the pulse generator have an amplitude of 53 V which produces discharge pulses with a charge content of 7155 pC .

The winding is terminated in its characteristic impedance at one terminal and a 20 ohm impedance at the other . Pulses are injected at a frequency of 4.2 kHz with a scan interval at each delay increment of 250 msec .

Figure 4.4.4.1 shows the location scans at each of the injection points collectively . It is readily seen from this result that the way in which pulses are injected greatly effect the performance of MICA . Location peaks are no longer uniform in shape and the pulse count at each location varies markedly . The observed and expected channel positions of pulse locations are given in the table in figure 4.4.4.2 along with the pulse count at each location peak .

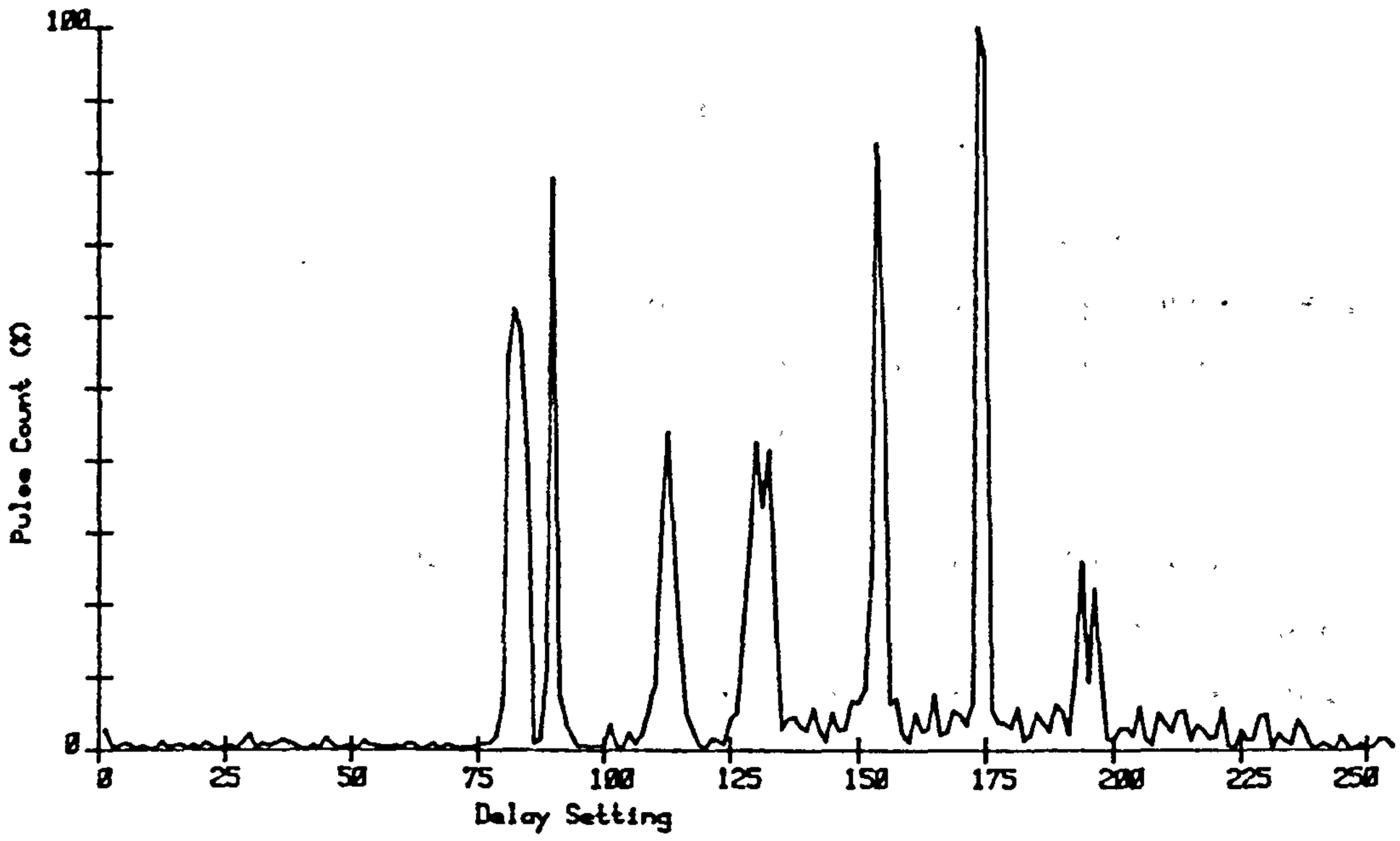

Figure 4.4.4.1 – Scan of Endwinding Injected Pulses

Pulse Injection Point	Channel Position Observed	Expected	Delay Difference t (nsec.)	Pulse Count
c1	82	87	520	678
c2	89	94	440	887
c3	112	112	200	488
c4	129	141	180	473
c5	153	163	460	931
c6	173	178	650	1112
	193	-	-	287

Figure 4.4.4.2 - Error in Locations

A spurious discharge location peak occurs at a position close to the end of the winding which is terminated in the winding impedance . It is likely that this irregularity is due to changes in the shape of the pulse causing accidental coincidence triggering .

To obtain a clear understanding of the results it is necessary to compare the scan obtained in this experiment with the scan produced in figure 4.4.3.1 for the same termination conditions . This is shown on the composite scan in figure 4.4.4.3 .

The position of the location peaks from the first scan indicate the positions of the coil interconnections and serve as a reference to assertain the true location peaks of pulses injected in the endwindings . The positions of location peaks 5 and 6 are at the intermediate positions as expected , however , the location peaks 2,3, and 4 are almost in line with location peaks 1,2, and 3 in the previous experiment which are at the coil inter-connections . This error in locations represents a shift in the location peaks towards the low impedance terminal . Location peak 1 is closer to the low impedance terminal position than the first loaction peak in the previous experiment , which is consistent with what is expected .

Although the scan , showing pulses injected at the coil endwindings , appears to have irregularities in the location and shape of peaks and variations in the pulse counts , it must be appreciated that the mode of pulse injection is complex , since each of the conductors in the coil are excited simultaneously by the injected pulse . In a motor in which partial discharges take place it is reasonable to say that

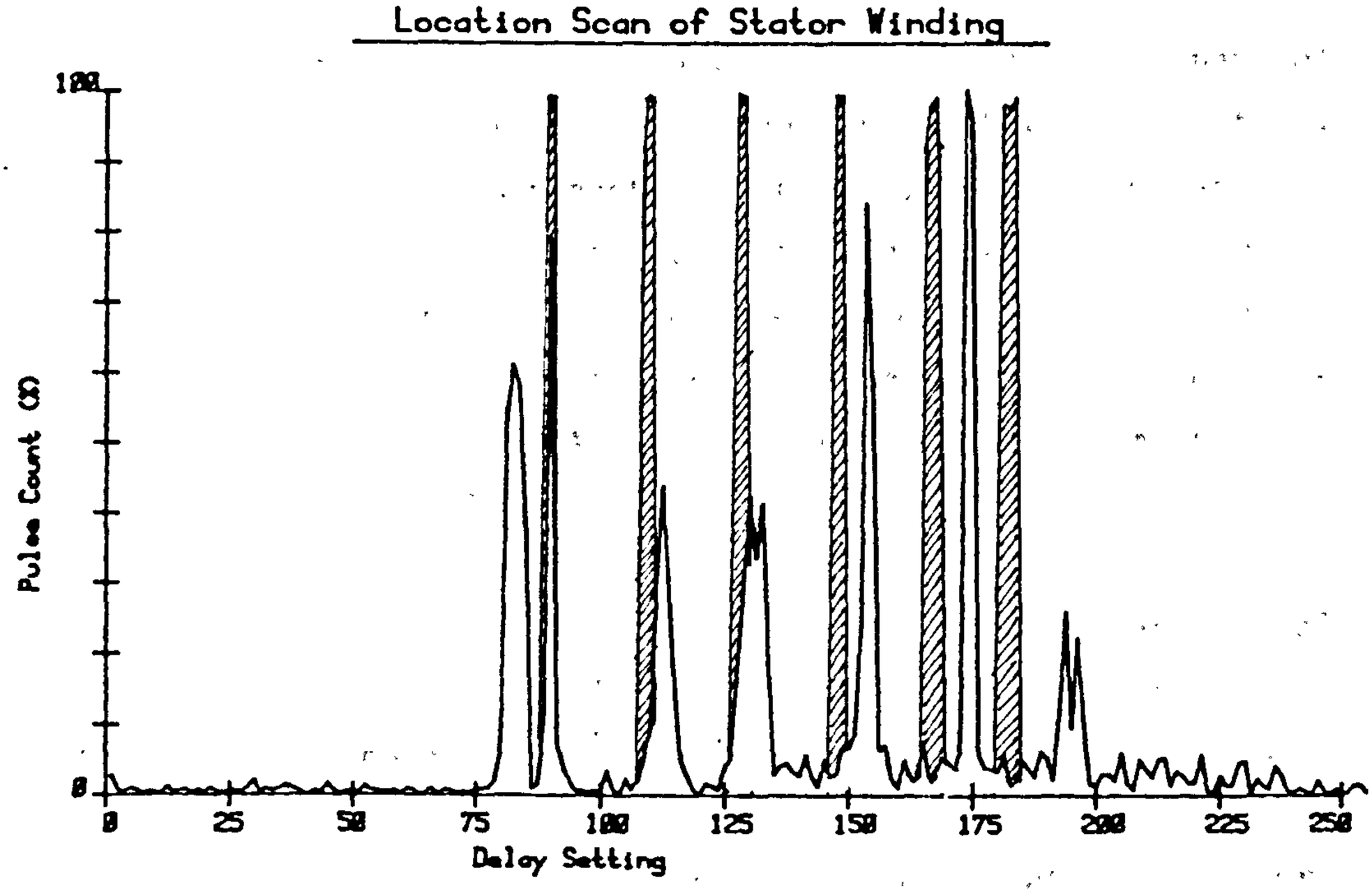

Figure 4.4.4.3 – Composite Scans

internal partial discharges and surface discharges are unlikely to affect more than two coil turns since the area of the region in to which charge is transferred is very small .

In the light of these findings , the performance of the location technique is promising .

4.4.5 Simultaneous Discharge Pulse Injection

In an electrical motor connected to a high voltage supply , partial discharges will normally take place , some of which will inevitably occur at or around the same moment in time . It is reasonable to expect that the number of instances of simultaneously occuring discharges will reduce for larger discharges since these are fewer in number . The object of this series of experiments is to assess the behaviour of the instrument MICA to the presence of simultaneous discharges in a machine winding .

Simultaneous discharges are simulated by injecting artificial discharge pulses from a single pulse source into two different points on the test winding through a coupling capacitor of 500 pF , as shown in figure 4.4.5.1 . The pulses injected at the two points are time coincident with a fixed repetition rate so that stationary oscilloscope traces may be observed and used to explain the resulting behaviour of the location instrument .

In the following experiments the winding is terminated in a 20 ohm resistance at terminal c1 and a 150 ohm resistance at terminal c7 . The coincidence threshold levels are as follows :-

Channel A : 100mV.
Channel B : 30mV.

Pulses are injected at a frequency of 8.4 kHz . One source is located at point c7 whilst the other source is connected in turn to positions c6,c5,c4,c3, and c2 . The purpose of this is to demonstrate the effect coincident pulses injected at different points on the winding has on the accuracy of pulse location .

In the first test , pulses are injected at points c6 and c7 on the

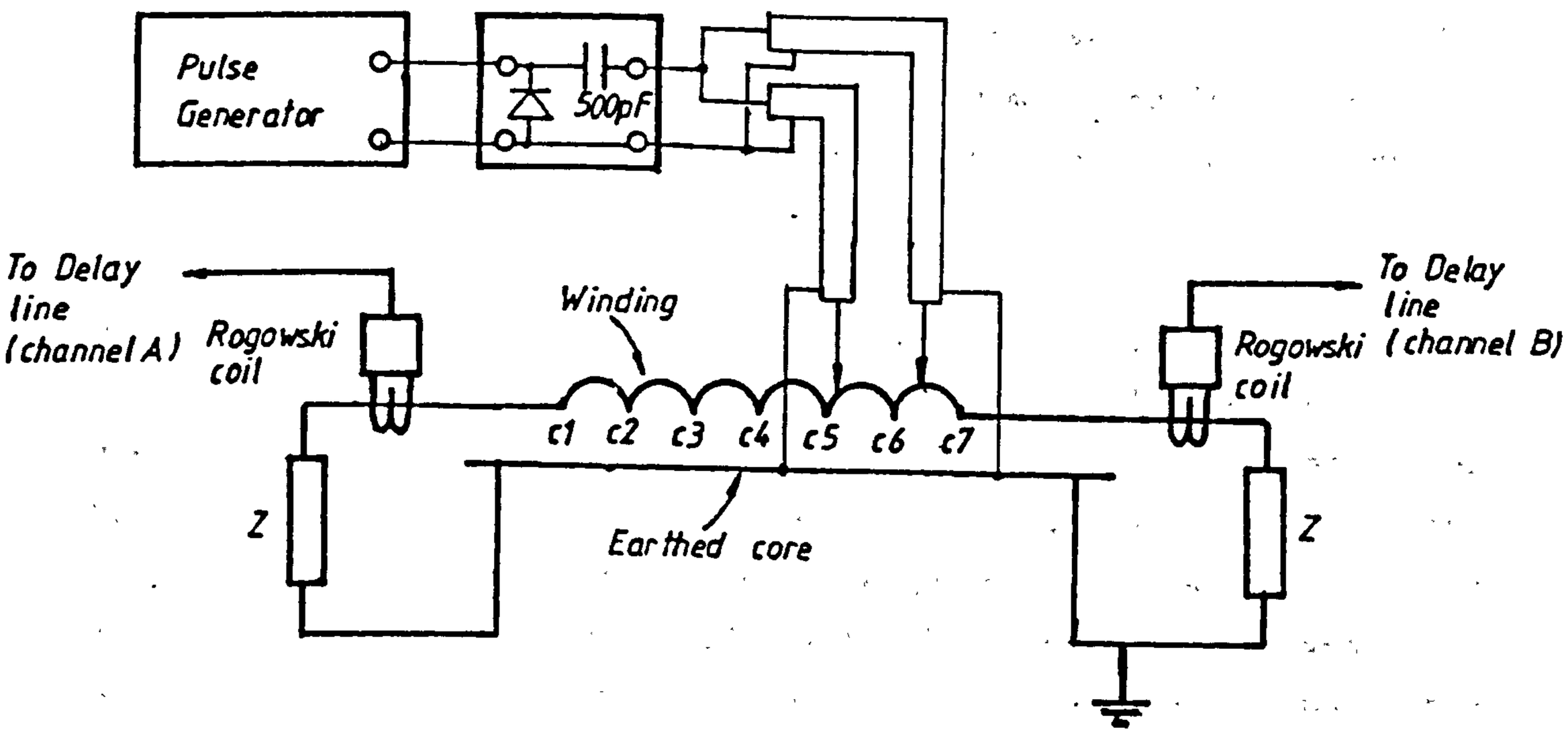

Figure 4.4.5.1 - Simultaneous Pulse Injection Circuit

winding . The corresponding location scan shown in figure 4.4.5.2 indicates that there is only one source of discharges at channel position 87 . This is the location of the pulse source at point c6 on the winding .

To explain why only the pulse source at c6 is sucessfully located it is necessary to examine the current waveforms observed at either of the winding terminals . These waveforms are displayed in the oscilloscope traces in figure 4.4.5.3. The current waveform observed at c7 shows the pulse injected at c7 arrives at the terminal immediately . This pulse is the amalgamation of the pulses from both sources since they are separated by a small time interval of only 100 nsec . The rising edge of this pulse is of the pulse injected at position c7 since this is the first pulse to arrive at terminal c7 . This pulse is followed 1300 nsec later by a much smaller pulse which is the reflection of the initial pulse at the low impedance terminal c1 .

The waveform observed at terminal c1 is similar . A single pulse arrives at terminal c1 after a delay of 650 nsec . This pulse is also the combination of the two pulses injected at c6 and c7 and has longer duration due to transmission line distortion . Again the the rising edge of this pulse is that of the pulse injected at position c6 since this pulse arrives at terminal c1 first . This pulse is followed by an attenuated pulse about 1300 nsec. later which is the reflection of the same pulse at terminal c7 .

From the waveforms it is clear that only one pulse location can be determined since the coincidence detector is unable to discriminate between two amalgamated pulses . The reason the location peak appears at position c6 is simple to explain . The coincidence detector sees on one input the rising edge of the pulse injected at c7 and at the other input , the rising edge of the pulse injected at c6 since , as stated previously , these fronts arrive at the respective terminals c7 and c1 first . It is on these edges that the coincidence detector discriminates .

For a delay dwell time of 250 msec and a pulse frequency of 8.4 kHz the expected pulse count is 2100 pulses compared to an actual count of 2016 pulses .

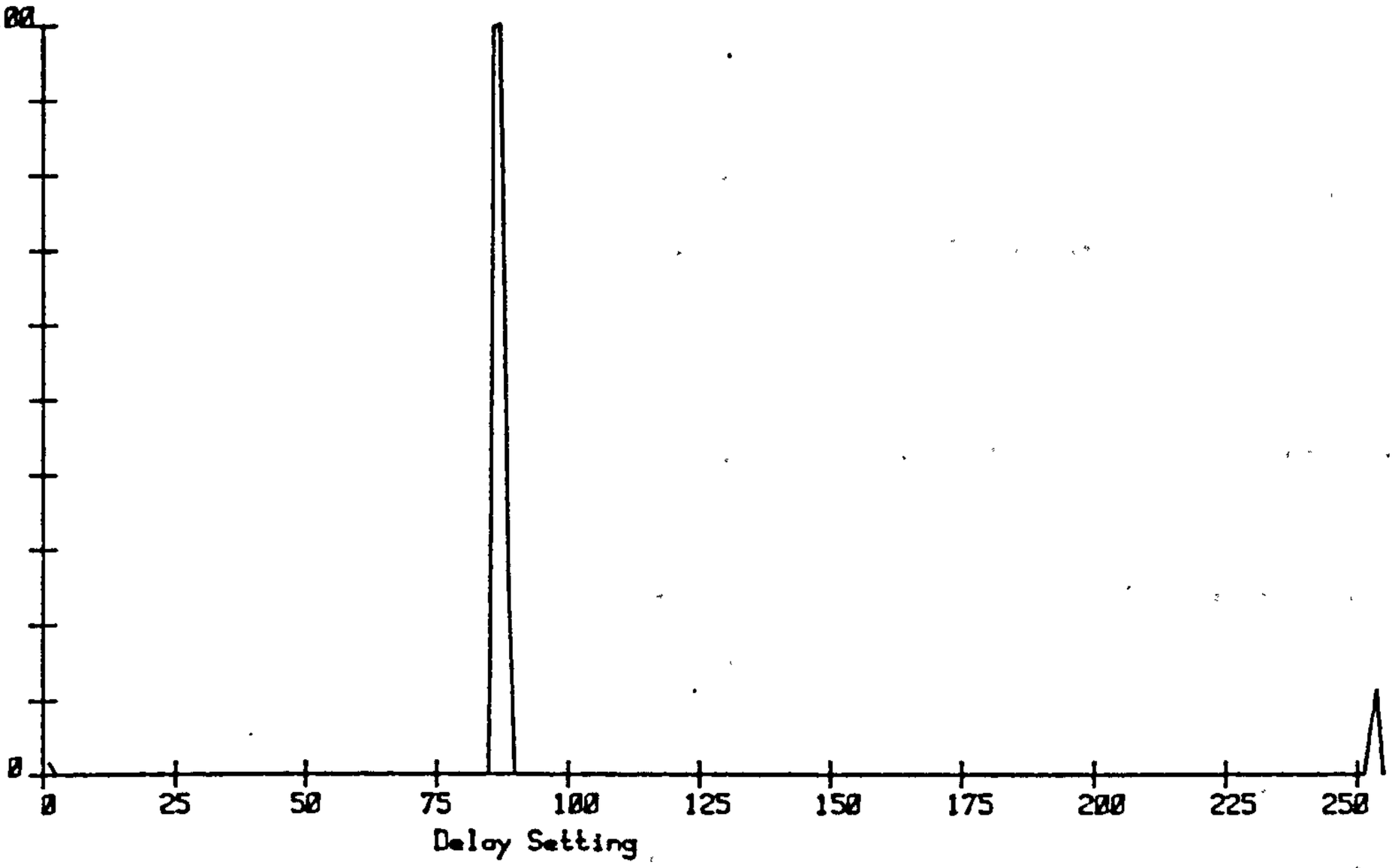

Figure 4.4.5.2 - Scan of Pulse Injected at Positions c6 and c7

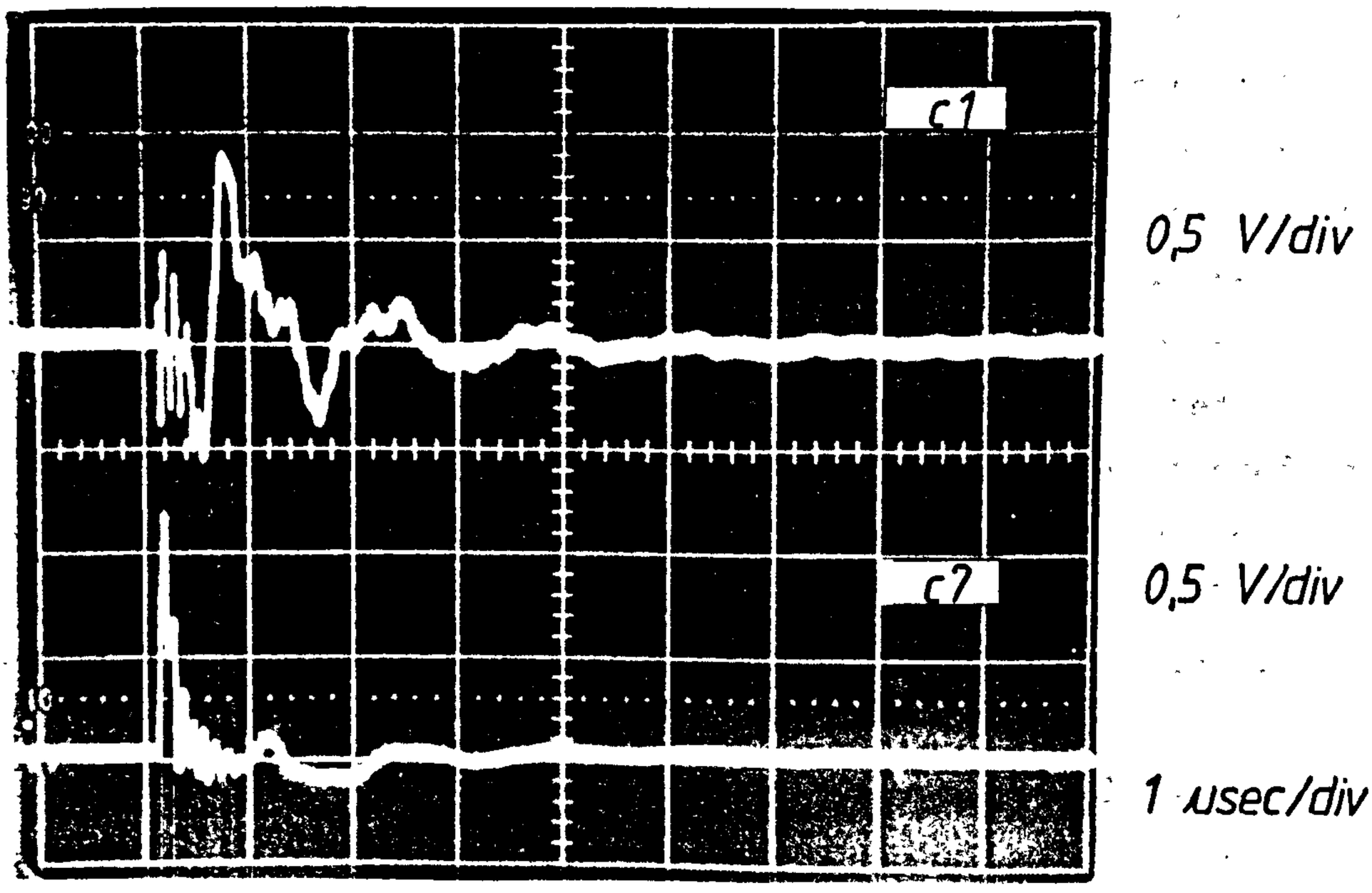

Figure 4.4.5.3 - Pulse Waveforms

The spurious location on channel 253 is unaccounted for since it is difficult to see any possible pulse coincidence from the current waveforms observed in figure 4.4.5.3 .

In this next scan , the pulse sources are positioned at the coil connections c7 and c5 , a distance of two coil lengths apart . The corresponding location scan is shown in figure 4.4.5.4 .

Only one location peak is detected , which is at a delay setting of 98. This location appears half way between expected locations at 72 and 107. The reason for this behaviour is explained with reference to the signal waveforms shown in figure 4.4.5.5 .

It is seen from the signal observed at terminal c7 that a pulse arrives at c7 immediately , followed by the pulse injected at c5 which is approximately 240 nsec later . Soon afterwards the reflection of the pulse injected at c5 is detected , which is followed closely by the pulse injected at c7 . The pulse lattice diagram in figure 4.4.5.6 shows the sequence of pulse events . Similarily at terminal c1 the pulse injected at c5 is observed initially , followed 240 nsec. later by the pulse entered at c7 . The subsequent reflections of these pulses follow .

As regards the location instrument these two pulses are still sufficiently close as to appear as a single pulse . The origin of this pulse is determined from the time delay difference between the rising edges of the pulses which arrive first at the end terminals . At terminal c7 the first pulse front is detected immediately whereas at terminal c1 the first pulse front is detected after approximately 440 nsec. , which is the transit time of the pulse injected at c5 travelling to terminal c1 .. The time delay difference is therefore -440 nsec . By using the expression 4.13 ,the position of the location peak which corresponds to this delay difference is expected to be at a delay setting of 94 which is very close to the recorded position .

The measured pulse count of 2070 also compares well with the calculated value of 2100 pulses .

The experiment is repeated with the two pulse sources injected at connections c7 and c4 on the winding .

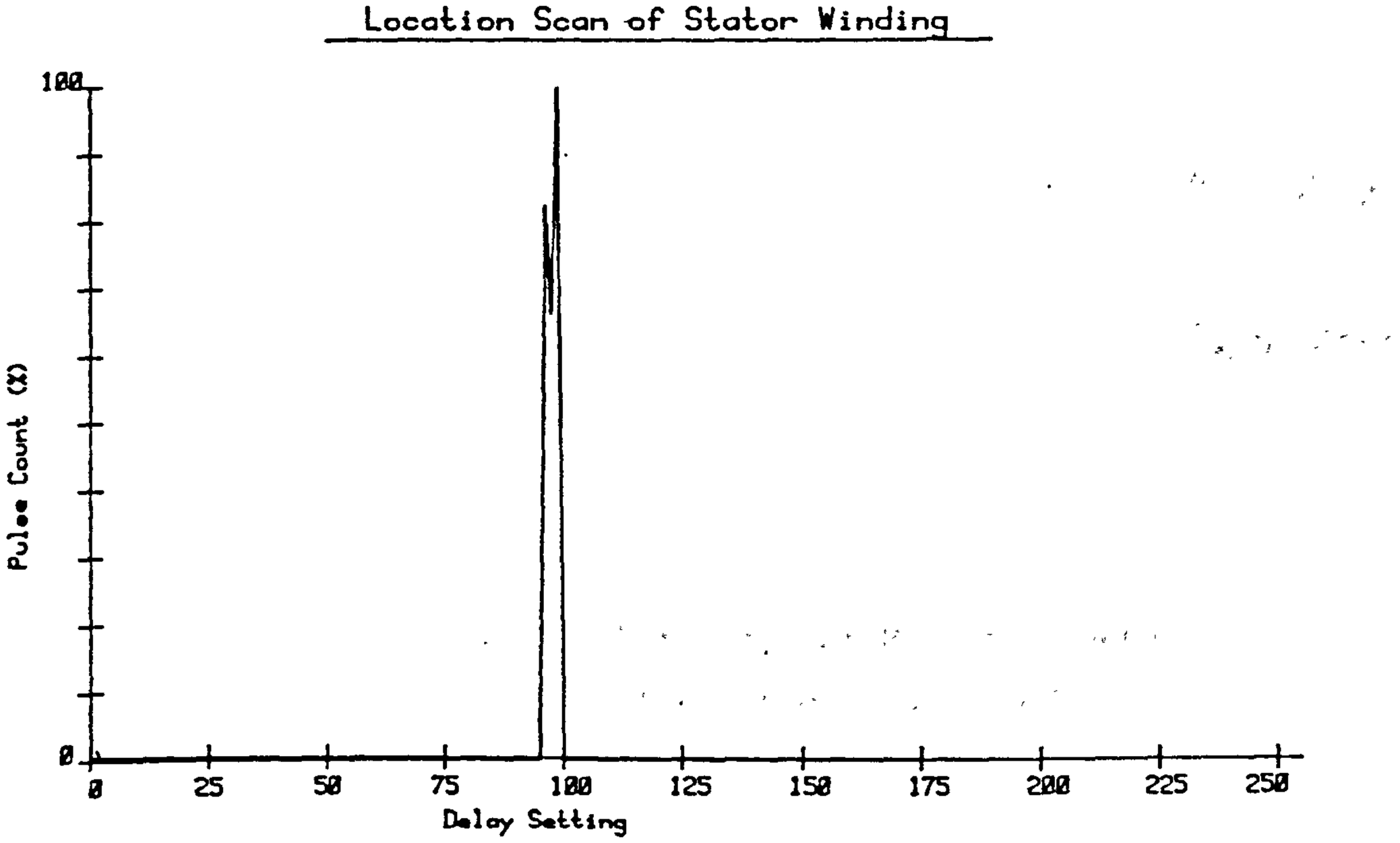

Figure 4.4.5.4 - Scan of Pulses Injected at Positions c5 and c7

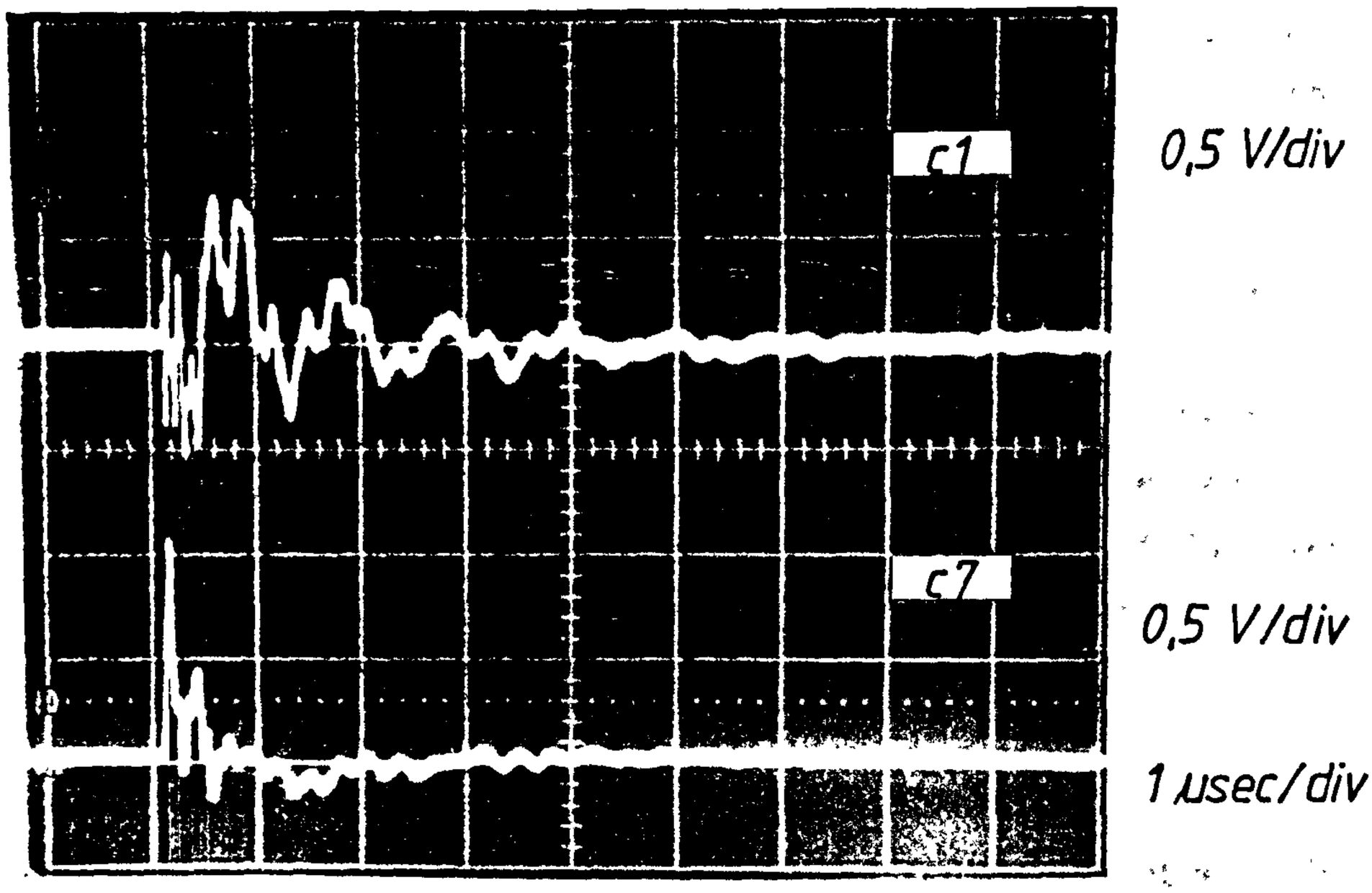

Figure 4.4.5.5 - Waveforms of Pulses Injected at Positions c5 and c7

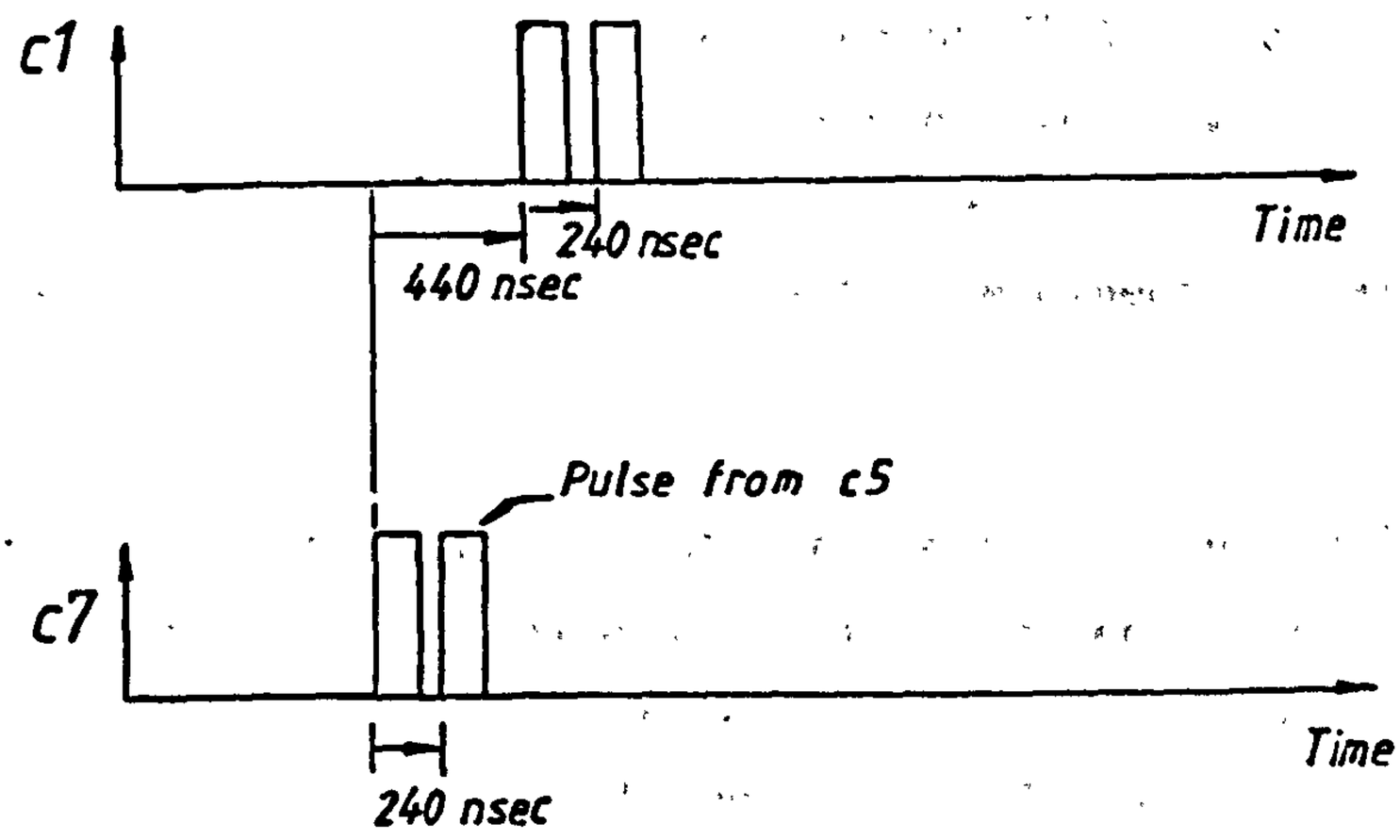

Figure 4.4.5.6 - Pulse Reflection Diagram

Similar to the previous results the location scan in figure 4.4.5.7 identifies a single discharge source at the channel position 107 . Expected location peaks are at channel positions 72 and 126 . The corresponding current waveforms are displayed in figure 4.4.5.8, along with the pulse lattice diagrams , in figure 4.4.5.9, which provide the pulse timing relationships .

As before, the pulse entered at c7 is detected immediately, followed 3 coil transit times, (330 nsec) later, by the pulse injected at c4. After 660 + 330 nsec. , the reflection at terminal c1 of the pulse injected at c7 arrives at c7 . Likewise at terminal c1 the waveform shows the arrival after 330 nsec. of the pulse injected at c4 followed by the pulse injected at c7 , 330 nsec. later . The first pulse injected at c4 follows 660 nsec. later , after being reflected at terminal c7 .

Even with a separation of 330 nsec. of propagation delay between the two injected pulses the location instrument is unable two discriminate between these two adjacent pulses at the given discrimination levels in the coincidence detector .

The pulse front arriving first at terminal c7 is that of the pulse injected at that point and the pulse front which arrives initially at terminal c1 is that of the pulse injected at c4 . This corresponds to a time delay difference of 330 nsec. as observed by the coincidence detector . From expression 4.13 , the expected location position of the apparent, single pulse source detected by MICA is calculated to be at channel position 103 . This compares well with the measured location at channel position 107 . The pulse count of 2112 at the location peak also compares well with the expected value of 2100 pulses .

In this next scan the separation of the two pulse sources is 4 stator coils in which the pulse sources are injected at points c7 and c3 on the winding . A scan of the winding yields the locations of two discharge sources at channel positions 72 and 117 which are shown in figure 4.4.5.10. The first location at channel position 72 is the correct location of the pulse source entered at terminal c7 .

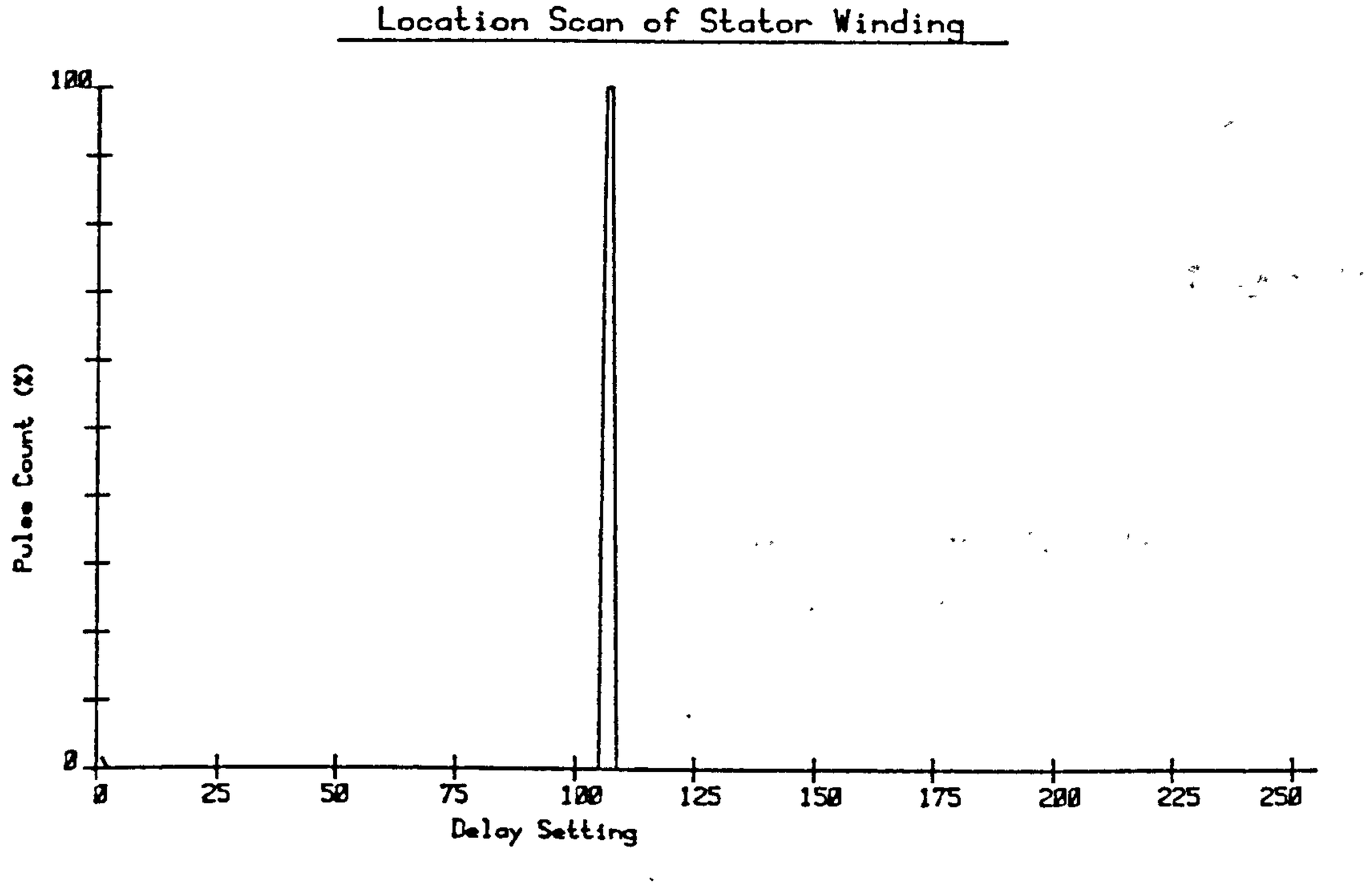

Figure 4.4.5.7 - Scan of Winding with Pulses Injected at Positions c4 and c7

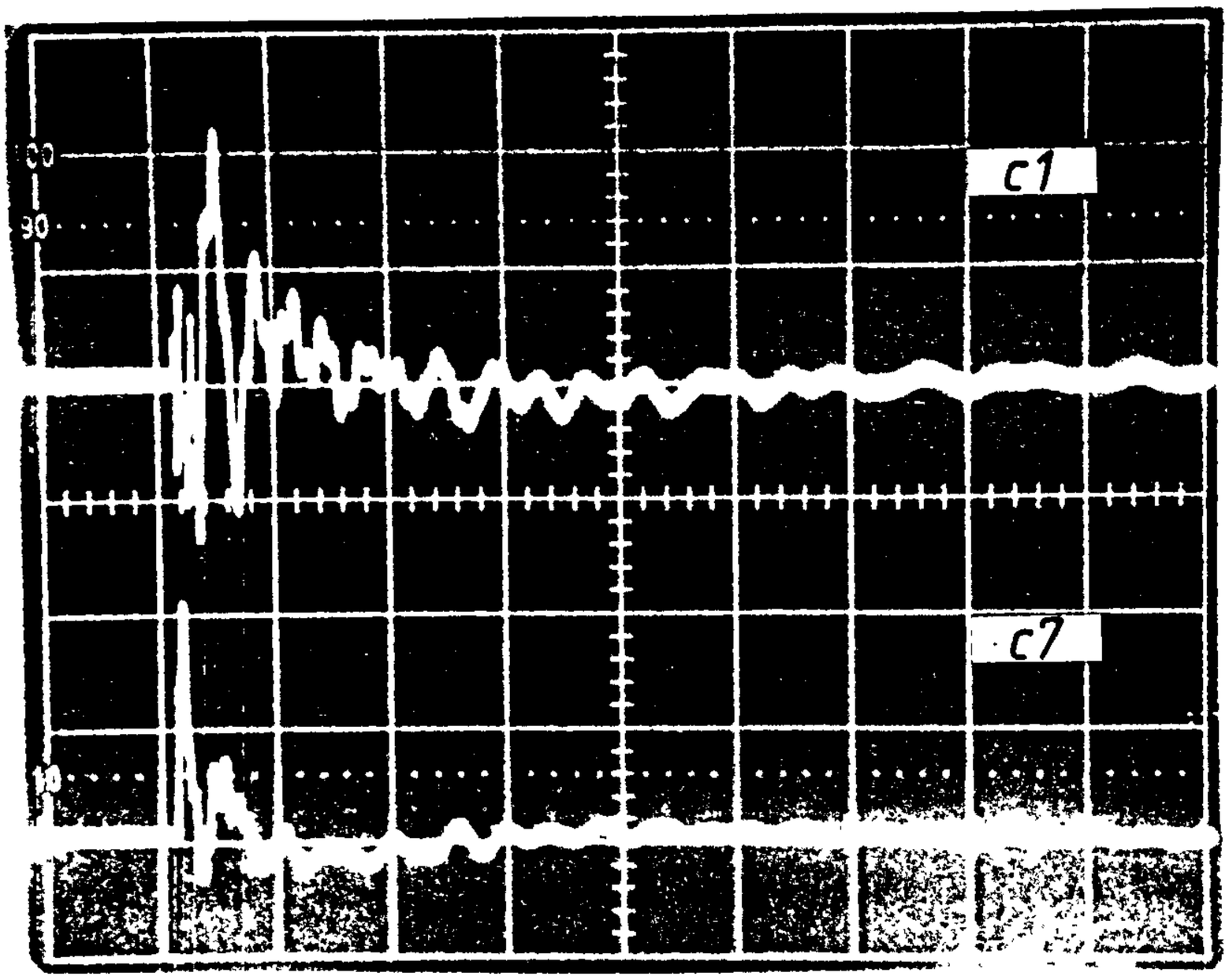

Figure 4.4.5.8 - Waveforms of Pulses Injected at Positions c4 and c7

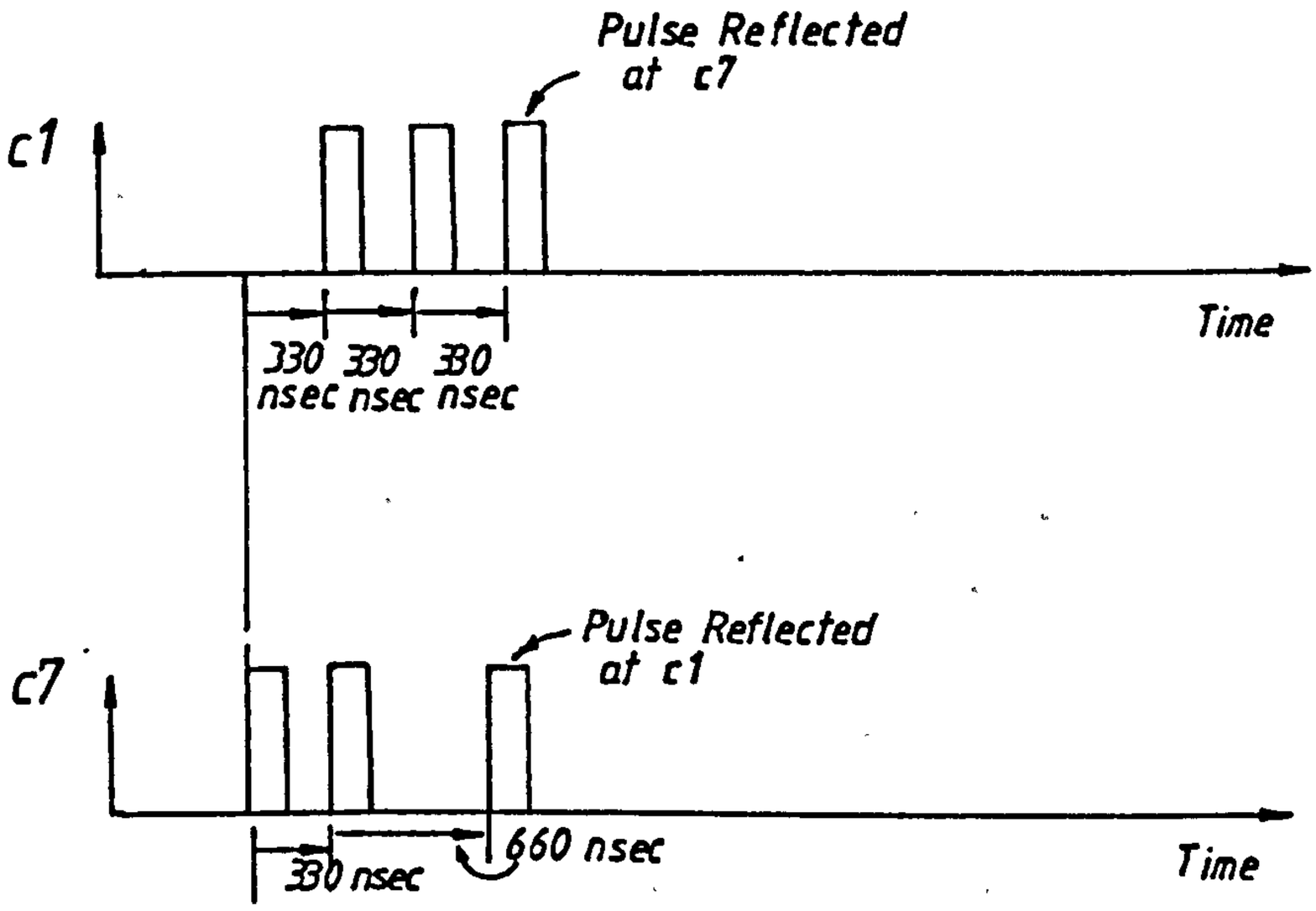

Figure 4.4.5.9 - Pulse Reflection Diagram

However , the second location is not the true location of the pulse source at connection c3 which is expected to be at channel position 145 . The pulse waveforms observed at the winding terminals, shown in figure 4.4.5.11, are used to explain this characteristic .

At terminal c7 , the pulse injected at that point arrives initially , followed 4 coil transit times (440 nsec.) later by the pulse originating at point c3 . Subsequently, the reflection at terminal c1 of the pulse injected at point c3 , arrives after a delay of 440 nsec. Further pulse reflections occur . Similarily , at terminal c1 the first pulse arrives from the source at point c3 after a period of 220 nsec . After a further 440 nsec. , the pulse injected at terminal c7 arrives . This pulse is followed 220 nsec. later by the pulse from c3 which is reflected at terminal c7 . This pulse reflection process continues as shown in figure 4.4.5.11 .

In this experiment the results are more difficult to explain since the correlator is able to discriminate between the two simultaneous pulses . However, at a delay setting of 72 , the pulse fronts which are discriminated are of the pulse injected at terminal c7 observed at terminals c1 and c7 . This results in the correct location of the pulse source at c7 . The location peak at a delay setting of 117 implies that the coincidence detector discriminates on the rising edge of the following pulses :

i. The pulse injected at terminal c7 which is detected at terminal c7 , and ,
ii. The pulse injected at point c3 which is detected at terminal c1 .

The time interval between the arrival of these pulses at their respective terminals is around 220 nsec. When substituted into expression 4.13 the location should be at a delay setting of 112 . This is comparible with the location on the scan , 117 .

The pulse count for the location peaks at channel positions 77 and 117 are 2085 and 2102 respectively ; both of which are close to the calculated value of 2100 pulses .

In the final scan of this experiment the two pulse sources are injected at points c7 and c2 on the winding . The scan of the winding

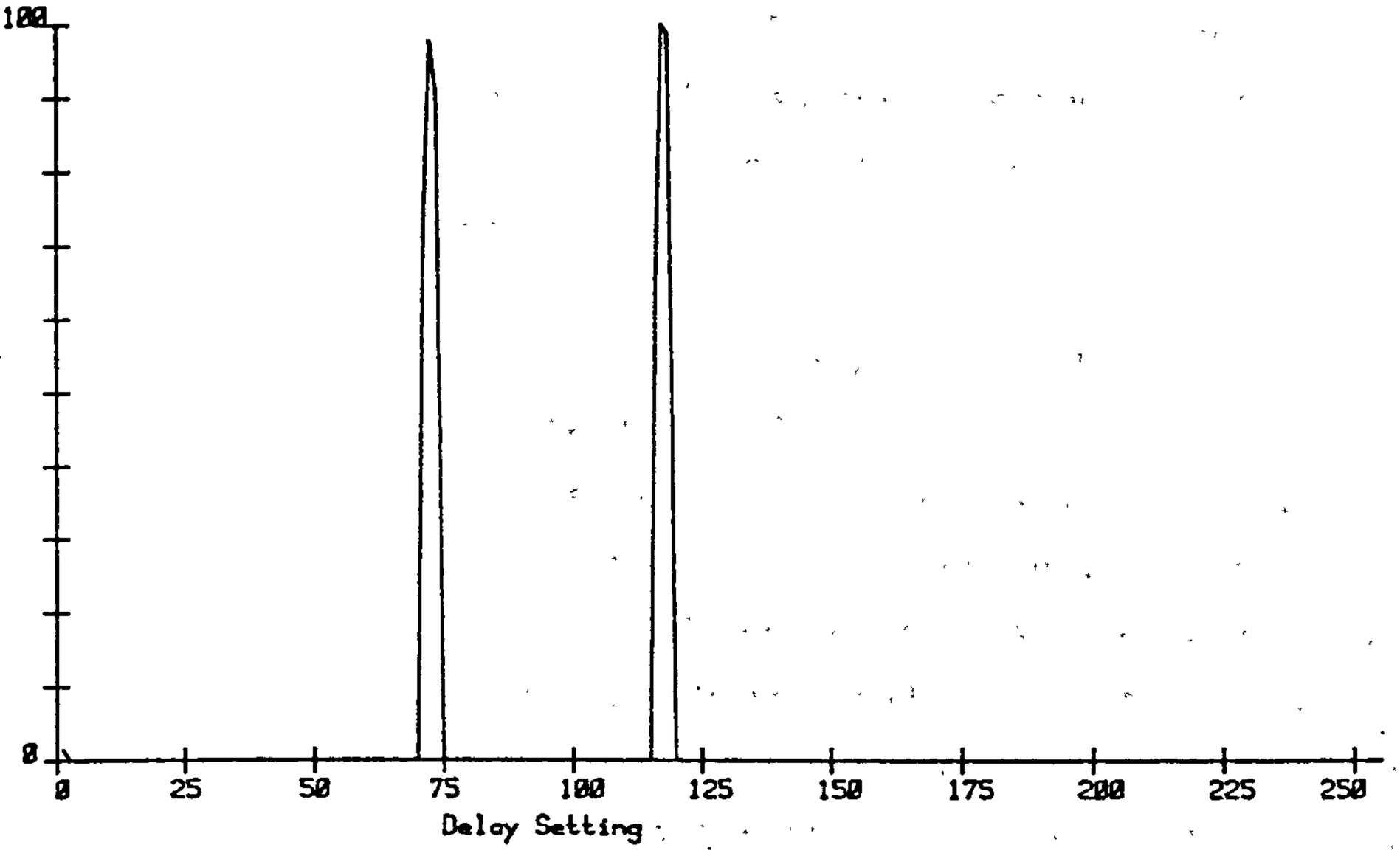

Figure 4.4.5.10 - Scan of Winding with Pulses Injected at Positions c3 and c7

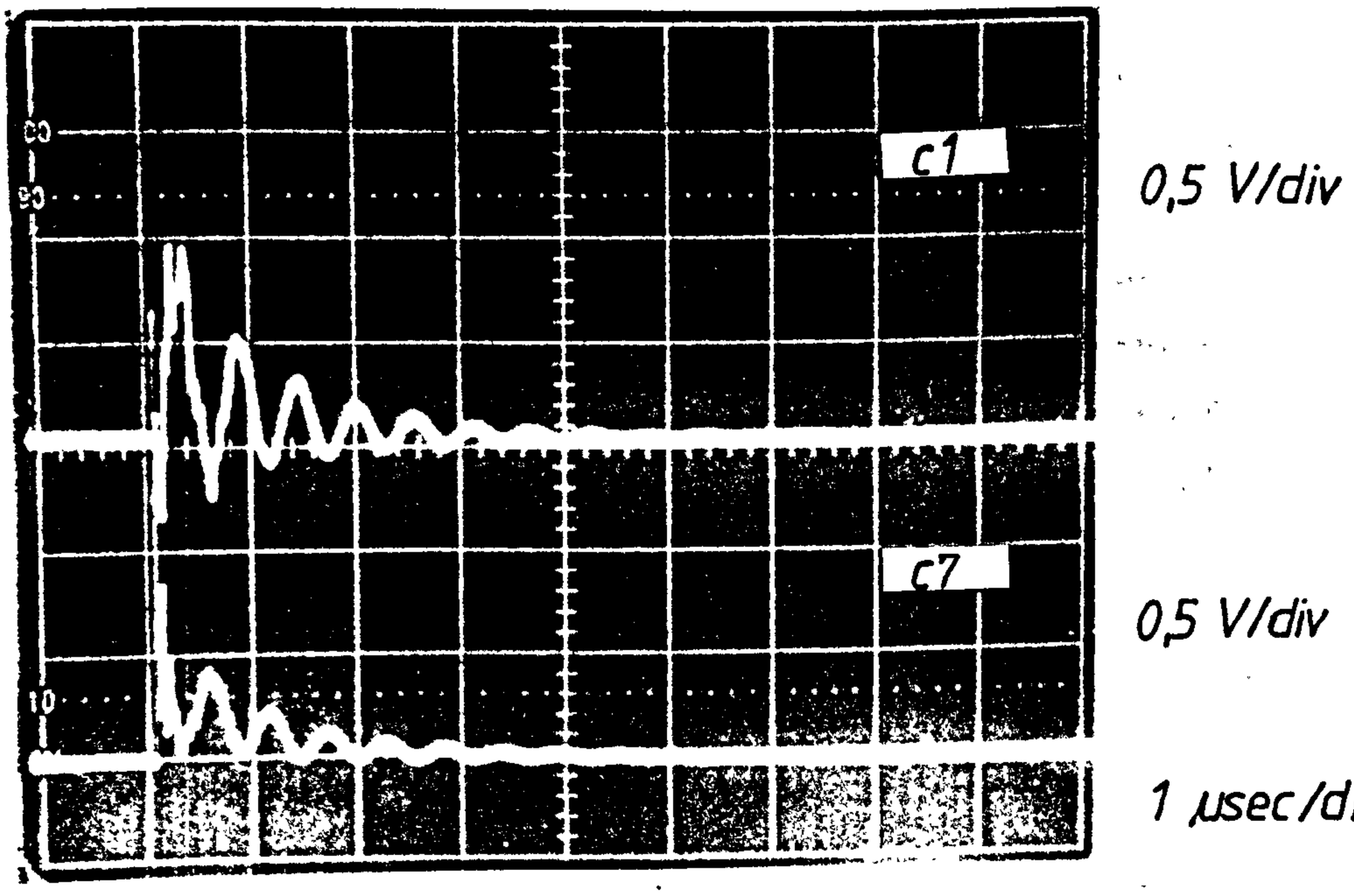

Figure 4.4.5.11 - Waveforms of Pulses Injected at Positions c3 and c7

shown in figure 4.4.5.12 indicates the location of two pulse sources at channel positions 77 and 128 . The first of these is the approximately the location of the pulse source injected at terminal c7 and the latter is the location of a discharge source at point c4 which is the mid point of the winding .

The waveforms observed at either terminal are shown in figure 4.4.5.13. The waveform at terminal c7 indicates that the pulse injected at that terminal arrives initially , followed 559 nsec. after by the pulse from the source at point c2 . Likewise , at terminal c1 the pulse from the source at c2 is detected after a time delay of 110 nsec. This current pulse is greater in amplitude since it is developed across one coil and the low 20 ohm terminal resistor . The initial pulse is followed 550 nsec. later by the pulse injected at point c7 .

At a delay setting of 77, the fronts of the pulse injected at c7 which is observed at the winding terminals, are time coincident giving the correct location . In addition, the threshold level at the input of the correlator which monitors terminal c1 is marginally below that of the peak of the pulse which travels from c7 to c1 . Thus , any small variation of the pulse amplitude from the pulse generator results in no coincidence , which explains the low pulse count of 158 at that particular location .

When the delay is set at 128 , the pulse fronts which are coincident at the correlators inputs are those from the pulse injected at c7 and observed at that terminal, and the pulse injected at point c2 and observed at terminal c1 . The difference in delay between these two pulse fronts is approximately 110 nsec. , which is the delay through one coil . Using expression 4.13 the expected delay setting for coincidence is 120 which is close to the location obtained . The pulse count at this position is correct at a value of 2065 counts .

From this group of experiments with simultaneously injected pulses it is possible to form the following general conclusions :-

i. Two pulse sources separated by a distance of 3 coils or less will interfere and produce a single pulse . In the tests undertaken the transit time between 3 coils is comparable with the width of the injected pulses .

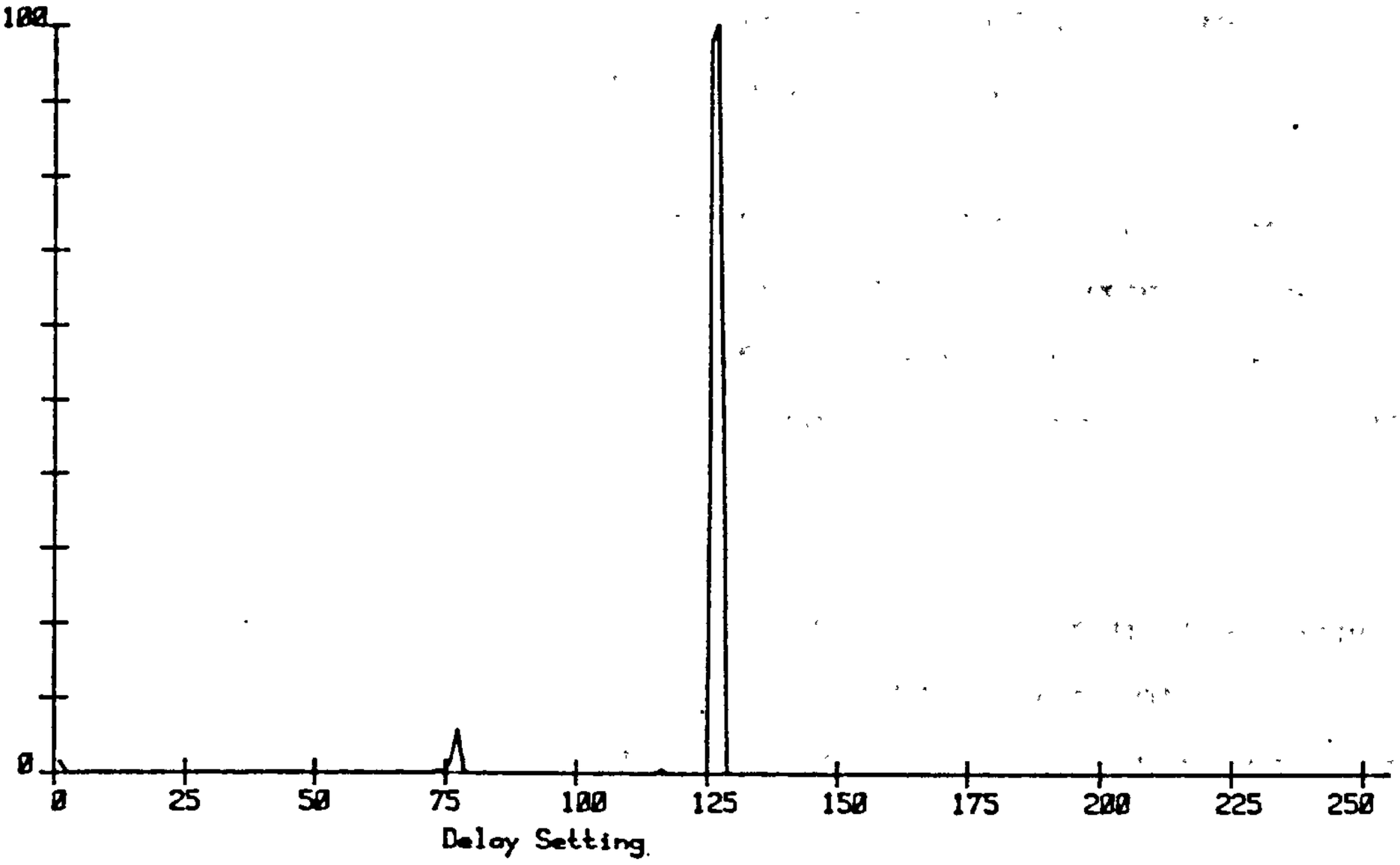

Figure 4.4.5.12 - Scan of Winding with Pulses Injected at Positions c2 and c7

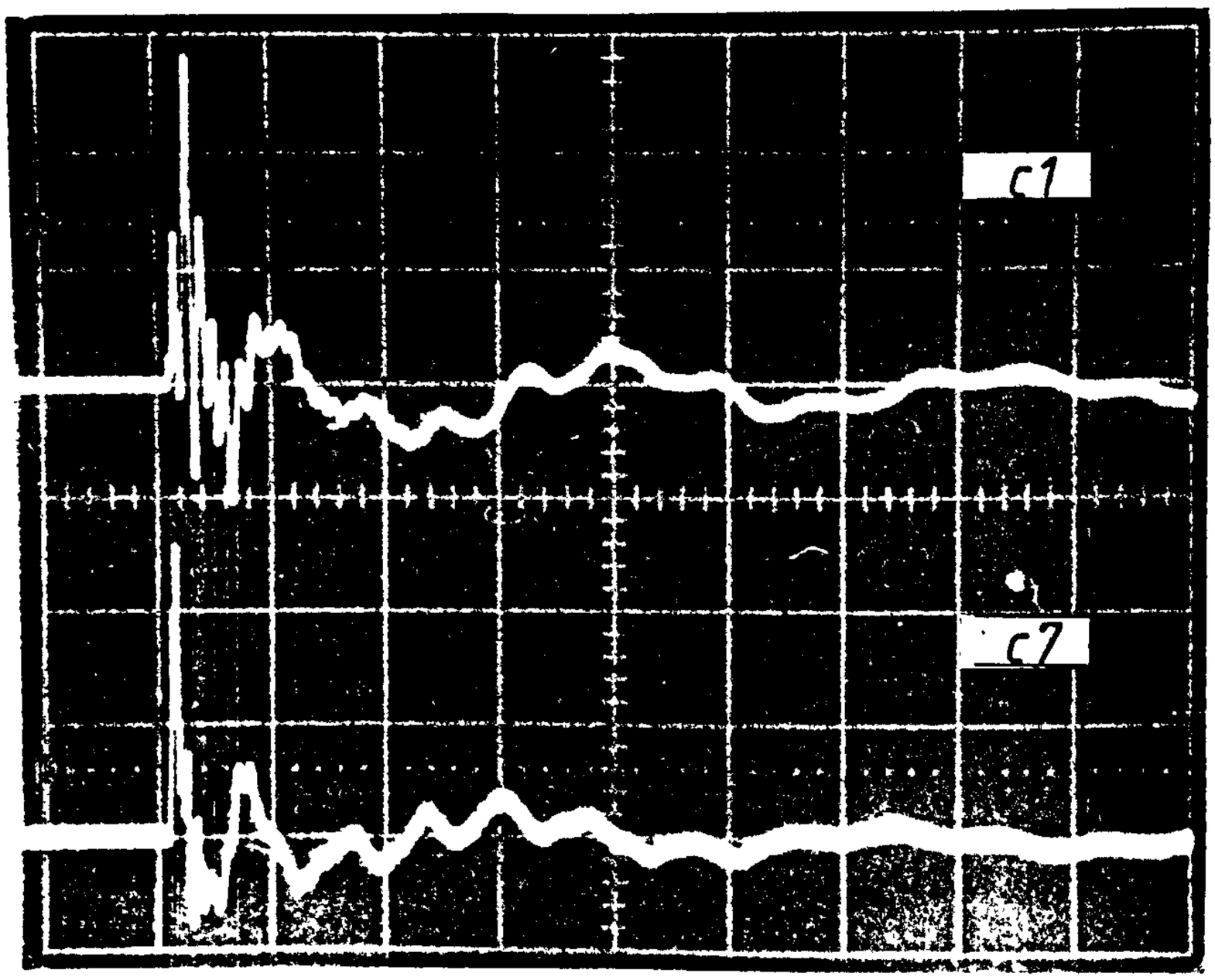

Figure 4.4.5.13 - Waveforms of Pulses Injected at Positions c2 and c7

ii. At a distance between sources of 3 coils and greater , (or when the transit time between sources exceeds the injected pulse width the correlation of the two pulse sources is possible .

iii. These sources will not correspond in general to their true positions since the coincidence correlator will examine the pulse fronts of both pulse sources to produce a false coincidence and not the pulse fronts of each individual source observed at the winding terminals .

iv. Pulse sources located at points equidistant from the winding terminals will appear to originate from the centre of the winding since the pulse fronts that arrive first at the terminals are coincident in time .

4.4.6 Injection of Two Random Discharge Sources

In practice partial discharge sources are entirely independent of each other . In such a situation the phase relationships , with respect to time , between partial discharge sources are random and the likelyhood therefore , of simultaneously occuring discharges is very small . It is the purpose of the next series of experiments to simulate as closely as possible the condition when random discharges are present in a winding and to investigate the behaviour of the correlator .

In this first set of experiments , only two independent pulse sources are injected into the winding , as shown in figure 4.4.6.1 . The pulse repetition frequencies for the two pulse sources are set at different levels in order to distinguish each source in the location scan . In addition to the difference in pulse repetition frequency the magnitude of the discharges differ by a ratio of 2:1 . The pulse source details are as follows :-

i. Discharge pulse source (a) : 1600 Hz . (T = 600 µsec.)
   Discharge magnitude : 10000 pC. (20V , 500 pF.)
   Expected pulse count : 416 pulses .

ii. Discharge pulse source (b) : 5000 Hz . (T = 200 µsec.)
   Discharge magnitude : 5000 pC. (10V , 500 pF.)
   Expected pulse count : 1250 pulses .

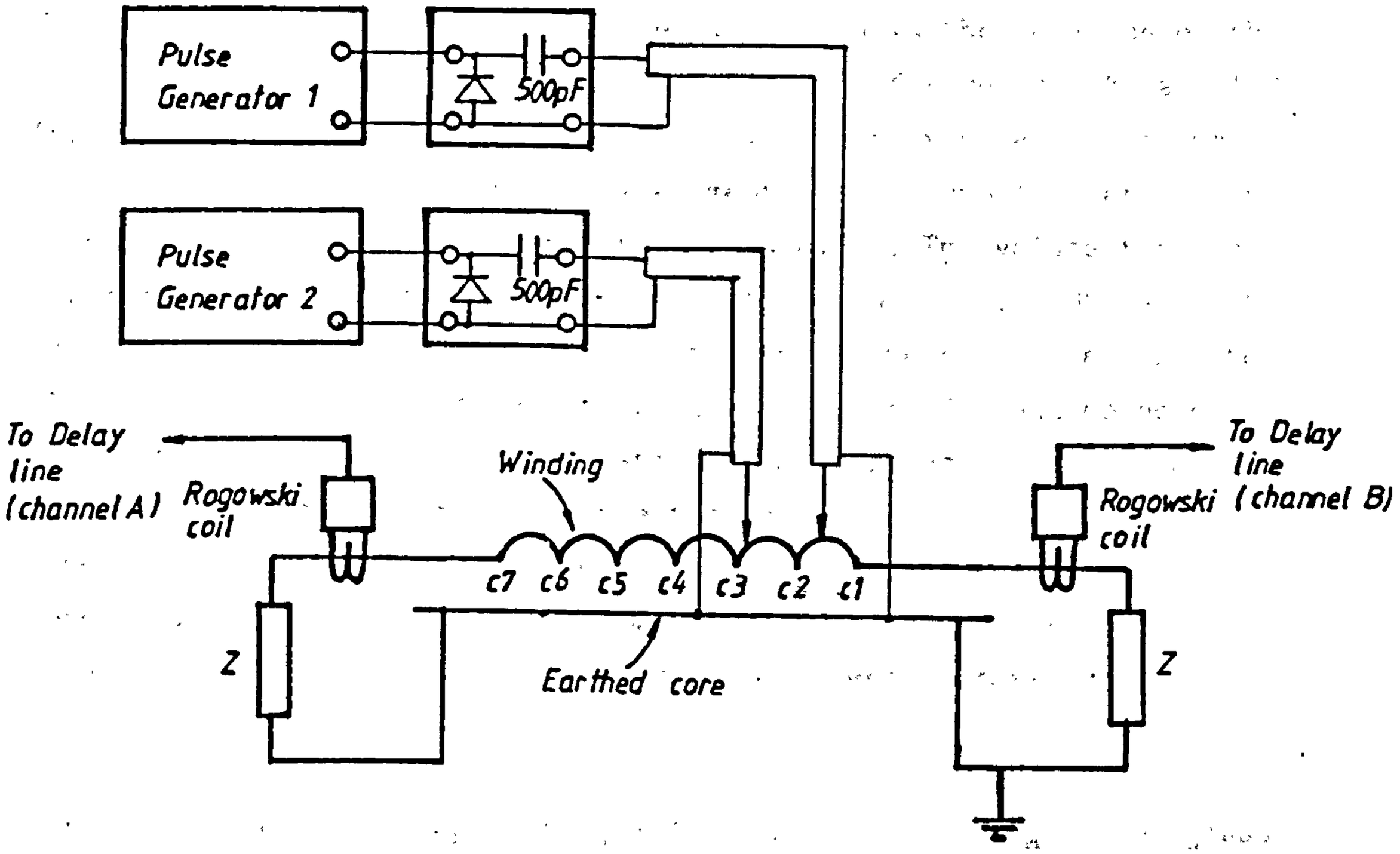

Figure 4.4.6.1 – Test Circuit with Two Independent Discharge Pulse Sources

The threshold voltage levels at the coincidence detector inputs are 65 mV and 75 mV respectively for channels A and B , and the channel dwell time is 250 msec .

The winding is terminated as a typical star connected motor with a 150 ohm resistor at the neutral end and a 20 ohm resistor at the line end to represent the surge impedances at these terminals . Discharge source (a) is injected at point c2 whilst discharge source (b) is injected at point c6 on the winding .

The resulting scan as seen in figure 4.4.6.2 shows the location of the two discharge sources at channel positions 87 for source (b) and 170 for source (a) , which correspond well with the expected positions as determined from the previous experiment ,(with similar terminating impedances), as described in section 4.4.2 . The values from this experiment were, for the same injection points , 88 and 165 respectively . If pulses from both sources were to be injected simultaneously at some instant then it is expected that coincidence detection would indicate the location of a spurious pulse source at the centre of the winding and hence the scan . This is clearly not the case in this test since there are no accidental coincidences detected. It is reasonable to assume therefore that the probability of simultaneous pulse injection from two independent sources is extremely small .

Pulse counts for sources (b) and (a) are 1167 pulses and 380 pulses respectively compared with the corresponding expected values of 1250 and 416 pulses . This represents at least 93% and 91% correlation of all the incident pulses .

To increase the probability of accidental coincidences from simultaneously occuring pulses , the pulse repetition frequency of source (a) is increased to 8000 Hz ,(T = 125 μsec.) , to give an expected pulse count of 2000 pulses . The scan in figure 4.4.6.3 indicates the locations of the same two pulse sources at channel positions 87 and 170 for sources (b) and (a) as before with the exception of a much higher pulse count for pulse source (a) of 2029 pulses . This shows that all the incident pulses are processed by the correlator . More importantly , there are no accidental pulse coincidences at the centre position on the scan plot .

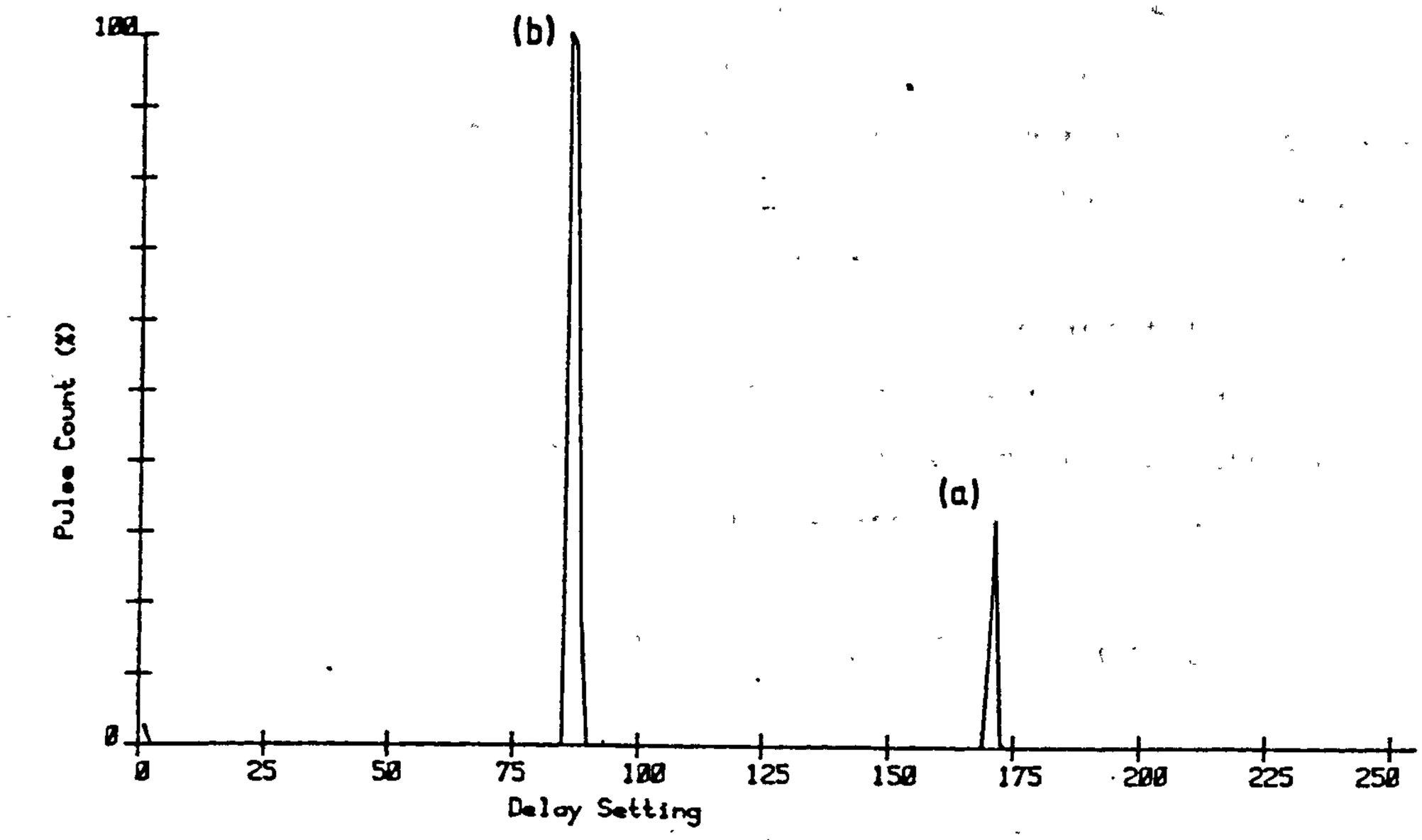

Figure 4.4.6.2 - Scan of Winding with Pulse Source at c2 and c6

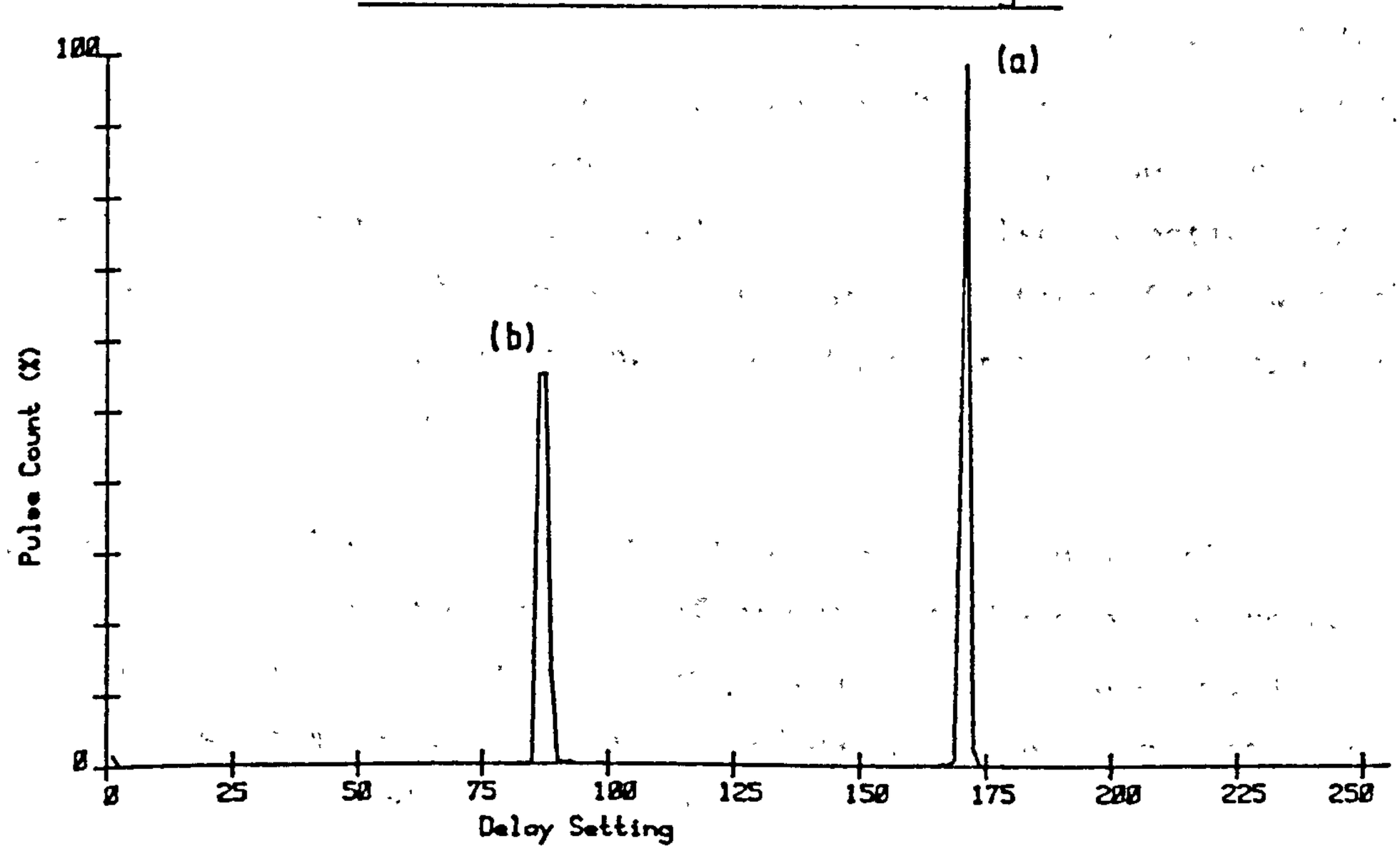

Figure 4.4.6.3 - Scan of Winding - Pulse Injection Rate Increased

It is recalled , from the previous discussion in section 4.4.5 on simultaneous pulse injection , that pulse sources separated by transit times close to the width of the injected pulses merge to form a single pulse source due to pulse interference . In this next test two independent pulse sources are injected at positions c3 and c5 which are a distance of 2 coil lengths , hence 2 coil transit times , apart. Pulse source (a) is injected at point c5 and source (b) at point c3 . The same termination conditions and discharge amplitudes are preserved whilst the pulse repetition frequencies are as follows :-

i. Pulse source (a) : 10000 Hz , (T = 100 μsec.)
   Expected count : 2500 pulses .

ii. Pulse source (b) : 8000 Hz , (T = 125 μsec.)
   Expected count : 2000 pulses .

The scan in figure 4.4.6.4 shows two pulse source locations at channel positions 111 and 154 which correspond to the positions of sources at points c5 and c3 respectively . The expected locations from the previous scan performed with the same terminating impedances in section 4.4.2 , are 107 and 145 which indicates errors of 4 and 9 channel positions . Translated into distance along winding these values are approximately 2.8 metres and 6.3 metres (one coil length is 11.5 metres). The error therefore in the location is greatest towards the low impedance end of the winding , the line end , as demonstrated before . It is thought that the pulse injection circuits effect a change in the transmission characteristics of the winding . The addition of the coupling capacitance must alter the shunt capacitance of the winding .

The measured pulse counts for the two pulse locations are 2083 and 1866 pulses which correspond to 84% and 93% of the expected values . The scan also indicates that there are no accidental pulse coincidences from pulses occuring close together in time since no spurious location peaks are observed .

To further this investigation the two discharge sources are injected into the winding a distance of a single coil length apart and a scan of the winding is performed . This proceedure is repeated with the two pulse sources injected one coil apart at regularly spaced intervals of one coil length along the entire winding .

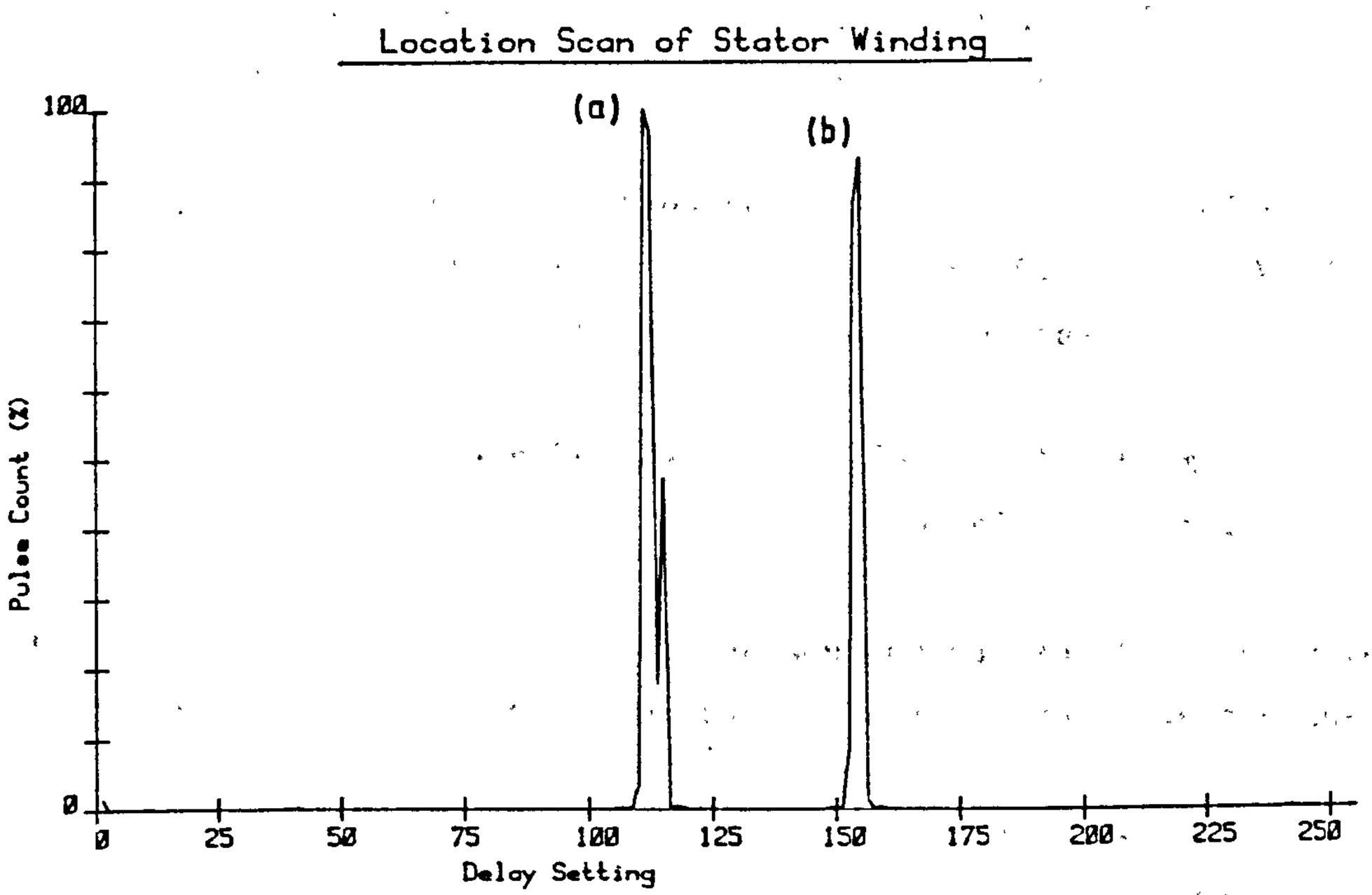

Figure 4.4.6.4 – Scan of Winding with Pulse Sources at Positions c3 and c5

There are five scans which correspond to the injection of pulse sources (a) and (b) into the winding at the following positions : c7 and c6 ; c6 and c5 ; c5 and c4 ; c4 and c3 ; c3 and c2 . These scans are shown in figures 4.4.6.5 , 4.4.6.6 , 4.4.6.7 , 4.4.6.8 , and 4.4.6.9 .

The discharge source parameters for this experiment are as follows :-

i. Discharge source (a) frequency : 10000 Hz ,(T = 100 µsec.)
Discharge magnitude : 5000 pC. ,(10V ,500 pF.)
Expected pulse count : 2500 pulses

ii. Discharge source (b) frequency : 5000 Hz , (T = 200 µsec.)
Discharge magnitude : 10000 pC. ,(20V ,500 pF.)
Expected pulse count : 1250 pulses

iii. Threshold Voltage Levels : Channel A - 65 mV.
Channel B - 75 mV.

Location positions and pulse counts for sources (a) and (b) are given in the table in figure 4.4.6.10 for ease of comparison between scans .

Injection point		Channel location		Pulse count	
(a)	(b)	(a)	(b)	(a)	(b)
c6	c7	95	75	2718	2151
c5	c6	118	96	2287	761
c4	c5	136	117	2149	636
c3	c4	155	136	2090	1540
c2	c3	175	156	2240	1323

Figure 4.4.6.10 - Location Positions and Associated Pulse Counts

One can readily see from these results that the locations of the pulse sources (a) and (b) injected at each position on the winding compare well , and lie within 1 channel position , (0.7 metres) between each other at the most . To assertain the accuracy of these location positions , it is necessary to compare the values with those obtained from the first experiment in which a single pulse source is used with identical terminating conditions . Figure 4.4.6.11 tabulates the

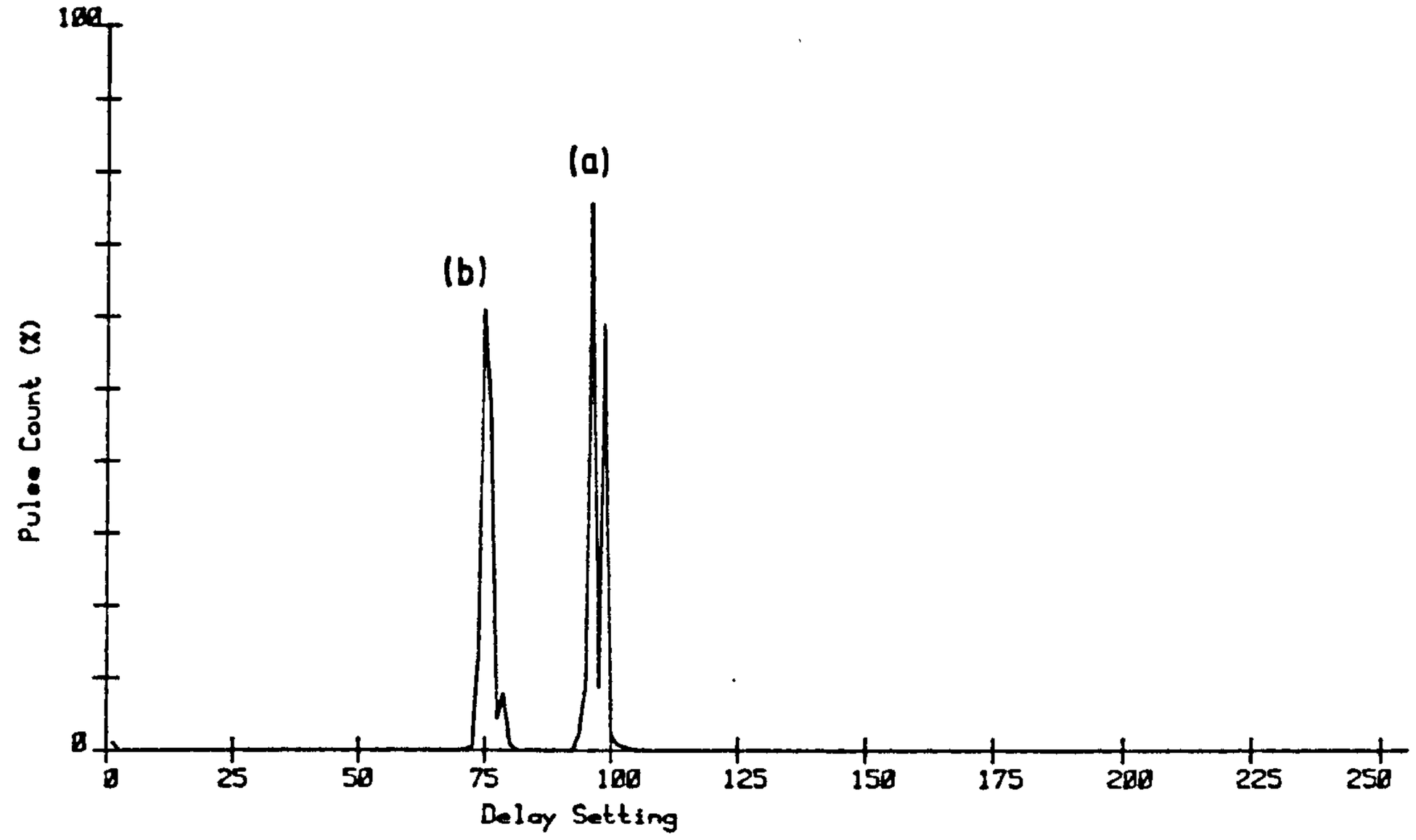

Figure 4.4.6.5 - Scan of Winding with Pulses Injected at c6 and c7

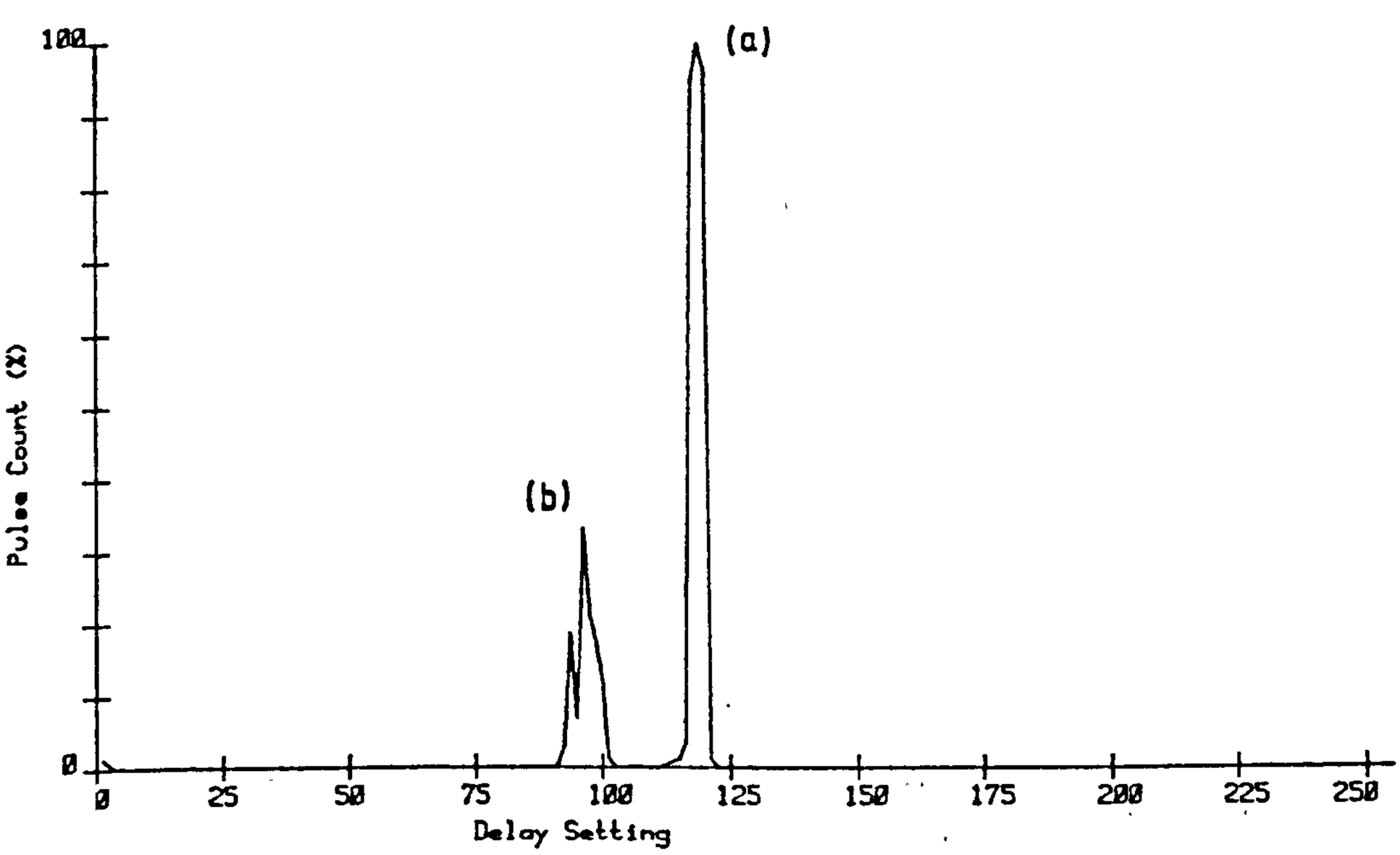

Figure 4.4.6.6 - Scan of Winding with Pulse Sources at c5 and c6

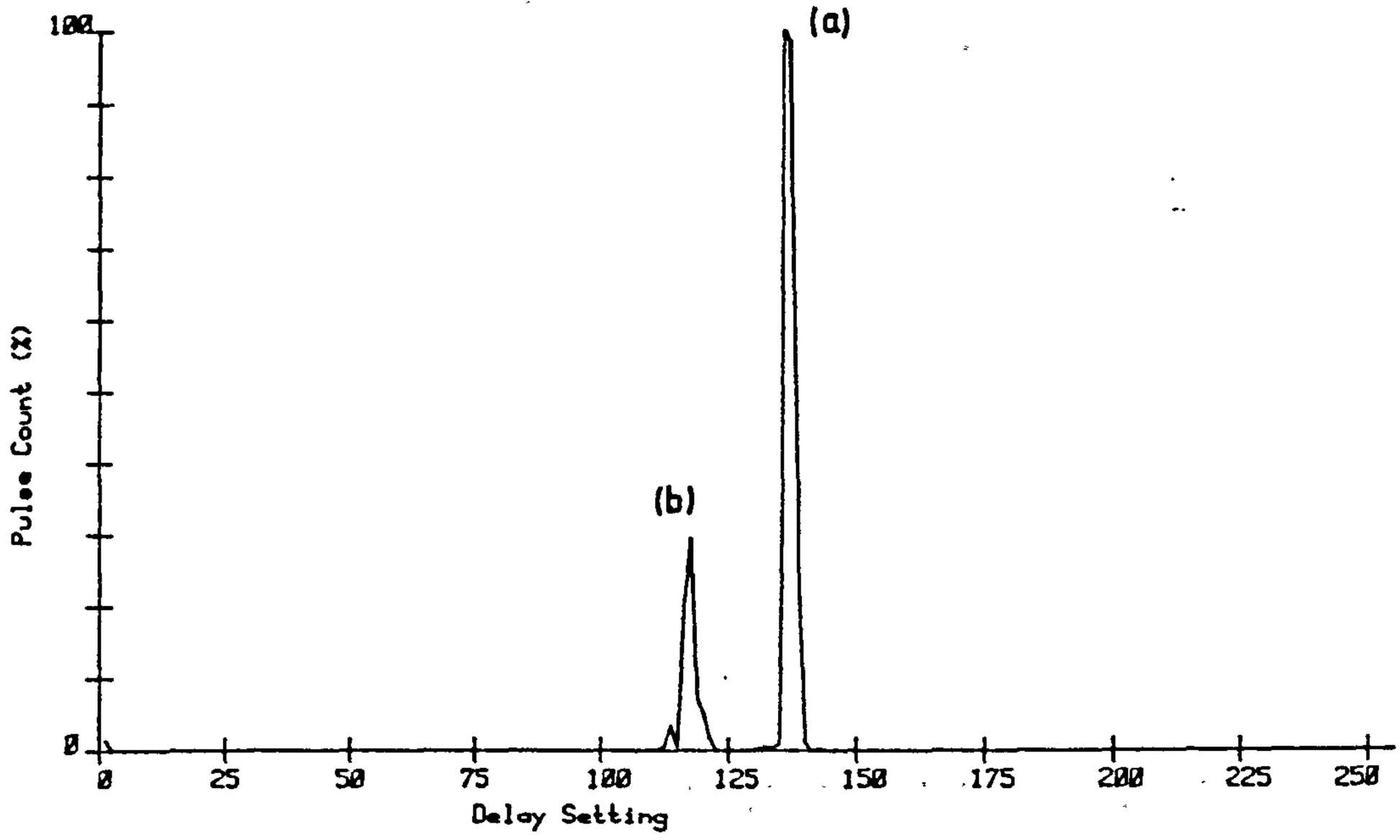

Figure 4.4.6.7 - Scan of Winding with Pulse Sources at c4 and c5

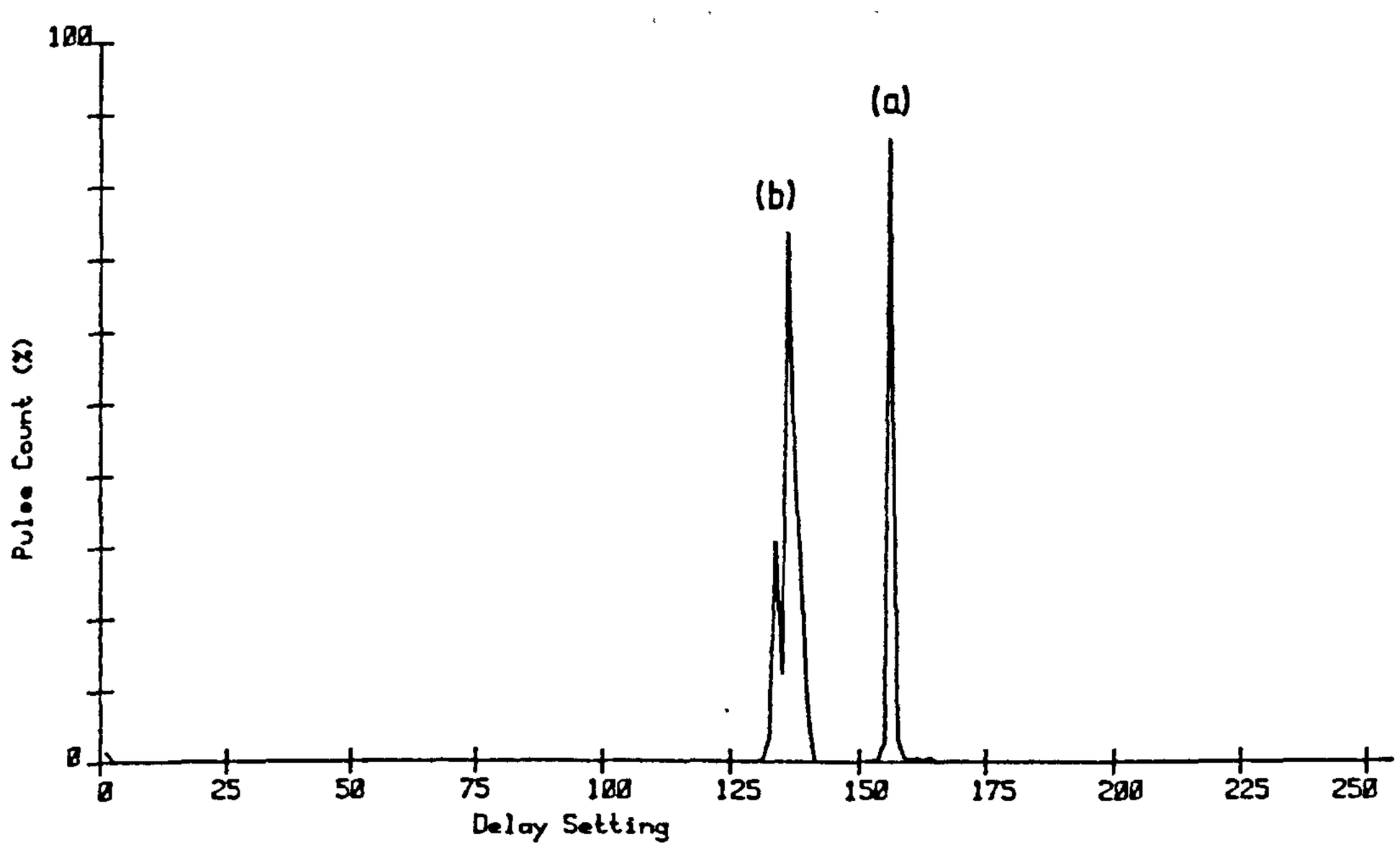

Figure 4.4.6.8 - Scan of Winding with Pulse Sources at c3 and c4

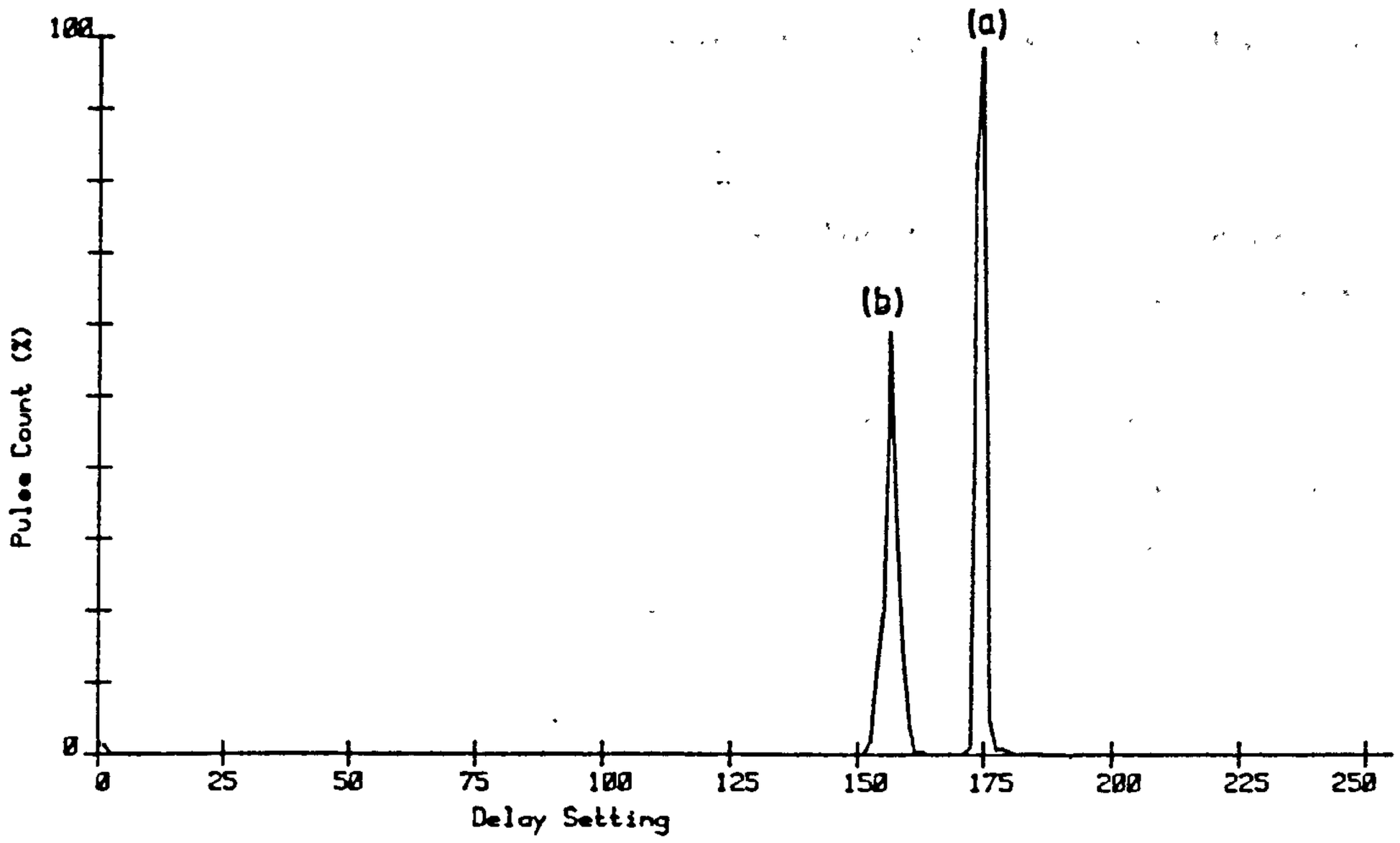

Figure 4.4.6.9 - Scan of winding with Pulse Sources at c2 and c3

correct locations obtained from the scan in figure 4.4.3.4 in section 4.4.3 and indicates the differences between these and the values in figure 4.4.6.10 above .

Injection point		Expected location		Error	
(a)	(b)	(a)	(b)	(a)	(b)
c6	c7	88	72	7	3
c5	c6	107	88	11	8
c4	c5	126	107	10	10
c3	c4	145	126	10	10
c2	c3	165	145	10	10

Figure 4.4.6.11 - Errors in Scan Locations

The difference between the expected locations from previous results and the values obtained is a maximum of 11 channel positions , 7.7 metres of winding . Error in location is greater towards the low impedance end of the winding . The only explanation for this behaviour is that the addition of one pulse injection circuit causes a significant change in the transmission characteristics of the winding which alters the discharge source locations on the winding scan .

Another observation from these scans is that significant errors appear in the measured pulse counts , particularily those from pulse source (b) when injected at points c5 and c6 . Pulse counts of 636 and 761 respectively are roughly half the expected value of 1250 . A possible explanation for this behaviour is that the threshold level in channel A of the coincidence detector is too low to discriminate the attenuated discharge pulse which travels from the sites at c5 and c6 to terminal c1 .

In summarising , it is fair to say that MICA is able to locate the positions of two independent discharge sources injected a single coil distance apart to reasonable accuracy . Although locations are different from those obtained from a single discharge source , locations of discharge sources at each coil interval are spaced correctly , with respect to each other , on the winding scan . One must also take into account the effect an additional pulse injection circuit has on the transmission characteristics of the winding .

4.4.7 Injection of Three Independent Discharge Sources

In this set of experiments three independent discharge pulse sources are injected into the winding which is terminated at the line end by a 20 ohm resistor and at the neutral end by a 150 ohm resistor . The discharge sources are applied to the winding , a distance of one coil apart . The magnitudes of the discharge pulses are of the same order whilst the pulse repetition frequency for one of the sources is five times lower than the other two to help identify the pulse source . The characteristics of the three pulse sources are given in the table in figure 4.4.7.1 . Coincidence detector threshold levels are as before : channel A is 65 mV and channel B is 75mV .

Discharge Source	Discharge Magnitude	Pulse Frequency
(a)	6000 pC.	1000 Hz.
(b)	5000 pC.	5000 Hz.
(c)	5000 pC.	5000 Hz.

Figure 4.4.7.1 - Pulse Source Characteristics

In the first test discharge sources (a), (b), and (c) are injected at positions c1, c2, and c3 respectively on the winding . The winding scan for this test is shown in figure 4.4.7.2 . The pulse sources are then displaced one coil to points c2, c3, and c4 on the winding . Figure 4.4.7.3 shows the resulting scan of the winding . The three pulse sources are again moved along one coil to the next position , a scan is performed and the process is repeated until source (c) is positioned at c6 on the winding . Figures 4.4.7.4 and 4.4.7.5 show the winding scans for these cases .

The pulse source location and pulse count data associated with the scans obtained are given in the table in figure 4.4.7.6 .

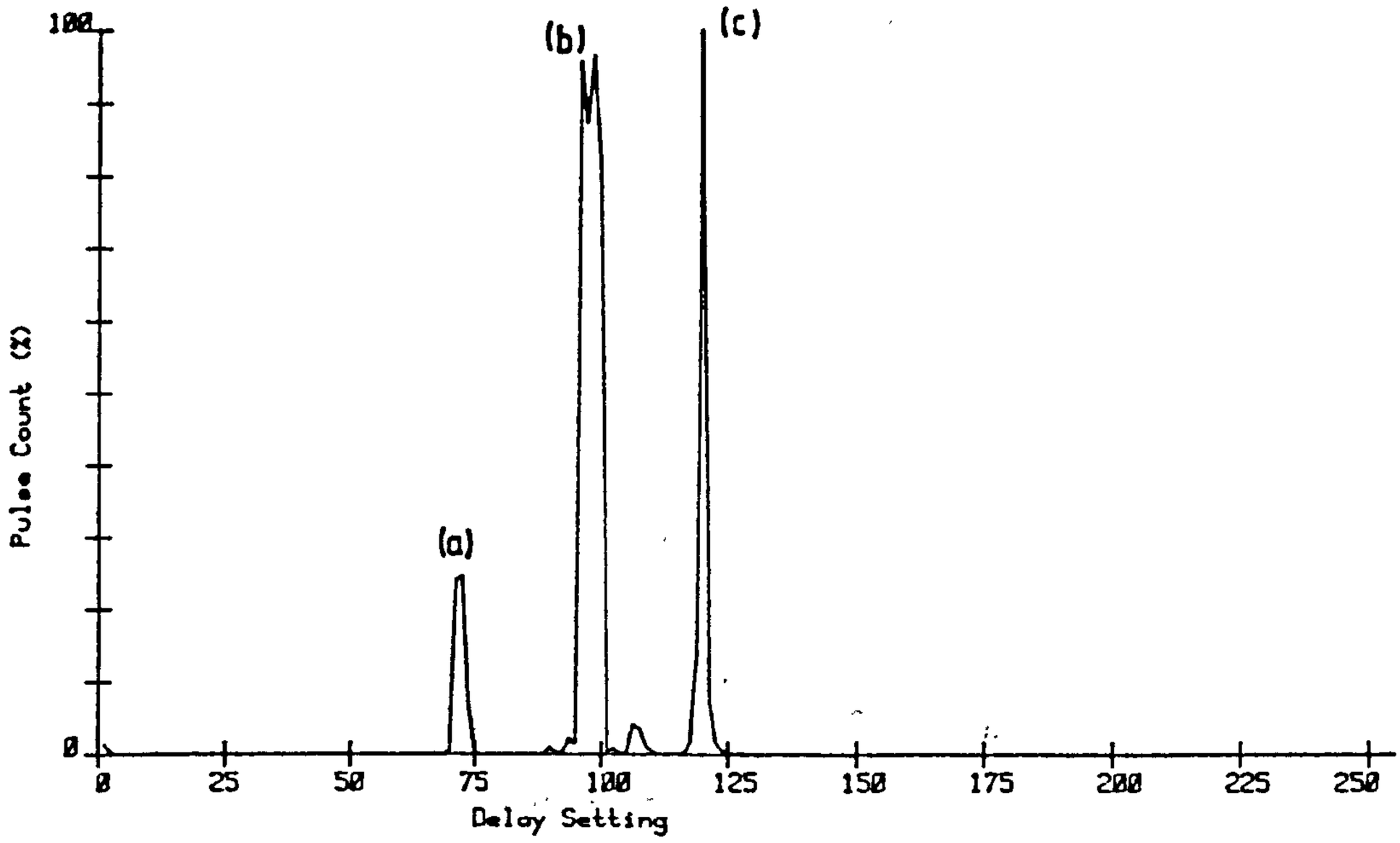

Figure 4.4.7.2 - Scan of Winding with Pulse Sources at c1,c2 and c3

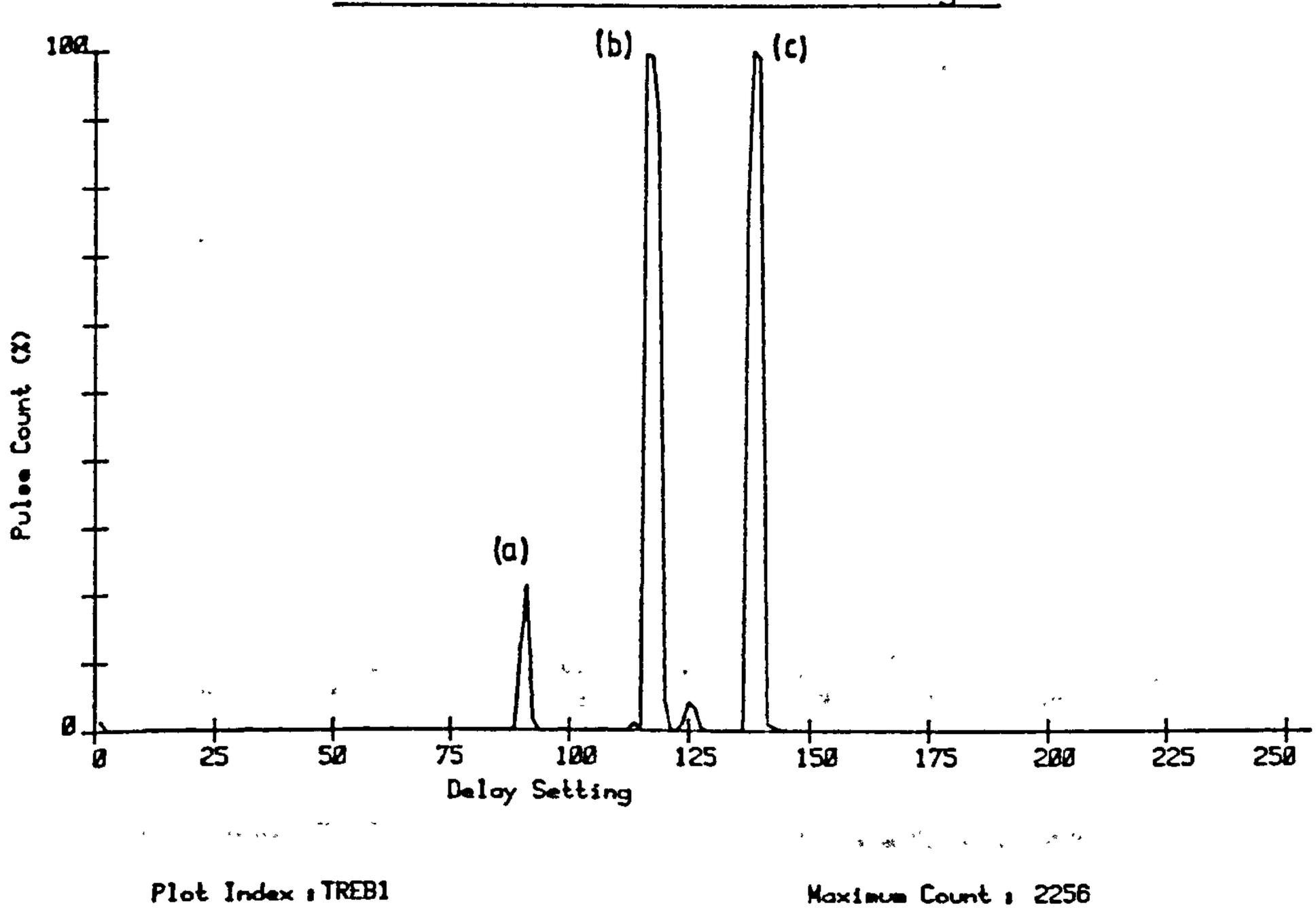

Figure 4.4.7.3 - Scan of Winding with Pulse Sources at c2,c3 and c4

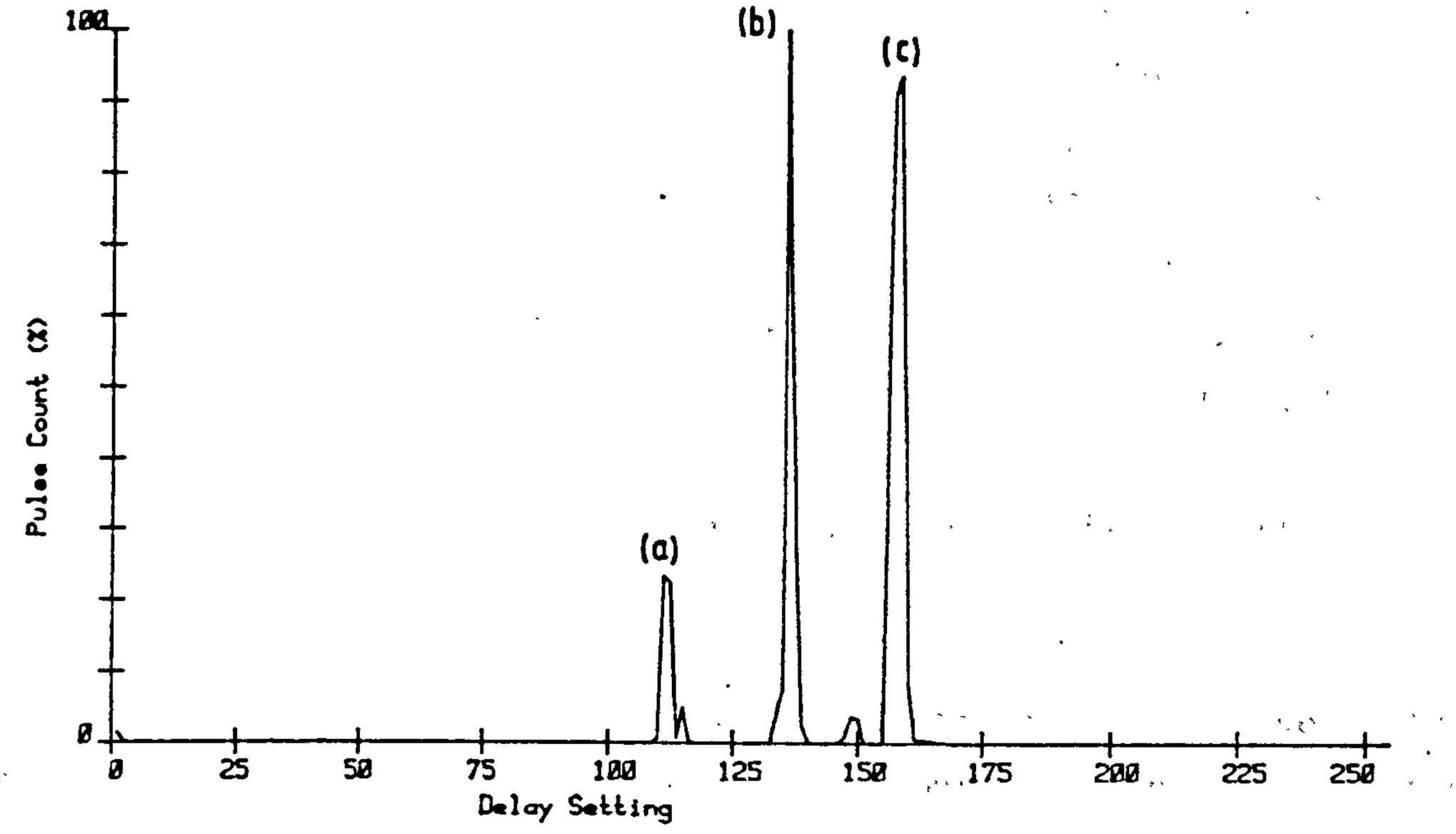

Figure 4.4.7:4 - Scan of Winding with Pulse Sources at c3,c4 and c5

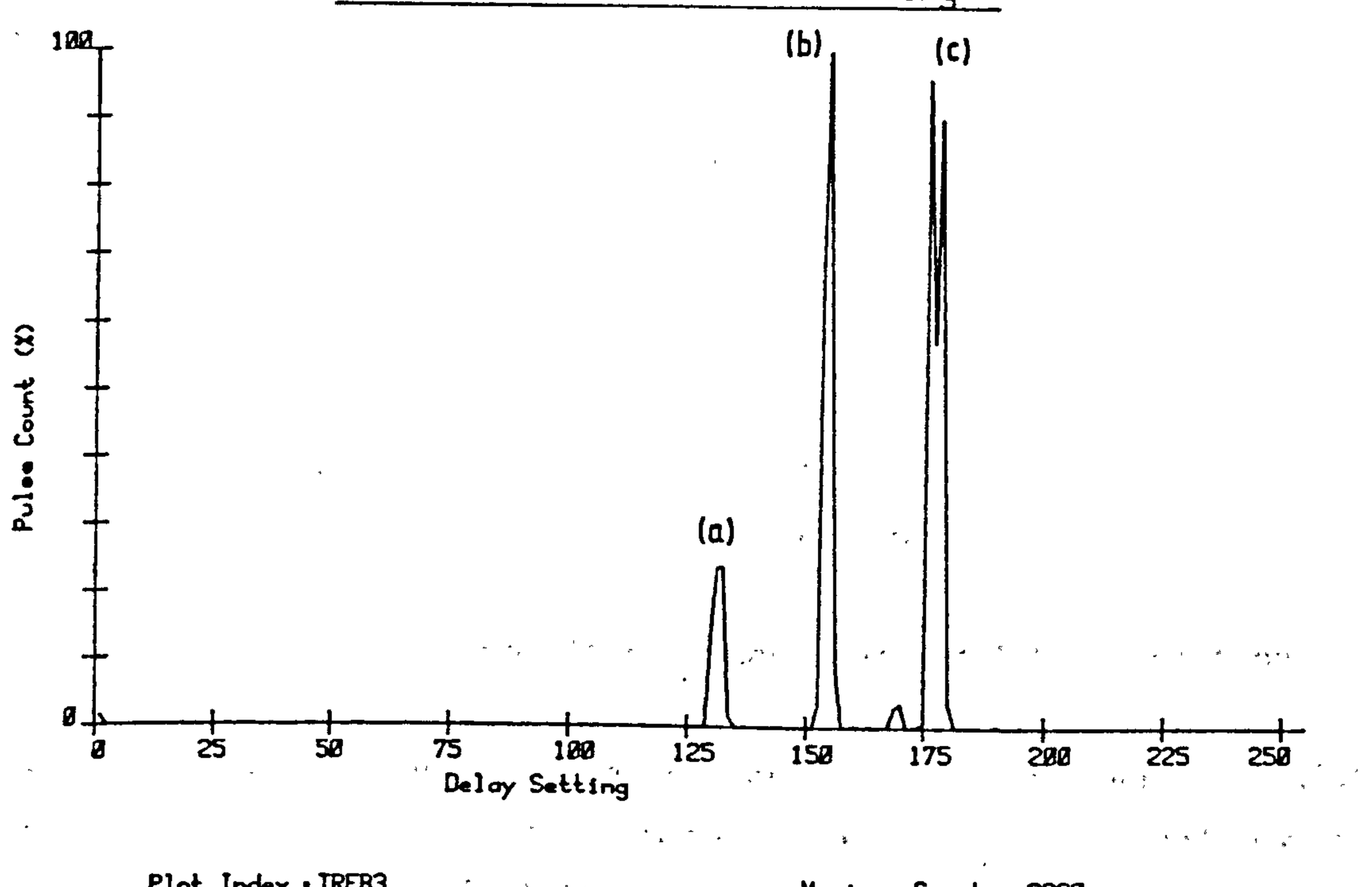

Figure 4.4.7:5 - Scan of Winding with Pulse Sources at c4,c5 and c6

Injection Points			Channel Position			Pulse Count		
Source			Source			Source		
(a)	(b)	(c)	(a)	(b)	(c)	(a)	(b)	(c)
1	2	3	75	98	119	551	2173	2248
2	3	4	90	117	138	514	2240	2256
3	4	5	111	136	158	544	2306	2161
4	5	6	132	155	176	543	2111	2189

Figure 4.4.7.6 - Pulse Source Location and Pulse Count Data

From the scans , source (a) is easily identified by the lower pulse count at its peak whilst the other two sources have consistently similar peak pulse counts .

The accuracy of discharge source location is assessed by comparing the results in figure 4.4.7.6 with the location positions obtained from the previous experiment with single pulse source injection on a winding with identical terminating impedances , (refer to section 4.4.3) . The expected discharge source locations are given in the table in figure 4.4.7.7 .

Injection Points			Channel Position		
Source			Source		
(a)	(b)	(c)	(a)	(b)	(c)
1	2	3	72	88	107
2	3	4	88	107	126
3	4	5	107	126	145
4	5	6	126	145	165

Figure 4.4.7.7 - Comparison of Measured and Actual Locations

From a comparison of the discharge source locations in figures 4.4.7.6 and 4.4.7.7 it follows that the observed positions are biased towards the low impedance terminal of the winding by an average of 10 channel positions , (7 metres of winding length) . This is a shift in the expected location spectrum of approximately three quarters of the length of a coil . This shift can only be explained by the fact that the amalgamated impedance of the pulse injection circuits significantly changes the pulse propagation characteristics of the winding so as to alter the location properties of the correlator .

Although a shift in the discharge location spectrum occurs , the shift is linear and discharge locations at coil connections are correctly positioned with respect to one another . The technique is therefore able to locate the discharge sources in the winding accurately since only the reference position of the scan changes .

In each of the winding scans a spurious pulse count occurs at a position midway between the locations of discharge sources (b) and (c). Because the spurious peak occurs between the locations of sources (b) and (c) , it is assumed that it is due to the interference of pulses from these sources which happens randomly .

In all the winding scans the observed pulse count at the location peaks for each discharge source is double the value expected since for a channel dwell period of 250 msec the pulse counts expected for pulse sources (a), (b), and (c) are 250, 1250, and 1250 respectively . This behaviour is explained with reference to the waveform diagrams in figure 4.4.7.8 .

The rectangular pulse from the pulse generator is differentiated with respect to time by the injection coupling capacitor C to produce a positive and negative polarity pulse . A signal diode clips the negative pulse at the forward bias voltage of the diode , approximately 0.7 volts . This waveform enters the winding and travels to the winding terminals after undergoing some intermediate distortion in shape . The resultant signal is then differentiated with respect to time again by the Rogowski coil before it is passed through the programmable delay line to the coincidence detector . After the second stage differentiation at the Rogowski coil the negative polarity pulse exhibits a overshoot . This overshoot appears to the coincidence detector as a small positive polarity pulse since the peak amplitude is above the threshold level of the detector . Therefore for every rectangular pulse , pulse cycle , from the pulse generator two positive polarity discharge pulses will be produced which is reflected in the pulse counts obtained .

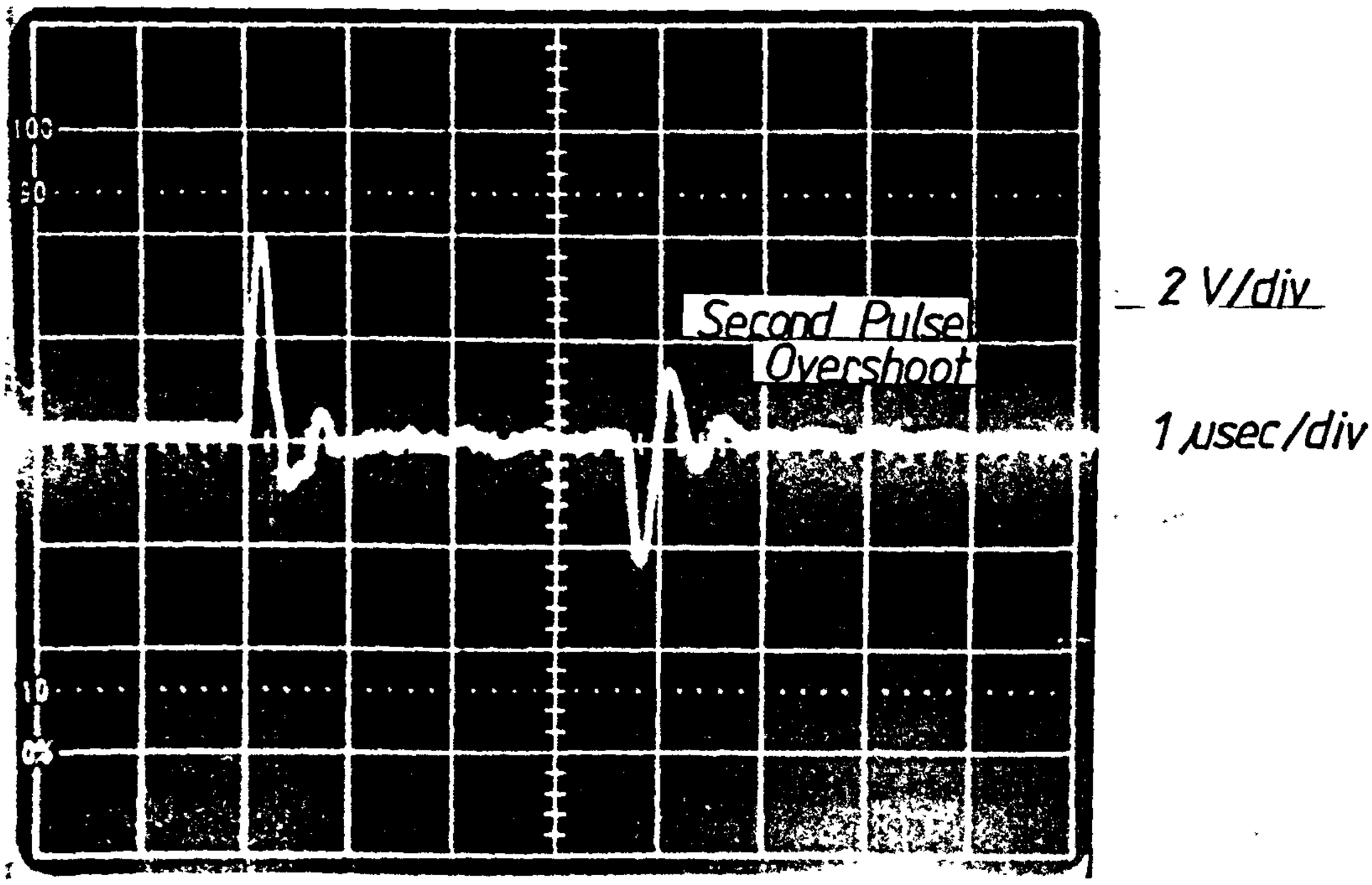

Figure 4.4.7.8 - Waveforms Showing Pulse Overshoot

4.4.8 Injection of Six Independent Discharge Sources

In this final experiment with artificial discharges six independent discharge pulse sources (a), (b), (c), (d), (e), and (f) are injected into the winding at coil connections c1, c2, c3, c4, c5, and c6 . The discharge pulse magnitude developed at each source is 5000 pC , (10 V through 500 pF) , and the pulse repetition frequencies for each source is shown in the table in figure 4.4.8.1 .

Discharge Source	Pulse Frequency (Hz)
(a)	9000
(b)	4600
(c)	4600
(d)	9000
(e)	9000
(f)	4600

Figure 4.4.8.1 - Discharge Source Repetition Rates

The threshold voltage levels in the coincidence detector for channels A and B are 65 mV and 75 mV respestively .

Figure 4.4.8.2 shows the scan of the winding which indicates the location of all the pulse sources injected . The channel positions of these location peaks and the expected source locations are given in the table in figure 4.4.8.3 , along with the pulse counts for each source .

Discharge Source	Channel Location	Expected Location	Pulse Count
(a)	63	72	2081
(b)	87	88	860
(c)	108	107	1058
(d)	135	126	2236
(e)	159	145	1988
(f)	181	165	1080

Figure 4.4.8.3 - Expected and Measured Locations and Pulse Counts

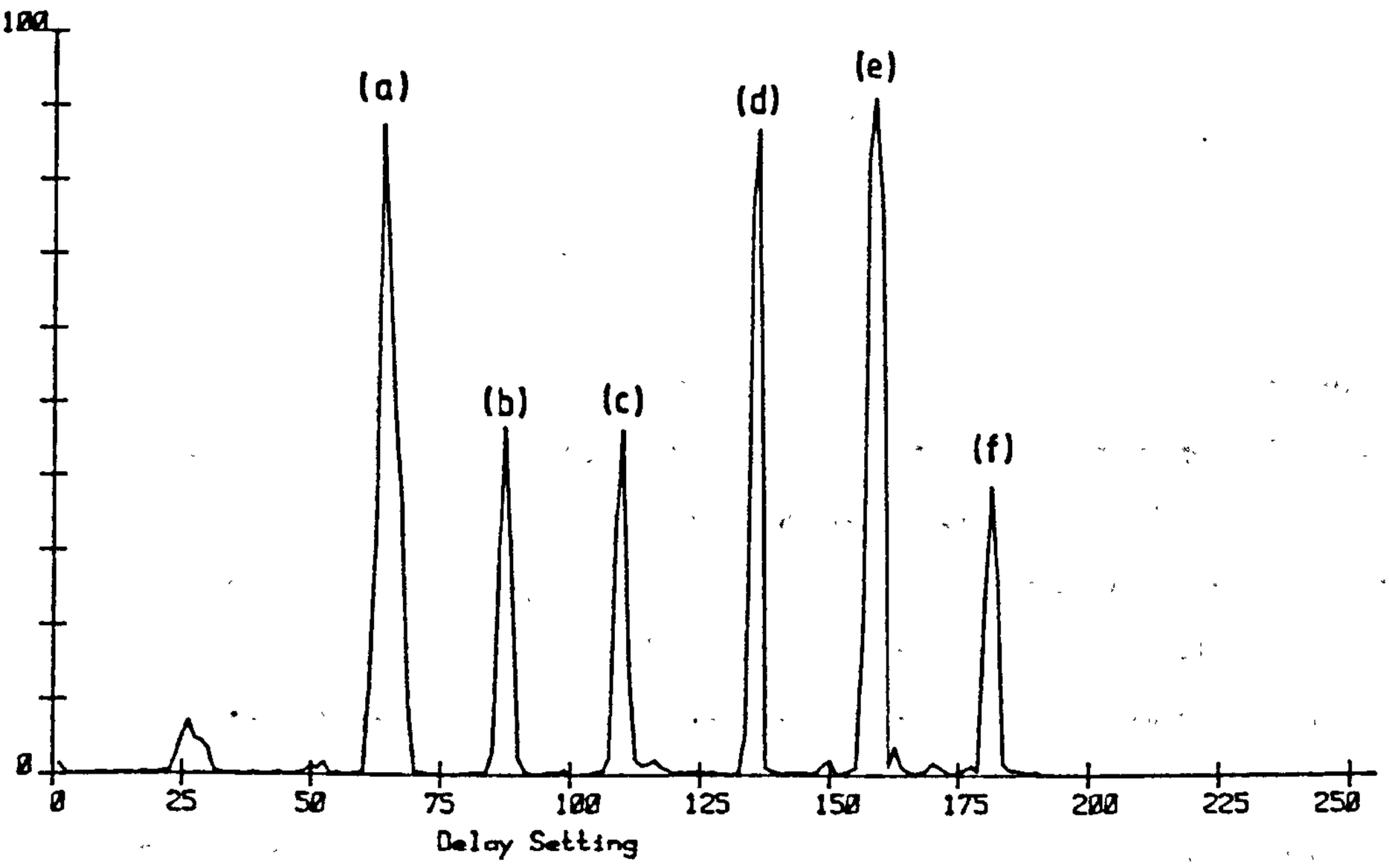

Figure 4.4.8.2 – Scan of Winding with Six Independent Pulse Sources

From these results it can be seen that correlation between location positions and expected positions for the discharge sources (a), (b), and (c) are good . However , as in previous experiments errors occur in locations of sources closer to the low impedance terminal of the winding , the maximum error being 16 delay settings or 11.2 metres of winding . Although this discrepancy is of the order of one coil length the technique is still able to indicate the approximate positions of the discharge sources relative to the winding terminals and to each other . The errors in the locations are due to the influence of the additional coupling capacitance of each discharge circuit on the transmission characteristics of the winding .

Pulse counts for each source is close to the expected values of 1150 and 2250 pulses for 4600 Hz and 9000 Hz sources respectively .

4.5 High Voltage Discharge Source

The correlator has been shown to be effective in the location of artificially generated discharge pulse sources within a model stator winding . As a natural progression in the assessment of the correlator as discharge location technique , the next series of experiments demonstrate the behaviour of the location instrument when partial discharges derived from a high voltage source are injected into the winding model . This is as close to a real motor in which there are partial discharges as is possible with a model representation of a stator winding .

The source of high voltage discharges is a spark gap in series with a parallel plate capacitor as shown in the photogragh in figure 4.5.1 . The magnitude of the partial discharges produced is controlled by varying the separation between the plates of the capacitor thus varying the injection capacitance C . The breakdown voltage at which discharges occur is controlled by the separation between the two needle electrodes in the spark gap , the closer the distance between the electrodes the lower the breakdown voltage . An equivalent circuit for the components of the discharge injection circuit is shown in figure 4.5.2 .

From the circuit , V is the supply voltage and δV is the discharge breakdown voltage as dictated by the spark gap separation d . C is the capacitance of the parallel plate capacitor and C_s is the

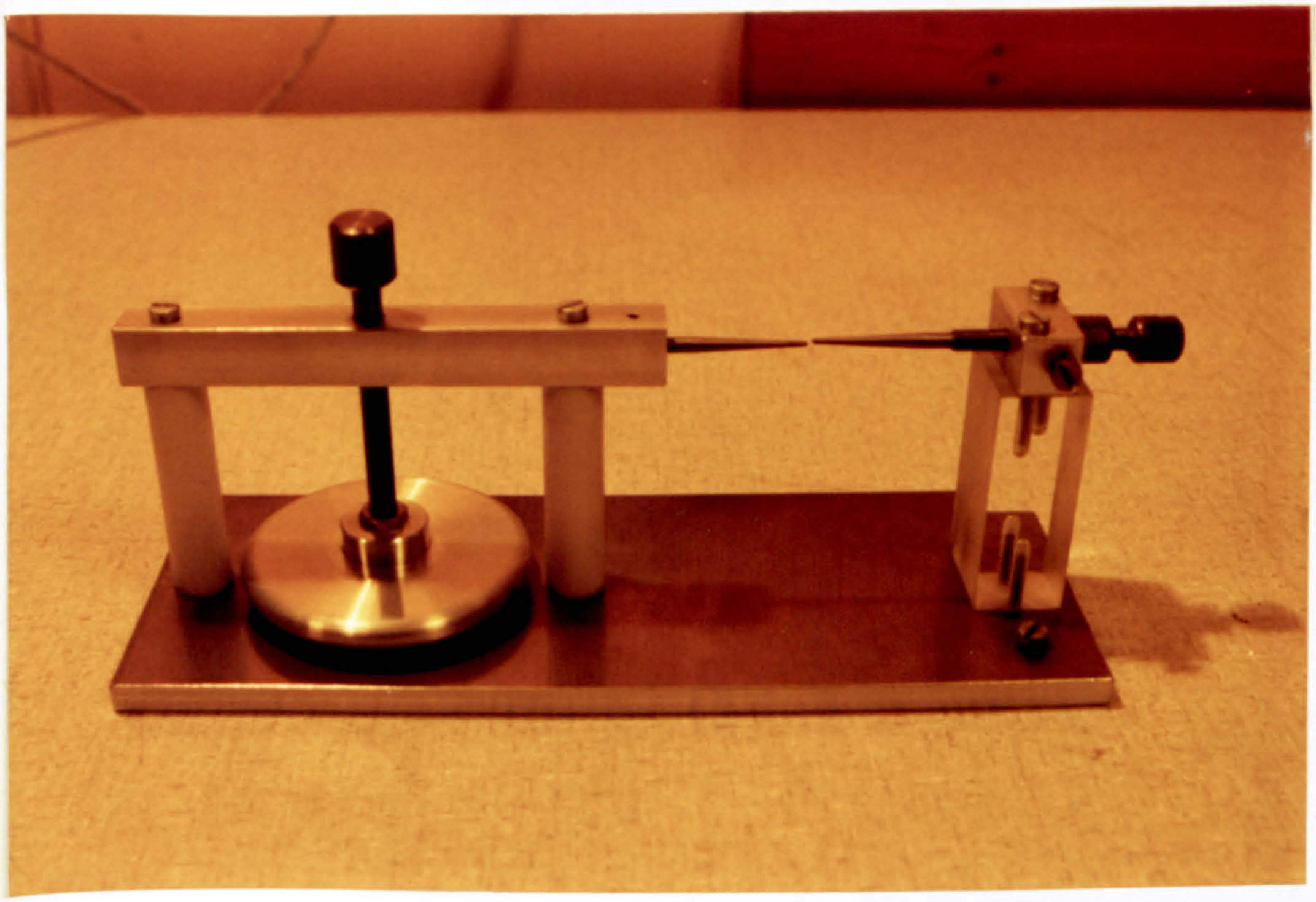

Figure 4.5.1 - Spark Gap Discharge Source

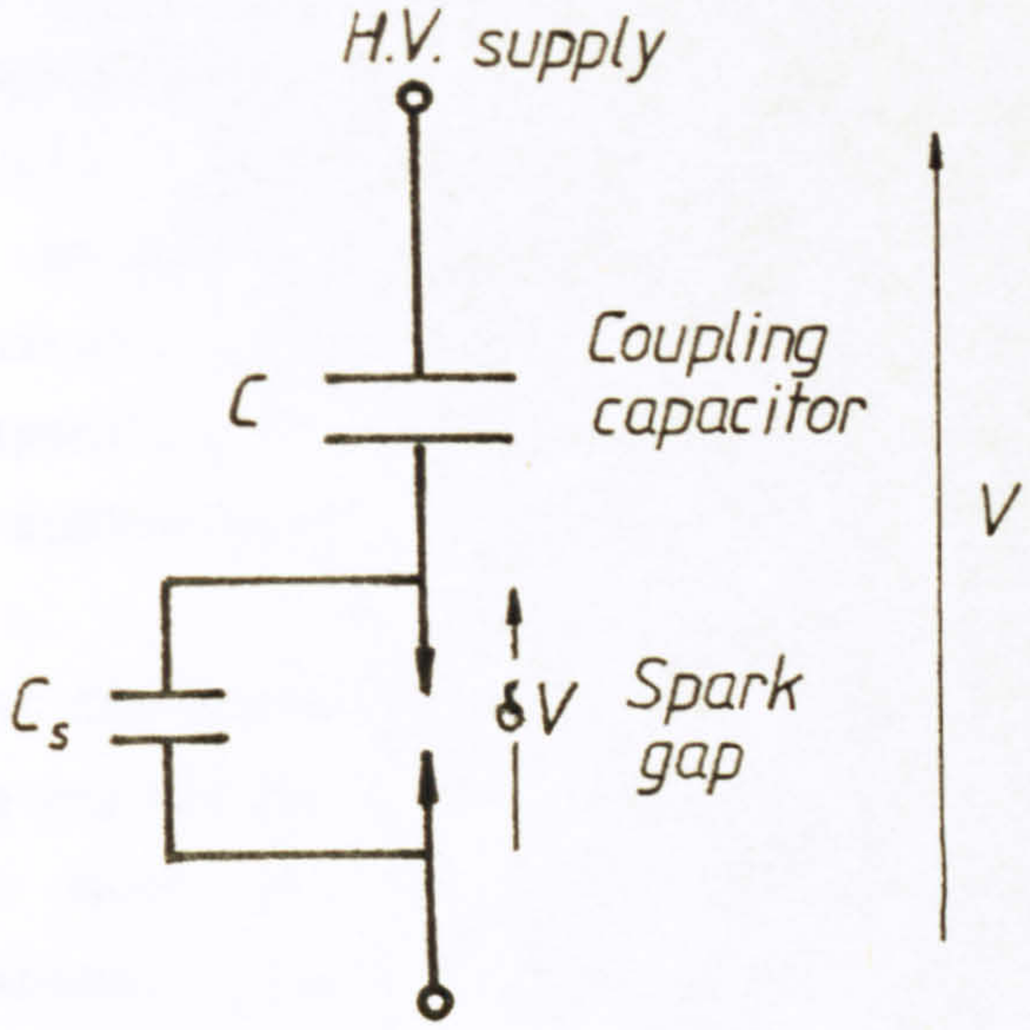

Figure 4.5.2 - Spark Gap Equivalent Circuit

capacitance of the spark gap . Assuming that the capacitance of the gap C_s is completely discharged at the breakdown voltage of the gap then the magnitude of the discharge is given by ;

$$Q = C_s.\delta V$$

This is equivalent to the charge on the plates of the variable capacitor C which is ;

$$Q = C .(V - \delta V)$$

Both the supply and discharge breakdown voltages can be measured whilst the capacitance C can be calculated to give the discharge magnitude produced in the spark gap . If D is the diameter of the plate capacitor and d is the plate separation then the capacitance is given by the expression :

$$C = \frac{\epsilon.\pi.D^2}{4d}$$

D is 70 mm and the capacitor plate separation is variable in the range 2 mm to 30 mm , so that the range in capacitance is from 1.15 pF to 17 pF .

In the high voltage experiments the supply voltage is the nominal phase voltage , 3.8 kV, (6.6 kV line voltage). The discharge breakdown voltage is measured at 2.5 kV . From these parameters the range in discharge magnitude is 2875 pC to 4250 pC . The plate separation of the capacitor C is 20 mm which corresponds to a discharge magnitude of approximately 2200 pC .

In the first experiment the discharge source is connected in series with the stator winding across the H.V. supply as shown in figure 4.5.3 . In doing so most of the voltage is developed across the discharge source circuit since the combined capacitance of the plate capacitor and the spark gap is less than 2 pF . Therefore , no discharges can be generated in the winding since the voltage from the winding to earth is to small . The main conducted source of high voltage discharge must be the spark gap . The winding terminals are terminated in resistors which match the characteristic impedance of the winding which is 330 ohms .

In the first scan the discharge source is connected to c1 on the winding . The scan of the winding is displayed in figure 4.5.4 which shows a location peak at channel 73 which is close to the expected position of a source at c1 for the matched terminating impedance case (channel 72) . However , there are two other distinct location peaks at channel positions 208 and 242 which are outwith the limits of the scan plot for a six coil winding since these locations correspond to a delay time difference of greater than the transit time through six coils . That is to say that these spurious discharge sources must have originated outwith the six coil winding . However , since this is not possible it must be deduced that these spurious counts must be due to the effects of interference on the location instrument . It may be the case that the interference pulses generated by the spark gap cause erroneous switching of the relays in the programmable delay line circuit .

The manner in which the interference pulses enter the instrument must be via the interface cable conductors which links MICA to the microcomputer and the multi-channel analyser . Figure 4.5.5 demonstrates the probable mode of interference coupling . This problem is highlighted by the fact that very frequent spurious switching of relay contacts occurs when a high voltage discharge source is in close proximity to the interface cable , controlling the programmable delay line from the microcomputer . Under such conditions it is not possible to perform a scan of the winding since interference pulses trigger the channel advance signal to the multi-channel analyser . This is eliminated to an extent that only signals from the microcomputer advance the channel position on the multi-channel analyser scan by minimising the loop area formed by the interface cables . Clearly some mode of interference coupling remains since spurious location peaks are obtained , however , the mechanism by which these peaks occur is difficult to assess .

The discharge pulse count at the location peak is 61 pulses which corresponds to 244 pulses per second which is approximately 4 - 5 discharges every cycle of the mains supply . This is the expected discharge pulse rate which is derived from the model of the discharge injection circuit in figure 4.5.2 and the resultant voltage waveform

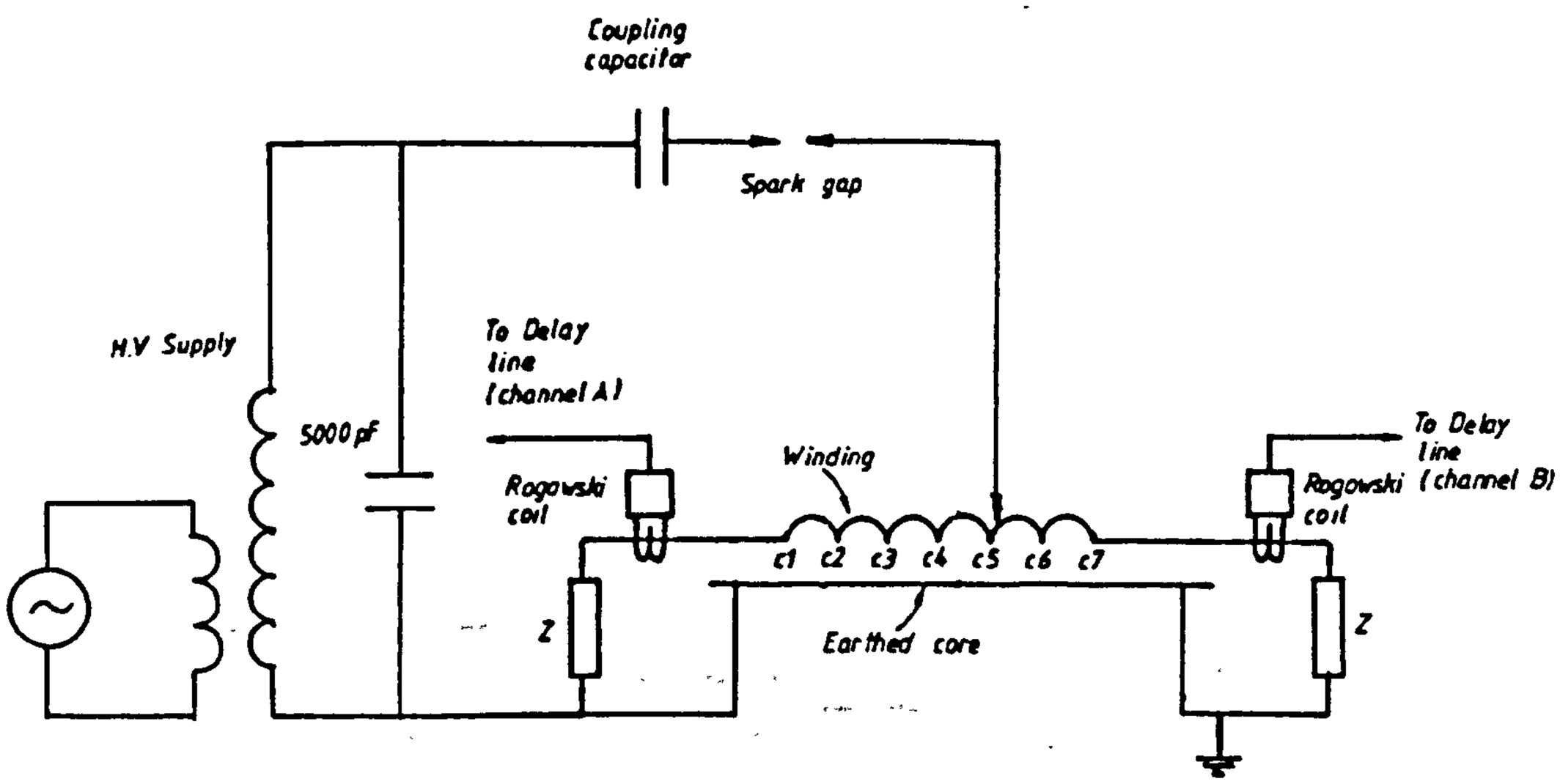

Figure 4.5.3 - High Voltage Discharge Injection Circuit

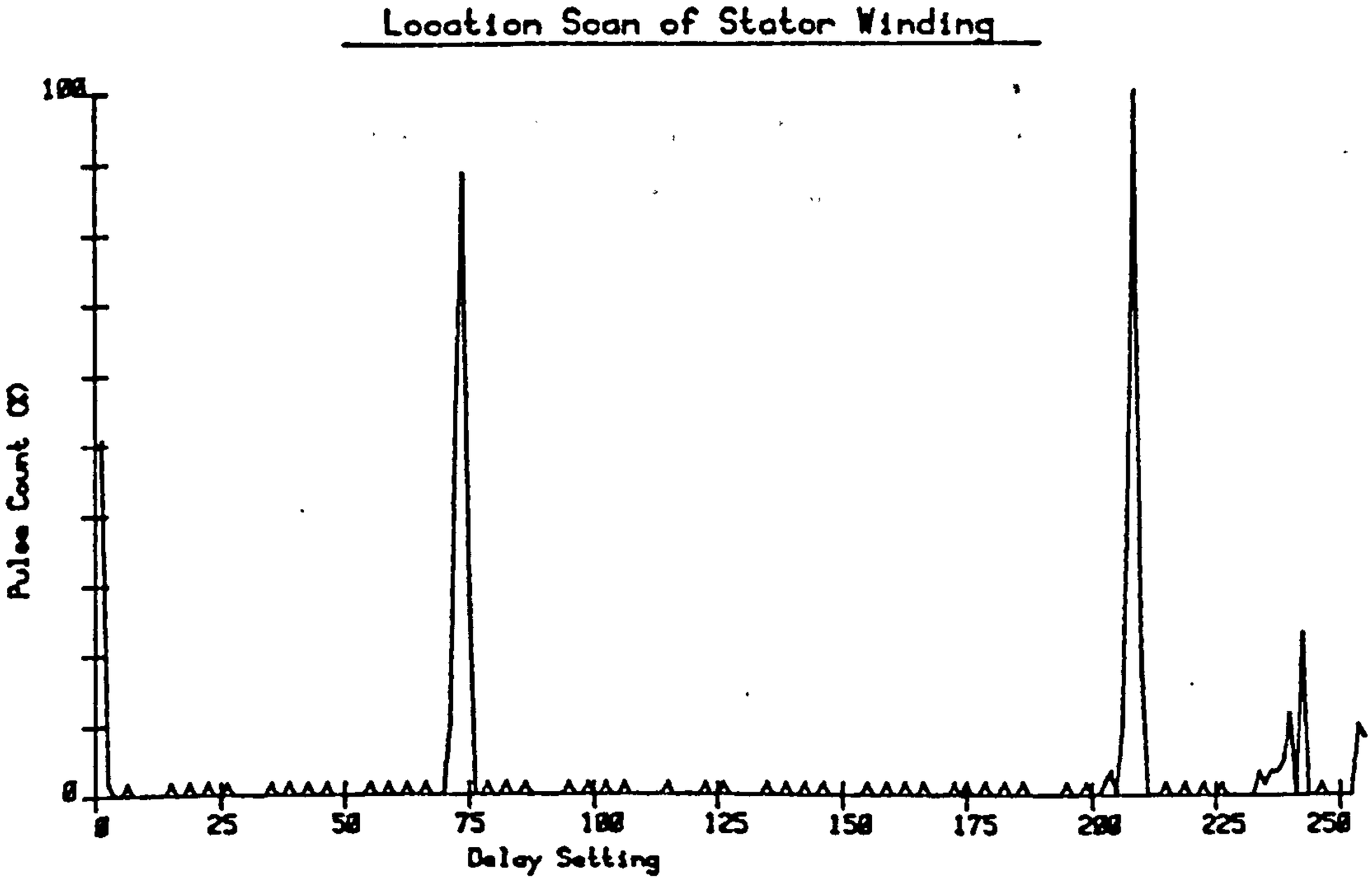

Figure 4.5.4 - High Voltage Discharge Injected at Position c1

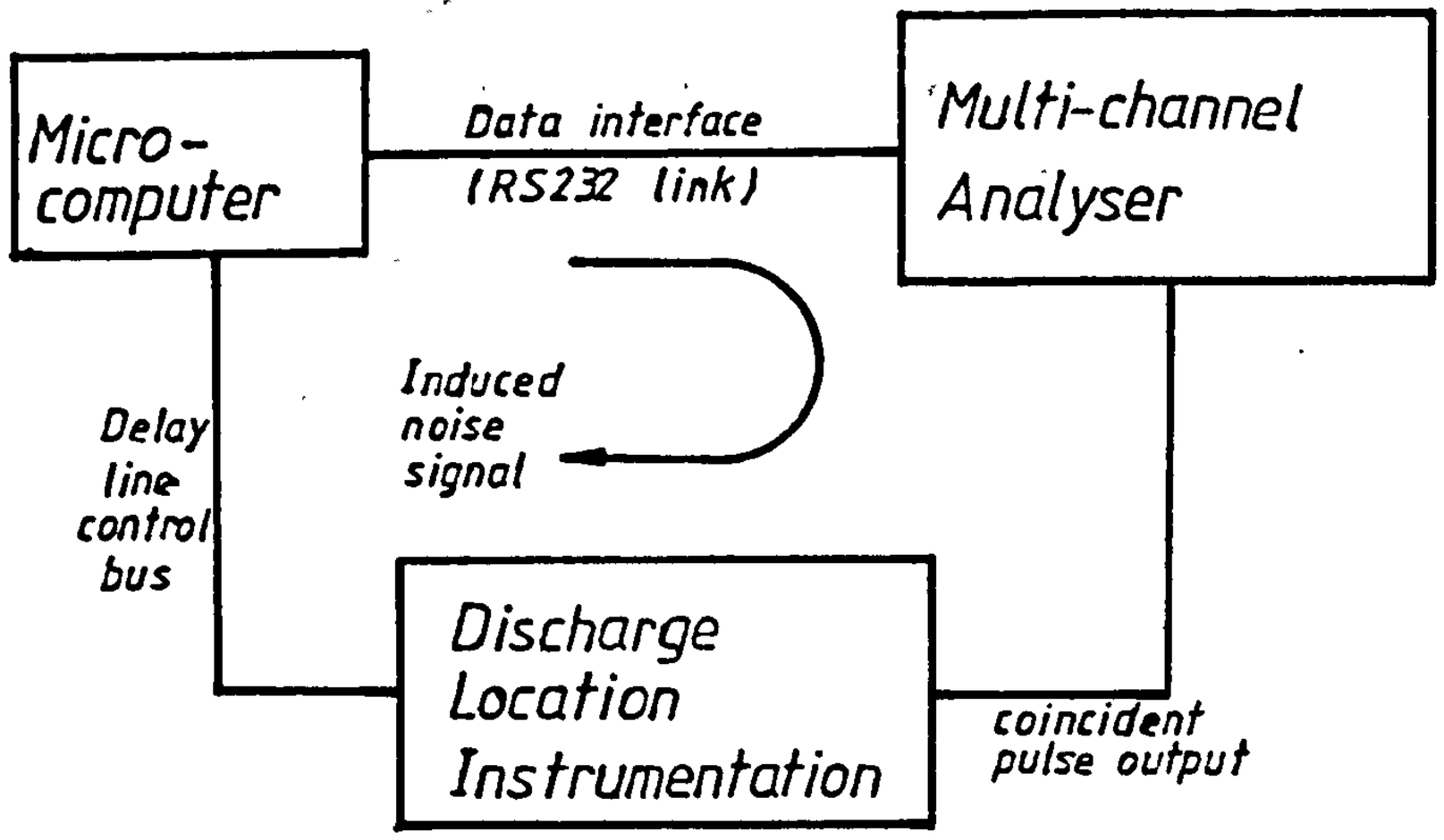

Figure 4.5.5 - Mode of High Voltage Discharge Interference

across the spark gap , as shown in figure 4.5.6 . A spark gap capacitance of 2 pF is assumed and the measured discharge inception voltage is 2.5 kV . Since the parallel plate capacitance for the test is 11 pF , then 85 % of the supply voltage is developed across the spark gap .

In the next test the scan is performed with the discharge source injected at point c2 on the winding . The results are displayed in the scan in figure 4.5.7 . Similarily , the test is repeated with the discharge source injected at positions c3, c4, c5, c6, and c7 . The respective scans for these are shown in figures 4.5.8, 4.5.9, 4.5.10, 4.5.11, and 4.5.12 . Positions of the location peaks are summarised in the table in figure 4.5.13 along with the pulse count of the largest peak for each scan .

Injection Point	Location Positions					Pulse Count
c2	81	214				42
c3	90	215				63
c4	53	136	97			67
c5	27	56	72	226		64
c6	35	58	189			54
c7	6	35	149	162	196	61

Figure 4.5.13 - Location Scan Data

In the previous experiment with artificial pulses injected into a winding with matched impedance terminations , section 4.4.1 , the limits of the scan for a six coil winding are 72 and 186 for points c1 and c7 respectively . It may then be deduced that location peaks at positions on the scans outwith these limits are false and are due to interference .

The remaining locations are listed in the table in figure 4.5.14 along with the expected locations of discharges injected at the coil connections .

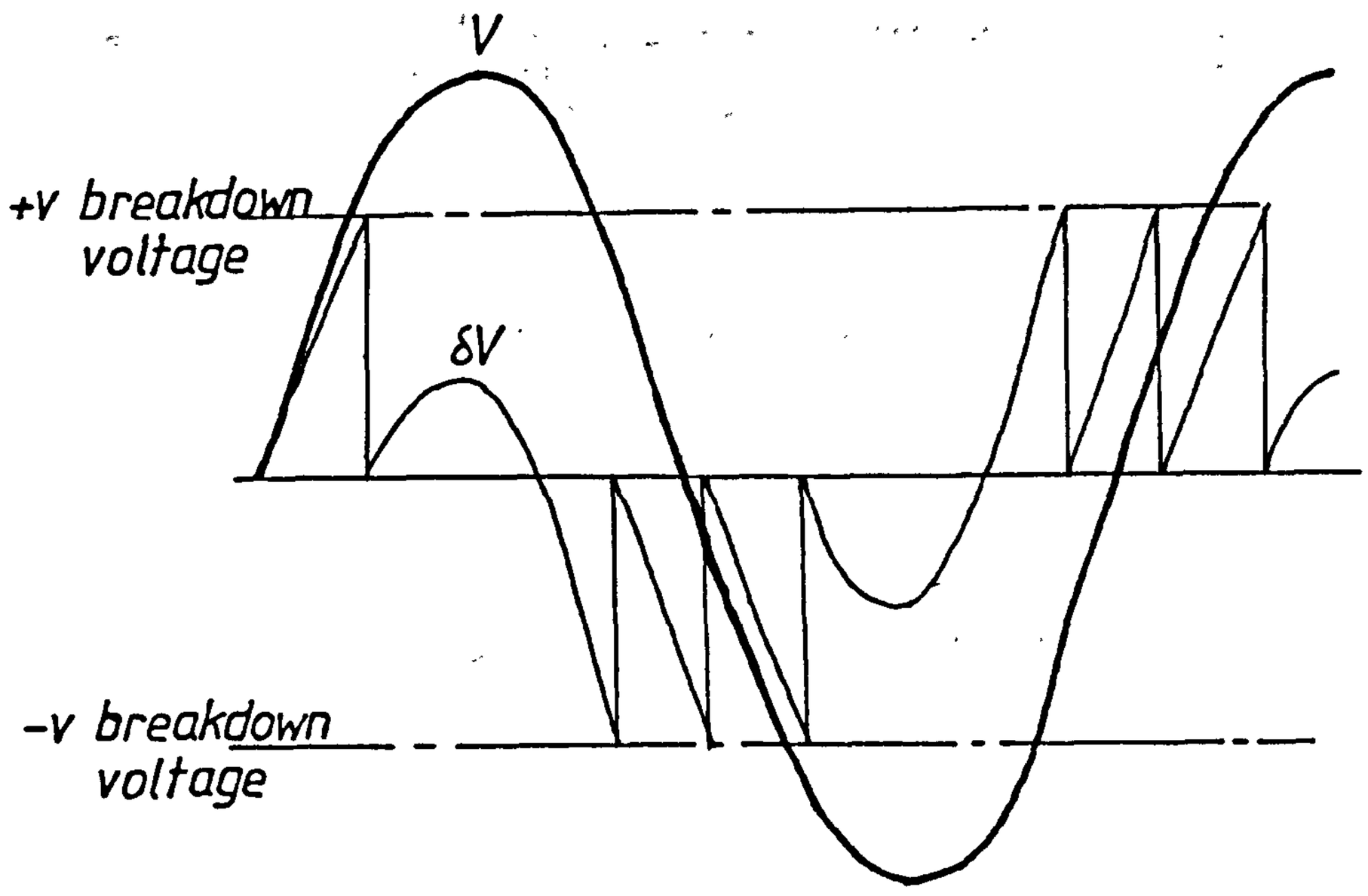

Figure 4.5.6 - Discharge Repetition Rate in Spark Gap Circuit

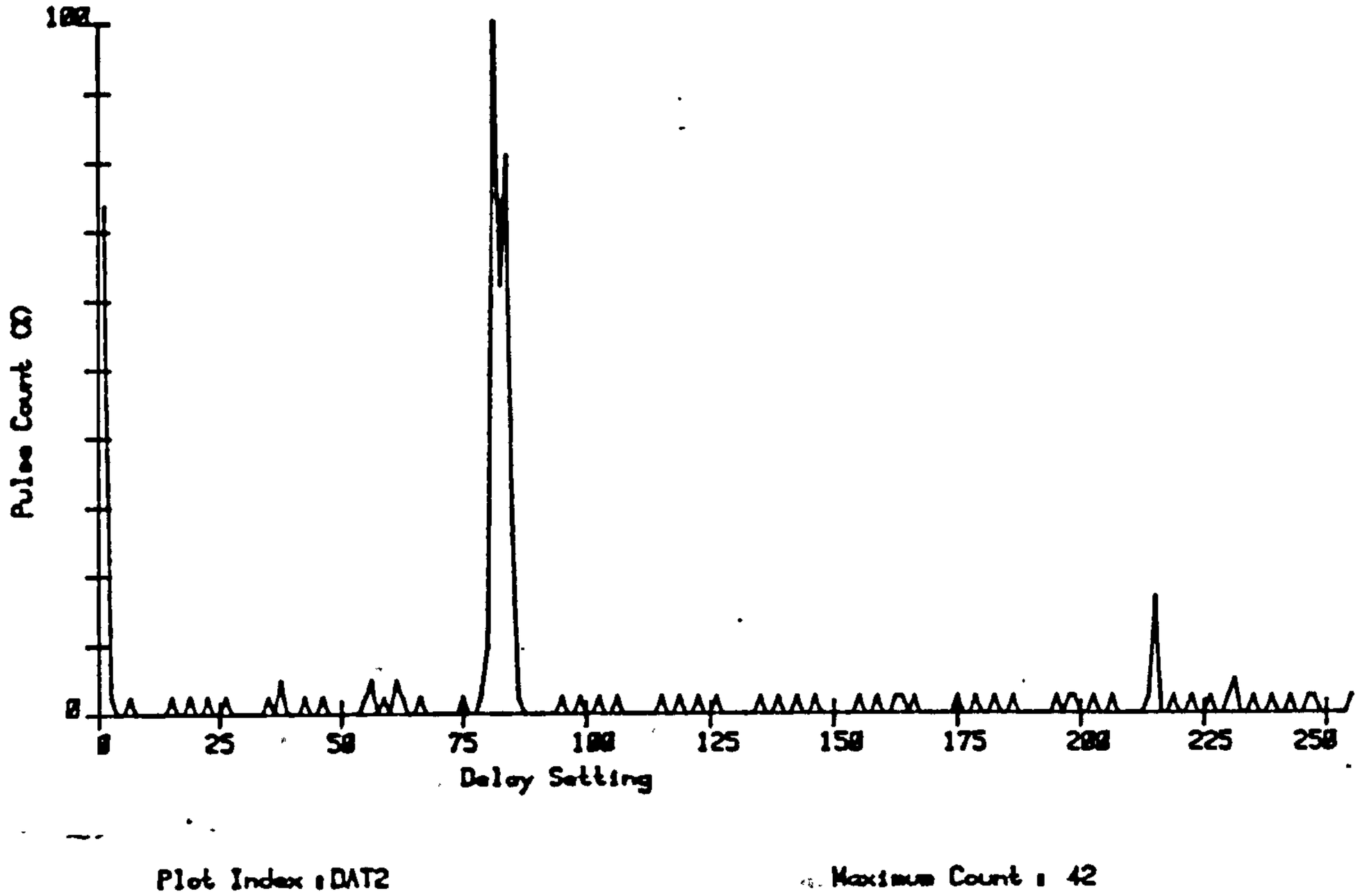

Figure 4.5.7 – Scan of Winding with Discharge Source at c2

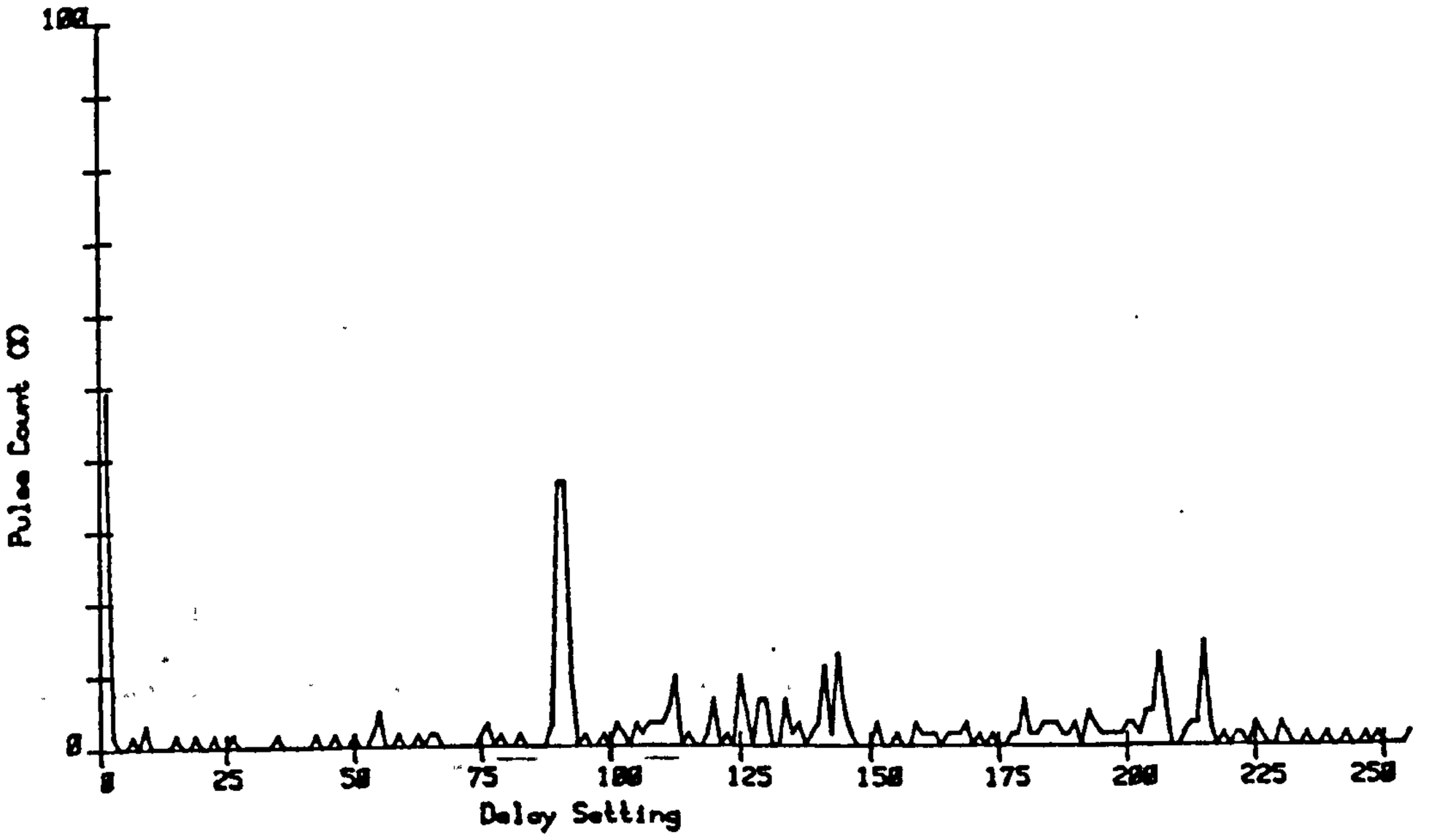

Figure 4.5.8 – Scan of Winding with Discharge Source at c3

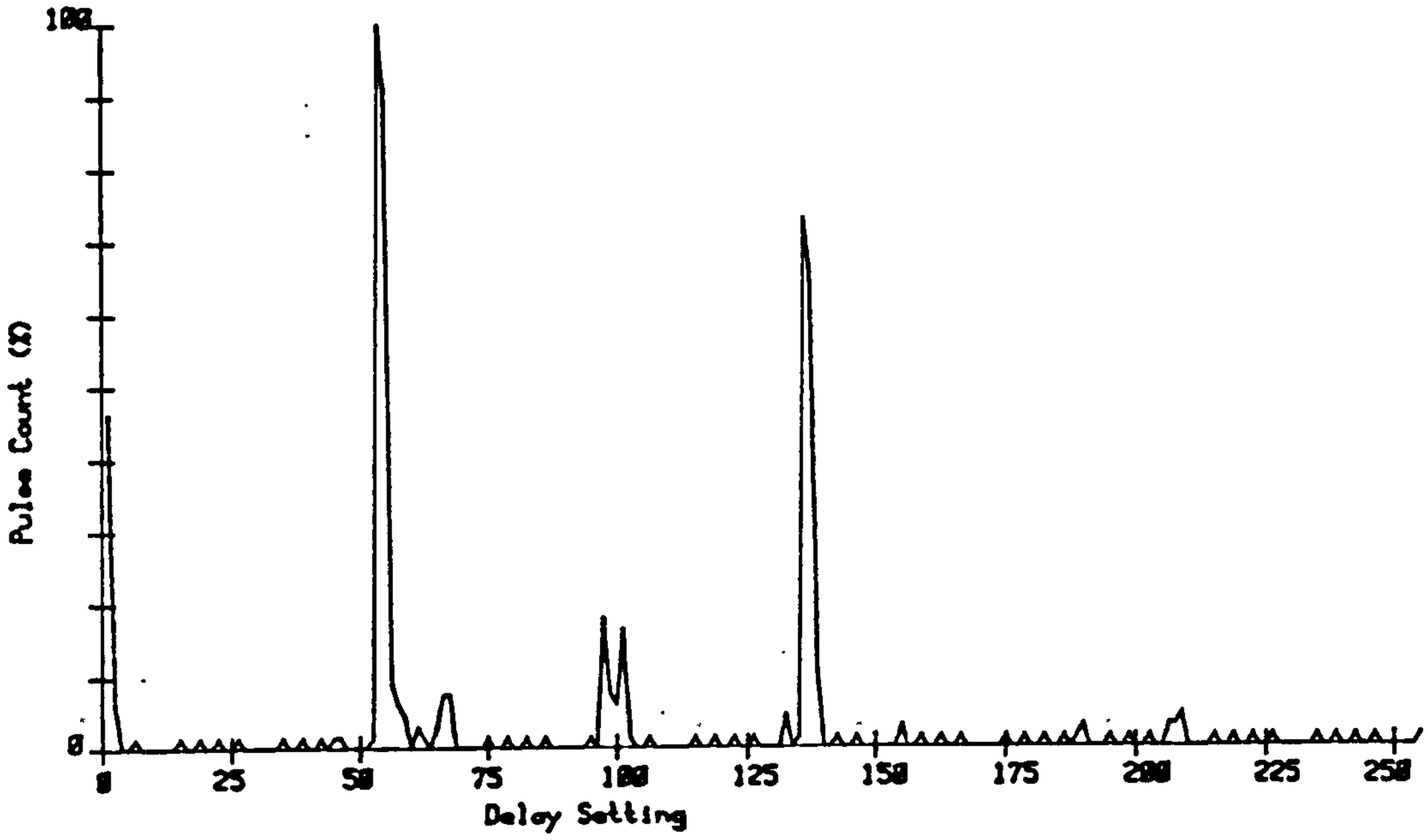

Figure 4.5.9 – Scan of Winding with Discharge Source at c4

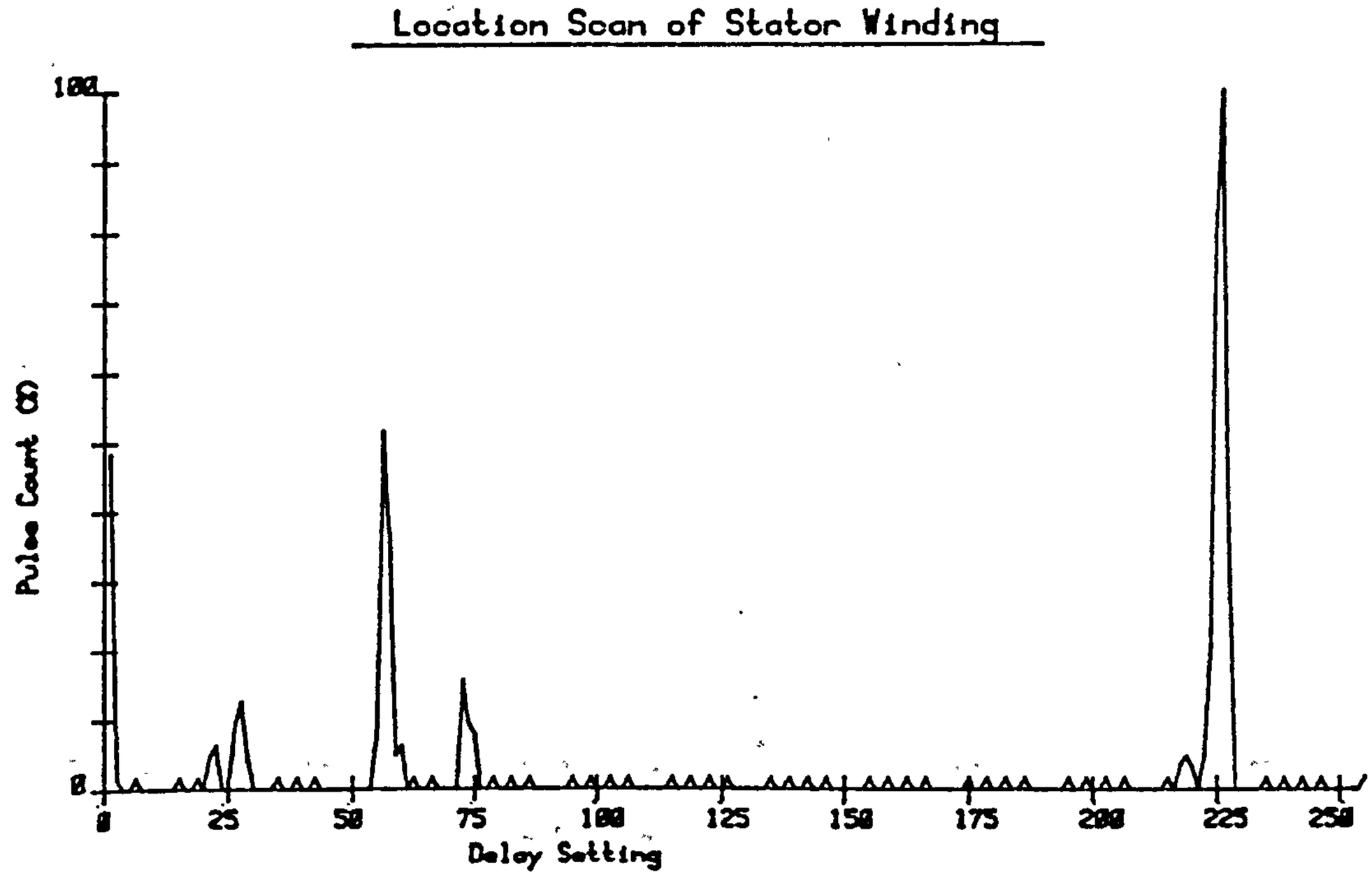

Figure 4.5.10 – Scan of Winding with Discharge Source at c5

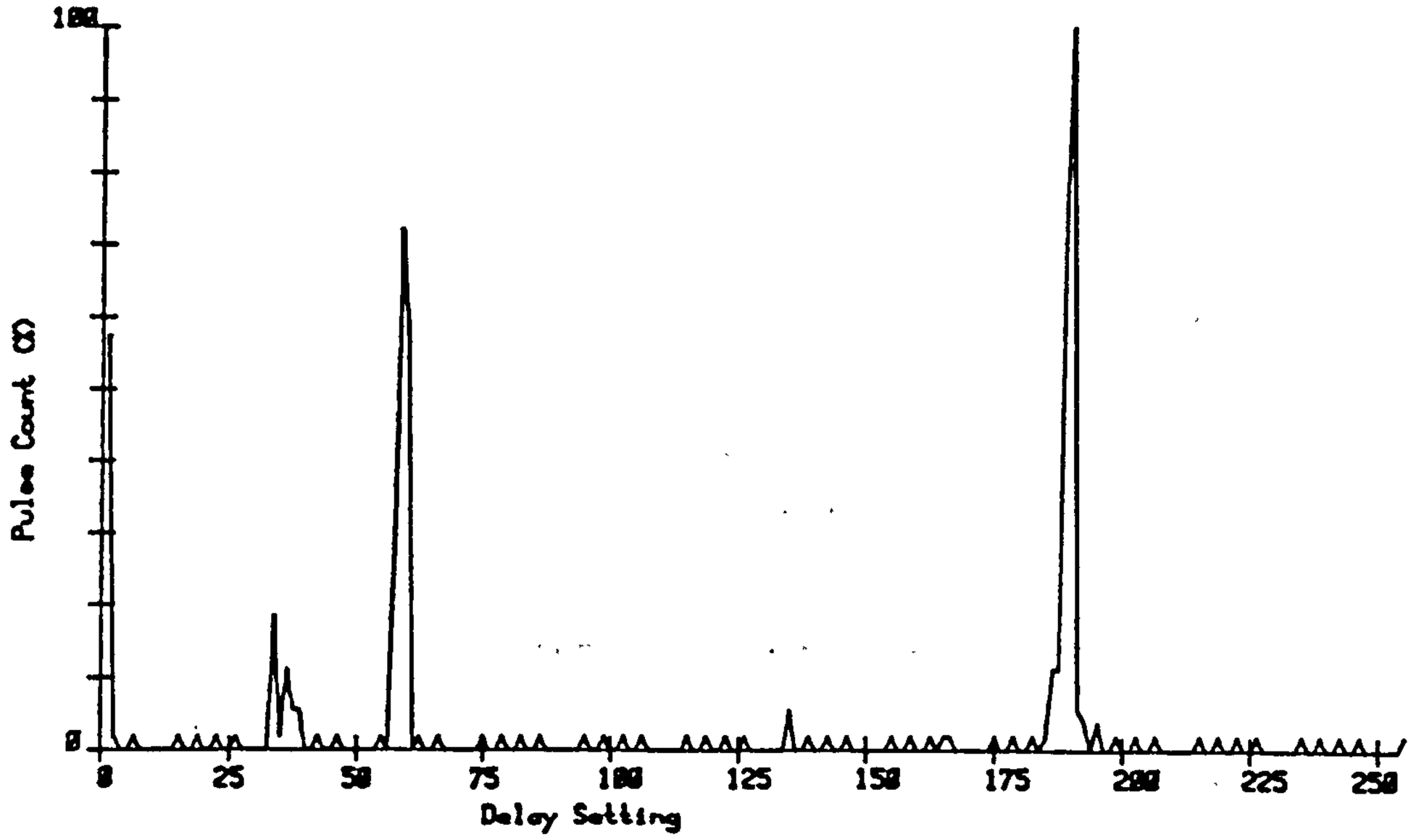

Figure 4.5.11 - Scan of Winding with Discharge Source at c6

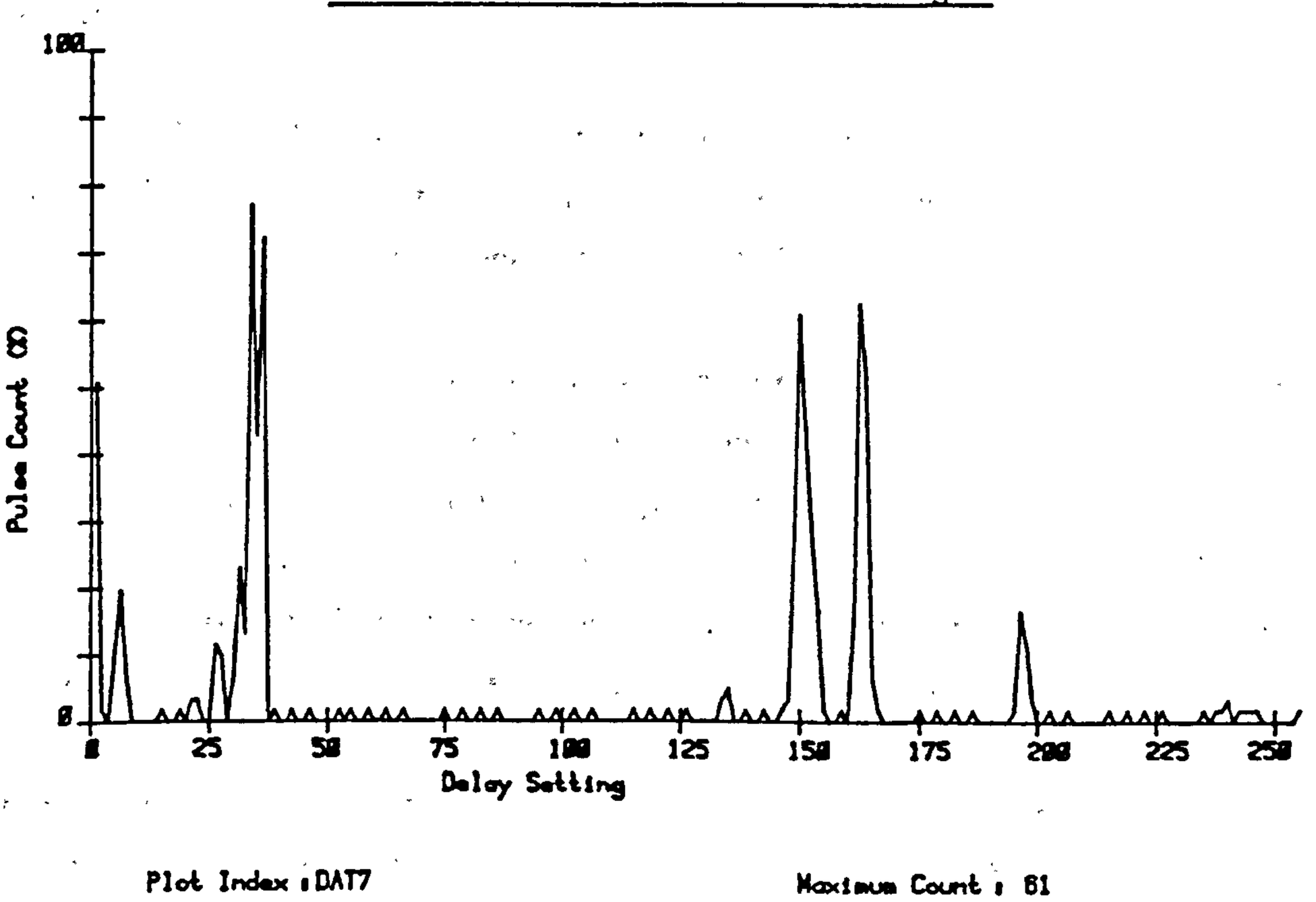

Figure 4.5.12 - Scan of Winding with Discharge Source at c7

Injection Point	Location Positions Observed		Location Positions Expected
c1	73		72
c2	81		90
c3	90		111
c4	97	136	131
c5	72		152
c6	189		170
c7	149	162	186

Figure 4.5.14 - Expected and Measured Discharge Locations

Locations for discharges at positions c1 and c2 are reasonably close to the expected values . An error of 9 delay increments , half a coil length , occurs in the location of the source at point c2 on the winding . This error in location increases to 21 delay increments ; that is just over one coil length or 18 % of the total winding length, for the source injected at point c3 . The location peak at this position is the most definitive one and must be the discharge source , however , the error in the location of this source can only be explained in terms of the effects of interference .

It is also observed that there is a high level of spurious pulse counts over the scan from the largest peak up to channel 255 , which suggests a high interference susceptability .

In the next scan in which discharges are injected at point c4 on the winding , one location peak appears only 4 channel positions from the expected location which is equivalent to 2.8 metres form the true location . One much smaller location peak occurs at channel position 97 , and another distinctive peak outside the limits on the scan for a six coil winding which must be an interference effect .

When discharges are injected at position c5 , two main location peaks are detected at channels 56 and 226 on the scan which are outwith the limits for a six coil winding and must therefore be regarded as spurious interference counts . A discharge location does occur at the position where pulses injected at point c1 on the winding are expected, (channel 72), however this must be regarded as a spurious count since pulses are injected at the opposite end of the winding .

The observed location for discharges injected at point c6 is 19 channel increments from the expected value which is an error of 13.3 metres or just over one coil's length . Although the error is substantial the peak on the scan must correspond to the discharge source . Two other location peaks appear outside the limits for the winding and are therefore products of interference pulses .

Finally , when the discharge source is positioned at point c7 , five distinct pulse location peaks occur , the nearest to the expected discharge location being 10 channel positions away and also being the location with the lowest pulse count . It is however difficult to determine which of these is the true location . Interference effects seem to be more severe when discharges are positioned at this point on the winding .

4.5.1 Influence of Discharge Source Circuit

In this series of tests the influence of the high voltage test ciruit on the generation of interference and hence the resultant effects on the discharge location scans are discussed . The tests are essentially the same as the previous with the exception that changes are made in the high voltage circuit . In each of the scans the discharge source is connected to point c4 on the winding , the centre .

In the first scan the high voltage source and spark gap are moved to a location 5 metres from the instrument and the connection between the spark gap and the winding is made by a length of coaxial cable as shown in figure 4.5.1.1 . The scan of the winding obtained is displayed in figure 4.5.1.2 .

This result appears to be worse than the previous test result in the scan in figure 4.5.9 . Location peaks occur at positions 51, 103, 119, and 239 . Peaks at 51 and 239 are false since they are outwith the limits of the six coil winding . The nearest peak to the expected value is at channel 119 which is 17 channel positions in error , (equivalent to 11.9 metres) . Clearly , removing the high voltage source circuit from the close vicinity of the location instrument does not improve the performance of the instrument with respect to pulse

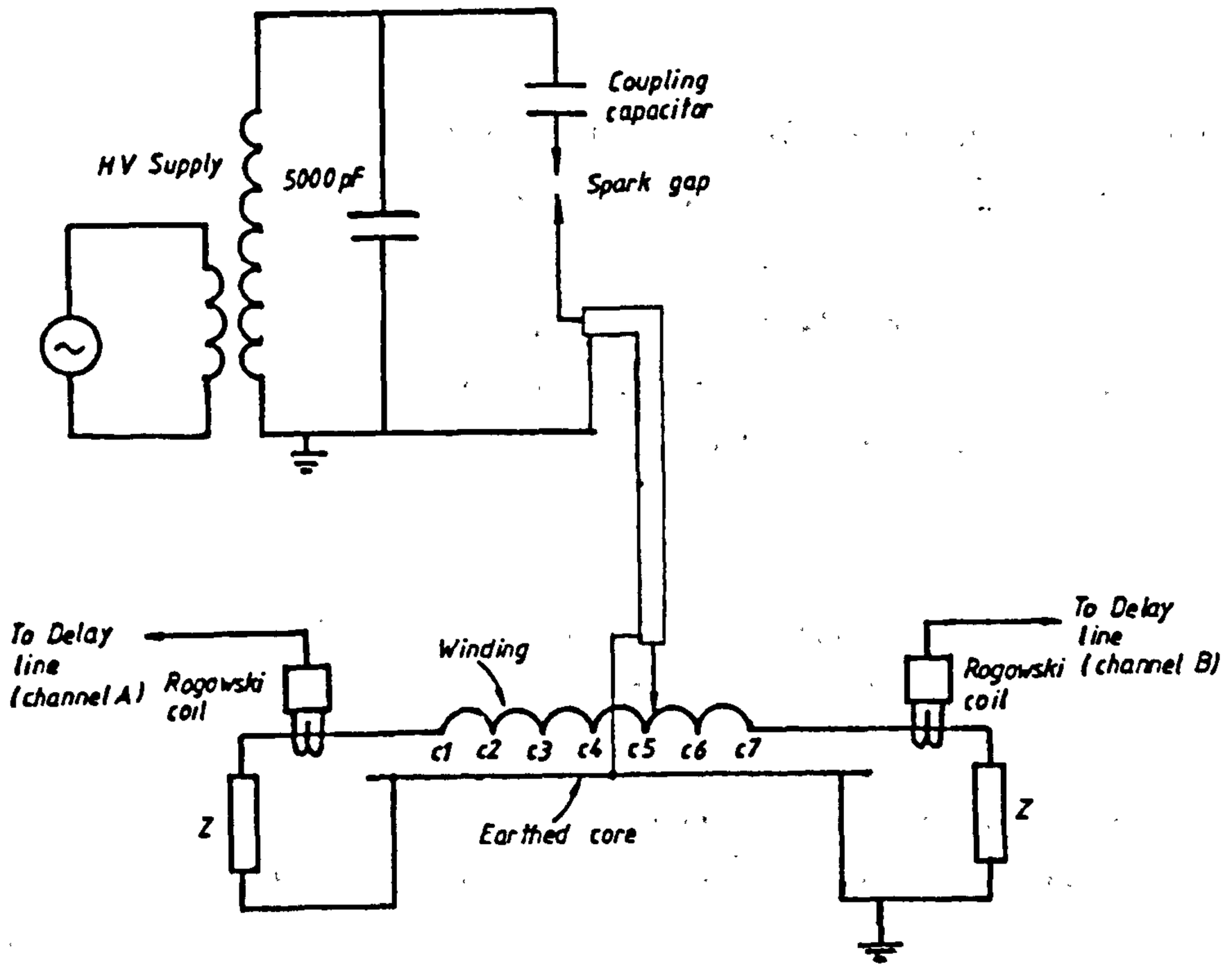

Figure 4.5.1.1 - High Voltage Discharge Injection Circuit

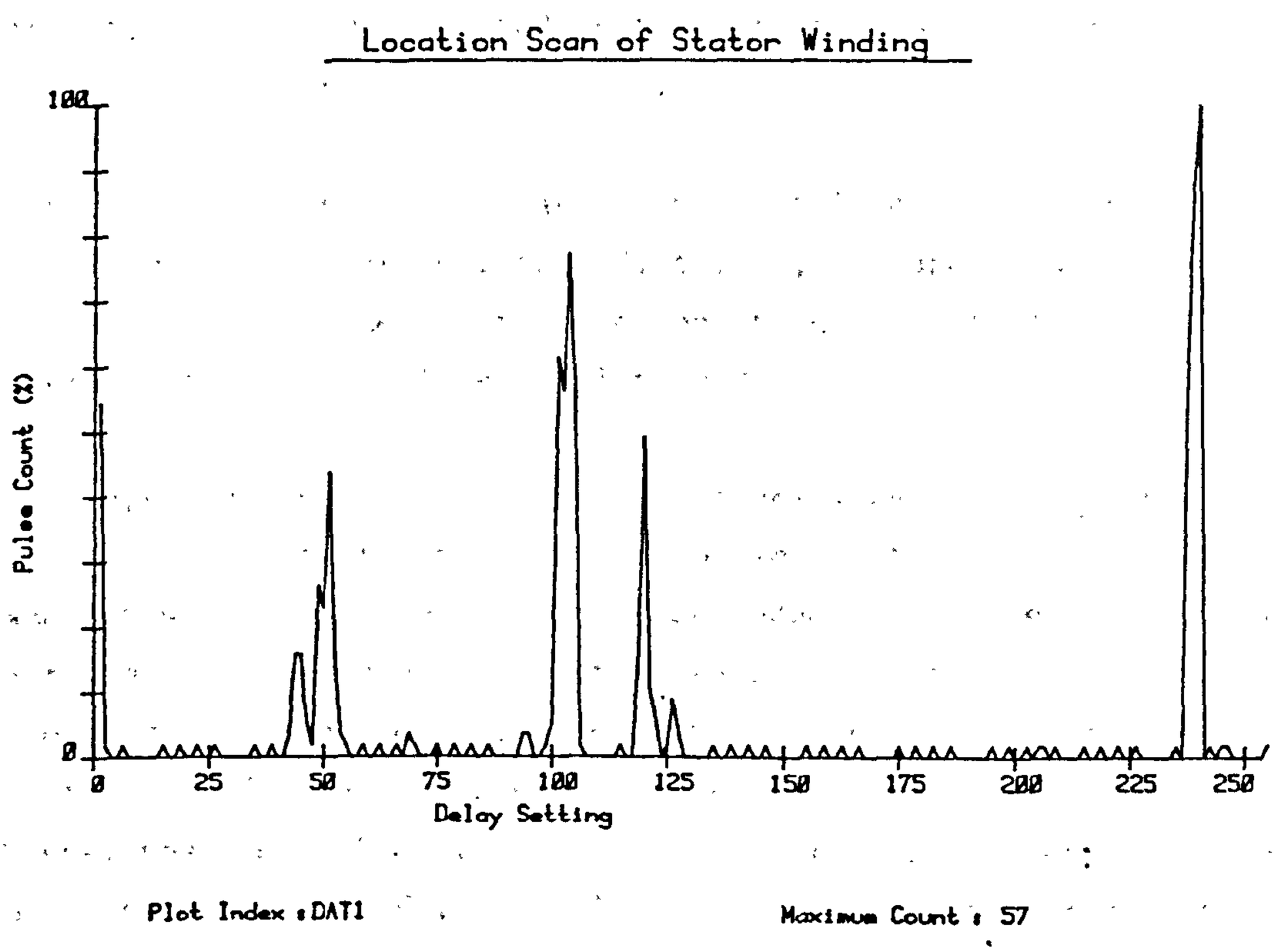

Figure 4.5.1.2 - Scan of Winding with Discharge Source at Winding Centre

interference .

In the second test , the characteristics of the source circuit are altered by the inclusion of a second discharge source in the form of a spark gap across the high voltage supply . A scan of the winding for this test is shown in figure 4.5.1.3 , in which it can be seen that there is a marked increase in the number of location peaks . The location peaks on the scan are at channel positions 20, 45, 54, 104, 121, 160, 214, and 239 .

This experiment simply emphasises the fact that the location instrument is susceptible to external, radiated interference since increasing the effective number of discharges injected at the same position on the winding does not increase the pulse count at the location of the discharge source but serves to increase the effects of interference .

4.5.2 Effect of Screening High Voltage Circuit

To eliminate as far as possible the effect of radiated interference the high voltage source and spark gap are placed in a screened enclosure which is connected to earth potential . The spark gap discharge source is connected to the winding via a coaxial cable as shown in the diagram in figure 4.5.2.1 .

In this experiment the discharge source is injected into each of the coil interconnections c1, c2, c3, c4, c5, c6, and c7 sequentially and a scan is performed for each position . The scans obtained are superimposed on a single scan plot as displayed in figure 4.5.2.2 .

It is apparent that there is still a significant level of interference present since there are spurious pulse counts across the whole scan base , however this level has been reduced from the previous by the fact that very pronounced location peaks occur at regularly spaced intervals in the scan . The first three peaks correspond to the positions of discharges injected at points c5, c6, and c7 which are at channel positions 76, 89, and 102 respectively . The expected channel positions are 72, 90, and 111 which represents errors in these locations of 4, 1, and 9 channels , (a maximum error of 6.3 metres). The results of the scans of discharges injected at the remaining positions are not so favourable , as the scan in figure 4.5.2.2 shows

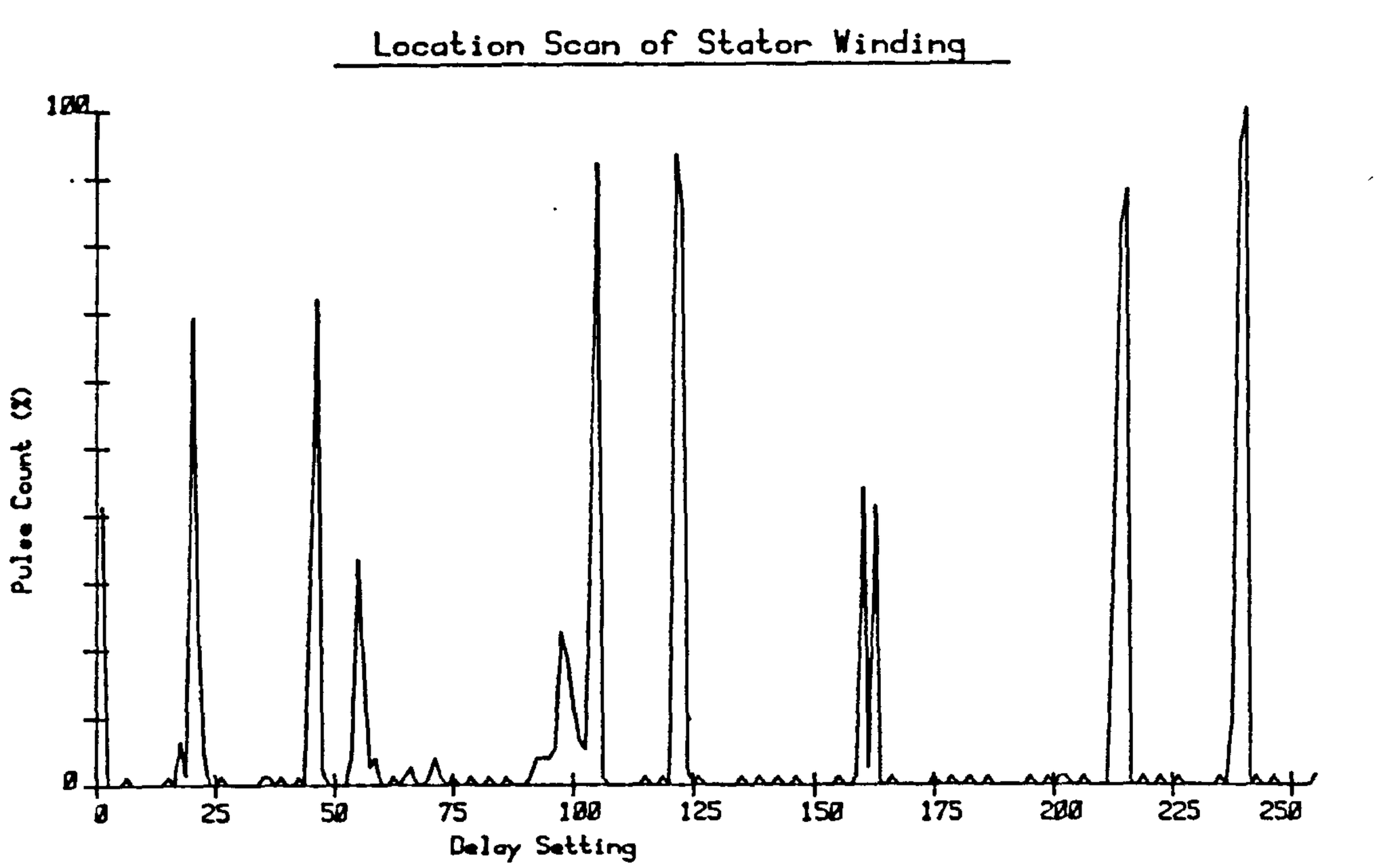

Figure 4.5.1.3 - Scan of Winding with Two High Voltage Sources Connected to Winding Centre

a cumulative pulse count at channel 132 for discharge sources at these positions . The reason for this is not clear , however , since the pulse counts occur at the same channel positions for each source it is assumed that interference pulses have affected the relays which control the programmable delay line or the coincidence detector circuit , both of which operates from a relatively low voltage power supply of 5 volts .

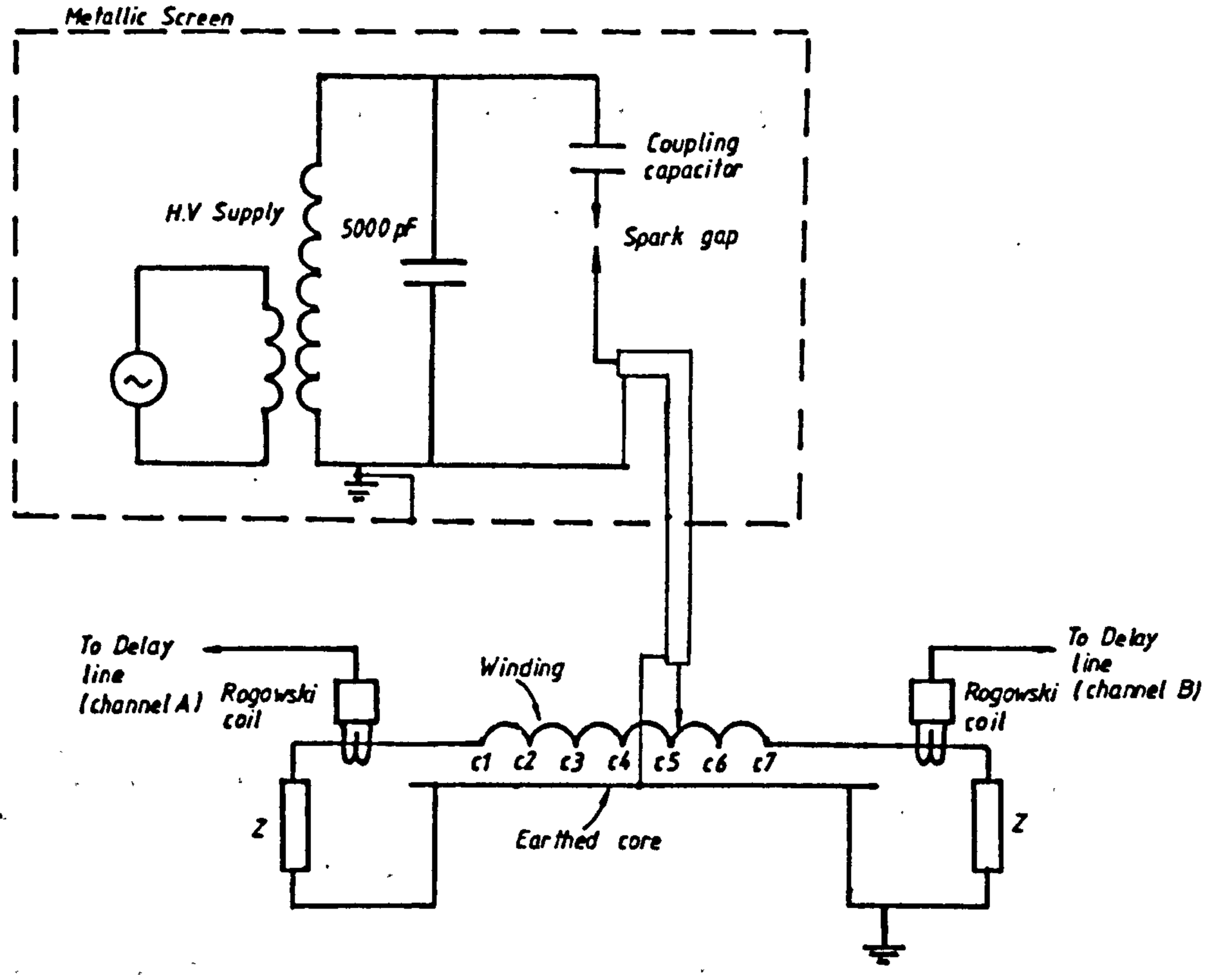

Figure 4.5.2.1 - Test Circuit with High Voltage Discharge Source Screened

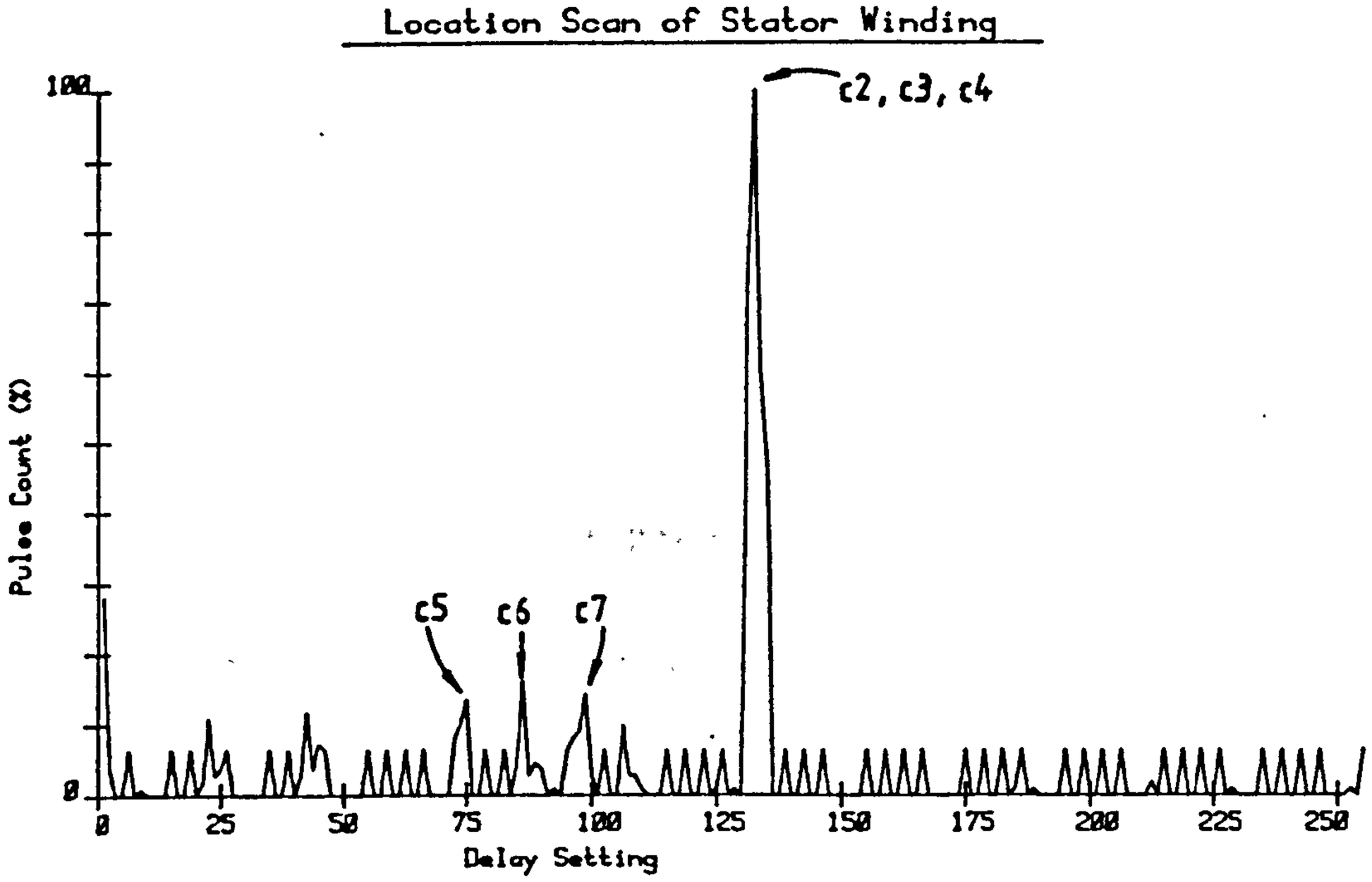

Figure 4.5.2.2 – Composite Scan of Winding with Discharge Source at each Winding Connection

CHAPTER FIVE

THEORETICAL MODEL OF A STATOR WINDING WITH ENDWINDING COUPLING

5.1 Review of Previous Investigations.

All previous investigations have been concerned with the study of the surge voltage distribution (especially interturn voltage distribution), within the line end coils of stator windings . Surges originate from switching operations and lightning strokes, and in general have rise times as low as 100 nsec followed by a long tail which lasts tens of microseconds. Although these surges are slower rising and longer duration waveforms than most partial discharge pulses, their behaviour in windings are similar . Therefore models developed to describe their transmission within machine windings may be used to demonstrate the propagation of discharge pulses in the same winding structures .

Until very recently, the stator winding has been treated either as a simple transmission line or as a ladder network of lumped parameter sections, each section representing a single coil or coil turn. Earliest investigations were directed to a more fundamental study of the behaviour of surges in coils and windings which was more akin to transformer windings. Analyses developed were extended, with certain additional assumptions and modifications to motor coils and windings.

The concepts of travelling waves in coils and windings was first applied by R. Rudenberg [95] . A distributed parameter model , (figure 5.1.1) , was based on single layer coil which incorporated mutual inductance and capacitance between adjacent turns. The following partial differential equations were derived for voltage and current in the coil.

$$-\frac{\partial i}{\partial x} = p.\frac{\partial e}{\partial t} - k.w.\frac{\partial e}{\partial t \partial x} \qquad .....(5.1)$$

$$-\frac{\partial e}{\partial x} = l.\frac{\partial i}{\partial t}$$

where p - slot capacitance per unit length

k - interturn capacitance per unit length

w - length of winding element or turn

l - self inductance per unit length

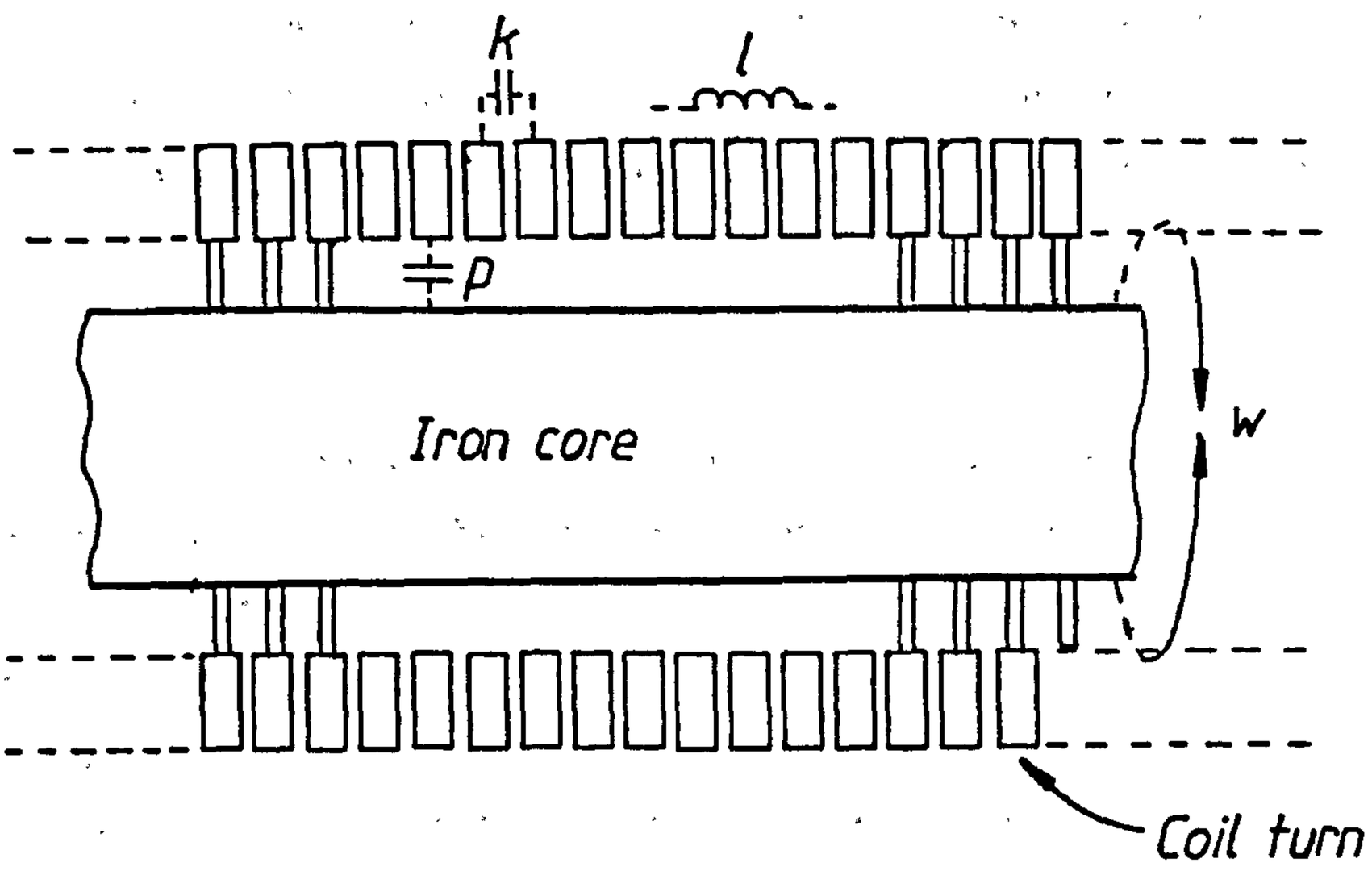

Figure 5.1.1 - Rudenberg's Distributed Parameter Model

The solution to these equations was given by a set of travelling waves which oscillate in time with frequency, ω , and propagate along the conductor with a velocity, v, given by :

$$v = \left[\frac{1}{p.l} - \frac{k.w^2.\omega^2}{p}\right]^{1/2} \qquad .....(5.2)$$

This is true for sinusoidal waves below a critical frequency , ω_c, given by,

$$\omega_c = \frac{1}{w\sqrt{k.l}} \qquad .....(5.3)$$

In the 'sub-critical' frequency range the coil behaves like a lossless transmission line . However, at 'super-critical' frequencies , the voltage to current ratio becomes imaginary and the coil acts as a capacitance network. In this frequency range no travelling waves penetrate the coil but, rather results in an exponential attenuation of the voltage from the terminal to the coil interior.

In the analysis of machine windings Rudenberg [82] , treated each coil as an elemental section of the transmission line representing the winding ,(see figure 5.1.2) . This approach is questionable since machine coils are distributed around a cylindrical iron core whilst the analysis is founded upon closely spaced concentric coils/turns like those in a transformer. In addition validity of the analysis is doubtful with regard to machine windings since the assumption is made in deriving the model that the equations " are valid to a good degree of approximation if the number of turns, or layers, or coils is relatively large " [95] . It is thought that there are an insufficient number of coils in a phase winding for this to be true . There is also no provision for the endwinding coupling that exists between adjacent coils in a winding . The analysis is however , useful in giving the general behaviour of low frequency waves within machine windings .

A comprehensive analysis of single turn coils was undertaken by Robinson , [96] , in which the basic section of the network representing a winding was a single coil, (figure 5.1.3). Each coil section comprised a capacitance to ground C_1 , a mutual capacitance C_f between adjacent coils in the same slot, a capacitance C_2 to the coil

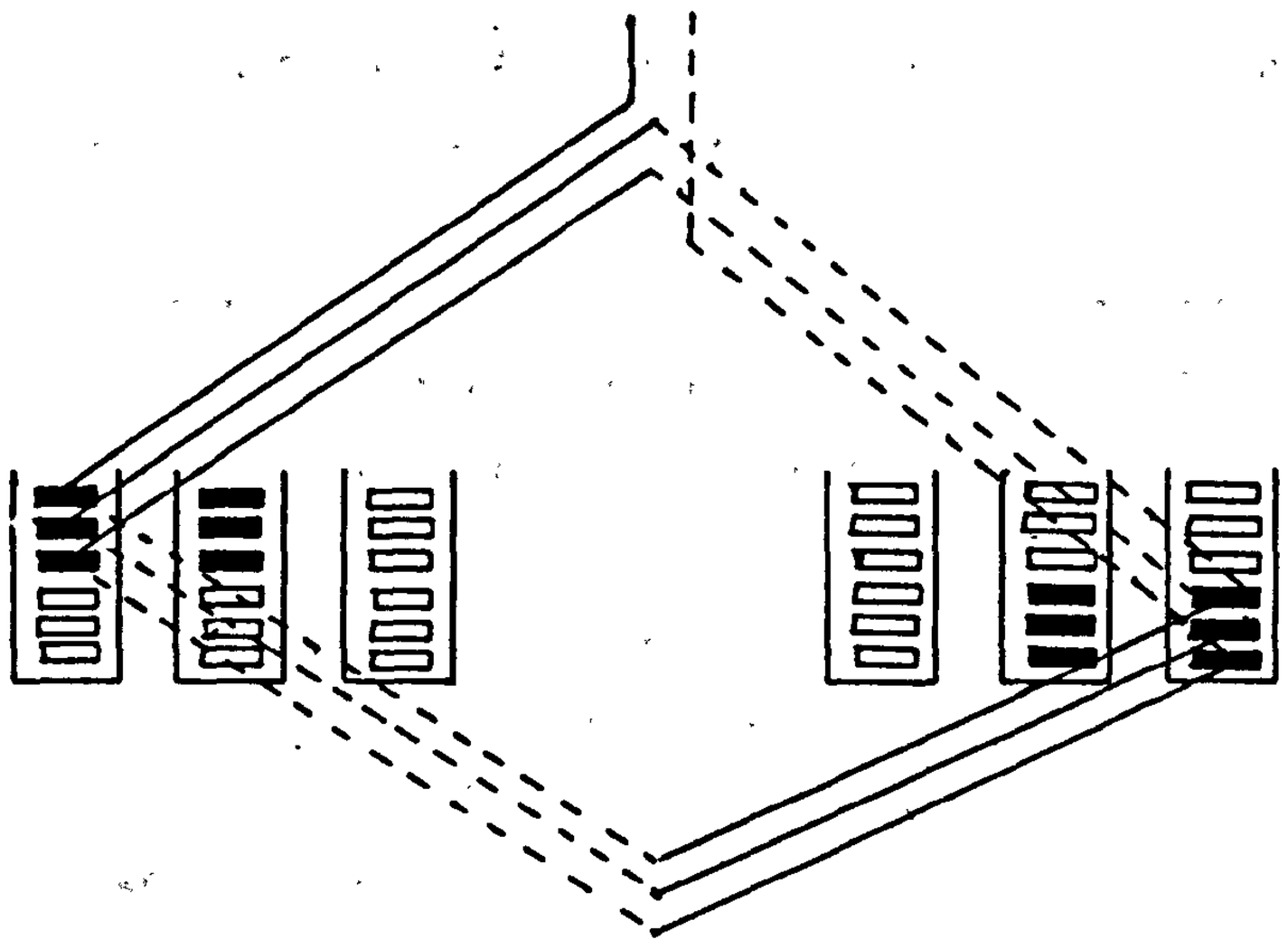

Figure 5.1.2 - Rudenberg's Machine Winding Model

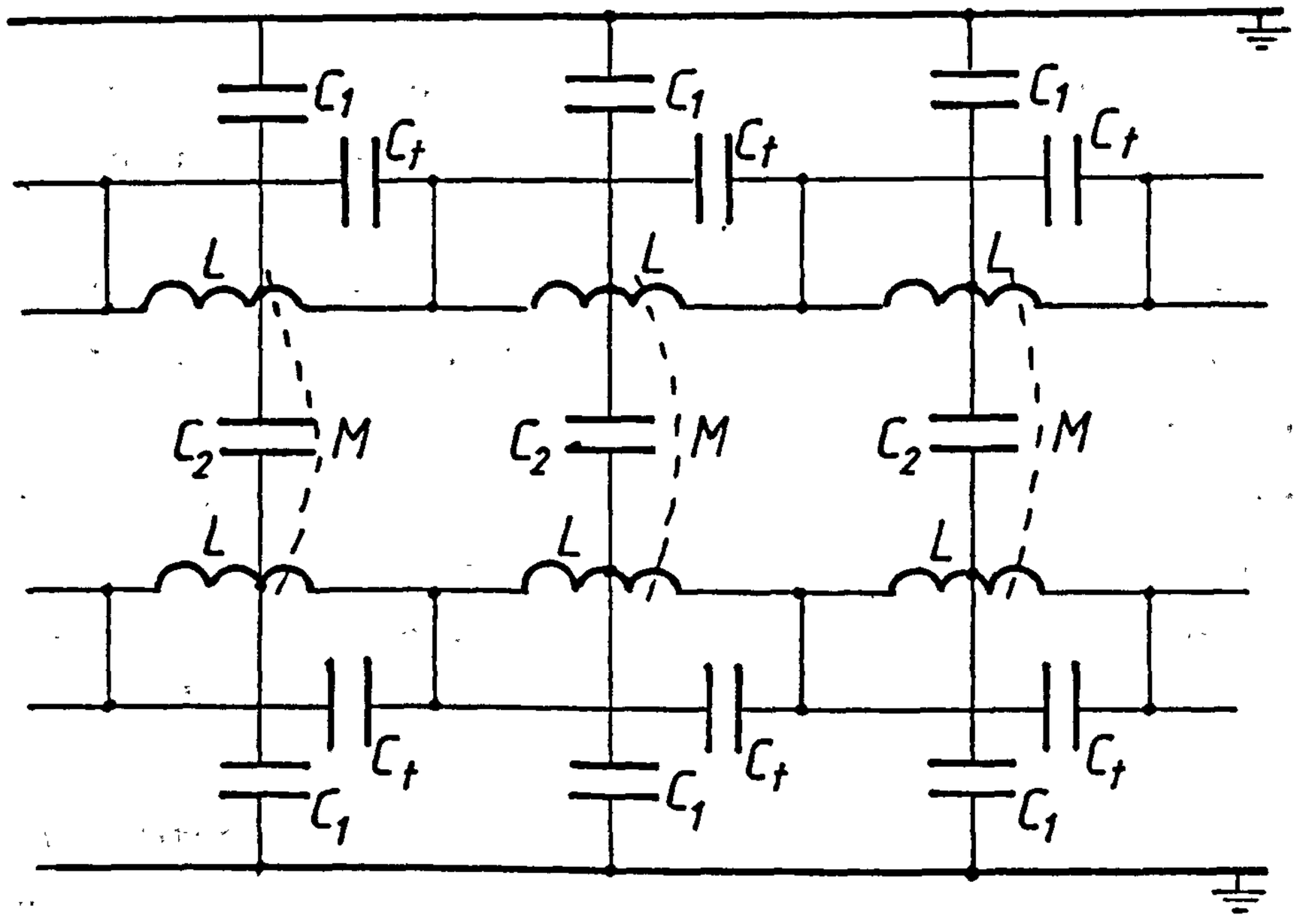

Figure 5.1.3 - Robinson's Machine Winding Model

in the adjacent slot (through the endwindings), a self inductance L and a mutual inductance M between coils in the same slot. Partial differential equations were derived in a similar fashion to Rudenberg. The velocity of propagation of travelling sinusoidal waves was determined and a critical frequency defined.

Whilst it is useful for turbo-generator windings, the major draw back with this analysis is that it cannot be extended to model multi-turn coils which are found in large induction motors .

Lewis [97] , developed a ladder network of lumped parameter sections to represent a machine winding, (figure 5.1.4). The section comprised a self inductance L , the slot capacitance to ground C_g, and mutual capacitance C_s, between adjacent coils. Equations were solved using transformation methods and solutions were expressed in either an ensemble of sinusoidal, standing or travelling waves. Results similar to the previous studies were obtained in which the velocity of propagation was defined along with a critical frequency. Unfortunately, propagation within individual coils was not taken into account in the treatment .

Even if this analysis was extended to model a single coil using a turn as a section of the network no provision is made to include mutual inductive coupling between sections, hence coils and turns. This makes the analysis unsuitable for the present purpose.

A much simpler ladder network was adopted by Meyer [98] , in which a coil formed the lumped parameter T - section , (figure 5.1.5) , in an artificial transmission line. Only the slot capacitance to earth and coil self inductance was considered, all other mutual field couplings being assumed to have negligible effect on surge propagation. The same general results were derived in which a cut off frequency and velocity of propagation were derived.

A comprehensive experimental investigation into surge distribution within the line end coils of two motors was carried out by Parrot [22] . In this study, a comparison was also made of previous theoretical analyses [95,96,97,98] . This led to the conclusion that the results from these methods "differ considerably from measurements".

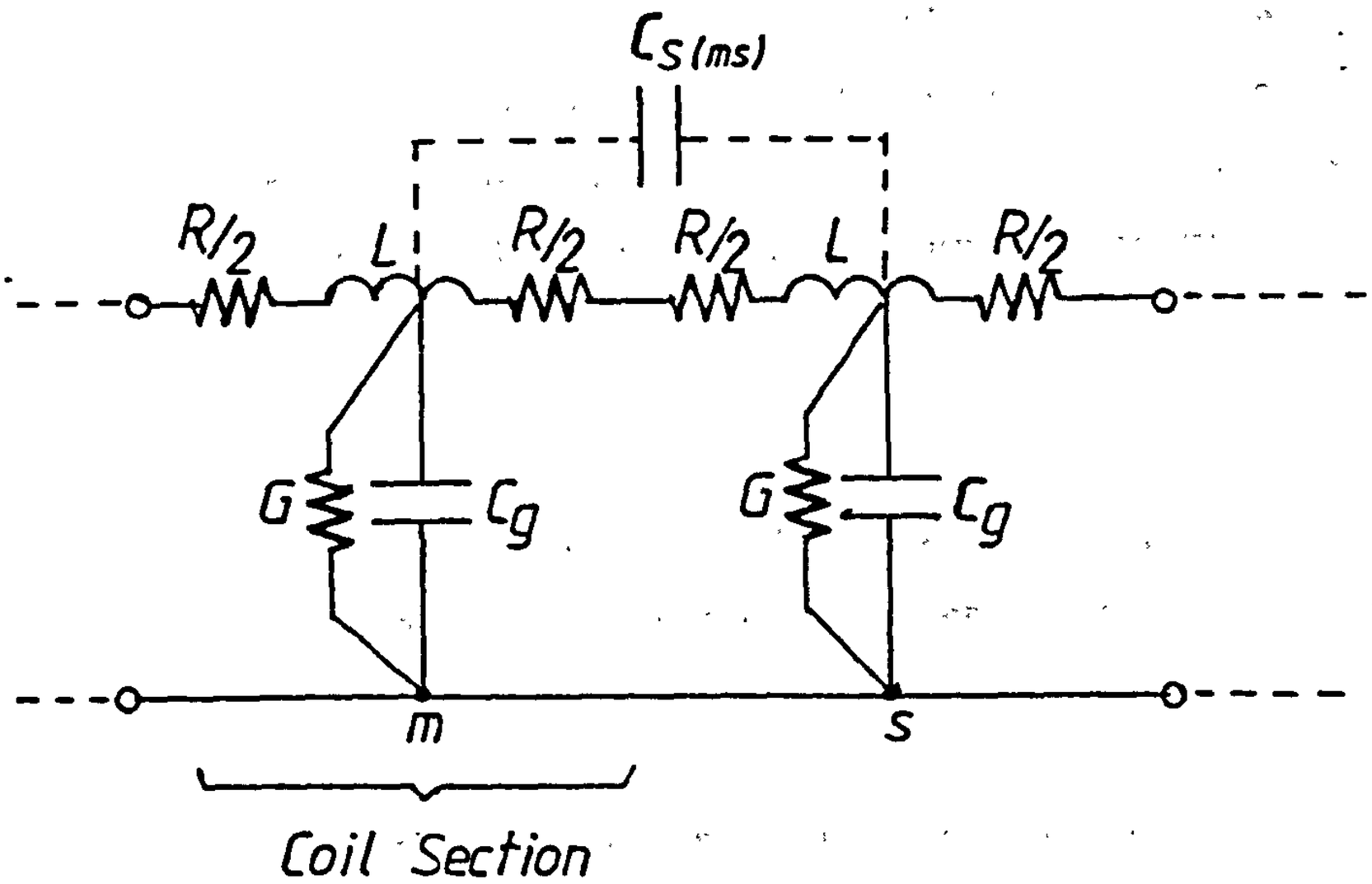

Figure 5.1.4 - Ladder Network of Machine Winding
by Lewis

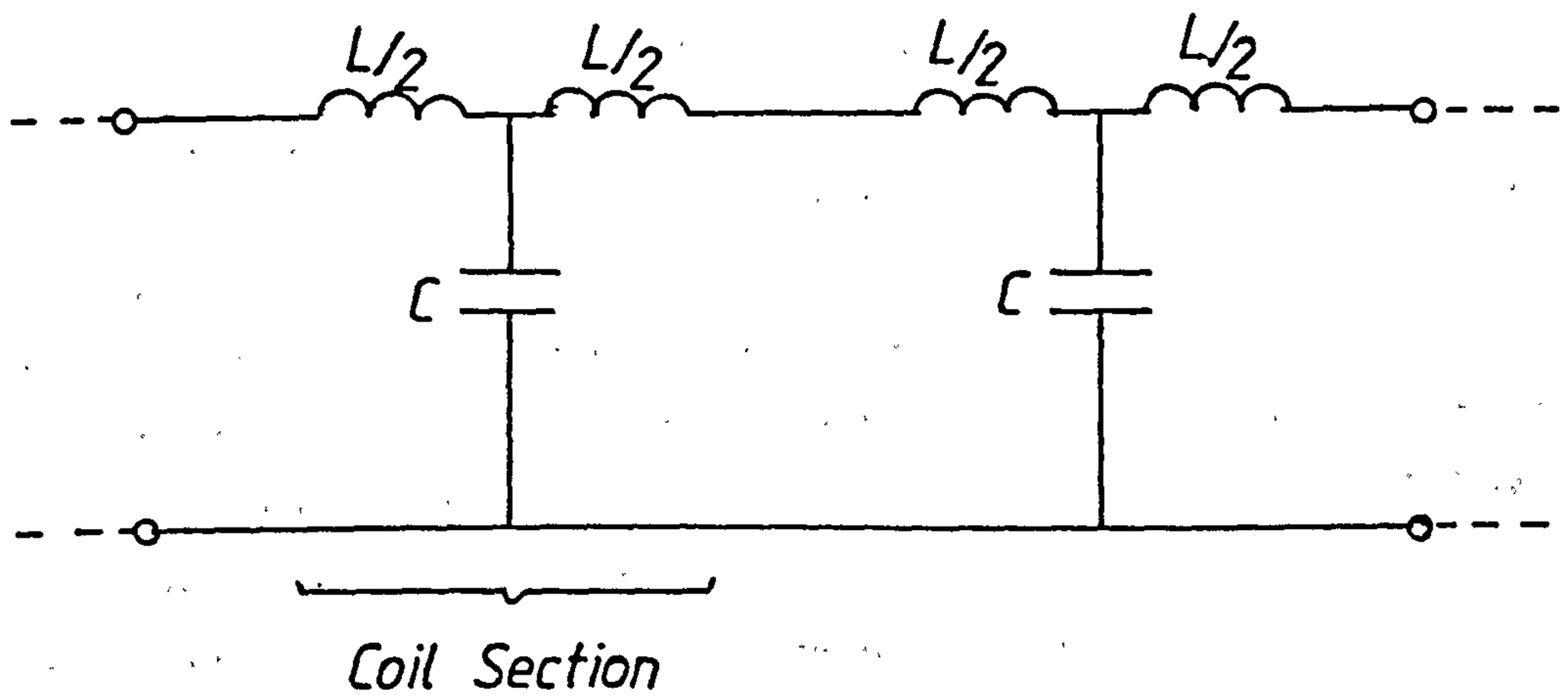

Figure 5.1.5 - Lumped Parameter Winding Model
by Meyer

A comprehensive study was carried out by Adjaye and Cornick [99] in which two-port networks were used to represent a complete system of source , supply switchgear , connecting cables and the motor winding . In addition the frequency dependence of inductances and the effects of dielectric losses were included in the analysis. Again however the basic unit modelled was a coil and no provision for mutual inductance and capacitance between coils and turns was made , (figure 5.1.6).

A very similar investigation was done by V.Chura, [100], in which procedures for determining the frequency dependence of circuit parameters were established.

In all of the forementioned treatments the influence of mutual inductance linking turns and adjacent coils on surge propagation has been neglected. In addition , no distinction has been made between the slot region where conductors are embedded in a highly permeable iron core and the endwinding region where conductors are situated in an air dielectric. The first investigation to incorporate these features into a mathematical model was done by Wright et al., [23] . An entirely new approach was made to the representation of a coil through the application of multi-conductor transmission line theory with junction scattering matrices.

The coil was considered to comprise five distinct sections of lossless multi-conductor transmission line corresponding to the different physical regions; the endwinding, the slot, and the coil terminals, (figure 5.1.7). A Scatter matrix was developed to characterise each of the five junctions in order to determine the magnitude and polarity of reflected and refracted impulses impinging on a junction. The response of the coil model to a single idealised impulse was found. This was then convolved numerically with an impulse input function to obtain the overall response of the coil. In this way the behaviour of a coil to a surge of any general shape was achieved. Analysis was performed entirely in the time domain. The treatment could be extended to model a whole machine winding by connecting a chain of multi-conductor coil sections. Accuracy was also improved by including resistive and dielectric losses as lumped parameters at the junctions of the lossless lines such that predicted and computed waveforms differed by a few percent.

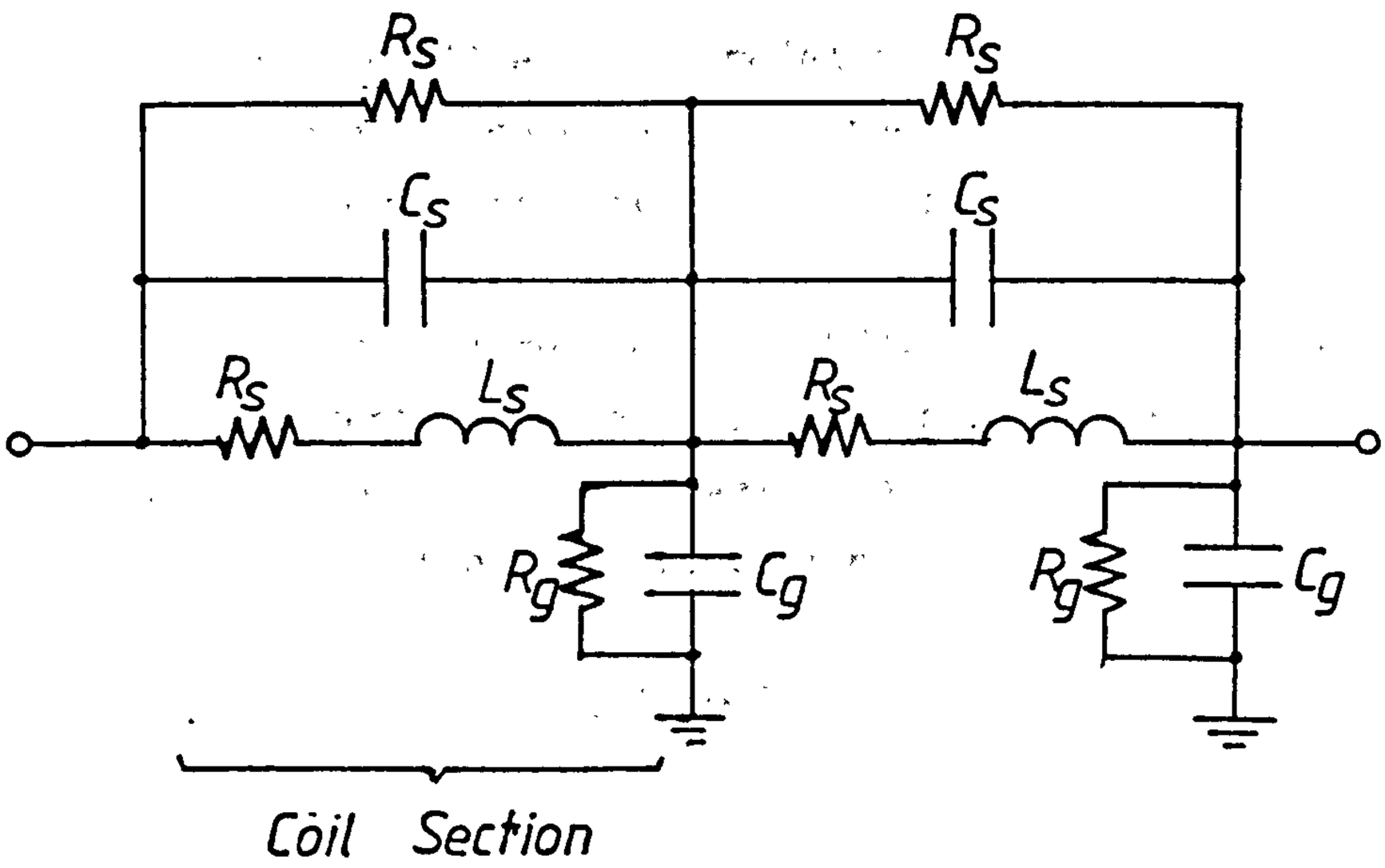

Figure 5.1.6 - Two-Port Network Model of Winding
by Adjaye and Cornick

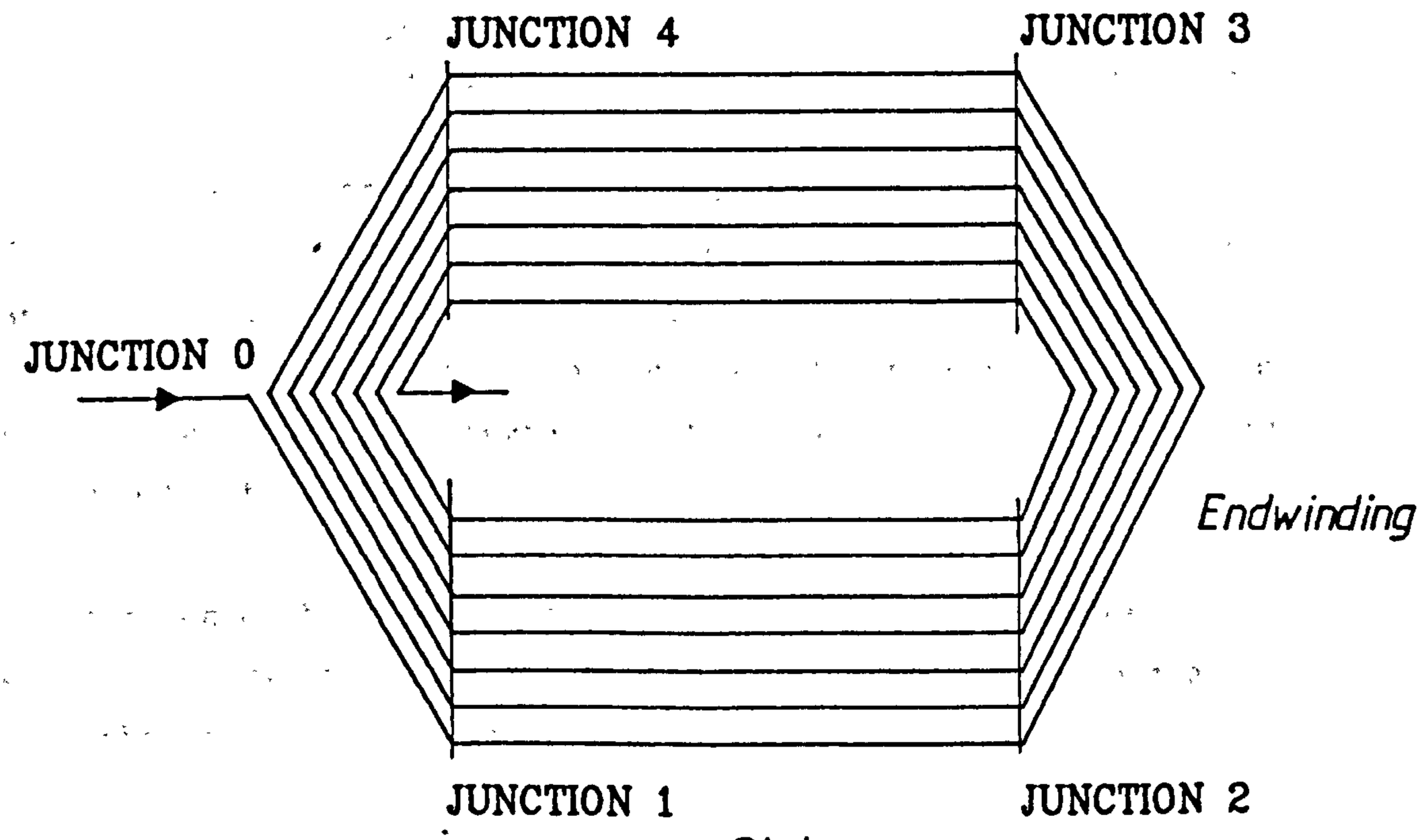

Figure 5.1.7 - Multi-conductor Model of Coil

Oraee & McLaren [101] followed the work by Wright et al with a multi-conductor transmission line coil model similar to the previous with the exception of an extra section due to the transposition of the conductors in the coil endwinding region, (figure 5.1.8) . The mathematical analysis however was entirely different. Modern multi-conductor transmission line theory, [102], was applied to solve the voltage and current at any point in the coil. Each multi-conductor section of the coil was considered as a two port network described by the partial differential equations;

$$\frac{\partial^2 v}{\partial x^2} = [Z].[Y].v = [R+j\omega L].[G+j\omega C].v \qquad \ldots\ldots (5.4)$$

$$\frac{\partial^2 i}{\partial x^2} = [Y].[Z].i = [G+j\omega C].[R+j\omega L].i \qquad \ldots\ldots (5.5)$$

[Z] and [Y] are the complex impedance and admittance matrices which characterise the lines at a particular frequency . A mathematical transformation on equations 5.4 and 5.5 results in a set of independent differential equations. Solution of these equations yield the expressions for voltage in each section ;

$$V = [S].\exp(-[\gamma]x)[S]^{-1}.[V_s] + [S].\exp([\gamma]x)[S]^{-1}.[V_r] \qquad \ldots\ldots (5.6)$$

V_s and V_r are the sending and receiving end voltages respectively, and $[\gamma]$ and [S] are the eigenvalue and eigenvector matrices of [Z] and [Y]. Analysis requires the determination of the network voltages at each particular frequency, in a Fourier series representing the input waveform. The Fourier integral is then used to transform the solution into the time domain.

From a comparison of both multi-conductor models of a stator coil , the one developed by Wright et al. is the simplest to apply to a given system for the following reasons .

i. Formulation of the model is considerably simpler since only the capacitance parameters describing the coil are required. Inductance values have to be determined at a number of frequencies in McLarens model . This necessitates the calculation of the magnetic field distribution at different frequencies with

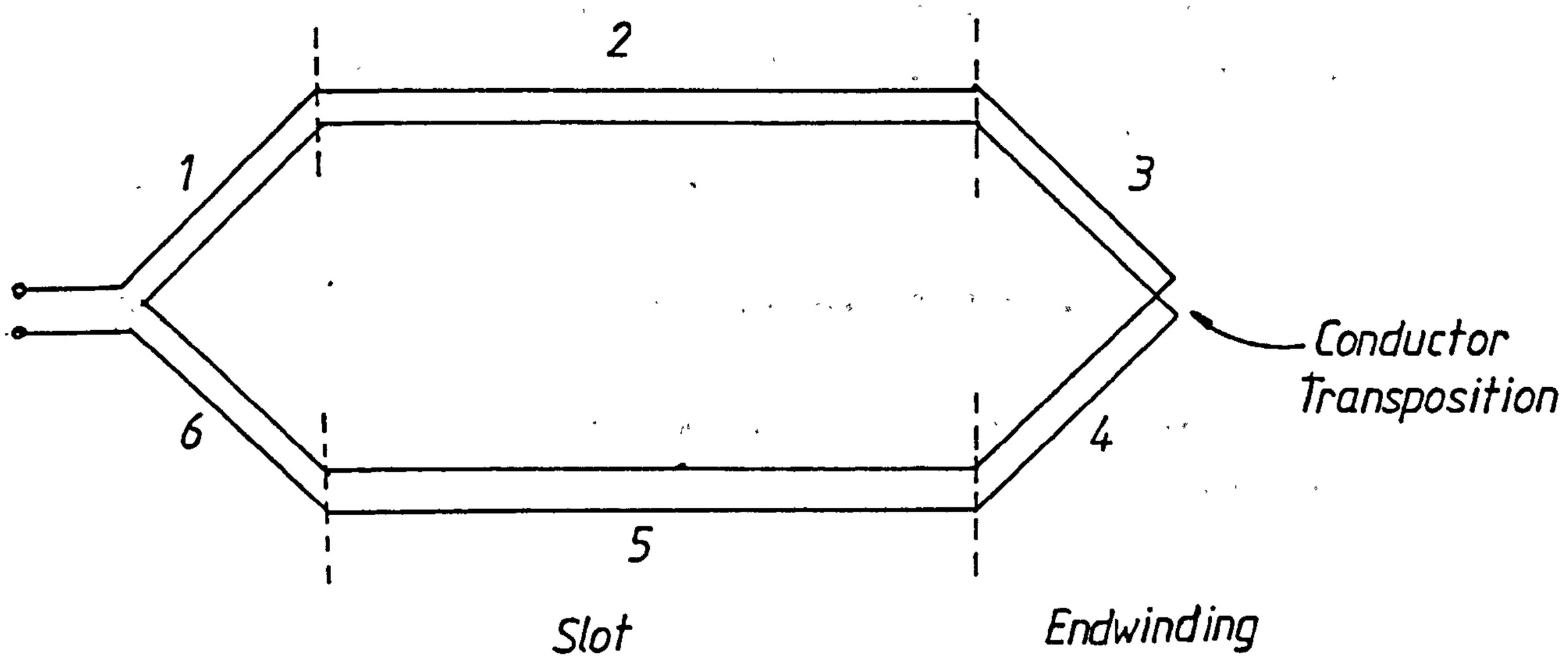

Figure 5.1.8 - Multi-conductor Model of Coil with Endwinding Transposed

a complex , electromagnetic , finite-element computer program.

ii. Solution is considerably easier in the time domain than in the frequency domain , [103], for comparable study times. There is no need, with the time domain approach , to evaluate eigenvalue and eigenvector matrices for each frequency of interest, for each section of transmission line.

iii. A better understanding of pulse propagation in coils is obtainable , since analysis is entirely in the time domain.

iv. Storage requirements on computer is considerably less .

The model developed by Wright et al. is selected as the basis for the development of a model for a complete phase winding since interturn coupling is incorporated in the analysis , and the model can be extended to include the effects of inter-coil coupling in the endwinding region .

5.2 Development of Lossless Multi-conductor Coil Model

Certain assumptions have to be made before development of a mathematical model can take place and these are discussed in the following paragraphs.

5.2.1 Iron Core Flux Barrier

At high frequencies the stator iron core behaves in a completely different manner to that at power frequencies. It becomes effectively a barrier to magnetic flux since eddy currents induced in the slot wall iron , modify the resultant magnetic field ,(skin effect), so that its depth of penetration into the iron is limited .

The skin depth may be calculated at the frequency of interest, f, from the skin effect equation ,

$$d = \frac{1}{\sqrt{(\sigma.\pi.\mu.f)}} \qquad \text{.....(5.7)}$$

σ - conductivity of steel ($\Omega^{-1}m^{-1}$)

μ - permeability (Hm^{-1})

d - depth of penetration (m)

If the conductivity of steel is taken to be 3.6 $\Omega^{-1} m^{-1}$, (resistivity of 270 Ωm), the calculated skin depth is :

53.1	µm	at	100 kHz
16.7	µm	at	1 MHz
5.3	µm	at	10 MHz
1.6	µm	at	100 MHz

Clearly, at a relatively low frequency (100 kHz) there can be very little magnetic field coupling between adjacent slot conductors and so the iron behaves as a impenetrable earth sheath.

Machine stator cores are laminated structures in which each iron lamination is separated from an adjacent lamination by a thin layer of insulation. Some justification is required to explain how a laminated structure supports current flow at right angles to the laminations. At high frequencies under consideration there is close capacitive coupling between iron laminations which provides a low impedance path for axial return currents. In the insulation the current is a displacement current and has equivalent effect to the conduction current in the iron [101].

5.2.2 Rotor Effects

Since at the frequencies of concern the magnetic field does not penetrate iron appreciably , the rotor will have negligible effect on pulse propagation in the winding . This is especially true when magnetic wedges are installed in slots .

5.2.3 Mode of Wave Propagation

The rise time of a partial discharge pulse is unlikely to be less than 1 nsec so that the maximum frequency contained in the pulse is about 1000 MHz . At this frequency, the wavelength of propagation with an epoxy resin / mica dielectric, with a typical relative permittivity of 6.6 , is 0.117 metres . The minimum wavelength in the dielectric region is therefore of the order of a few centimetres , 11.7 cm , whilst the separation between the conductor and the slot is generally only a few millimetres , 2 - 5 mm approximately. Consequently, the principle mode of propagation which needs to be considered is the TEM

mode (transverse electromagnetic mode), as any transverse electric (TE), or transverse magnetic, (TM), modes are not supported [104] .

5.2.4 Multi-conductor Transmission line theory

Any lossless transmission line formed by N conductors and a reference earth conductor can be represented mathematically by the "generalised telegraphers " equations [105] :

$$\frac{\partial [V_n(x,t)]}{\partial x} = - [L_{nm}] \frac{\partial [I_m(x,t)]}{\partial t} \quad \text{.....(5.8)}$$

$$\frac{\partial [I_n(x,t)]}{\partial x} = - [C_{nm}] \frac{\partial [V_m(x,t)]}{\partial t} \quad \text{.....(5.9)}$$

where $n = 1,2,...,N$ and $m = 1,2,...,N$.

$[L_{nm}]$ and $[C_{nm}]$ are the per unit length inductance and capacitance matrices, respectively. D'Alembert's solution to these equations takes the form of a set of forward and backward travelling waves expressed as :-

$$[v_n(x,t)] = [F_1\delta(x-v_m t)] + [F_2\delta(x+v_m t)] \quad \text{....(5.10)}$$

$$[i_n(x,t)] = [F_1\delta(x-v_m t)]/Z_{nm} + [F_2\delta(x+v_m t)]/Z_{nm} \quad \text{....(5.11)}$$

δ is the delta impulse function and F_1 and F_2 are arbitrary functions.

In general, for a uniform multi-conductor transmission line with, insulated conductors having different dielectric materials and geometries , N conductors and a ground , there are N modes of wave propagation, each having a unique propagation velocity, v_m . These modes are separated in time as they travel in the transmission line conductors .

In a system with a single dielectric , propagation modes degenerate to a single mode with a single velocity of propagation :

$$v = \frac{c}{\sqrt{\epsilon_r}} \qquad \text{.....(5.12)}$$

5.2.5 Multi-conductor Coil Sections

A stator coil occupies two distinct regions: the endwinding and the slot region, where the coil is situated in air and iron respectively. This forms four sections of a multiconductor line . However, one of the endwinding sections is interrupted by the coil terminals at or close to the coil evolute . The coil can therefore be subdivided into a series of five multi-conductor transmission line sections as shown in the diagram of figure 5.2.5.1 .

5.2.6 Multi-conductor Junction in a Stator Coil

A junction is formed at the interconnection of two multi-conductor line sections and there are five of these junctions in a lossless coil model. There are two forms of junction in a stator coil : the slot/endwinding region junction and the terminal junction. The slot/endwinding junction is a junction of two dissimilar N conductor lines of which there are four in a single coil. This is shown for a 7 turn coil in figure 5.2.6.2 . The terminal junction comprises the junction of two similar N conductor lines and two single conductor lines and is shown for a 7 turn stator coil in figure 5.2.6.1 .

5.3 Scatter Matrix Analysis of a Lossless Coil

The behaviour of a stator coil to a fast risetime pulse, is determined by the reflections and refractions of the pulse wave at the transmission line junctions and by interturn coupling . A scatter matrix, for a junction, embodies the relationships between the incident and reflected voltages , (and currents), and from it, the magnitudes and polarities of reflected and transmitted waves are obtained .

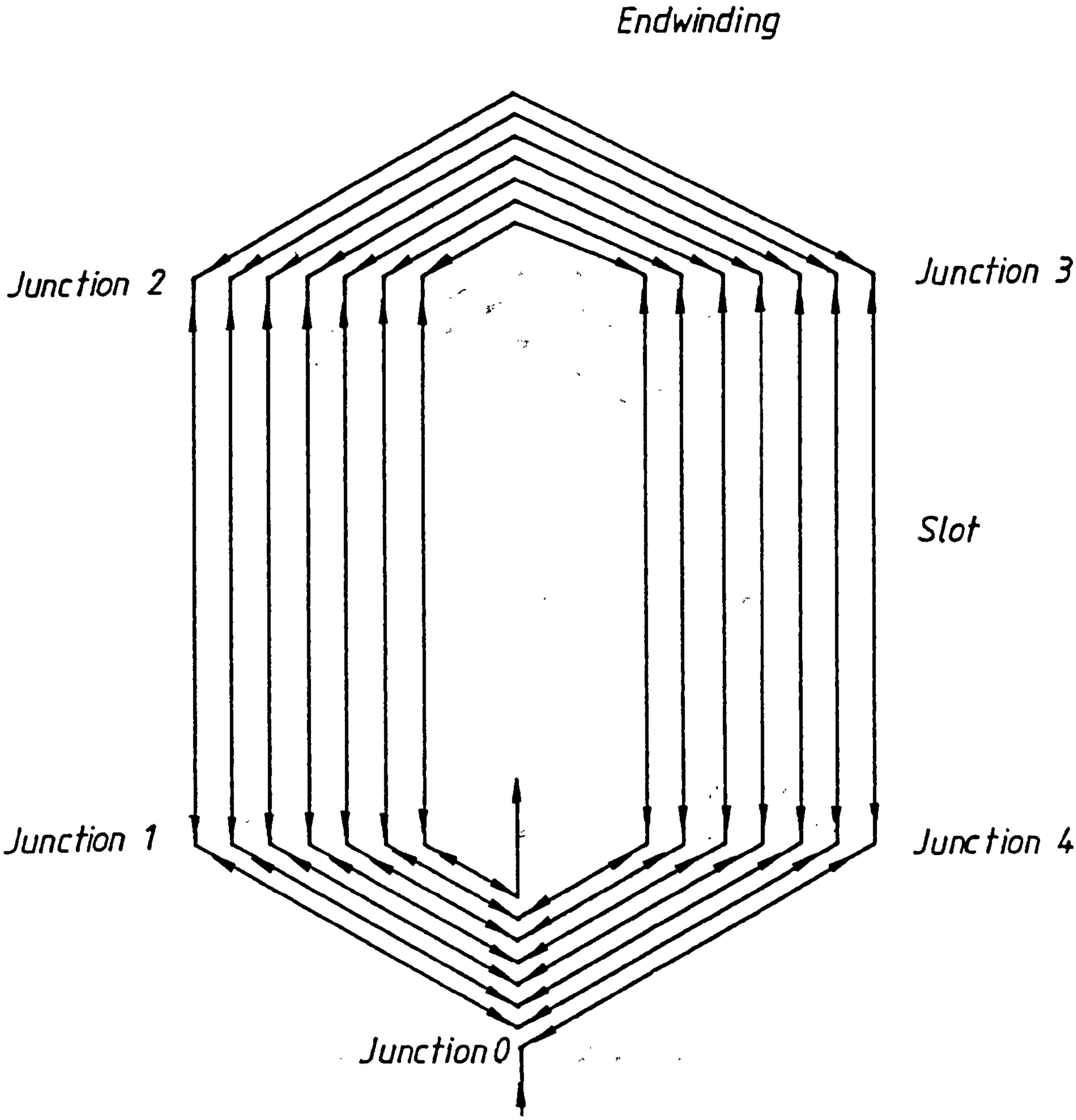

Figure 5.2.5.1 - Multi-conductor Model of
7-turn Coil

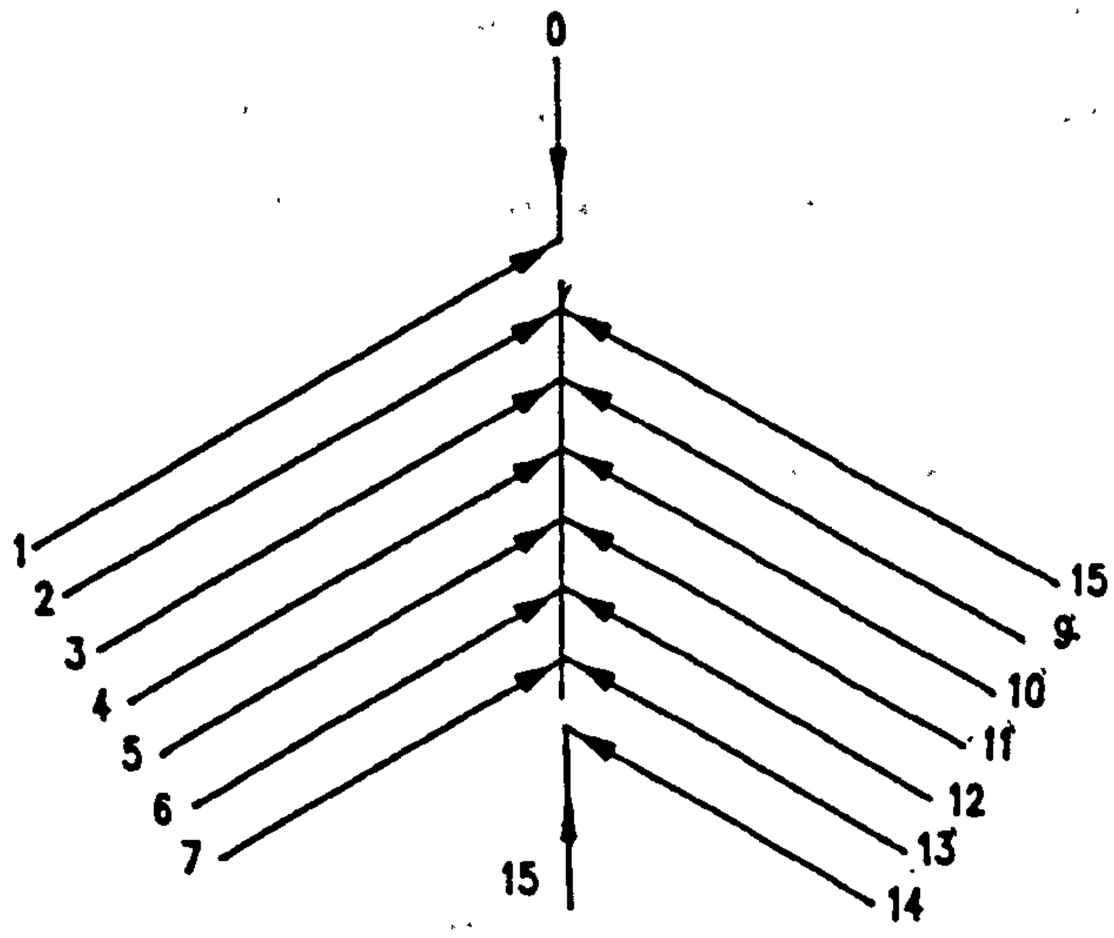

Figure 5.2.6.1 - Coil Terminal Junction

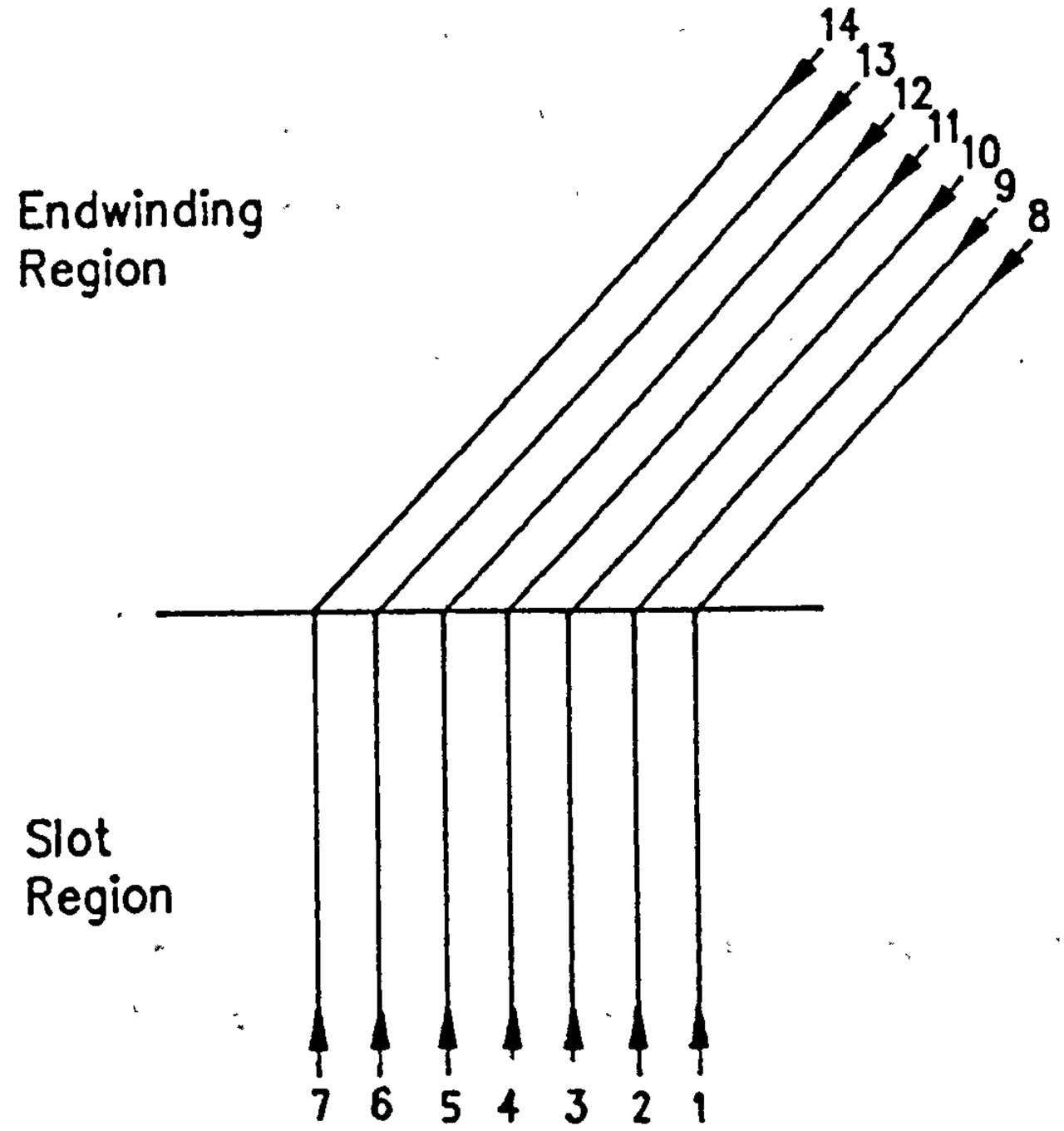

Figure 5.2.6.2 - Slot/Endwinding Junction

5.3.1. Derivation of Scatter Matrix

Scatter matrices derived in this section, define the relationship between incident and reflected voltages. The same procedure applies to the definition of scatter matrices relating conductor currents.

Consider first, the terminal junction of a 7 turn stator coil as in figure 5.2.6.1 . Using Kirchoffs law, the relationships for voltages at the junction are given by:

$$v_0 - v_1 = 0 \quad ; \quad v_2 - v_3 = 0 \quad ; \quad v_4 - v_5 = 0 \qquad \text{and so on.}$$

Expressed in matrix form this becomes :

$$[V] = \begin{bmatrix} v_0 \\ v_1 \\ v_2 \\ v_3 \\ v_4 \\ v_5 \\ v_6 \\ v_7 \\ v_8 \\ v_9 \\ v_{10} \\ v_{11} \\ v_{12} \\ v_{13} \\ v_{14} \\ v_{15} \end{bmatrix} \quad \text{and} \quad [C_v] = \begin{bmatrix} 1 & -1 & 0 & 0 & . & . & & & & & & & & & & \\ . & 0 & 1 & 0 & 0 & 0 & 0 & 0 & -1 & 0 & . & . & & & & \\ . & . & 0 & 1 & 0 & 0 & 0 & 0 & 0 & -1 & 0 & . & . & & & \\ & . & . & 0 & 1 & 0 & 0 & 0 & 0 & 0 & -1 & 0 & . & . & & \\ & & . & . & 0 & 1 & 0 & 0 & 0 & 0 & 0 & -1 & 0 & . & . & \\ & & & . & . & 0 & 1 & 0 & 0 & 0 & 0 & 0 & -1 & 0 & . & \\ & & & & & & & & & & & . & . & 0 & 1 & -1 \end{bmatrix}$$

$[C_v]$ is the voltage connection matrix for the junction, and is related to the voltage matrix [V] by the expression :

$$[C_v].[V] = 0 \qquad \ldots\ldots(5.13)$$

Similarly, for the junction currents, taking positive current flow as towards the junction and applying Kirchoffs current law we can say,

$$i_0 + i_1 = 0 \quad ; \quad i_2 + i_3 = 0 \quad ; \quad i_4 + i_5 = 0 \; ; \; \ldots\ldots \qquad \text{and so on.}$$

Again expressing in matrix form we have :

$$[I] = \begin{bmatrix} i_0 \\ i_1 \\ i_2 \\ i_3 \\ i_4 \\ i_5 \\ i_6 \\ i_7 \\ i_8 \\ i_9 \\ i_{10} \\ i_{11} \\ i_{12} \\ i_{13} \\ i_{14} \\ i_{15} \end{bmatrix} \quad \text{and} \quad [C_i] = \begin{bmatrix} 1\ 1\ 0\ 0\ .\ .\ . & & & & & & & & & & & & & & & \\ 0\ 0\ 1\ 0\ 0\ 0\ 0\ 1\ 0\ .\ . & & & & & & & & & & & & & & & \\ .\ 0\ 1\ 0\ 0\ 0\ 0\ 1\ 0\ .\ . & & & & & & & & & & & & & & & \\ .\ .\ 0\ 1\ 0\ 0\ 0\ 0\ 1\ 0\ .\ . & & & & & & & & & & & & & & & \\ .\ .\ 0\ 1\ 0\ 0\ 0\ 0\ 1\ 0\ .\ . & & & & & & & & & & & & & & & \\ .\ .\ 0\ 1\ 0\ 0\ 0\ 0\ 1\ 0\ . & & & & & & & & & & & & & & & \\ .\ .\ .\ 0\ 0\ 1\ 1 & & & & & & & & & & & & & & & \end{bmatrix}$$

$[C_i]$ is the current connection matrix and is related to the junction currents in the expression,

$$[C_i].[I] = 0 \qquad \ldots.(5.14)$$

Voltage and current vectors at the junction can then be decomposed into their incident and reflected components :

$$[V] = [V]^{in} + [V]^{re} \qquad \ldots.(5.15)$$

$$[I] = [I]^{in} + [I]^{re} \qquad \ldots.(5.16)$$

The relationship between [V] and [I] is embodied in the characteristic admittances , (similarly the impedances) , of the multiconductor transmission lines at the junction. Considering the diagram for the terminal junction in figure 5.2.6.1 this relationship for the incident voltages is expressed as follows :

$$
\begin{bmatrix} v_0 \\ v_1 \\ v_2 \\ v_3 \\ v_4 \\ v_5 \\ v_6 \\ v_7 \\ v_8 \\ v_9 \\ v_{10} \\ v_{11} \\ v_{12} \\ v_{13} \\ v_{14} \\ v_{15} \end{bmatrix}^{in} = \begin{bmatrix} y_0 & 0 & & & & & & & & & & & & & & \\ 0 & y_1 & y_{12} & & & & & & & & & & & & & \\ & y_{12} & y_2 & y_{23} & & & & & & & & & & & & \\ & & y_{23} & y_3 & y_{34} & & & & & & & & & & & \\ & & & y_{34} & y_4 & y_{45} & & & & & & & & & & \\ & & & & y_{45} & y_5 & y_{56} & & & & & & & & & \\ & & & & & y_{56} & y_6 & y_{67} & & & & & & & & \\ & & & & & & y_{67} & y_7 & y_{78} & & & & & & & \\ & & & & & & & y_{78} & y_8 & y_{89} & & & & & & \\ & & & & & & & & y_{89} & y_9 & y_{910} & & & & & \\ & & & & & & & & & y_{910} & y_{10} & y_{1011} & & & & \\ & & & & & & & & & & y_{1011} & y_{11} & y_{1112} & & & \\ & & & & & & & & & & & y_{1112} & y_{12} & y_{1213} & & \\ & & & & & & & & & & & & y_{1213} & y_{13} & y_{1314} & \\ & & & & & & & & & & & & & y_{1314} & y_{14} & 0 \\ & & & & & & & & & & & & & & 0 & y_{15} \end{bmatrix} \begin{bmatrix} i_0 \\ i_1 \\ i_2 \\ i_3 \\ i_4 \\ i_5 \\ i_6 \\ i_7 \\ i_8 \\ i_9 \\ i_{10} \\ i_{11} \\ i_{12} \\ i_{13} \\ i_{14} \\ i_{15} \end{bmatrix}^{in}
$$

that is: $[I]^{in} = [Y].[V]^{in}$ .....(5.17)

and, $[I]^{re} = [Y].[V]^{re}$ .....(5.18)

Alternatively , the impedance matrix may be used in which case,

$$[V]^{in} = [Z].[I]^{in}$$

$$[V]^{re} = [Z].[I]^{re}$$

where,

$$[Y] = [Z]^{-1}$$

Once these basic relationships have been defined it only remains to express them in a single expression to describe voltage scattering . Taking equations (5.15) and (5.13) the expression ,

$$[C_v].[V] = [C_v].[V]^{in} + [C_v].[V]^{re} = 0$$

is obtained . From this we have,

$$[C_v].[V]^{in} = - [C_v].[V]^{re} \qquad .....(5.19)$$

Similarly,

$$[C_v].[I]^{in} = -[C_v].[I]^{re} \qquad .....(5.20)$$

Substituting equations (5.17) and (5.18) into equation (5.20), it follows that,

$$[C_i].[Y].[V]^{in} = [C_i].[Y].[V]^{re} \qquad .....(5.21)$$

Thus two expressions relating $[V]^{in}$ and $[V]^{re}$ are derived , (5.19) and (5.21), neither of which allows extraction of $[V]^{re}$ as a function of $[V]^{in}$ since matrices $[C_i]$ and $[C_v]$ are not symmetrical . However, combining these equations we find :

$$\begin{bmatrix} -[C_v] \\ [C_i].[Y] \end{bmatrix} [V]^{re} = \begin{bmatrix} [C_v] \\ [C_i].[Y] \end{bmatrix} [V]^{in}$$

Since these matrices are now square we obtain from rearrangement ,

$$[V]^{re} = \begin{bmatrix} -[C_v] \\ [C_i].[Y] \end{bmatrix} . \begin{bmatrix} [C_v] \\ [C_i].[Y] \end{bmatrix} [V]^{in} \qquad .....(5.22)$$

which is, $[V]^{re} = [S].[V]^{in}$ .....(5.23)

[S] is the voltage scatter matrix for the junction which was developed by A.K. Agrawal et al [105] . In this fashion , the scatter matrix completely describes the voltage reflection and transmission properties of a junction.

By considering the diagram in figure 5.2.6.2, the scatter matrix can be obtained for a slot/endwinding junction . By inspection the current and voltage connection matrices are :

$$[C_i] = \begin{bmatrix} 1 & 0 & 0 & 0 & 0 & 0 & 0 & 1 & & & & & & & & \\ & 1 & 0 & 0 & 0 & 0 & 0 & 0 & 1 & & & & & & & \\ & & 1 & 0 & 0 & 0 & 0 & 0 & 0 & 1 & & & & & & \\ & & & 1 & 0 & 0 & 0 & 0 & 0 & 0 & 1 & & & & & \\ & & & & 1 & 0 & 0 & 0 & 0 & 0 & 0 & 1 & & & & \\ & & & & & 1 & 0 & 0 & 0 & 0 & 0 & 0 & 1 & & & \\ & & & & & & 1 & 0 & 0 & 0 & 0 & 0 & 0 & 1 & & \\ & & & & & & & 1 & 0 & 0 & 0 & 0 & 0 & 0 & 1 & \end{bmatrix}$$

$$[C_v] = \begin{bmatrix} 1 & 0 & 0 & 0 & 0 & 0 & 0 & -1 & & & & & & \\ & 1 & 0 & 0 & 0 & 0 & 0 & 0 & -1 & & & & & \\ & & 1 & 0 & 0 & 0 & 0 & 0 & 0 & -1 & & & & \\ & & & 1 & 0 & 0 & 0 & 0 & 0 & 0 & -1 & & & \\ & & & & 1 & 0 & 0 & 0 & 0 & 0 & 0 & -1 & & \\ & & & & & 1 & 0 & 0 & 0 & 0 & 0 & 0 & -1 & \\ & & & & & & 1 & 0 & 0 & 0 & 0 & 0 & 0 & -1 \end{bmatrix}$$

The admittance matrix is,

$$[Y] = \begin{bmatrix} y_1 & y_{12} & & & & & & & & & & & & \\ y_{12} & y_2 & y_{23} & & & & & & & & & & & \\ & y_{23} & y_3 & y_{34} & & & & & & & & & & \\ & & y_{34} & y_4 & y_{45} & & & & & & & & & \\ & & & y_{45} & y_5 & y_{56} & & & & & & & & \\ & & & & y_{56} & y_6 & y_{67} & & & & & & & \\ & & & & & y_{67} & y_7 & y_{78} & & & & & & \\ & & & & & & y_{78} & y_8 & y_{89} & & & & & \\ & & & & & & & y_{89} & y_9 & y_{910} & & & & \\ & & & & & & & & y_{910} & y_{10} & y_{1011} & & & \\ & & & & & & & & & y_{1011} & y_{11} & y_{1112} & & \\ & & & & & & & & & & y_{1112} & y_{12} & y_{1213} & \\ & & & & & & & & & & & y_{1213} & y_{13} & y_{1314} \\ & & & & & & & & & & & & y_{1314} & y_{14} \end{bmatrix}$$

The same analysis may be performed to derive the scatter matrix for this and the remaining junctions.

In general for a stator coil with N turns, [S] will be a (2N+2)x(2N+2) matrix for the terminal junction , and a (2N) x (2N) order matrix for the slot/endwinding junction .

5.3.2 Computation of Capacitance Matrix.

In order to derive the admittance , (or impedance), matrix for the junction , only the capacitance parameters for the junction need to be determined.

For a lossless multiconductor transmission line it has been shown [104] that,

$$[L].[C] = \frac{1}{v^2}$$

and that $[Z] = v.[L]$,

Hence,

$$[Z] = \frac{1}{v}.[C]^{-1}$$

It follows that the admittance matrix is given by ,

$$[Y] = v.[C] = \frac{c}{\sqrt{\epsilon_r}}.[C] \qquad .....(5.24)$$

The great advantage of this technique over frequency domain analysis is that the inductance parameters need not be evaluated in the formation of the admittance matrix .

The shape of the conductors of high voltage stator coils are sufficiently regular , to permit the conductor stack to be represented by an arrangement of parallel plate capacitors, (see figure 5.3.2.1) . The equivalent circuit of figure 5.3.2.1 can be further reduced to that shown in figure 5.3.2.2 to simplify the analysis .

Derivation of the capacitance matrix is performed from the equivalent circuit and using the simple relationship :

$$q = CV$$

Consider the charge , q_1 , on the first conductor . It can be defined by the expression,

$$q_1 = C_{s1} V_1 + C_i.(V_1 - V_2)$$

$$= (C_{s1} + C_i).V_1 - C_i V_2$$

similarly the charge , q_2 , on the adjacent conductor is given by,

$$q_2 = (C_{s2} + C_i).V_2 - C_i V_3 - C_i V_1$$

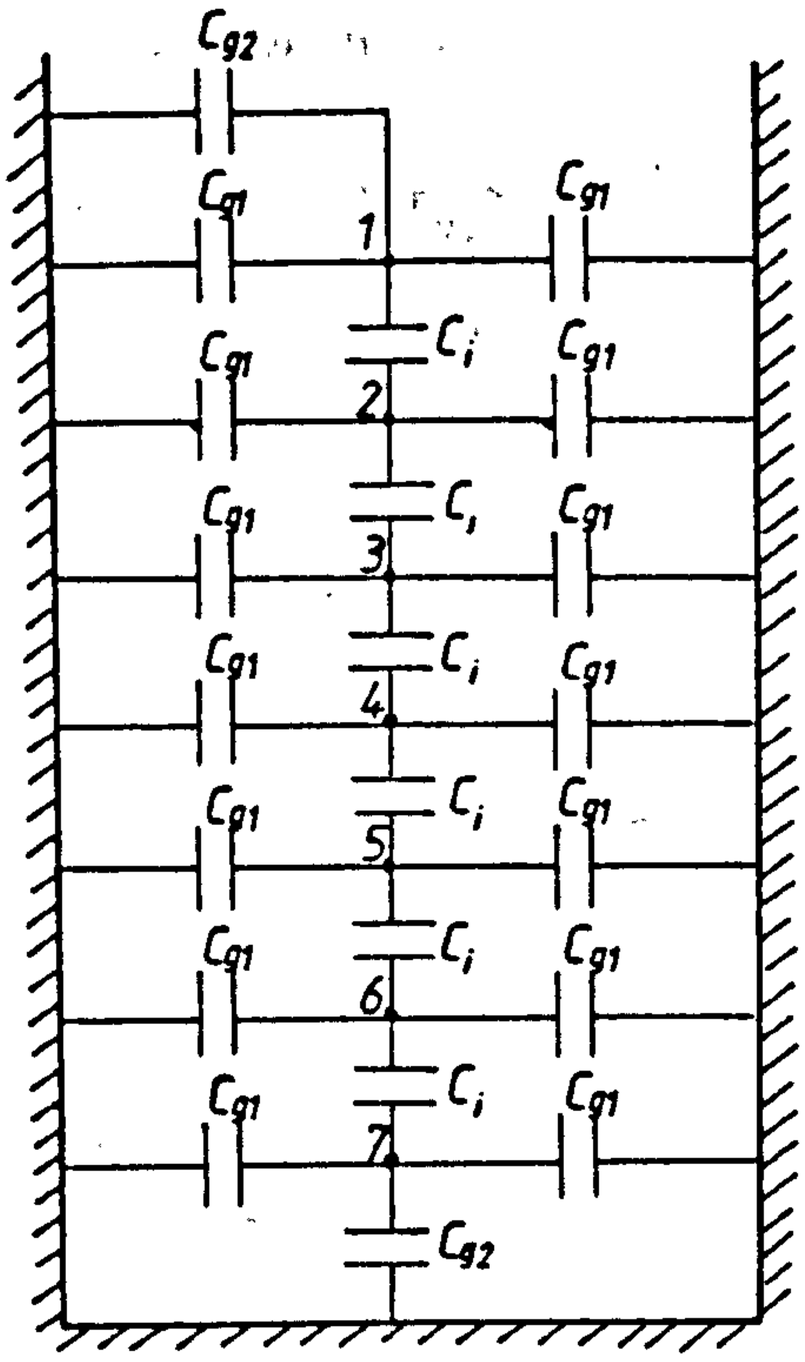

Figure 5.3.2.1 - Equivalent Circuit of Coil Conductors

$C_{s1} = C_{g2} + 2C_{g1}$

$C_{s2} = 2C_{g1}$

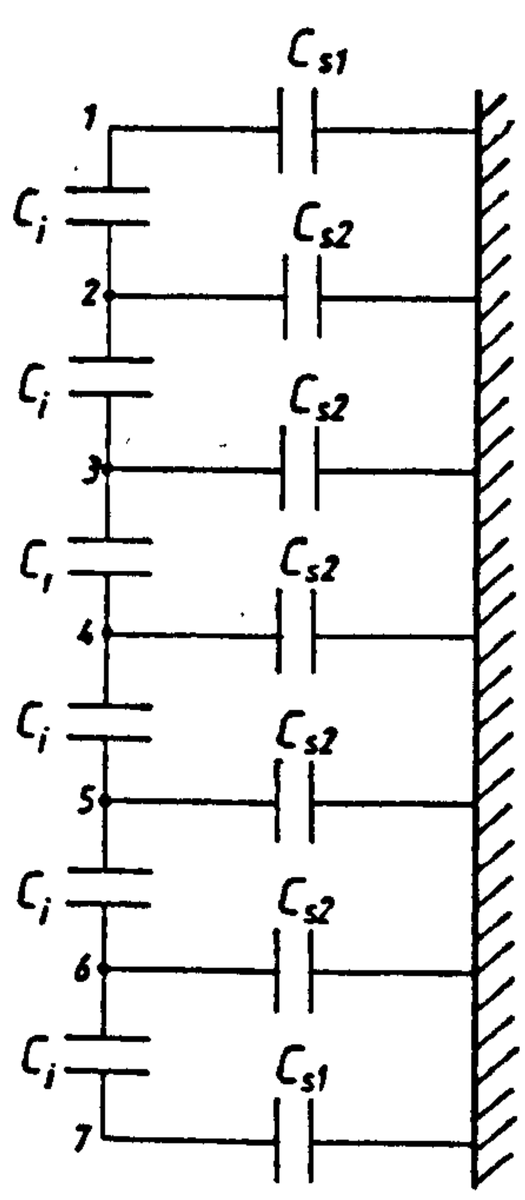

Figure 5.3.2.2 - Reduced Equivalent Circuit

Expressing this in matrix form we have :

$$\begin{bmatrix} q_1 \\ q_2 \end{bmatrix} = \begin{bmatrix} C_{s1} + C_i & - C_i & 0 \\ - C_i & C_{s2} + C_i & - C_i \end{bmatrix} \cdot \begin{bmatrix} v_1 \\ v_2 \\ v_3 \end{bmatrix}$$

This process is repeated to obtain the complete capacitance matrix [C] .

$$[C] = \begin{bmatrix} C_{s1}+C_i & -C_i & & & & & & \\ -C_i & C_{s2}+C_i & -C_i & & & & & \\ & -C_i & C_{s2}+C_i & -C_i & & & & \\ & & -C_i & C_{s2}+C_i & -C_i & & & \\ & & & -C_i & C_{s2}+C_i & -C_i & & \\ & & & & -C_i & C_{s2}+C_i & -C_i & \\ & & & & & -C_i & C_{s1}+C_i & \end{bmatrix}$$

When calculating the interturn capacitance, C_i , field fringing may be neglected owing to the large conductor width to interturn separation ratio . With reference to figure 2.3.1.1 of chapter two, the capacitance C_i is given by :

$$C_i = \frac{\epsilon_0 \epsilon_r w}{b} \quad \text{(Farads/metre)}$$

Similarly, the slot capacitances , C_{s1} and C_{s2} , are given by :

$$C_{s1} = \frac{\epsilon_0 \epsilon_r (w+2a)}{b} \qquad C_{s2} = \frac{\epsilon_0 \epsilon_r 2a}{b} \quad \text{(Farads/metre)}$$

5.4 Computer Analysis

A suite of FORTRAN programs were developed to model a single lossless coil initially, as the basic unit in a winding model . The programs can be separated into three distinct sections:

i. Formulation of scatter matrices .
ii. Determination of the impulse response of the coil .
iii. Convolution of the impulse response with the input function to give the actual response of the coil to a discharge pulse .

5.4.1 Scatter Matrix Formulation

The scatter matrix is defined in equation (5.22) as ;

$$[S] = \begin{bmatrix} -[C_v] \\ [C_i].[Y] \end{bmatrix}^{-1} . \begin{bmatrix} [C_v] \\ [C_i].[Y] \end{bmatrix}$$

Construction of [S], the scatter matrix, takes place in two stages.

i. Input and storage of the matrices $[C_v]$, $[C_i]$ and [Y]

ii. Inversion of the sub - matrix $\begin{bmatrix} -[C_v] \\ [C_i].[Y] \end{bmatrix}$

followed by the multiplication of the two sub - matrices.

A routine called ENTER, (see appendix A); allows the operator to define the current and voltage connection, and admittance matrices , (C_i , C_v and Y), for a coil with a limit of 9 turns. This is an arbitrary limit and may be increased to accommodate a coil with a greater number of turns. These matrices, for a particular junction, are then stored in a data file on a permanent storage medium for use in the subsequent stage.

The second stage is handled by a routine called TOM, (listed in appendix A). The matrices $[C_i]$, $[C_v]$ and [Y], are read from data file, after which the scatter, sub-matrices are constructed. A Gaussian elimination technique is then used to find the inverse of the sub-matrix . For this purpose a routine, F04 AEA, was used, which was

part of a set of the NAG, (Numerical Algorithm), package within the computer library.

To check the accuracy of the inversion process the sub-matrix is pre-multiplied by its inverse to give the identity matrix. The zero elements on the off diagonals are no greater than 0.465×10^{-13} for single precision arithmetic, giving an inversion which is acceptable.

The scatter matrix, having been constructed, is stored in a data file and the process is repeated for each junction . The scatter matrices for each of the five junctions in the single coil model are given in appendix B .

5.4.2 Time Convolution Analysis

Any arbitrary time function x(t) can be approximated by a series of ideal impulses, which over the time interval $-\infty$ to ∞, is expressed as :

$$x(t) = \int_{-\infty}^{\infty} x(\lambda).\delta(t-\lambda)d \qquad \ldots.(5.25)$$

The function x(t) is thus represented as the summation (integral) of a continuum of impulses where each impulse is of the form $x(\lambda).\delta(t-\lambda)d\lambda$.

Using the concept of impulse response, h(t), for a linear, time - invariant system, it is possible to determine the system output for an arbitrary input. The response of the system, (in this case the coil multiconductor transmission line), to each elementary impulse is, $h(t-\lambda)$ multiplied by the magnitude of the impulse $x(\lambda)d\lambda$. The output response y(t) , is the summation of all the elementary responses which is given by,

$$y(t) = \int_{-\infty}^{\infty} x(\lambda).h(t-\lambda)d \qquad \ldots..(5.26)$$

The integral expression (5.26) is termed the convolution of x(t) and h(t).

Therefore, by computing the response of the coil transmission line system to each member of a continuum of impulses which represent an arbitrary input function, and summing up these responses, the output function may be obtained .

5.4.3. Impulse Response of a Lossless Coil

The Bewley Lattice technique , [106], for time domain analysis of transmission lines provides the means of obtaining the impulse response h(t) of a coil to a single impulse input. The Bewley Lattice technique is basically a timetabling exercise in which the path of every impulse travelling in a complex transmission line system is documented.

The coil is characterised by a series of lossless transmission lines, with impulse transit times calculated from equation (5.12) as indicated in figure 5.4.3.1 . Each junction is numbered as shown and has a scatter matrix associated with it.

When a single impulse enters the coil terminal, it results in a number of impulses propagating from junction 0 towards junctions 1 and 4 determined by the voltage scattering at that junction. These impulses arrive at junctions 1 and 4 at time $t + t_0$ seconds later. Each of these impulses result in sets of reflected and transmitted impulses scattered at junctions 1 and 4 , and the process continues . Therefore the impulse response at a particular point on the coil is a series of relatively small impulses which are separated in time by unequal time intervals , (see figure 5.4.3.2) .

The program developed to incorporate this anaylsis is called IMPL1 and constitutes the largest routine in the program suite, (see appendix A). The function of the program is best described with reference to the flow diagram in figure 5.4.3.3 .

Each voltage scattering operation at a junction is done in chronological order . The reflected and transmitted impulse magnitudes are stored in an array STORE along with the number of the junction to which they travel and the corresponding time of arrival, (the current time plus the line transit time) .

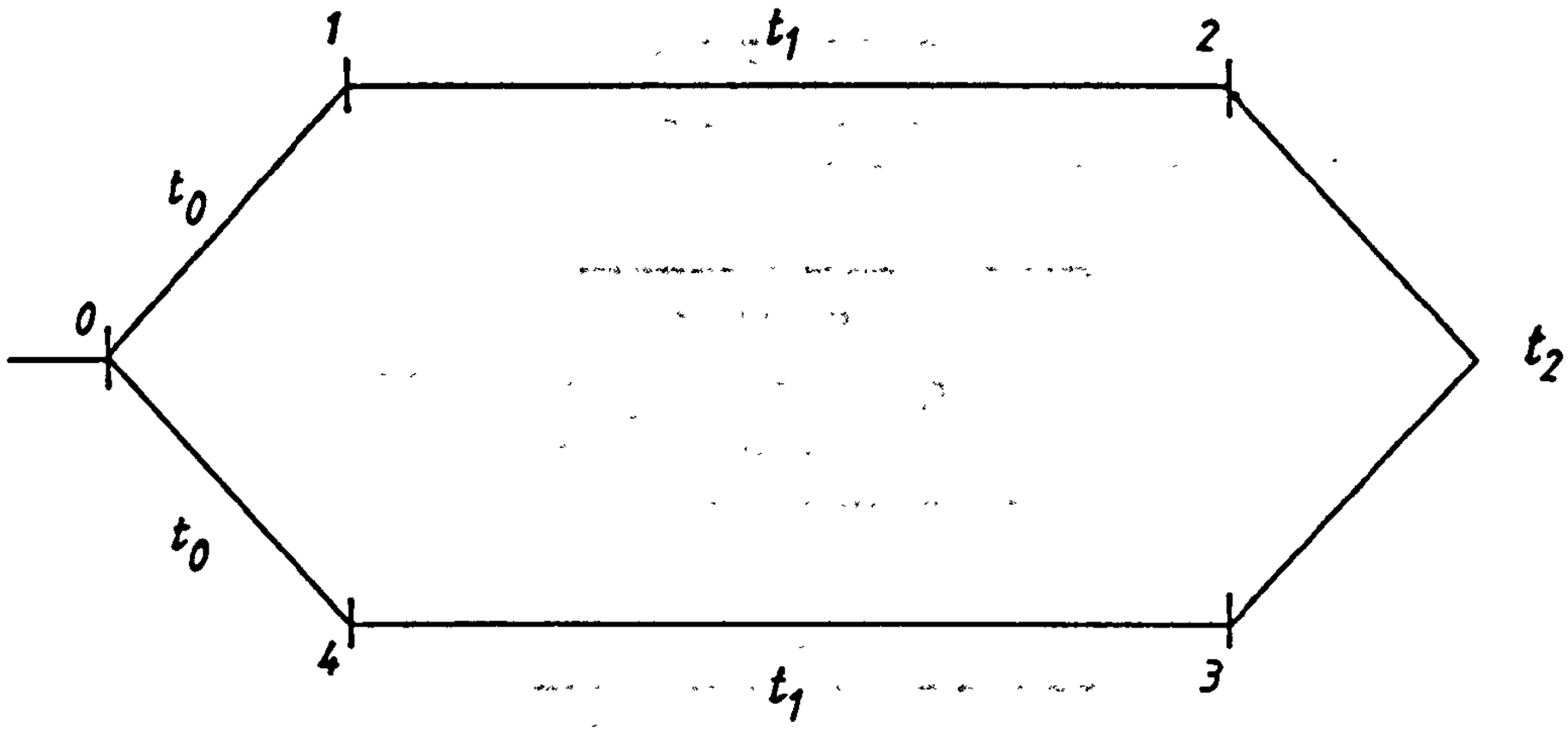

Figure 5.4.3.1 - Coil Section Transit Times

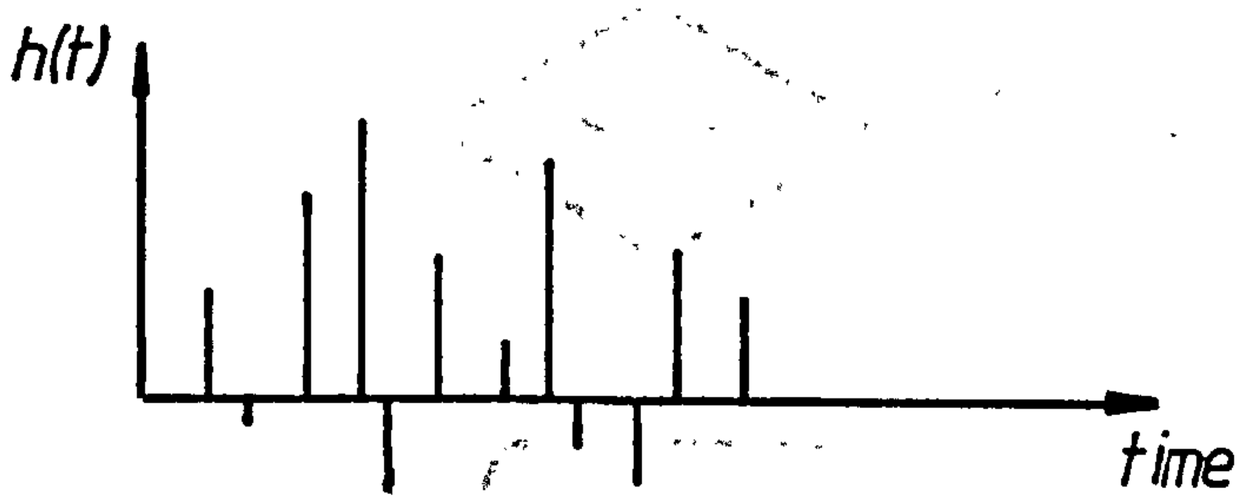

Figure 5.4.3.2 - Typical Impulse Response

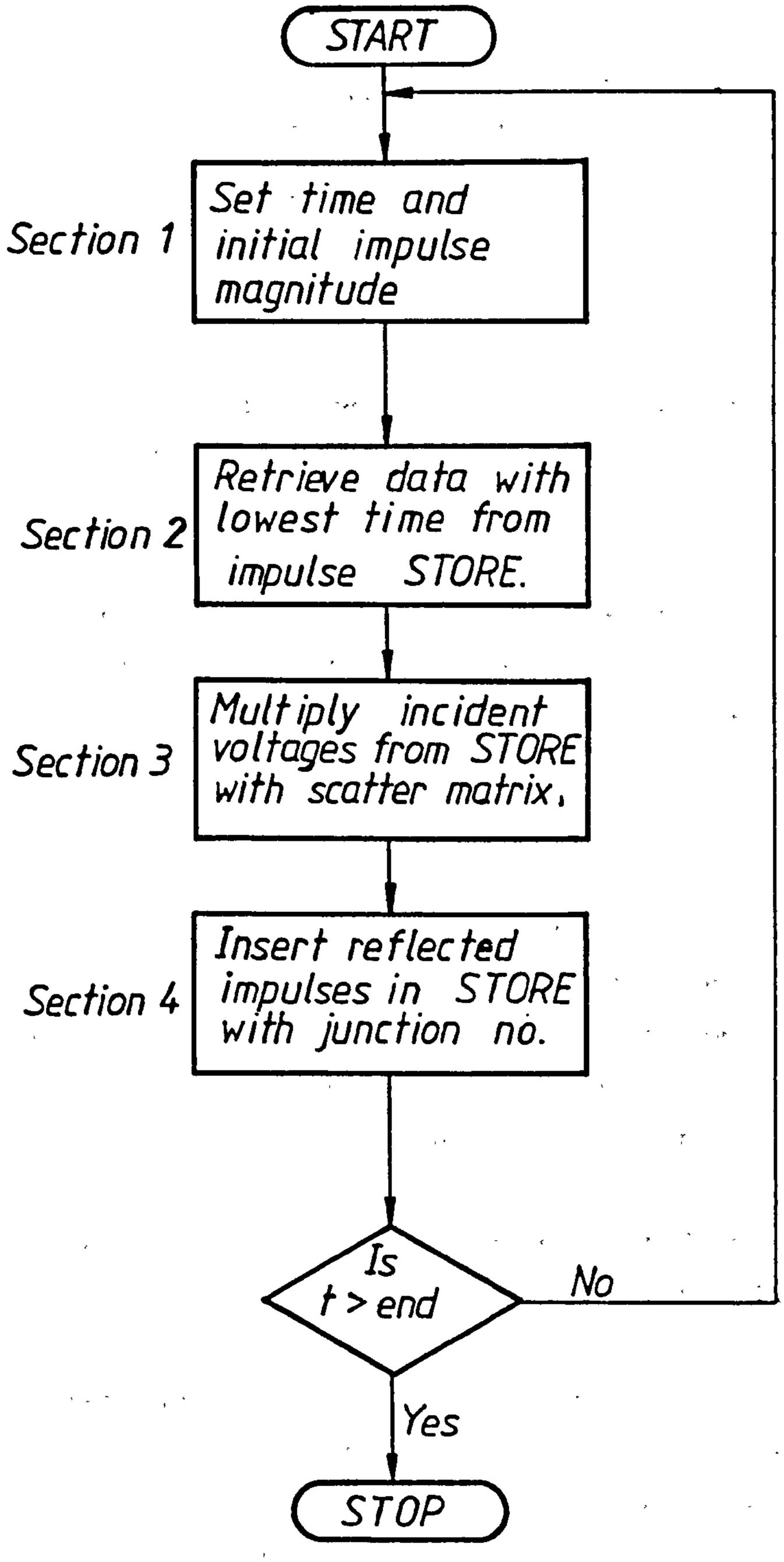

Figure 5.4.3.3 - Flow Diagram For Impulse Response Computer Program

An entry in the array STORE comprises a location for the junction number, a location for the time of arrival, t, and 2N + 2 locations for the impulse magnitudes . The location size 2N+2 corresponds to the number of impulses generated at the terminal junction. This is shown in figure 5.4.3.4 .

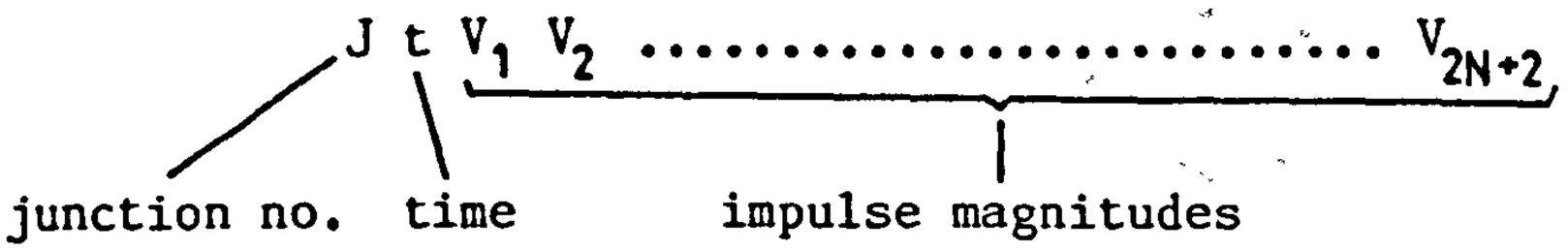

Figure 5.4.3.4 - Single Entry in STORE

Initially time is set to zero and the unit impulse is incident on junction 0 . Voltage scatter takes place and the first entry is placed in STORE.

Section 2 of the program searches STORE for the next scattering operation to take place in time, by finding the entry with the lowest time t . This operation is outlined in the flowchart in figure 5.4.3.5. Provision must be made for entries which have identical times t but different junction numbers .

The impulse magnitudes in STORE are then transferred to another array VIN which forms the incident voltage vector V^{in} in equation (5.22) . The store is searched again for impulses that arrive at the particular junction at or about the same time t . These impulses are added to the incident voltage array VIN, for use in the next section.

In section 3 the scatter matrix for the junction and the incident impulses in VIN are multiplied to obtain the scattered voltages [V] , which are placed in an array VRE. This is performed by a subroutine TIMES. It remains to put the impulse data in array VRE into an appropriate position in STORE for the purpose of data retrieval. This operation is best described by example. Consider the junction and conductor configuration in figure 5.4.3.6 .

In a voltage scattering operation at junction 2, sets of impulses will be reflected towards junctions 1 and 3 which means two entries will be placed in STORE. It is the function of a subroutine, STORE 2, to transfer the impulse voltages in array VRE to the appropriate positions in the entries (a) and (b) . This depends on the numbering

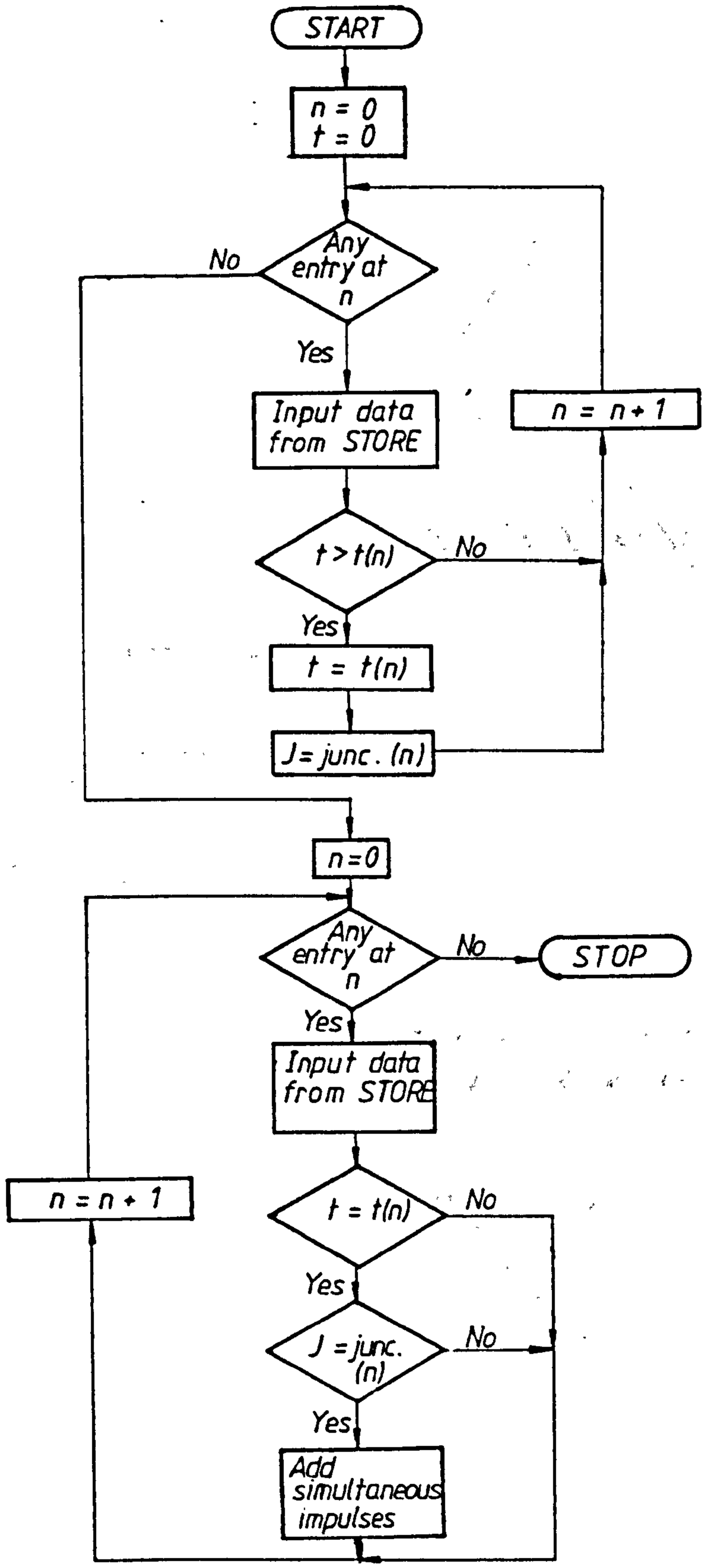

Figure 5.4.3.5 - Flow Diagram For STORE Program

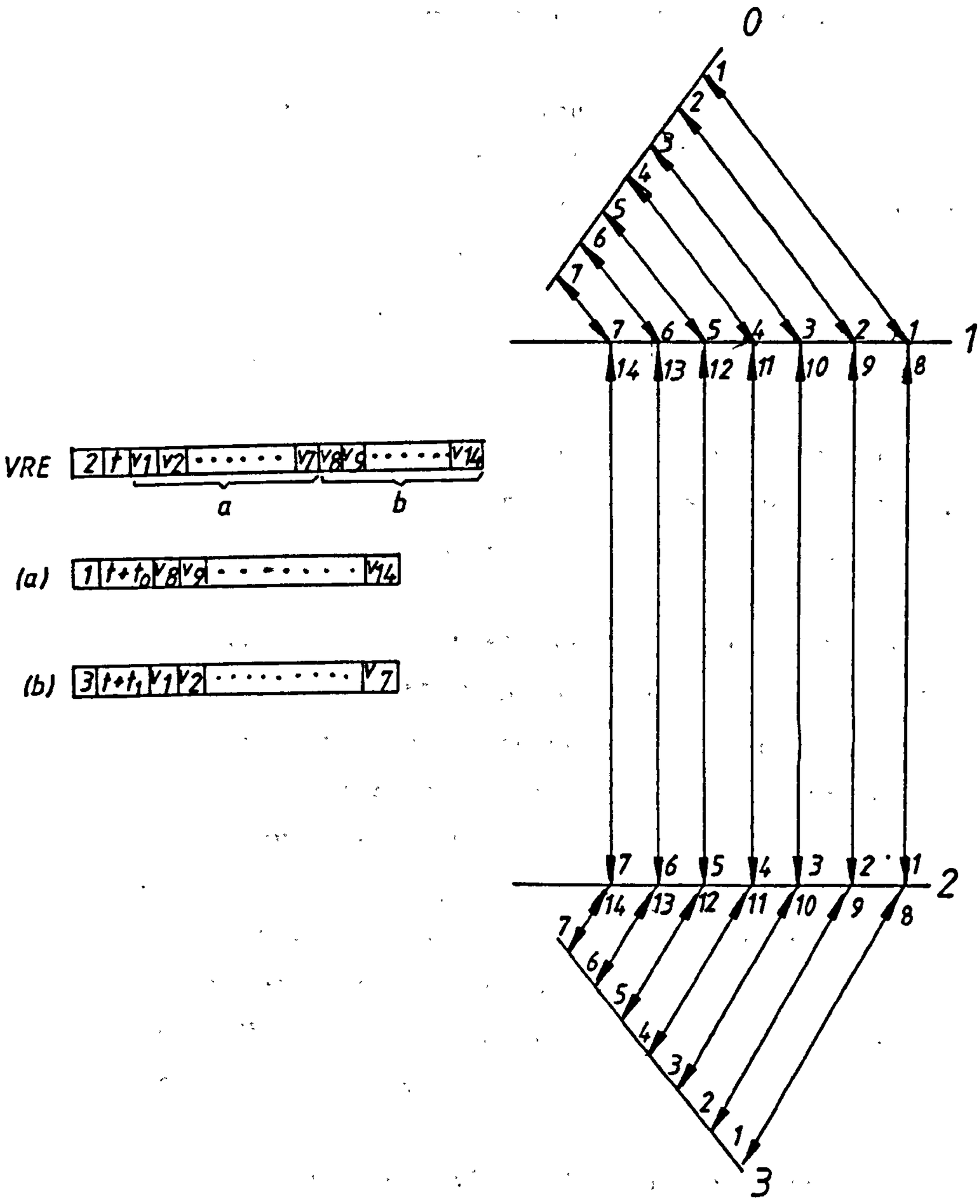

Figure 5.4.3.6 - Impulse Scattering at Junction 2

system for conductors in the coil model . By specifying a number of parameters in the subroutine when it is called from the main program, controls the way impulse voltages are mapped from the array VRE to the arrays in STORE . This flexibility allows any numbering system to be used. For slot/endwinding junctions , 2 entries are placed in STORE whilst 3 entries result in STORE for the terminal junction. The entire process is repeated until the specified time of study elapses.

To store every event in permanent storage would be wasteful and so only the impulse response at a particular point (junction) on the coil is retained . A data file RESPONSE is used to store the impulse response used in the next stage of the anaylsis.

5.4.4 Impulse Convolution.

The predicted response of the coil to an arbitrary waveform is obtained by convolving the impulse response with the input function. This operation is described mathematically by equation (5.26) .

Having obtained the impulse response h(t) it follows that the input x(t) must be defined. A program INPUT allows one to define the input function by specifying the magnitude and time of occurrence of each impulse which constitutes the input function . These parameters are stored in a data file for subsequent use .

Convolution , in this context, is basically the summation of the responses of the coil to each impulse in the input function which is performed by a program CONVL, (see appendix A) . The process of convolution is divided into five stages.

In the first stage the input waveform and coil impulse response are extracted from the appropriate data files.

In the second stage the weighted impulse response to each impulse in the input waveform is obtained . This is achieved by multiplying the impulse response by the normalised magnitude of the impulse in the input waveform and storing the resultant weighted impulse response in an array OUTPUT along with the corresponding impulse times . Impulse times are computed from the addition of the input impulse time, t_i, with the times, t_n associated with the impulse, and stored in an array TIME . This is shown in the flow diagram in figure 5.4.3.7 . The

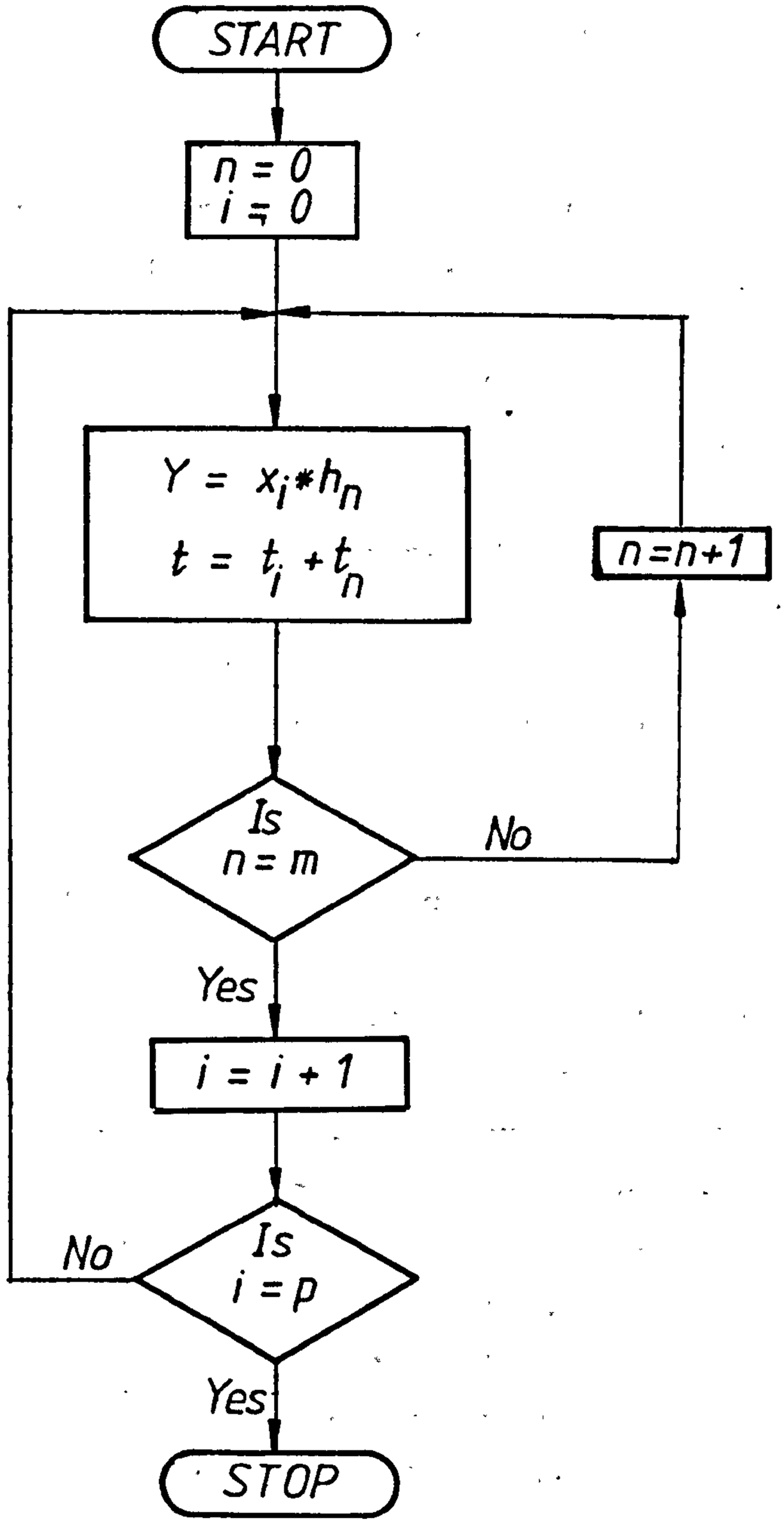

Figure 5.4.3.7 – Flow Diagram For Impulse Times Search in Convolution Program

variables x_i and h_n are the impulse magnitudes of the input function and impulse response respectively. The resulting weighted impulses are not in the order in which they occur in time .

In stage three, a subroutine called SORT, rearranges the impulses into chronological order . To sort impulses into chronological order, after determining all the weighted impulse responses, would require repeated searches throughout the entire array store TIME . Instead the subroutine SORT is called by the main program after each weighted impulse response is computed . This saves a large amount of computer time .

Impulse data is further compressed by searching the array store for impulses which occur simultaneously in time or within a small time interval of each other . This forms the fourth stage of the convolution process . The resulting impulse data represents the convoluted function which is the predicted response of the coil.

The impulse data which is obtained is excessive in size and is compressed, to a more useable length for ease of information presentation . The data is effectively filtered by selecting either every second or third impulse data from the array store. This completes the impulse convolution stage.

5.5 Extended Model to Include Intercoil Coupling

Previous investigations have concluded that intercoil electromagnetic coupling has a negligible influence on the propagation of steep-fronted surges in machine windings . However, experimental evidence ,(see chapter 2), has shown that coupling between adjacent coils in a winding has a significant effect on the shape , (hence behaviour), of short duration pulses travelling in a winding . A portion of the pulse is transferred instantaneously from one coil to the terminals of an adjacent coil by a route other than the conduction path . In this section, a model is proposed which attempts to take into to account the intercoil coupling effect on pulses propagating in a winding.

Experimental evidence shows that intercoil coupling is strongest between adjacent coils in a winding . The effect of intercoil coupling between one coil and the next adjacent coil is not so significant and

is neglected in the analysis . Therefore intercoil coupling is only considered for two adjacent coils in a winding group.

In the slot region of a stator core, two adjacent coils are electromagnetically isolated from each other due to eddy current flow in the iron . Any field coupling must exsist in the endwinding regions of the coils . It is this assumption which provides a basis for the two coil model .

Consider the two adjacent coils in the diagram of figure 5.5.1 . The coils are in close proximity to one another, being situated in adjacent core slots. Conductors numbered 1 and 8 through to conductors 7 and 14 run parallel to one another in the endwinding region, separated by a short air space , (normally a few millimetres). In addition, the two coils are connected in series .

In this configuration, the two, 7 turn, coils may be regarded as a single 14 turn coil. Applying the same philosophy, as in a single coil model, this coil may be divided into five multiconductor transmission line sections with corresponding junctions . The scatter matrices for each junction are derived in the following sections .

5.5.1 Terminal Junction Scatter Matrix.

The diagram in figure 5.5.1.1 depicts the terminal junction for the two coils. Analysis is identical to the single coil case in which the voltage and current connection matrices are defined first. Both will have dimensions (N+1)x(2N+2) which is (15x30).

In order to derive the admittance matrix for the junction it is necessary to obtain the capacitance matrix . In the endwinding region the coil conductors run parallel to one another. It is assumed that the influence of the transposition of conductors in the endwinding section on the electric field is negligible , along the length of the section.

With this assumption the two coil conductor stacks may be regarded as a system of parallel plate capacitors . Figure 5.5.1.2 shows the cross section of the two coils in the endwinding region . The corresponding capacitance equivalent circuit is exactly the same for two, 7-turn, coils as it is for a single, 14 turn, double stack coil.

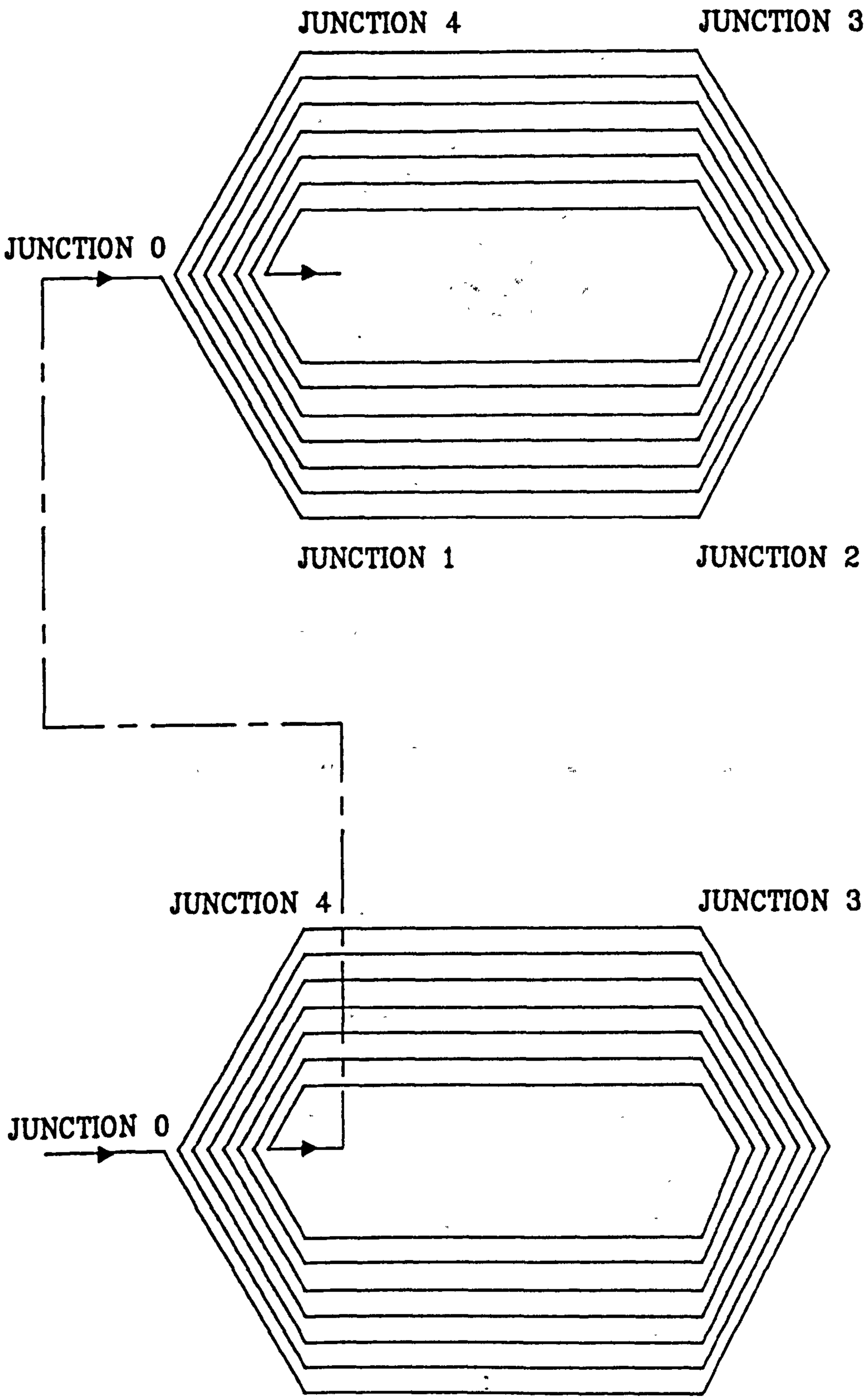

Figure 5.5.1 - Model of Two Adjacent Coils

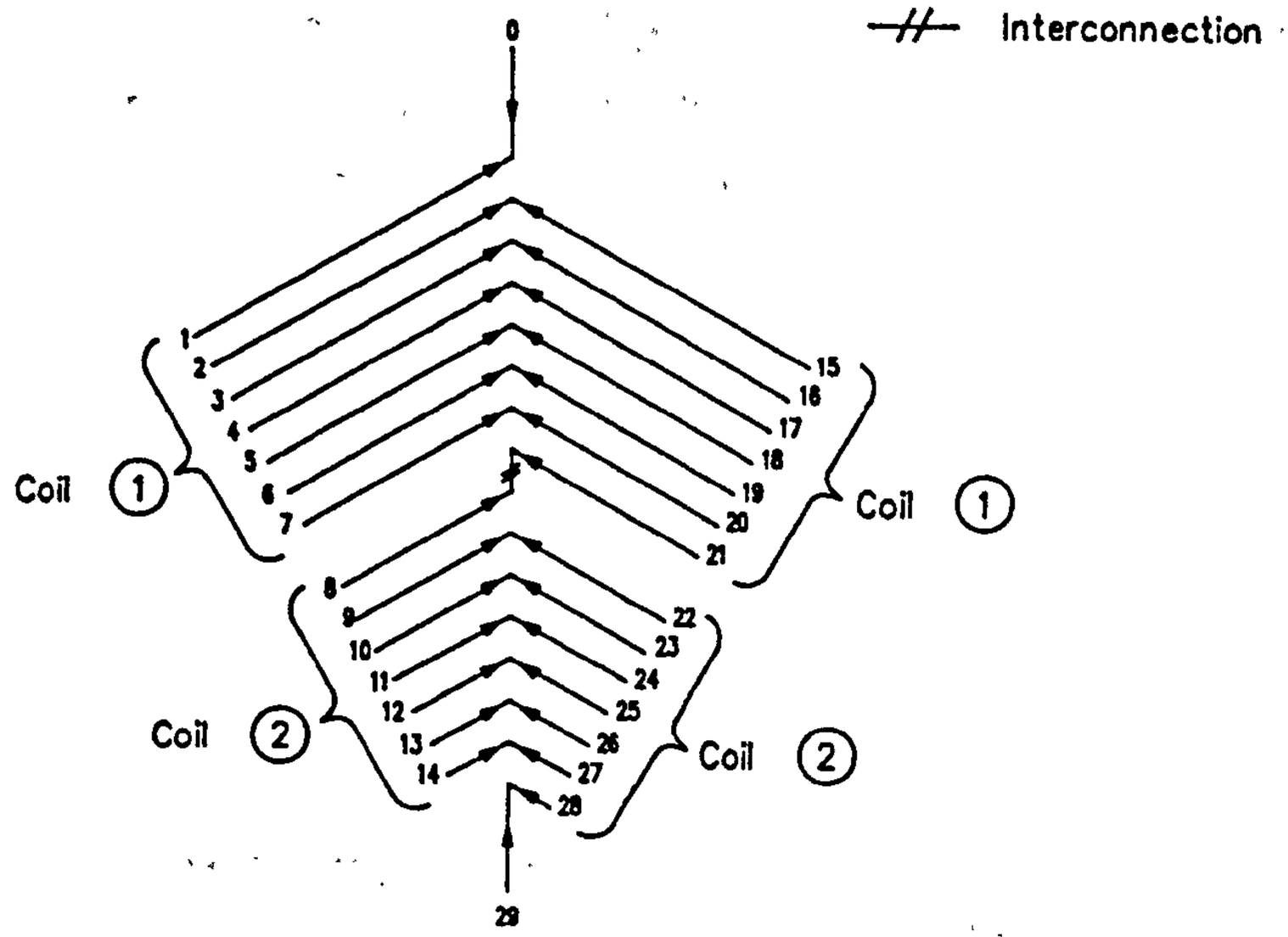

Figure 5.5.1.1 - Terminal Junction for Two Coils

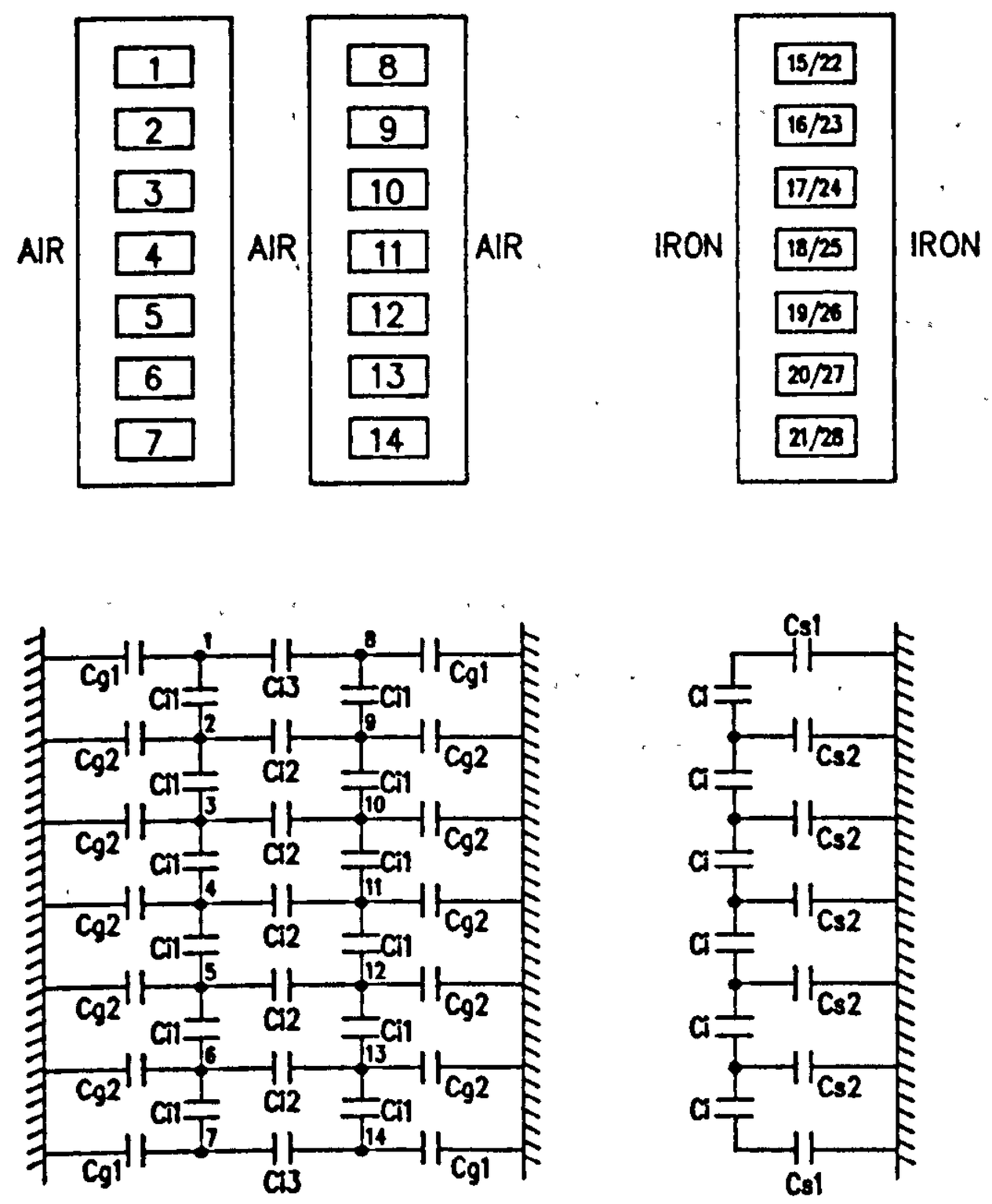

Figure 5.5.1.2 - Equivalent Circuit

The only difference is the inclusion of an air dielectric in the calculation of the capacitances C_{i2} and C_{i3}. The capacitance matrix [C] may be derived directly from the equivalent circuit and is given in figure 5.5.1.3 . Matrix capacitances are as follows :

C_0 : terminal lead capacitance.
C_1 : C_{s1}, $+ C_{i1} + C_{i3}$
C_2 : $C_{s2} + 2C_{i1} + C_{i2}$
C_3 : $- C_{i1}$
C_4 : $- C_{i2}$
C_5 : $- C_{i3}$

Calculation of these capacitance values is difficult and requires the exact electric field solution for the conductor/dielectric system.

The scatter matrix is obtained by following the same route as described previously.

5.5.2. Slot/Endwinding Junction Scatter Matrix

The slot/endwinding junction is shown in figure 5.5.2.1 . The same assumptions are made for the endwinding conductors, for which, the equivalent circuit is given , (see figure 5.5.1.2) . In the slot region, the two coil conductor systems are electromagnetically isolated so that the resulting equivalent circuit is that shown in figure 5.5.2.2.

Comparision of the two circuits reveals the difference between two closely coupled coils situated in both air and iron . This difference is the inclusion of the intercoil capacitances C_{i2} and C_{i3} . Derivation of the capacitance matrix for the junction follows directly from the equivalent circuit and is shown in figure 5.5.2.3 .

The matrix capacitances are as follows :

$$C_1 : C_{s1} + C_{i1} , + C_{i3}$$
$$C_2 : C_{s2} + 2C_{i1} , + C_{i2}$$
$$C_3 : - C_{i1}$$
$$C_4 : - C_{i2}$$
$$C_5 : - C_{i3}$$
$$C_6 : C_{s1} + C_i$$
$$C_7 : C_{s2} + 2C_i$$
$$C_8 : - C_i$$

Once the admittance matrix is obtained , the scatter matrix for the junction can be derived .

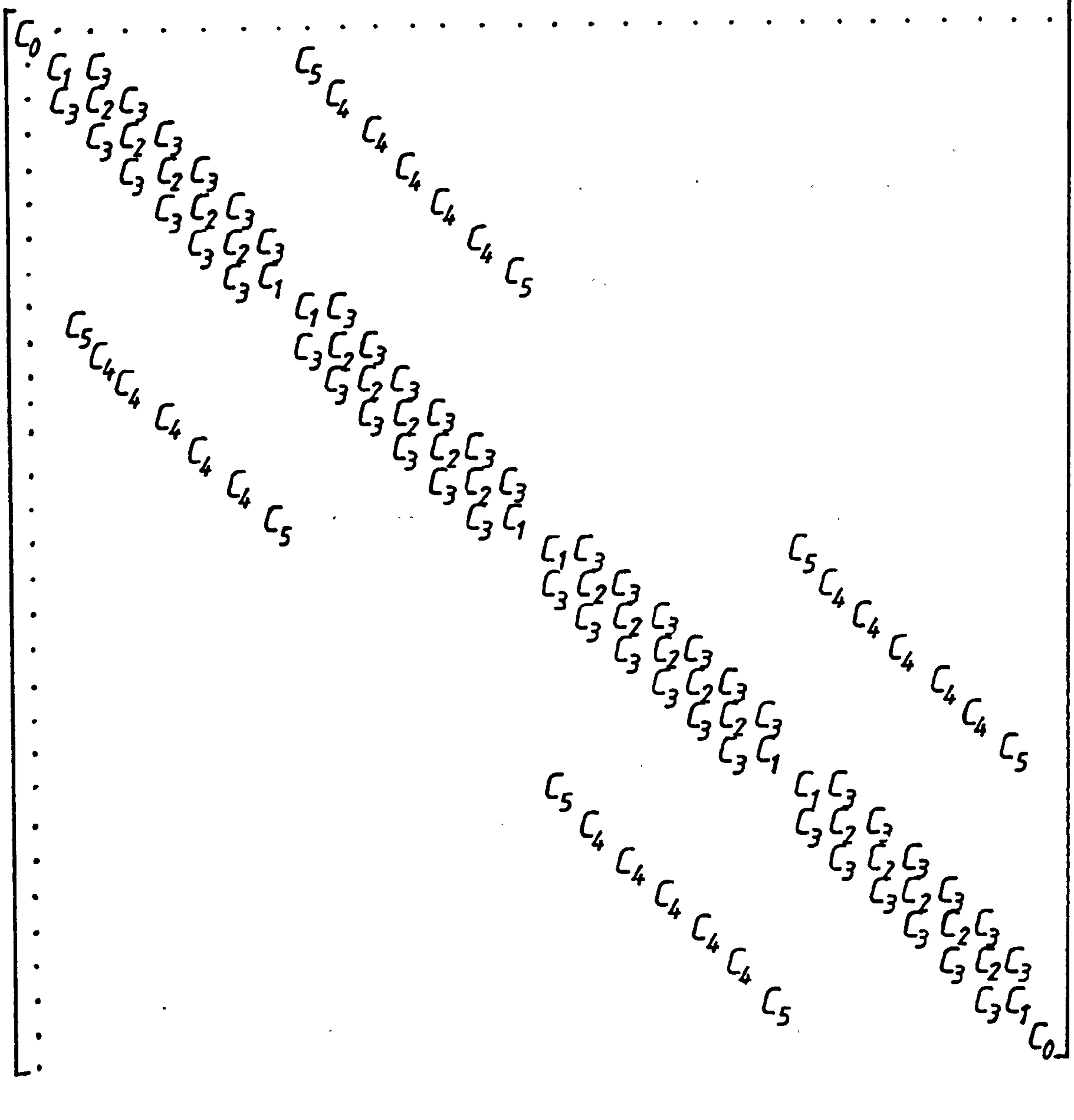

Figure 5.5.1.3 - Capacitance Matrix for Terminal Junction

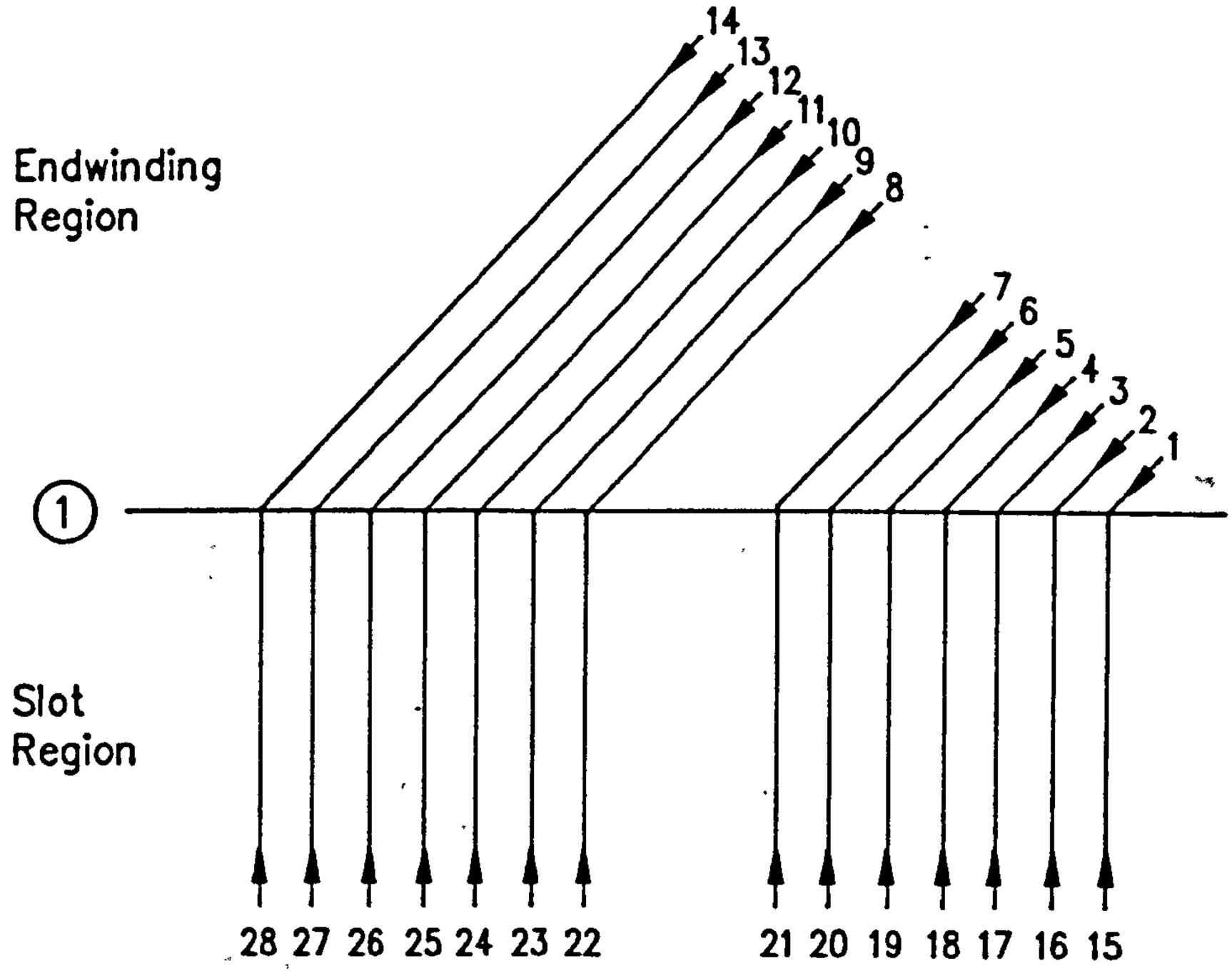

Figure 5.5.2.1 - Slot/Endwinding Junction for Two Coils

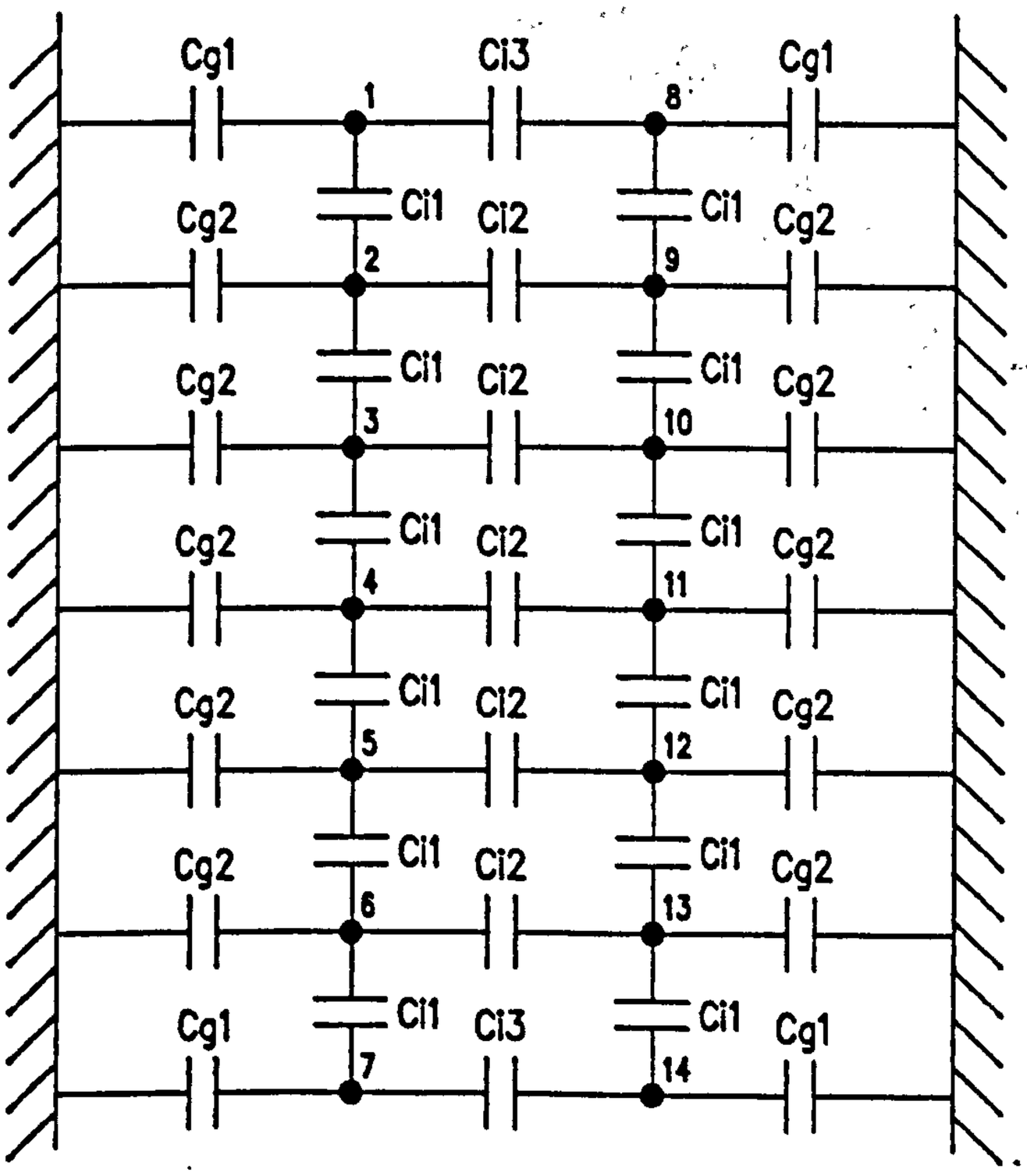

Figure 5.5.2.2 - Equivalent Circuit

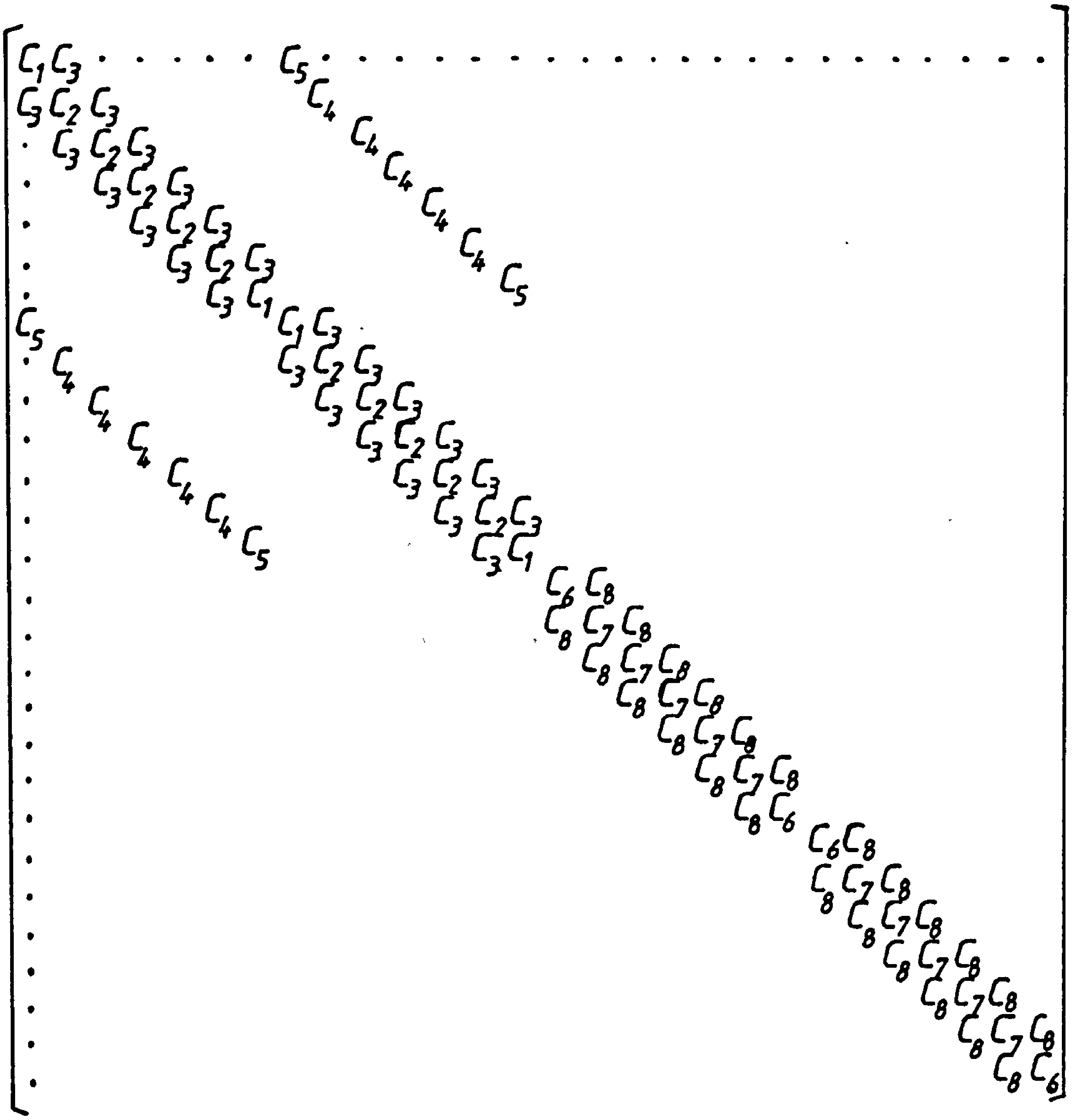

Figure 5.5.2.3 - Capacitance Matrix for Slot/Endwinding Junction

CHAPTER SIX

CONCLUSIONS

6.1 Conclusions

The work presented in this thesis was concerned with the development of an on-line technique for detecting and locating partial discharges in the stator windings of high voltage machines . This technique is to form part of an on-line health monitoring strategy for the insulation of high voltage machine stator windings .

The introduction has presented an outline of existing techniques for assessing the state of machine stator winding insulation and systems used for detecting partial discharges in high voltage equipment .

It was shown that there is a requirement for a diagnostic system to monitor the condition of high voltage machine insulation . In addition, there is also a requirement for a partial discharge location technique for application to high voltage machine stator windings to aid diagnosis of the insulation condition . This objective has been achieved on a model phase winding of a machine.

Before developing a system to detect and locate partial discharges in a stator winding , an investigation was made of the propagation characteristics of high frequency pulses within the model phase winding . In the investigation , time and frequency measurements were made with typical partial discharge pulses generated artificially .

The results prove that a machine phase winding behaves like a low pass filter circuit to high frequency pulses so that propagation is only supported at signal frequencies below a certain cut-off frequency , which for the model winding was approximately 3.5 MHz . Below the cut-off frequency , three modes of wave propagation have been identified and are listed as follows :-

i. Transmission line wave propagation .
ii. Electromagnetic and electrostatic coupling between adjacent turn conductors within a single coil .
iii. Electromagnetic coupling between the endwinding conductors of adjacent coils in a winding .

Studies have shown that the velocity of propagation of waves is dependent on frequency . At relatively low frequencies , (below 900 kHz), associated with the transmission line mode of wave propagation,

the velocity is approximately 38 m/μsec and can be calculated from the relationship :

$$v = \frac{1}{\sqrt{LC}}$$

L is the winding inductance per unit length and C is the winding slot capacitance per unit length .

At higher frequencies , electromagnetic waves travel by a combination of transmission line propagation and endwinding coupling . This occurs at a higher velocity of approximately 116 m/μsec which can be calculated using the expression :

$$v = \frac{c}{\sqrt{\epsilon_r}}$$ (c - velocity of light in a vacuum)

Investigation has also shown that wave propagation through the endwinding conductors of coils takes place within a relatively narrow bandwidth of signal frequencies , between 900 kHz and 3.5 MHz .

Frequency response measurements have indicated that transmission line resonance occurs in a phase winding which is terminated at one or both ends by an impedance other than the characteristic impedance of the winding . The frequencies at which resonance occurs is when the half or quarter wavelength of the wave oscillation is a multiple of the winding length . This effect depends on the terminating conditions . These resonant frequencies have been calculated from the relationship, $v = f\lambda$, where the velocity is the transmission line value of 38 m/μsec .

Identical behaviour occurs when waves propagate through the endwindings . However , calculation has shown that transmission line resonant frequencies associated with this mode of propagation can be calculated from the expression , $v = f\lambda$, but the velocity of propagation in this case is around 116 m/μsec .

In addition to these findings on the propagation of high frequency pulses , two properties of pulse propagation have been identified which can provide the basis for a partial discharge location technique. The time delay of signals travelling through a winding from

a discharge source to the winding terminals can be used to determine the location of the source . The time delay measured depends on the mode of wave propagation selected for the location technique , which is either the transmission line mode or the endwinding coupling mode .

In the development of a location technique , a means of detecting the partial discharge signals at the machine terminals is required . An investigation of the Rogowski coil for use in a partial discharge detection scheme was therefore undertaken .

The study has shown that the Rogowski coil can provide wideband measurement of partial discharge current pulses in the self-integrating mode . In this mode the risetime of the coil is in the sub-nanosecond region . The Rogowski coil must be enclosed in a metallic housing in order to provide a uniform distribution of capacitance to earth around the coil . Otherwise severe resonance occurs in the response of the coil to high frequency pulses .

Charge measurement was achieved using an integration circuit in which the peak value of the integrated signal from the Rogowski coil is related to the discharge magnitude .

When the Rogowski coil is connected to a capacitor and a damping resistor , the response to a discharge pulse is a damped oscillation . The peak amplitude of the first oscillation is related to the peak discharge current . Two types of narrowband detection circuits can be implemented , in which the Rogowski coil is connected in series or in parallel with the capacitor and damping resistor . Higher resonant detection frequencies can be achieved with the series circuit since it is less affected by the stray capacitance that exists across the load resistor .

The disadvantage of the use of the narrowband Rogowski coil detector is that it is unable to be calibrated in terms of discharge magnitude. Charge measurement is not possible since the oscillatory response of the narrowband detector does not preserve the shape of the current pulse and integration to obtain charge magnitude cannot be done .

The wideband self integrating Rogowski coil is therefore the most suitable for partial discharge measurements .

A partial discharge location instrument has been developed in which the location of a discharge source is obtained by correlation of the time delay difference between the high frequency pulses , detected at the winding terminals , that propagate from the discharge site . Investigation of the performance of the location system with artificial discharge pulses injected into a winding comprising six stator coils has been undertaken .

Results show that when the winding is terminated at both ends in the characteristic impedance , the location of a discharge source injected at each of the coil interconnections can be determined to within a distance of 2.1 metres , (2.9 % of the winding length).

Experiment has shown , that the introduction of a high or low impedance at one end of the winding causes a shift in the measured discharge source locations on the winding scan from the expected locations . In the case of the low impedance termination the shift is towards the low impedance terminal . This shift is progressively larger for sources connected away from that terminal .

The discharge source was also injected into the coil endwindings through an aluminium foil coupling capacitor . The discharge sources were successfully located but errors occurred in a few of the locations due to the mode of pulse injection , since all of the turn conductors were excited simultaneously by the discharge pulse injected.

An investigation with two simultaneous discharge sources injected at various points on the winding showed that pulse sources separated by 3 coils distance apart or less appear as a single pulse source . This single discharge source does not correspond to either of the two injected discharges but rather occurs at a false location determined by the time difference between the wavefronts of each of the discharge pulses observed at the winding terminals .

An experiment with six independent discharge sources positioned at each of the coil interconnections has shown that the technique can locate these sources successfully . Small errors occurred in the locations due to the effect the coupling capacitance of each discharge injection circuit has on the pulse propagation characteristics of the winding .

Tests were performed using a single high voltage discharge source . Results showed that the system is susceptible to interference from high voltage discharges , causing maloperation of the location instrument . Interference was manifested in the form of spurious location peaks appearing on the winding scan . However , when the source of high voltage discharge was placed in a shielded enclosure , the positions of the discharge source injected at three of the coil interconnections were located successfully .

The location technique has been proven to be capable of locating the positions of partial discharges within a stator winding comprising six coils .

In the final stage of the work , a theoretical model of a single stator coil was developed based on an existing model . This model was then developed to include inductive and capacitive coupling between two adjacent coils in a winding . However , time constraints did not permit completion of the analysis .

6.2 Future Work

The results of the work carried out provide scope for the future investigation and development of the partial discharge location system.

At present the discharge location system , MICA, is capable of locating discharges within a six coil stator winding ,(approximately 72 metres of winding). Development work is required to improve the performance of the location system to allow successful location in a winding of greater length . This would require investigation of the two modes of wave propagation in a winding , transmission line or endwinding coupling , to determine which of the two provides the most useful basis for development of the location technique .

Some investigation is required to determine the behaviour of the location system when used in conjunction with a narrowband Rogowski coil detector .

Further study of the application of high voltage discharge sources is

necessary to obtain an understanding of the mechanisms of interference coupling . The results of such a study could be used to develop the location system for use in an industrial environment where high levels of interference are present . Ultimately , the technique needs to be proven on a real high voltage machine on-line .

Development of a theoretical model to predict the propagation characteristics of discharge pulses in a stator winding is required . This model must incorporate the electromagnetic coupling between adjacent coils in a machine winding . The theoretical model should represent a complete phase winding and should be valid over the frequency range of partial discharge signals .

Finally, further work could include an investigation into the possible diagnostic measurements that may be used in assessing the condition of stator winding insulation . The partial discharge pulse information provided by the location instrument could be presented in the form of a pulse height analysis . This could then be related to the condition of the insulation .

REFERENCES

1 Thomson , W.T., Deans , N.D., Leonard , R.A., and Milne , A.J.: 'Condition monitoring of induction motors for availability assessment in offshore installations', 4th Eurodata Conference, Venice, Italy, 1983.

2 Albrecht , P.F. , Appiarius , J.C. , and Sharma , D.K. : 'Assessment of the reliability of motors in utility applications - updated', IEEE Trans. on Energy Conversion, vol EC-1, no.1, 1986, pp. 39-46.

3 Hardy-Bishop , B.A., Connolly , B.P.F., and Courtney , R.G.: 'The reliable offshore motor - an outline sketch',

4 Neale , M., and Associates,: 'Guide to the condition monitoring of machinery', Dept. of Industry report ISBN011 5121269 , London, England, 1979.

5 Hemmings , R.C., and Smith , J.D. : 'Information from bearing vibration', Inst. Mech.E., Conference Publications, 1976.

6 Boyd , J., and Kaufman , H.N.: 'The causes and control of electrical currents in bearings', Lubrication Eng., January , 1959, pp. 28-35.

7 Lloyd , O.: 'Wear debris in lubrication systems ; Evaluation of a Smith's industries in-line chip detector', C.E.G.B. Report R/M/N1094, March 1980.

8 Burns , R.L., 'Rotor bar failures in large ac squirrel cage motors', Electrical Engineer, October, 1977, pp. 11-14.

9 Cameron , J.R., Thomson , W.T., and Dow , A.B.:'Vibration and current monitoring for detecting airgap eccentricity in large induction motors', IEE Proc. , vol.133 , pt.B , no.3 , 1986, pp. 155-163.

10 Rolls , T.B.: 'Protection of induction motors', IEE Proc., Electric Power Applications , 1978 , Vol.1 , no.3 , pp. 72-76.

11 Bonnett , A.H.: 'Analysis of winding failures in three - phase squirrel cage induction motors', IEEE Trans. on Industry Applications, vol. IA-14, no.3, 1978, pp. 223 - 226.

12 Sillars , R.W.: 'Electrical insulating materials and their application', IEE Monograph, series 14, (Peter Peregrinus Ltd.) 1973.

13 Galpern , H.N.: 'A new thermal aging facility for the evaluation of generator stator insulation systems', IEEE paper CH1952/83, pp. 258-263.

14 Kelen , A.; 'Functional testing of MICAPACT II insulation', ASEA Journal, vol. 54, no.2, 1981, pp. 36-41.

15 Flynn , E.J., Kilbourne , C.E., and Richardson , C.D. : 'An advanced concept for turbine - generator stator winding insulation', Trans. AIEE, vol.PAS-77 , 1958, pp. 358-371.

16 Evans , D.L.: 'IEEE working group report of problems with hydrogenerator thermoset stator windings Part I - analysis of survey', IEEE Trans. on Power App. and Syst., vol. PAS-100, no.7, 1981, pp. 3284 - 3291.

17 Forster , J.A., and Klataske , L.F.: 'IEEE working group report of problems with hydrogenerator thermoset stator windings', Part II - Detection, correction and prevention', IEEE Trans. on Power App. and Syst., vol.PAS-100, no.7, 1981, pp. 3292-3300.

18 Hogg , W.K., and Halsall , C.L.: 'Functional multiple ageing experiments on HV high power machines stator insulation systems', NRC Conference, PA, U.S.A., Oct. 1979.

19 Wood , J.W., Hindmarch , R.T., Frame , F., and Halsall , C.L.: 'Slot discharges in class B and F stator insulating systems', Proceedings of CEA International Symposium in Generator Insulation Tests', 1980, pp. 17-23.

20 Campbell , J.J., Clark , P.E., McShane , I.E., and Wakeley , K.: 'Strains on motor endwindings', Vol. IA-20, no.1, 1984, pp. 37-45.

21 Cornick , K.J., and Thompson , T.R.: 'Steep-fronted switching voltage transients and their distribution in motor windings Part 1 : Systems measurements of steep-fronted switching voltage transients', Proc. IEE , vol.129 , Pt.B , no.2 , 1982 , pp. 45-55.

22 Parrott , P.G. : 'Switching surge measurements on two high voltage induction motor installations', ERA report 72-159, 1972.

23 Wright, M.T., Yang, S.J., and McLeay, K.: 'General theory of fast-fronted interturn voltage distribution in electrical machine windings', Proc. IEE, Pt.B, vol. 130, no.4, 1983, pp. 245-256.

24 Salvage , B.: 'Electric stresses in gaseous cavities in solid dielectrics', Proc. I.E.E. , vol 111 , 1964 , pp. 1162-1173 .

25 Mason , J.H.: 'Discharges', Trans. Elect. Insul., vol. EI-13, no. 4, 1978, pp. 211-238.

26 Gallagher , T.J., and Pearmain, A.J.:'High voltage measurement, testing and design, J. Wiley and sons, 1983, chapter 7.

27 Hiley , J., and El Gendy , O.A.: 'A comparison of the discharge resistance of epoxy resins', 3rd Int. Symposium on High-Voltage Engineering, Milan, 1979, paper 22.03.

28 Ryder , D.M., Wood , J.W., and Hogg , W.K.: 'The deterioration of mica under the action of electrical discharges', Trans IEEE, vol. PAS-94, no. 3, 1975, pp. 1013-1020.

29 Stone , G.C., Gupta , B.K., Kurtz , M., and Sharnea , D.K.: 'Investigation of turn insulation failure mechanisms in large AC Motors', Trans IEEE. on Power App. and Systems, vol.PAS-103, no.9, 1984, pp. 2588-2595.

30 Jackson , R.J., and Wilson , A.: 'Slot discharge activity in air-cooled motors and generators', IEE Proc., vol.129, Pt.B. no.3, 1982, pp. 159-167.

31 Wilson , A.: 'Discharge damage in air cooled stator windings', 5th International BEAMA Conference on Electrical Insulation, Brighton, England, May 1986, pp. 7-12.

32 Simons , J.S.: 'Diagnostic testing of high-voltage machine insulation - A review of ten years experience in the field', Proc. I.E.E., vol. 127, Pt.B, no.3, 1980, pp. 139-154.

33 Childs,S.E., Wilson, A.:'CERL looks into insulation troubles in high-voltage motors', Elect. Times, vol.213, no.18, Nov. 1983, p.32 and p.37.

34 Dakin , T.W.: 'The relation of capacitance increased with high voltage to internal electric discharges and discharging void volume', Trans. AJEE, IIIA Vol.78, 1959, pp/ 790-795.

35 British Standards Institution, BS 4999 ,'General requirements for rotating electrical machines', part 60, 'Tests'.

36 Johnstone , D.R., and Gyaja , N.V.: 'Hazards of interpretation of dissipation - factor tip - up determinations', IEEE Trans. on Electrical Insulation, Vol. EI-13, No.1, 1978, pp. 9-13.

37 Orbeck , T.: 'Discussion of Practical value of internal partial discharge measurements on high voltage insulation systems for rotating machines', IEEE Trans. on Electrical Insulation , vol. EI-8, no.3, 1973, pp. 98-107.

38. Schwab., A.J.: 'High-voltage measurement techniques', M.I.T. Press, 1972, chapter VI.

39 Simons , J.S., and Richards , M.T.: 'Non-destructive electrical test methods for evaluating high-voltage stator insulation', Proc. IEE, 109A. Supplement 3, 1962, pp. 71-79.

40 Dakin , T.W., and Malinaric , P.J.: 'A capacitance bridge method for measuring integrated corona. Charge transfer and power loss per cycle', AIEE Trans. , PAS-79, pt.3 , 1960, pp. 648-652.

41 Simons , J.S.: 'Recent advances in diagnostic testing equipment and measuring techniques for large machine insulation', 5th BEAMA International Electrical Insulation Conference, 19-22 May, 1986, pp. 13-19.

42 Whitehead , S. : 'Dielectric breakdown of solids' , Oxford University Press, London, chapter IV, 1951.

43 Dakin , Y.W. , and Lim , J. : ' Corona measurement and interpretation', AIEE Trans., PAS - 76, 1957, pp/ 1059-1065.

44 Mole , G. : ' Basic characteristics of corona detector calibrators', IEEE Trans on Power Apparatus and Systems , vol. PAS-89, no.2, 1970, pp. 198-204.

45 Hogg , W.K., and Walley , C.A.: 'An assessment of the point - hemisphere discharge gap as a partial discharge reference', Journal of Scientific Instr., vol 43, 1966. pp. 11-15.

46 'Recognition of Discharges', Recommedations of CIGRE Study Committee No.2, Cables, Working group on Discharge Detection. Electra, no.11, pp. 61-98.

47 'Elimination of interference in discharge detection', Report by CIGRE Working group 03 of Study Committee 21 , H.V. insulated cables, Electra, no.21, pp.55-72.

48 Wilson , A.: 'Discharge detection under noisy conditions', Proc. IEE, vol.121, no.9, 1974, pp. 993-996.

49 Black , I.A.: 'The pulse discrimination system for partial discharge measurements in electrically noisy enviroments', BEAMA International Conference on Electrical Insulation, Brighton, England, May, 1978, pp. 300-308.

50 Discussions on 'Diagnotic testing of high-voltage machine insulation', Proc. IEE , vol. 127, Pt. B, no.6 , 1980, pp. 386-388.

51 Knoll , G.F.: 'Radiation detection and measurement', J.Wiley and sons, 1979, chapter 18.

52 Starr, W.T., and Johnstone, L.W.: 'Pulse distribution analyser for corona analysis', General Electrical Company , Report R55GL94, October, 1955.

53 Wijsman, R.A.:'Breakdown probability of a low pressure gas discharge', Physical Review, vol.75, no.5, 1949, pp. 833-838.

54 Karkkainen , S. : ' Internal partial discharges - pulse distributions, physical mechanisms and effects on insulations', Electrical and Nuclear Technology, Technical Research Centre of Finland, publication 14, 1976.

55 Karkkainen, S.:'Physical mechanisms of partial discharges', Electrical and Nuclear Technology, Technical Research Centre of Finland, publication 6, 1974.

56 Hogg, W.K., Miller, R., Rabach, G., and Ryder, D.M.:'The relationship of partial discharge amplitude distributions with dielectric damage at diffrent levels of voltage and frequency', IEEE Symposium on Electrical Insulation, Philadelphia, USA, June 1982, pp. 1-7.

57 Kurtz, M., Lyles, J.F., and Stone, G.C.:'Application of partial discharge testing to hydro-generator maintenance', IEEE Trans. on Power Apparatus and Systems, vol.PAS-103, no.8, 1984, pp. 2148-2157.

58 Kelen, A.:'Partial discharge pulse distribution analysis as a tool for assessing defects in high-voltage rortating machine insulation', CEA Symposium on Generator Insulation Diagnostic Testing, Toronto, Canada, June 1980, pp. 29-34.

59 Emery, F.T., and Harrold, R.T.:'Radio frequency response of a large turbine-generator stator winding', IEEE Trans. on Energy Conversion, vol. EC-1, no.2, 1986, pp. 172-179.

60 Timperley, J.E.:'Detection of insulation deterioration through electrical spectrum analysis', 16th EEIC, IEEE publication no. 83CH1952-1, 1983, pp. 60-64.

61 Harrold, R.T., Emery, F.T., Murphy, F.J., and Drinkut, S.A. 'Radio frequency sensing of incipient arcing faults within large turbine generators', IEEE Trans. on Power App. and Syst., vol. PAS-98, no.4, 1979, pp. 1167-1173.

62 Timperley, J.E.:'Incipient fault identification through neutral r.f. monitoring of large rotating machines', IEEE Trans on Pwr. App. and Syst., vol.PAS-102, no.3, 1983, pp. 693-697.

63 Banks, M.J.J.:'On-line detection of discharges in stator insulation', International Power Generation, vol.7, pt.3, 1984, p.35.

64 Malik, A.K., and Banks, M.J.J.:'The use of a loop probe for the radio frequency detection of discharges in the insulation of power plant in service', CEGB Technical Disclosure Bulletin, no. 364. 1981.

65 Dembinski, E.M., and Douglas, J.L.:'Calibration and comparison of partial discharge and radio interference measuring circuits' Prco. IEE, vol.115, no.9, 1968, pp. 1332-1340.

66 Dakin, T.W., Works, C.N., and Johnson, J.S.:'An electromagnetic probe for detecting and location discharges in large rotating-machine stators', vol. PAS-88, no.3, 1969, pp. 251-257.

67 McDermid, W.:'Review of the applications of the electromagnetic probe method for the detection of partial discharge activity in stator windings', Proceedings of CEA International Symposium on Generator Insulation Tests, Toronto, Canada, 1980, pp.47-50.

68 Miller, R. , Black, I.A., and Hogg, W.K. : ' Development of tecniques for detecting and locating the source of partial discharges in stator windings of electrical machines', 4th BEAMA International Electrical Insulation Conference, Brighton, England, May 1982, pp. 228-232.

69 Hickling, G.H.:'Measuring and locating partial discharges', Electrical Times, Sept. 1964, pp.443-444.

70 Tangen, K.O.:'Maling og lokalisering av partielle utladninger i transformatorer', Elektorteknisk Tidsskrift, 78 , nr.20 , 1965, pp. 365-371.

71 Talvio, E.:'Partial discharge carrier currents', Sahko, vol.41, 1968, pp. 50-53.

72 Salvage, B., and Tapupere, O.:'Measurement of current pulses due to discharges in a gaseous cavity in solid dielectric', Electronic Letters, vol. 6, no. 18, 1970, pp. 569-570.

73 Boggs, S.A., and Stone, G.C.:'Fundamental limitations in the measurement of corona and partial discharge', IEEE Trans. on Elect. Insul., vol. EI-17, no.2, 1982, pp. 143-150.

74 Franke, E., and Czekaj , E. : ' Wide-band partial discharge detector', IEEE Trans. on Elect. Insul., vol.EI-10, no.4, 1975, pp. 112-116.

75 Devins, J.C.: 'The physics of partial discharges in solid dielectrics', J.B. Whitehead Memorial Lecture, Conference on Elect. Insul. and Dielectric Phenom., IEEE Trans. on Electrical Insulation, vol. EI-19, no.5, 1984, pp. 475-499.

76 Harrold,R.T., and Sletten,A.M.:'Corona location in transformers by radio frequency spectrum analysis , Part I : Theory', IEEE Trans. on Pwr. App. and Syst., vol. PAS-89, no.7, pp.1584-1590.

77 James, R.E., Trick, F.E., Phung, B.T., and White, P.A. :' Interpretation of partial discharge quantities as measured at the terminals of H.V. transformers', IEEE Trans. on Elect. Insul., vol. EI-21, no.4, pp. 629-638.

78 Jackson, R.J., Wilson,A., and Geisner, D.B.:'Partial discharges in power cable joints : their propagation along a crossbonded circuit and methods for their detection', Proc. IEE, vol. 127, Pt.C, no.6, 1980, pp.420-429.

79 McDermid, W.:'Estimate of the attenuation of partial discharge pulses in stator windings of waterwheel generators', Proc. of CEA International Symposium on Generator Insulation Tests, Toronto, Canada, June 1980, pp.73-76.

80 Miller, R., Hogg, W.K., and Black, I.A.:' Measuring techniques for identifying partial discharges in stator windings of electrical machines', IEE Conf. on Electrical Machines : Design and Application, London, July 1982, pp. 221-234.

81 Wilson, A., Jackson, R.J., and Wang, N.: ' Discharge detection techniques for stator windings', Proc. IEE, vol.132, Pt.B, no.5 1985, pp. 234-244.

82 Rudenberg, R. : ' Electric shock waves in power systems - travelling waves and distributed circuit elements', Harvard University Press, Cambridge, Massachusetts, 1968 , chapter 17 , pp. 147-160.

83 Pellinen, D.G., Di Capua, M.S, Sampayan, S.E., Gerbracht,H. and Wang, M.:'Rogowski coil for measuring fast, high level pulsed currents', Rev. Sci. Instrum., vol.51, no.11, 1980 , pp. 1535-1540.

84 Stygar, W., and Gerdin, G. : ' High frequency Rogowski coil response characteristics', IEEE Trans. on Plasma Science, vol. PS-10, no.1, 1982,pp. 40-44.

85 Anderson. J.M.:'Wide frequency range current transformers', Rev Sci. Instrum., vol.42, no.7, 1971, pp. 915-926.

86 Rogowski, W., and Steinhaus, W. : ' Die messung magnetischen spannung', Archiv. Electortech., 1, 1912, pp. 141-150.

87 Bogle, A.G. : ' The effective inductance and resistance of screened coils', IEE Journal, 187, 1940, pp. 299-316.

88 Weeks, W.L., and Steiner, J.P. : ' Instrumentation for the detection and location of incipient faults on power cables', IEEE Trans. on Pwr. App. and Syst., vol. PAS-101, no.7 , 1982 , pp. 2328-2335.

89 Blewett, J.P., and Rubel, J.H.:'Video delay lines', Proc. IRE, - waves and electrons section, vol.35, 1947, pp. 1580-1584.

90 Lewis , I.A.D., and Wells , F.H. : ' Millimicrosecond pulse techniques', 2nd Edition, Pergamon Press, 1959, chapter 2.

91 Brown, D., and Neumann, U.: ' An improved programmable delay line', Nuclear Instr. and Methods, 158, 1979, pp. 281-288.

92 Connor, F.R.: ' Wave transmission - introductory topics in electronics and telecommunications' , Edward Arnold , 1978 , chapter 1.

93 Herbst, L.J.:'Electronics for nuclear particle analysis',Oxford University Press, 1970.

94 Kowalski, E.:'Nuclear Electronics', Springer-Verlag, 1970.

95 Rudenberg, R.:'Performance of travelling waves in coils and windings', AIEE Trans., vol. 59, 1940, pp. 1031-1040.

96 Robinson, B.C.:'The propagation of surge voltages through high-speed turbo-alternators with single-conductor windings', Proc. IEE, vol.100, Pt.II, 1953, pp. 453-467.

97 Lewis, T.J.:'The transient behaviour of ladder networks of the type representing transformer and machine windings', Proc. IEE, vol.101, Pt.II, 1954, pp. 541-553.

98 Meyer, H.:'The behaviour of rotating machinery windings on the occurence of travelling waves', Brown Boveri Review , vol.30 , no.9, 1943, pp. 279-286.

99 Adjaye, R.E., and Cornick, K.:'Distribution of switching surges in the line-end coils of cable-connected motors' , Proc. IEE , Electric Power Applications, vol.2, no.1, 1979, pp. 11-21.

100 Chura, V.:'Computation of surge phenomena in H.V. induction motors', Acta Technica Csav, vol.27, 1982, pp.568-584.

101 McLaren, P.G., and Oraee, H.:'Multi-conductor transmission line model for the line-end coil of large A.C. machines', Proc. IEE, vol.132, Pt.B, no.3, 1985, pp. 149-156.

102 Wedepohl, L.M.:'Applications of matrix methods to the solution of travelling wave phenomena in polyphase systems', Proc. IEE , vol. 110, no.12, 1963, pp. 2200-2212.

103 Bickford, J.P., Sanderson, J.V.H., Abdelsalem, M.M., Mohamed, S.E.T., Morias, S.A., and Olipade, O. : ' Developments in the calculation of waveforms and frequency spectra for transient fault currents and voltages', Proc. IEE, vol.127, Pt.C , no.3 , 1980, pp. 145-152.

104 Weeks, W.T.:'Multi-conductor transmission line theory in the TEM approximation,' IBM Journal of Research and Development, 2, no.1, 1972, pp. 11-21.

105 Agrawal, A.K., Fowles, H.M., Scott, L.D., and Gurbaxani, S.N. : 'Application of modal analysis to the transient response of multiconductor transmission lines with branches' , IEEE Trans. on Electromagnetic Compatibility, vol. EMC-21, no.3, 1979, pp. 256-262.

106 Bickford, J.P., Mullineux, N., and Reed, J.R.:' Computation of power system transients', IEE Monograph 18 , Peter Peregrinus , 1976, chapter 6.

Appendix A

Computer Programs

```
C     ***************************************************************
C     *  THE CURRENT AND VOLTAGE CONNECTION MATRICES AND THE        *
C     *  ADMITTANCE MATRIX FOR EACH SCATTERING JUNCTION IS          *
C     *  ENTERED FROM THE TERMINAL AND STORED ON DISK.              *
C     ***************************************************************
C
      DOUBLE PRECISION CI(20,20),CV(20,20),Y(20,20),FILE
      INTEGER M,N,NT,L,NS,NUM
      WRITE(5,10)
10    FORMAT(1H-,'ENTER THE NUMBER OF TURNS PER COIL :',$)
      READ(5,20)NT
20    FORMAT(I)
      KCOUNT = 0 ; NUM = 20
C
C     ***************************************************************
C     *       CHECK FOR THE TERMINAL JUNCTION 0                     *
C     ***************************************************************
C
22    IF (KCOUNT.GT.0) GOTO 25
      L=NT+1 ; N=(2*NT)+2
      GOTO 23
25    L=NT ; N=2*NT
C
C     ***************************************************************
C     *       ENTER JUNCTION MATRIX PARAMETERS.                     *
C     ***************************************************************
C
23    WRITE(5,26)KCOUNT
26    FORMAT(1H-,'JUNCTION NUMBER',I)
      WRITE(5,27)
27    FORMAT(1H ,'--------------------')
C
C     ***************************************************************
C     *      ENTER THE CURRENT CONNECTION MATRIX                    *
C     ***************************************************************
C
      WRITE(5,29)
29    FORMAT(1H ,'ENTER CURRENT CONNECTION MATRIX ?')
      WRITE(5,31)
31    FORMAT(1H ,'TYPE : 1- YES  OR  2- NO ')
      READ(5,32)NS
32    FORMAT(I)
      IF (NS.EQ.2) GOTO 51
      WRITE(5,30)
30    FORMAT(1HO,' CURRENT CONNECTION MATRIX DATA FILE NAME :',$)
      READ(5,45)FILE
45    FORMAT(A)
46    OPEN(UNIT=NUM,DEVICE='DSK',FILE=FILE)
      DO 50 I=1,L
      READ(5,40)(CI(I,J),J=1,N)
      WRITE(NUM,40)(CI(I,J),J=1,N)
40    FORMAT(G)
50    CONTINUE
      CLOSE(UNIT=NUM,DEVICE='DSK',FILE=FILE)
      WRITE(5,47)
47    FORMAT(1H ,'CORRECT MATRIX ?')
      WRITE(5,31)
      READ(5,32)NS
      IF (NS.EQ.1) GOTO 51
      WRITE(5,52)
52    FORMAT(1H ,'RE-ENTER THE MATRIX ELEMENTS')
      GOTO 46
51    NUM=NUM+1
```

Figure A.1 - Program to Enter Scatter Matrix Parameters - ENTER

```
C
C       ***************************************************
C       *     ENTER THE VOLTAGE CONNECTION MATRIX         *
C       ***************************************************
C
        WRITE(5,53)
53      FORMAT(1H ,'ENTER VOLTAGE CONNECTION MATRIX ?')
        WRITE(5,31)
        READ(5,32)NS
        IF (NS.EQ.2) GOTO 81
        WRITE(5,60)
60      FORMAT(1HO,'VOLTAGE CONNECTION MATRIX DATA FILE NAME:',$)
        READ(5,65)FILE
65      FORMAT(A)
66      OPEN(UNIT=NUM,DEVICE='DSK',FILE=FILE)
        DO 80 I=1,L
        READ(5,70)(CV(I,J),J=1,N)
        WRITE(NUM,70)(CV(I,J),J=1,N)
70      FORMAT(G)
80      CONTINUE
        CLOSE(UNIT=NUM,DEVICE='DSK',FILE=FILE)
        WRITE(5,47)
        WRITE(5,31)
        READ(5,32)NS
        IF (NS.EQ.1) GOTO 81
        WRITE(5,52)
        GOTO 66
81      NUM=NUM+1
C
C       ***************************************************
C       *     ENTER THE ADMITTANCE MATRIX                 *
C       ***************************************************
C
        WRITE(5,88)
88      FORMAT(1H ,'ENTER ADMITTANCE MATRIX ?')
        WRITE(5,31)
        READ(5,32)NS
        IF (NS.EQ.2) GOTO 111
        WRITE(5,90)
90      FORMAT(1HO,' ADMITTANCE MATRIX DATA FILE NAME :',$)
        READ(5,95)FILE
95      FORMAT(A)
96      OPEN(UNIT=NUM,DEVICE='DSK',FILE=FILE)
        DO 110 I=1,N
        READ(5,100)(Y(I,J),J=1,N)
        WRITE(NUM,100)(Y(I,J),J=1,N)
100     FORMAT(G)
110     CONTINUE
        CLOSE(UNIT=NUM,DEVICE='DSK',FILE=FILE)
        WRITE(5,47)
        WRITE(5,31)
        READ(5,32)NS
        IF (NS.EQ.1) GOTO 111
        WRITE(5,52)
        GOTO 96
111     NUM=NUM+1
C
C       ***************************************************
C       * REPEAT MATRIX STORAGE FOR EACH OF THE COIL JUNTIONS  *
C       ***************************************************
C
        KCOUNT=KCOUNT+1
        IF (KCOUNT.LT.5) GOTO 22
        END
```

```
C
C     ****************************************************
C     *  DEFINE ALL PROGRAM VARIABLES AND DIMENSION ARRAYS   *
C     ****************************************************
C
      REAL CI(20,20),CV(20,20),Y(20,20),A(20,20),B(20,20)
      REAL U(20,20),D(20,20),C(20,20),S(20,20),T(20,20)
      REAL AA(20,20),BB(20,20),WKSPCE(40),ST,STORE
      DOUBLE PRECISION FILE
      INTEGER IA,IB,IC,IAA,IBB,M,N,IFAIL,NT,L,NUM,CHAN
C
C     ****************************************************
C     * THIS PROGRAM FORMULATES THE MULTICONDUCTOR JUNCTION  *
C     * SCATTER MATRICES OF AN H.V. STATOR WINDING COIL.     *
C     ****************************************************
C
      WRITE(5,5)
5     FORMAT(1H-,'THIS PROGRAM FORMULATES THE MULTI-')
      WRITE(5,7)
7     FORMAT(1H ,'CONDUCTOR JUNCTION SCATTER MATRICES OF A')
      WRITE(5,8)
8     FORMAT(1H ,'STATOR WINDING COIL.')
      WRITE (5,10)
10    FORMAT(1H-,'ENTER THE NUMBER OF TURNS PER COIL :',$)
      READ(5,20)NT
20    FORMAT(I)
      KCOUNT = 0 ; NUM=20 ; CHAN=50
C
C     ****************************************************
C     *    CHECK FOR THE TERMINAL JUNCTION                *
C     ****************************************************
C
22    IF (KCOUNT.GT.0) GOTO 25
      L=NT+1 ; N=(2*NT)+2
      GOTO 23
25    L=NT ; N=2*NT
C
C     ****************************************************
C     *    ENTER JUNCTION MATRIX PARAMETERS FROM DISK      *
C     ****************************************************
C
23    WRITE(5,26)KCOUNT
26    FORMAT(1H-,'JUNCTION NUMBER',I)
      WRITE(5,27)
27    FORMAT(1H ,'------------------')
C
C     ****************************************************
C     *     ENTER THE CURRENT CONNECTION MATRIX            *
C     ****************************************************
C
      WRITE(5,30)
30    FORMAT(1HO,' CURRENT CONNECTION MATRIX DATA FILE NAME :',$:
      READ(5,45)FILE
45    FORMAT(A)
      OPEN(UNIT=NUM,DEVICE='DSK',FILE=FILE)
      DO 50 I=1,L
      READ(NUM,40)(CI(I,J),J=1,N)
40    FORMAT(G)
50    CONTINUE
      CLOSE(UNIT=NUM,DEVICE='DSK',FILE=FILE)
      NUM=NUM+1

C     ****************************************************
C     *     ENTER THE VOLTAGE CONNECTION MATRIX            *
C     ****************************************************
C
      WRITE(5,60)
60    FORMAT(1HO,'VOLTAGE CONNECTION MATRIX DATA FILE NAME:',$)
      READ(5,65)FILE
65    FORMAT(A)
      OPEN(UNIT=NUM,DEVICE='DSK',FILE=FILE)
      DO 80 I=1,L
      READ(NUM,70)(CV(I,J),J=1,N)
70    FORMAT(G)
80    CONTINUE
      CLOSE(UNIT=NUM,DEVICE='DSK',FILE=FILE)
      NUM=NUM+1
```

Figure A.2 - Program to Form Scatter Matrices - TOM

```
C
C     ****************************************************
C     *     ENTER THE ADMITTANCE MATRIX                  *
C     ****************************************************
C
      WRITE(5,90)
90    FORMAT(1H0,' ADMITTANCE MATRIX DATA FILE NAME :',$)
      READ(5,95)FILE
95    FORMAT(A)
      OPEN(UNIT=NUM,DEVICE='DSK',FILE=FILE)
      DO 110 I=1,N
      READ(NUM,100)(Y(I,J),J=1,N)
100   FORMAT(G)
110   CONTINUE
      CLOSE(UNIT=NUM,DEVICE='DSK',FILE=FILE)
      NUM=NUM+1
C
C     ****************************************************
C     *          FORM THE INTERMEDIATE MATRICES :        *
C     *                                                  *
C     *            MULTIPLY MATRICES CI & Y              *
C     ****************************************************
C
      DO 149 I=1,L
      DO 149 J=1,N
      D(I,J)=0.0
149   CONTINUE
      ST=0.0 ; STORE=0.0 ; TEMP=0.0 ; TOL=0.0
      DO 150 I=1,L
      DO 150 J=1,N
      DO 150 K=1,N
      ST = CI(I,K)*Y(K,J)
      D(I,J) = D(I,J) + ST
150   CONTINUE
C
C     ****************************************************
C     *   FORM FIRST SUB-MATRIX OF SCATTER MATRIX        *
C     ****************************************************
C
      DO 160 I=1,N
      DO 160 J=1,N
      U(I,J)=0.0
160   CONTINUE
      DO 170 I=1,L
      DO 170 J=1,N
      U(I,J) = CV(I,J)
170   CONTINUE
      DO 180 I=1,L
      DO 180 J=1,N
      U(I+L,J) = D(I,J)
180   CONTINUE
C
C     ****************************************************
C     *   FORM SECOND SUB-MATRIX OF SCATTER MATRIX       *
C     *                                                  *
C     *   INVERT THE VOLTAGE CONNECTION MATRIX           *
C     ****************************************************
C
      DO 195 I=1,N
      DO 195 J=1,N
      A(I,J)=0.0
195   CONTINUE
      DO 190 I=1,L
      DO 190 J=1,N
      A(I,J) = -CV(I,J)
190   CONTINUE
      DO 200 I=1,L
      DO 200 J=1,N
      A(I+L,J)=D(I,J)
200   CONTINUE
      DO 999 I=1,N
      WRITE(5,991)A(I,1),A(I,2),A(I,3),A(I,4),A(I,5),A(I,6),A(I,7)
     &,A(I,8),A(I,9),A(I,10),A(I,11),A(I,12),A(I,13),A(I,14),A(I,15)
     &,A(I,16)
991   FORMAT(16F8.5)
999   CONTINUE
C
```

```
C     ***************************************************************
C     *       INVERT SCATTER SUB-MATRIX A(I,J)                      *
C     *                                                             *
C     *       INITIALISE SUBROUTINE PARAMETERS                      *
C     ***************************************************************
C
C     ***************************************************************
C     *  FORM THE UNIT MATRIX B WITH M RIGHT-HAND SIDES             *
C     ***************************************************************
C
      DO 201 I=1,N
      DO 201 J=1,N
      B(I,J)=0
      IF (I.EQ.J) GOTO 202
      GOTO 201
202   B(I,J)=1.0
201   CONTINUE
C
C     ***************************************************************
C     * DIMENSION MATRICES A ,B ,C ,AA ,BB                          *
C     ***************************************************************
C
      IA=20 ; IB=20 ; IC=20 ; IAA=20 ; IBB=20 ; M=N
C
C     ***************************************************************
C     *   INTEGER IFAIL CONTAINS ERROR CODE FOR F04AEF              *
C     *  0- NO ERROR, 1- ROUNDING ERROR, 2- ILL CONDITIONED         *
C     ***************************************************************
C
      IFAIL=1
C
C     ***************************************************************
C     *    CALL MATRIX INVERSION SUBROUTINE F04AEF                  *
C     ***************************************************************
C
      CALL F04AEF(A,IA,B,IB,N,M,C,IC,WKSPCE,AA,IAA,BB,IBB,IFAIL)
C
C     ***************************************************************
C     *    CHECK FOR FAILURE OF LIBRARY ROUTINE F04AEF              *
C     ***************************************************************
      IF (IFAIL.EQ.0) GOTO 101
      WRITE(5,98) IFAIL
98    FORMAT(1H ,'ERROR IN F04AEF : ',I)
      GOTO 280
C
C     ***************************************************************
C     *   FORM THE SCATTER JUNCTION MATRIX S(I,J)                   *
C     ***************************************************************
C
101   DO 209 I=1,N
      DO 209 J=1,N
      S(I,J)=0.0
209   CONTINUE
      DO 210 I=1,N
      DO 210 J=1,N
      DO 210 K=1,N
      STORE = C(I,K)*U(K,J)
      S(I,J) = S(I,J) + STORE
210   CONTINUE
C
C     ***************************************************************
C     * CHECK ON INVERSION ACCURACY USING A.A-1=I                   *
C     ***************************************************************
C
      DO 78 I=1,N
      DO 78 J=1,N
      T(I,J)=0.0
78    CONTINUE
      DO 77 I=1,N
      DO 77 J=1,N
      DO 77 K=1,N
      TEMP=C(I,K)*A(K,J)
      T(I,J)=T(I,J)+TEMP
      IF (K.LT.N) GOTO 77
      IF (I.EQ.J) GOTO 77
      IF (ABS(T(I,J)).LT.TOL) GOTO 77
      TOL=ABS(T(I,J))
77    CONTINUE
      WRITE(5,88)TOL
88    FORMAT(1H ,'MAXIMUM OFF DIAGONAL ELEMENT :',G)
```

```
C
C       ***************************************************************
C       *     ASK FOR THE DATA FILE NAME FOR THE JUNCTION              *
C       ***************************************************************
C
        WRITE(5,250)
250     FORMAT(1H ,1H ,1H ,'GIVE A NAME FOR THE DATA FILE :',$)
        READ(5,260)FILE
260     FORMAT(A)
C
C       ***************************************************************
C       *   OPEN THE DATA FILE FOR SCATTER MATRIX DATA                *
C       ***************************************************************
C
        OPEN(UNIT=CHAN,DEVICE='DSK',FILE=FILE)
        DO 270 I=1,N
        WRITE(CHAN,265)(S(I,J),J=1,N)
265     FORMAT(G)
270     CONTINUE
C
C       ***************************************************************
C       *   CLOSE THE DATA FILE AND SAVE THE DATA ON DISK             *
C       ***************************************************************
C
        CLOSE(UNIT=CHAN,DEVICE='DSK',FILE=FILE)


        CHAN=CHAN+1
C
C       ***************************************************************
C       *   REPEAT PROCESS FOR THE NEXT SCATTER JUNCTION              *
C       ***************************************************************
C
280     KCOUNT = KCOUNT+1
        IF (KCOUNT.LT.5) GOTO 22
        END
```

```
C
C     ****************************************************
C     *  THIS PROGRAM CALCULATES THE RESPONSE OF A SINGLE  *
C     *  STATOR COIL TO AN IMPULSE FUNCTION USING THE      *
C     *  BEWLEY LATTICE TECHNIQUE WITH SCATTER MATRIX      *
C     *  THEORY.                                           *
C     ****************************************************
C
C     ****************************************************
C     * DIMENSION ARRAYS AND INITIALISE PROGRAM VARIABLES.*
C     ****************************************************
C
      COMMON/BLOCK1/STORE(20,5000),STACK,TIME
      COMMON/BLOCK2/VIN(20)
      COMMON/BLOCK3/VRE(20)
      DIMENSION S0(20,20),S1(20,20),S2(20,20)
      DIMENSION S3(20,20),S4(20,20),S(20,20)
      REAL TIME,TIMEND,T0,T1,T2,T3,TEMP,JUNC,JUNCT,TEMPO
      INTEGER L,N,CHAN,STACK,POINT,K1,K2,J1,J2,ADD,MARK,M,STEP,INC,N
       CHAN=50
C
C     ****************************************************
C     * INITIALISE IMPULSE FUNCTION ON TERMINAL JUNCTION 0*
C     ****************************************************
C
      VIN(1)=1.0
      DO 5 I=2,20
      VIN(I)=0
5     CONTINUE
C
C     ****************************************************
C     * ENTER THE NUMBER OF TURNS IN A STATOR COIL.       *
C     ****************************************************
C
      WRITE(5,6)
6     FORMAT(1H-,'ENTER THE NO. OF TURNS IN A COIL ......',$)
      READ(5,30)NT
      N=2*NT ; L=(2*NT)+2
C
C     ****************************************************
C     * ENTER TRANSIT TIMES FOR EACH OF THE COIL SECTIONS *
C     ****************************************************
C
      WRITE(5,7)
7     FORMAT(1HO,'ENTER TRANSIT TIME BETWEEN SOURCE AND ')
      WRITE(5,8)
8     FORMAT(1H ,'JUNCTION 1 .........',$)
      READ(5,30)T0
      WRITE(5,10)
10    FORMAT(1HO,'ENTER TRANSIT TIME BETWEEN JUNCTION 1 AND')
      WRITE(5,20)
20    FORMAT(1H ,'JUNCTIONS 2 & 5 ......... ',$)
      READ(5,30)T1
30    FORMAT(G)
      WRITE(5,40)
40    FORMAT(1HO,'ENTER TRANSIT TIME BETWEEN JUNCTIONS 2 & 3')
      WRITE(5,50)
50    FORMAT(1H ,'AND JUNCTIONS 4 & 5 ......... ',$)

      READ(5,30)T2
      WRITE(5,60)
60    FORMAT(1HO,'ENTER TRANSIT TIME BETWEEN JUNCTIONS 3 & 4 .......'
$)
      READ(5,30)T3
C
C     ****************************************************
C     * ENTER MAXIMUM TIME LIMIT FOR THE SIMULATION.      *
C     ****************************************************
C
      WRITE(5,70)
70    FORMAT(1HO,'ENTER TIME LIMIT ON SIMULATION ......... ',$)
      READ(5,30)TIMEND
C
C     ****************************************************
C     * READ IN ALL JUNCTION SCATTER MATRICES FROM DISK DATA *
C     * FILES AND STORE THEM IN SEPARATE ARRAYS ; S0, S1, S2 *
C     * S3, S4.                                           *
C     ****************************************************
C
```

Figure A.3 - Program to Find Impulse Response of Coil - IMPL1

```
C       READ IN SCAT0.DAT AND TRANSFER S TO S0
C
        OPEN(UNIT=CHAN,DEVICE='DSK',FILE='SCAT0.DAT')
        DO 80 I=1,L
        DO 80 J=1,L
        READ(CHAN,85)S(I,J)
85      FORMAT(G)
        S0(I,J)=S(I,J)
80      CONTINUE
        CLOSE(UNIT=CHAN,DEVICE='DSK',FILE='SCAT0.DAT')
        CHAN=CHAN+1
C
C       READ IN SCAT1.DAT AND TRANSFER S TO S1
C
        OPEN(UNIT=CHAN,DEVICE='DSK',FILE='SCAT1.DAT')
        DO 90 I=1,N
        DO 90 J=1,N
        READ(CHAN,95)S(I,J)
95      FORMAT(G)
        S1(I,J)=S(I,J)
90      CONTINUE
        CLOSE(UNIT=CHAN,DEVICE='DSK',FILE='SCAT1.DAT')
        CHAN=CHAN+1
C
C       READ IN SCAT2.DAT AND TRANSFER S TO S2
C
        OPEN(UNIT=CHAN,DEVICE='DSK',FILE='SCAT2.DAT')
        DO 100 I=1,N
        DO 100 J=1,N
        READ(CHAN,105)S(I,J)
105     FORMAT(G)
        S2(I,J)=S(I,J)
100     CONTINUE
        CLOSE(UNIT=CHAN,DEVICE='DSK',FILE='SCAT2.DAT')
        CHAN=CHAN+1
C
C       READ IN SCAT3.DAT AND TRANSFER S TO S3
C
        OPEN(UNIT=CHAN,DEVICE='DSK',FILE='SCAT3.DAT')
        DO 110 I=1,N
        DO 110 J=1,N
        READ(CHAN,115)S(I,J)
115     FORMAT(G)
        S3(I,J)=S(I,J)
110     CONTINUE
        CLOSE(UNIT=CHAN,DEVICE='DSK',FILE='SCAT3.DAT')

        CHAN=CHAN+1
C
C       READ IN SCAT4.DAT AND TRANSFER S TO S4
C
        OPEN(UNIT=CHAN,DEVICE='DSK',FILE='SCAT4.DAT')
        DO 120 I=1,N
        DO 120 J=1,N
        READ(CHAN,125)S(I,J)
125     FORMAT(G)
        S4(I,J)=S(I,J)
120     CONTINUE
        CLOSE(UNIT=CHAN,DEVICE='DSK',FILE='SCAT4.DAT')
        CHAN=CHAN+1

C
C       ***************************************************
C       * SET UP STACK AND STORE ENTRY POINTERS AND       *
C       * PLACE THE INPUT IMPULSE VECTOR VIN 'STORE'.     *
C       ***************************************************
C
        POINT=1 ; STACK=1
        STORE(1,1)=1.0
        STORE(2,1)= T0
        DO 121 I=1,16
        STORE(I+2,1)=VIN(I)
121     CONTINUE
C       :
```

```
C     ************************************************************
C     * SEARCH FOR THE NEXT JUNCTION SCATTERING OPERATION TO     *
C     * TAKE PLACE IN TIME .                                     *
C     ************************************************************
C
      TIME=T0
77    DO 130 I=POINT,STACK
      TEMPO=ABS(STORE(2,I))
      DIFF=ABS(TEMPO - TIME)
      IF (DIFF.LT.0.0001) GOTO 132
130   CONTINUE
      TIME=TIME +0.2 ; POINT=1
      GOTO 77
132   JUNC=STORE(1,I) ; MARK=I
      IF (JUNC.NE.6.0) GOTO 133
      POINT=MARK+1
      GOTO 77

C
C     ************************************************************
C     * PLACE ENTRY FROM STORE IN THE INCIDENT IMPULSE           *
C     * VOLTAGE VECTOR VIN AND SET TIME EQUAL TO TMIN.           *
C     ************************************************************
C
133   DO 140 I=1,16
      VIN(I)=0.0
      IF (JUNC.EQ.1.0) GOTO 145
      IF (JUNC.EQ.0.0) GOTO 145
      VIN(I) = STORE(I+3,MARK)
      GOTO 140
145   VIN(I) = STORE(I+2,MARK)
140   CONTINUE
C
C     ************************************************************
C     * FIND OTHER IMPULSE WAVES THAT ARRIVE AT THE JUNCTION     *
C     * SIMULTANEOUSLY AND ADD THESE TO IMPULSES IN VIN.         *
C     ************************************************************
C
88    DO 155 I=MARK+1,STACK

      SUB=ABS(STORE(2,I)-TIME)
      IF (STORE(1,I).NE.JUNC) GOTO 155
      IF (SUB.GT.0.1) GOTO 155
      DO 160 K=1,16
      IF (JUNC.EQ.1.0) GOTO 165
      IF (JUNC.EQ.0.0) GOTO 165
      VIN(K) = VIN(K) + STORE(K+3,I)
      STORE(K+3,MARK)=STORE(K+3,MARK) + STORE(K+3,I)
      GOTO 160
165   VIN(K) = VIN(K) + STORE(K+2,I)
      STORE(K+2,MARK)=STORE(K+2,MARK) + STORE(K+2,I)
160   CONTINUE
      LOCK=I
      DO 157 K=LOCK,STACK-1
      DO 157 J=1,20
      STORE(J,K)=STORE(J,K+1)
157   CONTINUE
      DO 158 J=1,20
      STORE(J,STACK)=0.0
158   CONTINUE
      STACK=STACK-1
      GOTO 88
155   CONTINUE
      POINT=MARK+1
C
C     ************************************************************
C     * MULTIPLY INCIDENT IMPULSE VOLTAGE VECTOR VIN WITH        *
C     * THE JUNCTION SCATTER MATRIX TO FIND THE REFLECTED        *
C     * VOLTAGE VECTOR VRE .                                     *
C     ************************************************************
C

      IF (JUNC.EQ.1.0) CALL TIMES(S0,L)
      IF (JUNC.EQ.2.0) CALL TIMES(S1,N)
      IF (JUNC.EQ.3.0) CALL TIMES(S2,N)
      IF (JUNC.EQ.4.0) CALL TIMES(S3,N)
      IF (JUNC.EQ.5.0) CALL TIMES(S4,N)
```

```
C
C       ************************************************************
C       * SEND THE REFLECTED IMPULSE VOLTAGES VRE TO THE           *
C       * APPROPRIATE JUNCTIONS AND STORE THEM IN 'STORE'.         *
C       ************************************************************
C
        IF (JUNC.EQ.0.0) GOTO 170
        IF (JUNC.EQ.1.0) GOTO 180
        IF (JUNC.EQ.2.0) GOTO 190
        IF (JUNC.EQ.3.0) GOTO 200
        IF (JUNC.EQ.4.0) GOTO 210
        IF (JUNC.EQ.5.0) GOTO 220
C
C       ************************************************************
C       * REFLECTIONS FROM THE SOURCE TRAVEL TO JUNCTION 1         *
C       * WITH A TRANSIT TIME TO.                                  *
C       ************************************************************
C
170     CALL STORE0(T0,1.0)
        GOTO 99
C
C       ************************************************************
C       * REFLECTIONS FROM JUNCTION 1 TRAVEL TO JUNCTIONS 0        *
C       * 2 & 5 WITH TRANSIT TIMES T0,T2 & T5.                     *
C       ************************************************************
C
180     CALL STORE1(T0,0.0)
        CALL STORE2(T1,2.0,4,10,11,17,-2,1,0)
        CALL STORE2(T1,5.0,17,11,4,10,-8,-1,1)
        CALL STORE6(0.0,6.0)

        GOTO 99
C
C       ************************************************************
C       * REFLECTIONS FROM JUNCTION 2 TRAVEL TO JUNCTIONS 1 & 3    *
C       * WITH TRANSIT TIMES T1 & T2.                              *
C       ************************************************************
C
190     CALL STORE2(T1,1.0,4,10,11,17,-3,1,0)
        CALL STORE2(T2,3.0,4,10,11,17,4,1,0)
        GOTO 99
C
C       ************************************************************
C       * REFLECTIONS FROM JUNTION 3 TRAVEL TO JUNCTIONS :         *
C       * 2 & 4 WITH TRANSIT TIMES T2 & T3 RESPECTIVELY.           *
C       ************************************************************
C
200     CALL STORE2(T2,2.0,11,17,4,10,-10,1,0)
        CALL STORE2(T3,4.0,10,4,11,17,-2,-1,1)
        GOTO 99
C
C       ************************************************************
C       * REFLECTIONS FROM JUNCTION 4 TRAVEL TO JUNCTIONS:         *
C       * 3 & 5 WITH TRANSIT TIMES T3 & T2 RESPECTIVELY.           *
C       ************************************************************
C
210     CALL STORE2(T3,3.0,17,11,4,10,-16,-1,1)
        CALL STORE2(T2,5.0,4,10,11,17,4,1,0)
        GOTO 99
C
C       ************************************************************
C       * REFLECTIONS FROM JUNCTION 5 TRAVEL TO JUNCTIONS:         *
C       * 1 & 4 WITH TRANSIT TIMES T1 & T2 RESPECTIVELY.           *
C       ************************************************************
C
220     CALL STORE2(T1,1.0,17,11,4,10,-9,-1,1)
        CALL STORE2(T2,4.0,11,17,4,10,-10,1,0)
        GOTO 99
C
C       ************************************************************
C       * CHECK FOR STOPPING CRITERIA .                            *
C       ************************************************************
C
99      IF (TIME.GT.TIMEND) GOTO 230
        IF (STACK.GT.4999)  GOTO 230
        GOTO 77
```

```
C
C       ************************************************************
C       * PLACE ARRAY 'STORE' IN A DATA FILE 'RESPONSE'.           *
C       ************************************************************
C
230     WRITE(5,221)
221     FORMAT(1H-,'CHOOSE THE POSITION ON THE COIL WHICH')
        WRITE(5,222)
222     FORMAT(1H ,'IS TO BE ANALYSED.')
        WRITE(5,223)
223     FORMAT(1H ,'ENTER JUNCTION NUMBER .........',$)
        READ(5,235)JUNC
        OPEN(UNIT=CHAN,DEVICE='DSK',FILE='RESPONSE')
        WRITE(CHAN,235)JUNC
        WRITE(CHAN,235)TIMEND
        WRITE(CHAN,350)STACK
235     FORMAT(G)
        KCOUNT=0
        DO 240 I=1,STACK
        IF (STORE(1,I).NE.JUNC) GOTO 240
        KCOUNT=KCOUNT+1
240     CONTINUE
        WRITE(CHAN,350)KCOUNT
350     FORMAT(I)
        DO 290 I=1,STACK
        IF (STORE(1,I).NE.JUNC) GOTO 290
        WRITE(CHAN,295)(STORE(J,I),J=1,20)
295     FORMAT(G)
290     CONTINUE
        CLOSE(UNIT=CHAN,DEVICE='DSK',FILE='RESPONSE')
        WRITE(5,310)TIMEND
310     FORMAT(1H-,'FOR A SIMULATION TIME.......',F4.1)
        WRITE(5,320)STACK
320     FORMAT(1H ,'THE NO. OF ENTRIES IN "STORE" WERE......',I)
        WRITE(5,330)JUNC
330     FORMAT(1H ,'AT JUNCTION .........',F3.1)
        WRITE(5,340)KCOUNT
340     FORMAT(1H ,'THE NO. OF ENTRIES WERE .......',I)
        END
```

```
C       ************************************************************
C       * SUBROUTINE TO MULTIPLY INCIDENT VOLTAGE VECTOR WITH      *
C       * THE APPROPRIATE JUNCTION SCATTER MATRIX TO GIVE THE      *
C       * REFLECTED VOLTAGE VECTOR.                                *
C       ************************************************************
C
        SUBROUTINE TIMES(S,NO)
        DIMENSION S(20,20)
        COMMON/BLOCK2/VIN(20)
        COMMON/BLOCK3/VRE(20)
        REAL TEMP
        TEMP=0.0
C       RESET REFLECTED VOLTAGE ARRAY VRE.
        DO 300 J=1,20
        VRE(J)=0.0
300     CONTINUE
        DO 500 I=1,NO
        DO 500 J=1,NO
        TEMP = S(I,J)*VIN(J)
        VRE(I) = VRE(I) + TEMP
500     CONTINUE
        RETURN
        END
```

```
C
C     ************************************************************
C     * THE FOLLOWING SET OF SUBROUTINES STORE THE REFLECTED     *
C     * IMPULSE WAVES IN 'STORE' ALONG WITH THE JUNCTION TO      *
C     * WHICH THEY TRAVEL AND THE TIME OF ARRIVAL THERE.         *
C     ************************************************************
C
      SUBROUTINE STORE0(T,JUNCT)

      COMMON/BLOCK1/STORE(20,5000),STACK,TIME
      COMMON/BLOCK2/VIN(20)
      INTEGER STACK
      REAL TIME,T,JUNCT
      STACK=STACK+1
      STORE(1,STACK)=JUNCT
      STORE(2,STACK)= TIME + T
      STORE(3,STACK)= VIN(1)
      DO 250 K=4,18
      STORE(K,STACK)= 0.0
  250 CONTINUE
      RETURN
      END

      SUBROUTINE STORE1(T,JUNCT)

      COMMON/BLOCK1/STORE(20,5000),STACK,TIME
      COMMON/BLOCK3/VRE(20)
      INTEGER STACK
      REAL TIME,T,JUNCT
      STACK=STACK+1
      STORE(1,STACK)= JUNCT
      STORE(2,STACK)= TIME + T
      STORE(3,STACK)= VRE(1)
      DO 260 K=2,16
      STORE(K+2,STACK)=0.0
  260 CONTINUE
      RETURN
      END

      SUBROUTINE STORE2(T,JUNCT,K1,K2,J1,J2,M,STEP,INC)
      COMMON/BLOCK1/STORE(20,5000),STACK,TIME
      COMMON/BLOCK3/VRE(20)
      INTEGER STACK,M,INC,STEP,ADD
      REAL TIME,T,JUNCT
      STACK=STACK+1
      STORE(1,STACK)= JUNCT
      STORE(2,STACK)= TIME + T
      ADD = 0
      DO 270 K=K1,K2,STEP
      STORE(K,STACK) = VRE(K+M+ADD)
      ADD=ADD+INC+INC
  270 CONTINUE
      DO 280 J=J1,J2
      STORE(J,STACK)= 0.0
  280 CONTINUE
      RETURN
      END

      SUBROUTINE STORE6(T,JUNCT)

      COMMON/BLOCK1/STORE(20,5000),STACK,TIME
      COMMON/BLOCK3/VRE(20)
      INTEGER STACK
      REAL TIME,T,JUNCT
      STACK=STACK+1
      STORE(1,STACK)= JUNCT
      STORE(2,STACK)= TIME+T
      STORE(18,STACK)= VRE(16)
      RETURN
      END
```

```
C
C       ************************************************************
C       * THIS PROGRAM PERFORMS A TIME DOMAIN CONVOLUTION OF       *
C       * THE IMPULSE RESPONSE OF STATOR COIL MULTI-CONDUCTOR      *
C       * TRANSMISSION LINE WITH AN INPUT IMPULSE FUNCTION OF      *
C       * ANY GENERAL FORM TO GIVE THE OUTPUT FUNCTION.            *
C       ************************************************************
C
        DIMENSION STORE(20,2000),TIMES(50)
        COMMON/BLOCK1/TEMPT(1000),TEMPO(1000),TIME(50000),OUT(50000)
        COMMON/BLOCK2/NUM,KPILE,NPILE,IN,KC1
        DOUBLE PRECISION FILE
        INTEGER CHAN,STACK,NPILE,KPILE,NUM,IN,KC1,KC2
        REAL INPUT(50),TIMEND,JUNC,PROD
C
C       ************************************************************
C       * READ THE IMPULSE RESPONSE FROM DATA FILE 'RESPONSE'      *
C       ************************************************************
C
        CHAN=55
        OPEN(UNIT=CHAN,DEVICE='DSK',FILE='RESPONSE.DAT')
        READ(CHAN,21)JUNC
        READ(CHAN,21)TIMEND
        READ(CHAN,15)STACK
        READ(CHAN,15)KCOUNT
21      FORMAT(G)
15      FORMAT(I)
        DO 10 I=1,KCOUNT
        READ(CHAN,20)(STORE(J,I),J=1,20)
20      FORMAT(G)
10      CONTINUE
        CLOSE(UNIT=CHAN,DEVICE='DSK',FILE='RESPONSE.DAT')
        CHAN=CHAN+1
C
C       ************************************************************
C       * READ THE INPUT FUNCTION FROM DATA FILE 'INPUT'.          *
C       ************************************************************
C
        OPEN(UNIT=CHAN,DEVICE='DSK',FILE='INPUT')
        READ(CHAN,25)KTOP
25      FORMAT(I)
        DO 30 I=1,KTOP
        READ(CHAN,40)INPUT(I),TIMES(I)
40      FORMAT(2G)
30      CONTINUE
        CLOSE(UNIT=CHAN,DEVICE='DSK',FILE='INPUT')

        WRITE(5,41)TIMEND
41      FORMAT(1H-,'FOR A SIMULATION TIME OF.......',F5.1)
        WRITE(5,42)STACK
42      FORMAT(1H ,'THE NO. OF ENTRIES IN 'STORE' WERE.....',I)
        WRITE(5,43)JUNC
43      FORMAT(1H ,'AT JUNCTION........',F3.1)
        WRITE(5,44)KCOUNT
44      FORMAT(1H ,'THE NO. OF IMPULSES WERE.......',I)
        IF (JUNC.EQ.6.0) NTURN=18
        IF (JUNC.EQ.0.0) NTURN=3
        GOTO 55
        WRITE(5,46)
46      FORMAT(1H-,'ENTER COIL TURN NO. TO BE ANALYSED.....',$)
        READ(5,47)NT
47      FORMAT(I)
        NTURN=NT+2
```

Figure A.4 - Program to Perform
Convolution - CONVL

```
C
C       ************************************************************
C       * CONVOLUTION OF INPUT FUNCTION WITH IMPULSE RESPONSE.     *
C       ************************************************************
C
55      NPILE=0 ; NUM=0 ; KPILE=0
        WRITE(5,222)NTURN
222     FORMAT(I)
        DO 50 IN=1,KTOP
        DO 60 K=1,KCOUNT
        TMOD=ABS(STORE(NTURN,K))
        IF (TMOD.GT.0.0000001) GOTO 65
        NTURN=NT+9
65      PROD=INPUT(IN)*STORE(NTURN,K)
        IF (ABS(PROD).LT.0.001) GOTO 60
        TEMPO(K)=PROD
        TEMPT(K)=STORE(2,K)+TIMES(IN)
        WRITE(5,888)TEMPO(K),TEMPT(K)
888     FORMAT(3X,G,3X,G)
        NUM=NUM+1
60      CONTINUE
        CALL SORT
50      CONTINUE

C
C       ************************************************************
C       * ADD SIMULTANEOUS IMPULSES IN THE OUTPUT RESPONSE.        *
C       ************************************************************
C
        GOTO 555
        DO 70 I=1,KPILE-1
        SUB=ABS(TIME(I)-TIME(I+1))
        IF (SUB.GT.0.1) GOTO 70
        OUT(I)=OUT(I)+OUT(I+1)
        OUT(I+1)=0.0 ; TIME(I+1)=0.0
        DO 80 J=I+1,KPILE
        OUT(J)=OUT(J+1)
        TIME(J)=TIME(J+1)
80      CONTINUE
70      CONTINUE
C
C       ************************************************************
C       * FILTER THE OUTPUT FUNCTION BEFORE IT IS PLOTTED.         *
C       ************************************************************
C
555     DO 77 I=1,200
        WRITE(5,88)TIME(I),OUT(I)
88      FORMAT(2G)
77      CONTINUE

        END
C
C       ************************************************************
C       * SUBROUTINE TO ARRANGE IMPULSES IN CHRONOLOGICAL ORDER*
C       ************************************************************
C
        SUBROUTINE SORT
        COMMON/BLOCK1/TEMPT(1000),TEMPO(1000),TIME(50000),OUT(50000)
        COMMON/BLOCK2/NUM,KPILE,NPILE,IN,KC1
        INTEGER NUM,NPILE,KPILE,IN,KC1,KC2
        KC2=1 ; KC1=1 ; NPILE=NPILE+NUM
        IF (IN.EQ.1) GOTO 100
        WRITE(5,111)IN,NUM
111     FORMAT(2I)
        GOTO 120
110     KC1=KC1+1
130     IF (KC1.GT.KPILE) GOTO 100
120     IF (TEMPT(KC2).GT.TIME(KC1)) GOTO 110
        DO 140 I=NPILE,KC1
        TIME(I+1)=TIME(I)
        OUT(I+1)=OUT(I)
140     CONTINUE
        TIME(KC1)=TEMPT(KC2)
        OUT(KC1)=TEMPO(KC2)
        KC2=KC2+1 ; KPILE=KPILE+1
        GOTO 120
100     DO 150 J=KC1,NPILE
        TIME(J)=TEMPT(KC2)
        OUT(J)=TEMPO(KC2)
        KC2=KC2+1 ; KPILE=KPILE+1
150     CONTINUE
```

```
      NUM=0
      DO 1000 J=1,NFILE
      WRITE(5,1001)OUT(J),TIME(J)
1001  FORMAT(3X,F15.12,3X,F15.12)
1000  CONTINUE
      RETURN
      END
```

```
C
C     ************************************************************
C     * THIS PROGRAM FORMULATES THE INPUT IMPULSE FUNCTION       *
C     * FOR USE IN THE CONVOLUTION PROGRAM 'CONVL'.              *
C     ************************************************************
C
      REAL INPUT(50),TIMES(50)
      DOUBLE PRECISION FILE
      INTEGER CHAN
      CHAN=56
      WRITE(5,10)
10    FORMAT(1H-,'THIS PROGRAM FORMULATES THE INPUT IMPULSE')
      WRITE(5,20)
20    FORMAT(1H ,'FUNCTION FOR USE IN THE CONVOLUTION PROGRAM.')
      WRITE(5,30)
30    FORMAT(1H-,'ENTER THE NO. OF IMPULSES WHICH FORM')
      WRITE(5,31)
31    FORMAT(1H ,'THE INPUT FUNCTION :',1)
      READ(5,35)N
35    FORMAT(I)
      WRITE(5,40)
40    FORMAT(1H-,'ENTER THE MAGNITUDE AND TIME OF EACH IMPULSE WHI
      WRITE(5,50)
50    FORMAT(1H ,'FORM THE INPUT FUNCTION ,ONE AT A TIME :')
      DO 60 I=1,N
      READ(5,45)INPUT(I),TIMES(I)
45    FORMAT(2G)
60    CONTINUE
C
C     ************************************************************
C     * STORE THESE VALUES IN A DATA FILE 'INPUT'.               *
C     ************************************************************
C
      KTOP=N
      OPEN(UNIT=CHAN,DEVICE='DSK',FILE='INPUT')
      WRITE(CHAN,75)KTOP
75    FORMAT(I)
      DO 70 I=1,N
      WRITE(CHAN,80)INPUT(I),TIMES(I)
80    FORMAT(2G)
70    CONTINUE
      CLOSE(UNIT=CHAN,DEVICE='DSK',FILE='INPUT')
      END
```

Figure A.5 - Program to Form Input
Impulse Function - INPUT

Appendix B

Scatter Matrices

```
PROGRAM TO PRINT SCATTER MATRICES.
ENTER NO. OF COIL TURNS !?

ENTER DATA FILE NAME !SCAT0
```

(Junction 1)

```
 -0.02036 1.02036-0.47559 0.00000 0.00000 0.00000 0.00000-0.17582 0.47559 0.00000 0.00000 0.00000 0.00000 0.17582-0.34360 0.34360
  0.97964 0.02036-0.47559 0.00000 0.00000 0.00000 0.00000-0.17582 0.47559 0.00000 0.00000 0.00000 0.00000 0.17582-0.34360 0.34360
  0.77775-0.77775 0.39798 0.00000 0.00000 0.00000 0.00000-0.22256 0.60202 0.00000 0.00000 0.00000 0.00000 0.22256-0.43494 0.43494
  0.69478-0.69478 0.35552 0.00000 0.00000 0.00000 0.00000-0.25108-0.35552 1.00000 0.00000 0.00000 0.00000 0.25108-0.49066 0.49066
  0.61984-0.61984 0.31717 0.00000 0.00000 0.00000 0.00000-0.28249-0.31718 0.00000 1.00000 0.00000 0.00000 0.28249-0.55206 0.55206
  0.55206-0.55206 0.28249 0.00000 0.00000 0.00000 0.00000-0.31718-0.28249 0.00000 0.00000 1.00000 0.00000 0.31717-0.61984 0.61984
  0.49066-0.49066 0.25108 0.00000 0.00000 0.00000 0.00000-0.35552-0.25108 0.00000 0.00000 0.00000 1.00000 0.35552-0.69478 0.69478
  0.43494-0.43494 0.22256 0.00000 0.00000 0.00000 0.00000-0.39798-0.22256 0.00000 0.00000 0.00000 0.00000 1.39798-0.77775 0.77775
  0.77775-0.77775 1.39798 0.00000 0.00000 0.00000 0.00000-0.22256-0.39798 0.00000 0.00000 0.00000 0.00000 0.22256-0.43494 0.43494
  0.69478-0.69478 0.35552 1.00000 0.00000 0.00000 0.00000-0.25108-0.35552 0.00000 0.00000 0.00000 0.00000 0.25108-0.49066 0.49066
  0.61984-0.61984 0.31717 0.00000 1.00000 0.00000 0.00000-0.28249-0.31718 0.00000 0.00000 0.00000 0.00000 0.28249-0.55206 0.55206
  0.55206-0.55206 0.28249 0.00000 0.00000 1.00000 0.00000-0.31718-0.28249 0.00000 0.00000 0.00000 0.00000 0.31717-0.61984 0.61984
  0.49066-0.49066 0.25108 0.00000 0.00000 0.00000 1.00000-0.35552-0.25108 0.00000 0.00000 0.00000 0.00000 0.35552-0.69478 0.69478
  0.43494-0.43494 0.22256 0.00000 0.00000 0.00000 0.00000 0.60202-0.22256 0.00000 0.00000 0.00000 0.00000 0.39798-0.77775 0.77775
  0.34360-0.34360 0.17582 0.00000 0.00000 0.00000 0.00000 0.47559-0.17582 0.00000 0.00000 0.00000 0.00000-0.47559 0.02036 0.97964
  0.34360-0.34360 0.17582 0.00000 0.00000 0.00000 0.00000 0.47559-0.17582 0.00000 0.00000 0.00000 0.00000-0.47559 1.02036-0.02036

ENTER DATA FILE NAME !SCAT1
```

(Junction 2)

```
 -0.42870-0.14552-0.10160-0.07147-0.05104-0.03753-0.05966 1.42870 0.14552 0.10160 0.07147 0.05104 0.03753 0.05966 0.00000 0.00000
 -0.29823-0.18759-0.13097-0.09213-0.06579-0.04838-0.07691 0.29823 1.18759 0.13097 0.09213 0.06579 0.04838 0.07691 0.00000 0.00000
 -0.20822-0.13097-0.17812-0.12529-0.08947-0.06579-0.10459 0.20822 0.13097 1.17812 0.12529 0.08947 0.06579 0.10459 0.00000 0.00000
 -0.14647-0.09213-0.12529-0.17546-0.12529-0.09213-0.14647 0.14647 0.09213 0.12529 1.17546 0.12529 0.09213 0.14647 0.00000 0.00000
 -0.10459-0.06579-0.08947-0.12529-0.17812-0.13097-0.20822 0.10459 0.06579 0.08947 0.12529 1.17812 0.13097 0.20822 0.00000 0.00000
 -0.07691-0.04838-0.06579-0.09213-0.13097-0.18759-0.29823 0.07691 0.04838 0.06579 0.09213 0.13097 1.18759 0.29823 0.00000 0.00000
 -0.05966-0.03753-0.05104-0.07147-0.10160-0.14552-0.42870 0.05966 0.03753 0.05104 0.07147 0.10160 0.14552 1.42870 0.00000 0.00000
  0.57130-0.14552-0.10160-0.07147-0.05104-0.03753-0.05966 0.42870 0.14552 0.10160 0.07147 0.05104 0.03753 0.05966 0.00000 0.00000
 -0.29823 0.81241-0.13097-0.09213-0.06579-0.04838-0.07691 0.29823 0.18759 0.13097 0.09213 0.06579 0.04838 0.07691 0.00000 0.00000
 -0.20822-0.13097 0.82188-0.12529-0.08947-0.06579-0.10459 0.20822 0.13097 0.17812 0.12529 0.08947 0.06579 0.10459 0.00000 0.00000
 -0.14647-0.09213-0.12529 0.82454-0.12529-0.09213-0.14647 0.14647 0.09213 0.12529 0.17546 0.12529 0.09213 0.14647 0.00000 0.00000
 -0.10459-0.06579-0.08947-0.12529 0.82188-0.13097-0.20822 0.10459 0.06579 0.08947 0.12529 0.17812 0.13097 0.20822 0.00000 0.00000
 -0.07691-0.04838-0.06579-0.09213-0.13097 0.81241-0.29823 0.07691 0.04838 0.06579 0.09213 0.13097 0.18759 0.29823 0.00000 0.00000
 -0.05966-0.03753-0.05104-0.07147-0.10160-0.14552 0.57130 0.05966 0.03753 0.05104 0.07147 0.10160 0.14552 0.42870 0.00000 0.00000

ENTER DATA FILE NAME !SCAT2
```

(Junction 3)

```
  0.42870 0.14552 0.10160 0.07147 0.05104 0.03753 0.05966 0.57130-0.14552-0.10160-0.07147-0.05104-0.03753-0.05966 0.00000 0.00000
  0.29823 0.18759 0.13097 0.09213 0.06579 0.04838 0.07691-0.29823 0.81241-0.13097-0.09213-0.06579-0.04838-0.07691 0.00000 0.00000
  0.20822 0.13097 0.17812 0.12529 0.08947 0.06579 0.10459-0.20822-0.13097 0.82188-0.12529-0.08947-0.06579-0.10459 0.00000 0.00000
  0.14647 0.09213 0.12529 0.17546 0.12529 0.09213 0.14647-0.14647-0.09213-0.12529 0.82454-0.12529-0.09213-0.14647 0.00000 0.00000
  0.10459 0.06579 0.08947 0.12529 0.17812 0.13097 0.20822-0.10459-0.06579-0.08947-0.12529 0.82188-0.13097-0.20822 0.00000 0.00000
  0.07691 0.04838 0.06579 0.09213 0.13097 0.18759 0.29823-0.07691-0.04838-0.06579-0.09213-0.13097 0.81241-0.29823 0.00000 0.00000
  0.05966 0.03753 0.05104 0.07147 0.10160 0.14552 0.42870-0.05966-0.03753-0.05104-0.07147-0.10160-0.14552 0.57130 0.00000 0.00000
  1.42870 0.14552 0.10160 0.07147 0.05104 0.03753 0.05966-0.42870-0.14552-0.10160-0.07147-0.05104-0.03753-0.05966 0.00000 0.00000
  0.29823 1.18759 0.13097 0.09213 0.06579 0.04838 0.07691-0.29823-0.18759-0.13097-0.09213-0.06579-0.04838-0.07691 0.00000 0.00000
  0.20822 0.13097 1.17812 0.12529 0.08947 0.06579 0.10459-0.20822-0.13097-0.17812-0.12529-0.08947-0.06579-0.10459 0.00000 0.00000
  0.14647 0.09213 0.12529 1.17546 0.12529 0.09213 0.14647-0.14647-0.09213-0.12529-0.17546-0.12529-0.09213-0.14647 0.00000 0.00000
  0.10459 0.06579 0.08947 0.12529 1.17812 0.13097 0.20822-0.10459-0.06579-0.08947-0.12529-0.17812-0.13097-0.20822 0.00000 0.00000
  0.07691 0.04838 0.06579 0.09213 0.13097 1.18759 0.29823-0.07691-0.04838-0.06579-0.09213-0.13097-0.18759-0.29823 0.00000 0.00000
  0.05966 0.03753 0.05104 0.07147 0.10160 0.14552 1.42870-0.05966-0.03753-0.05104-0.07147-0.10160-0.14552-0.42870 0.00000 0.00000

ENTER DATA FILE NAME !SCAT3
```

(Junction 4)

```
 -0.42870-0.14552-0.10160-0.07147-0.05104-0.03753-0.05966 1.42870 0.14552 0.10160 0.07147 0.05104 0.03753 0.05966 0.00000 0.00000
 -0.29823-0.18759-0.13097-0.09213-0.06579-0.04838-0.07691 0.29823 1.18759 0.13097 0.09213 0.06579 0.04838 0.07691 0.00000 0.00000
 -0.20822-0.13097-0.17812-0.12529-0.08947-0.06579-0.10459 0.20822 0.13097 1.17812 0.12529 0.08947 0.06579 0.10459 0.00000 0.00000
 -0.14647-0.09213-0.12529-0.17546-0.12529-0.09213-0.14647 0.14647 0.09213 0.12529 1.17546 0.12529 0.09213 0.14647 0.00000 0.00000
 -0.10459-0.06579-0.08947-0.12529-0.17812-0.13097-0.20822 0.10459 0.06579 0.08947 0.12529 1.17812 0.13097 0.20822 0.00000 0.00000
 -0.07691-0.04838-0.06579-0.09213-0.13097-0.18759-0.29823 0.07691 0.04838 0.06579 0.09213 0.13097 1.18759 0.29823 0.00000 0.00000
 -0.05966-0.03753-0.05104-0.07147-0.10160-0.14552-0.42870 0.05966 0.03753 0.05104 0.07147 0.10160 0.14552 1.42870 0.00000 0.00000
  0.57130-0.14552-0.10160-0.07147-0.05104-0.03753-0.05966 0.42870 0.14552 0.10160 0.07147 0.05104 0.03753 0.05966 0.00000 0.00000
 -0.29823 0.81241-0.13097-0.09213-0.06579-0.04838-0.07691 0.29823 0.18759 0.13097 0.09213 0.06579 0.04838 0.07691 0.00000 0.00000
 -0.20822-0.13097 0.82188-0.12529-0.08947-0.06579-0.10459 0.20822 0.13097 0.17812 0.12529 0.08947 0.06579 0.10459 0.00000 0.00000
 -0.14647-0.09213-0.12529 0.82454-0.12529-0.09213-0.14647 0.14647 0.09213 0.12529 0.17546 0.12529 0.09213 0.14647 0.00000 0.00000
 -0.10459-0.06579-0.08947-0.12529 0.82188-0.13097-0.20822 0.10459 0.06579 0.08947 0.12529 0.17812 0.13097 0.20822 0.00000 0.00000
 -0.07691-0.04838-0.06579-0.09213-0.13097 0.81241-0.29823 0.07691 0.04838 0.06579 0.09213 0.13097 0.18759 0.29823 0.00000 0.00000
 -0.05966-0.03753-0.05104-0.07147-0.10160-0.14552 0.57130 0.05966 0.03753 0.05104 0.07147 0.10160 0.14552 0.42870 0.00000 0.00000

ENTER DATA FILE NAME !SCAT4
```

(Junction 5)

```
  0.42870 0.14552 0.10160 0.07147 0.05104 0.03753 0.05966 0.57130-0.14552-0.10160-0.07147-0.05104-0.03753-0.05966 0.00000 0.00000
  0.29823 0.18759 0.13097 0.09213 0.06579 0.04838 0.07691-0.29823 0.81241-0.13097-0.09213-0.06579-0.04838-0.07691 0.00000 0.00000
  0.20822 0.13097 0.17812 0.12529 0.08947 0.06579 0.10459-0.20822-0.13097 0.82188-0.12529-0.08947-0.06579-0.10459 0.00000 0.00000
  0.14647 0.09213 0.12529 0.17546 0.12529 0.09213 0.14647-0.14647-0.09213-0.12529 0.82454-0.12529-0.09213-0.14647 0.00000 0.00000
  0.10459 0.06579 0.08947 0.12529 0.17812 0.13097 0.20822-0.10459-0.06579-0.08947-0.12529 0.82188-0.13097-0.20822 0.00000 0.00000
  0.07691 0.04838 0.06579 0.09213 0.13097 0.18759 0.29823-0.07691-0.04838-0.06579-0.09213-0.13097 0.81241-0.29823 0.00000 0.00000
  0.05966 0.03753 0.05104 0.07147 0.10160 0.14552 0.42870-0.05966-0.03753-0.05104-0.07147-0.10160-0.14552 0.57130 0.00000 0.00000
  1.42870 0.14552 0.10160 0.07147 0.05104 0.03753 0.05966-0.42870-0.14552-0.10160-0.07147-0.05104-0.03753-0.05966 0.00000 0.00000
  0.29823 1.18759 0.13097 0.09213 0.06579 0.04838 0.07691-0.29823-0.18759-0.13097-0.09213-0.06579-0.04838-0.07691 0.00000 0.00000
  0.20822 0.13097 1.17812 0.12529 0.08947 0.06579 0.10459-0.20822-0.13097-0.17812-0.12529-0.08947-0.06579-0.10459 0.00000 0.00000
  0.14647 0.09213 0.12529 1.17546 0.12529 0.09213 0.14647-0.14647-0.09213-0.12529-0.17546-0.12529-0.09213-0.14647 0.00000 0.00000
  0.10459 0.06579 0.08947 0.12529 1.17812 0.13097 0.20822-0.10459-0.06579-0.08947-0.12529-0.17812-0.13097-0.20822 0.00000 0.00000
  0.07691 0.04838 0.06579 0.09213 0.13097 1.18759 0.29823-0.07691-0.04838-0.06579-0.09213-0.13097-0.18759-0.29823 0.00000 0.00000
  0.05966 0.03753 0.05104 0.07147 0.10160 0.14552 1.42870-0.05966-0.03753-0.05104-0.07147-0.10160-0.14552-0.42870 0.00000 0.00000
```

Figure B.1 - Scatter Matrices.

PUBLICATIONS

1. Buchan, J.G., and Edwards, D.G.:'A technique for the location of partial discharge in the stator winding of a high-voltage motor', 5th BEAMA International Electrical Insulation Conference, Brighton, England, May 1987, pp.225-229.

A TECHNIQUE FOR THE LOCATION OF PARTIAL DISCHARGE IN THE STATOR WINDING OF A HIGH-VOLTAGE MOTOR

J G Buchan and D G Edwards
Robert Gordon's Institute of Technology, Aberdeen

1 INTRODUCTION

If a large electric motor fails in service the cost of repair is often secondary to the loss of production which ensues. This is especially so in high-cost operations such as offshore oil and gas production where the harsh environment and severe duty cycles have contributed to a higher than expected failure rate of high power drives (1). For this reason, there is an increasing interest in on-line condition monitoring techniques applicable to large electric motors. Some monitoring techniques, based on measurement of vibration and temperature, are well established, and, more recently, it has been shown that spectral analysis of the supply current waveform can give information on rotor problems (2,3). A survey has shown that almost a half of all large motor failures are due to insulation breakdown, but there is, as yet, no generally available on-line technique for monitoring stator winding insulation. Some off-line diagnostic techniques are well established (4), but the majority of insulation failures which have occurred in machines with epoxy-mica insulation systems have been the result of degradation processes which have developed too rapidly to be predicted by tests carried out during routine maintenance shut-down periods.

The most obvious basis for a condition monitoring technique for high voltage insulation is a measurement of partial discharge activity, since the discharge characteristic of the insulation structure may be expected to change with the development of any one of a number of possible degradation processes. An on-line technique should be non-invasive so that it cannot itself detract from the drive reliability. Furthermore it should be able to separately identify the discharge characteristic of one machine in a situation where several high-voltage motors are connected to the same supply busbars via short lengths of cable, and it should preferably give information concerning the location of high-energy discharge sites in the stator winding structure.

2 GENERAL CONCEPT

The new technique developed for detection and location of partial discharges in the stator winding structure is based upon the behaviour of the winding as a transmission line when subjected to high-frequency disturbances. Signals arriving at the line and neutral ends of the phase winding are detected by means of Rogowski coils and transmitted via fibre optic links to a processing unit. A block diagram of the system is shown in Figure 1.

Each of the programmable delay lines has a maximum delay equal to the propagation time for a pulse to travel the length of the phase winding. The delay lines are switched in synchronism, under control of a microcomputer, and in a manner such that the sum of the two delays is always just equal to the winding propagation time. Thus, for a given combination of delay line settings, the coincidence unit

will only recognise pulses originating from one local area of the phase winding.

The output from the coincidence unit is fed to a multichannel analyser which has options of multichannel scaling or pulse height analysis modes. The MCA also operates under control of the microcomputer and, when multichannel scaling is implemented in synchronism with delay line switching the resultant display on the MCA screen is a scan of discharge activity along the phase winding.

In the multichannel scaling mode the system can only count pulses above a chosen threshold level, but when an area of interest has been located by the scan technique the discharge activity at this locality can be examined in greater detail by freezing the scan at that point and implementing pulse height analysis mode on the MCA.

Since the technique rejects pulses from all positions on the winding other than the one focussed by the delay line settings, it follows that pulses originating from discharge sources external to the machine under examination will also be rejected. Accidental coincidences will occur but the resolution of the coincidence unit can be fine enough to ensure that this is not a serious problem.

3 EXPERIMENTAL SYSTEM

For the purposes of development of the location technique, a model winding was constructed of a group of 6.6 kV, 7-turn coils supported in a cradle of sheet copper which had the correct slotted profile of a stator core. Since the pulse penetration depth for steel is less than 50 μm at 100 kHz, it was not considered necessary to include an iron core in the model. A similar conclusion has been reached by previous workers (5). The model winding was terminated in a resistance representative of the surge impedance of the supply cable.

The Rogowski coils were wound onto polythene formers and enclosed in copper screening cans. Each coil had 200 turns and was terminated by a resistor of sufficiently low ohmic value to give the coil a self-integrating characteristic.

The programmable delay lines were made up of binary weighted lengths of low-loss coaxial cable. Each line had a total delay of 1.6 microseconds and was variable in 256 steps of 6.3 nanoseconds each. An IEEE bus system was used to interconnect the microcomputer, the delay lines, and the digital plotter. Control of the multichannel analyser was via an RS 232 link.

Pulse generators were capacitively coupled to the model winding as required to simulate partial discharge sources.

4 PULSE PROPAGATION IN A STATOR WINDING

The success of the location technique is dependent on the winding behaving as a transmission line to high-frequency disturbances and the pulse still being identifiable at the termination after frequency-selective attenuation in the winding. A study of pulse propagation in the model winding was therefore undertaken prior to the development of the location technique.

Each coil behaves as a multiconductor transmission line to high speed transients (6) and the precise mode of propagation is complex. The speed of travel in the slot portion of the winding will be somewhat lower than in the end winding region, but an effective propagation velocity can be established to form the basis of a location technique. Figure 2 shows an idealised pulse which was injected into the model winding at a point six coils away from one termination and the resultant pulse detected at the termination after a delay of 660 nanoseconds. The effective propagation velocity is therefore 120 metres/microsecond based on the coil dimensions.

5 DISCHARGE LOCATION TEST RESULTS

The scan plots of Figures 3-5 illustrate the results of tests carried out on a group of six 6.6 kV coils. Artificial discharge sources were applied as necessary to the intercoil connection points. For the first test, a single source was connected to each of the intercoil links and to each end of the winding in turn. A location scan was carried out in each case and all seven results are plotted for convenience of comparison in Figure 3. Full scale on the Channel Position axis represents 256 delay increments, each of 6.3 nanoseconds, so that the well-defined peaks on the plot indicate the positions of connection of the pulse source to within 2-3 delay increments, or, in terms of position, of the order of one turn of the coil. The precision of location is governed essentially by the resolution of the coincidence unit (15-20 ns).

Figure 4 shows the result of applying two pulse sources to the winding simultaneously. A source of 5 kHz repitition frequency was applied to the link between coils 1 and 2, and a second source of 1.6 kHz repetition frequency was connected to the link between coils 5 and 6. The positions of the peaks accord with predicted positions and the amplitudes, in terms of pulse count, are 1167 and 380 respectively, which are reasonably close to the pulse counts of 1250 and 416 calculated from the dwell time of 250 milliseconds for each channel position. The dwell time was arbitrary for this test, but in a situation where a motor winding is excited by a power frequency test voltage, or normal supply source, the dwell time for each scan position should be an integral multiple of the period of the supply waveform. Thus for a 256 position scan and a 50 Hz supply, the minimum value of total scan time would be 256 x 0.02 = 5.12 seconds. In practice it would be desirable to have a dwell time of several supply cycles to allow for random variations in discharge generation, so that a typical scan time for 256 channels might be of the order of one minute.

Figure 5 shows the result of a scan test with six independent sources of different repetition frequencies connected to the model winding.

6 CONCLUSIONS

A new technique has been described for the location of partial discharge sites in the stator winding of a high-voltage motor. The method has been shown to be accurate and reliable when applied to a model winding under controlled conditions with artificial discharge sources.

Further development of the work will be aimed at proving the technique on a real stator winding with partial discharges generated by a high-voltage source. Owing to the multiplicity of discharge sites in a machine in normal service, it is not anticipated that the technique will be able to give an accurate scan of low level discharge activity throughout the winding, but it essentially counts pulses above a chosen energy threshold level and should therefore find application particularly in the location of local areas of high-energy discharge activity in an otherwise reasonably healthy winding. A requirement for this facility has been highlighted previously (1,7).

Although the new location technique, when fully developed, should be a useful addition to the range of off-line diagnostic procedures currently applied during routine maintenance shut-down periods, potentially its greatest value is as an on-line condition monitoring technique which would give early warning of a developing problem.

7 ACKNOWLEDGEMENTS

The authors wish to express their gratitude to SERC for financial support for the work, to Brioil plc for sponsorship of Mr J G Buchan and to Mr A J Low for technical assistance.

8 REFERENCES

1 Hardy Bishop, B A, Connolly, B P F, and Courtney, R G "The Reliable Offshore Motor - an Outline Sketch" Offshore Europe '85, Conference and Exhibition, Aberdeen, September 1985

2 Thomson, W T, Leonard, R A, Deans, N D and Milne, A J "Monitoring Strategy for Discriminating Between Different Types of Rotor Defects in Induction Motors" 18th UPEC Proc University of Surrey, 1983, pp 241-246

3 Cameron, J R, Thomson, W T and Dow, A B "Vibration and Current Monitoring for Detecting Air Gap Eccentricity in Large Induction Motors" IEE Conference Publication No 254 : Electrical Machines - Design and Applications, 1985, pp 173-179

4 Simons, J S "Diagnostic Testing of High-Voltage Machine Insulation" IEE Proc, Vol 127, Pt B, No 3, May 1980, pp 139-154

5 Miller, R, Black, I A and Hogg, W K "Development of Techniques for Detecting and Locating the Source of Partial Discharges in Stator Windings of Electrical Machines" 4th BEAMA International Electrical Insulation Conference, Brighton, May 1980, pp 228-232

6 McLaren, P G and Oraee, H "Multiconductor Transmission Line Model for the Line-End Coil of Large A.C. Machines" IEE Proc, Vol 132, Pt B, No 3, May 1985, pp 149-156

7 Wilson, A and Jackson, R J "Discharge Detection Techniques for Stator Windings" IEE Proc, Vol 132, Pt B, No 5, September 1985, pp 234-244

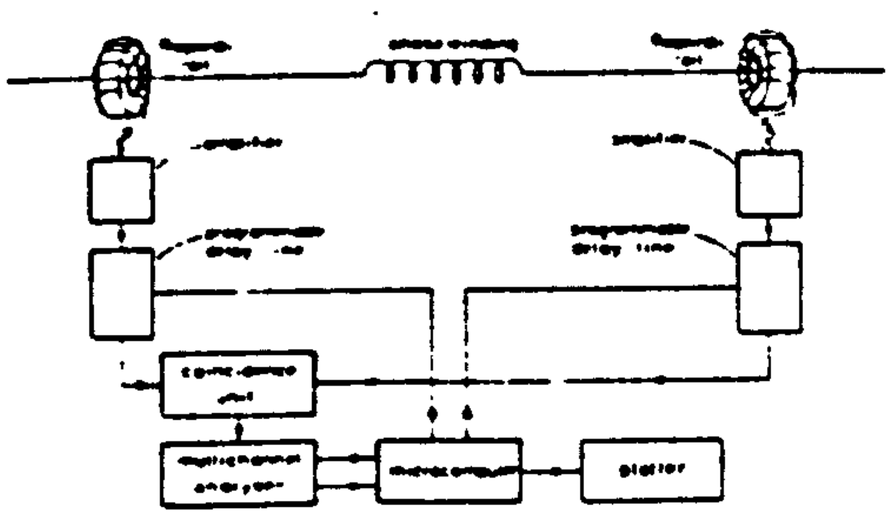

Figure 1 Discharge detection and location system

Figure 2 Pulse transmission through 6 coils

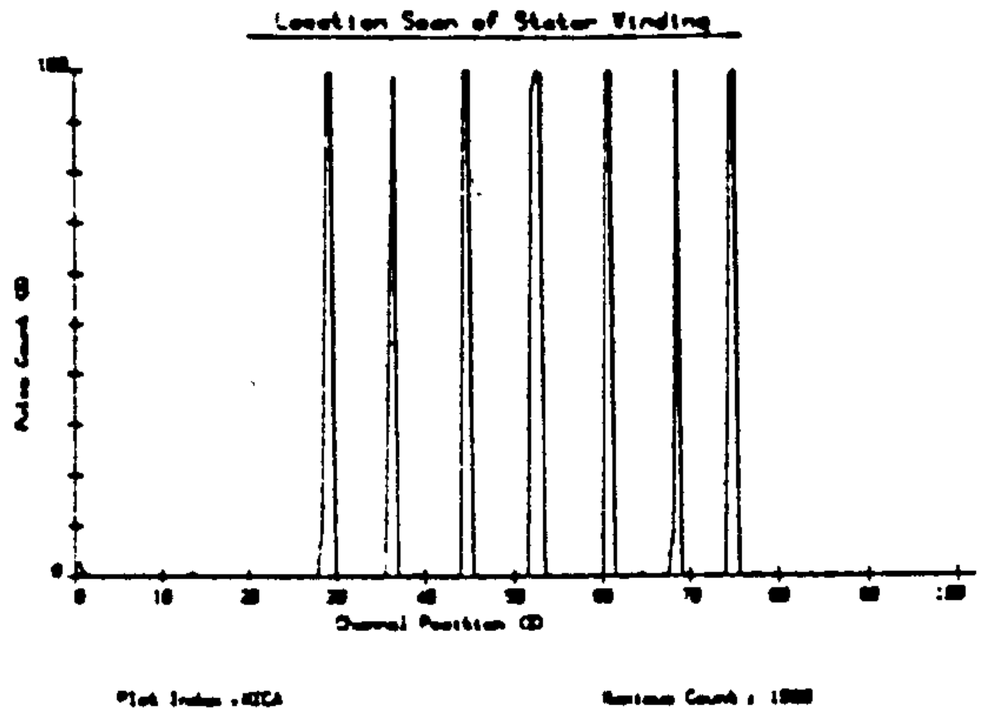

Figure 3 Scan Plot for One Pulse Source

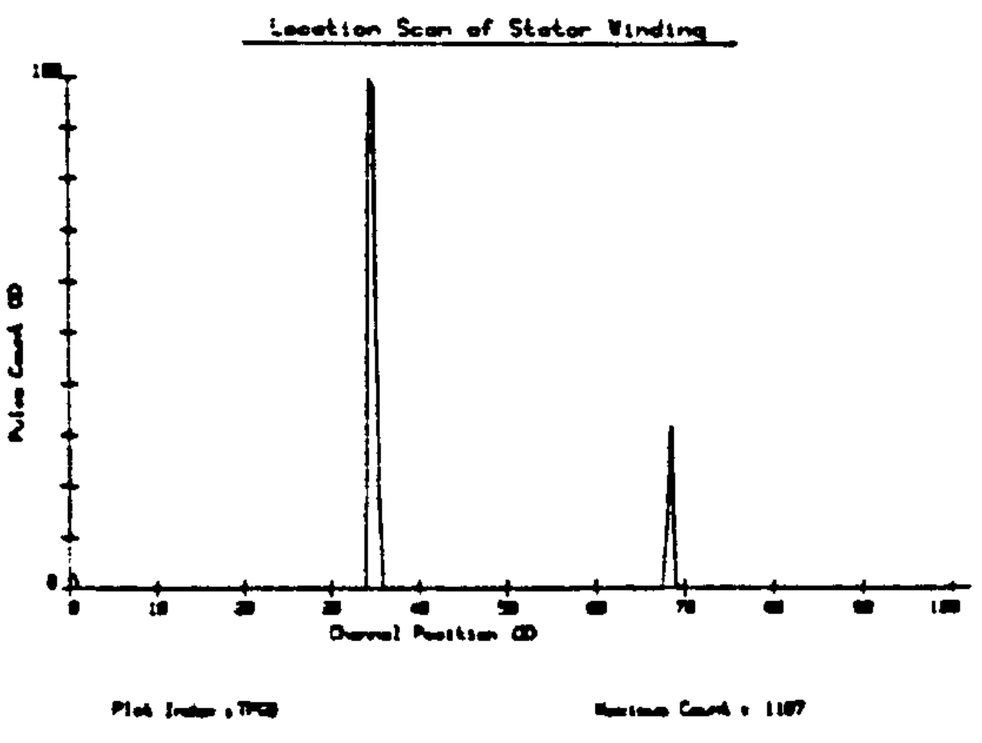

Figure 4 Scan Plot for Two Pulse Sources

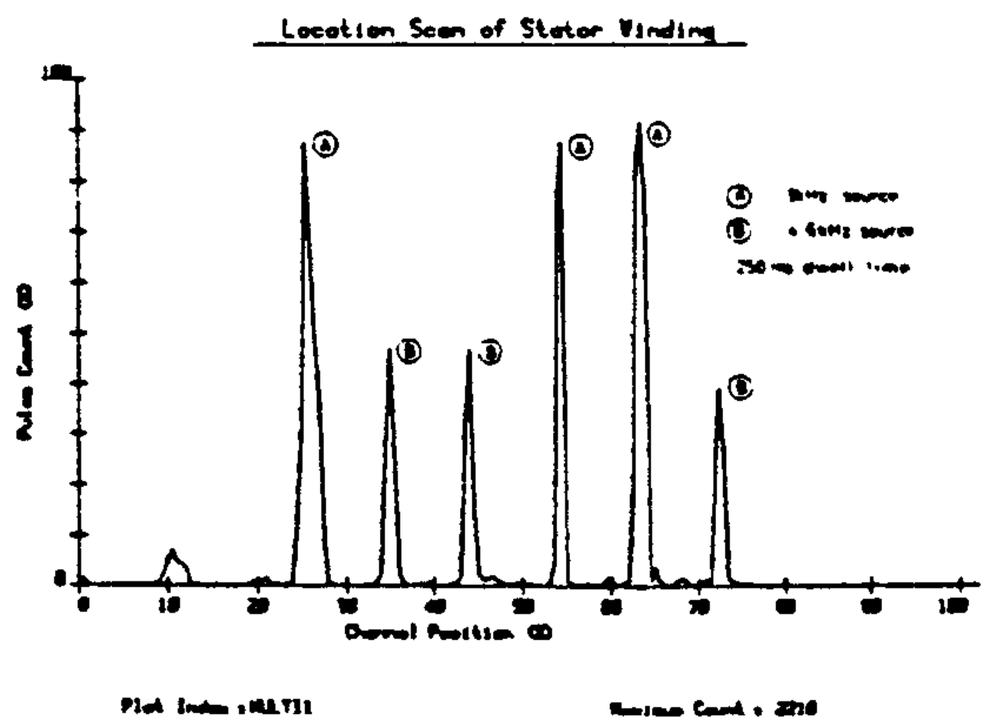

Figure 5 Scan Plot for Six Pulse Sources